71

THE CAPE RAPIDLY OSCILLATING Ap STAR SURVEY

by

PETER MARTINEZ

Thesis presented to the Faculty of
Science at the University of Cape Town
for the Degree of
DOCTOR OF PHILOSOPHY

UNIVERSITY OF CAPE TOWN

August 1993

Abstract

The cool peculiar A-type stars occupy only a small region of the HR diagram, but it is a region rich in interesting astrophysical behaviour. These stars, referred to as Ap stars, for "A peculiar", have peculiar spectra with anomalously strong lines of Si, Sr, Cr, Eu and other rare earth elements. They also have global magnetic fields with strengths of typically a few kG. The line strength anomalies reflect real abundance anomalies in the upper atmospheres of these stars. The origin of these abundance anomalies is thought to lie in magnetically guided chemical diffusion. The "classical" Ap phenomenon ranges in temperature from about spectral type B8 to spectral type F0. Towards the cool end of their temperature range, the Ap stars overlap the classical instability strip, where both radial and non-radial low-overtone pulsation occur in the δ Scuti variables.

The rapidly oscillating Ap (roAp) stars are cool Ap stars which exhibit rapid broadband photometric oscillations with periods in the range of 6 - 15 min and peak-to-peak amplitudes ≤ 0.016 mag in Johnson B light. The oscillations are non-radial p-modes of low degree ($\ell \leq 3$) and very high overtone ($n \approx 10 - 80$). The study of these oscillations, asteroseismology, opens a window to the interior structure, dynamics and magnetic fields of roAp stars. The pulsations can also be used to probe the outer layers to provide further clues to the physics of the Ap phenomenon. The roAp stars are currently the only upper main sequence stars whose high-overtone oscillations are routinely studied.

In the past 20 years, a number of searches for pulsation in the Ap stars have been conducted. The earlier searches were aimed at finding low-overtone (*i.e.* δ Scuti-like) pulsation. The discovery of high-overtone pulsations in the cool Ap stars in the late 1970's motivated a number of searches for roAp stars in the 1980's. A literature survey of surveys has been conducted. Although all searches for pulsation in Ap stars are listed, emphasis is placed on the searches for high-overtone pulsation in Ap stars. A list of Ap stars with null results in searches for high-overtone pulsation is presented.

This thesis describes a survey, the Cape Survey, which was started with the intention of discovering more roAp stars suitable for asteroseismological studies and also to identify the limits of the roAp phenomenon in temperature and luminosity. This is the most extensive survey of the roAp phenomenon to date. Prior to the start of the Cape Survey, only 14 roAp stars, discovered over a

period of 12 years, were known. The Cape Survey has yielded another 10 new roAp stars in the past three years. The candidates for the Cape Survey were mostly drawn from the Ap SrCrEu stars in the Michigan Spectral Catalogue. All the candidates were observed in the Strömgren $uvby\beta$ photometric system in order to obtain their Strömgren photometric indices. One of the major results of this survey is a catalogue of Strömgren $uvby\beta$ photometry for all the southern Ap SrCrEu stars in the Michigan Spectral Catalogue for declination $\delta \leq -12^{o}$.

The second phase of the observing program in the Cape Survey was to search for rapid oscillations in a large subset of stars chosen to sample the range of photometric indices as broadly as possible. This was done in order to determine the photometric limits of the roAp phenomenon. We searched for rapid oscillations in 148 Ap SrCrEu stars and were rewarded with the discovery of 10 new roAp stars. These new roAp stars are presented in this thesis and preliminary frequency analyses of their oscillations are given.

The null results of our searches for rapid oscillations are also presented in the form of an atlas of high-speed photometry of Ap SrCrEu stars. We emphasize that the appearance of a star in our atlas of null results *does not exclude the roAp phenomenon in that star*. All that one is entitled to conclude is that the star was constant for the duration of the observations. In many cases, only a single light curve of 1 - 2 hr duration exists for a given star. Such results should be seen as inconclusive rather than as secure negative results. Indeed, several roAp stars may lie in the atlas awaiting discovery. There are a number of stars in the atlas that show intriguing variations on the same timescales as roAp star oscillations; such stars should be observed again.

Several of the new roAp stars suffer multi-mode pulsations and, as such, are of interest asteroseismologically. Two of the new roAp stars, HD 42659 and HD 196470, are equatorial stars. Since most roAp stars are in the south and most roAp star observers are in the northern hemisphere, these stars should be of interest to some northern observers. The rapid oscillations in two of the new roAp stars, HD 84041 and HD 119027, have been studied in detail. Analyses of these observations reveal that these stars are multi-mode pulsators with non-stationary amplitude spectra.

An examination of the distribution of the roAp stars in various Strömgren photometric diagrams has allowed us to identify the photometric limits of the roAp phenomenon. The null results of pulsation searches, when plotted on these diagrams, show that the parameter space has been well explored. We are thus fairly confident that these limits represent true astrophysical limits and are not a selection effect.

The standard photometric calibrations of temperature and luminosity derived for chemically normal A stars cannot be applied reliably to the heavily blanketed Ap stars. Fortunately, asteroseismology offers a means of estimating the luminosities of the roAp stars. In this thesis, estimates of the effective temperatures of the roAp stars are derived using the Cape Survey β photometry. These estimates of T_{eff} are combined with the observed p-mode spacings and theoretical A-star models to estimate the asteroseismological luminosities of the roAp stars. The temperatures and luminosities derived in this way are used to plot the positions of the roAp stars in a temperature-luminosity diagram. This diagram suggests that the roAp stars are all sightly evolved main sequence objects lying within the δ Scuti instability strip. This implicates the κ-mechanism as the source of pulsational driving.

The oscillation spectra of the roAp stars are nonstationary on timescales of days to years. Short-term changes in the structure of the amplitude spectrum are caused by changes from one pulsation mode to another. Long-term changes are usually changes in frequency and are caused by evolution, orbital motion or a stellar cycle of some kind (*e.g.* a magnetic cycle).

An exciting recent idea is the possibility of using multicolour photometry of the rapid oscillations to probe the outer layers of the roAp stars. By observing the oscillations in the *UBVRIJHK* passbands, it should be possible to construct an empirical $T(\tau)$ relation for the atmosphere of an Ap star. Since the oscillation amplitudes of the roAp stars drop sharply towards the infrared, the viability of this idea depends on the precision that can be attained in high-speed infrared photometry. Trial high-speed infrared observations of the roAp star HR 1217 are presented. These observations constitute the first convincing detection of the oscillations of a roAp star in the infrared and it is argued that the aforementioned project is viable at a good infrared site.

Finally, we discuss the estimation of main sequence ages using asteroseismology and we compare the results of model calculations with the observations for three roAp stars.

Foreword

This thesis is intended to be a working document for astronomers engaged in roAp star research. As such, it lists virtually all of the available data on the roAp stars and provides bibliographical references to the original sources of data. Extensive tabular material is presented in this thesis. Since this material forms the core of the thesis, it has been integrated into the main body of the thesis instead of being relegated to a lengthy series of appendices at the end. To facilitate access to the data, a list of Tables is included on page *xii*.

This style of presentation has been motivated by our experiences of observing roAp stars in the past where it has usually been the case that the basic data for the roAp stars (and roAp star candidates) were scattered over a number of different bulky catalogues. Observers searching for new roAp stars would often go to the telescope armed with a box of catalogues. One of the aims of this presentation is to replace that box of catalogues with just this thesis - for a few years, at least.

In this thesis I have taken care to emphasize the observations and to limit the range of interpretations. The reason for this is that many facets of the roAp phenomenon are not yet well understood, so it is to be expected that the interpretations may change as new data are collected. The data, however, will not change and any later interpretations will have to accommodate them also.

A complete appreciation of the roAp stars requires an understanding of the Ap phenomenon. For this reason, chapter 1 provides a fairly detailed introduction to the chemically peculiar stars of the upper main sequence. Readers with a knowledge of the Ap phenomenon may wish to commence reading in chapter 2. On a first reading, readers wishing to grasp only the essentials of the Ap phenomenon may wish to read only sections 1.1 to 1.3 and sections 1.15 and 1.16 before moving on to chapter 2.

Acknowledgements

This dissertation has taken just over three years to produce and it is my pleasant duty to acknowledge the assistance of many fine people during that time. Firstly, I acknowledge the enormous amount of support, encouragement and advice from my thesis advisor, Prof. Don Kurtz. I have the greatest respect for him, both as a friend and as a scientist. Over the past three years, Don has used most of his observing time in support of the Cape Survey to provide about a third of the high-speed photometric observations reported in this thesis. His contributions of data are acknowledged in the text and references. It was Don who originally suggested that I should present this thesis as a working document for roAp star observers, rather than just presenting the results of the Cape Survey. It was a lot of work, but I'm glad I followed his advice - I really think this compilation will be useful to roAp star observers, especially those engaged in searching for new roAp stars. Don was also an influential source of support dealing with bureaucratic problems and in securing funding. Most importantly, I've learnt a lot of astronomy from him.

The investigation reported in this thesis was done at the Sutherland site of the South African Astronomical Observatory (SAAO). I say without reservation that it could probably not have been done anywhere else in the world. There are several reasons for this. Firstly, Sutherland is an *excellent* photometric site. Secondly, the policy of the SAAO to support long-term observing projects of this nature made it possible to complete this survey in three years. The observations reported in this thesis were acquired during about 50 weeks of telescope time over a time-span of three years. In this regard, I thank the former Director of the SAAO, Prof. Michael Feast, for his support of this project. Thirdly, the equipment at Sutherland is well maintained and excellent technical backup is available at all times. I acknowledge the friendly and competent assistance of the SAAO technicians, particularly Piet Fourie, Willie Koorts and Mike Fouché, who were called out on many a cold night.

With such a large survey, it was not possible for me to do all the observations alone. Don Kurtz searched for oscillations in many of my candidate roAp stars. UCT students G. Kauffmann, P. Tripe and R. Ashley contributed a number of light curves of roAp star candidates. SAAO astronomers Greg Roberts, Fred Marang and Francois van Wyk obtained a large number of *UBVRI*

observations of several roAp stars to determine their rotations periods. Where data contributed by these observers is used in frequency analyses, the source is acknowledged in the text and/or references. To all these people I offer my thanks in the hope that I might one day aid them in a similar fashion.

Back in Cape Town, I acknowledge many informative discussions with SAAO astronomers Dave Kilkenny and Luis Balona. Dave provided much advice on photometry as well as arranging for service observations of roAp stars to be made for me. Mrs Joyce Westerhuys did the basic reductions for the all-sky photometry reported in this thesis. Without her assistance, I would never have kept pace with the vast amount of data that this survey has produced. I thank Dr Kazuhiro Sekiguchi for offering to observe HR 1217 in the infrared for me and Dr Patricia Whitelock for doing the basic reductions of those data. I also had very long, interesting and informative discussions with Dr Allen Cousins and I thank him for providing me with lists of his secondary $uvby\beta$ standards prior to publication.

Closer to home, several people in the Astronomy Department at UCT have assisted or influenced this investigation from time to time. In particular, I have had informative discussions with Brian Warner and Darragh O'Donoghue as well as the occasional 1-hr light curve on a promising roAp star candidate or two. I would like to thank Brian for supporting me in my attempts to secure funding for this project and for providing a pleasant and stimulating environment in which to work. I gratefully acknowledge financial support from the Foundation for Research Development and from the University of Cape Town.

Table of Contents

List of Tables

List of Tables (continued)

Chapter 1

The chemically peculiar stars of the upper main sequence

1.1 Introduction

The main sequence A-type stars occur in a region of the HR diagram where the classical assumptions of hydrostatic and radiative equilibrium ought to be most successful at explaining the observed spectra. A-type stars possess no extensive surface convection zones, hydrogen is the primary source of opacity and rotation is moderate. Yet, the A stars exhibit the most bewildering diversity of spectra of all the classes in the spectral sequence. Approximately one fifth of the stars in the temperature range equivalent to spectral types B8 - F0 show anomalously strong (or weak) lines conspicuous enough to be identified on low resolution spectrograms (Bonsack & Wolff 1980). In her book on the A stars, Sidney Wolff (1983) begins her discussion of the normal A stars by defining a normal A star as follows:

> *"...a normal A-type star is one that at classification dispersions shows none of the anomalies characteristic of the Ap, Am, λ Boo, or other types of peculiar stars; that when subjected to local thermodynamic equilibrium (LTE) analysis, appears to have a composition like the Sun's; and that exhibits no variability, either regular or irregular."*

The extensive, exclusive nature of these criteria for normalcy underscores what a significant fraction of A stars are deemed "abnormal" in some way or another.

This thesis concerns itself with the Ap stars which were discovered nearly a century ago when astronomers identified a distinct subclass of peculiar A-type stars that distinguished themselves from the normal A-type stars by having abnormally strong lines of one or more of the following elements: Si, Sr, Cr, Eu and other rare earths. In the past 40 years, strong magnetic fields have been found in many of these stars and these magnetic fields hold the key to understanding many of their unusual characteristics.

The chemically peculiar stars can be divided into several groups according to their dominant spectral peculiarities (Fig. 1.1). The most fruitful attempts to construct a unified description of all these groups of peculiar stars has focussed on the high stability which prevails in A star atmospheres.

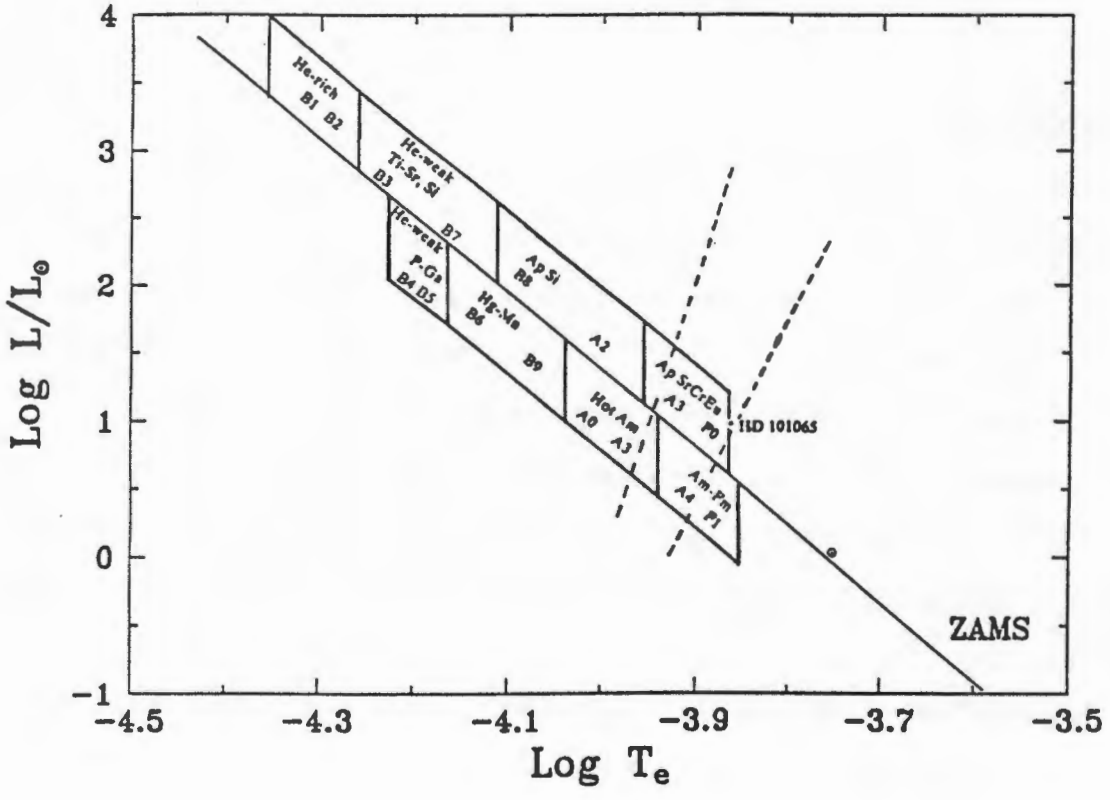

Figure 1.1 A schematic HR diagram showing the positions of the chemically peculiar stars of the upper main sequence. The stippled lines indicate the observed borders δ Scuti instability strip. The positions of the Sun and HD 101065 (see section 2.2) are indicated. The magnetic Bp - Ap stars are indicated as lying above the ZAMS line and the non-magnetic Am stars below. The luminosity borders are schematic and the separation in luminosity is for display purposes only; there is no systematic luminosity difference between these two groups of stars.

Although our discussion will focus on the chemically peculiar A-type stars, brief descriptions of these other peculiarity classes will be given later in this chapter for completeness. There are two groups of chemically peculiar A-type stars, the Ap stars and the Am stars. These stars can be distinguished at classification dispersions since the characteristically strong (or weak) absorption lines differ for the two groups. The Ap stars have strong (~kG) global magnetic fields. They are spectrum, radial velocity, magnetic and photometric variables with an unusually low binary frequency. In contrast, the Am stars are usually non-magnetic, usually constant in luminosity and spectral appearance and have and unusually high binary frequency.

In this chapter we will describe the discovery of the Ap phenomenon and the historical development of our knowledge of Ap stars. Emphasis has been placed on the discoveries that were essential to the development of the now universally accepted *oblique rotator model* of the Ap stars. This model will be presented before going on to discuss the systematics of Ap stars in detail. The reason for presenting the model first is to facilitate the reader's assimilation of a large amount of otherwise confusing observational minutiae. The discussion of Ap star systematics will end with a discussion of the detection and measurement of magnetic fields in Ap stars. This will then permit us to list several alternative theories for the origin of the anomalous spectral features. Only the most fruitful theory, *radiative diffusion*, will be discussed in detail and a case study showing the application of this theory to the Ap star 53 Cam will be presented. The chapter concludes with an overview of the other groups of chemically peculiar upper main sequence stars.

This chapter cannot hope to do justice to the immense literature that the Ap phenomenon has spawned. Readers interested in a more detailed discussion are referred to the proceedings of the following meetings: IAU Colloquium 32 (1975), Liège Colloquium 23 (1981), IAU Colloquium 90 (1985), the meeting 'Magnetic Stars' held at Nizhnij Arkhyz in Oct. 1987, the meeting 'Elemental abundance analyses' held at Lausanne 1987, IAU Symposium 145 (1991) and IAU Colloquium 138 (1992). Recent reviews have been written by Wolff (1983), Faraggiana (1987), Maitzen (1989). The most detailed recent treatment of the Ap stars appears in the book by Wolff (1983), titled *The A-type stars: Problems and perspectives*. Readers wishing to work on the A-type stars are referred to this book for the wealth of material it contains. Chapter 1 of this thesis is modelled on Wolff's treatment of the Ap stars except that I have tended to emphasize developments since 1983.

1.2 The Discovery of the Ap stars

Nearly a century ago Miss Antonia Maury, one of the early HD classifiers, first noted the peculiar nature of the spectrum of the bright northern star α^2 CVn. In particular, she remarked (Maury 1897) on the weakness of the Ca K line and the abnormal strength of the Si doublet at 4128.5 Å and 4131.4 Å. Interest in this star grew when Ludendorff (1906) discovered that the lines of Fe, Cr & Mg vary in intensity. In a further investigation of spectrum variability in α^2 CVn, Belopolsky (1913) discovered that the variations in the λ4129 Å line (attributed to Eu by Baxandall (1913)) were periodic with a period of 5.5 days. Moreover, the radial velocity was observed to vary in quadrature with the changes in intensity. Interestingly, Belopolsky's interpretation of the observations was surprisingly close to the modern interpretation of the Ap phenomenon. He postulated the existence of a gaseous satellite or a ring of circumstellar material with a condensation at one point as being the source of the spectrum and radial velocity variations. As the satellite or condensation appeared around one limb of the star, the radial velocity would be at its minimum extreme and the line intensity would be a minimum. Later in its orbit, when the satellite or condensation passed over the central meridian of the visible hemisphere, the radial velocity would pass through its mean value and the line intensity would be at a maximum. As the satellite or condensation rotated away from the observer towards the opposite limb, the radial velocity would increase while the intensity decreased. In the first photoelectric study of α^2 CVn, Guthnick & Prager (1914) discovered periodic photometric variations that varied in phase with the Eu line strength variations. Thus, by 1914 it was known that α^2 CVn is a photometric and spectrum variable, that the line intensities vary in quadrature with the radial velocity and that the light curve varies in phase with the Eu line strength variations.

In the three decades that followed, similarly correlated spectrum and photometric variations were identified in numerous other chemically peculiar stars and it began to seem that such variations were a feature of these objects. To test this, Deutsch (1947) conducted a survey of 61 stars classified as peculiar in the *Henry Draper*, or HD, catalogue to search for spectrum variability and to determine the period of variation for those stars that turned out to be variables. Deutsch's survey demonstrated that spectrum variability is indeed ubiquitous among the chemically peculiar stars. This led him to suspect that several spectrum variables had passed undetected in his study and that with continued observation, all Ap stars would prove to be spectrum variables of greater or lesser amplitude, a suspicion now known to be correct.

Deutsch's study also revealed some of the important systematics of the spectral variations in Ap stars. The lines that vary most strongly are usually those anomalously strong lines which mark the spectrum as peculiar (*e.g.* Sr, Cr, Eu and, to a lesser extent, Si). Another important feature of the variations is that although not all elements vary in phase, lines of a given ion always do. Moreover, the phase relationships of the various elements are not the same from star to star. As much as this study served to reveal some of the systematics of the Ap phenomenon, it also served to underscore the great diversity of Ap star spectra.

By the early 1930's, it was clear that the Ap stars did not form a single homogeneous group of stars and that there were different types of peculiarity that were readily identifiable at classification dispersions. This prompted Morgan (1933) to make the first attempt to define different classes of peculiarity. He identified five peculiarity classes in the spectral range B8 - F0 and found that these classes could be arranged in a temperature sequence. In order of decreasing degree of ionization these classes were the Mn II, λ4200, Eu II, Cr II and Sr II stars. Although Morgan's (1933) original classification is no longer in use, it directed further classification efforts which resulted in the classification scheme we use today (section 1.5). The lasting contribution of Morgan's classification attempts was to reveal a temperature-peculiarity relation in the Ap stars. This relationship is illustrated in Figure 1.2.

A key piece in solving the puzzle of the Ap stars fell into place when Babcock (1947) discovered that the Ap star 78 Vir has a variable magnetic field with a maximum polar field strength of 1500 G. In the same year, he also discovered a variable magnetic field in HD 125248 which underwent periodic polarity reversals (Babcock 1947b). Later work showed that most other sharp-lined Ap stars, including α^2 CVn, have variable magnetic fields which vary with the same period as the spectrum, radial velocity and photometric variations. Babcock (1947c) realized that the measured field strengths in the Ap stars were so high that they must be global fields, and not highly localized fields as in sunspots. That these fields must be low-order global magnetic fields is readily appreciated if one bears in mind the physical requirement that the net magnetic flux through the surface is zero. Field strengths of a few kG are unlikely to be measured in the integrated light of the stellar disk in high-order magnetic geometries. A more complete discussion of the observation of the magnetic fields of the Ap stars will be given in section 1.13. For our purposes here, it is sufficient to know that the Ap stars have global magnetic fields of a few kG which vary in strength with the same period as the spectrum, radial velocity and photometric variations.

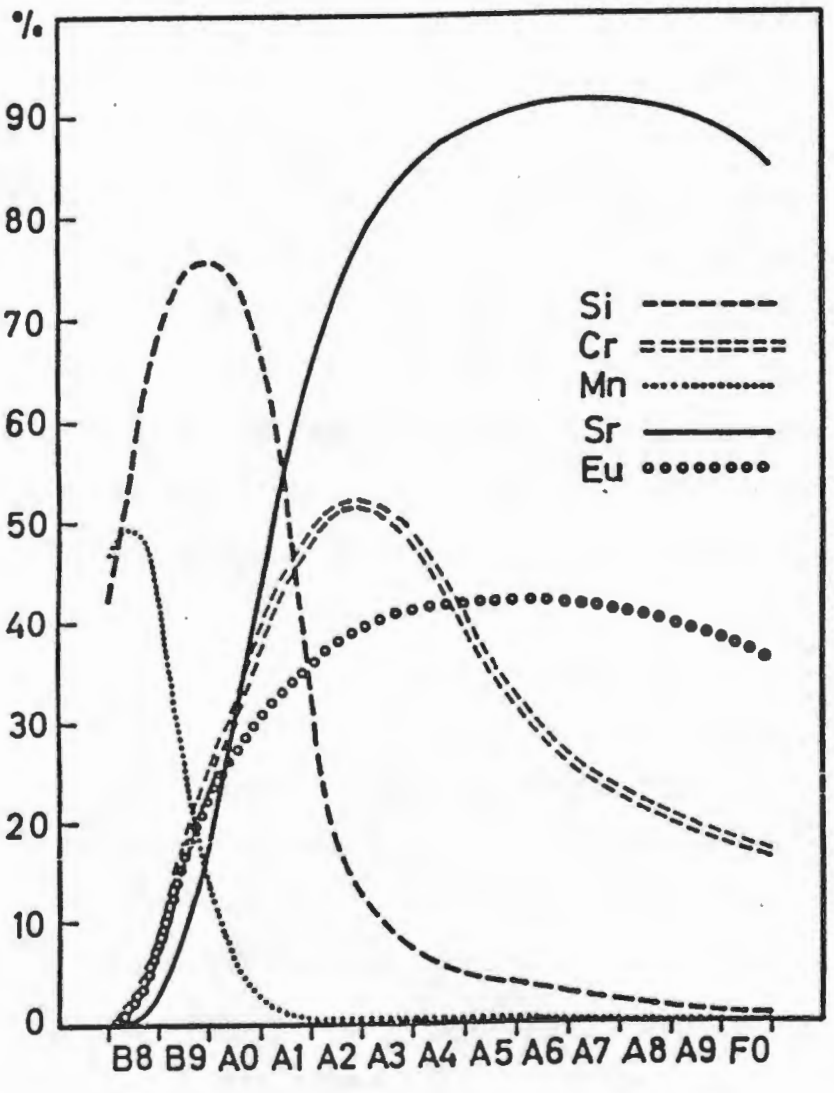

Figure 1.2 The relative percentage, per spectral class, of magnetic stars showing especially strong overabundances of Si, Cr, Mn, Sr and Eu. We will see later that the rapidly oscillating Ap stars are mostly Ap SrCrEu stars, so they are mostly late A stars. (Taken from Ledoux & Renson 1966)

1.3 The Oblique Rotator Model

Babcock's magnetic observations suggested, for the first time, that the Ap stars might possess an axis of symmetry other than the rotation axis. This is a key realization that must be reached in order to understand the variations in the Ap stars. This realization did not elude Babcock and he came tantalizingly close to developing a successful model for the variations. Babcock visualized the magnetic variations as some kind of magnetic activity correlated with rapid stellar rotation, but he realized that there was a much simpler geometrical interpretation of the observations. In a remarkably prescient letter to the journal *Observatory*, Babcock (1949) proposed what is now known as the oblique rotator model, but he did not follow it up:

> *It is true that I have suggested as a revised working hypothesis that intense magnetic activity may be correlated with rapid stellar rotation, but at this stage an equally good case can probably be made for the alternative hypothesis that the spectrum variables of type A are stars in which the magnetic axis is more or less highly inclined to the axis of rotation and that the period of magnetic and spectral variation is merely the period of rotation of the star.*

Working independently, it was Stibbs (1950) who proposed in detail the *oblique rigid rotator model* which has become the universally accepted model to explain all the variations observed in the Ap stars. This model postulates that the star is permeated by a stationary global dipole magnetic field which is frozen into the star and corotates with it. This field is inclined at some angle β to the rotation axis, in analogy to the tilt of the Earth's magnetic axis with respect to its spin axis. To a distant observer, the magnetic field will appear to vary in intensity as the star rotates. The magnetic variations will only arise if the magnetic field is inclined at an angle to the rotation axis, hence the appellation *oblique rotator*. The geometry of this model is shown in Fig. 1.3.

The magnetic polarity reversals observed in some Ap stars arise in those favourable cases where the stellar rotation axis is roughly in the plane of the sky ($i \sim 90^{\circ}$) and the dipole component of the field makes a large angle $\beta \sim 90^{\circ}$ with respect to the rotation axis. In such cases, the rotation of the star allows the observer to examine the field structure from one magnetic pole to the other.

The spectrum variations are explained by assuming that the anomalously strong lines are produced in small areas, or *spots*, on the stellar surface. When rotation brings one of these spots into

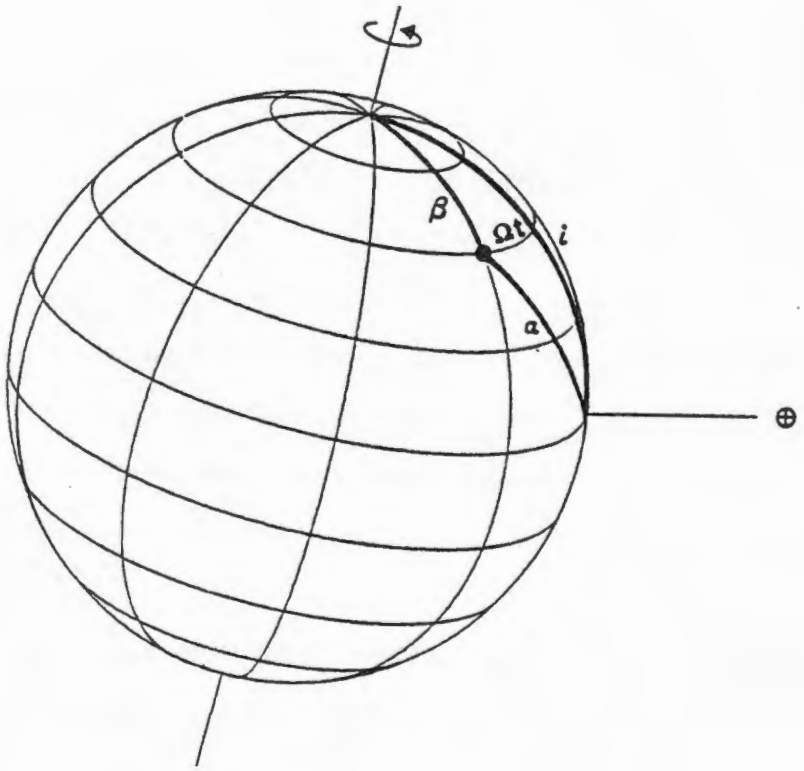

Figure 1.3 The geometry of the oblique rotator and oblique pulsator models. The direction of the observer is indicated by the Earth symbol, i is the inclination of the rotation axis to the line of sight, β is the magnetic obliquity (magnetic co-latitude), Ω is the circular rotation frequency and α is the angle between the line of sight and the magnetic pole.

the visible hemisphere, the anomalous lines become stronger as the spot moves towards the central meridian. As the spot comes into view on the limb, its radial velocity is at its minimum value (since it is directed towards the observer) and as the spot moves towards the central meridian the radial velocity increases. When the spot passes over the central meridian, the intensity of the anomalous lines passes through a maximum and the radial velocity passes through its mean value. The radial velocity then increases as the spot moves away from the centre of the disk towards the opposite limb and the lines weaken. With this hypothesis we can understand why, in some Ap stars, the lines of some elements vary with half the period of others. These lines originate in two spots on the star and have, therefore, two maxima. The coincidence of rare earth maxima with magnetic extrema indicates that these spots are at the same rotational longitude as the magnetic poles. Notice that the oblique rotator model assumes only that the anomalous lines are produced in localized regions on the surface. The physical mechanism producing the anomalous lines is completely unspecified.

1.4 Frequency

The frequency of Ap stars among the field A-type stars is a maximum for colours that correspond to normal stars of spectral type B8 - A0 and falls off rapidly outside these limits as illustrated in Table 1.1. In perusing this Table, we must bear in mind that any determination of the frequency of Ap stars obviously depends on the criteria one adopts to classify stars as peculiar or normal. This point is discussed further in section 1.5.

Table 1.1

Fraction of Ap stars in a sample of field A-type stars. (From Wolff 1983)

Colour Index	Fraction
$-0.19 \leq B-V \leq -0.10$	0.06
$-0.09 \leq B-V \leq -0.00$	0.13
$0.01 \leq B-V \leq 0.10$	0.05
$0.11 \leq B-V \leq 0.20$	0.01

The frequency of Ap stars in clusters is lower (perhaps by half) than in the field stars (Hartoog 1976, Abt 1979, Maitzen 1981, North & Cramer 1981). A possible explanation for this is that the frequency

of Ap stars increases with age as the Ap phenomenon develops in some cluster members. One way to test this hypothesis is to search for Ap stars in binaries with normal O - A-type stars. Indeed, the frequency of Ap secondaries in binaries with O5 - A1 primaries seems to be higher for the later spectral types, in support of the notion that the number of Ap stars in clusters increases with time (Abt & Cardona 1983). There is also marginal evidence for a deficit of hot Ap stars in young clusters ($< 10^7$ yr) while the frequency of cool Ap stars appears to be constant with age (North & Cramer 1981, Abt & Cardona 1983). None of the results from the studies just quoted are very secure, so the question of correlations between the incidence of peculiarity and age is still not settled.

1.5 Spectral Classification

The anomalously strong (or weak) lines in the Ap stars exhibit differences that are readily discernible at classification dispersions (normally ~ 100 Å/mm) and it is possible to form groups of Ap stars which have broadly similar spectral peculiarities. The first systematic attempts to define peculiarity classes for the Ap stars were initiated by Morgan in the 1930's. Morgan (1933) sorted the Ap stars into five groups named according to the dominant spectral peculiarity in each group and found that these groups could be arranged in a temperature sequence. Morgan's pioneer classification scheme has been superseded by more modern classification schemes, but his discovery of a colour - peculiarity type relation has been confirmed (see Fig. 1.2). The classification scheme currently in use (Jaschek & Jaschek 1958) employs five classes which, when arranged in order of colour from blue to red, are: λ4200 Si, Si, SiCrEu, EuCrSr & Sr. These five classes of Ap stars are often collectively referred to as CP2 stars, especially among European astronomers (see section 1.17 for a description of the CP notation).

It is important to appreciate that the stars in any one of these classes are not exactly alike. The spectra of these stars appear to be similar at classification dispersions (~ 100 Å/mm), but at higher resolutions, say ~ 10 Å/mm, no two Ap star spectra are exactly alike. Consequently, the number of spectral classes that can be defined depends on the resolution adopted for classification purposes. Much work has been done to find statistical correlations among certain elements from star to star and within the peculiarity classes (*e.g.* see Wolff 1983 and references therein). If anything, this work has reaffirmed the great diversity of Ap star spectra.

In the ongoing quest for better classification schemes, it is important to establish whether the Ap stars form a population distinct from the apparently normal A-type stars. Fine spectroscopic

classification has been used to demonstrate that there is no sharp border between the normal A stars and the Ap stars. The classification of peculiarity thus rests on the detection threshold defined by instrumental limitations. This apparently continuous transition from the normal A stars to the Ap stars suggests that by studying very mildly peculiar stars we may be able to learn something about the way in which the peculiarities arise.

Cowley (1991), who has worked on the problems posed by the A-type stars for many years, has summarized the diversity of their spectra as follows:

> *Normal A stars are rather like normal people. If you don't look too hard, there seem to be quite a few of them. After you get to know them well, most seem a little crazy.*

In this section, we have dealt only with the classification of stars classically defined as Ap stars, that is, stars in the spectral range B8 - F0. The classification of the other chemically peculiar stars of the upper main sequence will be dealt with in section 1.17.

1.6 Spectrum variations

Spectrum variations in the Ap stars were first noted 90 years ago and studies of these variations continue to the present day. In those Ap stars for which spectrum observations spanning many years and thousands of cycles exist, no period or phase changes are detected. This means that the Ap stars are truly rigid rotators, in sharp contrast to the Sun, which exhibits differential rotation. This rigid rotation implies that the spectrum variations can also be used to model the surface distribution of the areas or spots on the surface in which the anomalously strong lines originate. Because this endeavour requires an accurate knowledge of the surface magnetic field geometry, we will defer our discussion of surface mapping techniques until after discussing the magnetic fields in the Ap stars.

It is not only the line intensities that change in the Ap stars, but also the line profiles. In those stars with magnetic fields strong enough to broaden the lines significantly, the line widths vary periodically and in phase with the magnetic variations. Ap stars that reverse their magnetic polarity also display a very interesting change in their line profiles called the *crossover effect* (Babcock 1956). At the time of magnetic crossover, when the observed field is changing from one polarity to the other, there is a difference in the line widths in the two senses of circular polarization. This effect will be discussed in greater detail in section 1.13.

1.7 Photometric variations

It is well established that the vast majority of magnetic Ap stars are photometric variables. The amplitudes of variation are typically 0.01 to 0.10 mag (Catalano *et al.* 1993). The lower limit on the amplitude is set by the observational errors and there is good reason to believe that more precise observations (*e.g.* Kurtz *et al.* 1990) will detect photometric variations in heretofore apparently constant Ap stars. The amplitude of the variations is not correlated with period, colour, line widths, spectral peculiarity class or magnetic field strength. The light curve can vary either in phase or antiphase with the magnetic curve. The luminosity variations are detected in the *UBVRI* and *JHK* passbands, but the amplitude and character of the oscillations is strongly wavelength dependent. Figure 1.4 shows a few sample light curves from the ultraviolet to the infrared. Well defined light curves often reveal quite complex oscillations with double waves in some passbands and single waves in others. In many Ap stars, a null wavelength can be identified for which the amplitude of the variations is zero (Molnar 1973). On either side of this wavelength, the variations are in antiphase. An example of this can be seen in the top diagram in Fig 1.4.

Many of the existing light curves of the Ap stars were acquired through standard broadband Johnson UBVRI filters. For sufficiently bright stars, there are advantages to using the intermediate-band *uvby* filters because they are more likely to isolate wavelength regions where the photometric amplitude is large. This facilitates the astrophysical interpretation and modelling of the observations.

What is the cause of these photometric variations? The most generally accepted view is that the luminosity variations are a direct consequence of the spectrum variations. Enhanced continuum and line opacity in the ultraviolet causes a redistribution of flux to longer wavelengths, so variations in blanketing cause variations in the visible flux. It is possible to test this hypothesis by demonstrating that the total flux integrated over all wavelengths is a constant. Not all Ap stars pass this simple test, indicating the presence of further unknown complications. Exactly which elements are responsible for the enhanced ultraviolet blanketing is uncertain, but suspicion falls naturally on the Fe peak elements and rare earth elements as the sources of line blanketing (Muthsam 1979a, b) and Si as a source of continuous opacity (Molnar & Wu 1978).

The photometric variations discussed thus far are readily explained in terms of the oblique rotator model in which the stellar surface is inhomogeneous. The period of variation is simply the rotation period of the star. Several observers (e.g. Percy 1975, Weiss 1978) have sought photometric variations on shorter timescales and the results of their searches are discussed in chapter 3. Here we

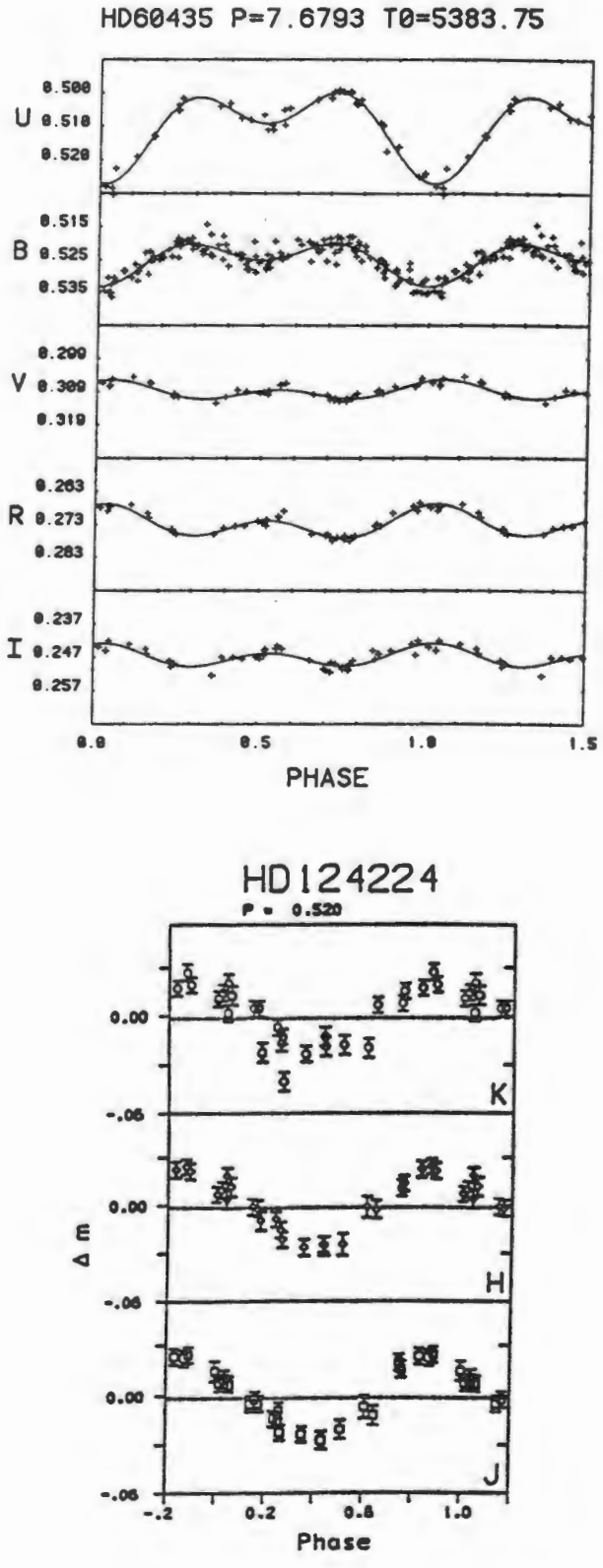

Figure 1.4 The light variations caused by rotation in the Ap stars. The top diagram shows the *UBVRI* light curve for HD 60435 (Kurtz *et al.* 1990) and the bottom diagram shows the *JHK* light curve for HD 124224 (Kroll 1989).

summarize those results by saying that the majority of Ap stars do not vary on timescales of hours to minutes with amplitudes in excess of 0.01 mag.

1.8 Radio variations

An interesting recent development is the discovery that the Ap stars are also radio variables. Drake *et al.* (1987) observed 34 chemically peculiar stars on the VLA at 2, 6 & 20 cm and detected radio emission of a few mJy in 5 of them. Of these five stars, three are He-rich and two are Ap Si stars. This radio variability shows evidence of having the same period as the light, spectrum and magnetic variations in two stars where both optical and radio observations exist (Leone 1991). In HD 37107, radio emission maximum coincides with the negative extremum of the magnetic field while radio emission minimum coincides with zero magnetic field. In σ Ori E, the sparse observations suggest that radio emission minimum occurs near a zero of the magnetic field. The origin of these radio variations is unclear. Leone (1991) postulates that the radio emission comes from the magnetic poles and is caused by the electron component of the wind flowing along open lines of the magnetic field. Drake *et al.* (1987) have postulated that the radio emission is due to gyrosynchrotron emission from continuously injected mildly relativistic particles trapped in an equatorial belt. In this picture, a distant observer would see the relativistic electrons radiating forward into a narrow cone and would observe radio maximum at magnetic crossover. This expectation is not supported by Leone's observation (in Drake *et al.*'s data) of the coincidence of radio minimum with zero longitudinal magnetic field.

1.9 Binary frequency

The frequency of Ap stars in spectroscopic binaries is significantly lower than the frequency of normal A stars in binaries. Of the Si and SrCrEu stars, only 20% are members of spectroscopic binaries, whereas the frequency of normal A-type stars in spectroscopic binaries is 43% (Abt & Snowden 1973, Floquet 1983 & Gerbaldi *et al.* 1985). The frequency of Ap stars in visual binaries is the same as the frequency of normal A-type stars in visual binaries. In contrast to the low binary frequency of the Ap stars, all A4 - F1 luminosity class IV-V stars that are primaries of binaries with periods in the range of $2.5 \leq P \leq 100$ days are Am stars (Abt 1961, 1965, Abt & Bidelman 1969).

1.10 Rotational velocities

The Ap stars rotate much slower as a group than do normal A-type stars of the same temperature. Indeed, it is the sharpness of their lines that permits the detection of their magnetic fields. Although slow rotation is associated with the Ap phenomenon, it is not a sufficient condition for the appearance of spectral anomalies. This is evinced by the existence of many slowly rotating chemically normal A-type stars and numerous rapidly rotating Ap Si and Ap SiCr stars (Wolff 1983).

One important property of the rotational velocities in Ap stars is that $v \sin i$ appears to decrease as the mass decreases (Wolff 1981). This property is evident in a plot of the distribution of $v \sin i$ for different classes of Ap stars (Wolff 1983). The slow rotation of the Ap stars is attributed to magnetic braking. Thus a natural, though not proven, explanation for the decrease in $v \sin i$ with decreasing mass is that the less massive stars evolve more slowly and so experience magnetic braking for longer. However, this result is not well established since an independent study by North (1984) found that the rotational velocities of Ap stars do not depend on age and that the Ap stars spin down before reaching the main sequence. Further work is required before any secure conclusions can be reached regarding correlations of rotation with age in Ap stars.

Measurement of rotation periods for Ap stars offers a way to test the oblique rotator model. If this model is correct, Ap stars with short rotation periods must generally have broader lines than stars with long rotation periods. The expected equatorial rotation velocity v for an oblique rotator of radius R rotating with period P is

$$v\,(\mathrm{km/s}) = 50.6\, R(R_\odot) \,/\, P\,(\mathrm{days}).$$

Thus, the line widths are expected to be inversely related to the rotation periods. In practice, it is the projected rotation velocity, $v \sin i$, that is measured, so the above relation should define an upper envelope to the observations (Fig. 1.5). This test was first conducted by Deutsch (1952) at Mt Wilson and the results were in agreement with expectations based on the oblique rotator model. Whilst this did not constitute a proof that Ap stars are oblique rotators, it was an early source of support for the model.

The rotation periods of the Ap stars fall mostly into the 1- to 10-day range, but some stars have *much* longer periods. Examples of such stars are HR 465 ($P \sim 24$ yr, Rice 1988) and γ Equ ($P \sim 72$ yr, Wolff 1983). The existence of such slow rotators implies that the braking mechanism active in Ap stars can be very efficient.

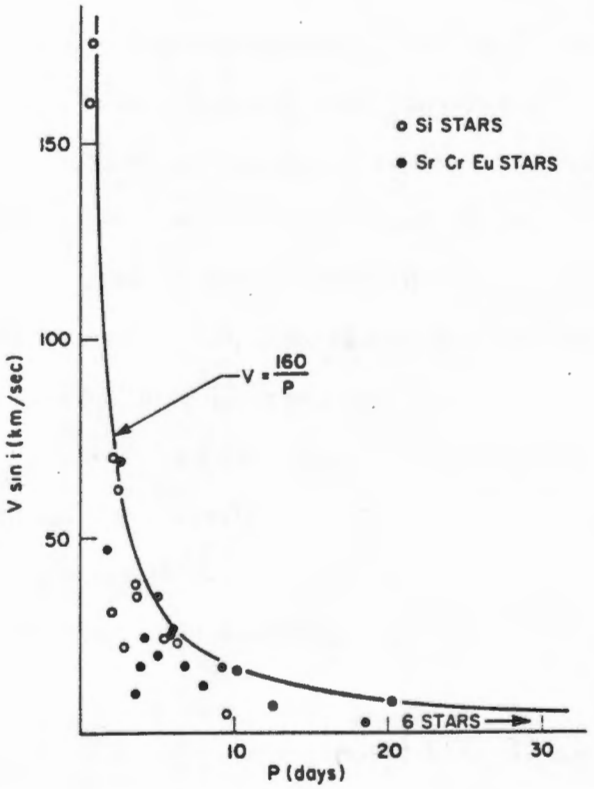

Figure 1.5 A plot of the projected rotation velocity v sin i versus rotation period P for the Ap stars. The curve represents the relation between equatorial rotation velocity and rotation period for stars with radius 3.2 $R_{\odot}$. (Taken from Preston 1971.)

1.11 Effective temperatures

The energy distributions of the Ap stars show marked departures from those of the normal A-type stars. In some cases, two different temperatures are required to describe the Balmer jump and the slope of the Paschen continuum in the same star (*e.g.* Adelman 1985). The result of this is that the usual temperature calibrations derived for chemically normal stars do not work when applied to Ap stars. The generally accepted explanation for the distorted energy distributions is that the large overabundances of metals enhance line and continuum opacity in the ultraviolet thus causing an ultraviolet flux deficiency. This blocked flux reappears in the visual and infrared. The effects of enhanced ultraviolet opacities have been explored by Muthsam (1979a, b) in a series of models which have chemical composition similar to those of a "typical" Ap star. These model atmospheres produce spectra that mimic those of normal stars with higher effective temperatures. Another interesting result of Muthsam's models is that the $T(\tau)$ relation appears to be a lot steeper in a heavily blanketed Ap star atmosphere than in a normal A star.

To date, the best method for determining the effective temperatures of the Ap stars is through detailed atmospheric modelling of the star to produce self-consistent computed spectra that match the observations. To do so, an accurate knowledge of the atmospheric chemical composition is required as well as the energy distribution from the ultraviolet to the infrared. These strong requirements restrict the use of this technique to a very limited number of Ap stars (*e.g.* Muthsam & Stepien 1980, Stepien & Muthsam 1981, 1987).

To circumvent this problem, a number of techniques requiring a more modest knowledge of the star (such as multicolour photometry) have been devised. The techniques available up until the end of 1982 have been reviewed and appraised by Wolff (1983). More recent temperature calibrations have been developed by Lanz (1985), Mégessier (1988) and Stepien & Dominiczak (1989). The different temperature calibrations agree rather well and suggest that reliable determinations of the effective temperatures of Ap stars are indeed possible. Taking the results of all these techniques together, the Ap stars can be said to occupy the following temperature ranges:

Ap SrCrEu (7500 K - 12000 K)

Ap Si (10000 K - 16000 K)

1.12 Masses, radii and evolutionary status

The most reliable data on masses and radii come from eclipsing binaries. At present, ten eclipsing binaries with Ap primaries known. Lebedev (1989) has presented effective temperatures, masses and radii for 8 of them. These 8 stars all fall within the main sequence band. The other two eclipsing binaries are ω UMa (Hric 1988) and TV Nor (Renson 1989). Further evidence for the main sequence nature of the Ap stars comes from studies of radii by Stepien (1989) and Hensberge *et al.* (1991) and a study of surface gravities by North & Kroll (1989) which shows that the Ap stars all have $\log g > 3.0$ and lie within the main sequence band.

Are the Ap stars on the main sequence for the first time, or are they highly evolved objects that have returned to the main sequence as suggested by Fowler *et al.* (1965)? The presence of Ap stars in even the youngest associations strongly suggests that the Ap stars are on the main sequence for the first time. (It also argues against the possibility that Ap stars formed out of material of anomalous composition.)

The demonstration that any of the properties of Ap stars change with time would provide useful constraints for models of these stars. At present, no simple, indisputable correlations with stellar age have been established. The discovery by Wolff (1981) of a decrease in rotational velocity with decreasing mass can be equated to a decrease in rotational velocity with increasing age. However, North (1984) has found that the rotational velocity of Ap stars does not depend on age and that an Ap star should lose its angular momentum before reaching the main sequence. Another way to search for age effects in Ap stars is to compare the Ap stars in different clusters. As yet, no indisputable correlations with age have emerged from such studies. In particular, Abt's (1979) finding of an increase in the number of Ap stars in clusters with increasing age has not been confirmed by Maitzen (1981). It is not clear whether the intrinsic diversity of the Ap phenomenon masks age effects or whether the Ap phenomenon develops very quickly and Ap stars arrive on the main sequence in their "adult" form.

1.13 Magnetic fields

A) Basic physics

If an atom is placed in an external magnetic field, then, assuming LS coupling, each energy level characterized by the quantum numbers (n,L,J) is split into $2J + 1$ sublevels characterized by a quantum number $M = J, J-1, J-2, \ldots -(J-1), -J$. The sublevels will have energy shifts given by

$$\Delta E = e\hbar BgM/2mc, \tag{1.1}$$

where e is the electronic charge, B is the magnetic field strength, g is the Landé g factor and the other symbols have their usual meanings and values in cgs units. The Landé g factor is evaluated using the expression (Aller 1963)

$$g = 1 + [\,\{J(J+1) + S(S+1) - L(L+1)\} / \{2J(J+1)\}\,]. \tag{1.2}$$

The observable consequence of this splitting of energy levels is that a spectrum line is broken up into several components whose separation depends on the strength of the applied field and on the J, S and L values involved in the transition. The components produced by transitions for which $\Delta M = \pm 1$ are called σ components and the components produced by transitions for which $\Delta M = 0$ are called π components. In general, each of the π and σ groups has several lines. In any specific Zeeman pattern, the Landé g values of the two spectroscopic terms involved determine the number of components, their relative positions and intensity. The scale of the pattern depends linearly on the field strength. In Figure 1.6 we show the Zeeman effect for the singlet $^1D_2$ - $^1F_3$ transition.

In the simple case where the line of sight is perpendicular to the local field vector (the so-called *transverse Zeeman effect*), the line is split into three components (Fig 1.7c). The central component remains at the original unperturbed wavelength λ and the other two components are displaced symmetrically to either side of the central component by an amount

$$\Delta\lambda(\text{Å}) = 4.67\times10^{-13}\, z\lambda^2 B, \tag{1.3}$$

where z is the intensity-weighted average displacement of the Zeeman components relative to the displacement for a "normal" Zeeman triplet (see Babcock 1962). The unshifted central component is the π *component* and it is linearly polarized parallel to the field. The shifted components are the σ *components* and they are polarized perpendicular to the local field vector. If we observe along the field vector, we see the *longitudinal Zeeman effect* where only the σ components are visible and the central π component vanishes (Fig. 1.7b). The light in the two σ components is circularly

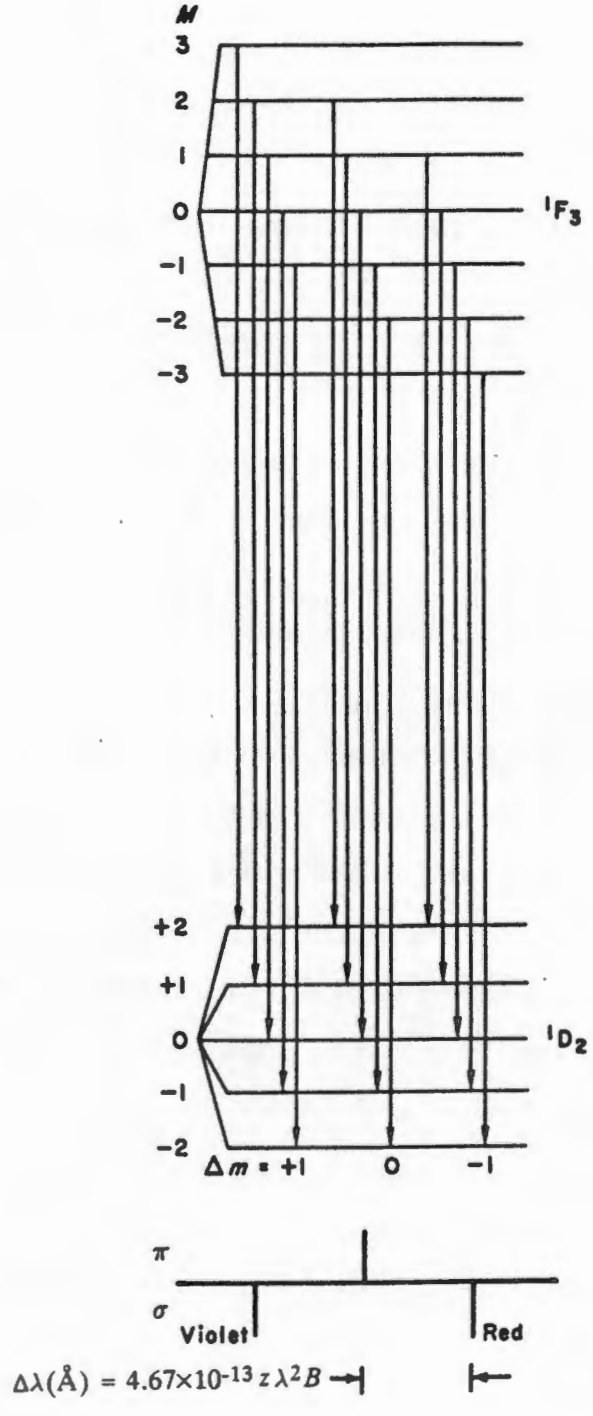

Figure 1.6 The Zeeman effect for a $^1D_2$ - $^1F_3$ transition. (Taken from Aller 1963.)

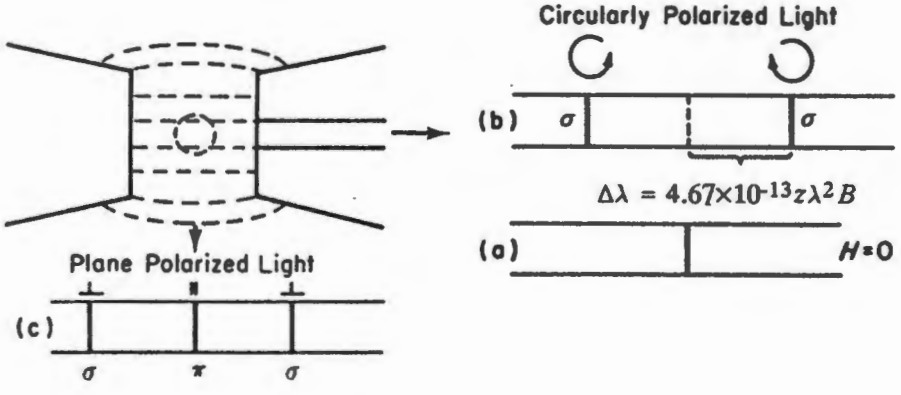

Figure 1.7 The simple Zeeman effect. Spectrum (a) shows the position of a spectrum line in the absence of a magnetic field. Spectrum (b) illustrates the longitudinal Zeeman effect and spectrum (c) illustrates the transverse Zeeman effect. (Taken from Aller 1963.)

polarized in opposite directions and the sense of polarization depends on whether the field lines are pointing towards the observer or away.

Since the line components are polarized, they absorb polarized light selectively. Thus the depth from which radiation in the line wings emerges depends on its polarization. Fig. 1.8 shows the wavelength dependence of the emergent intensity and polarization across a spectral line split by a longitudinal (left) and transverse (right) magnetic field. In practice, the observed line profiles are more complex than indicated in Fig. 1.8 for two reasons. Firstly, the magnetic fields are usually observed obliquely, and not longitudinally or transversely. Figure 1.9 shows the effect of viewing the same field at varying aspect. Secondly, the rotation of the star Doppler-shifts the contributions to the flux from the various parts of the photosphere.

B) Techniques of magnetic field measurement

1) Spectroscopy of Stars with Resolved Zeeman Structure

The most direct means of detecting a magnetic field is to observe Zeeman splitting or broadening of the spectral lines. Since the amount of splitting depends on the magnetic field strength only, and not on its direction, a measure of the splitting yields an integrated measure of the scalar field strength over the visible hemisphere of the star. This measure is called the *mean surface field* or *mean field modulus*,

$$B_s = \int BI dA \,/\, \int I dA, \tag{1.4}$$

where B is the local field strength, I is the local surface brightness, dA is an element of area on the surface and the integrals are carried out over the visible hemisphere. The quantity B_s can be estimated from eq. (1.3) if the separation of the Zeeman components can be measured and if the g values of the transition producing the line can be determined.

However, the detection of Zeeman splitting in main sequence stars is not easy. From eq. (1.3), the π-σ splitting for a triplet line of $g_i = g_f = 1$ is 0.016 Å/kG. This very small amount of splitting must compete with other line broadening processes, the most important of which is usually rotation. As a useful rule of thumb, the Zeeman splitting in the visible will only be detected in stars where B(kG) > v sin i (km/s). This condition is rarely fulfilled for the Ap stars. In the upper main sequence v sin i values of ~30 km/s are quite common while the magnetic field strengths in the Ap/Bp stars are rarely more than ~3 kG. The strongest magnetic field known in any Ap star is 34 kG in Babcock's

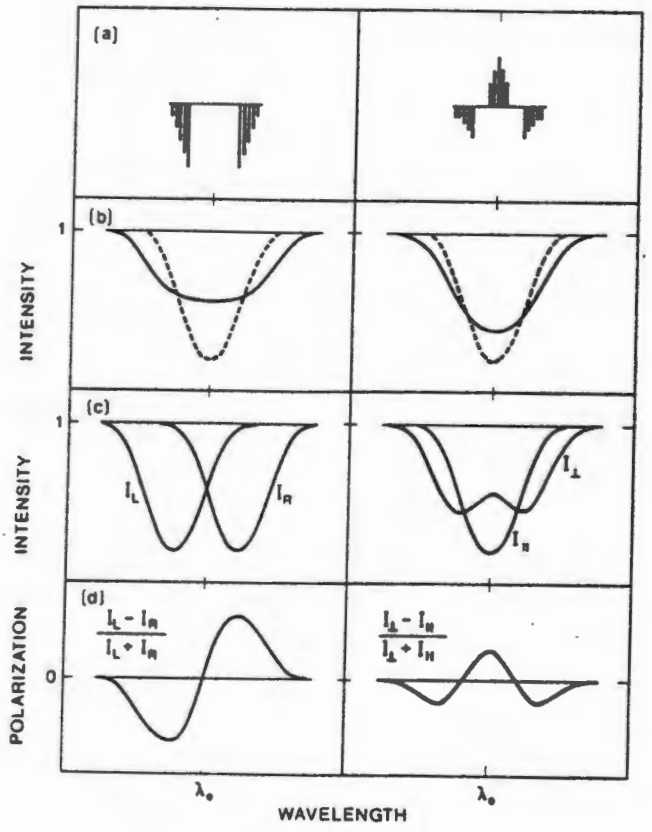

Figure 1.8 The emergent intensity and polarization across a spectral line split by a longitudinal (left panels) and transverse (right panels) magnetic field. Panels (a) show the splitting of a spectral line for a $^3P_2$ - $^3D_3$ transition, π components above the line and σ components below, with the lengths of the bars indicating the relative strengths. Panels (b) show the appearance of the stellar absorption line with a field present (solid line) and absent (dashed lines). Panel (c) (left) shows the line profile as seen in left and right circularly polarized light. Panel (c) (right) shows the line profile as seen in light polarized linearly parallel and perpendicular to the field. Panels (d) show the net circular and linear polarization across the line. (Taken from Landstreet 1980.)

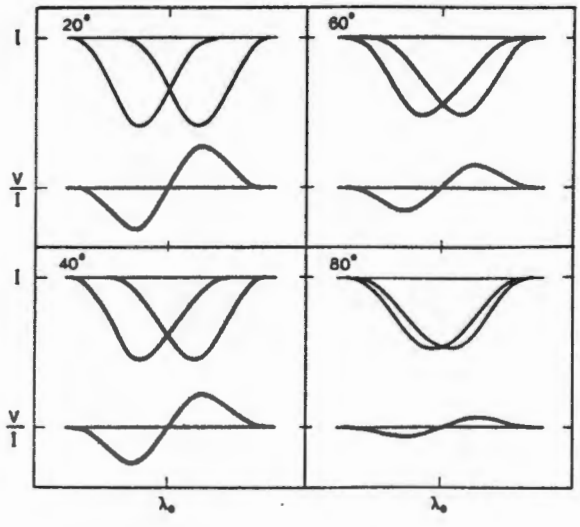

Figure 1.9 Changes in the emergent intensity and circular polarization profile of a simple triplet line viewed in right and left circularly polarized light as the angle between the uniform magnetic field and the line of sight varies from 20° to 80°. (Taken from Landstreet 1980.)

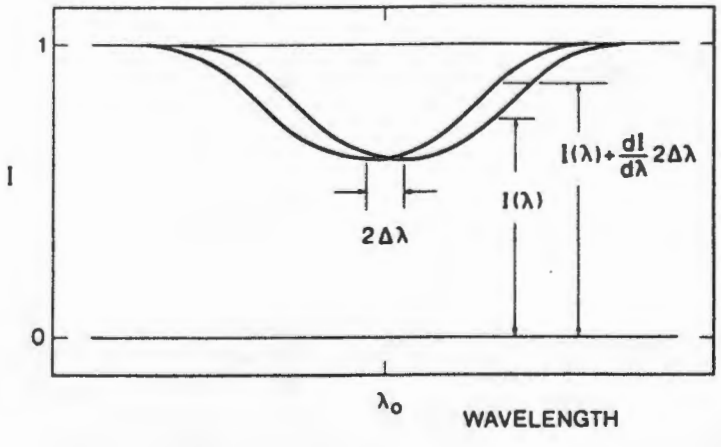

Figure 1.10 Changes in the line depth of an absorption line when viewed in left and right circularly polarized light in a narrow wavelength band. The difference in the intensity seen in right and left circularly polarized light at a specific wavelength is indicated. The field is assumed to be longitudinal. (Taken from Landstreet 1980.)

star, HD 215441, which has a rotation velocity of only 5 km/s. In this case Zeeman splitting is readily seen. Resolved Zeeman patterns are detectable in a few other Ap stars (Landstreet *et al.* 1989, Mathys 1990, Mathys & Lanz 1992).

In some very sharp-lined stars, fields not large enough to produce resolved Zeeman patterns may nonetheless produce measurable magnetic broadening. By comparing the profiles of magnetically broadened lines with those of lines unaffected by the magnetic field (either magnetic null lines or the same lines in a non-magnetic comparison star), one may estimate the magnitude of the mean field modulus. A detailed discussion of magnetic field measurements where the Zeeman splitting is not large compared to the field-free line width is given in section 3.2 of Mathys' (1989) review.

2) Photographic Zeeman Polarimetry

The classical photographic technique developed by Hale (1908) for measuring the magnetic fields of sunspots was adapted for stellar work by Babcock (1962). The technique consists of obtaining two spectra of opposite circular polarization on the same plate and measuring the centroid separation, $2\Delta\lambda_c$, usually with the aid of a measuring engine. The field is then inferred from eq. (1.3). Babcock (1947) has shown that $\Delta\lambda_c$ is proportional to the surface brightness-weighted average of the longitudinal field, also known as the *effective field*,

$$B_e = \frac{1}{\pi}\int_0^{2\pi} d\phi \int_0^{\pi/2} \frac{\cos\theta \sin\theta (1+a_2\cos\theta)(B\cos\psi)}{1+2a_1/3} d\theta; \qquad (1.5)$$

where the integrals are taken over spherical polar coordinates ϕ (azimuth measured around an axis parallel to the line of sight and passing through the centre of the visible disk) and θ (colatitude measured from the same axis), ψ is the angle between the magnetic field vector and the line of sight and a_2 is a constant in the source function approximated by $S(\lambda) = a_1[1 + a_2\tau]$.

3) Photoelectric Spectropolarimetry of Metal Lines

In this technique, one uses a coudé spectrograph with a polarization modulator and a photoelectric line profile scanner to measure the polarization in the wing of a single line, usually a metal line. If the polarization is defined as

$$V = (I_L - I_R) / (I_L + I_R), \qquad (1.6)$$

where I_L and I_R are the intensities viewed in left and right circularly polarized light, respectively, then from Fig. 1.10 the polarization of an observed line profile $I(\lambda)$ is

$$V(\lambda) \approx [I(\lambda) + (dI/d\lambda)2\Delta\lambda - I(\lambda)] / [I(\lambda) + (dI/d\lambda)2\Delta\lambda + I(\lambda)] \qquad (1.7)$$
$$= \Delta\lambda(dI/d\lambda)/I(\lambda).$$

The field, inferred from eq. (1.3), is the *mean longitudinal field* (Landstreet 1982).

$$B_l = \frac{1}{\pi}\int_0^{2\pi} d\phi \int_0^{\pi/2} \cos\theta \sin\theta \left(\frac{3}{2}\cos\theta B \cos\psi\right) d\theta, \qquad (1.8)$$

where the symbols have the same meaning as for eq. (1.5). This method of magnetic field measurement is susceptible to two complications which modify the line profile so that eq. (1.7) is longer applicable. The first is stellar rotation and the second is the magnetic field strength; if the field is too strong, the line may be split too widely for eq. (1.7) to apply.

4) Balmer-Line Zeeman Analyzer

In this technique devised by Angel and Landstreet (1970), one measures the polarization in the wing of a Balmer line of hydrogen using a Cassegrain filter polarimeter and a narrow ($\approx$ 5 Å) interference filter to isolate the line wings. The field inferred from these measurements is B_l. This is essentially identical to photoelectric spectropolarimetry except that since the Balmer lines are much broader than metal lines in a sharp-lined star the technique is virtually insensitive to rotational broadening. Another advantage of this method is that hydrogen is not expected to have appreciable abundance fluctuations over the surface, unlike the metal lines.

5) Transverse Zeeman Effect

It is also possible to attempt measurements of the transverse component of the magnetic field by measuring the linear polarization. Very few such measurements exist because for typical line profiles and field strengths, the transverse Zeeman effect is hard to measure. The transverse Zeeman effect has been detected in the Ap star β CrB by Borra & Vaughan (1977), but has not otherwise attracted much attention until recently when Leroy *et al.* (1992) began a systematic program to study this effect in Ap stars.

C) Systematics of the magnetic fields in the Ap stars

The Ap stars have strong (300 G - 34000 G) magnetic fields whose structures do not change by detectable amounts on time-scales < 100 yr. It appears that the magnetic field strengths increase with T_{eff} along the upper main sequence (Bohlender *et al.* 1987). The observations also provide strong constraints on the magnetic geometries. From the early work of Babcock in the 1940's it was obvious that the fields must be predominantly dipolar. For higher order magnetic geometries, there is too much cancellation in the integrated light of the stellar disk for there to be an appreciable net magnetic field. For instance, in order to produce the observed values of B_l ~ 1-2 kG, a magnetic quadrupole must have a strength of ~30-40 kG (Wolff 1983). Such strong fields would produce larger Zeeman splitting than is actually observed in the Ap stars. The sharpness of the lines and the purity of the Zeeman effect rule out the possibility that the light is produced in small areas of the stellar disk with very intense fields.

Further evidence for the predominantly dipole nature of the fields comes from the observed field strength variations. If B_l and B_s can be measured as a function of rotation phase, they provide information about the surface magnetic geometry of the star. The most common situation is that B_l can be measured but B_s cannot. The variation of B_l with rotation is usually found to be a simple sine wave. This modulation of field strength is taken as evidence that the field is predominantly dipolar. Schwarzchild (1950) has shown that higher multipoles have sufficient field cancellation over the observed hemisphere to make only a small contribution to B_l unless the field distribution is actually dominated by a non-dipolar component.

For strictly dipolar fields, B_s should exhibit a double-wave variation during the rotation cycle if B_l reverses its sign. In many stars B_s exhibits a *single* maximum closely in phase with one of the extrema of B_l. This indicates that the magnetic fields are hemispherically asymmetric. The asymmetry may be represented by an off-axis decentred dipole (Stift 1975), but also equally well by a sum of axisymmetric dipole and quadrupole components. At present, the best constrained models are restricted to a three-term expansion with colinear dipole, quadrupole and octupole components (*e.g.* Landstreet 1988). The quadrupole components are often a significant fraction of the dipole components (*e.g.* in 53 Cam Landstreet (1988) finds $B_q/B_d = 0.45$).

An interesting question concerning the magnetic variations is whether there are intrinsic fluctuations in magnetic field strength superimposed on an otherwise regular periodicity. Several

workers have attacked this problem, but Wolff (1983) considers the evidence for intrinsic magnetic variations to be inconclusive.

D) Magnetic relations for an oblique rotator

The longitudinal component of the magnetic field, B_e, is related to the polar field strength B_p by

$$B_e \propto B_p P_\ell(\cos\alpha), \tag{1.9}$$

where $P_\ell(\cos\alpha)$ is the Legendre polynomial appropriate to the magnetic field configuration. From Fig. 1.3, $\cos\alpha$ is readily shown to be

$$\cos\alpha = \cos i \cos\beta + \sin i \sin\beta \cos\Omega t, \tag{1.10}$$

where all the symbols are defined graphically in Fig. 1.3. Detailed calculations (Stibbs 1950) lead to the following relations for a dipole and a quadrupole field:

$$B_e = [\, B_p \cos\alpha\,(15+u)\,] / [\,20(3-u)\,] \;\; \& \tag{1.11}$$

$$B_e = [\, uB_p(1 + 3\cos 2\alpha)\,] / [\,16(3-u)\,], \tag{1.12}$$

respectively, where u is the coefficient of limb darkening. Landstreet (1982) has shown that the value of B_e derived from polarization data is not weighted by limb darkening, so for such measurements $u \equiv 1$ in the above formulae.

The magnetic fields in the Ap stars are often characterised by the parameter (Preston 1967)

$$r = B_e(\text{min}) \,/\, B_e(\text{max}) \qquad -1 \le r \le +1, \tag{1.13}$$

where, from eq. (1.9) and (1.10),

$$\tan i \tan\beta = (1-r) \,/\, (1+r). \tag{1.14}$$

Thus, an estimate of r from the magnetic data allows us to constrain i and β.

E) Origins of the magnetic field

The origin of the magnetic fields is in the Ap stars is still uncertain. We outline three of the better known theories which have been proposed, the dynamo, fossil and battery theories.

The Battery: In an atmosphere with ionized atoms and free electrons, the lighter electrons are more likely to diffuse upwards and the heavier protons and ionized atoms are more likely to sink. This charge separation gives rise to an electric field which prevents further charge separation. If the atmosphere is chemically inhomogeneous with molecular weight not a function of radius alone, the

gravitationally induced charge separation causes circulation currents that generate a magnetic field.

The Dynamo: This theory postulates that the magnetic field is produced by a contemporaneous dynamo operating in the convective core which extends over 15 - 20 per cent of the stellar radius.

The Fossil Field: These theories postulate that the magnetic field is either a slowly decaying relic of a condensed interstellar field (only a fraction of which survived the star formation process) or of a pre-main sequence phase dynamo.

A detailed review of these rival theories is given by Moss (1986). Moss (1989) has devised a set of time dependent numerical models to place constraints on the dynamo and fossil field theories. The calculations suggest that the dynamo theory has difficulty in transporting the fields observed in very young cluster Ap stars from the core to the surface in the time available. However, Moss' calculations indicate that the observed magnetic properties of the Ap stars are consistent with fossil fields left over from the epoch of star formation. These fields might have been produced by compressing the weak interstellar field during the collapse of the protostellar cloud, or by dynamo action during the convective pre-main sequence phase. During the main sequence phase, the initial field structures are further modified by global hydrodynamical flows inside the star, by structure changes due to evolution and by ohmic decay.

F) The crossover effect

A major source of support for the oblique rotator model is its natural ability to explain the so-called *crossover effect*, first noted in HD 125248 by Babcock (1951). This effect appears as a difference in the sharpness of most spectral lines with sense of circular polarization. If two spectra are recorded, one for each sense of circular polarization, then, in one spectrum, lines are broad and shallow while in the other they are narrow and deep. This phenomenon occurs at and near phases when the mean magnetic field passes through zero; hence its appellation. The effect does not manifest itself equally strongly for all lines.

The explanation for the crossover effect is that there are two areas of opposite magnetic polarity on the surface giving rise to the lines. The line profiles then reflect the combined Zeeman and Doppler effects that arise when both regions are visible and a differential radial velocity prevails between them. Figure 1.11 illustrates the idea. Whatever model of Ap stars is assumed, spectroscopic

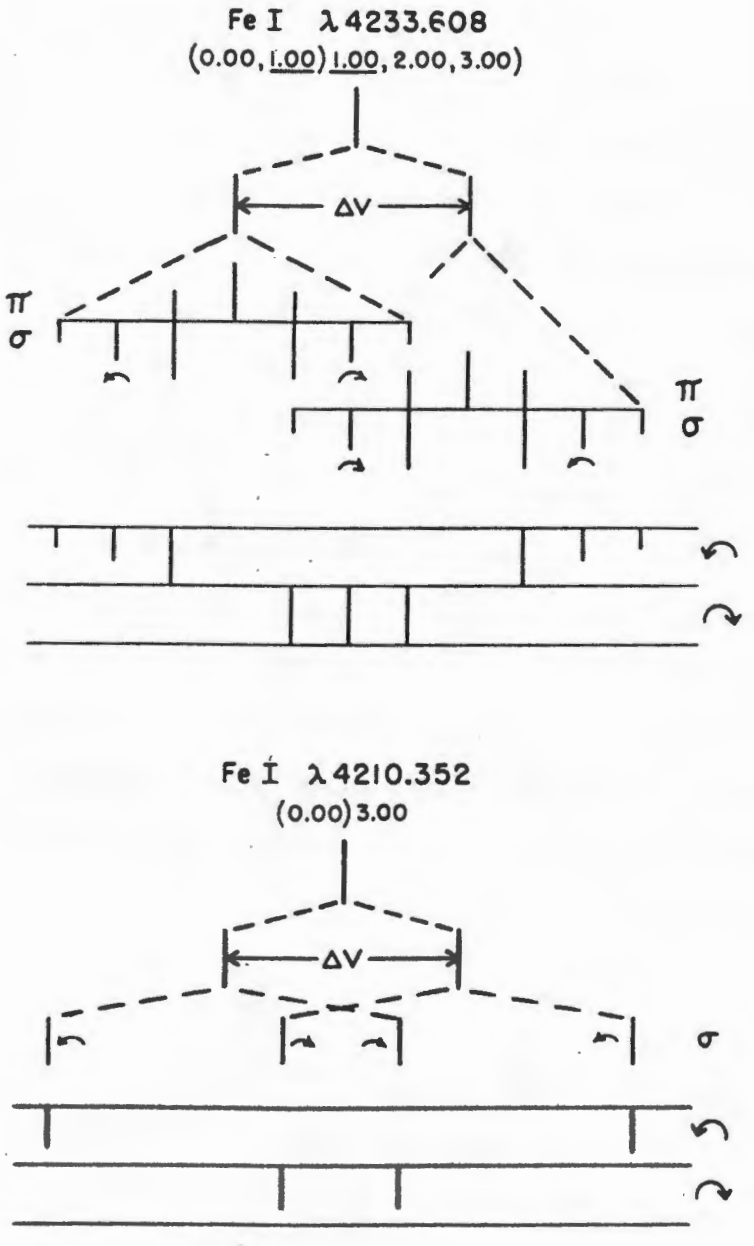

Figure 1.11 Diagrams illustrating the development of the crossover effect. The line is first split by the Doppler effect corresponding to a differential velocity, Δv, between two areas on the star. If these two areas have longitudinal magnetic fields of opposite polarity, the lines are further split into their Zeeman patterns. The σ components are sorted out by the analyzer according to their sign of circular polarization, leading to a "broad" and a "sharp" profile in the two strips. If the field is not strictly longitudinal, the π components appear in both strips of the spectrum. In general, there occurs considerable overlapping of the profiles represented by the "lines" in the diagrams. (Taken from Babcock 1956.)

patches are required to explain the crossover effect. The oblique rotator model accounts naturally for the magnitude of the effect and the details of its effect on the spectrum.

1.14 Mapping the surface abundance distributions

The impetus for mapping the surfaces of Ap stars was provided by the introduction of the oblique rotator model with its assumption of the existence of abundance patches on the surface of the star. As these abundance patches rotate with the star, they produce variations in the line profiles as well as the equivalent widths. The amount of blue shift as a patch comes into view depends on the latitude of the patch. Matter near the rotation pole has a much smaller blue shift than matter at the equator. This means that detailed line profiles contain information about the two-dimensional distribution of an element over the stellar surface, information that may be recoverable by suitable modelling.

The first mapping technique to be developed for the Ap stars was the harmonic analysis technique of Deutsch (1958). In this technique, the observed variations of equivalent width are described with a Fourier series whose coefficients are related to a truncated series of spherical harmonics describing the local equivalent width on the surface of the star. This technique makes no use of the information contained in the line profile. To keep the problem tractable, few terms are carried in the expansions, so while the resulting models are mathematically elegant, they are also highly constrained.

An alternative model is that of Khokholva (1975) where an initial guess of the abundance pattern is made. The number of spots and their approximate longitudes can be obtained from the observations but their sizes and abundances have to be guessed. One then computes the line profile for the whole disk and iterates until the observed and computed line profiles match.

Mégessier *et al.* (1979) have shown that the maps produced using the methods outlined above are not necessarily unique. The latitudes of the spots, the areas and the abundances are all linked. Thus a change in one quantity can always be matched by a corresponding change in the other two so that the observations are still reproduced. This lack of uniqueness makes it very difficult to relate the surface abundance distribution to the magnetic geometry.

More recently, new indirect imaging techniques have been devised which use maximum entropy image reconstruction principles to map the surface abundance distributions from line profile variations. This technique, called *Doppler Imaging*, has proved to be an accurate and efficient means of mapping the surface structure of some Ap stars (Rice *et al.* 1989, Hatzes *et al.* 1989, Rice

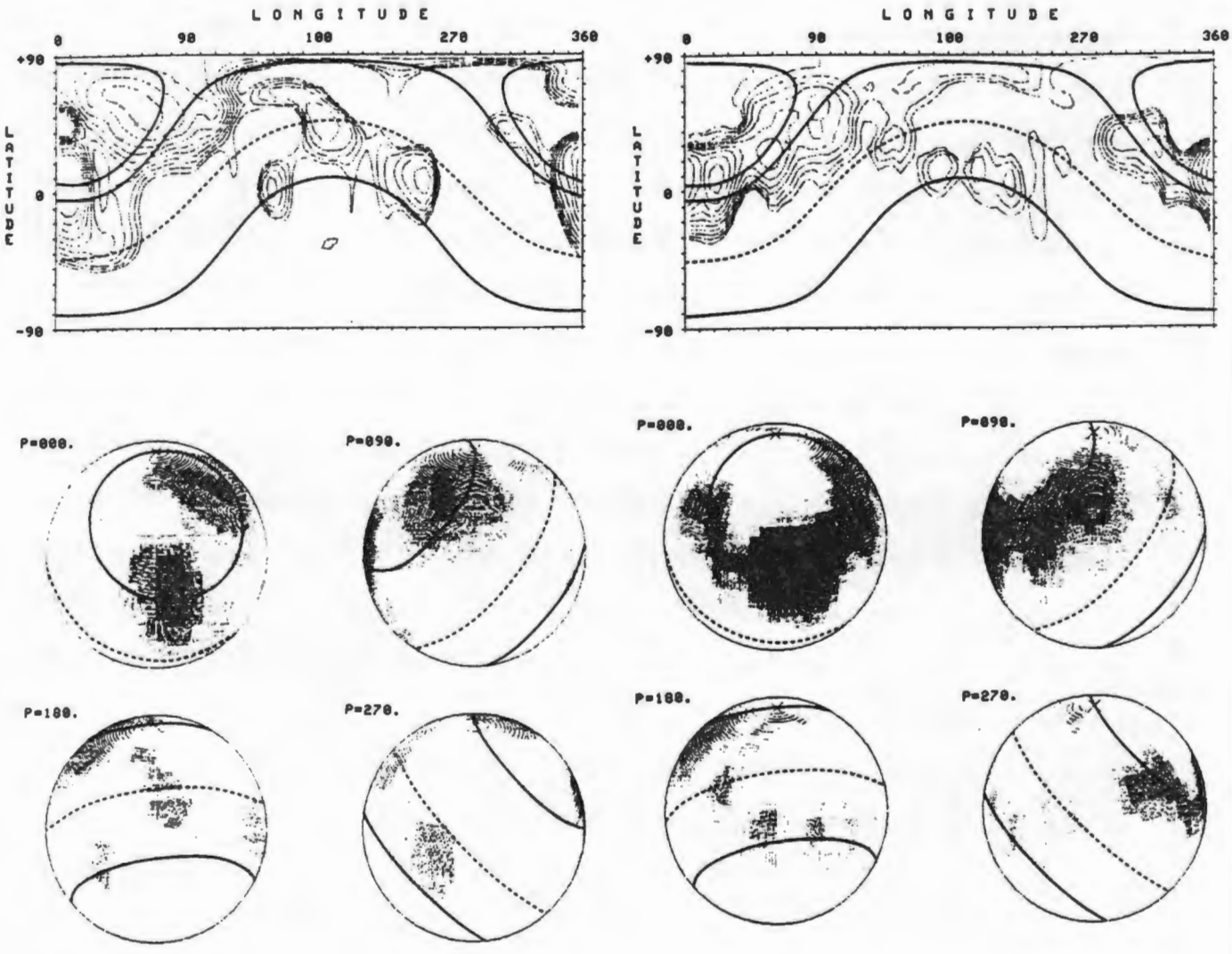

Figure 1.12 Maps of the distribution of Cr (left) and Fe (right) on the surface of the star ϵ UMa as seen at four phases during the rotation cycle. (Taken from Rice & Wehlau 1990.)

& Wehlau 1990). The resulting maps (e.g. Fig. 1.12) indicate annular abundance distributions of some elements about the magnetic axis and depletion at the magnetic equator of other elements. Semel (1989) has taken these ideas further by proposing the application of Doppler Imaging to the circularly polarized profiles V of Zeeman split spectral lines. This method, called *Zeeman-Doppler Imaging* promises to yield accurate, detailed images of the surface magnetic fields on rapidly rotating stars. Brown *et al.* (1991) have applied this technique to spotted model test stars and find that both circular and linear polarization measures are necessary in order to derive reliable results for Ap stars.

A rather different approach has been to calculate accurate local line intensity profiles as the solution to depth-dependent equations of transfer. These local profiles are integrated over the disk and the resulting profile is compared to the observed one. For such modelling one requires well defined magnetic curves and very high signal-to-noise spectra which contain information about both Doppler shifts and magnetic field structure. In this work the magnetic field is usually modelled by a three-term expansion of colinear dipole, quadrupole and octupole components. Typically, three or more elements are modelled and the abundance distribution of each element is assumed to be axisymmetric about the magnetic axis. The resolution in magnetic latitude is typically ~ 30°. Examples of this work are reported for 53 Cam (Landstreet 1988), HD 215441 (Landstreet *et al.* 1989) and HD 64740 (Bohlender & Landstreet 1990). This technique yields essentially correct, unique low resolution representations of the surface of the star.

Abundance distributions on 53 Cam

53 Cam is an Ap star with a well determined magnetic geometry and for which reliable abundance maps for several elements exist (Landstreet 1988). The magnetic field is modeled with an axisymmetric dipole + quadrupole + octupole combination with the components determined by Landstreet (1988) to be $(H_d/H_q/H_o)$ = (-16300/-7300/4900) G at the strong (negative) pole (Fig. 1.16). The pattern of abundance anomalies in magnetic coordinates may be summarized as follows:

Ca has 30 times solar abundance at the weak magnetic pole and is a factor of 2 underabundant elsewhere.

Sr is overabundant by a factor of ~2000 at the strong negative pole and by a factor of ~500 elsewhere.

Sc is present at about solar abundances, or just slightly below. The distribution of Sc cannot be determined.

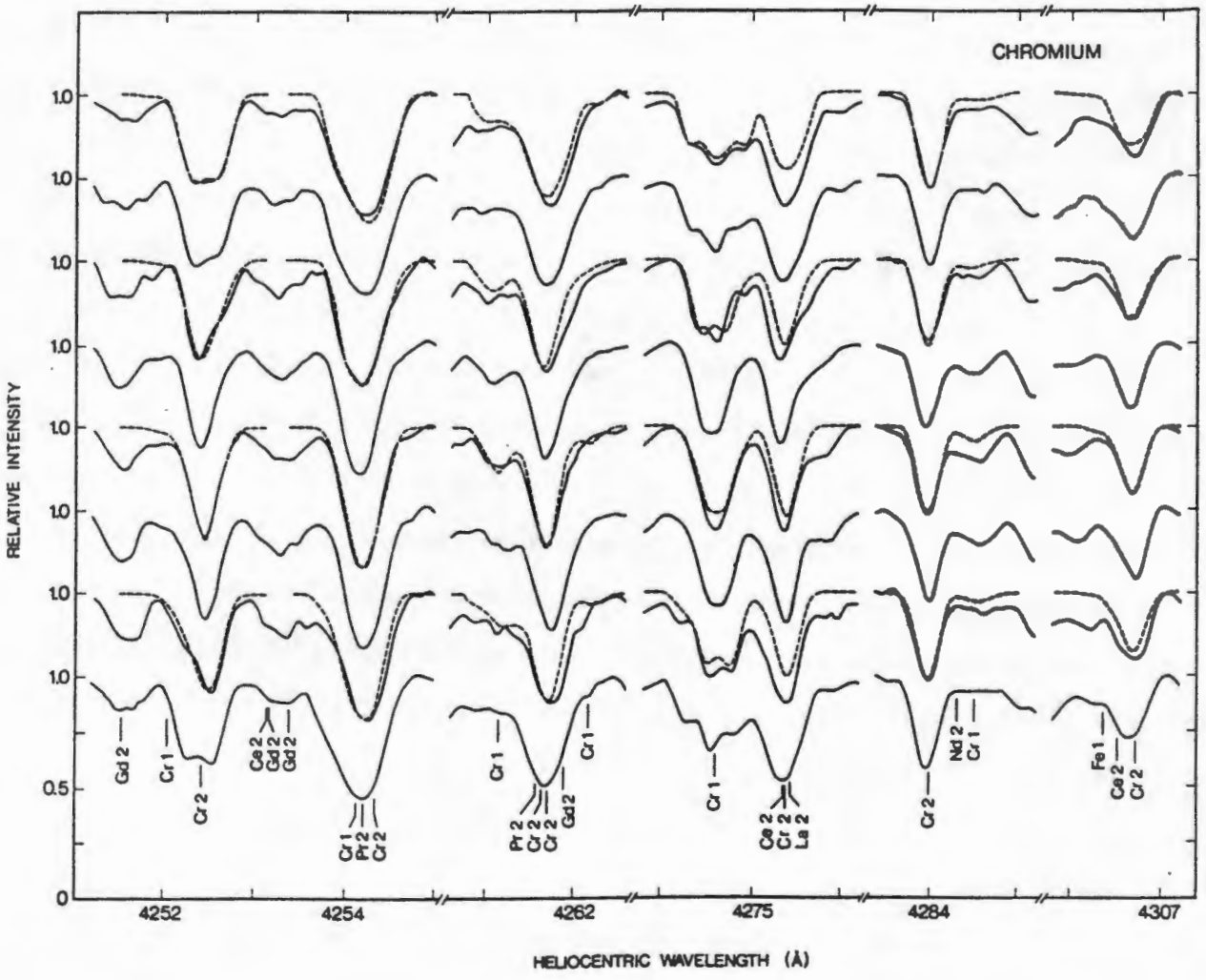

Figure 1.13 Observed profiles (*solid curves*) of several lines in the spectrum of 53 Cam that are primarily due to Cr. The eight rows are eight successive phases of the rotation of the star starting with $\phi = 0.798$ when the strong negative pole is close to the line of sight. Identifications of contributing lines are shown below the bottom spectrum. The dashed curves are the models computed by Landstreet (1988). (Taken from Landstreet 1988.)

Mn is present with an overabundance of ≤ 5 times solar. Only an upper limit can be established and Landstreet concludes that Mn is not as overabundant as Cr.

Fe is overabundant by a factor of 4 at the equator and 10 at the poles.

Cr is overabundant by a factor of 15 at the equator and 40 at the poles.

Figure 1.13 shows the observed profiles for Cr in 53 Cam (solid lines) and the models (dashed lines) computed by Landstreet (1988).

1.15 Origin of the line strength anomalies

It is universally believed that the line strength anomalies in the Ap stars are real abundance anomalies and are not due to abnormal excitation and ionization conditions in their atmospheres. One of the reasons for this belief is that no one has yet been able to produce self-consistent models of the observed spectra by using a peculiar atmospheric structure with a normal (solar) chemical composition.

There are several reasons to believe that the anomalous abundances are confined to the stellar surface. One of the most compelling of these reasons is that if the abundance peculiarities in the Ap stars were truly compositional, then virtually the entire galactic abundance of rare earths would be locked up inside Ap stars. Another reason is that it is difficult to explain the coexistence of Ap stars with chemically normal stars in binary systems or open clusters.

Several models for the origin of the abundance anomalies have been proposed. These models all have the common feature that they assume the anomalies are confined to the surface. Where they differ is in how the anomalies are produced. The models can be divided into two broad classes, the nucleosynthetic and non-nucleosynthetic models. The nucleosynthetic models differ mainly in the site of nucleosynthesis:

1) *Interior:* This model posits that Ap stars are highly evolved objects and the anomalies are produced by dredging up highly processed material from the interior (Fowler *et al.* 1965).
2) *Surface:* The magnetic fields accelerate protons and α particles to produce spallation reactions on the surface (Brancazio & Cameron 1967).
3) *Binary companion:* These models propose that the nuclear reactions occur in a more massive binary companion that evolves faster than the A star and explodes in a supernova. The light elements such as H, He, C, N & O reach the secondary first with

velocities well in excess of the escape velocity so very little of this material is deposited on it. The heavier elements coat the secondary to produce the abundance anomalies (van den Heuvel 1967, Guthrie 1971).

The non-nucleosynthetic models achieve the peculiar abundances by one of five mechanisms.

1) *Magnetic accretion:* Ionized heavy elements in the interstellar medium, perhaps enriched by a nearby supernova, are captured by the star and guided magnetically towards the poles (Havnes & Conti 1971).
2) *Accretion of comets:* (Joss 1974)
3) *Accretion of interplanetary dust:* (Krishna-Kumar *et al.* 1989)
4) *Infall of planets or planetesimals:* (Cowley 1977)
5) *Radiative diffusion:* (Michaud 1970)

Of all these models, nucleosynthetic and non-nucleosynthetic alike, the most promising by far is radiative diffusion (Wolff 1983).

1.16 Radiative Diffusion

The most promising explanation for the origin of the abundance anomalies is based on the separation of elements, or *diffusion*, in the atmosphere. The astrophysical significance of diffusion processes was recognized as long ago as 1926 by Sir Arthur Stanley Eddington in his seminal work *The Internal Constitution of the Stars*. In his book, Eddington (1926) discussed contemporary ideas on diffusion with references to the earlier literature. However, it is to Michaud (1970) that we are indebted for the first detailed treatment of diffusion in an Ap star atmosphere.

In a slowly rotating A star with a stable atmosphere devoid of turbulence and convection, the dominant forces on ions are pressure (specifically including radiation pressure) and gravity. Elements with many lines near flux maximum will experience excess pressure transferred through either bound-bound or bound-free atomic transitions. Such elements will be pushed upwards through the atmosphere and concentrate in the line forming regions thus appearing to be overabundant. The low abundance elements with many lines near flux maximum will only depress the flux slightly and will be preferentially supported. Elements with few lines near flux maximum or with saturated lines will tend to sink in a sea of hydrogen and therefore appear to be underabundant. In the A stars very little flux is emitted in the Lyman continuum. Thus elements which are naturally abundant and whose ionization potentials exceed 13.6 eV should show marked deficiencies. Indeed, elements such as He, Ne, N and

O *do* show marked deficiencies (Ryabchikova 1991). On the other hand, the early calculations of Michaud (1970) show how even the most rudimentary diffusion model predicts overabundances of Mn, Y, Zr, Sr and other rare earths in the temperature ranges in which they are observed. Diffusion affects the various elements differently as T_{eff} changes because the degree of ionization and the radiation field change as the temperature changes. Thus diffusion can account in a qualitative way for the various types of spectral peculiarity observed. Diffusion also accounts for the temperature range of the Ap phenomenon, which is from spectral type B2 to F0. Earlier than B2, the star suffers from extensive mass loss and F0 marks the onset of an extensive surface convection zone. Both surface convection and mass loss would destroy the chemical separation set up by the frail diffusion process. Diffusion is also consistent with the presence of Ap stars in even the youngest clusters since the typical time scale required to develop chemical composition gradients is ~ 10^4 yr. The diffusion hypothesis is also consistent with the observation that Ap stars rotate slowly as a class. Indeed, diffusion *requires* slow rotation, for only then is the disruptive mixing effect of meridional circulation minimized. Prior to the onset of peculiarity, the magnetic A stars will experience magnetic braking which reduces meridional circulation currents. Once the mixing processes at the base of the He II ionization-convection zone are sufficiently reduced, this allows the gravitational settling of He under the He II ionization zone to proceed until eventually this convection zone disappears. With the atmosphere thus stabilized, diffusion processes are free to produce the other abundance anomalies. This chain of events is neatly summarized in a flow diagram devised by Alecian (1986) which is shown in Fig. 1.14.

In the absence of a magnetic field, and for neutral states of ionization, diffusion is predominantly vertical and is governed by the imbalance of radiation pressure and gravity. Magnetic fields influence the diffusive separation of elements by influencing the motions of ionized particles. The basic physics of particle diffusion in the presence of a magnetic field has been studied by Michaud, Mégessier & Charland (1981). The salient features of their work may be summarized as follows: For non-neutral states of ionization, the magnetic field acts differently on the components of the diffusion velocity parallel and perpendicular to the field lines. The parallel component of the diffusion velocity is not modified by the field, but the perpendicular component is modified in a way which depends on the field strength, the collision frequency, temperature and charge-to-mass ratio of the given ion. Michaud *et al.* (1981) show that the magnetic field can only guide diffusing elements effectively once they are pushed above the region where the continuum forms. In the continuum-

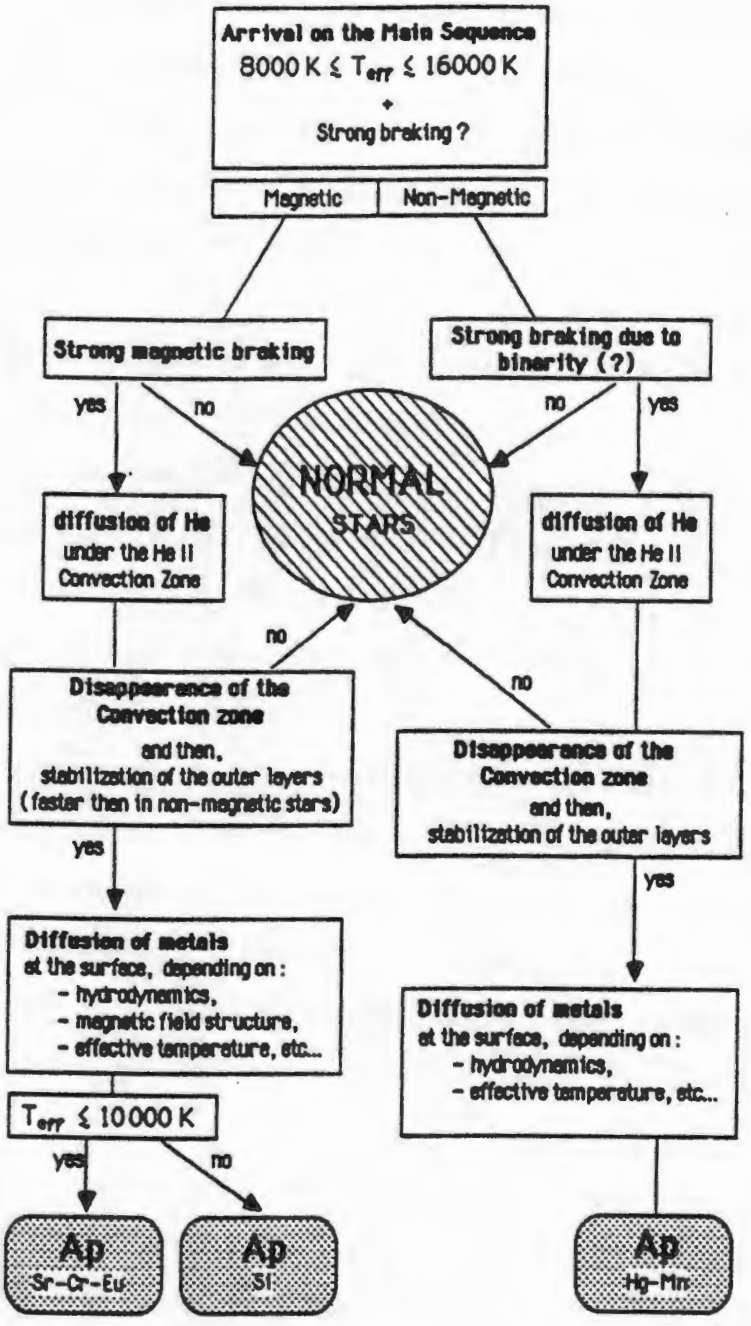

Figure 1.14 A possible scenario for the development of the Ap phenomenon through diffusion. (Taken from Alecian 1986.)

forming region, the number density and collision frequency are both high, so the perpendicular velocity is comparable to the parallel velocity and magnetic field does not significantly influence diffusion. As the ion diffuses into the upper regions of the atmosphere, the lower density reduces the importance of the perpendicular diffusion velocity and the ion is able to follow the field lines more closely. Upward diffusion of the ion stops when the field lines are horizontal because the magnetic field resists the motion charged particles across the field lines. Another way the magnetic field influences diffusion is by Zeeman splitting which desaturates lines and increases the radiative acceleration of the diffusing elements.

The azimuthal symmetry in the atmosphere is broken by an oblique magnetic field. This effectively increases the opacity in certain directions and leads to a horizontal component of the radiative acceleration that only appears in treatments that deal correctly with the problem of polarized transfer. Babel and Michaud (1991) have examined the implications of this and find that the horizontal acceleration resulting from polarized transfer is very small relative to the vertical acceleration, so much larger distances must be travelled horizontally than vertically to lead to observable effects. Horizontal radiative acceleration can only play a significant role for elements whose flux from the interior is limited because the effects of a horizontal flux will be wiped out whenever a vertical flux is present.

Another subtle effect that has to be incorporated into diffusion calculations is ambipolar diffusion of hydrogen (Babel & Michaud 1991b). In a cool Ap star hydrogen is only partially ionized and the protons and electrons develop drift velocities with respect to the neutral H atoms. The ambipolar proton drift affects the drift velocities of minor species by dragging them upwards to produce overabundances in the line-forming region. The efficiency of ambipolar diffusion is strongly affected by the local orientation of the magnetic field. Babel & Michaud's (1991b) calculations indicate that the effect is much stronger in regions where the magnetic field is vertical than where it is horizontal. This could partly explain the relative enrichment of chemical elements observed at the magnetic poles of Ap stars relative to the equator.

In addition to expediting and influencing diffusion processes in the ways described above, the magnetic field also has a strong influence on the eventual form of the surface abundance distribution. The magnetic fields of the Ap stars can be modelled as simple combinations of axisymmetric dipoles (predominantly) and quadrupoles. Because of the cylindrical symmetry of these magnetic geometries,

the diffusing elements tend to concentrate in spots or rings centered on the magnetic axis. The latitudes of these features will depend on the ratio of the dipole to quadrupole field strengths.

One may wonder, if the magnetic field were strong enough, would it prevent the diffusing ions from reaching the surface? Michaud *et al.* (1981) have considered this possibility and their models reveal that changing the strength of the magnetic field changes the depth at which the elements accumulate but, for realistically strong fields ($\leq 4\times10^5$ G), the diffusing ions cannot be prevented from rising to the surface. Moreover, the magnetic field is also what makes a peculiar star *stay* peculiar. In the absence of a magnetic field, calculations show that the ionized elements will leave the star on a time-scale of 10^4 yr, whereas the presence of a strong magnetic field lengthens this time scale to longer than the stellar lifetime. So, to sum up, the magnetic field cannot prevent the accumulation of diffusing elements on the stellar surface but it does prevent the diffusion-induced loss of such elements.

The reader may at this point recall our earlier mention of the *nonmagnetic* chemically peculiar stars, the Am stars. If the magnetic field is so important in forming the peculiarities in the Ap stars, how is it possible that the nonmagnetic Am stars also show extreme spectral peculiarities? In this case we recall that the Am stars are all in binaries with periods in the range $2.5 \leq P \leq 100$ days. Here the atmosphere is stabilized by rotational braking via tidal interactions. Once this happens, diffusion proceeds in more or less the same way as in the Ap stars except that the emergence of spectral peculiarities takes longer. This is because the magnetic field has a stronger stabilizing effect and one thus expects peculiarities to develop faster in magnetic stars than in nonmagnetic ones. In agreement with this expectation, Abt (1979) found a higher incidence of Ap stars than Am stars in young clusters.

Various authors have modelled the diffusion of specific elements. We will not report these calculations in detail here, but only summarize the salient results. Michaud (1980), modelling diffusion in the presence of a magnetic field, found that the Fe peak elements should be concentrated in regions of vertical field (poles). Other elements, like Si and the rare-earths, can be supported only in regions with a horizontal magnetic field, that is, near the magnetic equator. Further time-dependent calculations by Mégessier (1984) showed that as more and more Si arrives on the surface from below, horizontal diffusion makes the Si migrate to the magnetic poles where it sinks (since it is not supported there). This takes $\sim 10^8$ yr, so we should expect to see age effects in the Si abundance and surface distribution. Detailed diffusion calculations have also been performed for the following

elements: B (Borsenberger *et al.* 1979) Be, Mg, Ba (Borsenberger *et al.* 1984), Ca & Sr (Borsenberger *et al.* 1981), Ga (Alecian & Artru 1987), Mn (Alecian & Michaud 1981). These diffusion calculations show a temperature dependence in the overabundances of Y, Zr, Sr, Si, Mn & Ga in fair agreement with the temperature ranges in which they are observed. A detailed review of the observed chemical abundances and a comparison of the observations with the predictions of diffusion calculations in the Ap stars is given in a recent review by Ryabchikova (1991). Other recent reviews have been written by Maitzen (1989), Wolff (1983), Vauclair & Vauclair (1982), Michaud (1986) and Alecian (1986). Other papers of interest appear in the proceedings of IAU Colloquium 90 and IAU Symposium 145 and the references therein.

53 Cam - An important case study in diffusion

53 Cam is one of the two Ap stars which have well determined magnetic geometries *and* good abundance maps for several elements (Landstreet 1988). The other star is ϵ UMa (Bohlender & Landstreet 1990b, Donati *et al.* 1990, Rice & Wehlau 1990, 1991). Landstreet's reliable determinations of surface abundances and magnetic geometry for 53 Cam (presented in section 1.14) have opened the way to more accurate tests of the diffusion model for Ap stars. In this section we will discuss the attempts of Babel and Michaud to model these observations.

Babel & Michaud (1991c) have tried to account for the observed surface abundance anomalies on 53 Cam by assuming that the level of the anomalies, and their distributions relative to the magnetic field, are the product of diffusion. The model they used was developed by Michaud, Mégessier and Charland (1981) to describe diffusion in a magnetic Ap star atmosphere. It is a parameter-free model which makes as few assumptions as possible. The model uses the observed magnetic field geometry and assumes the atmosphere is stable enough for diffusion to be significant. The existence of abundance spots on the surface also indicates that overshooting above the HII convection zone is suppressed, otherwise the photosphere would be homogenized horizontally (Michaud 1980). Babel & Michaud show that this model can account for the *average* observed abundance anomalies assuming the hydrogen convection zone is partially suppressed. This is a reasonable assumption for 53 Cam where the observed field strengths imply that the magnetic pressure is larger than the gas pressure down to depths $\tau_R = 10^4$ ($T = 80000\ K$, $\Delta M/M = 4\times10^{-8}$) at the strong magnetic pole and to depths $\tau_R = 10^3$ ($T = 45000\ K$, $\Delta M/M = 3\times10^{-9}$) at the weak pole, deeper than the HII convection zone in both cases. Although the model can explain the *average*

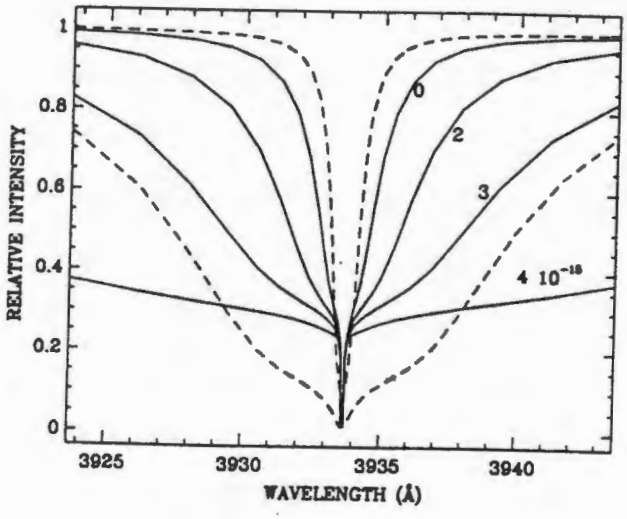

Figure 1.15 Spectral profiles of the Ca II K line for equilibrium abundances with mass loss rates of 0, 2, 3 and 4×10^{-15} $M_\odot$/yr (*solid lines*), and for non-stratified abundances of $10^{-6.5}$ and $10^{-4.3}$ (*dashed lines*). (Taken from Babel 1992.)

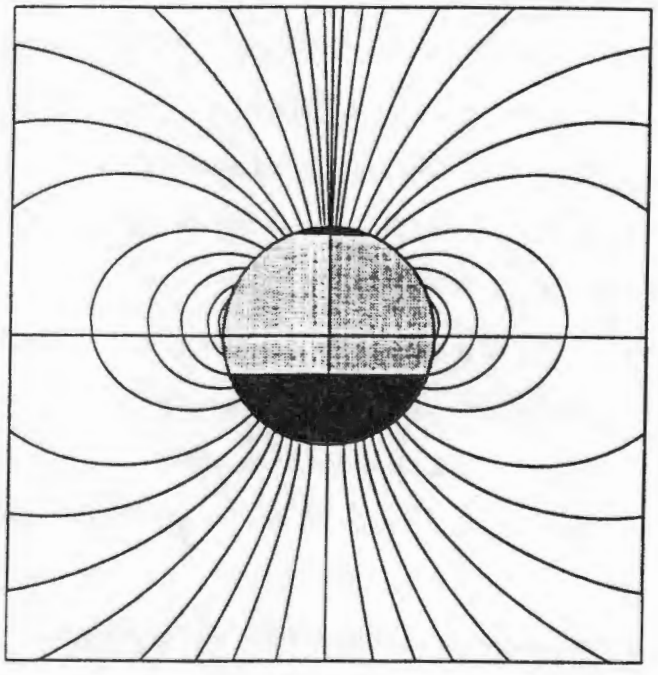

Figure 1.16 Schematic representation of the magnetic field of 53 Cam from the dipole, quadrupole and octupole components ($H_d/H_q/H_o$ = -16300/-7300/+4900 G) obtained by Landstreet (1988). The strong (negative) pole is at the top. The two shaded areas are the diffusion mass loss caps inferred by Babel (1992) where the mass loss rate is ~ 10^{-13} $M_\odot$/yr. The small mass loss cap at the strong pole extends from α = 0° to 20° (α, the magnetic colatitude, is measured from the top), while the cap at the weak pole extends from 180° to 110°. (Taken from Babel 1992.)

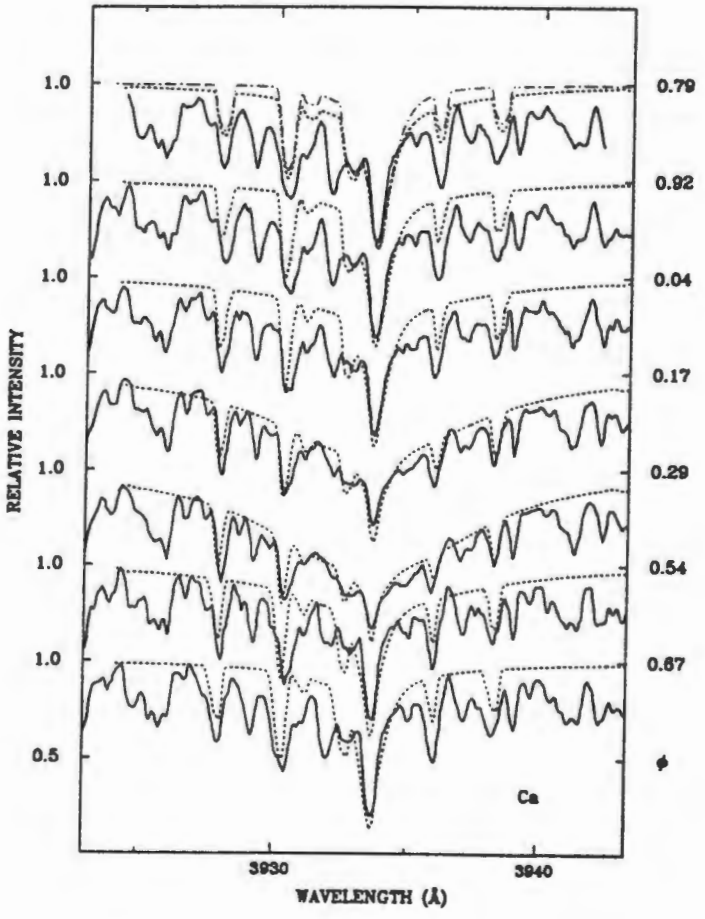

Figure 1.17 Observed profiles (*solid lines*) of the Ca II K line (Landstreet 1988) and the theoretical profiles (*dashed lines*) from Babel's (1992) diffusion model with mass loss. The dashed-dotted curve at phase $\phi = 0.79$ is for a model without mass loss at the strong pole. Observation phases are given on the right side of the Figure. (Taken from Babel 1992.)

observed abundance anomalies, it cannot explain the observed surface distribution of elements, whatever assumption is made about the effect of the magnetic field on the convection zone.

Babel (1992) has investigated the effects of including a magnetically controlled wind in the diffusion models for 53 Cam. As no detailed wind model for the Ap stars is available, Babel assumed a wind that is modulated by the magnetic field with a mass loss rate as a free parameter. In such a model, larger mass loss rates must be present at the magnetic poles than at the magnetic equator, leading to larger abundance variations between the magnetic poles and the equator than in the absence of such a wind.

The mass loss rates were the constrained using the Ca lines in Landstreet's (1988) observations. Babel used Ca because of its strongly nonuniform distribution on the surface of 53 Cam and because the Ca abundance distribution is very sensitive to the mass loss rate; slight variations in the mass loss rate or geometry lead to observable changes in the intensity and profiles of the Ca lines. Because of its high saturation, the Ca II K line is very sensitive to abundance stratification (*e.g.* see Borsenberger *et al.* 1981). For cool Ap stars like 53 Cam, the line centre is formed at optical depths where the abundance is very different from the abundance where the wings are formed. Figure 1.15 shows the profile of the K line for equilibrium abundance distributions corresponding to various mass loss rates and for non-stratified abundances. These profiles are for $B = 0$ and $v \sin i = 0$ and for uniform abundance across the disk. In the presence of stratification, the K line shape differs markedly from the shape for the non-stratified case. The line wings depend crucially on the mass loss rate whereas the core is relatively unaffected. By watching the time dependence of the K line profile one can in principle separate the effects of stratification from the effects of abundance spots.

Babel (1992) finds that the time variation of the K line profile is well reproduced with a mass loss rate of $3\times10^{-15}\ M_{\odot}$/yr at the two magnetic poles. Not surprisingly, since the polar field strengths differ, the sizes of the polar mass loss caps also differ. Figure 1.16 illustrates the magnetic geometry of 53 Cam and the two mass loss caps. The cap at the strong (negative) pole extends from magnetic co-latitude $\alpha = 0^{\circ}$ to $\alpha = 20^{\circ}$ while the cap at the weak pole extends from $\alpha = 110^{\circ}$ to 180°. Fig 1.17 shows the observed (solid line) and theoretical (dashed line) profiles of the Ca II K line for several rotation phases. The small wings at phases 0.54 and 0.92 imply that $dM/dt = 0$ at the equator. Observed and theoretical profiles for Cr are given in Fig. 1.18. (It is instructive to compare this Figure to Landstreet's (1988) model calculations shown in Fig. 1.13.) The agreement for Cr is excellent and we conclude that Landstreet's observations of the Cr abundance variations can be

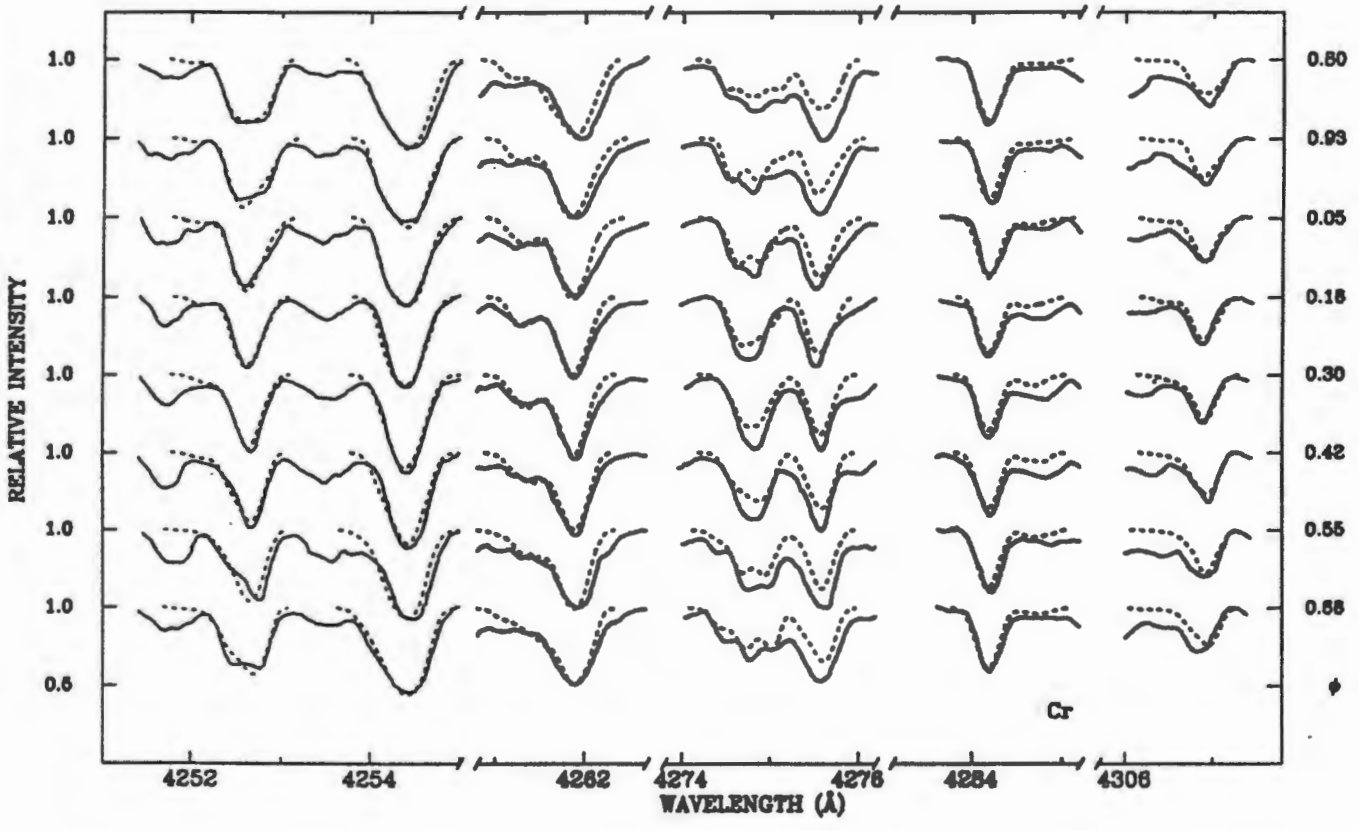

Figure 1.18 The solid lines are spectral profiles of Cr observed at various rotation phases of 53 Cam by Landstreet (1988). The dashed lines are theoretical profiles derived from the diffusion mass loss model. (Taken from Babel 1992.)

explained by the dependence of the Cr abundance distribution on the mass loss rate, which is influenced by the magnetic geometry.

Babel has demonstrated that this model can also reproduce the spectral profiles and variations of Sr. The abundance of Fe can also possibly be explained, but not that of Mn. The abundance and distribution of elements which have $g_{rad} > g$ cannot yet be satisfactorily modelled as their photospheric abundances depend (probably) on the characteristics of the wind region. The mass loss rates inferred by Babel are several orders of magnitude lower than can be observed directly. Thus the diffusion model can be a powerful tool to investigate the magnetohydrodynamics of the outer layers of the Ap stars.

1.17 The other chemically peculiar stars of the upper main sequence

The Ap stars form part of a continuum of chemically peculiar main sequence stars extending from spectral type B1 to F1. Since our discussion thus far has concentrated on what might be termed classical Ap stars, that is stars in the spectral range B8 - F0, we present, for completeness, a brief taxonomical overview of the other chemically peculiar stars. In the visible region, the line-strength anomalies are more conspicuous for the Ap stars than for the Bp stars and consequently the Ap stars have been scrutinized more carefully than the Bp stars. However, the difference in line-strengths may only be a consequence of the higher temperatures of the Bp stars. In the visible region, a Bp star will have less conspicuous lines of the ionized rare earths than an Ap star of identical composition because of the higher stages of ionization in the B star's atmosphere. Also, from the stellar atmospheric point of view, the division at A0 is an artificial one and it is now accepted that the Ap phenomenon (and the applicability of the oblique rotator model) extends to spectral types as early as B2 (Hensler 1979).

The diversity of Bp star spectra has led to the definition of several groups of Bp stars (Fig 1.1). The hottest group comprises the *Helium-rich* (also called *Helium-strong*) stars which have an abnormally high atmospheric abundance of helium and are mostly confined to spectral type B2. They also have strong magnetic fields and they exhibit luminosity, spectrum and magnetic variations in common with many Ap stars.

The He-rich stars are followed by a cooler group, the *He-weak* stars, which have spectral types in the range B3 to B7. This group is further subdivided into the *P-Ga*, *Ti-Sr* and *Si* He-weak subgroups. The names of these subgroups allude to the anomalously strong spectral lines which

characterize them. Like the He-rich stars and the Ap stars, the latter two subgroups have magnetic fields and exhibit magnetic, photometric and spectrum variability (Borra *et al.* 1983). Very little is known about the binary frequency among the He-rich and He-weak stars.

Wolff & Wolff (1976) argue that there are two distinct sequences of peculiar stars in the range 10000 K < T_{eff} < 16000 K (Fig. 1.1) and that the differences between these two groups mirrors the differences between the Ap and Am stars. Thus the coolest of the Bp stars, the HgMn stars which have spectral types in the range B6 to B9, appear to be non-magnetic counterparts of the Ap Si stars (Borra & Landstreet 1980, Borra *et al.* 1983). They are slow rotators, non-magnetic, non-variable and appear to have a much higher frequency of spectroscopic binaries than the Ap Si stars. One might say that they are hotter analogues of the Am stars. The P-Ga subgroup of the He-weak stars seems to constitute a hotter analogue of the HgMn stars. Like the HgMn stars, the P-Ga stars are non-variable and non-magnetic (Borra *et al.* 1983).

The *classical Am stars* are those main sequence stars of spectral type A4 - F1 in which the metallic-line and Ca II K-line spectral types differ by 5 or more spectral subclasses. The hydrogen line types range from A4 - F1 and are intermediate between the metal and K-line types. The spectra of the Am stars are characterized by anomalously strong metallic lines and marked deficiencies of Ca, C, O, Mg and Sc (Boyarchuk & Savanov 1986). In addition, Am spectra are less diverse than Ap spectra although several groups of Am stars are also defined. *Marginal Am stars* (designated Am:) are stars of spectral appearance similar to the classical Am stars, but in which the metallic and K-line spectral types differ by less than the required 5 subclasses. The *Hot Am stars* have H-line spectral types from A0 - A3 and show pronounced abundance anomalies but are not classified as classical Am stars owing to the general weakness of their line strength anomalies. This weakness is a consequence of the weaker metal lines which prevail at these higher temperatures.

The δ *Delphini stars* are A-type stars lying above the main sequence which have metallic line spectra. They are defined spectroscopically (Kurtz 1976) to be those late-A and early-F subgiants and giants with spectra similar to δ Del. Kurtz (1976) considers the δ Del stars to be evolved Am stars although this view is not universally accepted (Wolff 1983). Gray and Garrison (1989) argue that the δ Del class is spectroscopically inhomogeneous and that most stars classified as δ Del in the literature are either normal A-type, Am: or Am stars. They propose that the δ Del designation be dropped. Gray and Garrison have also identified a class of late, apparently evolved, Am stars which they designate the ρ Puppis stars after the bright prototype.

For many years, it was thought that Am stars were all non-magnetic. Recently, Mathys & Lanz (1990) discovered that the Am star *o* Peg has a magnetic field of order 2 kG which appears to have a complex structure. Interestingly, *o* Peg differs from the classical Am stars in that it is not very Ca deficient and it is not binary. If *o* Peg is not a mis-classified Ap star, then the discovery of a magnetic field raises a number of questions. Are other Am stars also magnetic? If so, have they eluded detection because they do not have simple field geometries as in the Ap stars? Is the field of *o* Peg or other Am stars variable in time? The counter example to *o* Peg in the Ap stars is HD 133792, a sharp-lined A0p SrCrEu star with little evidence of a magnetic field.

As a group, the Am stars are slow rotators (Abt & Moyd 1973, Abt 1975). Roughly, the Am stars have $v \sin i < 100$ km s^{-1} while spectroscopically normal stars have $v \sin i > 100$ km s^{-1}. Moreover, most Am stars are to be found in binary systems. Abt (1961, 1965) showed that 22 out of 25 Am stars were members of spectroscopic binaries with $P < 100$ days. Abt & Bidelman (1969) later suggested that all main sequence stars in the spectral range A4 - F1 that are primaries in binaries with periods in the range $2.5 < P < 100$ days have Am spectra while stars outside this period range are chemically normal with a few exceptions. Carcuillat (Vauclair 1983) has subsequently demonstrated the existence of 8 normal A stars with periods in the $2.5 < P < 100$ day range. Since slow rotation and a high binary frequency are both associated with the Am phenomenon and since slow rotation may be a consequence of binarity in many cases, it is important to test whether rotation is the key parameter that determines whether a given star will have a normal or an Am spectrum. In an attempt to establish whether *all* Am stars and *no* normal A stars are members of binary systems, Conti & Barker (1973) searched for and found radial velocity variations in only 2 out of 5 stars with Am characteristics in the Coma cluster. Unfortunately their sample is too small to rule out inclination effects.

The existence of Am stars in even the youngest associations (Abt 1979) indicates that the time required for the emergence of the Am phenomenon is substantially less than the nuclear evolution time-scale. Also, metallicism appears to be a main sequence phenomenon since Am stars are only found fairly close to the main sequence.

Several observers have sought variability in the Am stars. Initial variability studies indicated that the lack of spectrum and brightness variability and the Am star phenomenon go together. The lack of spectrum variability on time-scales of days seemed to exclude surface inhomogeneities as in the Ap stars, whilst the absence of brightness variability on time-scales of minutes to hours seemed to exclude pulsation. In fact, some δ Del and Am: stars *do* pulsate (Kurtz 1976, 1978a, 1984b) and so

does at least one classical Am star (Kurtz 1989b). We will return to this issue of pulsation and metallicism after discussing the δ-Sct stars.

The favoured working hypothesis of the origin of the abundance anomalies in the Am stars is diffusion (Wolff 1983, Vauclair 1983). The diffusion hypothesis provides a natural explanation for the absence of metallicism in rapid rotators; strong meridional circulation currents in rapid rotators destroy the atmospheric stability required for diffusion to operate effectively. The existence of Am stars in very young associations is consistent with the theoretical expectation that unimpeded diffusion can produce marked abundance anomalies in only 10^4 yr.

The λ *Boo stars* constitute yet another group of peculiar stars (Sargent 1967, Hauck & Slettebak 1983, Cowley 1991). They are characterized by the weakness of their metallic lines and their rather high rotational velocities, which range from 75 km/s to over 200 km/s. The criteria for membership in this class are: (1) an early A spectral type as determined from the hydrogen lines, (2) weak metallic lines for their colours and hydrogen line spectral types and (3) low (*i.e.* Population I) radial velocities. These stars are in a sense the alter-egos of the Am stars. It is not presently known whether these stars have ordered global magnetic fields or not.

The different types of peculiar stars described in this section are often referred to by their CP (for *chemically peculiar*) designations. The CP classification scheme was devised by Preston (1974) and extended by Maitzen (1984). This notation is especially popular among the European astronomers. The notation is as follows:

CP1 metallic line (Am)
CP2 magnetic Ap
CP3 HgMn
CP4 magnetic He-weak
CP5 nonmagnetic He weak
CP6 magnetic He strong
CP7 nonmagnetic He strong

This notation is easy to memorize if one notes that the even numbers go with the magnetic stars in order of increasing temperature. Note also that the CP classification scheme does not accommodate the λ Boo or δ Del stars.

1.18 The δ Scuti stars

The lower portion of the Cepheid instability strip crosses the main sequence around the late-A and early-F spectral types. The pulsating variables located here are called the δ Scuti stars. They are

population I low-amplitude (A < 0.8 mag), short-period (½hr < P < 7hr) pulsating variables of spectral types A and F which lie within 3 magnitudes of the main sequence. The pulsation driving mechanism in the δ Scuti stars, the so-called κ *mechanism*, stars is discussed in chapter 2. The distribution of v sin i in the δ Scuti stars is interesting. While the δ Scuti giants have a distribution of v sin i which is essentially the same as that for normal A stars, there is a dearth of slow rotators near the main sequence (Wolff 1983). This complements the observation that the chemically peculiar dwarfs are predominantly slow rotators. Because of the complexity of their light curves, some δ-Scuti stars have attracted extensive observational investigations, with several astronomers observing from sites widely separated in longitude. Among the most successful networks for δ Scuti observations have been STEPHI (STEllar PHotometry International programme) with three sites (Michel *et al.* 1992, Belmonte *et al.* 1991) and the 'δ Scuti Network' with up to 10 sites (Breger *et al.* 1989, 1990). The high quality data produced by these groups have shown that δ Scuti eigenmode spectra are much more complex than was previously thought. While the complex behaviour of these stars confounds classification attempts, Breger (1991) has found that δ Scuti stars fall into one of two broad categories:

1) *The radial pulsators*. These stars have only one or two dominant periods and undergo no obvious amplitude modulation. They are also slow rotators (v sin $i \leq 30$ km/s). These stars used to be called Dwarf Cepheids because of their large pulsation amplitudes.

2) *The non-radial pulsators*. These stars pulsate with many non-radial (and radial) modes and show significant amplitude modulation. The also tend to be faster rotators, with v sin i as high as 150 km/s.

There is a vast amount of observational material on these variables. Breger (1979) lists 129 δ Scuti stars in his review and new candidates are being added to the list all the time. The most up-to-date compilation of δ Scuti stars is now available in digital form (García *et al.* 1993). It is interesting that only about a third of the stars in this section of the instability strip pulsate with *detectable* amplitudes. The reason why I emphasize detectable pulsation is that the majority of δ Scuti stars pulsate with very low amplitudes. The histogram of pulsation amplitudes in Breger's (1979) review reveals that the number of pulsators increases exponentially with decreasing amplitude. This point is worth pursuing with a survey which should have a limiting amplitude considerably less than the 0.01 mag limit of existing surveys.

1.19 Metallicism and Pulsation

The definitions of the δ Del and Am stars imply nothing about pulsation in such stars and, conversely, the definition of a δ Scuti star implies nothing spectroscopic about such a star. As all three classes of object populate the same region of the HR diagram, one might suppose that pulsation and metallicism could coexist in some stars. In fact, for many years an apparent exclusion between the δ Scuti stars and the Am stars was observed (Breger 1970). That is, an exclusion between pulsation and metallicism was observed. The diffusion hypothesis is usually invoked to explain this observation. It is argued that in slowly rotating stars, He II diffuses out of the He II ionization zone and the star is stabilized against pulsation. If the star is magnetic, it becomes an Ap star, otherwise it becomes an Am star. On the other hand, rapid rotation gives rise to turbulent meridional circulation currents which destroy the effects of diffusion and leave the He II ionization zone with sufficient He to drive pulsation. According to this simple picture, all slowly rotating A stars should be chemically peculiar and should not pulsate. The rapidly rotating A stars should all be chemically normal and pulsate.

However, the situation is not this simple since some δ Del and Am: stars *do* pulsate (Kurtz, 1976, 1978, 1984b) and so does at least one classical Am star (Kurtz 1989b). One might argue that the Am, Am: or δ Del classifications of these stars are incorrect, but such an argument becomes much less tenable as the number of candidates increases. Cox, King and Hodson (1979) responded to the need for theoretical studies addressing the problem of pulsation in the presence of metallicism and found that the Am: and δ Del stars may possess sufficient residual He to drive pulsation in a narrow instability strip only 200-500 K wide situated in the coolest one-third of the δ Scuti instability strip. They conjectured that the residual He exists because of incomplete settling, or because of a small recent upward mixing of He.[1] They also argued that the classical Am and Ap stars should *not* pulsate because their He II ionization zones should be fully depleted of He. In the 14 years that have followed the publication of Cox *et al.*'s paper, the whole issue of pulsation and metallicism has become considerably clouded with exceptions to this rule.

The first pulsating metal-rich A star to be discovered was the extremely peculiar star HD 101065 (Kurtz 1978b). This star proved to be instrumental in the discovery of a new, and entirely unexpected, class of rapidly oscillating Ap stars. These stars oscillate with periods in the range 4-15 min and amplitudes of a few millimagnitudes (mmag). Kurtz (1979, 1980b) also discovered low-overtone multi-periodic δ Scuti pulsation in the metal-rich star HD 188136. It could be argued that

---

1 The co-existence of pulsation and mild metallicism in the Am: stars could also be a consequence of the metals diffusing upwards faster than the He diffuses downwards (Vauclair *et al.* 1978).

since this star is above the main sequence and displays enhanced metallicity it is a δ Del star, but Wegner's (1981) abundance analysis indicates that HD 188136 is spectroscopically akin to HD 101065. This means that HD 188136 is probably an Ap star which exhibits δ Scuti pulsation. Kreidl (1986) has reviewed the observational evidence for δ Scuti variability in about 20 candidate Ap stars. Although there do not seem to be any clear-cut cases of δ Scuti variability in a star with an unambiguous Ap designation, further observational work in this direction is justified. A most exciting recent development is Kurtz's (1989b) discovery of δ Scuti pulsation in the classical Am star HD 1097. Unless the Am classification of this star can be shown to be incorrect, Kurtz's observations constitute evidence that classical Am stars can pulsate.

It seems that just about the only general statement that can still be made about pulsation and metallicism is that where they co-exist, low pulsation amplitudes ($A \leq 0.05$ mag) prevail. This suggests that diffusion is still a viable underlying mechanism for producing the spectral peculiarities. One then requires that the turbulent velocities remain much lower than the diffusion velocity of ≈ 1 cm s^{-1} while pulsation in the Ap stars generates radial velocities as high as several hundred metres per second (Matthews *et al.* 1988, Libbrecht 1988 & Ando *et al.* 1988). The whole question of pulsation in the presence of metallicism is far from being resolved.

Chapter 2

The rapidly oscillating Ap stars

2.1 Introduction

This chapter consists of two parts. In the first part we describe the discovery of the rapidly oscillating Ap (roAp) stars and we present an overview of the general properties of the roAp stars. The second part of this chapter deals with the mathematical description and physics of the oscillations in the roAp stars. There are many excellent treatments of the physics of stellar pulsation. We will not reproduce these treatments here but present only some of the salient features that will be required in later chapters. We will begin by discussing the different types of stellar oscillations and the surface manifestation of these oscillations as well as their mathematical description. This is followed by a discussion of the expected eigenfrequency spectra for high-overtone pulsation. The chapter concludes with an examination of the models that have been proposed to explain the roAp phenomenon. The reader interested in a more detailed introduction to stellar pulsation than given here is referred to the excellent review articles by Christensen-Dalsgaard *et al.* (1985) and Gough & Toomre (1991) and the books by Cox (1980) and Unno *et al.* (1989). The two review articles focus on the solar oscillations, but they are also of relevance to the pulsations in the roAp stars. Readers interested in more details of the roAp phenomenon are referred to the recent reviews by Kurtz (1990), Matthews (1991) and Shibahashi (1991). Kurtz and Matthews emphasize the observations and Shibahashi emphasizes theoretical developments.

2.2 Przybylski's star (HD 101065) and the discovery of the roAp stars

Przybylski's star, HD 101065, is arguably the most peculiar non-degenerate star in the sky. It has an extremely complex spectrum which is dominated by lines of the rare earth elements, the strongest of which belong to holmium. Because of the extreme line blanketing, it is impossible to estimate where the continuum is and this gave rise to a decade-long controversy over the spectral type of this star. One gains an idea of the extremely peculiar nature of this star when referring to the literature where the suggested spectral types range from late A to early G with Przybylski, among others, favouring the later spectral types.

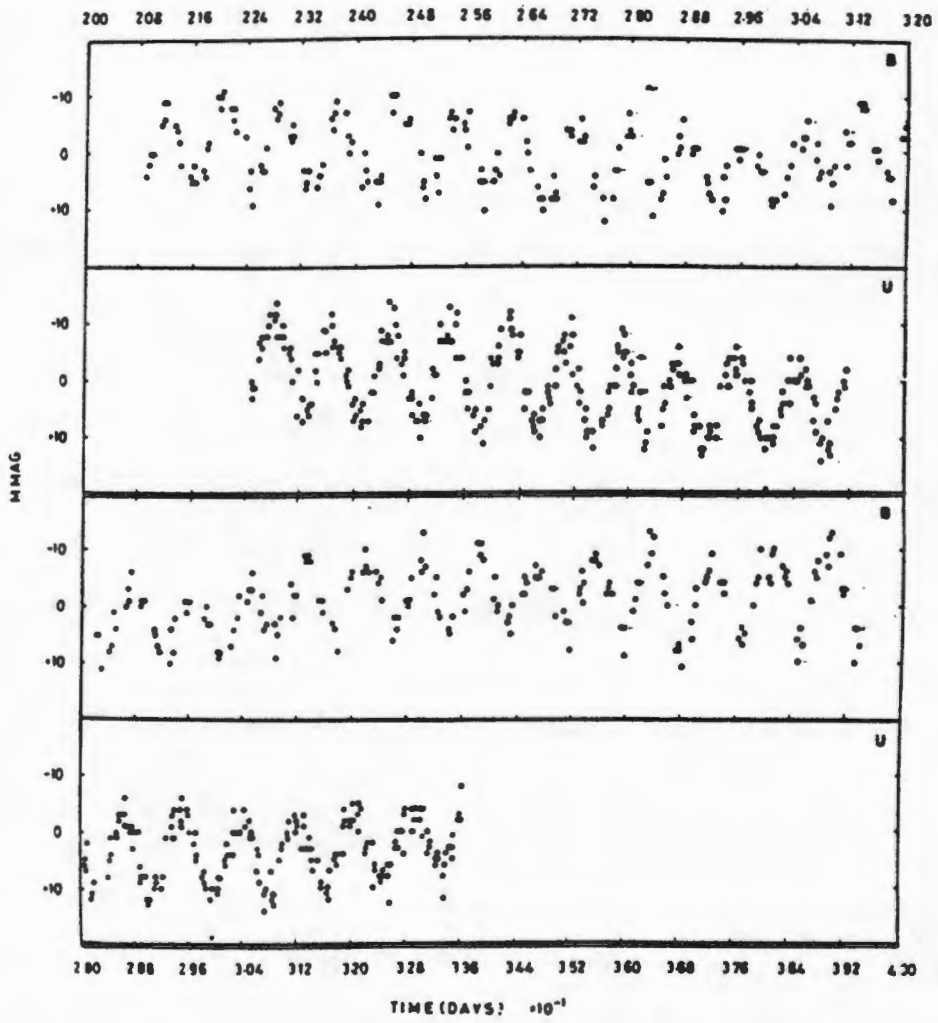

Figure 2.1 This is one of the earliest light curves of the roAp stars. After discovering rapid oscillations in HD 101065, Kurtz observed it simultaneously in Johnson *B* on the South African Astronomical Observatory (SAAO) 0.5-m telescope and Johnson *U* on the SAAO 1.0-m telescope. These observations demonstrated that there was no possibility that the variability was an instrumental artefact. Variations of this amplitude are obvious at the telescope. (Taken from Kurtz & Wegner 1979)

As we saw in chapter 1, roughly two out of every ten A-type stars exhibit some kind of spectral peculiarity. If the classification of HD 101065 as a late-type star were correct it would be a unique pathological object. However, if the earlier spectral classification were correct then it would be at the cool end of the sequence of peculiar stars and might just be an extreme example of an Ap star. Initially, the identification of HD 101065 as an extreme Ap star faced a number of difficulties which have largely fallen away over the years. The discovery of a -2200 G magnetic field by Wolff & Hagen (1976) was an important early source of support for the suggested Ap nature of this star. Later, ultraviolet observations taken by Gary Wegner *et al.* (1983) with the *International Ultraviolet Explorer* (*IUE*) satellite revealed a clear dominance of Fe peak elements and too much ultra violet flux to be consistent with a later spectral type. This resolved the contentious issue of whether the Fe abundance was normal or not. Previous estimates of the Fe abundance had ranged from normal to underabundant by several orders of magnitude; the dominance of Fe peak elements was another significant indication of the Ap nature of HD 101065. Further circumstantial evidence in support of the proposed extreme Ap nature of HD 101065 comes from the discovery of qualitatively similar spectra in the known magnetic Ap stars HD 51418 (Jones *et al.* 1974) and HR 465 (Hartoog *et al.* 1973).

In 1978, prior to the *IUE* observations, Don Kurtz and Gary Wegner were searching for a way to demonstrate that HD 101065 is an extreme member of the Ap stars. Kurtz reasoned that this star should be constant in brightness even though they believed it to be hot enough to lie inside the δ Scuti instability strip. The reason for this belief was that if HD 101065 was an Ap star, then its peculiarities were produced by diffusion processes and the exclusion between metallicism and pulsation (Sec. 1.20), then still thought to be absolute, should apply.

To confirm these expectations, Kurtz searched for the presence of δ Scuti-like oscillations in HD 101065 using conventional differential photometry. The cycle time for HD 101065 and the two comparison stars was about 7 minutes. While the comparison stars were constant to a scatter of σ = 0.002 mag, HD 101065 had a suspiciously regular scatter of σ = 0.003 mag about the mean value (Kurtz & Wegner 1979). Kurtz then switched to doing continuous 10-s integrations without comparison stars and found that HD 101065 is indisputably a variable star with a 12.14-min period and an amplitude of 0.010 mag peak-to-peak (Fig. 2.1).

It would probably be true to say that were it not for HD 101065, the roAp stars would still be undiscovered today. The technology necessary to study the roAp stars was readily available to

Table 2.1

The rapidly oscillating Ap stars: Names, positions, magnitudes, spectral types, oscillation periods and amplitudes

HD	HR	Name	α (2000)	δ (2000)	V	Spectral Type	Period (min)	ΔB_{max} (mmag)
6532			1 5 56	-26 43 43	8.445	Ap SrCrEu	7.1 ○	5
12932			2 6 13	-19 7 16	10.235	Ap SrEuCr	11.6	4
19918 •			3 1 24	-81 54 0	9.336	Ap SrEuCr	14.5	2
24712	1217		3 55 16	-12 5 54	6.001	Ap SrEu(Cr)	6.2 •	10
42659 •			6 11 21	-15 47 32	6.768	Ap SrCrEu	9.7	0.8
60435			7 31 0	-58 0 0	8.891	Ap Sr(Eu)	11.4 - 23.5 •	16
80316			9 18 25	-20 22 13	7.782	Ap Sr(Eu)	7.4	2
83368	3831		9 36 25	-48 45 3	6.168	Ap SrEuCr	11.6	10
84041 •			9 41 34	-29 22 26	9.330	Ap SrEuCr	15.0 •	6
101065	Przbylski's Star		11 37 37	-46 43	7.994	Controversial	12.1 •	13
119027 •			13 41 19	-28 47 23	10.022	Ap SrEu(Cr)	8.7 •	2
128898	5463	α Cir	14 42 30	-64 58 0	3.198	Ap SrEu(Cr)	6.8 •	5
134214			15 9 3	-13 59 58	7.464	Ap SrEu(Cr)	5.6	7
137949		33 Lib	15 29 35	-17 26 27	6.673	Ap SrEuCr	8.3 ○	3
150562 •			16 44 11	-48 39 16	9.816	A/F(p Eu)	10.8	0.8
161459 •			17 48 29	-51 55 2	10.326	Ap EuSrCr	12.0	1.3
166473			18 12 26	-37 45 6	7.923	Ap SrEuCr	8.8 •	2
176232	7167	10 Aql	18 58 47	+13 54	5.89	F0p SrEu	11.6 •	0.6
190290 •			20 14 0	-78 52 0	9.912	Ap EuSr	7.3 •	2
193756 •			20 24 11	-51 43 25	9.195	Ap SrCrEu	13.0	0.9
196470 •			20 38 10	-17 30 6	9.721	Ap SrEu(Cr)	10.8	0.7
201601	8097	γ Equ	21 10 21	+10 08	4.68	F0p	12.4 •	3
203932			21 26 4	-29 55 45	8.820	Ap SrEu	5.9 •	2
217522			23 1 47	-44 50 25	7.525	Ap (Si)Cr	13.9 •	4
218495 •			23 9 30	-63 40 0	9.356	Ap EuSr	7.4	1

Notes:

1) The HD numbers marked with a bullet (•) denote the 10 new roAp stars discovered in the Cape Survey.
2) The V magnitudes are as measured in the Cape Survey, except for the three stars, HD 128898, HD 176232 & HD 201601. For these stars, the V magnitudes from Table 1 of Kurtz's (1990) review were used.
3) The spectral types listed are from the Michigan Spectral Catalogue (Houk & Cowley 1975, Houk 1978, 1982, Houk & Smith-Moore 1988)
4) The periods given are for the principal oscillation frequency. The original sources of these periods are listed in Table 9.1. Stars which have been observed to pulsate in two, or more, independent pulsation modes are marked with a bullet (•). Stars in which there is evidence of further oscillation frequencies are marked with an open circle (○)
5) ΔB_{max} is the maximum peak-to-peak light variation observed in Johnson B light for the star to date.

Table 2.2

The rapidly oscillating Ap stars: Strömgren indices, magnetic field strengths and rotation periods.

HD	y	$b-y$	m_1	δm_1	c_1	δc_1	β	B_e (G)	P_{rot} (day)
6532	8.445	0.088	0.214	-0.014	0.879	-0.051	2.880		1.9448
12932	10.235	0.179	0.228	-0.024	0.765	-0.035	2.810		
19918	9.336	0.169	0.216	-0.010	0.822	-0.058	2.855		
24712	6.001	0.191	0.211	-0.023	0.626	-0.074	2.760	+400 to +1300	12.4572
42659	6.768	0.124	0.257	-0.050	0.765	-0.076	2.834		
60435	8.891	0.136	0.240	-0.034	0.833	-0.047	2.855	<1000	7.6793
80316	7.782	0.118	0.324	-0.118	0.599	-0.283	2.856		2.1?
83368	6.168	0.159	0.230	-0.024	0.766	-0.062	2.825	-700 to +700	2.851962
84041	9.330	0.177	0.233	-0.026	0.797	-0.061	2.844		3.69
101065	7.994	0.431	0.387	-0.204	0.002	-0.370	2.641	-2200	3.94?
119027	10.022	0.257	0.214	-0.034	0.557	-0.076	2.731		
128898	3.198	0.152	0.195	0.012	0.760	-0.077	2.831	-300	4.46
134214	7.464	0.216	0.223	-0.029	0.620	-0.108	2.774		
137949	6.673	0.196	0.311	-0.105	0.580	-0.236	2.818	+1400 to +1800	
150562	9.816	0.301	0.212	-0.015	0.659	-0.087	2.783		
161459	10.326	0.245	0.246	-0.040	0.679	-0.141	2.820		
166473	7.923	0.208	0.321	-0.118	0.514	-0.268	2.801		
176232	5.89	0.150	0.208	-0.004	0.829	0.031	2.809		
190290	9.912	0.289	0.293	-0.091	0.466	-0.306	2.796		
193756	9.195	0.181	0.213	-0.008	0.760	-0.040	2.810		
196470	9.721	0.211	0.263	-0.059	0.650	-0.144	2.807		
201601	4.68	0.147	0.238	-0.032	0.760	-0.058	2.819	-800 to +500	
203932	8.820	0.175	0.196	0.004	0.742	-0.020	2.791		
217522	7.525	0.289	0.227	-0.056	0.484	-0.015	2.691		
218495	9.356	0.114	0.252	-0.049	0.812	-0.098	2.870		

Notes:

1) The photometric data in this Table were acquired as part of the Cape Survey for all but three stars, HD 128898, HD 176232 and HD 201601. For these stars, the photometric data in Table 1 of Kurtz's (1990) review were used.

2) The magnetic field measurements tabulated here are from Table 2 of Kurtz's (1990) review.

3) The original sources of the rotation periods are listed in Table 9.1.

astronomers already in the late 1960's but there was no theoretical or empirical motivation to search for rapid oscillations in Ap stars. In fact, there was a strong theoretical expectation that Ap stars should *not* pulsate because this would be incompatible with the atmospheric stability required for radiative diffusion to produce the observed abundance anomalies. Nonetheless, on the belief that HD 101065 was a cool Ap star, Kurtz decided to search for rapid oscillations in other cool Ap stars and he was rewarded with the discovery of a new class of variable star which he presented in his seminal paper (Kurtz 1982) in 1982.

2.3 General properties of the roAp stars

In the 12 years following the discovery of rapid oscillations in Przybylski's star, Don Kurtz and his collaborators discovered another 14 roAp stars. The Cape Survey described in this thesis has led to the discovery of 10 new roAp stars. One other new roAp star was discovered independently by two other surveys that ran in parallel with the Cape Survey, bringing the total number of roAp stars to 25 as of this writing. Table 2.1 lists the names, positions, magnitudes, spectral types, oscillation periods and maximum amplitudes of the roAp stars. Table 2.2 lists their Strömgren indices, magnetic field strengths and rotation periods. The properties of these roAp stars may be summarized as follows:

1) The pulsation periods are in the range 5.6 to 15.0 min. The amplitudes are all ≤ 16 millimagnitudes (mmag) peak to peak. Because of the shortness of these periods, roAp stars are detected and studied using non-differential high-speed photometry. Experience has shown that it is possible to distinguish between real variations in the star and variations caused by sky transparency. Nonetheless, stable, well maintained equipment and an excellent photometric site are required for roAp star photometry. The observational techniques are discussed in greater detail in chapter 5.
2) Many roAp stars are multiperiodic. Fig 2.2 shows a sample light curve for one of the new roAp stars presented in this thesis; note the modulation in the amplitude of the oscillations during the course of the observations. This amplitude modulation is caused by three frequencies beating against each other.
3) The pulse shape in some roAp stars is nonsinusoidal. In such cases the harmonics of the principal oscillation frequencies are seen in the Fourier spectra of the light curves. Fig 2.3 shows an example of this.

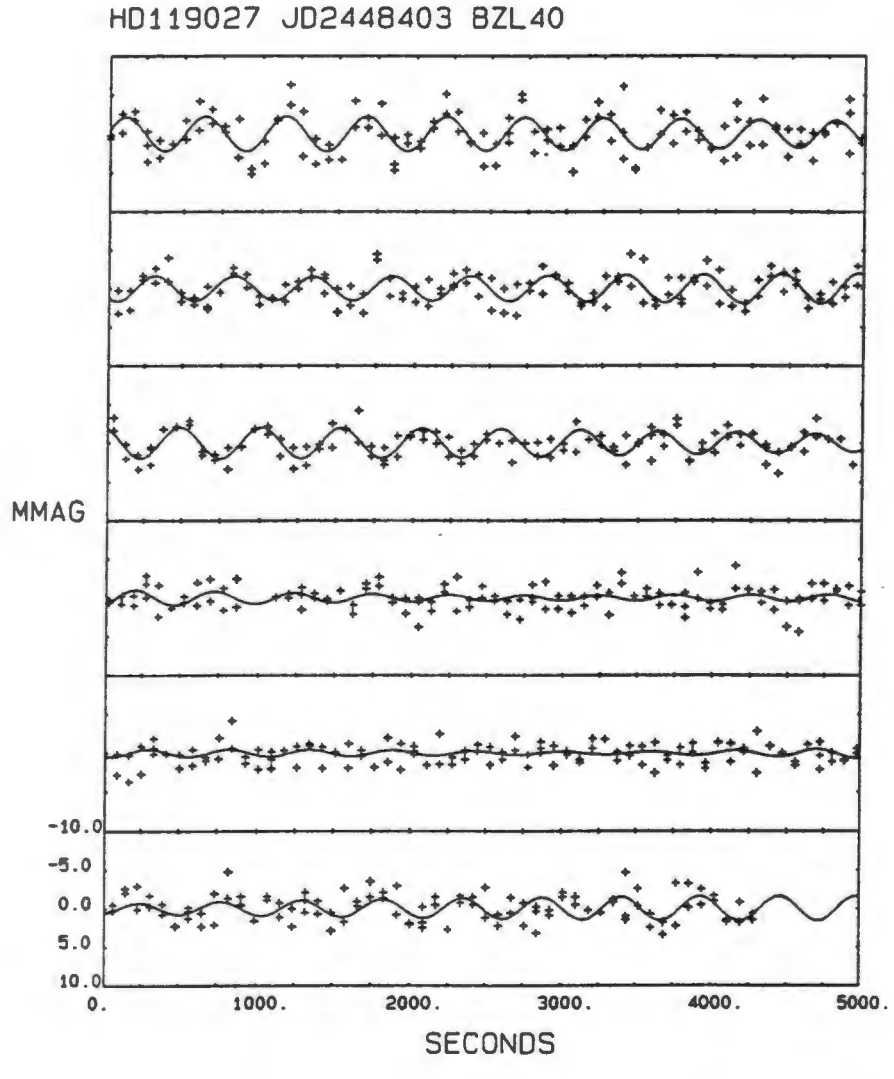

Figure 2.2 This continuous 8.15-hr record of the rapid Johnson *B* light variations in the roAp star HD 119027 illustrates the amplitude modulation that arises from the beating of three independent pulsation frequencies. This is especially evident when one compares the second and fourth panels. The light curve is continuous; the right edge of each panel coincides with the left edge of the panel below it. The solid line is a least-squares fit of the three oscillation frequencies to the data. The ordinate is scaled in millimagnitudes (mmag); each panel is 20 mmag high. This star is discussed in detail in Chapter 7.

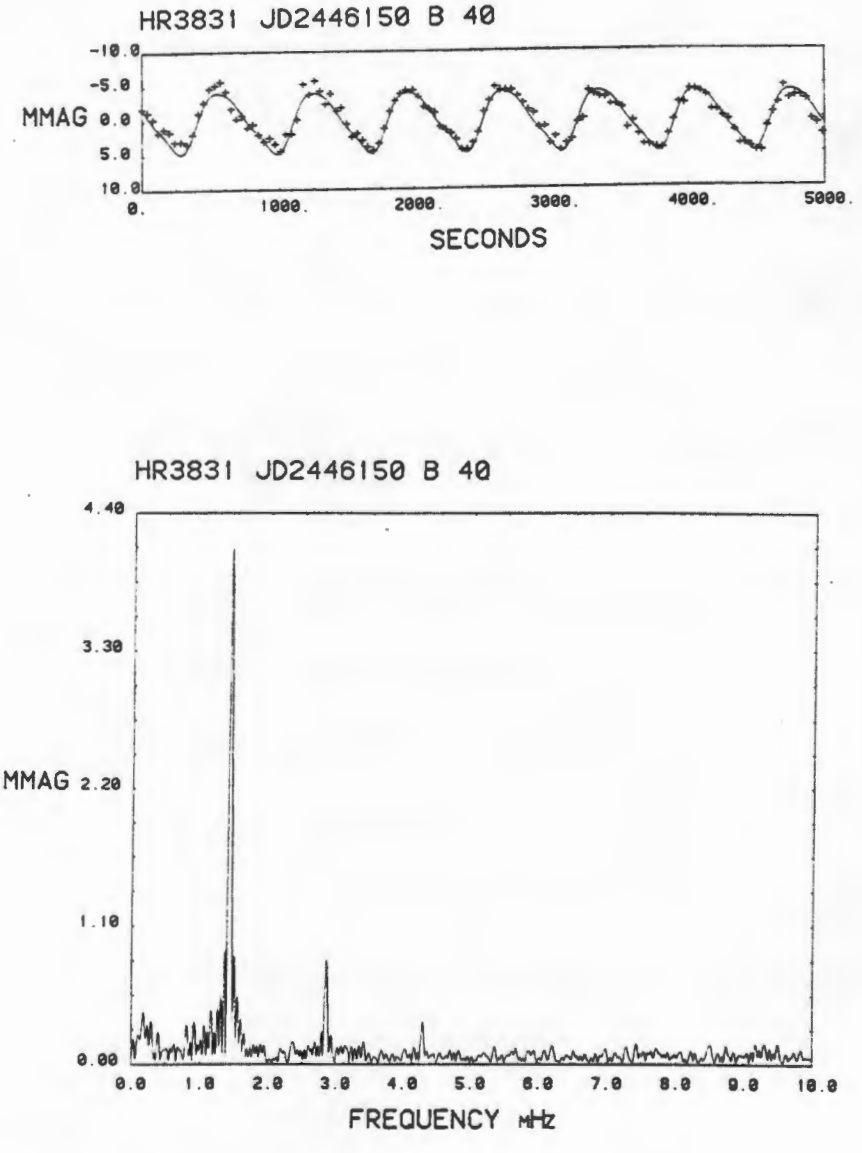

Figure 2.3 The top panel shows a portion of the *B* light curve of the roAp star HR 3831 on the night JD 2446150. Each point is an average of 4 10-s integrations. The bottom panel shows the Fourier transform of the entire light curve for that night. Notice that the light curve is non-sinusoidal; the rise is steeper than the fall. This non-sinusoidal behaviour shows up in the Fourier transform as the first and second harmonic of the principal frequency. The solid line in the upper panel is a least-squares fit of the principal frequency and its two harmonics to the data. (Taken from Kurtz 1990)

4) In addition to short-term amplitude modulation caused by beating of independent pulsation frequencies, the oscillations also undergo amplitude modulation on time scales of several days, or longer. Fig. 2.4 shows this for HR 3831. For those roAp stars with known magnetic (rotation) periods, the period of the amplitude modulation is always equal to the rotation period. For HR 3831, this agreement is better than 1 part in 150 (Kurtz *et al.* 1992). The pulsation amplitude is always a maximum at magnetic extremum (*i.e.* when one views one of the magnetic poles directly) and always a minimum at quadrature. This amplitude modulation manifests itself in the Fourier spectrum of the oscillations as an equally spaced frequency multiplet centered on the pulsation frequency. The spacing of the frequencies in the multiplet is equal to the rotation frequency.

5) At quadrature, when the oscillation amplitude dies down, the oscillation phase is observed to undergo a π radian phase reversal. This is shown for HR 3831 in Figure 2.5.

6) The oscillation spectra of the roAp stars are not stationary. In some stars, oscillation frequencies come and go on a time-scale of days. Figure 2.6 is series of Fourier amplitude spectra of the roAp star HD 60435 taken on 6 different nights by Matthews *et al.* (1987). Notice how the most prominent peaks are different on different nights. In other stars frequency changes are seen from one season to the next. In HD 217522 a new frequency emerged in 1985 observations which was not seen in 1982 data. Phase instabilities are also known in a few well-studied roAp stars and may be the norm, rather than the exception. We will discuss this feature of the oscillations in greater detail in chapter 9.

7) Even roAp stars which oscillate with only one frequency display non-stationary behaviour on timescales of years. Measurement of dP/dt values in roAp stars can potentially be used to determine their evolutionary status and evolutionary timescale. Periodic Doppler shifts in the oscillation frequencies can be used to detect the presence of low mass companions. There is also a possibility that subtle frequency shifts may be used to study gradual changes in the magnetic fields (chapter 9).

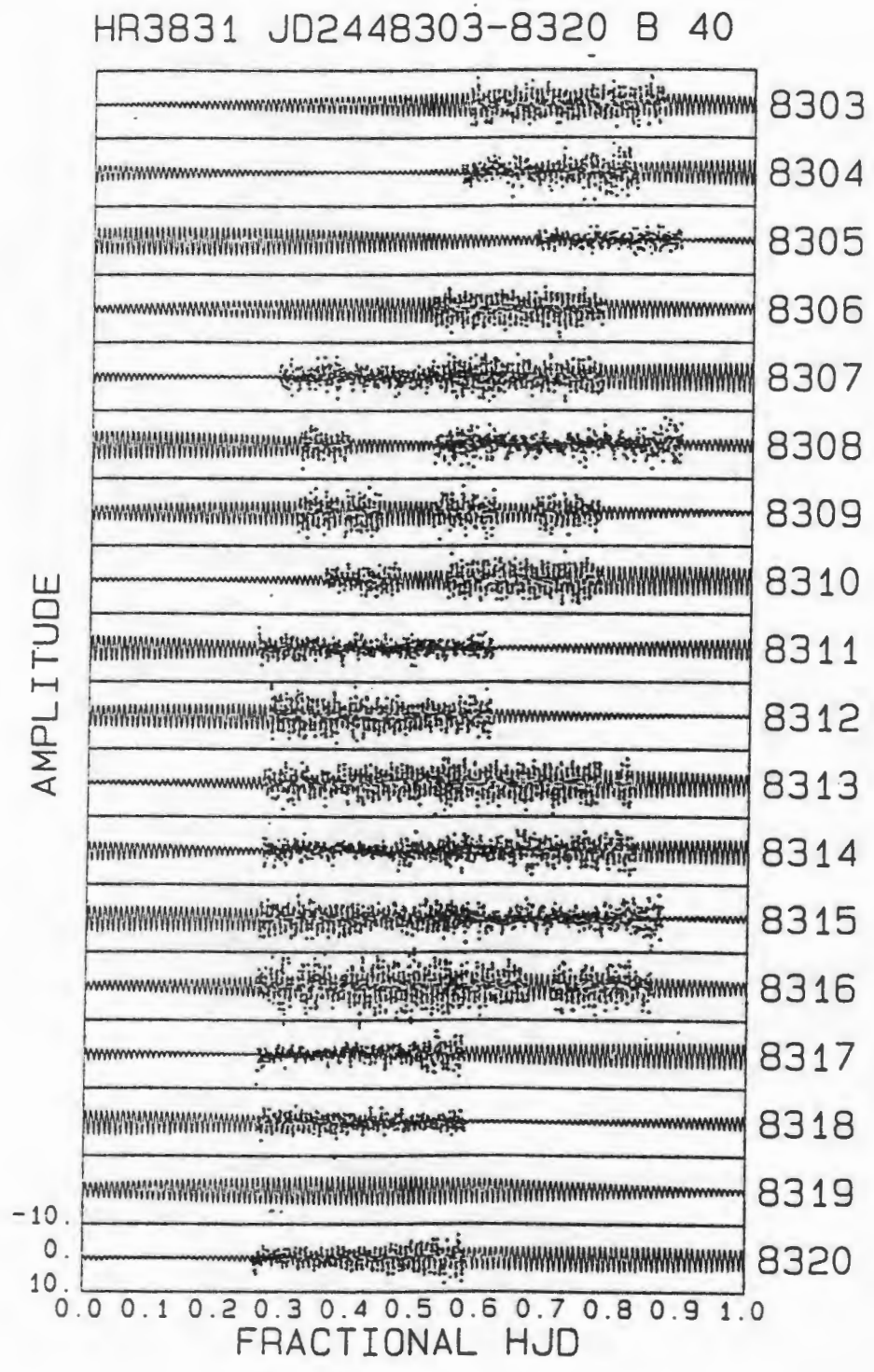

Figure 2.4 This is a record of the *B* light variations of HR 3831 on 18 consecutive nights during 1991. These multi-site observations were acquired at the South African Astronomical Observatory (SAAO) and the Cerro Tololo Inter-American Observatory (CTIO). The solid line shows the rotational amplitude modulation continuously. The number to the right of each panel shows the last 4 digits of the Heliocentric Julian Date, HJD244*nnnn* Each panel covers 24 hr and is 20 mmag high. (Taken from Kurtz, Kanaan & Martinez 1991)

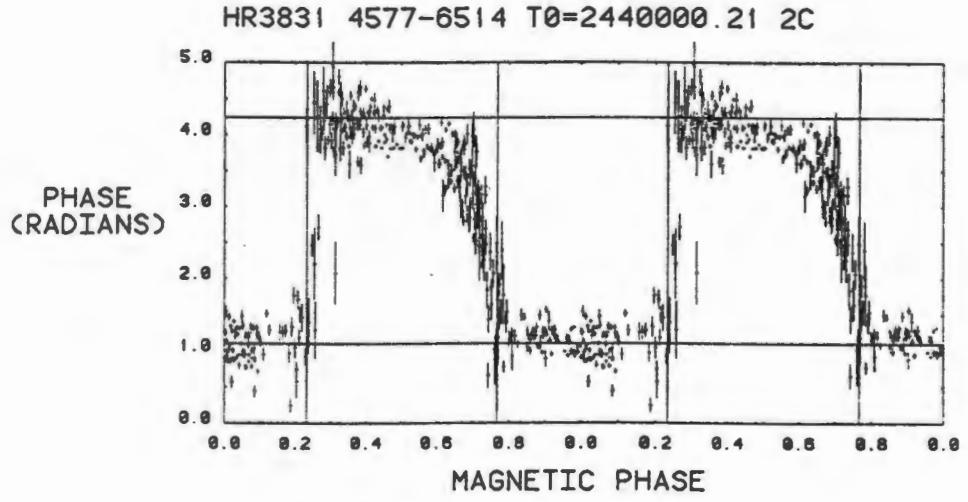

Figure 2.5 This diagram shows the behaviour of the pulsation phase vs. the magnetic (rotation) phase. The pulsation phases were obtained by fitting the oscillation frequency to two-cycle lengths of data by least squares. The magnetic phase was calculated independently using the magnetic ephemeris for this star. The vertical lines indicate the times of quadrature where the pulsation amplitude goes to zero and the pulsation phase flips by π radians. (Taken from Kurtz 1990)

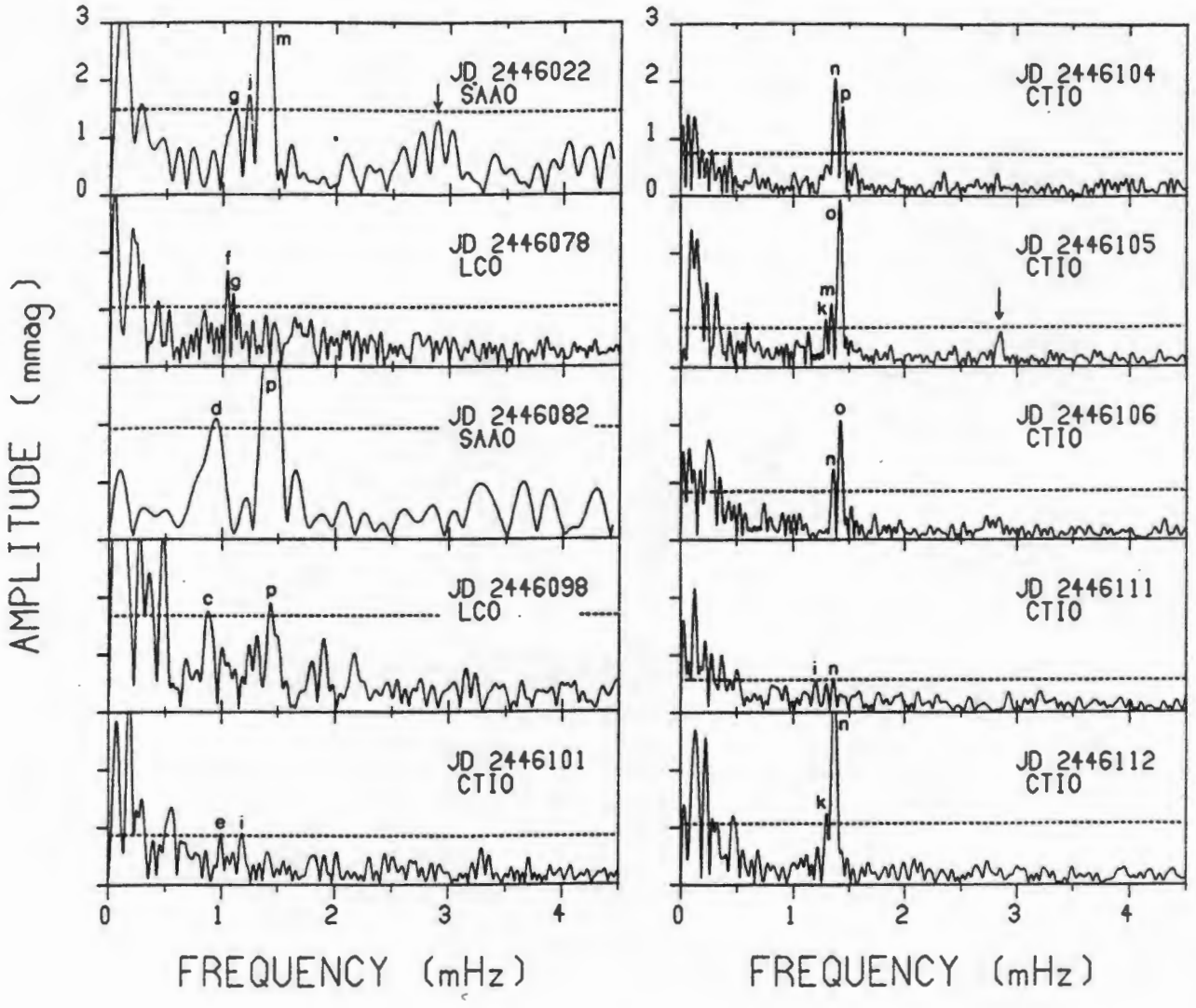

Figure 2.6 Fourier amplitude spectra for ten nights of high-speed Johnson *B* photometry of the roAp star HD 60435 taken at SAAO, CTIO and Las Campanas Observatory (LCO). The peaks of interest here are the labeled ones; the peaks at very low frequencies ($\nu < 1.0$ mHz) are caused by sky transparency variations during the observations. The point of this illustration is that different frequencies are excited to different amplitudes on a night-to-night basis in this star. In this case the amplitude modulation cannot be explained as an aspect effect that varies with rotation. (Taken from Matthews *et al.* 1987)

2.4 A stellar acoustic cavity

In a star whose outer layers are in hydrostatic equilibrium, the dominant restoring forces for oscillations are pressure and gravity. Which of these forces is the most important depends on the period and wavelength of the oscillation. At high frequencies, the pressure fluctuations dominate to produce acoustic modes, or *p-modes*. At low frequencies buoyancy dominates to produce internal gravity waves, the so-called *g-modes*. Examples of stars showing *g*-mode oscillations are the ZZ Ceti stars which are pulsating white dwarfs. In the Sun and the roAp stars, the shortness of the periods implies that the oscillations are high order *p*-modes.

These *p*-modes are standing oscillations in an acoustic cavity inside the star. Although the stellar interior lacks the solid walls of a musical instrument, it nonetheless has gradients of pressure, temperature and density which act to reflect and refract the acoustic waves. Fig 2.7 shows how a wavefront rising toward the surface is reflected back downwards by the sharp decrease in density at the surface. As the wavefront plunges into the stellar interior it traverses regions of increasing temperature and hence sound speed. The deeper portion of the wavefront travels faster and the wave is refracted back upwards. The depth to which the wave penetrates before it starts rising again marks the point where the horizontal phase speed of the wave, v_x, equals the local sound speed $c(r)$:

$$v_x = c(r) = \lambda/P = [kT(r)/\mu]^{1/2} \qquad (2.1)$$

where λ is the horizontal wavelength, k Boltzmann's constant, P the period, $T(r)$ is the temperature at radius r and μ the mean molecular mass. A wave that is thus trapped traces a series of arcs beneath the stellar surface. These trapped acoustic waves interfere constructively with themselves to produce a resonance, or standing wave, which produces the surface oscillations we see. Notice that if the horizontal wavelength of the surface disturbance is shorter, the waves travel more nearly horizontally and they are confined to a shallower cavity. Measuring the period and horizontal wavelength of these surface oscillations allows the inference of the average sound speed throughout the cavity.

Every acoustic cavity has a fundamental resonant period which is roughly equal to the time taken for a sound wave to propagate from the top to the bottom of the cavity and back. Shorter period waves with the same horizontal wavelength λ, the *overtones*, can also resonate but they will penetrate more deeply because their horizontal phase speed is greater. The speed and direction of propagation of the acoustic waves depends on the temperature, composition and motions within the stellar interior. Although we cannot trace the acoustic waves directly as they propagate into the stellar interior, their effects on the surface are evident in measurements of surface radial velocity and

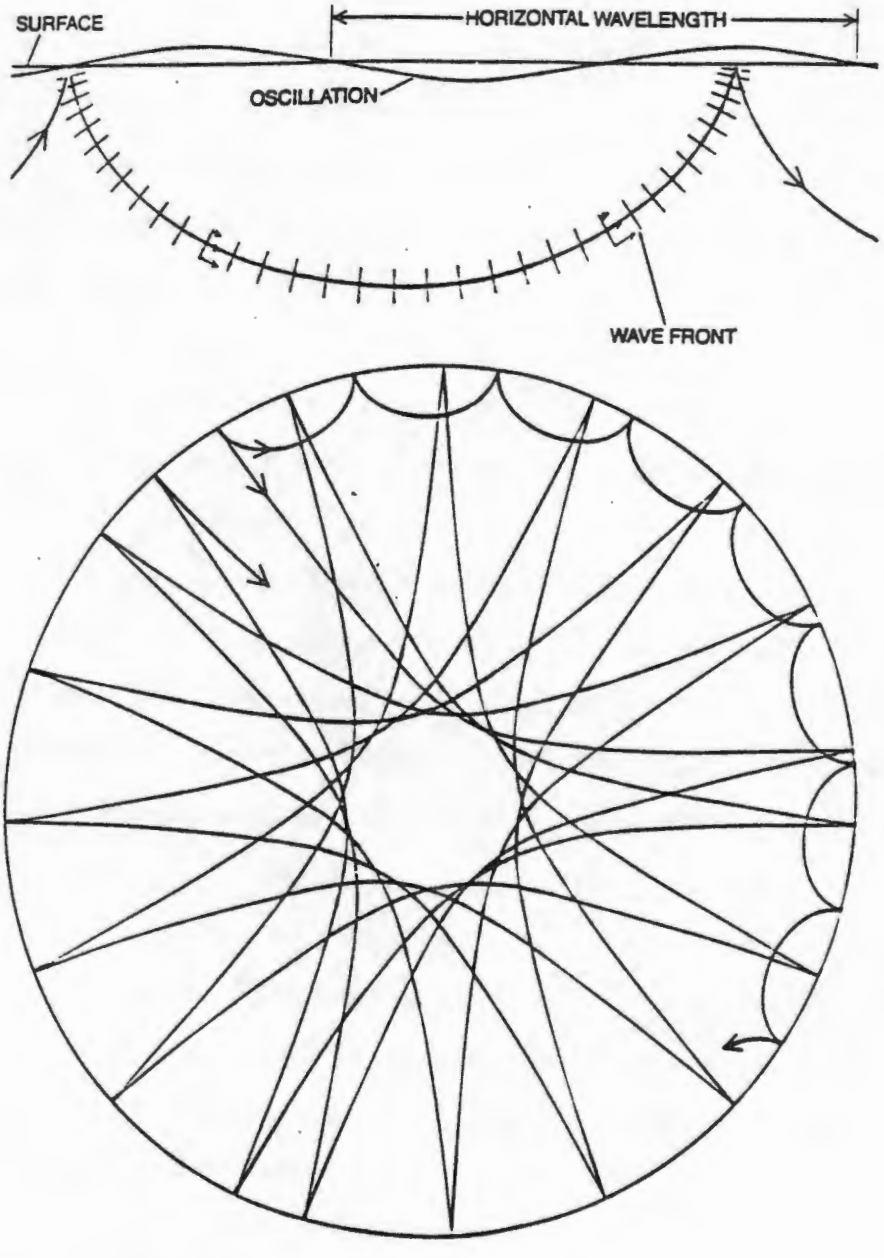

Figure 2.7 Reflection at the surface and refraction in the interior define the boundaries of a stellar acoustic cavity. Sound waves rising from the interior are reflected at the surface by the sharp decrease in density. As the reflected wave descends into regions of greater density and greater sound speed, the deeper part of the wavefront travels faster and the wave is refracted back upwards. Waves thus trapped interfere with each other creating resonances that are detectable as oscillations on the stellar surface. The horizontal wavelength and period of the surface oscillations depends on the period of the internal standing wave and the depth of the cavity. Modes of high ℓ (See Fig. 2.8) have short horizontal wavelengths λ, so they are confined to shallow acoustic cavities. Modes of low ℓ penetrate deep into the interior. It is the modes of low ℓ that are detectable with the techniques used in this thesis. (Adapted from Leibacher *et al.* 1990)

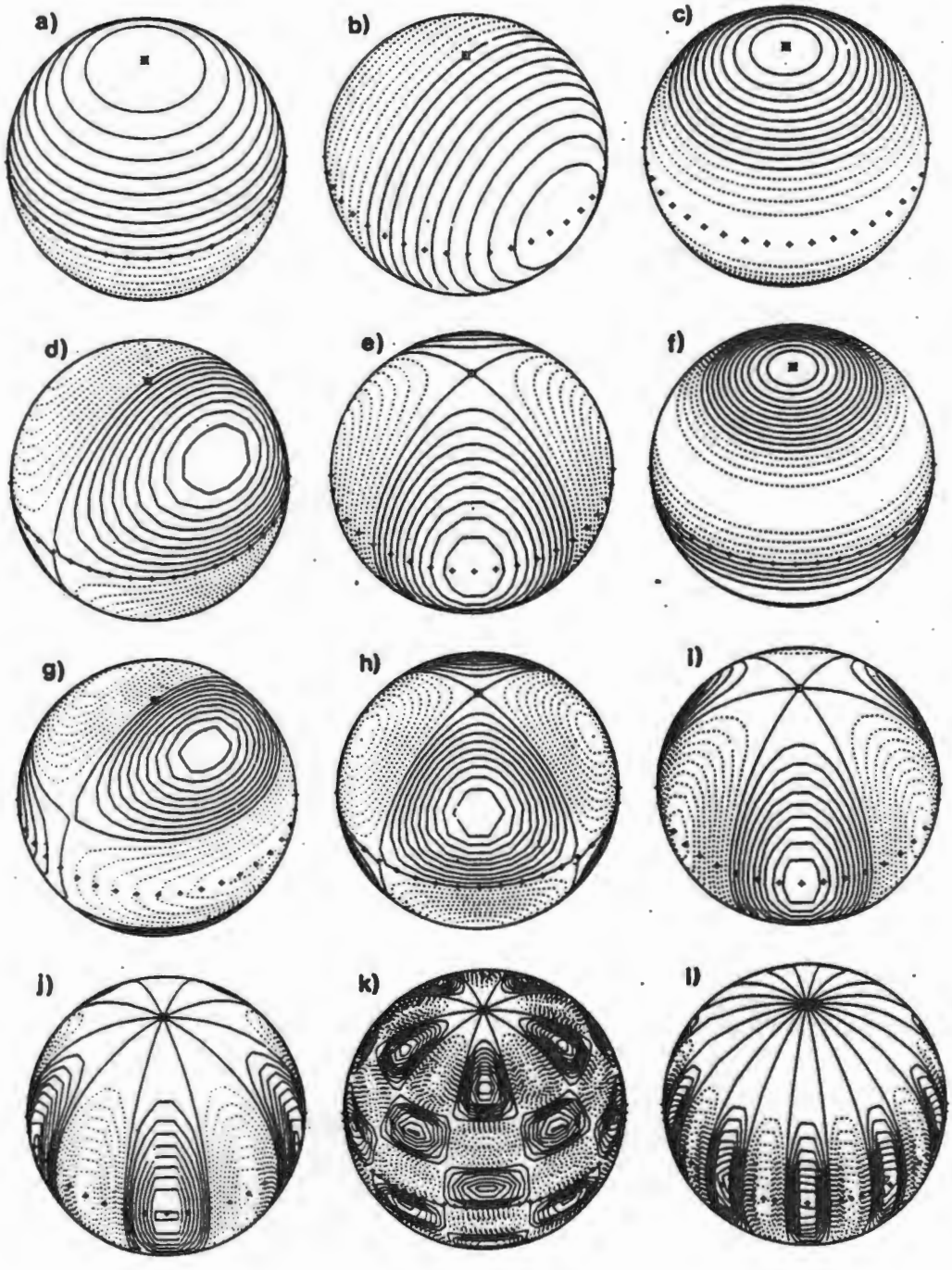

Figure 2.8 Contour plots of the real part of the spherical harmonics Y_ℓ^m. These are the normal modes of oscillation for a sphere. The nodal lines separate sectors that are pulsating out of phase with each other in a real star. The following normal modes are illustrated: a) $\ell = 1$, $m = 0$; b) $\ell = 1$, $m = 1$; c) $\ell = 2$, $m = 0$; d) $\ell = 2$, $m = 1$; e) $\ell = 2$, $m = 2$; f) $\ell = 3$, $m = 0$; g) $\ell = 3$, $m = 1$; h) $\ell = 3$, $m = 2$; i) $\ell = 3$, $m = 3$; j) $\ell = 5$, $m = 5$; k) $\ell = 10$, $m = 5$; l) $\ell = 10$, $m = 10$. In the Figure, the zonal modes are a, c & f. The sectoral modes are b, e, i, j & l. The tesseral modes are d, g, h & k. (Taken from Christensen-Dalsgaard 1989)

surface brightness. Thus these oscillations can be used to study the interior structure and dynamics of stars in much the same way that oscillations of the Earth are used to study its interior structure. Because of this similarity with terrestrial seismology, the study of these stellar oscillations is called *asteroseismology*.

The techniques of asteroseismology were first developed for use on the nearest star, the Sun, which gave rise to the term *helioseismology*. The success of helioseismology inspired many workers to extend these methods to the distant stars. Helioseismology has already provided measures of the sound speed and rotation rate throughout much of the solar interior. It has also yielded a He abundance that is essentially consistent with standard solar models. This is of relevance in solving the solar neutrino problem in that it points towards our understanding of neutrino physics as being the source of the problem.

The quantity of information contained in these stellar oscillations is immense. This can be illustrated with a simple musical analogy. We are accustomed to the rich variety of tones accessible to musical instruments like pianos and organs. In these instruments, the oscillations are one dimensional. In a star, however, unlike a piano string or organ pipe, the oscillations are three dimensional and this clearly permits a far richer spectrum of tones. Below we show how the surface oscillations are described mathematically. This is followed by a discussion of the expected and observed oscillation frequency spectra.

2.5 The description of the oscillations

In the roAp stars and the Sun, the oscillations can be treated as small perturbations about a spherical equilibrium state. This allows us to describe them as a series of normal modes using the spherical harmonics. Each mode is then characterized by three numbers:

1) *The radial quantum number* n. This index describes the radial structure of the oscillations and is the number of nodes in the radial direction (*caveat:* this is not strictly true for highly centrally condensed stars). The first value, $n = 0$, is called the *fundamental mode*, $n = 1$, the *first overtone*, $n = 2$, the *second overtone*, and so on.

2) *The spherical degree* ℓ. This is the number of nodal lines on the surface of the star. If $\ell = 0$, there are no nodal lines on the surface and the star pulsates radially like a Cepheid.

3) *The azimuthal quantum number m.* This is the number of nodal lines that cross the poles. These nodal lines are like lines of longitude. In a non-rotating star the m-modes are degenerate and each segment of the stellar surface will oscillate with a frequency $\nu(n,\ell)$ determined by n and ℓ only. In real stars this degeneracy is lifted by rotation through the Coriolis force and an inertial observer will see each $\nu(n,\ell)$ split into $(2\ell+1)$ m-modes whose frequencies are given to first order by the Ledoux (1951) relation

$$\nu(n,\ell,m) = \nu(n,\ell,0) - m\Omega(1-C_{n,\ell}) \qquad (2.2)$$

where $C_{n,\ell}$ is a constant dependent on the stellar structure and pulsation mode and Ω is the rotation frequency.

Fig 2.8 shows how several normal modes appear to the observer. At any instant the pattern is one of alternating regions of approach / high pressure / higher temperature and recession / lower pressure / lower temperature. Oscillation modes where $m = 0$ have nodal lines which are like lines of latitude and they are called *zonal modes*. Modes for which $\ell = m$ have nodal lines which are all like lines of longitude. Such modes are called *sectoral modes*. The modes for which $0 < m < \ell$ are called *tesseral modes*. All three of these types of modes are illustrated in Figure 2.8. In the case of the Sun, where the disk is resolved, thousands of modes are seen. For the distant stars, we see only the integrated light of the stellar disk. Such whole disk observations are sensitive only to low-order modes of $\ell \leq 3$; for higher ℓ modes, there are too many sectors pulsating out of phase with each other for there to be a net detectable signal. In the roAp stars, $\ell = 1$, $m = 0$ modes are indicated in most cases where a mode identification is possible. There are also indications that $\ell = 0$ and $\ell = 2$ modes might coexist in some roAp stars.

2.6 The eigenfrequency spectrum for high overtone pulsation

The asymptotic theory of low-degree, high overtone ($n >> \ell$) p-mode pulsation (Tassoul 1980, 1990) predicts that the eigenfrequencies will be given by

$$\nu_{n\ell} \approx \Delta\nu(n+\ell/2+\epsilon) + \delta\nu, \qquad (2.3)$$

where ϵ is a constant dependent on the equilibrium structure of the star and $\delta\nu$ is a second order term. To first order, the eigenfrequencies will have a uniform spacing $\Delta\nu$ given by

$$\Delta\nu = [2\int_0^R dr/c(r)\ ]^{-1}, \qquad (2.4)$$

where $c(r)$ is the sound speed. This spacing $\Delta\nu$ is the reciprocal of the time for sound to cross the star. For the Sun $\Delta\nu = 135\ \mu$Hz, which translates to a sound crossing time of 2.05 hr. The roAp stars have $\Delta\nu$ values between 30 and 70 μHz. The smaller $\Delta\nu$ values for the roAp stars relative to the Sun are consistent with the larger radii, and hence, longer sound crossing times. When $\Delta\nu$ is expressed in terms of structural parameters by $\Delta\nu \propto \sqrt{(GM/R^3)}$, one may readily show, using the mass-luminosity relation, that the loci of constant $\Delta\nu$ are straight lines in a theoretical H-R diagram. The p-mode oscillations in A-type stars have been modelled by Gabriel *et al.* (1985), Shibahashi & Saio (1985) and Heller & Kawaler (1988). Figure 2.9 is a series of evolutionary tracks for the A star models of Shibahashi & Saio (1985) showing how $\Delta\nu$ varies as the star evolves during its main sequence phase.

One of the properties of eq. (2.3) is that, to first order, it is degenerate for modes with the same value of $(n + \ell/2)$. Thus, consecutive overtones $(n, n+1)$ of modes with exclusively even or odd ℓ will be spaced by $\Delta\nu$, whereas alternating even and odd ℓ modes will be spaced by $\Delta\nu/2$. The problem is to decide whether the observed spacing corresponds to $\Delta\nu$ or $\Delta\nu/2$. A-star models such as the ones shown in Fig. 2.9 indicate that $\Delta\nu \approx 50$ - 80 μHz for a slightly evolved $2M_\odot$ star. In several roAp stars a frequency spacing of ~ 25 - 30 μHz is observed. In such cases, the theoretical overtone spacing and the fact that Ap stars are not highly evolved objects (see chapter 1), are used to argue that alternating even and odd ℓ modes are present. However, such conclusions are only secure if one has an independent luminosity estimate for the star. Matthews (1989) has noted that the ratio $\Delta\nu/\nu$ falls around the preferred values 0.040 and 0.025. This result, if confirmed, could be used to remove the ambiguity in determining $\Delta\nu$. Another way to determine $\Delta\nu$ is to measure the rate of frequency change due to evolution. A more evolved star will have a smaller value of $\Delta\nu$ and a higher rate of frequency change (see section 9.5)

We now turn to a discussion of the second-order term, $\delta\nu$. We have already noted that Tassoul's relation is degenerate for modes (n,ℓ) and $(n\pm1, \ell\mp2)$. The term $\delta\nu$ lifts this degeneracy by introducing a slight frequency spacing $\delta\nu << \Delta\nu$ between such modes. Physically, what is happening is that modes (n,ℓ) and $(n\pm1, \ell\mp2)$ have very similar mode structures outside the core but slightly dissimilar mode structures in the centre. Figure 2.10, which shows the two modes, ($\ell = 1$, $n = 19$) and ($\ell = 3$, $n = 20$), illustrates this. This difference in central mode structures is a measure of the sound speed gradient inside the star which is largely determined by the molecular mass gradient in the core. Since the molecular mass gradient changes as the star converts H to He, $\delta\nu$ is

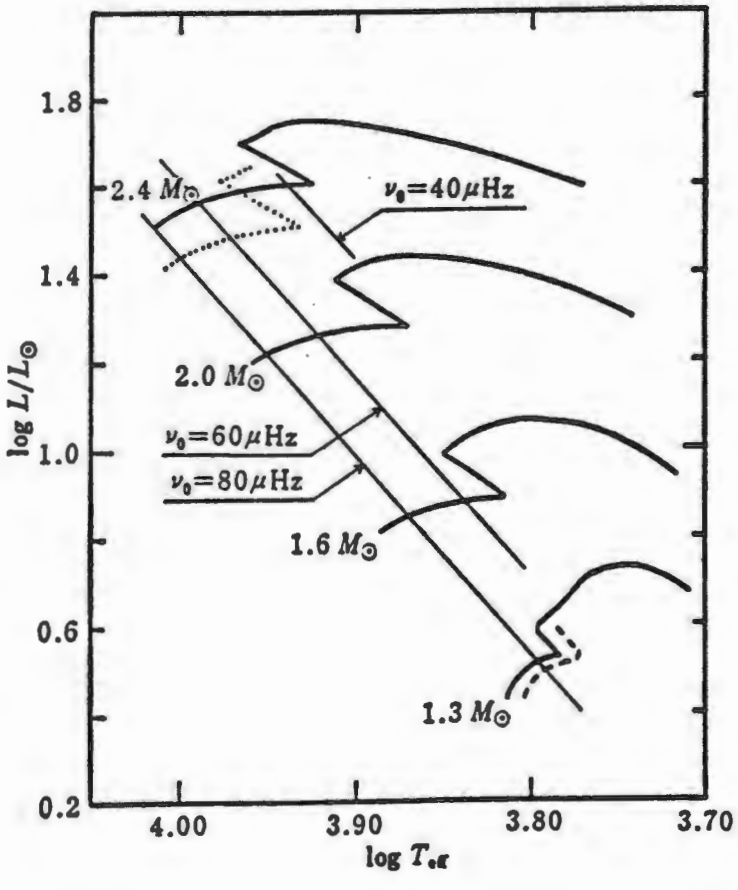

Figure 2.9 Evolutionary tracks of 1.3, 1.6, 2.0 and 2.4 $M_\odot$ stars. The nearly straight lines are lines of constant $\Delta\nu$. (Taken from Shibahashi & Saio 1985.)

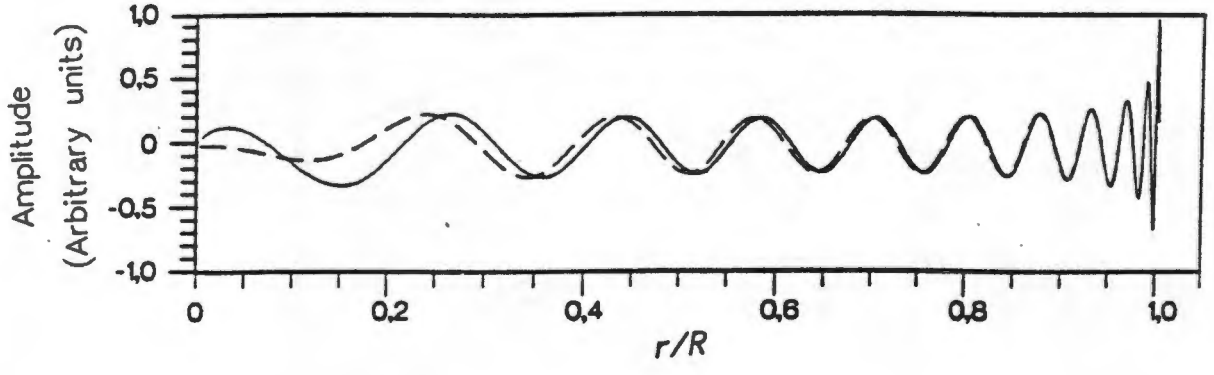

Figure 2.10 Mode structures for the p modes ($\ell = 1$, $n = 20$) (solid line) and ($\ell = 3$, $n = 19$) (dashed line). Although these modes have similar modes structures in the outer layers, they differ in the centre. The second-order spacing $\delta\nu$ is a measure of this difference. (Taken from Belmonte *et al.* 1991)

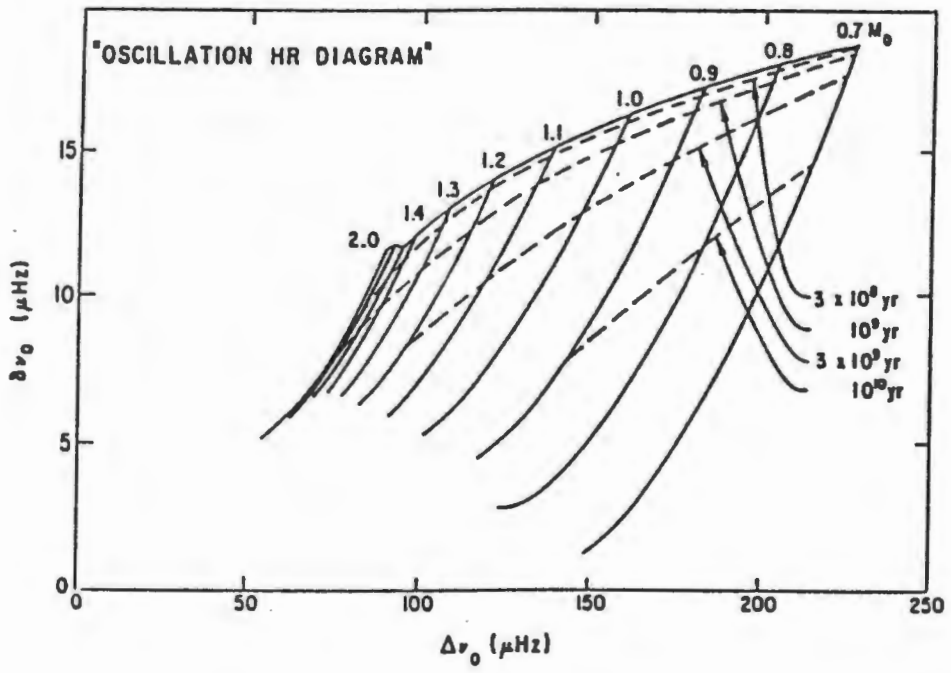

Figure 2.11 An asteroseismological HR diagram produced by Christensen-Dalsgaard (1986) showing the calculated first- and second-order frequency spacings of *p* modes for stars of different mass and age. One of the aims of the Cape Survey is to provide observational data for a diagram of this type for the roAp stars.

essentially an age indicator. This realization allowed Christensen-Dalsgaard (1984) to produce a theoretical asteroseismological H-R diagram by plotting $\Delta\nu$ against $\delta\nu$ as shown in Figure 2.11. At present, the Sun is the only star which can be plotted on this diagram with certainty.

2.7 The oblique pulsator model

The favoured model to explain the observed features of the roAp stars is the *oblique pulsator model* which was developed by Kurtz (1982). This model is a simple extension of the oblique rotator model of the Ap stars. It postulates that a roAp star is an oblique rotator which pulsates in a series of nonradial p-modes where the pulsation axis coincides with the magnetic axis. This very simple model can explain the observed amplitude modulation of the rapid oscillations (Fig. 2.4) and the oscillation phase flips at magnetic crossover (Fig. 2.5) whilst preserving our understanding of the magnetic, spectral and photometric variations in these Ap stars.

We will illustrate the oblique pulsator model for the simple case of dipole ($\ell=1$) pulsation. The luminosity variations over the surface of the star are given by (Kurtz 1982)

$\Delta L/L \propto P_\ell(\cos\alpha)\cos(\omega t+\phi)$

where $P_\ell(\cos\alpha)$ is an appropriate Legendre polynomial, $\omega=2\pi\nu$ is the oscillation frequency and α is the angle between the pulsation pole and the line of sight (Fig. 1.3). As the star rotates, this angle changes as

$$\cos\alpha = \cos i\cos\beta + \sin i\sin\beta\cos\Omega t \qquad (2.5)$$

where i is the rotational inclination, β the magnetic obliquity, Ω the rotation frequency and $t=0$ is defined at magnetic maximum. For an $\ell=1$ mode, $P_\ell(\cos\alpha) = \cos\alpha$ so that

$$\Delta L/L \propto A_0\cos(\omega t+\phi) + A_1\cos[(\omega-\Omega)t+\phi)] + A_1\cos[(\omega+\Omega)t+\phi)] \qquad (2.6)$$

where

$$A_0 = \cos i\cos\beta \qquad (2.7)$$

and

$$A_1 = \tfrac{1}{2}\sin i\sin\beta. \qquad (2.8)$$

Thus we see that an oblique pulsator pulsating in an $\ell=1$ mode will give rise to a frequency triplet with a spacing which is equal to the rotation frequency. The central frequency component, at ω, has amplitude A_0 and is flanked by sidebands of amplitude A_1 at frequencies $\omega\pm\Omega$. This type of frequency splitting has nothing to do with the m-mode splitting discussed in section 2.5; I will demonstrate this

in section 2.9 of this chapter. In the general case, each ℓ mode in an oblique pulsator will appear in the oscillation spectrum as a $(2\ell+1)$ frequency multiplet.

It is also possible to investigate the magnetic geometry of a system with this model. For a dipole oblique rotator,

$$\tan i \tan \beta = (1-r)/(1+r) \tag{2.9}$$

where $r = B_{e\ min}/B_{e\ max}$ is an observable quantity. Using the oblique pulsator model, for an $\ell = 1$ mode we may write

$$A_1/A_0 = \tfrac{1}{2} \tan i \tan \beta, \tag{2.10}$$

whence

$$r = (1-2A_1/A_0)/(1+2A_1/A_0) \tag{2.11}$$

where A_1/A_0 is an observable quantity. In the few cases where r values have been obtained both from magnetic measurements and from the rapid oscillations there is good agreement between the results. The oblique pulsator model also predicts the phase reversal of the oscillations at magnetic cross-over. For a dipole mode we have $\Delta L/L \propto \cos \alpha \cos(\omega t+\phi)$ which may be regarded as a sinusoid of constant phase ϕ until $\cos \alpha$ changes sign; this is equivalent to a phase-flip of ϕ by π radians. Physically, what is happening is that the visible hemisphere is initially dominated by one of the pulsation poles and the observer sees an oscillation of constant phase ϕ, but modulated in amplitude. At quadrature, the amplitude passes through zero and increases again with constant phase $\phi+\pi$ as the other pulsation pole comes into view. Matthews (1991) has prepared a schematic illustration showing how the amplitude and phase of the oscillation vary during the rotation cycle. His diagram is reproduced here as Fig. 2.12. The best studied roAp star, HR 3831 (HD 83368), is a textbook example of an $\ell = 1$ oblique pulsator where these effects are well illustrated (Figures 2.4 & 2.5).

The coincidence of the magnetic and pulsation axes in the basic oblique pulsator model developed by Kurtz (1982) was an *ad hoc* assumption motivated only by the observations. This led Dziembowski & Goode (1985, 1986) and Kurtz & Shibahashi (1986) to take into account the effects of rotation and an oblique magnetic field on the amplitudes of the nonradial oscillation modes. By assuming that the perturbation to the eigenfrequencies by the magnetic field dominates the perturbation due to rotation, they were able to show that the pulsation axis locks onto the magnetic axis. The inclusion of the Lorentz and Coriolis forces also predicts an inequality in the amplitudes of the rotational sidelobes.

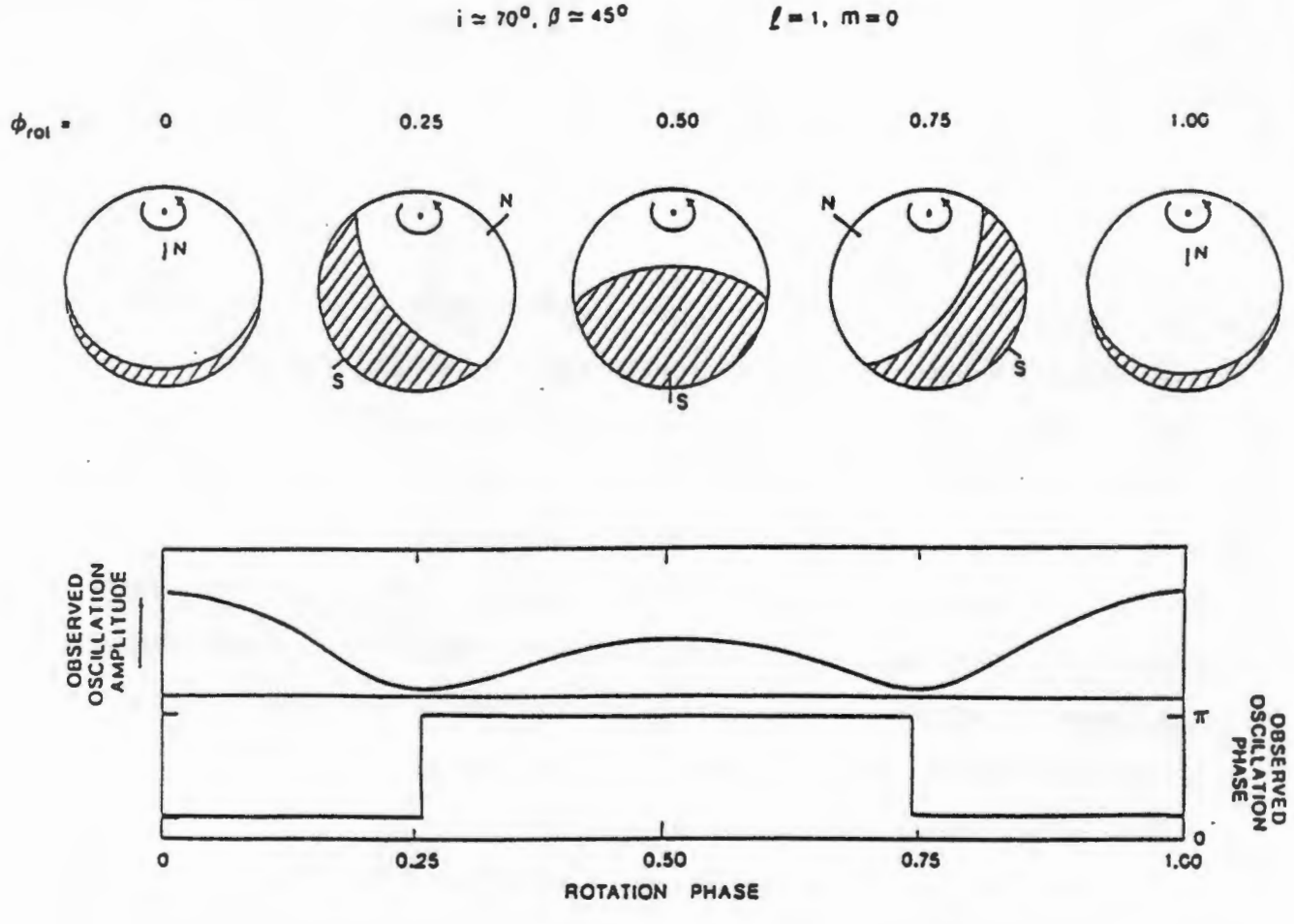

Figure 2.12 A schematic view of the way in which the pulsation amplitude and phase are modulated in the oblique pulsator model. The star is assumed to have a dipole magnetic field and to be pulsating in an $\ell = 1$, $m = 0$ mode; the shaded portion of the surface varies in antiphase with the rest of the star. The star's rotation axis is tipped toward the observer by 30° out of the plane of the page. The magnetic poles, indicated by "N" and "S", are tipped by 45° to the rotation axis. (Taken from Matthews 1991)

Without reproducing in detail the formalism developed by Dziembowski & Goode (1985), we sketch the essential results of their arguments. They show that a predominantly dipole magnetic field induces a perturbation to the eigenfrequencies of the form

$$\omega = \omega^{(0)} + \omega^{(1)mag}_{|m|}, \tag{2.12}$$

where $\omega^{(0)}$ is the unperturbed frequency in the rest frame of the star in the absence of a magnetic field and $\omega^{(1)mag}_{|m|}$ is the perturbation to the mode (ℓ,m) by the field. For a dipole magnetic field the magnitude of this perturbation is given by

$$\omega^{(1)mag}_{|m|} \propto K^{mag}[\ell(\ell+1)-3m^2]/[4\ell(\ell+1)-3] \tag{2.13}$$

where K^{mag} is a $|Y^{\ell}_{m}|^2$-weighted integration over the P_2 distortion caused by the magnetic field. If one recomputes the luminosity variations taking into account the magnetic perturbation for an $\ell = 1$, $m = 0$ mode one finds

$$\begin{aligned}\Delta L/L \propto\ & A_0 \cos[(\omega^{(0)}+\omega_0^{(1)mag})t+\phi] \\ & + A_{+1}\cos[(\omega^{(0)}+\omega_0^{(1)mag}+\Omega)t+\phi] \\ & + A_{-1}\cos[(\omega^{(0)}+\omega_0^{(1)mag}-\Omega)t+\phi],\end{aligned} \tag{2.14}$$

where

$$A_0 = \cos i \cos \beta, \tag{2.15}$$

and

$$A_{\pm 1} = \tfrac{1}{2} \sin i \sin \beta\,[\,1 \pm C_{n\ell}\Omega/(\omega_1^{(1)mag}-\omega_0^{(1)mag})]. \tag{2.16}$$

Note that when the Coriolis force and Lorentz force are neglected ($C_{n\ell} = 0$ and $\omega^{(1)mag}_{|m|} = 0$), equations (2.14) - (2.16) reduce to equations (2.6) - (2.8), the basic oblique pulsator model. This more detailed treatment still predicts that an $\ell = 1$ mode will give rise to a frequency triplet. The difference is that the amplitudes of the triplet components are now given by A_{-1}, A_0 and A_{+1} where, again for an $\ell = 1$, $m = 0$ mode,

$$(A_{+1} + A_{-1})/A_0 = \tan \iota \tan \beta \tag{2.17}$$

and

$$(A_{+1} - A_{-1})/(A_{+1} + A_{-1}) = C_{n\ell}\Omega/(\omega_1^{(1)mag}-\omega_0^{(1)mag}). \tag{2.18}$$

The different heights of the sidelobes is an integral measure of the magnetic field strength. Thus a knowledge of the ratio of the sidelobe amplitudes and a knowledge of the rotation period allows, in principle, the determination of the relative values of K^{mag} for different roAp stars showing a frequency triplet. This exercise has been done by Matthews (1991) for four roAp stars and he finds $1.0 \leq K^{mag} \leq 4.2$ μHz. More intriguing is the possibility that several determinations of K^{mag} for the

same star could be made by studying different (ℓ,m) modes; then given $C_{n\ell}$ and Ω, the internal magnetic field geometry could be modelled.

The distorted oblique pulsator model

Recently, it has become apparent that the situation is a good deal more complicated than has been outlined above. The formalism described above was developed, in a large part, to explain the observation of an equally spaced asymmetric frequency triplet in the roAp star HR 3831. However, recent observations by Kurtz *et al.* (1993) have revealed that the fine structure originally thought to be a triplet is in fact part of a septuplet. Kurtz *et al.* then used the spherical harmonic decomposition technique developed by Kurtz (1992) to express the oscillations as a sum of axisymmetric spherical harmonics of degree $\ell = 0$, 1, 2 and 3. Although the observations were well reproduced by this procedure, there was no physical justification for using it. To explain the septuplet in HR 3831, Shibahashi & Takata (1993) refined the treatment of the effects of the Lorentz and Coriolis forces on nonradial oscillations in a rotating magnetic oblique pulsator. Using their refined model, they showed that the effect of the magnetic field on an axisymmetric dipole mode is to distort the dipole oscillation pattern in such a way that axisymmetric octupole components arise; this leads to an asymmetric equally spaced frequency septuplet instead of a triplet. This distortion of the basic dipole pattern led Shibahashi & Takata to christen their model the *distorted oblique pulsator model*. Assuming a dipole oscillation as before, this model yields relations (2.15) and (2.17) above for the A_0, A_{+1} and A_{-1} components and it also yields relations for the A_{+2}, A_{-2}, A_{+3} and A_{-3} components which can be summarized as:

$$[\,(A_{+3} + A_{-3}) / (A_{+2} + A_{-2})\,] / [\,(A_{+1} + A_{-1}) / A_0\,] \approx 1/6 \qquad (2.19)$$

and

$$[\,(A_{+3} - A_{-3}) / (A_{+3} + A_{-3})\,] / [\,(A_{+2} - A_{-2}) / (A_{+2} + A_{-2})\,] = 3/2. \qquad (2.20)$$

The observed amplitude ratios for the frequency septuplet in HR 3831 are in good agreement with the expected value of 1/6 for relation (2.19). The agreement for relation (2.20) is not as good, but it is still consistent with the observations bearing in mind the tiny amplitudes under consideration.

The oblique pulsator model may have applications in stars other than roAp stars. Early in this century Blazhko discovered that the amplitude of the pulsations in some RR Lyrae stars is modulated on a time-scale of around 40 days. At about the same time that Kurtz developed the oblique pulsator model for the roAp stars, Cousens (1983) independently developed an identical model as a possible

explanation of the Blazhko effect in the RR Lyrae stars, calling it the *obliquely oscillating magnetic rotator model*. This does not mean to say that the question of the Blazhko effect in the RR Lyrae stars has been settled. More recently, Moskalik (1986) has suggested that the Blazhko effect may result from resonances in double-mode pulsating RR Lyrae stars.

2.8 The spotted pulsator model

One of the objections to the early oblique pulsator model was the *ad hoc* requirement that the pulsation and magnetic axes should coincide. Dolez and Gough (1982) pointed out that Coriolis force should induce a precession of the pulsation axis with respect to the magnetic axis since eastward and westward propagating waves are affected in opposite senses according to the well-known Ledoux (1951) relation (eq. 2.2). Mathys (1985) has managed to model the amplitude modulation without requiring that the magnetic and pulsation axes coincide. His *spotted pulsator model* assumes that the pulsations are symmetrical about the rotation axis, so that the pulsations are always seen from the same aspect, but that the ratio of flux to radius variations, f, and the phase lag, ψ, between the flux and radius variations are variable over the surface as a function of the magnetic field strength (or as a function of the spots associated with the rotational photometric variations). In this way, variations in f and ψ produce amplitude modulation with a frequency that is exactly the rotation frequency of the star.

The spotted pulsator model makes testable predictions which can be used to discriminate between it and the oblique pulsator model. In particular, the model predicts that although the light variations will be amplitude modulated, the radial velocity variations will not. The oblique pulsator model predicts that both variations will be modulated in the same way with changing aspect as the star rotates. Radial velocity measurements of HR 1217 by Matthews *et al.* (1988) with the Canada-France-Hawaii Telescope revealed modulation in the radial velocity amplitude in support of the oblique pulsator model. (*caveat:* HR 1217 is multi-periodic, so we cannot exclude the possibility that the radial velocity amplitude modulation was caused by beating among the independent pulsation frequencies. High-precision observations of a single-mode pulsator, such as HR 3831, would provide an unambiguous test.)

A further constraint on the applicability of the spotted pulsator model comes from the finding that although the times of pulsation amplitude maximum and magnetic extremum agree in HR 1217, there is a 3σ difference between the time of pulsation amplitude maximum and mean light extremum

(Kurtz *et al.* 1989). In the case of HR 3831 there is a 5σ difference in the times of pulsation amplitude maxima and mean light extrema (Kurtz *et al.* 1992). This excludes a spotted pulsator model in which the variations in f and ψ are functions of spots associated with the mean light variations, but it does not exclude a spotted pulsator model where the variations in f and ψ are governed by magnetic field strength variations. Clearly, the basic mechanism invoked by the spotted pulsator model *is* operating at some level. As more precise observations become available in future it may be necessary to incorporate the effects of flux inhomogeneities in the description of the pulsations.

2.9 Another look at rotational *m*-mode splitting

Fourier spectra of the oscillations in the roAp stars show equally spaced frequency multiplets so reminiscent of rotationally split m-modes that the reader might justifiably object to the way this possible interpretation was summarily rejected in section 2.7 of this chapter. We now return to examine this possibility in more detail.

The frequencies of rotationally split m-modes are given by the Ledoux relation, eq. (2.2). Model calculations by Shibahashi & Saio (1985) indicate that $10^{-2} \leq C_{n\ell} \leq 10^{-3}$ for the roAp stars. By studying the times of magnetic and oscillation amplitude maxima it has been determined that $C_{n\ell} \leq 6\times10^{-4}$ for HR 1217 (Kurtz *et al.* 1989) and $C_{n\ell} \leq 2\times10^{-5}$ for HR 3831 (Kurtz *et al.* 1992). Both of these determinations of $C_{n\ell}$, secure to the 3σ confidence level, are 2 to 3 orders of magnitude lower than theoretical expectations for rotational m-mode splitting. If $C_{n\ell}$ is not exactly zero, the times of pulsation amplitude maxima and magnetic maxima should drift apart at a rate $\sim C_{n\ell}^{-1}$ and the observed agreement in these times is purely fortuitous for both stars. Thus we conclude that rotationally split m-modes are a highly unlikely interpretation of the observed frequency splitting.

Chapter 3

The Cape Survey and other surveys for variability in Ap stars

3.1 Introduction

In the past two decades a considerable number of surveys have been conducted to search for variations in Ap stars on timescales shorter than typical rotation periods. Such short periods would be evidence for some kind of pulsational instability. The surveys that have been conducted can be divided into two broad classes, those that searched for low overtone (*i.e.* δ Scuti-like) pulsations and those that searched for high overtone (*i.e.* roAp-like) pulsations. The first half of this chapter describes these survey efforts and lists their results, both positive and negative. For ease of reference, the null results of all searches for high-overtone pulsation in Ap stars are gathered together in a single Table. There has also been one search for high overtone pulsation in chemically normal A stars. For completeness, we will discuss that survey as well. In the second half of this chapter, we present our survey, the Cape Survey. The methods, scope, goals and limitations of our survey are discussed and the null results are presented in tabular form (the positive results are tabulated in chapter 2, Tables 2.1 and 2.2).

3.2 A survey of surveys

A survey of the literature was done to find all the published surveys for variability in Ap stars on timescales < 1 day. The results of this survey of surveys are listed in Table 3.1. We caution that this list may not be a complete list of all the searches conducted because observers tend not to publish papers containing null results; such papers are not exciting to write or read! However, there is now a large enough sample of stars that has been observed by the different groups that much may be learned by collating all the results. Moreover, a star that is classified as a null result by one group may be discovered as a new roAp star by another group. This was the case for HD 42659 which was observed to be constant in the Lowell-Wisconsin survey (Kreidl, private communication) and was discovered to be a roAp star in the Cape Survey. For these reasons we describe in detail the observational effort and scope of all the survey programs we located in the literature even though some surveys did not produce any new roAp stars. Where possible, we have listed the candidates observed in each survey.

Table 3.1

Surveys for pulsation in the Ap stars

Searches for low overtone pulsations:

Percy (1975) Astronomical Journal **80**, 698
Weiss (1978) Astron. Astrophys. Suppl., **35**, 83.
Kreidl (1986) Lecture Notes in Physics, **274**, 134
Hildebrandt[2] (1992) Astron. Nachr. **313**, 233

Searches for high overtone pulsations:

Kurtz (1984) Mon. Not. R. astr. Soc. **206**, 247
Matthews & Wehlau (1985) Pub. Astron. Soc. Pacific **97**, 841
Matthews, Kreidl & Wehlau (1988) Pub. Astron. Soc. Pacific **100**, 255
Heller & Kramer (1988) Pub. Astron. Soc. Pacific **100**, 583
Kurtz (1989) Mon. Not. R. astr. Soc. **238**, 261
Schutt[1] (1991) Astron J, **101**, 2177
Nelson & Kreidl[2] (1993) Astron. J. **105**, 1903
Belmonte[2] (1989) PhD thesis, Universidad de La Laguna, Tenerife
Hildebrandt[2] (1992) Astron. Nachr. **313**, 233
Martinez, Kurtz & Kauffmann (1991), **250**, 666

Notes:

[1] This is a survey of chemically normal stars.
[2] Includes chemically normal stars of type late B to early F.

The surveys are described in more or less chronological order. It is hoped that this chapter will serve as a useful bibliographical reference of sources of data to observers who wish to select well-established null results or to re-examine old data. The Ap stars which showed no evidence of high-overtone pulsation in these surveys have been gathered together in Table 3.2.

Because surveys for rapid variability necessitate intensive observing programs requiring much telescope time, high-speed photometry has been the technique of choice for roAp star survey work (as opposed to radial velocity studies, say). Because of the short integration times required, broad pass-band Johnson filters, usually B and/or V, are almost universally used; the best signal to noise ratio is obtained in Johnson B (Kurtz 1982). Unless otherwise noted, all the surveys described below were conducted using high-speed photometry with Johnson B and/or V filters.

3.3 Search for low overtone pulsation in 15 cool Ap stars by Percy

The first search for *pulsations* in Ap stars was conducted by Percy (1975). In his paper, Percy lists the 15 cool Ap stars he observed differentially in B and V as well as the upper limits to any signals in his observations. Except for the star 21 Com which showed evidence of oscillations (2 periods, 30 min and 40 min), there were no convincing indications of coherent oscillations in the other stars. Percy concluded from this that pulsation in the Ap stars lying in the instability strip is vary rare and/or of very low amplitude.

3.4 Search for low-overtone pulsation in Ap stars by Weiss

Sixteen Ap stars (one of questionable Ap classification) and two Am stars were observed in B, V and occasionally U for time spans ranging from 2 to 4 hours with conventional differential photometry by Weiss (1978) Barring the long-term variability due to rotation, all 16 Ap stars and the 2 Am stars proved to be of constant brightness to within 0.003 mag and he concluded that the Ap stars are stable against pulsation. Interestingly, Weiss suspected that one of his program stars, HD 24712, showed evidence of short periodic variability in the U band, but he never followed up his hunch by observing this star continuously in high-speed mode. Had he done so, he would have discovered that this star is a roAp star.

3.5 The earliest searches for southern roAp stars by Kurtz

When Don Kurtz first searched for oscillations in HD 101065, his expectation was that it should *not* pulsate. This was because if HD 101065 was an extreme Ap star, then its spectral peculiarities were the product of diffusion. At that time it was thought that the exclusion between pulsation and metallicism was absolute, so HD 101065 should not pulsate. Having made the serendipitous discovery of high overtone pulsations in what he believed to be an Ap star, Kurtz reasoned that perhaps other Ap stars would also pulsate in the same manner. He then did a quick-look survey of the Ap stars and discovered rapid oscillations in 4 cool Ap SrCrEu stars. The results of this first brief survey are reported in Kurtz's seminal paper (Kurtz 1982) in which he announced this new class of variable star.

To maximize his chances of detecting further roAp stars, Kurtz concentrated on the cool Ap SrCrEu stars from 1982 to 1989 and in this period discovered a further 7 roAp stars using the facilities of the South African Astronomical Observatory (SAAO) where excellent photometric conditions obtain and ample time is available on small telescopes for such undertakings. This survey was confined to the southern hemisphere and the candidates were selected from the first 3 volumes of the *Michigan Spectral Catalogue* (Houk & Cowley 1975, Houk 1975, 1978). Because this early survey was conducted mostly using the SAAO 0.5-m telescope, most of the candidates observed were $m_{pg} \geq 8.5$ and had fairly high scintillation noise levels, usually about 0.6 mmag, but often as high as 1 mmag. On good nights, the scintillation noise is usually the factor that governs whether rapid oscillations are detected in a given star or not. Since the scintillation noise scales as the -2/3 power of the telescope aperture (Young 1967) there is a real advantage in using larger telescopes to reduce the level of the scintillation noise. In the Cape Survey, scintillation noise levels of 0.12 - 0.20 mmag are routinely obtained and many of the stars observed earlier by Kurtz and others using small telescopes are being observed again with 1-m class telescopes. Although Kurtz observed a large number of cool Ap stars, he only published four of his null results: HD 15233 & HD 51684 (Kurtz 1984), FG Sge (Kurtz 1986) and β CrB (HD 137909) (Kurtz 1989).

3.6 Search for northern roAp stars by Matthews & Wehlau

Matthews & Wehlau (1985) monitored 4 northern Ap stars for rapid variability in two colours (B and V) during six nights in March 1984 using the 0.9-m telescope at Kitt Peak National Observatory. The stars were HR 2977 (49 Cam), HR 3109 (53 Cam), HR 4330 and HR 4369. The results for 49 Cam and 53 Cam are of interest in the present context. The star 49 Cam has a spectral type of F0p SrEu and a

magnetic (rotation) period of 4.23 days. On two nights out of three, Matthews *et al.* identified a possible coherent oscillation in the data at ν = 0.27 mHz ($P \sim 62$ min). They consider it unlikely that the suspected oscillations were caused by an instrumental effect or sky transparency variations since a similar peak was absent in the data of two other stars on the same nights. The possible 1-hour period in 49 Cam implies that there may be a continuous distribution of periods linking the roAp stars and the δ Scuti stars. However, this result requires confirmation, especially as it was obtained using high-speed photometry without comparison stars. Although this is the best technique for studying roAp oscillations, the purported 1-hour period of 49 Cam is best studied using the technique of differential photometry.

The star 53 Cam was observed on three nights, the last of which was within 0.08 in phase of magnetic maximum . The oblique pulsator model predicts that maximum oscillation amplitude should be observed at magnetic extrema, but no oscillations were detected at this time in 53 Cam. In many ways 53 Cam would be an ideal roAp star because of its extensively documented spectroscopic and magnetic properties which would allow an all-encompassing study of the oscillations. Thus, while the null result at magnetic maximum is discouraging, it is worth repeating the search for rapid oscillations in this star.

3.7 The Lowell Observatory survey for low overtone pulsation in Ap stars

Tobias Kreidl of Lowell observatory used the 0.6-m, 0.8-m and 1.1-m Lowell telescopes and the CTIO 0.9-m telescope to search for δ Scuti (i.e. low overtone) pulsation in Ap stars. Kreidl (1986) lists 18 candidate Ap stars suspected by earlier authors of showing possible short-period oscillations. In fact, for several stars the Ap classification is questionable and they are probably either normal δ Scuti stars or Am stars. Kreidl did not find convincing evidence of low overtone pulsation in the remaining stars securely classified as Ap. Thus the limited observational evidence suggests that there is a dichotomy between the chemically normal δ Scuti stars which pulsate in low overtone modes and the chemically peculiar Ap stars which pulsate in high overtone modes.

3.8 Search for roAp stars in the open cluster NGC 2516

We saw in chapter 2 how, in principle, the asymptotic p-mode spacing, $\Delta\nu$, could be used to obtain a luminosity estimate for the roAp stars. Such asteroseismological luminosity estimates need to be checked against luminosities obtained using independent methods. The discovery of a roAp star in a

well-studied cluster of known reddening, age and distance would provide such an important check. In an attempt to discover a roAp star in a well-studied cluster Matthews *et al.* (1988) searched for rapid oscillations in 4 Ap stars, C52, C69, C93 & C96 (Cox 1955), in the open cluster NGC 2516. These stars were chosen because of the similarity of their Strömgren indices to those of the known roAp stars. The observations were acquired using a Cousins *B* filter and the 1.0-m telescope of the Cerro Tololo Inter-American Observatory (CTIO). No oscillations were detected, but their data are limited to a few 1- to 2-hr runs on a few nights. I conducted a similar brief survey in this cluster in 1989 (unpublished) and also obtained null results. Both studies, however, were brief and suffer from scintillation noise levels of about 0.5 - 0.8 mmag in the frequency range of interest and should be repeated with lower the noise levels. As of this writing, I have compiled a list of roAp candidate stars in several open clusters which have Strömgren photometric indices similar to those of the known roAp stars (Table 2.2) and it is hoped that these candidates will be observed in the near future using CCD photometry.

Matthews *et al.* also claimed that they had evidence for rapid oscillations with periods near 7 and 20 minutes in the field star HD 116763. I observed this star on 4 nights in 1988 using the 1.0-m telescope of the SAAO and found no evidence of the oscillations reported by Matthews *et al* (Martinez 1989). A careful reanalysis of the earlier CTIO data allowed me to argue that the purported coherent oscillations in those data were statistical 'false alarms' and I discussed this problem in general for these stars.

3.9 The European Southern Observatory survey by Weiss and collaborators

The Cape Survey is not the only current southern survey for roAp stars. Werner Weiss, Hartmut Schneider and collaborators are conducting a parallel survey at the La Silla site of European Southern Observatory (ESO) in Chile. This survey was initiated in 1978 (Schneider & Weiss 1990) and is a program under the auspices of the European Working Group on Chemically Peculiar stars. Candidate stars are observed on the 0.5-m Danish telescope and the 0.9-m Dutch telescope in the Walraven *VBLUW* system. To date, one new roAp star, HD 12932, has been discovered by this group. The roAp nature of this star was discovered independently by Tobias Kreidl observing at Lowell observatory and confirmed by the Cape Survey. As of this writing (January 1993), the selection criteria and null results of Weiss & Schneider's survey have not yet been published.

3.10 Heller & Kramer

In a further survey for rapid variability in northern Ap stars, Heller & Kramer (1988) observed four Ap stars in high-speed mode in B and V using the 1.0-m telescope at Mount Laguna Observatory. They discovered rapid oscillations with a period of 11.4 min in the F0p star 10 Aql (HD 176232) and obtained null results for 6 other Ap stars in the temperature range from A7 to F3. The stars are: HD 62140 (49 Cam), HD 119288, HD 137909 (β CrB, HR 5747), HD 165474, HD 176232, HD 184471 & HD 191742.

Two of their null results are worth mentioning here. For the star 49 Cam Heller & Kramer found no evidence in a single 4.06-hr light curve of the 0.27-mHz oscillations reported by Matthews & Wehlau (1985). This does not exclude the possibility that such oscillations are present and a more thorough search of the frequency domain below 0.5 mHz using differential photometry is required. The other null result of note is β CrB (HR 5747). This star has a polarity reversing magnetic field which varies from -500 gauss to +900 gauss with a period of 18.5 day. It also has the spectral peculiarities and colours associated with the roAp phenomenon. According to the oblique pulsator model, a roAp star attains maximum pulsation amplitude at times of magnetic extrema when one sees the star pulsation-pole on. Heller & Kramer observed β CrB for 4.53 hr at positive magnetic extremum and found no evidence for rapid oscillations. This is in agreement with the null results obtained for this star by Kurtz (1989) and Kreidl (1991), who also observed it at magnetic maximum. β CrB is one of the few Ap stars for which a well established null result exists and this is of interest because it has all the attributes of a roAp star (*cf.* Tables 2.1 & 2.2). This star would be a suitable null result star to use for a spectroscopic study aimed at finding subtle spectroscopic differences between the pulsating and constant Ap stars.

3.11 Instituto de Astrofisica de Canarias survey

As part of a program to search for rapid solar-type oscillations in the A-F, stars Belmonte (1989) observed 8 Fp/Ap stars using the 1.0-m Jacobus Kapteyn telescope on La Palma and the 1.5-m Carlos Sanchez telescope on Tenerife. No new roAp stars were discovered in this survey. The Ap stars he observed were 9 Tau, 49 Cam, HD 81009, 21 Com, HD 115606, HD 117708, β CrB and HD 220846. The scintillation noise levels attained in the frequency range of interest range from 0.5 mmag to 1.0 mmag.

3.12 The Potsdam-ESO Survey for rapid oscillation in stars in the spectral range A to F

Hildebrandt of the Astrophysicalisches Institut of Potsdam has searched for rapid oscillations in Ap stars using the ESO 0.5-m telescope at La Silla. As of this writing, no new roAp stars have emerged from the Potsdam survey. This survey has subsequently been extended to include solar and late-type stars as well. The first publication to emerge from this survey (Hildebrandt 1992) discusses HD 4849, HD 24712 (= HR 1217), HD 182475 (A9V), HD 184552 (A1m) and HD 215874 (A9 III-IV). HD 4849 is a δ Scuti star and HR 1217 is a known roAp star. In a somewhat generous interpretation of his observations, Hildebrandt argues that the last three stars, HD 182475, HD 184552 and HD 215874, show oscillations with periods of 112.3, 163.3 and 97.2 min, respectively. Given that these stars were observed only once each for $\leq$ 4 hr in *single-channel high-speed mode*, I feel that these results are insecure and require confirmation using conventional differential photometry. No null results are reported and the selection criteria for candidate stars are not specified.

3.13 The Wisconsin survey for rapid variability in normal A0-A5 stars

For completeness, we discuss a survey for rapid variability among chemically normal early (A0 - A5) main sequence A stars by Schutt (1991) of Wisconsin University. The survey was conducted using the University of Wisconsin Two-Star Photometer attached to a range of small (16"-24") telescopes at Pine Bluff Observatory and Table Mountain Observatory. Although about 50 stars were observed in this survey, Schutt lists only 36 stars by name. He concludes that there is no evidence for pulsation on a time scale of 4 - 16 min in the normal A stars. Surprisingly, Schutt also found evidence for δ Scuti-type variability in five of the survey stars, three of which have spectral types from A0 to A2. These results require confirmation since, if correct, they imply that the blue border of the δ Scuti instability strip extends as far as A0 on the main sequence, earlier than the commonly accepted spectral type A3.

The Wisconsin survey was a useful first step in the search for rapid variability in normal main sequence stars outside the instability strip. However, because this survey was done on small telescopes at less than ideal photometric sites, it suffers from noise levels 3 to 6 times higher than those in the Cape Survey. A follow-up survey with much lower noise levels is the next logical step in this process.

Table 3.2

Ap stars showing no evidence of high overtone pulsation in the surveys listed in this chapter.

HD	ref	HD	ref	HD	ref	HD	ref
315	1	51684	3	102333	1	171586	1
5797	1	52539	1	107180	1	171771	1
5823	1	59435	1	108283	1	176232	7
8441	1	62140	1 2 5 7	108945	1 2	177016	1
9050	1	62530	1	109030	1	184471	1 7
15089	1	62905	1	111133	1	188041	1
15144	1	62953	1	112528	1	188601	1
15233	3	65142	1	115606	2	188854	1
16145	1	65339	1 5	115708	1	190145	1
18078	1	68351	1	116114	1	191695	1
19653	1	68781	1	116763	6	191742	1 7
22374	2	68998	1	117708	2	192678	1
23393	1	69013	1	119213	1	200405	1
24786	1	70340	1	119288	7	204411	1
25354	1	72968	1	120198	1	206088	1
27285	1	73455	1	126365	1	207757	1
30020	1	74494	1	126515	1	209364	1
31225	1	76276	1	130559	1	213232	1
33011	1	76759	1	134793	1	213637	1
34452	1	77609	1	137909	1 2 4 7	216533	1
34514	1	78316	1	138426	1	220825	1
37308	1	81009	1 2	140160	1	220846	1 2
39658	1	82093	1	146998	1	221531	1
40142	1	86592	1	148112	1	224962	1
41385	1	91087	1	148898	1	Cox 52	6
42326	1	95811	1	149822	1	Cox 69	6
42605	1	96237	1	151199	1	Cox 93	6
42659	1	96707	1 5	165474	1 7	Cox 96	6
49976	1	98088	1 5	170397	1		

Notes:

The key to the references in the Table is given below. See Table 3.1 for the full references. The stars with "Cox" designations are in NGC 2516 (Cox 1955).

1. Nelson & Kreidl (1993)
2. Belmonte (1983)
3. Kurtz (1984)
4. Kurtz (1989)
5. Matthews *et al.* (1985)
6. Matthews *et al.* (1988)
7. Heller & Kramer (1988)

HD 22374 = 9 Tau
HD 62140 = 49 Cam
HD 108945 = 21 Com
HD 137909 = β CrB

3.14 The Lowell - Wisconsin survey for northern roAp stars

This survey is actually the amalgamation of two survey programs that began independently. It is, as of this writing, the most extensive northern sky survey of Ap stars for rapid variability. Nelson and Kreidl (1993) conducted their survey efforts during the seven-year period from 1985 to 1991. This survey examined 120 Ap stars in the spectral range from B8 to F4. Unfortunately, Nelson & Kreidl do not state clearly what their selection criteria were; their Table 1 contains stars that are not chemically peculiar as well as some luminosity class III and IV stars. Table 3.2 contains a list of null results taken from Table 1 of their paper, but for Ap stars only. Although no new roAp stars were reported by these authors, they draw some interesting conclusions from their observational data. They note the absence of pulsation in stars in the spectral range B8 - A3, a significant result given the number of stars observed and the overall quality of their data. This does not preclude the existence of roAp stars in this range, however, since Martinez *et al.* (1991) discovered rapid oscillations in the star HD 218495 which has a temperature corresponding to a spectral type of around A3. Interestingly, HD 42659, one of the new Cape Survey roAp stars was also observed by Nelson and Kriedl who found it to be constant, a poignant reminder that it can sometimes be rewarding to observe roAp star candidates several times over.

3.15 The Cape Survey

The above surveys were all conducted on a small scale and were far from being a systematic attempt to study the roAp phenomenon. Prior to the present survey, only 14 roAp stars were known. Because of this paucity we were still unsure of the systematics of the roAp phenomenon. In May of 1990 we began a survey which differed considerably from the earlier surveys in that it was designed to answer, or at least shed some light, on questions of the systematics of the roAp phenomenon such as:

1) What is the extent of the roAp phenomenon in the HR diagram?

2) What are the extremes of pulsation amplitude and frequency?

3) What is the distribution of amplitude with pulsation periods like?

4) What distinguishes pulsating Ap stars from apparently constant Ap stars which resemble them in all other respects?

5) What are the luminosities of the Ap stars? Can we determine them by studying the oscillations?

6) What is the driving mechanism?

7) Are there any cool Ap SrCrEu stars which are short period δ Scuti (i.e. low overtone) pulsators?

8) Do the roAp and δ Scuti stars overlap in luminosity?

9) Can a reliable photometric indicator of the roAp phenomenon be found?

10) What is the incidence of the roAp phenomenon among the cool Ap stars?

11) What can we learn by applying the techniques of asteroseismology to the roAp stars?

12) What is the relationship between the roAp stars and the other pulsating stars, particularly the δ Scuti stars which occupy the same region of the HR diagram?

13) Some roAp stars have non-stationary oscillation spectra. Is this the exception or the norm? What governs the mode lifetimes? Is non-stationary oscillatory behaviour correlated with some other observed quantity?

From the outset it was hoped that stars with rich *p*-mode oscillation spectra would be discovered. From an asteroseismological perspective the multi-mode pulsators are the most interesting because their oscillation spectra contain a wealth of astrophysical information. The seismological return will be greatest for stars with well determined properties such as members of clusters or binary systems[1].

It was also hoped that the survey might shed some light on the question of pulsation in the presence of metallicism (section 1.19). For many years it was thought that the exclusion between pulsation and metallicism is absolute; the pulsating δ Scuti stars were all chemically normal and no Am or Ap stars were observed to pulsate. However, in the last ten years this exclusion has blurred considerably. Several pulsating δ Delphini and marginal Am stars are now known (Kurtz 1976, 1978, 1984b) and the recent discovery of δ Scuti pulsation in the classical Am star HD 1097 (Kurtz 1989b) suggests that this survey may also provide a fresh perspective on the question of pulsation in the presence of metallicism.

---

[1] The discovery of a roAp star in a binary system is of special interest since the Ap stars have an unusually low binary frequency (Abt & Snowden 1973). The asteroseismology may lead to the detection of orbital companions through the Doppler shifts introduced into the oscillations by the orbital motion of the roAp star.

The strategy adopted in the Cape Survey was to first observe all the southern Ap SrCrEu stars in the Michigan Spectral Catalogue (Houk & Cowley, 1975, Houk 1978, 1982, Houk & Smith-Moore 1988) in the Strömgren $uvby$ and Hβ photometric systems and then to search for rapid oscillations in the subset of stars with indices similar to those of the known roAp stars. To avoid selection effects we also searched for rapid oscillations in many stars way outside this trial roAp photometric box; no new roAp stars were discovered in these searches. In addition we searched for rapid oscillations in a number of Ap stars without prior knowledge of their Strömgren indices. One roAp star was discovered in such a blind search; it later proved lie well inside the roAp candidate photometric box.

Table 3.3 is the list of 558 Ap SrCrEu stars selected from the Michigan Spectral Catalogue and Table 3.4 lists remarks for these stars from the Catalogue. Table 3.5 is a list of 71 equatorial SrCrEu stars selected from Bidelman & MacConnell's (1973) compilation of astrophysically interesting southern stars. There is no overlap between Table 3.3 and Table 3.5. At this point we must clarify our use of the term "SrCrEu star". In this thesis the precise spectroscopic designation Ap SrCrEu is used in a generic sense to mean an Ap star with line strength anomalies of one or more of these elements.

The observations for the Cape Survey were done at the Sutherland site of the South African Astronomical Observatory (SAAO). Computer controlled pulse-counting photometers were used for all the observations. In order to minimize the noise introduced into the light curves by scintillation and telescope tracking errors we employed long integration times (~10 s) and used large apertures (~30"). The Cape Survey stars are mostly bright enough (m_{pg} < 10) that photon statistics are not a dominant contributor to the noise. A real-time display allowed us to see the light curve, monitor changes in sky transparency and to check on tracking errors.

When searching for oscillations, we observed each star only long enough to define its light curve. When we started this program we thought that only an amplitude spectrum would show up the variability in most cases, but it turned out that with experience we were able to identify most new roAp stars by looking at the light curve on the real time display. For this reason, and to conserve telescope time, we monitored stars only for 1-2 hr to get the required frequency resolution. Another reason for observing roAp star candidates for only 1 - 2 hr is that a real roAp star can be down in amplitude for days if one happens to observe it near quadrature. For this reason we favoured acquiring several short runs on different nights as opposed to a single long run on only one night. If in the first hour we thought we saw something we would persist for another hour on the same star. On

many occasions what appeared to be a good signal during the first hour turned out to be a false alarm; for short time-spans, the sky transparency variations are remarkably good at mimicking exactly the kind of oscillations we wish to detect.

All the light curves were later subjected to Fourier analysis to reveal their component frequencies and to put detection limits on the stars. The detection threshold was influenced by the star's brightness, the size of telescope, the duration of the observations and the quality of the night. As a rule, most stars claimed to be constant did not show coherent oscillations with a semi-amplitude in excess of 0.5 mmag in the amplitude spectra. In a relatively small number of cases, the amplitude spectra exclude the presence of coherent oscillations in excess of 0.125 mmag. Chapter 5 gives a full discussion of the observing procedures and data reduction techniques used. All the null results of our survey are also listed in chapter 5.

The Cape Survey complements searches being conducted on a somewhat smaller scale by other observers as discussed earlier in this chapter. Previous searches have tended to concentrate on stars of 8th mag, or brighter. The Cape Survey includes many stars of 9th and 10th mag and it is to be expected that the yield of roAp stars should rise considerably simply by going to fainter limiting magnitudes. Indeed, several of the new roAp stars presented in this thesis are among the faintest ones known. To date there are 25 known confirmed roAp stars (Table 1.1). The Cape Survey has been responsible for the discovery of 10 of these. In addition, the survey has confirmed 1 new roAp star, HD 12932, which was discovered independently by Schneider & Weiss in their roAp survey at ESO and by Kreidl at Lowell. Interestingly, HD 12932 is also a Cape Survey star and on the basis of its colours it was on our short list of candidate roAp stars for high-speed photometry.

Table 3.3

Candidate SrCrEu stars from the Michigan Spectral Catalogue

HD NO	SPECTRAL TYPE	QUALITY & REMARK	PG MAG	POSITION (2000) α H	M	S	δ °	'	"	REMARKS
2202	*F0(P SR)	2D	10.4	0	25	43	-50	50	18	
2883	*AP SR	1	9.6	0	31	36	-61	21	0	
2957	*AP CR(EUSR)	1	8.2	0	32	44	-13	29	11	
3980	*AP SREUCR	A1 RB	6.5 V	0	41	42	-56	30	0	
3988	*AP CREUSR	1	8.4	0	39	18	-83	2	0	
5823	*AP SREU(CR)	2	10.4	0	59	42	-11	55	35	
6532	*AP SRCREU	1	8.4	1	5	56	-26	43	43	roAp
7676	*AP SRCREU	A1	8.2	1	16	7	-34	8	56	
8783	*AP SREU(CR)	1 R	7.5	1	24	0	-72	20	0	
9050	*AP EUSR	1	8.9	1	28	56	-14	1	58	
10081	*AP SR(EU)	1	9.8	1	36	12	-68	14	0	
11090	*AP SR	3 R	11.4	1	46	36	-67	28	0	
11346	*AP SREUCR	1	10.2	1	47	54	-74	5	0	
12932	*AP SREUCR	2	10.8	2	6	13	-19	7	16	roAp
14944	*AP EU(CR)	2 R	9.4	2	20	0	-77	13	0	
15144	*AP SRCREU	1BLD	5.9 V	2	26	0	-15	20	25	
16002	*A3(P SREUCR)	1	9.3	2	29	42	-73	15	0	
16145	*AP CREUSR	A1	7.85	2	35	4	-17	17	22	
18610	*AP EUCRSR	1 R	8.2	2	54	30	-73	27	0	
19817	*F0(P CREU)	A3R	8.7	3	9	22	-48	57	45	
19918	*AP SREUCR	1	9.5	3	1	24	-81	54	0	roAp
20505	*AP CRSR	1	10.3	3	15	6	-59	11	0	
20880	*AP SR(EUCR)	1	7.7	3	17	24	-73	32	0	
22488	*AP SREUCR	A2 R	8.2	3	32	42	-66	44	0	
23207	*AP SREUCR	2	7.6	3	42	45	-18	42	45	
23329	*A(P EUCRSR)	3	9.8	3	43	24	-26	21	16	
23393	*AP SRCREU	2R	8.5	3	44	29	-12	3	29	
23715	*AP SREUCR	2R	9.2	3	46	31	-24	2	59	
24712	*AP SREU(CR)	1BL	6.22V	3	55	16	-12	5	54	roAp
24786	*AP CREUSR	2R	9.8	3	55	37	-21	50	8	
24825	*AP CREU(SR)	1	6.8	3	55	15	-38	45	32	
26726	*AP SR	2R	9.8	4	12	46	-24	47	47	
27211	*AP SRCREU	1	9.0	4	15	18	-52	9	49	
27285	*AP EUSRCR	2	9.8	4	17	48	-19	52	57	
27463	*AP EUCR(SR)	2 B	6.1	4	16	24	-60	56	0	
27472	*AP EUCRSR	1	10.5	4	16	30	-61	4	0	
28430	*AP EUCRSR	2	8.3	4	27	22	-40	11	51	
29469	*A(P SREUCR)	2R	9.9	4	36	58	-35	50	25	
29578	*AP SREUCR	A1 R	8.8	4	36	30	-54	37	0	
30335	*AP SRCREU	2	9.8	4	44	31	-44	25	7	
30374	*AP SREUCR	A2	9.8	4	40	42	-75	6	0	
30849	*AP SRCREU	1R	9.5	4	48	38	-49	10	11	
31225	*AP SREUCR	1RB	6.9	4	53	12	-20	46	20	
31973	*AP SRCREU	1	10.0	4	57	50	-44	37	46	
33011	*AP EUCR(SR)	1	9.2	5	6	37	-15	46	52	
33629	*AP SRCR(EU)	2	9.7	5	10	6	-33	46	45	
34060	*B9 V(P SICR)	1	7.9	5	12	3	-49	3	40	
34205	*AP SRCREU	1R	9.3	5	15	7	-15	6	0	
34514	*AP SRCREU	1	8.9	5	17	15	-20	50	3	
35361	*AP CREU	A2 R	9.8	5	16	6	-75	7	0	
36964	*A(P SR)	1R	9.5	5	34	17	-24	20	20	
37308	*AP SREUCR	1	8.6	5	36	53	-17	0	56	
38719	*AP CRSREU	A1	7.5	5	44	18	-56	55	0	
39575	*AP EUCRSR	1	8.4	5	52	24	-26	17	29	
40277	*AP SRCR(EU) PEC	1 R	8.6	5	51	48	-70	29	0	
40765	*AP SRCREU	2	9.9	5	59	41	-30	39	52	
40886	*AP SREU(CR)	1	8.0	6	0	28	-27	53	19	
41089	*B9 III(P SREUCR)	1R	6.5	6	0	51	-42	52	13	
41385	*AP SREUCR	A2	9.2	6	3	57	-20	51	33	
41511	*AP SHELL	1RBL	5.04V	6	4	59	-16	28	14	
41613	*AP EUCR	1	10.3	5	56	18	-77	51	0	
41757	*AP CREUSR	2	8.4	6	6	2	-24	54	8	
42075	*AP EUCRSR	2	9.2	6	7	37	-26	35	35	
42326	*AP EUCRSR	2R	7.66	6	9	17	-17	17	29	
42605	*AP SREUCR	1	9.2	6	11	7	-12	44	36	

HD NO	SPECTRAL TYPE	QUALITY & REMARK	PG MAG	POSITION (2000) α H	M	S	δ °	'	"	REMARKS
42659	*AP SRCREU	1	6.78	6	11	21	-15	47	32	roAp
42777	*AP EUSRCR	1	8.9	6	11	49	-20	29	58	
43226	*AP SR(EU)	1	9.4	6	9	18	-71	7	0	
43901	*AP SRCREU	1R	7.8	6	16	14	-47	49	46	
44226	*AP SREUCR	2	9.1	6	19	35	-25	19	41	
44290	*AP EUCR	1R	8.5	6	20	28	-14	11	48	
44550	*A(P SREUCR)	3RD	9.4	6	21	31	-20	2	41	
45698	*AP SREU(CR)	2	8.2	6	27	11	-37	6	7	
45870	*AP EUCRSR	2R	9.3	6	29	18	-18	1	49	
45961	*AP CREUSR	1	9.1	6	29	51	-17	22	23	
46649	*A(P EUCRSR)	2R	9.7	6	33	52	-16	37	30	
46665	*AP EUSRCR	1R	9.1	6	33	41	-22	41	43	
47009	*AP EUCR(SR)	1	8.5	6	35	49	-13	44	48	
49686	*AP CREU(SR)	1	9.3	6	47	58	-36	12	59	
50031	*AP SREUCR	1	10.1	6	50	46	-14	13	54	
50143	*AP EUSRCR	2R	9.4	6	50	57	-21	53	58	
50304	*AP EUCR	A1R	7.2	6	51	41	-23	48	8	
50620	*AP SREUCR	1	9.1	6	51	38	-47	19	40	
50627	*A(P EUSRCR)	3	10.5	6	45	48	-77	46	0	
50861	*AP SREU	1	9.6	6	51	18	-59	18	0	
51203	*AP SREUCR	3	11.0	6	55	10	-30	3	36	
51684	*AP SREUCR	2	8.1	6	56	30	-40	59	26	
52280	*AP SREUCR	1 R	9.5	6	55	54	-65	0	0	
52539	*AP EUSRCR	A1	8.9	7	0	59	-16	26	39	
52599	*AP SRCREU	1	8.3	7	0	46	-27	7	46	
52696	*AP SREUCR	1	8.3	7	1	29	-19	12	0	
52847	*AP CREU(SR)	1	8.4	7	1	46	-23	6	19	
54087	*AP SRCR	1	****	7	6	55	-15	53	11	
54399	*AP SR(CREU)	1	9.8	7	4	36	-61	50	0	
55540	*AP EUCR	A1	8.9	7	12	30	-21	3	52	
55719	*AP SREUCR	1LB	5.9	7	12	16	-40	29	55	
56026	*A4 V(P SREUCR)	2 R	10.2	7	11	0	-63	58	0	
56350	*AP EUCRSR	1	7.3	7	13	48	-53	39	0	
56809	*AP CREUSR	1	7.1	7	17	22	-29	7	53	
56882	*AP SRCREU	3R	8.4	7	16	41	-46	21	18	
56981	*AP SR	1	10.1	7	13	30	-72	1	0	
57040	*A(P EUSR)	4 R	9.5	7	16	42	-53	27	0	
57964	*AP (SI)	1RD	9.2	7	21	56	-37	29	33	
58868	*AP (SICR)	2	9.4	7	25	54	-35	35	35	
58935	*A(P SREUCR)	3R	10.1	7	26	11	-36	30	41	
58939	*AP SREUCR	A2R	10.0	7	24	59	-52	54	4	
59164	*AP SREUCR	2	8.4	7	27	42	-26	14	11	
59437	*AP CREU	2	9.2	7	29	24	-14	18	16	
59660	*AP EUCR(P SR)	1R	9.7	7	28	16	-52	4	34	
59776	*AP CRSR(EU)	2	8.8	7	30	10	-33	24	28	
59843	*F0 IV(P EUCR)	3	10.2	7	29	49	-44	24	44	
60220	*B9 V(P SRCREU)	2	9.0	7	32	20	-27	53	45	
60435	*AP SR(EU)	1	8.9	7	31	0	-58	0	0	roAp
60572	*AP EUCRSR	1	9.3	7	33	44	-34	35	24	
61468	*AP EUCR(SR)	2	9.2	7	38	21	-27	52	31	
61513	*AP CREUSR	2	9.7	7	38	28	-30	3	48	
61731	*AP CREU	2	9.8	7	39	57	-20	44	43	
61763	*AP SHELL	2R	7.8	7	38	47	-44	49	48	
62244	*AP SREUCR	1D	8.0	7	42	7	-24	6	53	
62399	*AP CREUSR	1	9.4	7	41	40	-45	19	11	
62530	*AP EUCRSR	2	7.5	7	43	55	-16	10	38	
62553	*AP SRCR	2	7.3	7	43	43	-22	10	4	
62556	*AP EUCR(SR)	2D	7.4	7	43	32	-27	10	45	
62562	*AP SREUCR	1	8.7	7	42	32	-45	2	0	
62905	*AP EUCR(SR)	1	9.5	7	45	37	-16	58	28	
62953	*AP EUCRSR	1R	9.2	7	45	54	-15	10	41	
63728	*AP EUCR	A1	9.1	7	46	36	-61	44	0	
63745	*AP EUCRSR	3R	10.6	7	47	50	-52	33	55	
63759	*AP SRCREU	1	8.6	7	49	29	-27	50	2	
64288	*AP EU(CRSR)	2R	9.8	7	50	57	-48	13	18	
64698	*AP CR(SI)	2	9.5	7	53	25	-40	15	58	
65142	*AP EUCRSR	1	8.7	7	56	41	-18	54	3	
65836	*AP SRCREU	2	6.5	7	47	30	-81	36	0	
65963	*AP (SRCR)	2R	9.0	7	59	54	-36	55	12	
66195	*AP SREUCR	1 R	8.5	7	57	36	-70	43	0	
66318	*AP (EUCRSR)	3 R	9.1	7	59	30	-60	48	0	

HD NO	SPECTRAL TYPE	QUALITY & REMARK	PG MAG	POSITION (2000) α H	α M	α S	δ °	δ '	δ "	REMARKS
67909	*AP CREU	2	8.9	8	7	36	-53	29	0	
67950	*AP EUSRCR	2	9.6	8	8	28	-45	19	23	
67975	*AP SR(CR)	2	9.3	8	9	31	-26	20	19	
68013	*AP EUCR(SR)	A1R	8.9	8	8	2	-52	48	7	
68419	*AP SRCREU	A1	8.1	8	10	0	-48	20	0	
68480	*AP EU(SR)	1 R	8.7	8	9	30	-57	59	0	
68781	*AP SREUCR	2	9.9	8	13	17	-18	46	59	
68807	*AP EUCRSR	A2D	8.7	8	12	3	-46	12	35	
68998	*AP SREUCR	1	8.5	8	14	21	-16	11	7	
69013	*AP EUSR	3	9.3	8	14	29	-15	46	29	
69204	*AP SR	2	9.5	8	15	7	-23	36	14	
69638	*AP EUCR	2R	9.2	8	17	3	-21	36	56	
69862	*AP SREUCR	2	10.1	8	15	30	-61	52	0	
70702	*AP EUCRSR	1	8.4	8	21	1	-51	32	37	
71058	*AP EUCRSR	2R	9.7	8	23	41	-41	51	9	
72316	*AP EUCR(SR)	1	8.6	8	30	57	-33	37	7	
72611	*AP EUCRSR	1R	7.3	8	32	17	-41	49	59	
72634	*AP CREUSR	2	7.9	8	29	48	-67	8	0	
72801	*AP CREUSR	1R	9.3	8	32	41	-50	12	35	
73063	*B9 III(P EUCR)	3	10.0	8	34	10	-49	33	34	
73101	*AP SREUCR	3	9.2	8	35	51	-21	59	31	
73403	*AP SRCREU	1R	8.6	8	36	53	-37	58	45	
73455	*AP SR(CREU)	2R	10.0	8	38	2	-16	1	53	
73850	*AP SRCREU	1D	8.9	8	38	22	-51	8	17	
74067	*AP (SICR)	2RBLD	5.15	8	40	19	-40	15	49	
74169	*AP EUCR(SR)	A2RO	7.2	8	39	59	-53	15	41	
74494	*AP EUCRSR	2	8.6	8	43	35	-24	31	37	
74555	*AP CRSI	2D	8.6	8	43	19	-38	41	43	
74629	*AP SR(CR)	1	9.5	8	44	28	-19	42	9	
74636	*B9 IV/V(P SICR)	1	8.9	8	42	53	-51	40	4	
74672	*AP SRCREU	1	9.4	8	44	23	-28	31	38	
75049	*AP EUCR	2R	8.7	8	45	33	-50	43	58	
75130	*A(P SICR)	2R	9.2	8	46	8	-49	34	48	
75163	*A5 V(P EU)	1R	9.4	8	47	31	-26	29	3	
75425	*AP SR(EUCR)	2RD	9.2	8	48	28	-42	1	19	
75445	*AP SREU(CR)	1	6.8	8	48	43	-39	14	3	
76225	*F7/G + A(P SR)	1R	9.5	8	54	0	-26	55	41	
76276	*AP SRCREU	2R	10.1	8	54	26	-22	56	59	
76460	*AP SR	2	10.0	8	53	6	-62	27	0	
76759	*AP EUSRCR	1RD	9.1	8	57	49	-13	5	34	
76877	*AP CRSREU	A2	9.6	8	56	43	-52	57	40	
77438	*AP EUCRSR	2	10.1	9	0	18	-52	26	55	
77609	*AP EUSRCR	2	8.0	9	3	7	-20	32	46	
77809	*AP SR(CR)	3	10.0	9	3	27	-39	17	42	
77830	*AP SRCR(EU)	2D	9.6	9	2	50	-51	50	49	
78651	*A(P EUCRSR)	4	10.2	9	7	35	-50	4	30	
78930	*B9 IV(P EUCR)	A2	9.1	9	8	49	-53	14	50	
79167	*A(P) SREUCR	3	10.3	9	11	47	-24	43	29	
79539	*AP SREUCR	1	9.3	9	13	43	-33	55	37	
79976	*AP SRCREU	A1	8.4	9	16	42	-16	50	12	
80211	*A(P EUCR)	2R	9.0	9	16	38	-50	56	37	
80249	*AP CREUSR	2	9.9	9	16	49	-50	57	1	
80316	*AP SR(EU)	3R	8.3	9	18	25	-20	22	13	roAp
80992	*AP SR(EUCR)	2	10.4	9	22	16	-27	48	31	
81076	*AP EUCR	2R	9.8	9	22	4	-45	38	35	
81289	*AP EUSRCR	1	8.4	9	23	25	-43	36	6	
81588	*AP SRCREU	A2	8.7	9	24	54	-48	29	7	
81877	*AP EUCRSR	1	8.8	9	27	9	-40	22	0	
82038	*AP SREUCR	2	9.7	9	27	6	-59	22	0	
82093	*AP EUSRCR	1B	7.11	9	29	26	-17	30	17	
82417	*AP EUSRCR	1R	9.0	9	30	23	-46	48	48	
82562	*AP EUCR(SR)	2	9.4	9	31	49	-36	32	14	
82749	*AP SRCREU	1	9.3	9	32	18	-50	30	12	
82989	*AP SRCR + G0/5	A1 R	8.8	9	32	24	-65	30	0	
83080	*A0/1 IV(P CRSI)	1	8.9	9	34	18	-50	36	7	
83181	*AP CREUSR	2	9.3	9	35	16	-44	36	52	
83368	*AP SREUCR	1RBD	7.2	9	36	25	-48	45	3	roAp
83817	*AP SR	2 R	9.1	9	37	0	-71	42	0	
84041	*AP SREUCR	2D	9.3	9	41	34	-29	22	26	roAp
85284	*AP EUCR(SR)	3	9.8	9	49	0	-55	2	0	
85453	*AP (SI)	3	8.0	9	50	22	-50	20	8	
85564	*AP (SICRSR)	3	9.6	9	51	12	-50	30	38	

HD NO	SPECTRAL TYPE	QUALITY & REMARK	PG MAG	POSITION (2000) α H	α M	α S	δ °	δ '	δ "	REMARKS
85733	*AP EUSRCR	A2	10.1	9	49	12	-75	24	0	
85766	*AP (SICR)	3	10.0	9	53	19	-30	54	12	
85812	*A(P EUSRCR)	3	9.8	9	52	36	-56	13	0	
86051	*AP EUSRCR	2	9.6	9	54	58	-42	22	43	
86181	*AP SR	3	9.4	9	54	54	-58	41	0	
86592	*AP SREUCR	2	7.68	9	59	14	-12	45	13	
86976	*AP SRCREU	1	8.6	10	1	4	-40	52	1	
87087	*AP SREUCR	2	10.3	10	1	0	-57	6	0	
87488	*A(P EUCR)	2R	7.9	10	4	49	-28	11	19	
88042	*AP EU(SRCR)	2 R	10.3	10	7	30	-55	31	0	
88241	*AP SR(EUCR)	1R	8.9	10	9	32	-40	28	24	
88385	*AP CREU(SR)	A1	8.6	10	9	48	-56	44	0	
88507	*AP SREU(CR)	2	9.3	10	11	14	-49	40	34	
88701	*AP CRSI	2R	9.8	10	13	0	-37	30	12	
89075	*A(P EU)	A2R	8.5	10	16	1	-26	35	39	
89192	*AP CREUSR	1 R	7.4	10	15	54	-55	31	0	
89385	*B8 V(P CREUSR)	2 R	7.8	10	17	30	-54	23	0	
89393	*AP SRCREU	A3D	8.6	10	18	6	-40	14	20	
89519	*AP EUCR(SR)	1	8.6	10	17	18	-68	8	0	
89680	*A(P CR)	2	8.2	10	19	53	-47	5	56	
89840	*AP (SI)	3 R	10.3	10	20	42	-53	53	0	
90131	*AP EUCR(SR)	1	9.3	10	23	33	-36	38	10	
91087	*AP SREUCR	2	8.9	10	30	35	-22	31	14	
91239	*AP EUCR(SR)	2R	7.7	10	31	13	-42	13	44	
91337	*AP SRCREU	2	9.9	10	32	10	-29	16	39	
91520	*AP SRCREU	A1R	9.7	10	33	24	-38	54	52	
91735	*AP EUSR(CR)	2 R	9.6	10	32	36	-74	5	0	
91982	*AP SRCREU PEC	1R	9.6	10	36	16	-50	8	50	
92106	*AP SREUCR	A2	7.6	10	32	54	-81	10	0	
92218	*AP SRCREU	1	8.9	10	36	36	-70	35	0	
92286	*AP EUCR	2 R	9.5	10	38	12	-54	40	0	
92315	*A1 V(P CRSREU)	1	8.3	10	37	24	-69	22	0	
92499	*AP SREUCR	1	9.0	10	40	9	-43	4	51	
92534	*AP CRSI LAM4200	A1	9.2	10	39	36	-61	35	0	
93500	*AP CREUSR	2	8.5	10	46	24	-59	27	0	
94052	*AP CREU	2	9.5	10	50	18	-55	13	0	
94111	*A2 V(P CRSREU)	2	9.5	10	50	42	-55	56	0	
94274	*AP CR(SI)	2	9.1	10	51	54	-55	31	0	
94455	*AP CREUSR	1	8.2	10	50	0	-80	56	0	
94660	*AP (SICR)	1RB	6.8	10	55	1	-42	15	4	
95158	*A9(P SRCR)	A1R	9.4	10	59	1	-21	10	11	
95491	*AP SRCREU	2	9.1	11	0	35	-51	38	37	
95508	*AP CR(EU)	1R	9.3	11	0	45	-50	25	47	
95699	*AP SREUCR	3	8.0	11	2	12	-42	29	54	
95811	*AP SRCREU	2R	10.1	11	3	8	-25	10	34	
96237	*AP SREUCR	1	9.8	11	5	34	-25	1	8	
96451	*AP SR(EU)	1 R	6.6	11	4	54	-75	9	0	
96537	*AP SRCREU	A1D	9.3	11	6	57	-44	2	38	
96616	*AP SRCREU	1LBD	5.4	11	7	17	-42	38	21	
96897	*AP SREUCR	3	9.7	11	8	36	-58	40	0	
97132	*AP SREUCR	2	9.6	11	10	15	-51	18	53	
97394	*AP EUCRSR	1	9.0	11	12	1	-43	40	36	
97987	*AP SREU	3	9.7	11	14	42	-72	58	0	
98340	*B9 IV(P SICR)	A2	7.3	11	17	54	-59	14	0	
100357	*AP EUCRSR	1	8.8	11	32	6	-67	2	0	
100587	*AP EUSRCR	2D	8.2	11	34	16	-41	9	16	
101189	*AP HGMN	A1 LB	5.32	11	38	12	-61	49	0	
101410	*AP EUCR	A1R	7.4	11	39	54	-50	29	10	
102333	*AP EUCRSR	1	8.9	11	46	39	-19	0	24	
102812	*A(P SR)	4	11.4	11	50	9	-28	36	19	
102983	*A0 III/IV(P CR)	A1RD	9.3	11	51	9	-53	26	7	
103210	*AP SRCREU	3	9.8	11	53	0	-52	37	57	
103302	*AP SRCREU	2	8.4	11	53	38	-49	19	14	
104044	*AP SREU(CR)	2	9.7	11	58	53	-43	22	55	
104402	*A(P EUCRSR)	2 R	9.3	12	1	18	-57	43	0	
105999	*AP SRCR(EU)	3	8.0	12	12	0	-63	22	0	
106215	*AP CREUSR	A1	9.4	12	13	13	-35	22	0	
106322	*AP EUCR	1R	9.2	12	14	2	-50	29	19	
106374	*A(P SRCREU)	2R	7.9	12	14	18	-33	46	44	
107107	*AP CREUSR	1	8.9	12	19	5	-40	9	46	
107180	*AP EUCRSR	1	10.0	12	19	32	-24	0	17	
109300	*AP (SI)	3 R	9.6	12	34	6	-58	51	0	

HD NO	SPECTRAL TYPE	QUALITY & REMARK	PG MAG	POSITION (2000) α H	M	S	δ °	'	"	REMARKS
109426	*AP SREUCR	2 R	9.3	12	35	24	-70	19	0	
109790	*AP (SI)	3	10.0	12	38	0	-58	22	0	
109989	*AP SRCREU	1R	9.2	12	39	25	-41	51	3	
110072	*AP SR(CR)	2R	10.8	12	39	50	-34	22	29	
110274	*AP EUCR	2	9.0	12	41	30	-58	55	0	
110446	*B9 V(P CREU)	2	9.4	12	42	42	-56	52	0	
110568	*A(P CREU)	2	9.7	12	43	36	-54	52	0	
111675	*AP EUSR	2	9.7	12	52	0	-66	2	0	
112528	*AP SREU(CR)	1	8.4	12	57	35	-19	45	0	
112616	*AP SR(EU)	1R	9.6	12	58	20	-27	20	33	
113149	*AP CREU	2	9.7	13	2	30	-55	44	0	
113588	*AP EUCR(SR)	A2	9.2	13	6	6	-66	45	0	
114035	*AP SREU(CR)	A1	8.0	13	15	48	-85	34	0	
114709	*AP EUCRSR	1	9.9	13	14	24	-73	4	0	
115226	*AP SR(EU)	1	9.5	13	18	0	-72	57	0	
115285	*AP CREU(SR)	1	8.8	13	17	54	-68	3	0	
115440	*AP (SI)	1	8.6	13	20	6	-76	26	0	
116114	*AP SR(EUCR)	1B	7.3	13	21	46	-18	44	29	
116423	*AP EUSR(CR)	1	8.6	13	25	24	-68	10	0	
116458	*AP HG(MN)	A1 RB	5.84	13	25	54	-70	37	0	
116729	*AP SREUCR	1	9.1	13	26	10	-37	13	45	
116763	*AP CRSREU	A1R	8.8	13	26	50	-53	28	8	
117025	*AP SREUCR	1 B	6.6	13	29	12	-64	41	0	
117227	*AP CRSR	2R	9.6	13	29	45	-47	25	5	
117290	*AP EUCRSR	1	9.3	13	30	13	-49	7	59	
117453	*AP SREUCR	2	10.3	13	31	1	-35	55	58	
117691	*F0/2(P SREU)	3	9.5	13	33	36	-63	30	0	
118231	*B9 III(P CR)	2	8.1	13	40	18	-79	51	0	
118470	*AP SREUCR	3	9.9	13	38	24	-54	39	0	
118683	*AP SRCR(EU)	2	9.7	13	40	36	-67	18	0	
118913	*AP EUCRSR	A1 R	7.4	13	42	18	-69	15	0	
119027	*AP SREU(CR)	2	9.9	13	41	19	-28	47	23	roAp
119158	*AP CREU(SR)	1R	9.6	13	42	42	-52	32	29	
119308	*AP SRCREU	2	7.4	13	43	13	-35	17	23	
119794	*AP CREUSR	1 R	9.4	13	47	0	-60	6	0	
120346	*AP SRCR(EU)	2	9.8	13	51	6	-66	33	0	
121276	*AP SICR(PEC)	1R	9.1	13	55	48	-51	42	58	
121661	*AP EUCR(SR)	1	7.9	13	58	48	-62	42	0	
121675	*AP CREUSR(PEC)	2R	9.7	13	57	57	-48	11	9	
121788	*AP (SRCR)	2R	8.9	13	58	17	-30	4	35	
121840	*AP EUCR(SR)	A3	9.4	13	59	54	-62	2	0	
122208	*AP SRCREU	1	8.2	14	1	17	-39	15	10	
122525	*AP SRCREU	1 R	9.1	14	3	54	-53	43	0	
122569	*AP CREUSR	1	8.8	14	3	40	-40	3	1	
123112	*A(P SICR)	1R	7.0	14	6	58	-47	35	19	
123164	*AP SREUCR	2	9.9	14	7	14	-46	24	16	
123627	*AP SREUCR	1	8.6	14	11	54	-70	10	0	
124437	*AP CRSREU	A2	8.9	14	16	18	-66	11	0	
124740	*A(P SICR)	3R	7.7	14	16	24	-41	14	0	
125467	*AP EUCRSR	A1 R	8.8	14	22	24	-66	19	0	
125555	*AP SREUCR(+ A)	1 R	9.8	14	24	48	-75	2	0	
125735	*AP EUCRSR	2	10.3	14	22	34	-45	29	11	
126297	*AP CREUSR	3	9.5	14	25	53	-44	40	6	
126365	*A(P SRCR)	3R	9.0	14	25	24	-14	5	5	
126936	*A(P CREUSR)	2R	9.7	14	29	53	-45	6	13	
127021	*AP SRCR(EU)	1	10.1	14	30	54	-54	33	0	
127154	*AP (SI)	1	7.6	14	31	18	-47	4	19	
127159	*A8/F0(P EUSR)	4 R	9.7	14	32	30	-63	58	0	
127210	*F2(P EU)	3	10.6	14	31	1	-33	55	44	
127241	*AP SRCR(EU)	1 R	9.2	14	33	36	-68	9	0	
127608	*AP EUSRCR	2R	10.0	14	33	47	-46	45	33	
128472	*AP CRSREU	1	9.9	14	38	41	-49	54	30	
128540	*AP SRCREU	1 R	8.6	14	39	48	-59	35	0	
128649	*AP CRSI LAM4200	1	9.4	14	39	23	-42	45	45	
128843	*A0 IV(P SICR)	3	10.1	14	43	42	-72	29	0	
128898	*AP SREU(CR)	4 LB	3.69	14	42	30	-64	58	0	roAp
129052	*A(P SREU)	4	10.6	14	41	26	-35	47	47	
129189	*B8/9 V(P CREU)	1	8.6	14	45	30	-72	6	0	
129994	*AP SR(CR)	3	10.4	14	47	48	-55	38	0	
130336	*AP	2 R	8.8	14	50	54	-66	31	0	
130382	*B9 IV(P EUCRSR)	3	9.7	14	50	24	-60	14	0	

HD NO	SPECTRAL TYPE	QUALITY & REMARK	PG MAG	POSITION (2000) α H	M	S	δ °	'	"	REMARKS
130559	*AP SREUCR	1RBD	5.44	14	49	19	-14	8	53	
131141	*A(P SREU)	A2	9.4	14	52	53	-35	22	49	
131750	*AP SRCREU	1	9.0	14	56	21	-30	52	36	
131870	*AP EU(CRSR)	2 R	9.8	14	58	30	-57	54	0	
131910	*AP EUCR	3	10.0	15	0	18	-69	8	0	
132205	*AP EUSRCR	1	9.3	15	0	0	-55	3	0	
132322	*AP SRCREU	A1 R	7.4	15	1	36	-63	56	0	
132673	*AP SREUCR	A1	8.8	15	4	48	-70	50	0	
132968	*AP SRCREU	1	8.8	15	5	36	-66	49	0	
132981	*AP SR(EUCR)	2R	10.7	15	3	36	-45	15	40	
133792	*AP SRCREU	1 B	6.2	15	9	24	-63	39	0	
133812	*AP SR	2	9.6	15	11	36	-73	2	0	
134214	*AP SREU(CR)	2	7.7 V	15	9	3	-13	59	58	roAp
134465	*AP SREUCR	2	10.4	15	12	18	-54	55	0	
134507	*AP SR(CR)	2 R	9.8	15	12	42	-56	48	0	
134640	*AP EUCR(SR)	2RD	9.5	15	12	44	-47	57	49	
135173	*AP CRSR	2	10.3	15	15	15	-43	7	30	
135396	*AP (SRCR)	2 R	8.6	15	18	30	-65	36	0	
135459	*AP EUCR(SR)	2	10.7	15	17	24	-53	44	0	
135480	*AP SR(CREU)	2	9.0	15	22	48	-77	43	0	
135512	*AP EUCRSR	2R	9.5	15	17	19	-48	8	46	
135728	*AP SREUCR	1	8.9	15	17	39	-31	27	30	
135815	*AP CREUSR	1	9.3	15	18	37	-41	7	23	
136575	*AP SR(EU)	2	9.5	15	30	0	-78	51	0	
137160	*AP SREUCR	A2	8.0	15	26	54	-55	0	0	
137401	*A(P EUSRCR)	3	9.8	15	27	41	-47	3	48	
137509	*AP (SICRFE)	A1 R	6.7	15	31	30	-71	4	0	
137581	*A1 V(P SREU)	A2	9.2	15	28	58	-51	1	8	
137802	*AP EUSRCR	1	9.5	15	32	6	-67	8	0	
137848	*AP CRSREU	1	9.4	15	29	49	-41	4	18	
137949	*AP SREUCR	1B	7.51V	15	29	35	-17	26	27	roAp
138146	*AP EUCR	3 R	9.7	15	35	30	-72	1	0	
138426	*AP SRCR(EU)	1	9.1	15	32	34	-19	24	8	
138497	*B9 IV(P CRSREU)	1	6.7	15	36	12	-65	6	0	
138927	*A(P CRSREU)	2R	9.9	15	36	53	-43	53	3	
139474	*AP EUSR(CR)	1	9.0	15	45	30	-75	55	0	
139631	*AP EUCRSR	1R	8.7	15	40	45	-40	4	57	
140220	*AP EUCRSR	A1R	8.2	15	44	11	-44	6	48	
140393	*A(P SREU)	4	9.9	15	48	24	-70	10	0	
140748	*AP EUCR(SR)	2	8.6	15	49	54	-68	8	0	
140959	*AP EUCRSR	A2	9.6	15	48	9	-43	18	1	
141249	*AP SREU(CR)	2	10.4	15	48	44	-18	25	29	
141317	*AP CREU	1	8.6	15	50	35	-49	21	8	
141981	*AP EUCRSR	1	9.7	15	53	39	-42	50	31	
142502	*AP SREUCR	1	10.0	15	55	26	-15	2	25	
142823	*AP CRSI	1R	8.7	15	58	52	-49	6	42	
143487	*APEC	2R	9.8	16	1	44	-30	54	54	
143654	*AP EUCRSR	1	8.7 V	16	4	9	-51	32	39	
144413	*AP SREU(CR)	2	10.4	16	6	32	-20	14	18	
144748	*AP EUCRSR	1	8.6	16	8	21	-25	7	34	
144897	*AP EUCR	2R	8.6	16	9	51	-41	9	27	
145074	*AP (EUCRSR)	3	10.5	16	10	31	-35	59	51	
145393	*A9 V(P EUCRSR)	2R	9.8	16	12	27	-41	19	45	
146631	*F0 IV/V(P CREU)	3	9.3	16	19	43	-52	9	46	
147105	*AP SRCREU	1	8.9	16	20	49	-25	23	38	
147863	*AP EUCR(SR)	3	9.5	16	27	42	-59	12	0	
148593	*AP SREUCR	1R	8.9	16	29	39	-14	35	5	
148848	*AP EUCRSR	2R	7.9	16	32	42	-41	2	4	
148898	*AP SREUCR	A3B	4.85V	16	32	8	-21	28	0	
149250	*AP EUCR(SR)	1	9.1	16	39	12	-70	9	0	
149769	*AP SREUCR	3	9.8	16	40	48	-62	26	0	
149887	*AP CREUSR	1	9.1	16	39	46	-46	51	43	
150035	*AP CREUSR	1	8.6	16	39	31	-27	17	8	
150562	*A/F(P EU)	3R	9.6	16	44	11	-48	39	16	roAp
150715	*A(P SRCREU)	3	10.1	16	43	47	-25	13	3	
150862	*F7 V + A(P SR)	1R	9.3	16	44	44	-25	12	53	
151301	*AP SRCREU	1	9.2	16	49	30	-54	27	0	
151560	*AP SR(EUCR)	2	9.8	16	49	15	-28	42	34	
151860	*AP SREU(CR)	2	9.5	16	52	54	-54	10	0	
151873	*APEC SHELL	A2 RL	9.2	16	53	24	-57	2	0	
151941	*A9(P SREUCR)	4	10.0	16	51	35	-26	42	20	
152137	*AP SRCREU	A2 R	9.8	16	54	48	-57	25	0	

HD NO	SPECTRAL TYPE	QUALITY & REMARK	PG MAG	POSITION (2000) α H	α M	α S	δ °	δ '	δ "	REMARKS
152387	*AP CREUSR	A1	8.5	16	55	18	-46	43	53	
153149	*AP SREUCR	1	9.4	16	58	21	-17	28	3	
153183	*AP SR(EU)	2	9.1	17	4	36	-72	24	0	
153192	*AP EUCR(SR)	1R	9.7	16	59	1	-27	4	17	
153201	*AP (SI)	2 R	6.4 V	17	1	12	-56	33	0	
153742	*A(P EUCRSR)	A3	10.1	17	2	3	-21	17	50	
153953	*AP SREUCR PEC	A1R	9.4	17	5	15	-51	32	50	
154075	*AP EUCR(SR)	1R	10.3	17	5	37	-47	54	57	
154253	*AP SRCREU	2	9.0	17	8	12	-60	45	0	
154308	*AP SRCREU	2	8.5	17	6	10	-33	3	18	
154645	*AP EUCRSR	A2D	8.4	17	8	40	-42	41	40	
154708	*AP SRCREU	2 R	8.5	17	10	30	-58	0	0	
155127	*AP EUCR	2	8.4	17	10	52	-26	27	4	
155171	*AP CREU(SR)	A4	10.2	17	13	24	-58	24	0	
155188	*AP SREUCR	1	9.4	17	13	12	-55	36	0	
155366	*AP SRCREU	1	9.1	17	13	42	-49	53	25	
156049	*AP CREU	A3	7.9	17	18	42	-57	27	0	
156366	*AP SREU(CR)	2	9.3	17	18	17	-28	7	35	
156495	*AP CRSREU	1 R	8.5	17	21	6	-56	6	0	
156808	*AP EUCR	A1R	9.3	17	21	24	-39	30	3	
156869	*AP SRCREU	A1	7.6	17	22	52	-52	58	41	
157208	*A(P SRCREU)	4R	9.9	17	24	21	-48	32	53	
157289	*A1 IV(P CREUSR)	1 R	8.5	17	26	24	-61	29	0	
158205	*AP SR(EUCR)	4 R	8.4	17	31	18	-56	45	0	
158293	*AP CREUSR	1	9.1	17	32	0	-58	36	0	
158979	*B9 V(P SREUCR)	2	10.4	17	32	50	-15	39	26	
159930	*AP EUCR(SR)	2	10.4	17	37	53	-14	7	42	
159992	*AP EUSRCR	1	9.1	17	41	42	-62	20	0	
160127	*AP SREUCR	1	8.0	17	40	9	-39	57	30	
160468	*AP SRCR	1	7.6	17	45	42	-68	39	0	
160544	*AP SRCR	2	8.9	17	41	19	-18	38	27	
161423	*AP SREU(CR)	2 R	9.2	17	52	6	-71	41	0	
161459	*AP EUSRCR	2	10.4	17	48	29	-51	55	2	roAp
161596	*A(P SICR)	4	9.6	17	48	18	-40	56	47	
161704	*A(P CREUSR) + (G)	A3R	8.7	17	48	51	-39	25	47	
161755	*AP SR(EUCR)	2	9.6	17	48	7	-18	17	28	
161998	*F0 V(P EUCRSR)	2	10.8	17	51	3	-44	49	58	
162265	*AP SR	3	9.8	17	51	0	-20	16	0	
162316	*AP SREU(CR)	1	9.5	17	59	12	-75	48	0	
162373	*AP SREUCR	1	8.8	17	52	4	-31	21	43	
162639	*AP SREUCR	A2R	10.1	17	54	41	-50	26	45	
163256	*AP SR(CR)	3R	10.1	17	57	34	-46	10	59	
163379	*A9 V(P CRSREU)	A1R	9.5	17	58	32	-50	34	18	
163583	*AP SRCREU	2	10.2	18	0	6	-55	38	0	
163712	*AP SR	2 R	9.3	18	0	42	-55	3	0	
163833	*AP (SI)	3	9.3	18	0	19	-42	36	1	
164231	*A2/3(P CREU)	4	8.9	18	2	23	-45	39	48	
164485	*AP SR	1R	8.8	18	1	56	-13	8	33	
165945	*AP SREUCR	1	9.2	18	9	2	-15	31	41	
166223	*AP CRSI	A2R	9.8	18	11	49	-44	18	1	
166469	*B9 IV(P SREUCR)	1RB	6.2 V	18	11	58	-28	54	4	
166473	*AP SREUCR	1	7.7	18	12	26	-37	45	6	roAp
166808	*AP SR(CREU)	1	9.2	18	13	31	-28	15	19	
167024	*AP SREUCR	1	9.1	18	15	7	-38	53	37	
167288	*A(P SICR)	2R	8.0	18	15	30	-23	7	0	
167700	*AP SREU(CR)	A2	9.1	18	17	26	-24	23	59	
168314	*AP EUCR(SR)	2	10.4	18	20	52	-39	39	34	
168767	*AP EUCR(SR)	2R	8.6	18	22	30	-26	54	39	
169380	*AP EUCRSR	2	9.2	18	26	3	-37	53	48	
169481	*AP CREUSR	1	9.4	18	26	59	-44	28	31	
169852	*AP CREUSR	3	9.6	18	28	3	-31	34	2	
169965	*A(P EUCRSR)	1RD	8.7	18	28	0	-21	35	27	
170044	*A(P SR)	4	10.6	18	30	24	-53	38	0	
170397	*AP EUCREU	2RB	5.99V	18	29	46	-14	34	53	
171771	*AP SREUCR	A2	8.2	18	37	27	-21	29	44	
172626	*AP SRCREU	1	9.5	18	42	51	-37	4	36	
172703	*AP EUCR(SR)	1	8.1	18	43	7	-33	29	35	
173562	*AP CREU(SR)	A2	8.1	18	49	36	-58	57	0	
173569	*A(P EUCR)	3	10.6	18	46	43	-17	23	43	
173600	*AP SREUCR	3R	10.6	18	48	28	-46	53	39	
176196	*AP EUCR(SR)	A2	7.9	19	6	54	-74	45	0	
176519	*AP CRSI	2R	10.0	19	3	6	-49	18	21	

HD NO	SPECTRAL TYPE	QUALITY & REMARK	PG MAG	POSITION (2000) H	α M	S	δ °	'	"	REMARKS
177013	*AP EUCRSR	2	9.3	19	3	27	-17	18	36	
177016	*AP EUSRCR	A1	9.0	19	3	40	-20	34	34	
177268	*AP CREU	1	8.8	19	5	25	-34	16	28	
177382	*AP EUCRSR	1	9.5	19	5	34	-28	10	5	
177765	*AP SREUCR	1	9.2	19	7	10	-26	19	53	
178246	*AP CRSI	2R	9.2	19	8	21	-13	47	6	
181810	*AP EUCRSR	2O	10.1	19	22	45	-21	25	40	
183806	*AP CREUSR	2B	6.3	19	33	22	-45	16	17	
184120	*AP EUCR	3D	10.1	19	33	42	-20	30	11	
184343	*AP SRCREU	A1	9.2	19	34	55	-23	22	2	
185204	*AP SREUCR	2	9.7	19	40	6	-46	54	26	
185256	*AP SR(EUCR)	3	9.9	19	39	24	-29	44	28	
186041	*F2 V(P SR)	1	9.1	19	43	10	-28	38	50	
186117	*AP SRCREU	1 R	7.8	19	49	24	-73	31	0	
186284	*A(P SRCR)	2R	9.7	19	44	15	-22	14	47	
187473	*AP (EUSRCR)	2R	7.4	19	51	10	-27	28	18	
187474	*AP CR(SI)	2RLB	5.39V	19	51	50	-39	52	27	
187761	*AP SREU	A1	9.5	19	53	16	-39	24	33	
188008	*AP CREUSR	2R	8.7	19	54	27	-36	34	31	
188518	*F(P EUCRSR) + (K)	2R	10.2	19	57	13	-40	34	38	
188601	*AP SREUCR	2	10.3	19	56	42	-22	0	18	
189832	*AP SRCREU	1	7.4	20	3	35	-38	51	5	
190290	*AP EUSR	3	9.7	20	14	0	-78	52	0	roAp
191439	*AP CREU(SR)	1	9.0	20	13	0	-58	47	0	
191695	*AP SREU(CR)	A2	9.8	20	12	2	-21	18	3	
191796	*AP EUCR(SR)	1	7.8	20	13	35	-45	35	26	
193756	*AP SRCREU	A1	9.1	20	24	11	-51	43	25	roAp
194623	*F2 V(P SR)	2R	8.9	20	27	35	-26	12	9	
194726	*A(P SRCREU)	1R	9.8	20	28	20	-29	52	14	
194750	*A(P SICR)	2R	8.7	20	29	2	-43	14	56	
195112	*AP EUCRSR	1	8.9	20	30	45	-38	34	40	
196470	*AP SREU(CR)	1	10.1	20	38	10	-17	30	6	roAp
197417	*AP CREU(SR)	1	7.5	20	48	48	-72	13	0	
200623	*AP SREUCR	1	9.1	21	5	34	-35	42	7	
201018	*AP CREUSR	2	8.7	21	8	7	-37	2	41	
202400	*AP SR	1 R	9.8	21	19	36	-70	5	0	
203006	*AP CREUSR	2RLB	4.98V	21	20	45	-40	48	34	
203932	*AP SREU	A1	8.9	21	26	4	-29	55	45	roAp
204367	*A(P SREUCR)	2R	7.7	21	28	41	-25	38	38	
207259	*AP EUSRCR	1	8.9	21	51	42	-73	10	0	
208217	*AP SREUCR	A1	7.6	21	56	54	-61	51	0	
208759	*AP SREUCR	1 R	10.1	22	0	54	-64	57	0	
209364	*AP SREUCR	1	9.9	22	3	15	-23	15	44	
209605	*AP SREUCR	1	9.2	22	5	14	-26	50	55	
212385	*AP SREUCR	A1R	6.9	22	24	37	-39	7	36	
213637	*A(P EUSRCR)	3	10.1	22	33	14	-20	2	8	
215185	*A(P SRCREU)	3R	11.4	22	44	4	-38	45	37	
215966	*AP EUCR(SR)	1	7.7	22	49	28	-34	59	4	
215983	*AP SREUCR	1	9.3	22	49	28	-32	33	33	
216113	*A3 V(P SREUCR)	A1R	9.3	22	50	32	-32	25	38	
217522	*AP (SI)CR	2R	7.5	23	1	47	-44	50	25	roAp
217704	*AP SR	1R	10.7	23	2	49	-26	54	44	
218495	*AP EUSR	1	9.3	23	9	30	-63	40	0	roAp
218994	*AP SR	2	8.1	23	13	18	-60	35	0	
219391	*A(P SREUCR)	2R	8.6	23	15	43	-27	10	42	
220352	*F0 V(P SRCR)	1	10.4	23	23	19	-38	4	21	
221127	*F6(P SR)	1R	9.6	23	29	32	-23	3	26	
221531	*AP SR	1	9.2	23	32	59	-11	59	12	
221760	*AP SRCREU	3RLB	4.86V	23	35	4	-42	36	54	
222638	*AP SREUCR	1	8.4	23	42	36	-57	29	0	
222925	*AP SREU	1	9.6	23	45	12	-61	55	0	
223967	*B8/9 III(P SICR)	A1	7.1	23	54	12	-59	33	0	
224962	*AP SR(CR)	3O	10.5	24	2	4	-22	19	37	

Table 3.4

Remarks on the Cape Survey stars from the Michigan Spectral Catalogue

2202	UNDETECTED VISUAL DOUBLE p = 172° d = 16.6" MAGS 9.5, 10.7
3980	Sr ESPECIALLY STRONG; χ PHE; HR 183; SUSPECTED VARIABLE 102327
8783	UNUSUALLY STRONG Sr 4077 AND 4216; SEE PHOTO IN ACCOMPANYING ATLAS.
11090	VERY FAINT, BUT SHOWS STRONG Sr 4077, 4216.
14944	WEAK CASE
15144	HR 710; AB CET; α^2 CVN; 5.71-5.88V; 2.997814 DAY; V SIN I=15; UNDETECTED VISUAL DOUBLE P=293 ° D=12.2 " MAGS 5.9, 8.9
18610	STRONG CASE, ESPECIALLY THE Cr AND Eu
19817	OVERLAPPED; POSSIBLY Fm δ DEL BUT OTHER UNUSUAL METAL LINES SEEM TO BE PRESENT
22488	OR SLIGHT POSSIBILITY IT IS Fm δ DEL
23393	RATHER WEAK CASE
23715	FUZZY; OVERLAPPED?; SLIGHT POSSIBILITY IT IS AN Am STAR
24712	HR 1217; DO ERI; α^2 CVN; 5.97-6.00V; 12.4580 DAY; V SIN I=5
24786	OR POSSIBLY B9 V + Ap; H WINGS MUCH BROADER THAN USUAL FOR Ap, AND Ca K IS BROAD OR WEAK
26726	STRONG CASE
27463	HR 1357
29469	PROBABLY A WEAK Ap STAR; UNDEREXPOSED
29578	Sr, Eu STRONGER THAN TYPICAL Ap; LIKE γ EQU; H LINES STRONGER, ESPECIALLY WINGS YLD. ABOUT A5; COMPOSITE?; ON PLATE 4CZ Sr EVEN STRONGER
30849	STRONG CASE, ESPECIALLY Sr
31225	BRIGHT STAR SUPPLEMENT; STRONTIUM LINES UNUSUALLY STRONG
34205	UNUSUALLY STRONG Sr
35361	DEFINITE Ap CrEu ON PLATE N BUT LOOKS LIKE NORMAL A2 IV ON PLATE Q (TAKEN THREE NIGHTS EARLIER).
36964	WEAK CASE; IF NORMAL, A7 III
40277	STRENGTH AND WINGS OF H YLD A0 BUT Ca K (FUZZY) YLD A4
41089	MAY BE Ap; WEAK CASE; Sr 4077 PRESENT
41511	HR 2148; 17 LEP; SS LEP; Z ANDROMEDAE TYPE; 4.82-5.06V; V SIN I=100; BIDELMAN TABLE 11; EMISSION CATALOGUE; Fe LINES UNUSUALLY STRONG; H CORES SHARP
42326	EARLIER TYPE THAN USUAL FOR Ap → A0 WITH BROAD H WINGS
43901	STRONG CASE
44290	OR POSSIBLY Si Cr
44550	UNDETECTED VISUAL DOUBLE AB d = 12.0" MAGS 9.1, 11.0; AC d = 20.0" MAGS 9.1, 11.1; BAD, TRICKY OVERLAP; MAY BE A NORMAL F0 STAR
45870	WEAK CASE
46649	WEAK CASE; POSSIBLY Ap SiCr
46665	OR POSSIBLY Si RATHER THAN Eu; THIS IS THE STRONGEST OF THE METAL LINES
50143	FUZZY; DUE TO OVERLAP OR POSSIBLY AN UNKNOWN DOUBLE
50304	WEAK CASE
52280	WEAK CASE
55719	HR 2727; V SIN I=66
56026	IF PECULIAR, VERY WEAK CASE; Sr STRENGTH SUGGESTS POSSIBLY Am INSTEAD
56882	OVEREXPOSED; VERY STRONG CASE
57040	VERY BAD OVERLAP; H LINES LOOK STRONG FOR STRENGTH OF METALS; MAY ALSO BE DUE TO VERY CLOSE OVERLAP.

57964 UNDETECTED VISUAL DOUBLE P=22 ° D=0.6 " MAGS 10.1, 10.2; WEAK CASE; BUT Si 4128 SEEMS STRONGER THAN IN NORMAL STARS
58935 OVERLAPPED; COULD BE Am INSTEAD
58939 BROAD H WINGS AS IN B9 OR A0 V, BUT Sr 4077 AND 4215 ARE STRONG
59660 OR A0 V; WEAK CASE
61763 H LINES FAIRLY SHARP; VERY SHARP METALLIC LINES OF Fe II, ETC., TYPICAL OF SHELL
62244 UNDETECTED VISUAL DOUBLE P=165 ° D=28.2 " MAGS 8.9, 10.0
62556 UNDETECTED VISUAL DOUBLE P=320 ° D=0.1 " MAGS 8.8, 9.1
62953 OR POSSIBLY WEAKLY Am, BUT LINE RATIOS SEEM WRONG
63745 UNDEREXPOSED AND OVERLAPPED; MAY BE Si INSTEAD OF Eu
64288 OVERLAPPED; WEAK CASE; MAY BE Ap Si INSTEAD
65963 VERY WEAK CASE
66195 K LINE LOOKS FILLED IN; Sr 4077, 4216 VERY STRONG
66318 BADLY OVERLAPPED; DEFINITELY Ap BUT ELEMENTS UNCERTAIN: Eu BY FAR STRONGEST; SLIGHT POSSIBILITY THAT IT IS Si INSTEAD
68013 OR POSSIBLY Ap SiCr
68480 OR COULD POSSIBLY BE Si
68807 UNDETECTED VISUAL DOUBLE P=324 ° D=4.0 " MAGS 9.4, 10.2
69638 WEAK CASE
71058 OVERLAPPED; WEAK CASE; VISUAL DOUBLE P=327 ° D=2.1 " MAGS 10.2, 11.8
72611 OR POSSIBLY Ap SiCr
72801 WEAK BUT DEFINITE CASE
73403 WEAK CASE
73455 Sr MUCH STRONGER THAN OTHER ELEMENTS
73850 UNDETECTED VISUAL DOUBLE P=48 ° D=2.6 " MAGS 9.5, 12.0
74067 HR 3439; V SIN I=50; UNDETECTED VISUAL DOUBLE P=64 ° D=4.0 " MAGS 5.2, 8.5; OVEREXPOSED; WEAK CASE
74169 OR POSSIBLY Ap SiCr; IN CLUSTER IC 2391
74555 UNDETECTED VISUAL DOUBLE P=311 ° D=6.7 " MAGS 9.4, 10.8
75049 OR VERY POSSIBLY Si RATHER THAN Eu
75130 OR COMPOSITE OF Ap Si + A? H HAS VERY STRONG DWARFISH WINGS UNLIKE USUAL Si STAR; ALSO OTHER LINES ARE PRESENT.
75163 PROBABLY Ap; STRONG FEATURE AT ABOUT 4128, BUT MAY BE COMPOSITE OR OVERLAP; FEATURES IN BLUE SOMEWHAT WASHED OUT
75425 WEAK CASE; UNDETECTED VISUAL DOUBLE P=288 ° D=0.4 " MAGS 9.9, 10.0
76225 PROBABLY COMPOSITE; Sr UNUSUALLY STRONG EVEN IF LATER COMPONENT IS A GIANT
76276 WEAK CASE
76759 UNDETECTED VISUAL DOUBLE P=256 ° D=0.8 " MAGS 9.3, 11.2; WEAK BUT DEFINITE Ap
77830 UNDETECTED VISUAL DOUBLE P=277 ° D=2.5 " MAGS 9.1, 11.4
80211 SOME CHANCE THAT Ap APPEARANCE IS DUE TO OVERLAP RATHER THAN Eu AND Cr
80316 VERY STRONG Sr
81076 WEAK CASE
82093 BRIGHT STAR SUPPLEMENT
82417 WEAK CASE; MAY BE WEAK Am INSTEAD
82989 COMPOSITE; STRONG Sr
83368 HR 3831; STRONG Sr; UNDETECTED VISUAL DOUBLE P=179 ° D=3.2 " MAGS 6.6, 9.0
83817 LOOKS LIKE Fm δ DEL EXCEPT THAT Ca H + K ARE NOT NARROW.
84041 UNDETECTED VISUAL DOUBLE D=8. " MAGS 9.2, 13
87488 WEAK CASE
88042 OR POSSIBLY Ap Si
88241 STRONG Sr
88701 FAIRLY WEAK BUT DEFINITE CASE
89075 OR POSSIBLY Ap Si OR Am; SOMEWHAT OVERLAPPED
89192 WEAK CASE
89385 IF Ap, A VERY WEAK CASE EXCEPT FOR Cr
89393 UNDETECTED VISUAL DOUBLE P=323 ° D=6.0 " MAGS 8.3, 9.4
89840 SPECTRUM OVERLAPPED, FAINTISH; POSSIBLY Eu INSTEAD; Ca K LINE STRONG (YLD A2) FOR Si STAR

91239 WEAK CASE
91520 FAIRLY WEAK CASE; H WINGS BROADER THAN USUAL FOR Ap STARS
91735 λ4300 IS UNUSUALLY STRONG, 4312 PRESENT BUT NOT=4300 AS IT IS IN A/F SUPERGIANTS; H LINES DWARFISH
91982 UNUSUALLY BROAD STRONG H YLD A3/5 V THOUGH Ca K STRENGTH YLD A9/F0
92286 OR POSSIBLY Si INSTEAD
94660 HR 4263; WEAK CASE; MAY BE Ap (EuCr)
95158 WEAK CASE BUT POSSIBLY Ap
95508 WEAK BUT DEFINITE CASE
95811 OR POSSIBLY A STRONG CASE OF Fm δ DEL
96451 WEAK CASE
96537 UNDETECTED VISUAL DOUBLE P=294 ° D=26.8 " MAGS 9.2, 11.2
96616 HR 4327; V SIN I=56; UNDETECTED VISUAL DOUBLE P=260 ° D=1.4 " MAGS 5.5, 8.0
100587 UNDETECTED VISUAL DOUBLE P=88 ° D=0.5 " MAGS 8.0, 10.0
101189 HR 4487; V SIN I=0
101410 WEAK CASE

102983 PROBABLY WEAK Ap; Sr AND Eu OR Si MAY ALSO BE WEAKLY PRESENT. UNDETECTED VISUAL DOUBLE p = 257° d = 0.9" MAGS 9.9, 11.6
104402 WEAK CASE; BROAD H WINGS
106322 WEAK BUT DEFINITE CASE
106374 OR POSSIBLY COMPOSITE OR Am
109300 OR COULD BE Ap Eu(Sr)
109426 H SEEMS STRONG (A7) FOR Ca K TYPE (F0).
109989 FAIRLY WEAK CASE
110072 SPECTRUM IN HD POSITION IS DEFINITELY OF TYPE Ap, RATHER THAN K AS GIVEN IN HD CATALOGUE
112616 WEAK CASE
116114 BRIGHT STAR SUPPLEMENT
116458 H LINES YLD B9 III; NO OTHER CONSPICUOUS LINES BUT MANY WEAK ONES, POSSIBLY Cr AND Si; NOT A NORMAL Ap STAR; HR 5049
116763 SLIGHT CASE
117025 HR 5069
117227 OR POSSIBLY Am
118913 λ4005 FEATURE ALSO PRESENT; PROBABLY NOT AS STRONG AS IN HD 96884
119158 WEAK CASE
119794 Cr, Eu, Sr ALL STRONG
121276 He 4026 IS FAIRLY STRONG, WITH Ca K BEING EVEN STRONGER (YLD A1). MAGNESIUM MAY ALSO BE STRONG; 4471 = 4481.
121675 H WINGS MUCH BROADER THAN USUAL IN Ap STAR; Ca K ALSO BROAD SO MAY BE COMPOSITE
121788 WEAK CASE; POSSIBLY Am INSTEAD
122525 STRONG CASE
123112 IF Ap, VERY WEAK CASE

124740 VERY WEAK CASE; MAY BE NORMAL B9 IV
125467 SLIGHTLY FUZZY; VISUAL DOUBLE P=249 ° D=1.8 " MAGS 9.5, 9.6
125555 SLIGHTLY FUZZY; STRONG H; NOT A KNOWN VISUAL DOUBLE
126365 OR POSSIBLY Fm δDEL BUT METALS IN GENERAL NOT STRONG THOUGH Ca H + K ARE NARROW
126936 WEAK CASE
127159 BADLY OVERLAPPED; POSSIBLY Ap
127241 SOME LINES BETWEEN Hβ AND Hγ SEEM STRONGER THAN USUAL.
127608 STAR HAS PG MAG ABOUT 8.5 RATHER THAN 10.0 AS LISTED IN THE HD CATALOGUE. CPD MAG IS BRIGHT (8.2) ALSO.
128540 WEAK CASE
128898 α CIR A; HR 5463; V SIN I=0; VISUAL BINARY P=232 ° D=15.7 " MAGS 3.4, 8.8
130336 OVERLAPPED, BRIGHT EARLY Ap SPECTRUM (NO Ca K) SEVERAL LINES AROUND Hδ INCLUDING TWO IN POSITIONS OF 4128 AND 4077 (WEAK) AND TWO OTHERS AROUND 4155 AND 4185

130559 HR 5523; μ LIB; UNDETECTED VISUAL DOUBLE P=355 ° D=1.8 " MAGS 5.8, 6.7; BUT ALSO DEFINITELY Ap
131870 OR POSSIBLY Ap Si
132322 Sr IS EXTREMELY STRONG.
132981 UNDEREXPOSED AND OVERLAPPED, BUT Sr (4077 AND 4216) EXTREMELY STRONG
133792 HR 5623
134507 WEAK CASE; POSSIBLY WEAK Am INSTEAD
134640 Ca H + K QUITE STRONG YLD F5/7; UNDETECTED VISUAL DOUBLE P=355 ° D=56.1 " MAGS 9.4, 10.4
135396 OR POSSIBLY Fm δ DEL, THOUGH METALLIC LINES ARE NOT PARTICULARLY STRONG.
135512 OR POSSIBLY Si RATHER THAN Eu; THERE ARE A NUMBER OF LINES BETWEEN Hβ AND Hγ
137509 DEFINITELY Ap, BUT NOT TYPICAL; MANY LINES MAY BE DUE TO Fe.
137949 BRIGHT STAR SUPPLEMENT; GZ LIB; α^2 CVN; 6.66-6.71V
138146 OR POSSIBLY Am
138927 OVERLAPPED; POSSIBLY Am INSTEAD
139631 RATHER WEAK CASE
140220 WEAKISH BUT DEFINITE CASE
142823 OR POSSIBLY Ap CrEu; ALSO THERE IS A RATHER STRONG LINE ABOUT 4145 -- He? BUT He 4026 IS ABSENT AND MOST LINES YLD B9 FOR SPECTRAL TYPE.
143487 OVERLAPPED; MANY LINES; PROBABLY Sr, Eu, Cr, BUT MANY OTHERS ALSO
144897 WEAK CASE; MAY BE Si RATHER THAN Eu
145393 POSSIBLY Ap
148593 UNUSUALLY STRONG Sr
148848 OR POSSIBLY Ap SiCr
148898 HR 6153; ω OPH; α^2 CVN; 4.44-4.51V; 2.99: DAY
150562 UNDEREXPOSED; DIFFERENT CRITERIA YIELD DIFFERENT SPECTRAL TYPES; H LINES AND Ca K YLD. A7/9; G BAND YLD. F3; THERE IS A STRONG FEATURE ABOUT 4128-30.
150862 COMPOSITE WITH A STAR WITH STRONG Sr; EITHER Ap OR GIANT; SPECTRUM IN GENERAL IS DWARFISH
151873 SPECTRUM SHOWS MANY Fe LINES AND OTHER TYPICAL SHELL LINES; Hβ IS SLIGHTLY FILLED IN; EMISSION CATALOGUE
152137 H WINGS MORE DWARFISH THAN IN MANY Ap STARS
153192 OR POSSIBLY Ap SiCr
153201 OR POSSIBLY Ap (EuCrSr); SUSPECTED VARIABLE 101618, 6.6V
153953 POSSIBLY ALSO COMPOSITE; SHOWS G BAND AND STRONGISH λ4226; STRENGTH OF PECULIAR LINES, H LINES AND Ca H + K SEEMS TO VARY FROM PLATE TO PLATE.
154075 OR POSSIBLY Ap SiCr
154645 UNDETECTED VISUAL DOUBLE P=291 ° D=13.7 " MAGS 8.7, 11.5
154708 OR POSSIBLY Si RATHER THAN Eu; SPECTRUM, ABOUT F0, SHOWS MANY LINES.
156495 VERY WEAK CASE
156808 WEAK CASE
157208 OR MAY BE Am; VERY OVERLAPPED AND UNDEREXPOSED
157289 POSSIBLY Ap BUT VERY WEAK CASE; COULD BE NORMAL A1 IVs
158205 EXTREMELY BAD OVERLAP
161423 STRONG H, BROAD WINGS
161704 PROBABLY COMPOSITE; EARLY-TYPE STAR PROBABLY Ap, BUT BADLY OVERLAPPED
162639 STRONTIUM EXTREMELY STRONG (4077 = Hδ)
163256 OR MAY BE Am
163379 PROBABLY A WEAK Ap STAR
163712 OR COULD BE LATE Am; Sr IS UNUSUALLY STRONG.
164485 OR POSSIBLY LATE Am OR Fm δ DEL WITH STRONG Sr
166223 OR POSSIBLY Eu RATHER THAN Si
166469 HR6802; V4045 SGR; AMPLITUDE 0.013v; 2.90^d; IF PECULIAR, VERY WEAK CASE
167288 RATHER WEAK CASE; ALSO POSSIBLY Sr
168767 OR POSSIBLY Ap SiCr
169965 UNDETECTED VISUAL DOUBLE p = 35° d = 4.6" MAGS 8.9, 10.9; WEAK CASE; POSSIBLY Ap SiCr INSTEAD

170397 HR 6932; V432 SCT; α CYGNI TYPE; MAX 5.96, AMPL. 0.012V; 2.1912 DAY; OR POSSIBLY Si RATHER THAN Eu
173600 UNDEREXPOSED; Ca K LOOKS STRONG FOR H-LINE TYPE.
176519 DOUBLE? NOT TYPICAL Ap; H WINGS VERY BROAD YLD A0 V
178246 OR POSSIBLY Ap CrEu
181810 CPD -21 ° 7349; NOT IN SD CATALOGUE
183806 HR 7416
184120 UNDETECTED VISUAL DOUBLE P=235 ° D=1.9 " MAGS 10.4, 12.5
186117 WEAK CASE
186284 OVERLAPPED; POSSIBLY Fm δDEL OR LATE Am INSTEAD
187473 WEAK BUT DEFINITE CASE
187474 HR 7552; V3961 SGR; ABUNDANCE, MNASSA, 23, 6, 1964; V SIN I=0; H=-1878 GAUSS (BABCOCK); WEAK CASE
188008 Ca K LOOKS FUZZY AS IF PERHAPS DOUBLE; NOT A KNOWN DOUBLE
188518 UNDEREXPOSED AND FUZZY; VISUAL DOUBLE p = 73° d = 2.9" MAGS 10.2, 10.9; ONE COMPONENT POSSIBLY PECULIAR
194623 Sr 4077 SEEMS VERY STRONG, BUT MAY BE DUE TO DEFECT
194726 WEAK CASE; POSSIBLY Am INSTEAD
194750 VERY WEAK CASE
202400 Sr 4077 STRONG BUT 4216 VERY WEAK
203006 HR 8151; θ MIC; α CVN TYPE; 4.77-4.87V; 1.062 DAY; V SIN I=48; H=-650 (VAR) GAUSS (BABCOCK)
204367 WEAK CASE; IF NORMAL, SPECTRAL TYPE IS A0IV/Vs
208759 Sr ESPECIALLY STRONG
212385 STRONG CASE
215185 BADLY OVERLAPPED; POSSIBLY Am INSTEAD OF Ap
216113 IF Ap, WEAK CASE
217522 MAY BE Eu RATHER THAN Si
217704 H WINGS MUCH STRONGER THAN USUAL FOR Ap STAR
219391 MAY BE COMPOSITE OR Am, BUT METALS WEAK FOR Am; Ca YLD. A1, BUT THERE SEEMS TO BE AN F3 TYPE G BAND
221127 COULD BE F6 III BUT OTHER METALS ARE DWARFISH; POSSIBLY COMPOSITE; Ca H AND K ARE NARROW FOR TYPE, BUT EQUAL
221760 HR 8949; ι PHE; α CVN TYPE; 4.70-4.75V; 12.5 DAY; V SIN I=22; WEAK POSITIVE MAGNETIC FIELD (BABCOCK); VERY OVEREXPOSED
224962 CoD -23 ° 18120 IF NUMBERING ERROR IN CoD CATALOGUE PAGE 117 IS CORRECTED

Table 3.5

Candidate SrCrEu stars from Table IV of Bidelman & MacConnell (1973) with $\delta > -12°$.

HD NO	SPECTRAL TYPE	VIS MAG	POSITION (2000) α H M S	δ ° ′ ″
9289	SrEu	9.6	1 31 15	-11 7 4
19712	CrEu	7.8	3 10 21	- 1 42 11
21799	SrEu(F)	9.3	3 30 44	- 2 0 27
22032	SrEu(F)	8.9	3 33 15	+ 4 40 14
25163	SrCr	8.7	3 59 51	- 4 30 57
28238	SrCrEu	9.2	4 27 32	+ 6 36 27
28520	SrEu	9.6	4 29 47	- 0 55 50
-	SrEu	8.8	4 44 5	- 0 57 46
-	SrCrEu	9.5	4 51 22	+ 9 36 13
-	SrCrEu(F)	9.0	5 3 36	- 2 57 30
-	CrEu(F)	9.5	5 15 1	+ 8 4 53
34162	SrCrEu(F)	9.0	5 15 32	+ 5 45 48
35353	SrCrEu	8.6	5 23 47	- 8 16 23
36955	CrEu	9.6	5 35 9	- 1 24 1
-	SrCrEu	9.3	5 35 11	- 0 50 1
38823	SrEu(F)	7.7	5 48 29	- 0 45 56
39082	SrCrEu	7.5	5 50 24	+ 4 56 44
40711	SrCrEu	8.3	6 1 1	+10 24 14
40759	CrEu	8.4	6 0 46	- 3 53 44
41403	SrCrEu	8.2	6 4 59	+ 2 6 38
-	SrCrEu(F)	9.5	6 9 4	- 1 5 56
42382	CrEu	9.1	6 10 32	+ 3 9 50
43408	SrEu	7.7	6 16 3	+ 0 52 1
44947	SrEu(F)	8.4	6 24 39	+ 0 53 46
45107	CrEu	8.9	6 25 33	+ 1 8 39
45564	CrEu	9.3	6 28 22	+ 3 56 14
-	SrCrEu	9.0	6 29 51	+ 6 10 2
-	SrEu	9.3	6 30 40	+ 3 51 54
47074	SrCrEu	8.9	6 36 52	+ 1 19 0
47612	SrEu	9.1	6 39 14	- 7 5 20
48668	SrCrEu	9.1	6 44 14	- 7 8 3
49223	SrEu	8.9	6 47 41	+ 7 19 28
49976	SrEu	6.2	6 51 18	+ 7 48 57
-	CrEu	9.5	6 51 56	+ 3 19 51
50169	SrCrEu	8.9	6 51 57	- 1 39 8
50733	Sr	8.9	6 54 36	- 0 26 30
-	SrCrEu(F)	9.3	6 54 59	+ 4 8 25
53116	SrEu	8.5	7 3 46	- 1 6 49
-	SrCrEu	-	7 5 56	- 5 7 7
55852	SrCrEu	8.9	7 14 26	- 7 34 18
-	SrCrEu	9.4	7 19 20	- 7 31 59
-	SrEu(F)	9.2	7 24 34	- 6 26 42
59021	CrEu	10.0	7 27 41	-11 48 8
59435	SrCrEu(F)	7.9	7 29 35	- 9 15 23
60210	SrEu	9.0	7 33 26	+ 0 14 5
62512	SrEu	9.0	7 44 18	- 0 45 20
-	CrEu	9.3	7 48 50	+ 0 17 3
-	SrCrEu	9.3	7 49 58	+ 1 35 54
-	SrEu	9.1	7 50 18	- 3 7 7
63843	CrEu(F)	9.6	7 50 43	- 6 3 11
66350	CrEu	8.3	8 3 1	- 2 43 45

HD NO	SPECTRAL TYPE	VIS MAG	POSITION (2000) α H M S	δ ° ′ ″
66533	CrEu	9.1	8 3 44	- 8 21 51
72295	SrCrEu	7.8	8 31 44	- 8 51 14
126515	SrCrEu	7.0	14 25 59	+ 0 59 55
135297	SrCrEu	8.0	15 14 24	+ 0 21 37
138218	Sr	9.1	15 30 53	- 5 49 31
138633	CrEu(F)	8.7	15 33 39	-11 4 12
138777	SrEu(F)	9.2	15 34 25	- 6 53 7
142070	SrCrEu	7.9	15 52 32	- 0 59 56
142544	CrEu	9.7	15 55 22	- 4 28 35
146971	SrCrEu	8.6	16 19 27	- 9 37 32
149046	SrCrEu	9.5	16 32 28	- 7 10 48
158450	SrCrEu	8.0	17 29 43	- 8 0 47
-	SrCrEu	9.3	17 33 58	+ 0 58 50
164258	SrCrEu	6.3	18 0 18	+ 0 37 40
164827	CrEu	9.1	18 3 2	- 0 26 55
170565	SrCrEu(F)	8.7	18 30 12	- 2 35 58
171279	SrEu	7.2	18 34 12	- 7 42 24
180058	Sr(F)	9.3	19 15 27	-11 43 34
189963	SrCrEu(F)	9.5	20 2 56	- 6 26 15
219831	Sr	9.9	23 18 59	- 9 4 11

Chapter 4

Strömgren *uvby* and Hβ photometry of the southern Ap stars

4.1 Introduction

The Cape Survey comprises two observational programs. The first program, a program of all-sky photometry, is to determine the Strömgren photometric indices of all the southern Ap SrCrEu stars. The second program is to search for rapid oscillations in as many Ap SrCrEu stars as possible to discover new roAp stars and, specifically, to determine the photometric temperature and luminosity limits of the roAp phenomenon. In this chapter we discuss the all-sky photometry component of the Cape Survey. The stars observed in this part of the survey were the 558 Ap SrCrEu stars in the four currently available volumes of the *Michigan Spectral Catalogue* (Houk & Cowley 1975; Houk 1978, 1982; Houk & Smith-Moore 1988) which covers all the southern HD stars up to a declination of -12°. We were able to supplement this list of candidates with a further 71 Ap SrCrEu stars north of δ = -12° taken from Table IV of Bidelman and MacConnell's (1973) compilation of astrophysically interesting southern stars. This extends our coverage to the celestial equator in a patchy fashion until further volumes of the Michigan Spectral Catalogue become available. We remind the reader that the *Ap SrCrEu* designation is used in a generic sense in this thesis to refer to Ap stars with line strength anomalies of one or more of these elements.

4.2 The *uvby* Hβ photometric system

The Strömgren (1966) *uvby* system is an intermediate bandwidth photometric system characterized by an astrophysically judicious choice of passbands. The system is designed to be entirely filter defined and independent of the spectral response of the detector. Manfroid & Sterken (1987) and Manfroid *et al.* (1991) have shown that this is not entirely true in practice. The Strömgren system is often supplemented with the Hβ index (Crawford & Mander 1966) which measures the strength of the Hβ line of the Balmer series of hydrogen. Two filters are used, $H\beta_{W(ide)}$ and $H\beta_{N(arrow)}$, and the index is computed as $\beta = m_W - m_N$ where m_W and m_N represent the magnitudes through the wide and narrow filters, respectively. Because the Strömgren *uvby* system is so often supplemented with a β index as well, the combination of these systems is referred to as the *uvbyβ* system. The filter

transmission curves published by Crawford (Golay 1974) are reproduced in Fig. 4.1 and the characteristics of the $uvby\beta$ system are summarized in Table 4.1

Table 4.1

Characteristics of the $uvby\beta$ photometric system

Filter	Central wavelength	Half-width
u	3500 Å	380 Å
v	4100 Å	200 Å
b	4700 Å	100 Å
y	5500 Å	200 Å
β_W	4860 Å	150 Å
β_N	4860 Å	30 Å

The $uvby\beta$ system was designed to be most useful for the B-, A- and F-type stars and it is well calibrated in this temperature range for normal stars. The $uvby\beta$ calibrations have been done by Crawford (1975, 1978, 1979) and Grønbech & Olsen (1976, 1977). The system is also well defined in terms of primary and secondary standard stars (Crawford & Barnes 1969, 1970, Crawford & Mander 1966, Perry Olsen & Crawford 1987, Cousins 1987, 1989). These features make the $uvby\beta$ system the ideal standard photometric system to use for the Cape Survey.

In the $uvby\beta$ system five parameters are used: y, $(b\text{-}y)$, m_1, c_1 and β. The y band gives the apparent visual magnitude. It is transformed to be the same as the V magnitude of the Johnson UBV system. Figure 4.2 is a schematic diagram devised by Crawford which shows the effects of line blanketing and the Balmer discontinuity on the intensity. For normal stars the blocking in the b and y bands is practically the same. Thus $b\text{-}y$ is reasonably insensitive to the abundance of lines in the spectrum and may be used as an indicator of effective temperature analogous to $B\text{-}V$ in the Johnson system. It is possible to devise indices which measure line blocking and the Balmer discontinuity:

$c_1 = (u\text{-}v) - (v\text{-}b)$ a measure of the Balmer discontinuity

$m_1 = (v\text{-}b) - (b\text{-}y)$ a metallicity or peculiarity indicator

The motivation for these definitions may be appreciated in Fig 4.2. The c_1 parameter is defined to eliminate the difference in blocking between u and v such that c_1 has little dependence on the chemical composition. The β index is a narrow-band index which measures the strength of the Hβ line

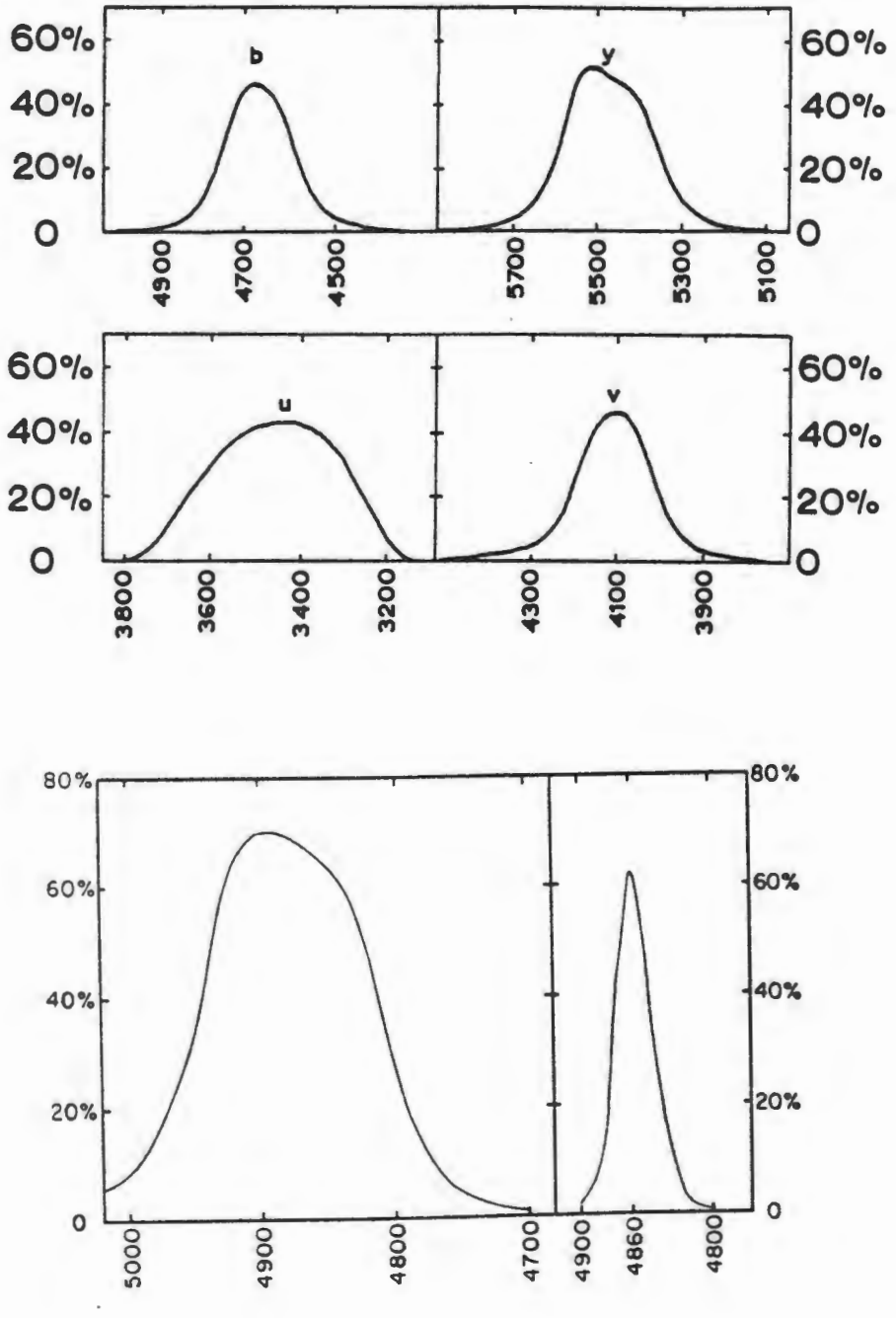

Figure 4.1 Transmission curves for the *uvby* filters (Crawford 1966) and the Hβ filters (Crawford & Mander 1966).

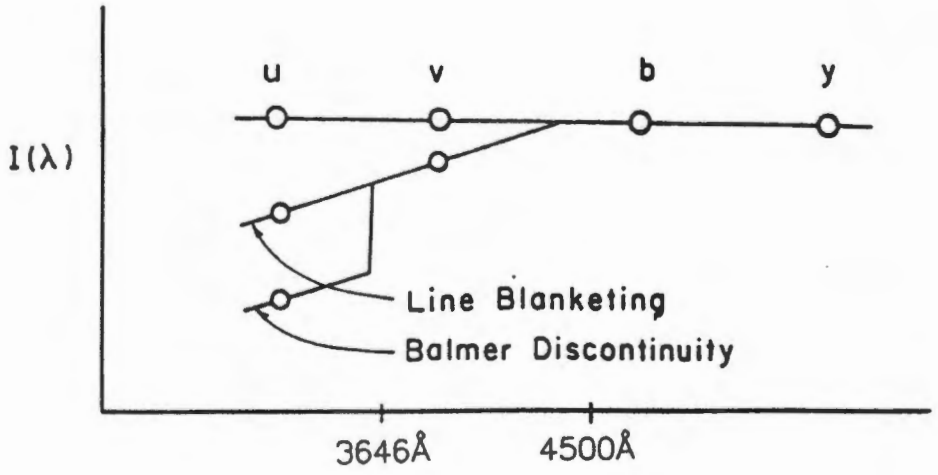

Figure 4.2 A schematic illustration by Crawford (Golay 1974) of the effect of line blanketing and the Balmer discontinuity on the intensities in the *uvby* passbands.

in the star's spectrum. It is free of extinction effects since both filters used to determine β have the same effective wavelength. For the A- to G-type stars β is a temperature indicator.

4.3 The instrumentation used for the all-sky *uvbyβ* observations

The photometry presented in this chapter was acquired using the Modular Photometer attached to the 0.5-m Boller and Chivens Cassegrain telescope of the South African Astronomical Observatory (SAAO) at Sutherland in the Karoo. The observations were acquired during 20 weeks of observing spanning the period May 1990 - June 1992. The Modular Photometer has been described in detail by Kilkenny *et al.* (1988) so we will give only a brief description of this instrument here. The Modular Photometer is a visual region single-channel photometer of conventional design except that the major components are all in the form of modules that plug into a chassis. This greatly facilitates filter changes, instrument testing and general maintenance. Backup modules for the mechanical and electronic units have been constructed and can be 'plugged in' in the event of a fault to minimize the amount of instrument down time. In practice, the Modular Photometer is the most stable and reliable of the SAAO instruments since it is permanently attached to the SAAO 0.5-m telescope and in continuous use.

The photo-detector is a Hamamatsu R943-02 GaAs photomultiplier tube housed in a thermoelectrically cooled unit to minimize the dark current. One disadvantage of these photomultiplier tubes is that they cannot tolerate high illumination levels; when they are over-illuminated, the sensitivity is enhanced in an unpredictable way. For the photomultiplier tube used in these observations, satisfactory results are obtained up to a counting rate limit of 4×10^5 Hz. This translates to a magnitude limit of $V \approx 6.5$; a series of neutral density filters is available for the observation of brighter stars. Another problem with these GaAs photomultiplier tubes is that they increase markedly in sensitivity when exposed to the first star at the start of the night. This problem is solved by exposing the photomultiplier tube to a bright E-region standard during evening twilight until the response stabilizes.

The instrument is controlled by an IBM AT microcomputer to which two SAAO-designed interface cards have been added. One of the cards is the instrument interface card which provides a 16-bit counter to count the incoming pulses as well as 16 TTL inputs and 16 TTL outputs to interrogate and control the instrument. The other card is a time and graphics display interface. Pulses from the photomultiplier tube are fed into an SSR discriminating amplifier whence they are routed to

the computer to be counted. The coincidence counting time, or 'dead time', during which two incoming photons produce only one count has been measured to be 40 ns for this system.

The observer controls the instrument and data acquisition from the computer console via menu-driven software (Balona 1988a,b) which allows the specification of the program of stars to be observed, the sequence of filters to be used for each star and the integration time per filter. Lists of $UBVR_CI_C$ and $uvby\beta$ standard stars are stored on disk so that rough zero points can be determined in real time. The computed magnitudes and colours are displayed at the end of each filter sequence. This provides a very useful check at the telescope that the correct star has been observed.

Telescope pointing and dome rotation are not automated for this telescope. Through the judicious selection of program stars we were able to minimize the amount of transition time between observations. On perfectly clear winter nights we were able to observe up to ~65 stars (including standards) and on summer nights ~45 stars. An automatic photoelectric telescope (APT) would probably observe at a considerably higher efficiency, especially for the fainter program stars in crowded fields. My observations were always acquired under the best photometric conditions. If I was the least bit suspicious about the quality of the sky, I would change to doing high-speed monitoring of a single star. As a result of this I have rejected only a very small number of observations, usually those acquired just before the switch to high-speed monitoring. It would be interesting to see whether an APT instrument could be as conservative since the recipients of APT data have to vet their data *post facto* without much knowledge of the atmospheric conditions under which the observations were done.

4.4 The $uvby\beta$ observations

The program stars were found using computer-generated finding charts produced from the electronic version of the *Michigan Spectral Catalogue*. These charts only show stars down to m_{pg} = 10 but they are adequate for identification purposes since, in most cases, the program stars are usually the brightest in their fields. In cases of confusion, photographic finding charts were produced using the ESO *B* southern sky survey plates.

The stars were observed in the filter sequence β_W, β_N, y, b, v, u, u, v, b, y, β_N, β_W, where β_N and β_W denote the Hβ narrow and Hβ wide filters, respectively. The filter sequence was defined in this way so that the effective time of the observation through all filters is the same. The u observations were done closest in time because the sky transparency changes most quickly in this

pass-band. Typical integration times were 25 s per filter for bright stars ($V < 7.0$) and 60 s per filter for faint stars ($V \geq 7.0$). Each filter sequence on the star was followed by a u, v, b, y, β_N, β_W sequence on the sky with an integration time of 10 s per filter. To average over the rotational photometric variations in these Ap stars we tried to acquire at least three observations of each star on different nights.

A 30 arcsec aperture was used for most of the observations presented in this chapter. This aperture is large enough to minimize the noise introduced by seeing fluctuations and telescope tracking errors; larger apertures were used when conditions dictated. Considerable care was taken to identify faint stars lying inside or on the edge of the aperture centered on the program star. For this purpose an image intensifier (VARO) tube was used. In quite a number of cases, one or more faint stars fell just within a 30 arcsec aperture centered on the program star. In such cases, the observations were done using smaller (say, 20 arcsec) apertures. Such observations were done only on nights where the seeing was judged to be ≤ 2 arcsec.

To monitor slight shifts in the zero points of the transformations we observed at least one standard star every half hour to 3/4 hour, depending on the quality of the night. The standard stars were selected from Cousins' (1987, 1989, 1990) compilations of secondary Harvard E-region $uvby\beta$ standards. We chose Cousins' standards because of the high quality of his observations and because of the need to use fainter standards to avoid excessive dead time corrections. Rather than reobserving the same pair of standards periodically, different standards were observed at a range of airmasses to allow the estimation of extinction. On nights when rapid extinction variations were noted, we switched to doing high-speed photometry of roAp star candidates. At least with high-speed photometry one gets all the information about the extinction variations. This is more efficient use of the telescope than having to do a standard star after every program star to monitor the extinction.

The observations were corrected for the 40 ns coincidence counting or 'dead time' losses and the sky background. Airmass corrections were then applied using extinction coefficients derived independently for each night. The resulting instrumental magnitudes were then transformed to the standard system using the following relations:

$$V = A + B(b-y) + y_*,$$
$$(b-y) = C + D(b-y)_*,$$
$$m_1 = E + Fm_{1*} + G(b-y),$$
$$c_1 = H + Ic_{1*} + J(b-y),$$
$$H\beta = K + LH\beta_*,$$

where the subscript * refers to the instrumental system. During the 1990 season, standard star reductions indicated that the telescope/photometer/filter characteristics remained constant. For this reason, only zero point corrections were applied to mean transformations on a nightly basis. During the 1991 season, the reductions had to be done on a more general basis for two reasons: (1) The Strömgren *y* filter began deteriorating gradually. This was first noted as a fine mottled "growth" that grew from the edges inwards. (2) The volcanic activity in the Philippines resulted in highly variable extinction at Sutherland for months afterwards. For reduction purposes, nights often had to broken up into chunks and analyzed piece-wise.

4.5 Observed and Intrinsic photometric indices for the Ap stars

The observed Strömgren and Hβ photometric indices of the Ap stars are given in Table 4.2. The rms residuals for the standard stars from the nightly transformations were found to be: $\sigma(y) = 0.015$, $\sigma(b\text{-}y) = 0.005$, $\sigma(m_1) = 0.008$, $\sigma(c_1) = 0.012$ and $\sigma(\beta) = 0.005$. The deteriorating *y* filter is reflected by the large standard deviations of the *y* observations for those data. Standard star residuals for all the nights are plotted in Figures 4.3 - 4.5. The scatter is slightly higher than one would hope, but it must be remembered that these are *all* the standard star observations done during 20 weeks of observing spanning 2 years. There are no obvious systematic effects in the range of interest for the residuals against $(b\text{-}y)$ and V. The standard star residuals with respect to time (Fig. 4.5) illustrate two points. Firstly, the deterioration of the *y* filter did not seriously affect the results; this deterioration started at the edges of the filter and was detected early enough to alert us to possible effects. The second point that these diagrams illustrate is a very mild seasonal variation in the residuals of the c_1 index. This variation is at such a low level that we elected not to remove it.

Table 4.2 was prepared as follows: No attempt was made to analyse program star data from the different runs separately. The observations were averaged and the internal consistency of the multiple observations provides an independent error estimate. The indices δm_1 and δc_1 were computed using the standard relations given by Crawford (1975):

$$\delta m_1 = m_1(\beta, \text{standard}) - m_1(\text{observed})$$

and

$$\delta c_1 = c_1(\text{observed}) - c_1(\beta, \text{standard}).$$

The parameter δm_1 measures differences in blanketing for stars of the same β. The δc_1 parameter measures the Balmer discontinuity difference for two stars of the same β. For normal stars it

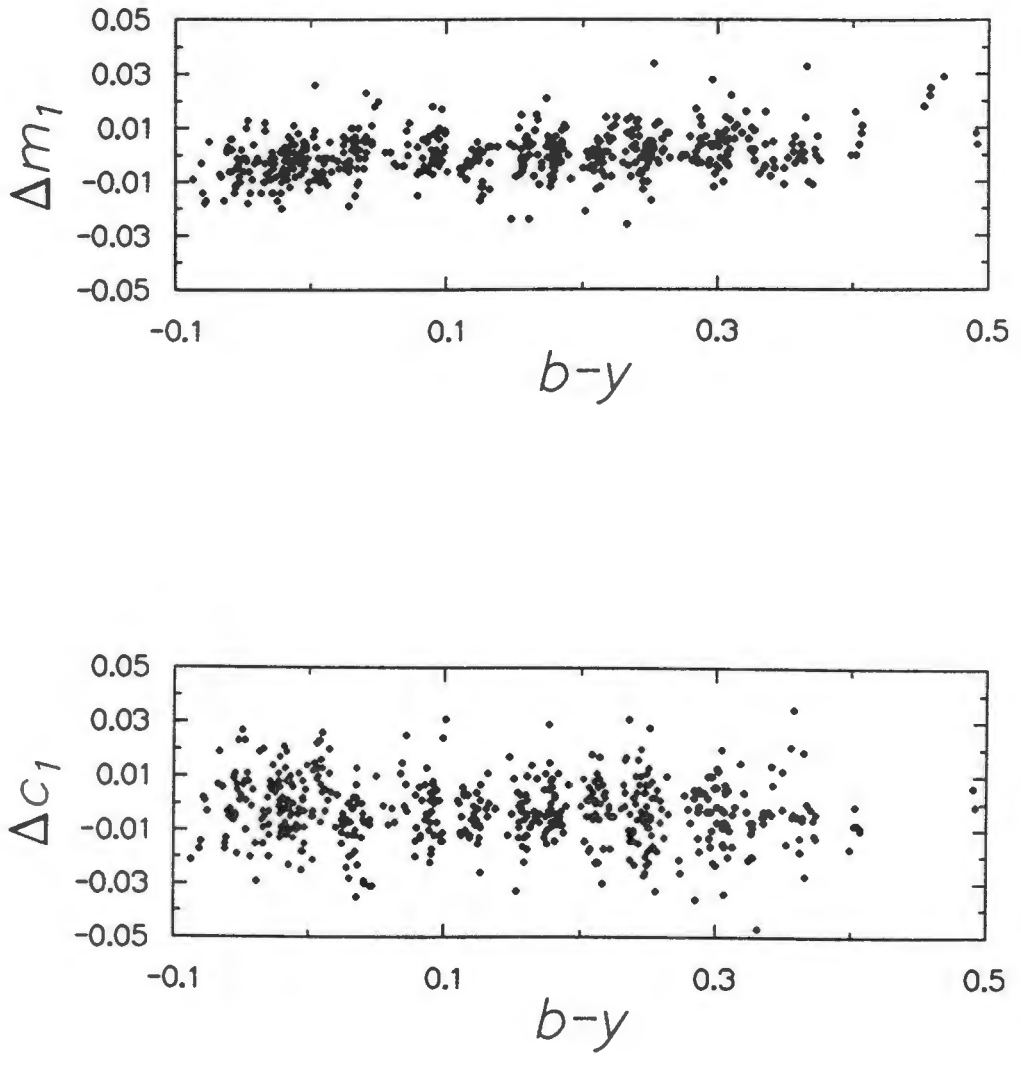

Figure 4.3 The m_1 and c_1 residuals for the standard stars from the nightly transformations as a function of $(b\text{-}y)$. There are indications that the m_1 residuals fall off slightly for $(b\text{-}y) < 0.05$ and rise slightly for $(b\text{-}y) > 0.35$. In the range of interest, $0.05 \leq (b\text{-}y) \leq 0.35$, there are no obvious systematic trends. For the c_1 residuals there are no systematic effects over the entire colour range shown.

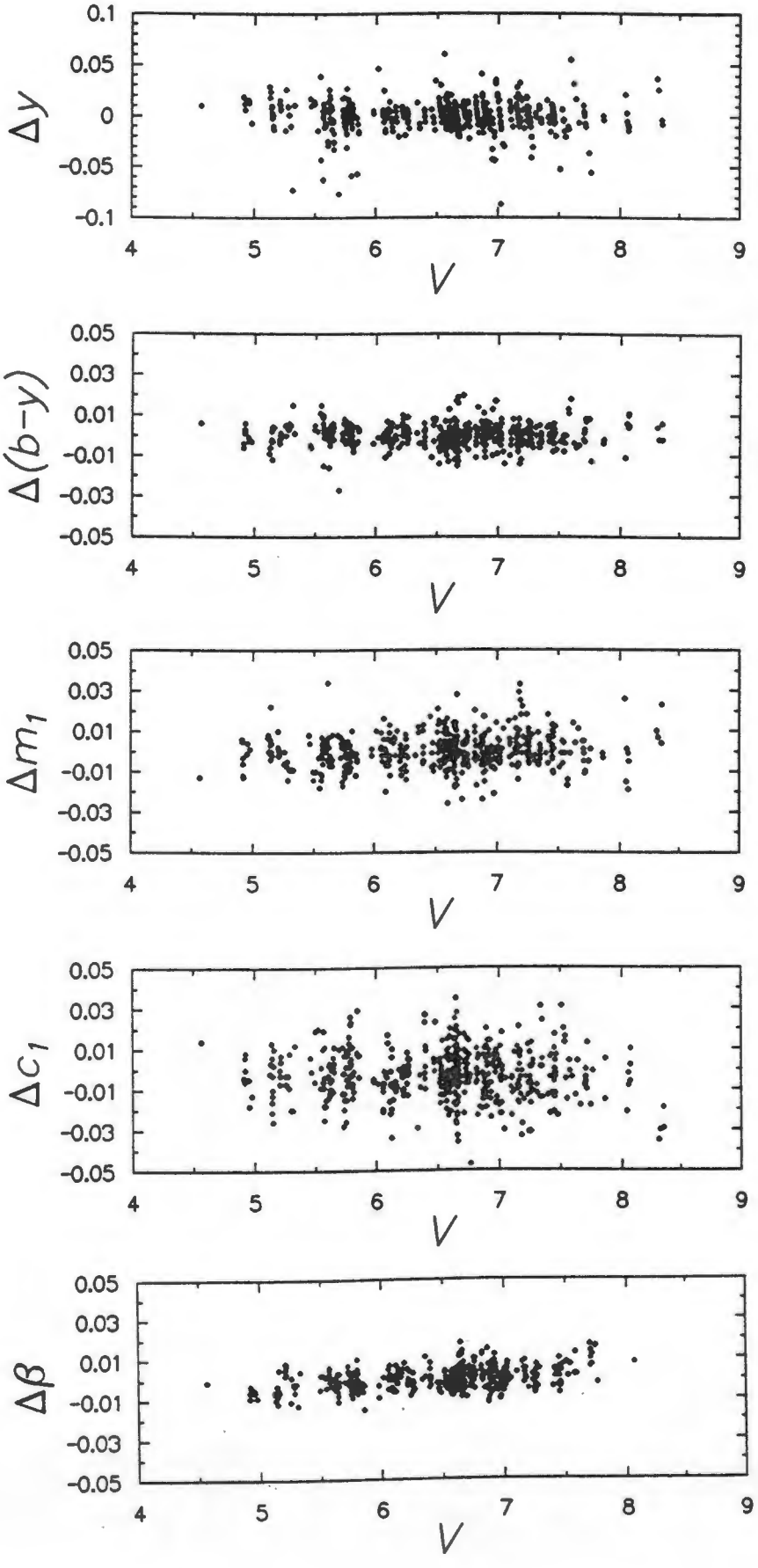

Figure 4.4 The residuals from the nightly transformations for all of the standard star observations plotted as a function of V.

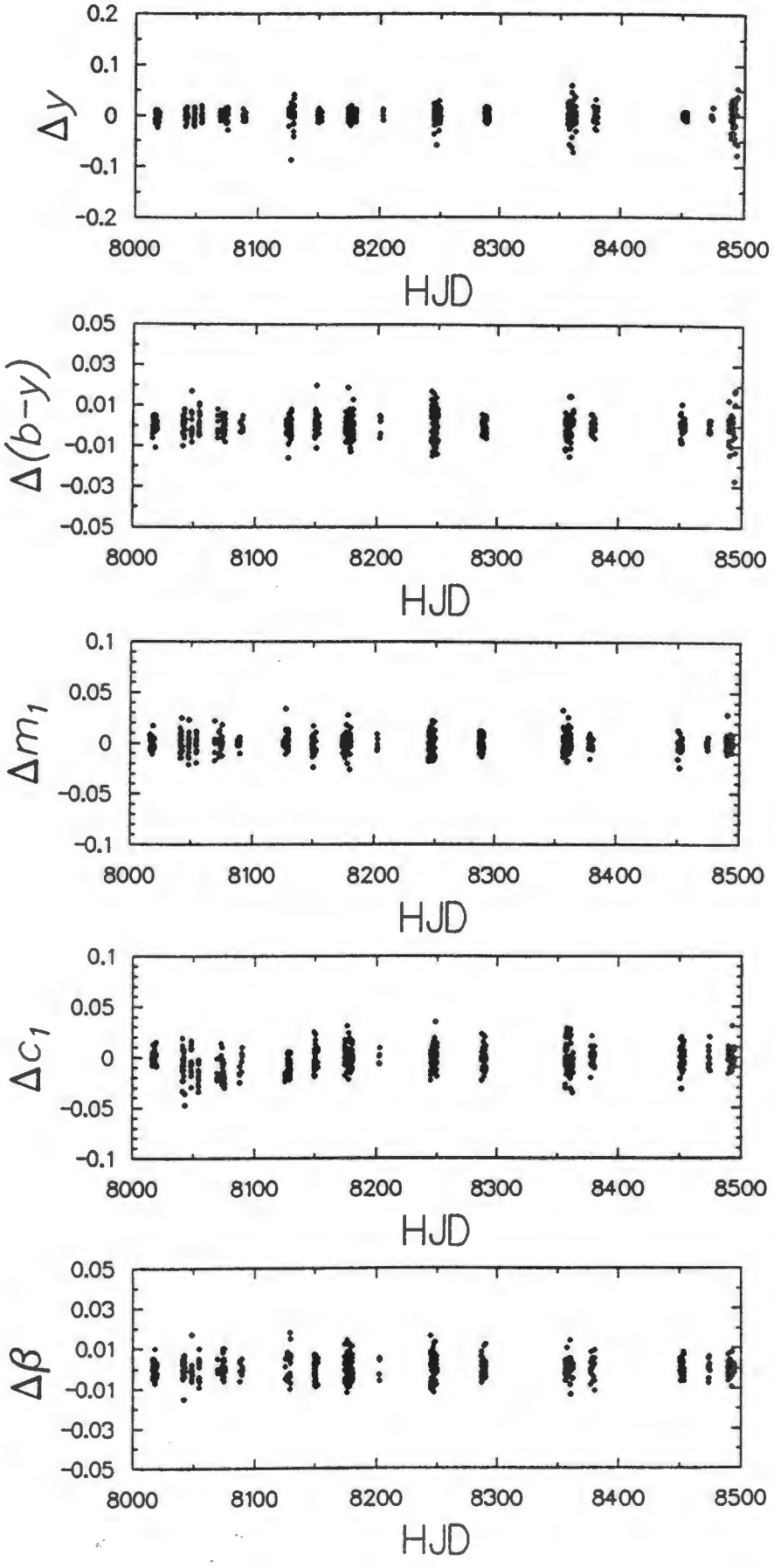

Figure 4.5 The residuals from the nightly transformations for all the standard stars observations shown as a function of time. The *y* residuals show that the deterioration of the *y* filter did not have an appreciable effect on the data. The c_1 residuals show a possible slight seasonal variation.

measures surface gravity or luminosity differences. The δm_1 and δc_1 indices are independent to first order. By this I mean that we expect that there is no luminosity effect on δm_1 and no blanketing effect on δc_1. This is true for normal stars near the main sequence but in the chemically peculiar Ap stars the severe line blanketing modifies the c_1 index to the point where it is no longer a reliable luminosity indicator. We will discuss this in greater detail in section 4.6 below.

The $(b\text{-}y)$, m_1 and c_1 indices are all affected by reddening. Using a standard extinction law it is possible to define the reddening free parameters (Golay 1974):

$$[c_1] = c_1 - 0.20(b\text{-}y),$$

$$[m_1] = m_1 + 0.18(b\text{-}y),$$

$$[u\text{-}b] = [c_1] + 2[m_1]$$

Table 4.3 gives the dereddened photometric indices of the Ap stars.

4.6 The effect of the peculiarities on the c_1 index.

For the chemically normal A-F stars c_1 is a luminosity indicator and β is a temperature indicator. Thus a plot of c_1 vs β is essentially an HR diagram. In Figure 4.6 we present the c_1 - β diagram for the Cape Survey stars, where the axes have been defined in accordance with the way HR diagrams are plotted; temperature increases towards the left and luminosity increases upwards. The fitted line is Crawford's (1975, 1979) standard relation for the zero age main sequence. The filled circles indicate the positions of the 14 roAp stars known prior to the start of the Cape Survey. The index δc_1, defined in section 4.5, is a luminosity parameter which measures the distance of a star above the standard relation. A naive interpretation of Fig. 4.6 is that many Ap SrCrEu stars and virtually all roAp stars have sub-dwarf luminosities. This is not the case; independent luminosity determinations show that the Ap stars are Population I H-core-burning stars (Wolff 1983), that is, they are on the main sequence. In chapter 9 we will use the asteroseismology of the roAp stars to provide further evidence that the roAp stars do not have sub-dwarf luminosities.

The reason for these apparent sub-dwarf luminosities is that severe line blanketing causes the continuum flux distributions in the Ap stars to deviate substantially from those of normal stars. In the cool Ap stars line blanketing depresses the continuum redward of the Balmer jump producing a rise in $(v\text{-}b)$. For the coolest Ap stars there is insufficient UV flux redistributed to longer wavelengths to compensate for the increase in v caused by blanketing and consequently the $(u\text{-}v)$ colour drops and the c_1 index is depressed relative to a normal A star of the same luminosity. In other words, the

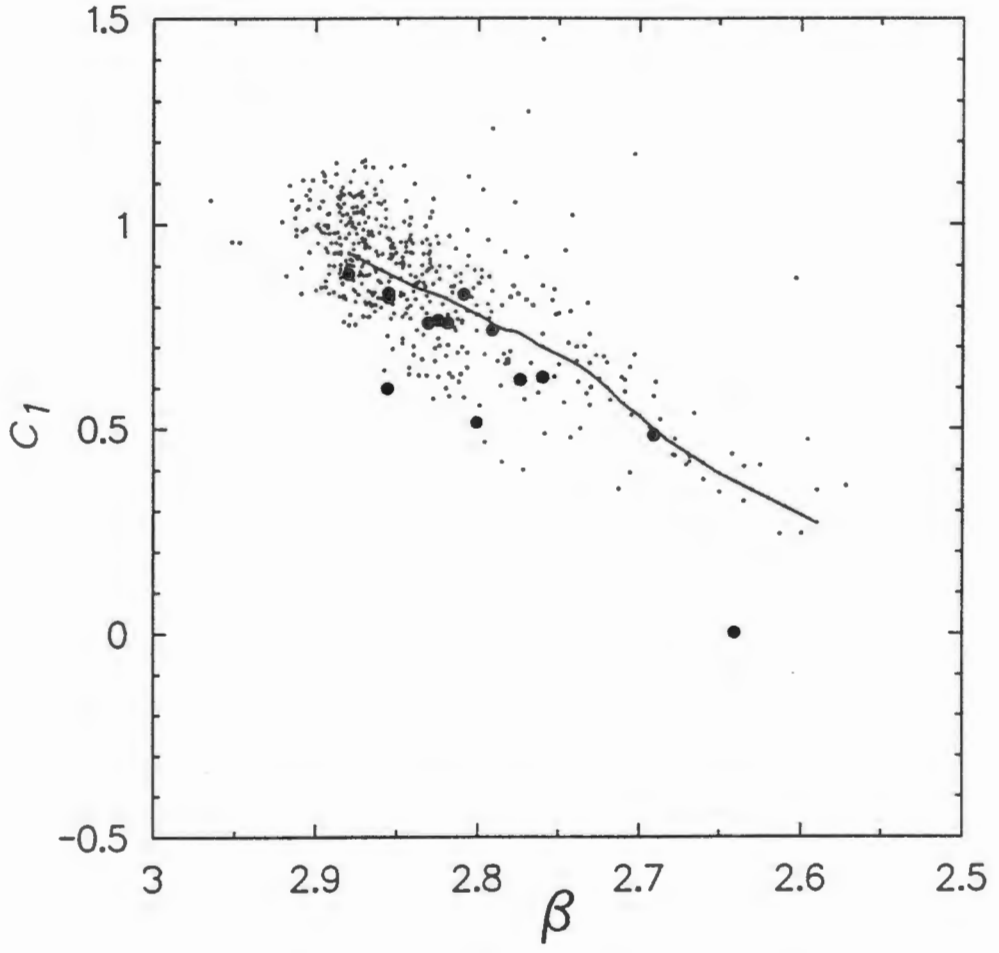

Figure 4.6 The relation between c_1 and β for the Cape Survey stars (Table 4.2). This diagram is similar to an HR diagram; temperature increases to the left and luminosity increases upwards. The fitted line is Crawford's (1975, 1979) standard relation for the A - F stars. The filled circles indicate the positions of the 14 roAp stars known prior to the start of the Cape Survey.

blanketing on the long wavelength side of the Balmer discontinuity reduces the apparent Balmer jump and this mimics a higher apparent surface gravity for the star. Because of this the c_1 index is not a reliable luminosity indicator for the Ap stars. Nevertheless, we note that the underlying main sequence trend is still evident in Fig. 4.6.

In the A - F stars the m_1 index is an indicator of the amount of blanketing due to metals in the stars' surface layers. In the heavily blanketed Ap stars the m_1 index can be thought of as a peculiarity indicator. For stars of the same β the δm_1 index measures metallicity differences from star to star. The m_1 - β diagram for the Cape Survey stars is shown in Figure 4.7. The fitted line is Crawford's (1975,1979) standard relation for the zero age main sequence. The filled circles indicate the positions of the 14 roAp stars that were known prior to the start of the Cape Survey. Note how the roAp stars almost all seem to lie above the standard line thus indicating extreme abundance anomalies. The filled circles here and in Fig. 4.6 define the photometric limits of the roAp phenomenon that served as the starting point of our search for new roAp stars.

There are several sources of scatter in these two diagrams. Firstly, the m_1 and c_1 indices are affected by reddening. Secondly, metallicity differences from star to star contribute to the variation in c_1 and m_1 for stars of a given β. Thirdly, the rotational photometric variations will not have been averaged out for many of the stars in these diagrams. Plots of c_1 vs $(b\text{-}y)$ and m_1 vs $(b\text{-}y)$ (not shown) are similar to Figures 4.6 and 4.7 since both $(b\text{-}y)$ and β are closely related to temperature for unreddened A - F stars.

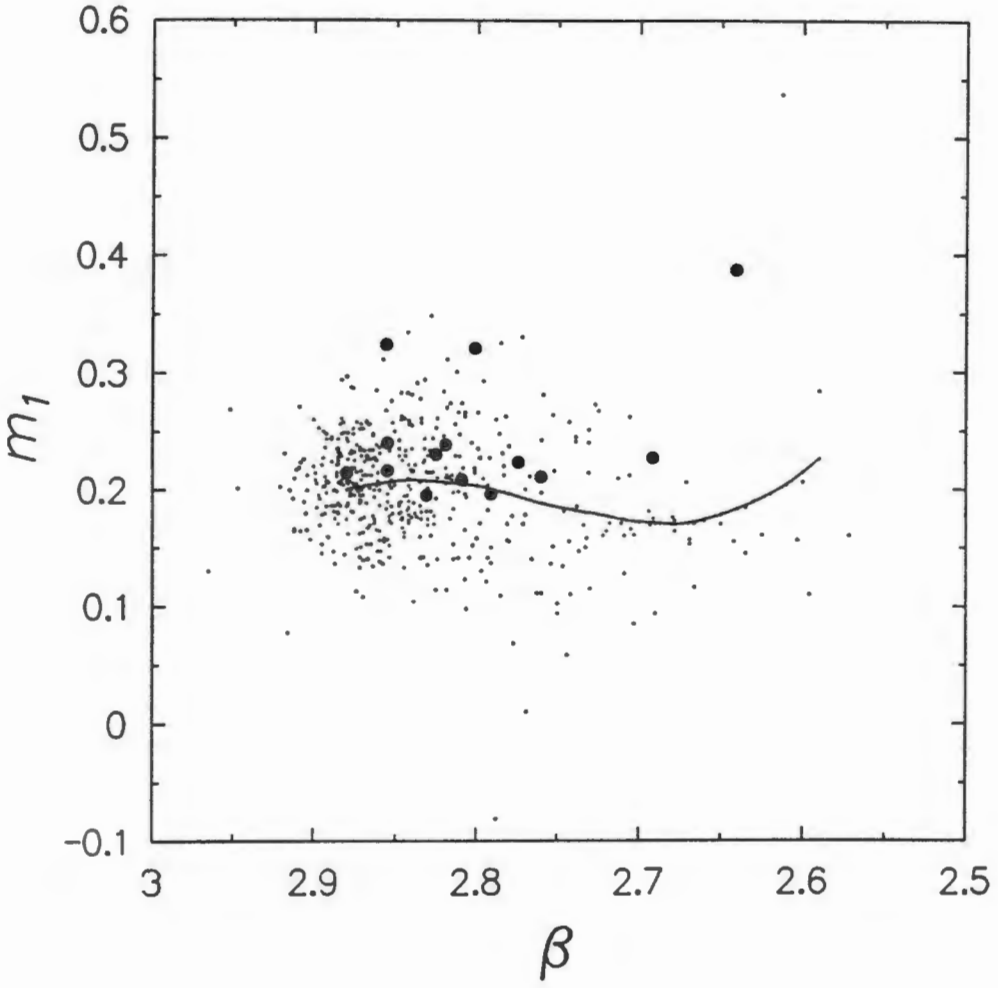

Figure 4.7 The relation between m_1 and β for the Cape Survey stars (Table 4.2). The fitted line is Crawford's (1975, 1979) standard relation for the A - F stars. The filled circles indicate the positions of the 14 roAp stars known prior to the start of the Cape Survey.

Table 4.2

Observed Strömgren photometric indices of the cool Ap stars

HD number	y	$b-y$	m_1	δm_1	c_1	δc_1	β	N
HD 2202	8.366	0.246	0.169	0.002	0.503	-0.003	2.693	1
HD 2883	9.369	0.295	0.173	0.001	0.376	-0.039	2.660	5
HD 2957	8.512	-0.001	0.208	-0.074	0.973	0.035	2.885	5
HD 3980	5.719	0.068	0.287	-0.086	0.757	-0.165	2.876	5
HD 3988	8.351	0.107	0.169	0.038	0.935	0.100	2.830	4
HD 5823	9.846	0.190	0.211	-0.020	0.661	-0.053	2.767	4
HD 6532	8.445	0.088	0.214	-0.014	0.879	-0.051	2.880	5
HD 7676	8.402	0.113	0.294	-0.087	0.630	-0.208	2.832	5
HD 8783	7.796	0.077	0.206	-0.012	1.051	0.114	2.883	4
HD 9050	8.965	0.147	0.218	-0.014	0.822	0.026	2.807	6
HD 9289	9.383	0.138	0.225	-0.018	0.826	-0.012	2.833	2
HD 10081	9.615	0.003	0.181	0.020	1.029	0.105	2.877	4
HD 11090	10.811	0.112	0.276	-0.070	0.696	-0.180	2.853	4
HD 11346	9.922	0.156	0.205	0.001	0.942	0.064	2.854	4
HD 12932	10.235	0.179	0.228	-0.024	0.765	-0.035	2.810	5
HD 14944	9.732	0.114	0.176	0.031	1.144	0.282	2.846	4
HD 15144	5.879	0.058	0.224	-0.042	0.930	-0.021	2.889	5
HD 16002	8.962	0.080	0.216	-0.011	1.036	0.152	2.857	1
HD 16145	7.668	0.033	0.199	-0.013	1.049	0.103	2.887	5
HD 18610	8.162	0.124	0.348	-0.141	0.574	-0.258	2.828	5
HD 19712	7.357	-0.076	0.248	-0.119	0.847	-0.046	2.867	1
HD 19918	9.336	0.169	0.216	-0.010	0.822	-0.058	2.855	5
HD 20505	9.901	0.019	0.226	-0.078	0.989	-0.002	2.906	4
HD 20880	7.957	0.097	0.212	-0.009	1.005	0.095	2.870	6
HD 22488	7.505	0.221	0.216	-0.030	0.780	0.096	2.752	5
HD 23207	7.568	0.113	0.259	-0.056	0.839	-0.067	2.868	4
HD 23393	8.299	0.225	0.156	0.028	0.788	0.122	2.743	4
HD 23715	9.477	0.154	0.231	-0.025	0.806	-0.017	2.822	4
HD 24712	6.001	0.191	0.211	-0.023	0.626	-0.074	2.760	5
HD 24786	9.757	0.047	0.179	-0.005	1.025	0.065	2.893	5
HD 24825	6.823	-0.046	0.187	-0.066	1.042	0.230	2.831	4
HD 26726	9.860	0.130	0.311	-0.106	0.644	-0.242	2.858	4
HD 27211	9.468	-0.027	0.194	-0.059	0.968	0.023	2.888	4
HD 27285	9.747	0.148	0.206	0.002	0.879	0.036	2.835	5
HD 27463	6.350	0.022	0.231	-0.030	0.872	-0.054	2.878	4
HD 27472	10.001	0.147	0.211	-0.007	0.850	0.040	2.815	4
HD 28430	8.221	0.118	0.182	0.023	0.968	0.085	2.856	4
HD 29578	8.507	0.173	0.229	-0.024	0.769	-0.037	2.813	4
HD 30335	9.717	0.063	0.208	-0.046	1.002	0.028	2.899	4
HD 30374	9.696	0.081	0.151	0.051	1.025	0.113	2.871	3
HD 30849	8.865	0.168	0.283	-0.076	0.721	-0.142	2.847	4
HD 31225	7.019	0.099	0.190	0.012	1.068	0.156	2.871	3
HD 31973	9.437	0.083	0.214	-0.018	0.966	0.031	2.882	3
HD 33011	9.579	0.171	0.216	-0.013	0.779	-0.003	2.801	3
HD 33629	9.064	0.200	0.231	-0.034	0.683	-0.065	2.784	3
HD 34205	9.264	0.134	0.219	-0.018	0.954	0.030	2.877	3
HD 34514	9.268	-0.007	0.198	-0.068	0.999	0.103	2.868	3
HD 35361	9.959	0.154	0.160	0.047	1.062	0.230	2.828	3
HD 36964	9.614	0.123	0.235	-0.028	0.826	-0.040	2.848	1
HD 37308	8.728	0.128	0.233	-0.026	0.897	0.064	2.829	3

HD number	y	$b-y$	m_1	δm_1	c_1	δc_1	β	N
HD 38719	7.510	0.017	0.207	-0.031	1.027	0.069	2.892	3
HD 39575	7.867	-0.059	0.248	-0.118	0.861	-0.035	2.868	3
HD 40277	8.333	0.046	0.250	-0.078	0.863	-0.100	2.894	3
HD 40765	9.577	0.271	0.241	-0.059	0.666	0.009	2.739	3
HD 40886	8.209	-0.021	0.242	-0.122	0.771	-0.008	2.818	3
HD 41385	9.434	0.154	0.281	-0.073	0.681	-0.169	2.840	3
HD 41511	4.894	0.220	0.010	0.182	1.274	0.556	2.769	3
HD 41613	9.689	0.202	0.159	0.048	0.933	0.073	2.845	3
HD 41757	8.489	-0.005	0.184	-0.059	1.137	0.288	2.847	3
HD 42075	8.968	0.205	0.260	-0.061	0.665	-0.091	2.788	3
HD 42326	7.708	0.010	0.243	-0.061	0.899	-0.052	2.889	3
HD 42605	8.934	0.146	0.218	-0.020	0.903	-0.029	2.881	3
HD 42659	6.768	0.124	0.257	-0.050	0.765	-0.076	2.834	3
HD 42777	9.166	-0.013	0.264	-0.132	0.785	-0.130	2.876	3
HD 43226	8.961	0.102	0.248	-0.047	0.812	-0.110	2.876	3
HD 43901	8.216	0.138	0.225	-0.020	0.927	0.032	2.862	4
HD 44226	9.492	0.161	0.259	-0.051	0.771	-0.083	2.842	3
HD 44290	8.533	-0.023	0.200	-0.072	0.899	0.021	2.860	2
HD 44550	9.626	0.269	0.161	0.012	0.682	0.143	2.703	1
HD 45698	8.162	0.072	0.248	-0.054	0.822	-0.115	2.882	2
HD 45870	9.802	-0.005	0.209	-0.081	0.969	0.089	2.861	2
HD 45961	9.424	0.062	0.202	0.001	0.964	0.054	2.870	2
HD 46649	9.564	0.036	0.186	0.022	0.797	-0.046	2.835	1
HD 46665	9.441	0.039	0.255	-0.047	0.702	-0.148	2.840	3
HD 47009	9.070	0.091	0.201	0.001	0.885	-0.031	2.873	1
HD 49686	9.797	0.063	0.197	0.003	1.042	0.116	2.878	2
HD 50031	9.668	0.125	0.253	-0.087	0.847	-0.123	2.897	1
HD 50143	9.781	0.145	0.247	-0.042	0.700	-0.100	2.810	1
HD 50304	7.574	0.005	0.137	0.063	1.232	0.470	2.791	1
HD 50620	9.743	0.085	0.243	-0.067	0.902	-0.056	2.892	1
HD 50627	10.633	0.239	0.176	0.032	0.862	0.017	2.837	1
HD 50861	9.718	0.150	0.174	0.033	0.915	0.080	2.830	1
HD 51203	10.500	0.207	0.256	-0.051	0.687	-0.119	2.813	3
HD 51684	7.950	0.139	0.256	-0.048	0.802	-0.052	2.842	1
HD 52280	9.793	0.039	0.179	-0.029	1.037	0.049	2.905	1
HD 52539	9.507	-0.056	0.228	-0.106	0.777	-0.045	2.835	1
HD 52599	8.506	0.130	0.195	0.013	0.965	0.109	2.843	1
HD 52696	8.549	0.095	0.200	0.002	1.074	0.156	2.874	1
HD 52847	8.157	0.101	0.334	-0.126	0.633	-0.223	2.843	1
HD 54087	9.431	0.222	0.200	-0.008	0.920	0.200	2.770	1
HD 54399	9.803	0.163	0.164	0.041	1.050	0.160	2.860	1
HD 55540	9.498	0.026	0.258	-0.055	0.774	-0.132	2.868	3
HD 55719	5.293	0.003	0.221	-0.033	1.030	0.086	2.886	1
HD 56026	9.851	0.132	0.201	0.005	0.953	0.077	2.853	1
HD 56350	6.705	-0.079	0.208	-0.088	0.781	0.017	2.813	1
HD 56809	7.102	0.034	0.196	0.005	1.131	0.207	2.877	1
HD 56882	8.378	0.111	0.234	-0.032	0.857	-0.057	2.872	1
HD 56981	10.015	0.489	0.206	0.008	0.245	-0.045	2.600	1
HD 57040	9.207	0.259	0.325	-0.127	0.419	-0.331	2.785	1
HD 57964	9.405	0.070	0.114	0.092	0.721	-0.107	2.825	1
HD 58868	9.592	0.086	0.231	-0.030	0.842	-0.082	2.877	1
HD 58939	10.131	0.113	0.181	0.003	1.122	0.173	2.888	1
HD 59164	8.365	0.002	0.200	0.001	1.067	0.143	2.877	1
HD 59437	9.260	0.029	0.252	-0.050	0.879	-0.035	2.872	1
HD 59660	10.033	0.067	0.174	0.028	1.032	0.120	2.871	1
HD 59776	8.913	0.217	0.169	0.011	0.703	0.061	2.734	1
HD 60435	8.891	0.136	0.240	-0.034	0.833	-0.047	2.855	1
HD 60572	9.338	0.007	0.256	-0.054	0.777	-0.135	2.871	1
HD 61468	9.844	-0.013	0.241	-0.119	0.770	-0.048	2.833	1

HD number	y	b-y	m_1	δm_1	c_1	δc_1	β	N
HD 61513	10.161	-0.046	0.252	-0.122	0.823	-0.075	2.869	1
HD 61731	9.767	0.123	0.283	-0.075	0.649	-0.207	2.843	1
HD 61763	7.958	0.025	0.110	0.073	1.023	0.359	2.742	1
HD 62244	8.276	0.035	0.213	-0.025	1.043	0.099	2.886	1
HD 62399	9.440	-0.033	0.254	-0.117	0.917	-0.051	2.897	1
HD 62530	8.156	-0.036	0.204	-0.084	0.856	0.077	2.818	1
HD 62553	7.857	0.045	0.206	-0.016	1.041	0.099	2.885	1
HD 62556	7.941	0.032	0.212	-0.008	0.828	-0.072	2.865	2
HD 62562	8.926	0.078	0.245	-0.063	0.836	-0.115	2.889	1
HD 62905	9.597	0.014	0.235	-0.027	0.837	-0.013	2.840	1
HD 62953	8.940	0.260	0.111	0.077	1.449	0.749	2.760	1
HD 63728	9.316	0.016	0.186	0.019	0.858	-0.032	2.860	1
HD 63745	10.683	0.020	0.268	-0.062	0.728	-0.154	2.856	1
HD 63759	8.292	0.063	0.206	-0.028	1.092	0.136	2.891	1
HD 64288	10.171	-0.040	0.272	-0.147	0.765	-0.082	2.846	1
HD 65142	8.522	-0.026	0.198	-0.074	1.013	0.177	2.841	1
HD 65836	6.788	0.063	0.212	-0.060	0.933	-0.053	2.904	1
HD 65963	9.281	0.006	0.185	0.021	0.923	0.047	2.853	1
HD 67909	8.961	0.110	0.224	-0.021	0.876	-0.032	2.869	1
HD 68013	9.185	-0.029	0.227	-0.099	0.832	-0.048	2.861	1
HD 68419	8.186	0.018	0.223	-0.079	0.984	-0.011	2.908	1
HD 68480	8.899	0.010	0.248	-0.050	0.605	-0.147	2.786	1
HD 68807	9.159	0.037	0.246	-0.042	0.789	-0.109	2.864	1
HD 68998	8.618	0.145	0.182	0.026	0.999	0.143	2.843	1
HD 69013	9.456	0.296	0.330	-0.137	0.400	-0.324	2.772	1
HD 69204	9.936	0.131	0.219	-0.077	0.895	-0.103	2.909	1
HD 69638	9.437	0.088	0.235	-0.045	0.929	-0.013	2.885	1
HD 69862	10.065	0.146	0.194	0.007	1.005	0.079	2.878	1
HD 70702	8.572	-0.076	0.305	-0.166	0.842	-0.143	2.904	1
HD 71058	9.436	0.599	0.284	-0.058	0.351	0.081	2.590	1
HD 72316	8.804	-0.001	0.248	-0.125	0.836	0.003	2.840	1
HD 72611	7.014	-0.062	0.200	-0.080	0.720	-0.019	2.805	1
HD 72634	7.280	-0.019	0.201	-0.071	0.987	0.089	2.869	1
HD 72801	9.586	0.120	0.135	0.072	0.906	0.071	2.830	1
HD 73101	9.367	-0.003	0.167	-0.047	0.890	0.086	2.827	1
HD 73403	8.877	-0.038	0.226	-0.095	0.896	-0.009	2.872	1
HD 73850	9.317	0.077	0.226	-0.023	0.810	-0.094	2.867	1
HD 74067	5.199	-0.052	0.237	-0.110	0.888	0.019	2.856	2
HD 74169	7.214	-0.041	0.214	-0.088	0.831	-0.027	2.851	2
HD 74494	8.863	-0.021	0.241	-0.121	0.793	-0.009	2.826	1
HD 74555	8.956	0.010	0.203	0.003	0.929	0.051	2.854	1
HD 74629	9.696	0.143	0.203	-0.029	0.999	0.039	2.893	1
HD 74636	9.210	0.027	0.159	0.049	0.901	0.058	2.835	1
HD 74672	9.801	0.122	0.221	-0.051	0.980	0.015	2.895	1
HD 75049	9.090	-0.054	0.249	-0.110	0.914	-0.076	2.906	1
HD 75425	9.584	0.112	0.247	-0.044	0.805	-0.094	2.864	2
HD 75445	7.131	0.165	0.215	-0.011	0.740	-0.042	2.801	2
HD 76276	9.725	0.223	0.188	0.020	0.856	0.007	2.839	1
HD 76460	9.805	0.221	0.210	-0.004	0.849	0.035	2.817	1
HD 76759	9.141	0.068	0.188	0.019	0.870	0.004	2.848	1
HD 76877	9.890	0.082	0.226	-0.022	0.973	0.073	2.865	1
HD 77438	10.131	0.122	0.250	-0.044	0.906	0.034	2.851	1
HD 77609	8.006	0.033	0.171	0.031	0.871	0.095	2.798	1
HD 77809	10.293	0.107	0.256	-0.064	0.855	-0.084	2.884	1
HD 77830	9.047	0.236	0.240	-0.060	0.732	0.099	2.731	1
HD 79539	9.226	0.077	0.228	-0.038	1.008	0.066	2.885	1
HD 79976	8.505	0.002	0.188	0.015	1.018	0.112	2.868	1
HD 80249	10.424	-0.081	0.304	-0.169	0.885	-0.065	2.890	1
HD 80316	7.782	0.118	0.324	-0.118	0.599	-0.283	2.856	1

HD number	y	$b-y$	m_1	δm_1	c_1	δc_1	β	N
HD 80992	9.867	0.088	0.205	-0.013	1.091	0.152	2.884	1
HD 81076	9.546	0.147	0.130	0.072	1.085	0.311	2.797	1
HD 81289	8.403	-0.008	0.234	-0.116	0.640	-0.041	2.787	1
HD 81588	8.445	0.125	0.263	-0.056	0.775	-0.089	2.847	1
HD 81877	8.873	-0.008	0.239	-0.119	0.849	0.067	2.819	1
HD 82038	9.568	0.168	0.167	0.036	1.054	0.150	2.867	1
HD 82093	7.095	0.064	0.190	0.011	1.069	0.155	2.872	2
HD 82417	9.181	0.150	0.162	0.040	1.152	0.238	2.872	1
HD 82562	9.213	0.014	0.195	0.008	0.942	0.032	2.870	1
HD 82749	9.364	0.019	0.178	0.030	0.975	0.121	2.842	1
HD 82989	8.320	0.418	0.164	0.013	0.663	0.063	2.720	1
HD 83181	9.467	0.008	0.199	-0.015	0.955	0.006	2.888	1
HD 83368	6.168	0.159	0.230	-0.024	0.766	-0.062	2.825	2
HD 83817	9.047	0.332	0.171	0.003	0.625	0.061	2.711	1
HD 84041	9.330	0.178	0.233	-0.026	0.797	-0.061	2.844	2
HD 85284	9.775	0.039	0.212	-0.006	0.896	0.080	2.818	1
HD 85453	8.144	-0.045	0.162	-0.052	0.520	-0.002	2.747	1
HD 85564	9.563	0.167	0.229	-0.022	0.812	-0.023	2.830	1
HD 85733	10.077	0.170	0.215	-0.027	0.824	-0.120	2.886	1
HD 85766	9.978	0.171	0.204	0.000	0.790	-0.004	2.807	1
HD 86051	9.790	-0.030	0.203	-0.083	0.840	0.098	2.806	1
HD 86181	9.323	0.172	0.205	0.001	0.757	-0.061	2.819	1
HD 86592	7.858	0.113	0.291	-0.083	0.630	-0.215	2.837	2
HD 86976	8.345	0.127	0.294	-0.100	0.762	-0.175	2.883	1
HD 87087	9.912	0.126	0.165	0.040	1.053	0.159	2.862	1
HD 87488	6.987	-0.030	0.213	-0.093	0.891	0.087	2.827	1
HD 88042	10.062	0.097	0.102	0.083	0.784	0.104	2.750	1
HD 88241	7.920	0.129	0.165	0.039	0.986	0.192	2.807	1
HD 88385	8.020	-0.007	0.273	-0.150	0.760	-0.069	2.838	1
HD 88507	9.697	0.135	0.196	0.010	0.918	0.038	2.855	1
HD 88701	9.258	0.002	0.225	-0.018	0.830	-0.032	2.846	1
HD 89075	8.488	0.001	0.123	0.081	0.900	0.106	2.807	1
HD 89192	6.850	0.019	0.186	-0.004	0.981	0.029	2.889	2
HD 89385	8.327	0.015	0.199	0.003	0.906	-0.006	2.871	1
HD 89519	8.266	0.032	0.150	0.050	0.838	0.076	2.791	1
HD 89680	8.368	0.053	0.174	0.028	1.081	0.167	2.872	1
HD 89840	9.855	0.156	0.163	0.040	1.047	0.137	2.870	1
HD 90131	9.517	0.030	0.288	-0.087	0.899	-0.025	2.877	1
HD 91087	9.426	0.058	0.261	-0.067	0.828	-0.109	2.883	1
HD 91239	7.366	-0.064	0.215	-0.088	0.848	-0.010	2.851	2
HD 91735	9.450	0.205	0.179	0.027	0.784	-0.090	2.852	1
HD 91982	9.431	0.085	0.241	-0.041	1.016	0.088	2.879	1
HD 92106	7.778	0.075	0.155	0.050	0.994	0.110	2.857	1
HD 92218	9.194	0.128	0.297	-0.097	0.755	-0.175	2.880	1
HD 92286	9.700	0.026	0.199	0.008	1.016	0.181	2.830	1
HD 92499	8.890	0.179	0.301	-0.096	0.615	-0.189	2.812	1
HD 92534	9.379	0.013	0.210	-0.004	0.706	-0.112	2.819	1
HD 93500	8.731	0.038	0.171	0.033	1.012	0.116	2.863	1
HD 94052	9.630	0.074	0.190	0.018	1.017	0.163	2.842	1
HD 94111	9.640	0.062	0.244	-0.044	0.890	-0.040	2.880	1
HD 94274	9.290	0.001	0.207	-0.006	0.912	-0.014	2.878	1
HD 94455	8.019	0.116	0.188	0.014	1.080	0.166	2.872	1
HD 94660	6.098	-0.081	0.240	-0.120	0.730	0.003	2.801	2
HD 95158	9.224	0.159	0.210	-0.004	0.900	0.074	2.824	1
HD 95491	9.208	0.169	0.193	0.011	0.923	0.131	2.806	1
HD 95508	9.521	0.005	0.205	-0.003	0.955	0.037	2.874	1
HD 95699	7.751	0.070	0.236	-0.034	0.966	0.052	2.872	1
HD 95811	9.502	0.281	0.245	-0.063	0.700	0.043	2.739	1
HD 96237	9.434	0.233	0.261	-0.055	0.704	-0.122	2.824	1

HD number	y	$b-y$	m_1	δm_1	c_1	δc_1	β	N
HD 96451	6.901	0.053	0.234	-0.047	0.968	0.024	2.886	2
HD 96616	5.155	0.001	0.198	0.004	1.031	0.115	2.873	1
HD 96897	10.121	0.935	0.537	-0.335	0.244	-0.072	2.613	1
HD 97132	9.727	0.121	0.229	-0.027	0.958	0.046	2.871	1
HD 97394	8.797	0.105	0.285	-0.081	0.821	-0.073	2.862	1
HD 97987	9.806	0.522	0.209	-0.034	0.353	-0.219	2.713	1
HD 98340	7.137	-0.031	0.168	-0.049	0.786	-0.006	2.822	2
HD100357	8.973	0.029	0.208	-0.003	0.749	-0.061	2.815	1
HD100587	7.378	-0.005	0.185	-0.065	0.957	0.155	2.826	1
HD101065	7.994	0.431	0.387	-0.204	0.002	-0.370	2.641	1
HD101189	5.127	-0.018	0.134	-0.014	0.878	0.123	2.810	2
HD101410	6.646	-0.002	0.150	-0.023	1.076	0.207	2.856	2
HD102333	9.046	0.068	0.232	-0.031	0.924	0.004	2.875	1
HD102812	10.763	0.140	0.258	-0.056	0.829	-0.089	2.874	1
HD102983	9.553	0.045	0.195	0.007	0.898	-0.016	2.872	1
HD103210	10.189	0.128	0.201	0.002	0.983	0.081	2.866	1
HD103302	8.284	0.017	0.197	-0.021	0.977	0.019	2.892	2
HD104044	9.577	-0.007	0.211	-0.091	0.972	0.181	2.822	1
HD104402	9.506	0.091	0.211	-0.037	0.992	0.032	2.893	1
HD105999	8.014	0.213	0.128	0.046	0.619	0.062	2.709	3
HD106215	9.323	0.034	0.211	-0.010	0.996	0.070	2.878	1
HD106322	10.187	0.126	0.226	-0.026	0.915	-0.013	2.879	1
HD106374	7.360	0.123	0.214	-0.007	1.030	0.196	2.829	1
HD107107	8.734	0.074	0.234	-0.030	0.835	-0.063	2.864	2
HD107180	9.846	0.180	0.238	-0.033	0.822	-0.072	2.862	1
HD109300	10.250	0.131	0.058	0.125	0.709	0.042	2.744	2
HD109426	9.217	0.227	0.174	0.033	0.905	0.043	2.846	3
HD109790	10.454	0.111	0.098	0.106	1.115	0.324	2.807	2
HD109989	9.086	0.053	0.212	-0.009	0.911	0.004	2.868	2
HD110072	10.104	0.227	0.281	-0.093	0.487	-0.211	2.759	2
HD110274	9.328	0.195	0.208	-0.002	0.805	-0.071	2.853	3
HD110446	9.382	0.136	0.153	0.017	1.119	0.154	2.895	1
HD110568	9.746	0.284	0.140	0.050	0.803	0.091	2.766	1
HD111675	9.756	0.143	0.217	-0.017	1.030	0.110	2.875	2
HD112528	8.249	0.199	0.216	-0.008	0.819	-0.029	2.839	3
HD112616	9.700	0.114	0.257	-0.051	0.942	0.068	2.852	1
HD113149	10.156	0.069	0.142	0.060	1.037	0.123	2.872	1
HD113588	9.618	0.154	0.069	0.127	1.053	0.319	2.778	2
HD114035	8.292	-0.007	0.173	-0.051	0.901	0.085	2.832	3
HD114709	9.943	0.087	0.195	0.006	1.043	0.123	2.875	2
HD115226	8.510	0.177	0.199	0.005	0.885	-0.011	2.863	2
HD115285	8.326	0.075	0.156	0.049	1.105	0.215	2.860	3
HD115440	8.235	0.056	0.134	0.050	0.563	-0.111	2.747	3
HD116114	7.024	0.174	0.223	-0.016	0.848	0.008	2.833	3
HD116423	8.472	0.100	0.182	0.019	0.770	0.004	2.793	3
HD116458	5.654	-0.030	0.203	-0.083	0.841	0.126	2.797	3
HD116729	8.951	0.066	0.260	-0.100	0.840	-0.137	2.899	2
HD116763	9.100	0.025	0.164	0.044	0.958	0.097	2.845	2
HD117025	6.106	0.044	0.231	-0.039	0.859	-0.080	2.884	3
HD117227	9.085	0.141	0.221	-0.013	0.878	0.023	2.842	2
HD117290	9.281	0.152	0.229	-0.026	0.879	-0.025	2.867	2
HD117453	10.380	-0.032	0.280	-0.155	0.758	-0.094	2.848	2
HD117691	9.446	0.244	0.220	-0.023	0.934	0.188	2.783	1
HD118231	8.902	0.053	0.109	0.089	0.802	0.052	2.785	1
HD118470	9.979	0.092	0.207	-0.007	0.977	0.047	2.880	2
HD118683	9.824	0.212	0.194	0.013	0.886	0.049	2.832	2
HD118913	7.692	0.034	0.193	0.011	0.935	0.039	2.863	3
HD119027	10.022	0.257	0.214	-0.034	0.557	-0.076	2.731	3
HD119158	9.778	0.135	0.208	-0.014	1.073	0.137	2.883	2

HD number	y	$b-y$	m_1	δm_1	c_1	δc_1	β	N
HD119308	7.853	0.005	0.204	-0.008	0.913	-0.022	2.882	3
HD119794	8.993	0.089	0.225	-0.024	0.917	-0.002	2.875	2
HD120346	9.813	0.121	0.142	0.065	0.995	0.155	2.833	2
HD121276	9.464	0.130	0.094	0.091	0.658	-0.022	2.750	1
HD121661	8.556	0.036	0.234	-0.030	0.805	-0.097	2.866	3
HD121675	9.676	0.150	0.200	0.008	0.953	0.101	2.841	3
HD121788	8.761	0.164	0.203	-0.002	0.872	0.106	2.793	2
HD121840	9.424	0.174	0.229	-0.026	0.974	0.068	2.869	2
HD122525	8.703	0.169	0.170	0.020	1.068	0.126	2.885	3
HD122569	9.008	0.003	0.222	-0.032	0.952	0.009	2.885	2
HD122659	9.024	0.005	0.204	-0.003	0.978	0.058	2.875	1
HD123112	6.974	0.046	0.133	0.074	1.057	0.197	2.845	1
HD123164	9.879	0.117	0.238	-0.036	0.875	-0.043	2.874	3
HD123627	8.139	0.140	0.186	0.000	1.069	0.123	2.887	3
HD124437	8.925	0.086	0.171	0.037	1.017	0.163	2.842	3
HD124740	7.826	0.004	0.141	0.063	0.823	0.035	2.804	1
HD125467	8.667	0.100	0.216	-0.014	0.875	-0.037	2.871	3
HD125555	9.400	0.217	0.177	0.030	0.971	0.142	2.826	2
HD125735	10.070	0.097	0.225	-0.035	0.903	-0.039	2.884	2
HD126297	9.456	0.188	0.181	0.026	0.928	0.091	2.831	2
HD126365	8.426	0.245	0.166	0.007	0.533	-0.012	2.705	1
HD126515	7.078	-0.052	0.278	-0.139	0.858	-0.134	2.907	1
HD126936	9.491	0.300	0.160	0.018	0.677	0.071	2.722	1
HD127021	9.754	0.169	0.153	0.050	0.983	0.077	2.868	2
HD127154	7.281	0.001	0.121	0.080	0.961	0.193	2.794	3
HD127159	9.707	0.189	0.174	0.033	0.910	0.046	2.847	1
HD127210	10.365	0.266	0.171	0.005	0.570	-0.022	2.718	1
HD127241	8.999	0.052	0.170	0.037	0.885	0.057	2.826	2
HD127608	8.546	-0.053	0.228	-0.105	0.850	0.023	2.837	3
HD128472	9.802	0.181	0.217	-0.009	0.929	0.078	2.841	2
HD128540	9.108	0.117	0.147	0.037	1.150	0.201	2.888	3
HD128649	9.478	0.000	0.233	-0.030	0.806	-0.102	2.869	2
HD128843	10.334	0.115	0.136	0.050	0.931	-0.015	2.887	1
HD129052	10.305	0.212	0.266	-0.062	0.686	-0.108	2.807	1
HD129189	8.523	0.016	0.199	0.006	0.820	-0.070	2.860	1
HD129994	10.066	0.125	0.136	0.069	1.057	0.171	2.858	2
HD130336	8.870	0.012	0.111	0.078	0.587	-0.119	2.763	3
HD130382	10.247	0.077	0.187	0.013	0.901	-0.027	2.879	1
HD130559	5.634	0.024	0.205	-0.005	0.903	-0.025	2.879	3
HD131141	9.426	0.178	0.261	-0.054	0.783	-0.077	2.845	1
HD131750	8.549	0.121	0.260	-0.053	0.710	-0.154	2.847	3
HD131870	9.420	0.057	0.174	0.033	0.858	0.017	2.834	2
HD131910	9.906	0.276	0.151	0.035	0.843	0.157	2.753	2
HD132205	8.715	0.225	0.270	-0.064	0.635	-0.181	2.818	2
HD132322	7.357	0.129	0.227	-0.055	0.943	-0.020	2.894	4
HD132673	8.472	0.176	0.186	0.021	0.906	0.040	2.848	3
HD132968	8.635	0.082	0.153	0.051	1.139	0.239	2.865	3
HD132981	10.503	0.227	0.180	0.027	0.929	0.088	2.834	3
HD133792	6.255	0.035	0.176	0.027	1.101	0.193	2.869	3
HD133812	9.662	0.300	0.171	0.000	0.522	0.036	2.687	3
HD134214	7.464	0.216	0.223	-0.029	0.620	-0.108	2.774	3
HD134465	9.962	0.072	0.205	-0.004	0.991	0.069	2.876	1
HD134507	9.629	0.187	0.171	0.035	0.990	0.114	2.853	3
HD134640	9.894	0.158	0.194	0.013	0.946	0.086	2.845	3
HD135173	9.758	0.126	0.203	0.000	0.952	0.044	2.869	3
HD135297	7.944	0.001	0.180	0.027	0.920	0.056	2.847	1
HD135396	8.279	0.259	0.136	0.050	0.815	0.127	2.754	4
HD135459	10.211	0.370	0.181	0.003	0.937	0.265	2.746	4
HD135480	8.907	0.092	0.214	-0.052	0.955	-0.019	2.899	3

HD number	y	$b-y$	m_1	δm_1	c_1	δc_1	β	N
HD135512	9.720	0.179	0.236	-0.031	0.820	-0.070	2.860	3
HD135728	8.602	0.236	0.203	0.005	0.931	0.077	2.843	4
HD135815	9.313	0.133	0.174	0.030	1.073	0.177	2.863	4
HD136575	10.222	0.129	0.186	0.006	1.023	0.084	2.884	3
HD137160	8.006	0.048	0.177	0.029	0.949	0.071	2.854	3
HD137401	9.886	0.211	0.209	-0.001	0.900	0.044	2.843	1
HD137509	6.859	-0.085	0.180	-0.080	0.356	-0.011	2.711	3
HD137581	9.500	0.087	0.139	0.064	1.140	0.230	2.870	1
HD137802	9.398	0.141	0.256	-0.054	0.775	-0.137	2.871	3
HD137848	9.377	0.081	0.199	-0.047	1.085	0.099	2.904	3
HD137949	6.673	0.196	0.311	-0.105	0.580	-0.236	2.818	3
HD138146	10.110	0.137	0.207	-0.002	0.979	0.087	2.861	3
HD138218	9.639	0.195	0.202	-0.001	0.805	0.037	2.794	1
HD138426	8.554	0.084	0.184	-0.020	0.990	0.018	2.898	3
HD138497	7.161	0.020	0.215	-0.007	0.854	0.004	2.840	1
HD138633	8.572	0.248	0.158	0.047	1.015	0.131	2.857	1
HD138777	9.690	0.249	0.263	-0.066	0.668	-0.076	2.782	1
HD138927	9.279	0.197	0.198	0.007	0.880	0.078	2.811	1
HD139474	9.163	0.021	0.179	0.029	0.855	0.008	2.838	3
HD139631	8.706	0.150	0.138	0.067	0.997	0.107	2.860	3
HD140220	7.980	0.069	0.142	0.064	1.138	0.260	2.854	3
HD140393	10.621	0.089	0.256	-0.052	0.800	-0.102	2.866	1
HD140748	9.214	0.089	0.231	-0.030	0.926	0.002	2.877	3
HD140959	9.884	0.056	0.271	-0.129	0.833	-0.165	2.909	3
HD141249	10.178	0.223	0.278	-0.070	0.670	-0.173	2.835	3
HD141317	8.900	0.048	0.179	0.028	0.957	0.091	2.848	3
HD141981	9.853	0.136	0.180	0.011	1.082	0.140	2.885	4
HD142070	7.939	0.084	0.248	-0.072	0.833	-0.125	2.892	1
HD142502	9.501	0.244	0.214	-0.009	0.861	-0.031	2.861	3
HD142544	9.707	0.113	0.220	-0.016	0.891	-0.007	2.864	1
HD142823	8.946	0.104	0.147	0.058	0.862	-0.030	2.861	3
HD143487	9.420	0.386	0.262	-0.089	0.393	-0.155	2.706	3
HD143654	8.978	0.180	0.145	0.025	0.999	0.034	2.895	3
HD144413	10.141	0.197	0.157	-0.001	1.109	0.128	2.902	3
HD144748	8.612	0.094	0.198	-0.010	1.062	0.118	2.886	3
HD144897	8.583	0.166	0.155	0.041	0.689	-0.051	2.780	3
HD145074	10.299	0.369	0.140	0.065	0.874	0.066	2.814	3
HD145393	9.763	0.300	0.152	0.051	0.888	0.104	2.802	1
HD146631	9.526	0.214	0.192	0.014	0.954	0.126	2.825	1
HD146971	8.589	0.160	0.165	-0.013	1.060	0.074	2.904	1
HD147105	8.783	0.342	0.113	0.089	1.002	0.084	2.874	3
HD147863	9.721	0.144	0.162	0.038	1.103	0.175	2.879	3
HD148593	9.111	0.348	0.215	-0.008	0.698	-0.133	2.827	3
HD148848	7.444	0.133	0.175	0.030	0.835	0.023	2.816	3
HD148898	5.384	0.064	0.180	0.010	1.072	0.130	2.885	3
HD149046	12.164	0.428	0.094	0.077	0.615	0.120	2.690	1
HD149250	9.263	0.033	0.197	0.008	0.741	-0.067	2.814	3
HD149769	9.735	0.154	0.252	-0.051	0.838	-0.084	2.876	4
HD150035	8.901	0.174	0.133	0.069	1.067	0.153	2.872	4
HD150562	9.816	0.301	0.212	-0.015	0.659	-0.087	2.784	2
HD150715	10.010	0.119	0.149	0.053	1.075	0.157	2.874	1
HD150862	9.162	0.334	0.170	0.008	0.346	-0.044	2.650	1
HD151301	8.541	0.222	0.244	-0.037	0.666	-0.165	2.827	3
HD151560	9.737	0.270	0.221	-0.027	0.831	0.101	2.775	3
HD151860	9.031	0.258	0.150	0.030	0.586	-0.053	2.733	4
HD151873	9.073	0.068	0.085	0.088	1.171	0.632	2.703	3
HD151941	9.801	0.202	0.215	-0.008	0.891	0.054	2.831	1
HD152137	9.635	0.039	0.217	-0.016	0.865	-0.059	2.877	3
HD152387	8.925	0.153	0.164	-0.020	1.109	0.114	2.908	3

HD number	y	$b-y$	m_1	δm_1	c_1	δc_1	β	N
HD153149	9.405	0.209	0.202	-0.030	0.848	-0.115	2.894	3
HD153183	8.968	0.142	0.167	0.040	1.006	0.144	2.846	3
HD153192	10.000	0.016	0.231	-0.026	0.798	-0.092	2.860	3
HD153201	6.390	0.009	0.115	0.065	0.602	-0.028	2.730	3
HD153742	10.095	0.317	0.140	0.066	0.868	0.042	2.824	2
HD153953	9.422	0.312	0.114	0.092	0.971	0.155	2.818	3
HD154075	10.030	0.113	0.170	0.022	0.572	-0.150	2.771	3
HD154253	9.011	0.113	0.227	-0.023	0.804	-0.092	2.863	3
HD154308	8.761	0.103	0.188	0.002	0.934	-0.008	2.885	3
HD154645	9.027	0.056	0.153	0.052	0.941	0.133	2.814	3
HD154708	8.744	0.277	0.258	-0.075	0.478	-0.188	2.743	3
HD155127	8.388	0.144	0.134	0.070	1.072	0.174	2.864	3
HD155171	10.209	0.267	0.227	-0.027	0.787	0.023	2.792	4
HD155188	9.877	0.050	0.235	-0.029	0.771	-0.107	2.854	3
HD155366	9.230	0.189	0.174	0.026	1.076	0.146	2.880	3
HD156049	8.245	0.003	0.176	0.032	0.848	-0.002	2.840	3
HD156808	8.614	0.640	-0.081	0.280	1.585	0.829	2.788	1
HD156869	7.926	0.046	0.173	0.033	0.963	0.085	2.854	4
HD157289	8.929	0.129	0.215	-0.013	0.924	0.006	2.874	3
HD158205	8.289	0.082	0.192	-0.024	1.127	0.160	2.896	3
HD158293	8.936	0.098	0.212	-0.012	1.005	0.075	2.880	3
HD158450	8.514	0.212	0.185	-0.009	0.880	-0.078	2.892	2
HD158979	10.258	0.124	0.157	0.049	0.965	0.085	2.855	2
HD159930	9.977	0.192	0.108	0.095	1.156	0.246	2.870	3
HD159992	9.394	-0.051	0.260	-0.128	0.835	-0.088	2.879	3
HD160127	8.089	0.134	0.180	0.021	1.070	0.148	2.876	3
HD160468	7.306	0.262	0.175	-0.004	0.580	0.081	2.691	3
HD160544	9.152	0.226	0.189	0.017	0.861	-0.019	2.855	3
HD161349	8.470	0.294	0.164	0.006	0.475	0.015	2.678	2
HD161380	9.653	0.436	0.160	0.032	0.411	0.071	2.625	2
HD161423	9.328	0.175	0.284	-0.078	0.599	-0.221	2.820	3
HD161459	10.326	0.245	0.246	-0.040	0.680	-0.141	2.820	4
HD161596	9.669	0.062	0.173	0.035	1.017	0.162	2.841	2
HD161704	8.368	0.298	0.171	0.001	0.430	0.000	2.666	2
HD161755	9.635	0.297	0.152	0.054	0.917	0.039	2.854	3
HD161998	9.848	0.210	0.227	-0.025	0.888	0.112	2.798	2
HD162265	10.062	0.394	0.158	0.045	0.857	0.077	2.800	3
HD162316	9.338	0.262	0.274	-0.070	0.576	-0.222	2.809	2
HD162373	9.017	0.079	0.211	-0.023	0.882	-0.062	2.886	3
HD162639	9.897	0.270	0.177	0.018	0.850	0.114	2.778	3
HD163256	9.884	0.210	0.178	0.014	0.816	0.096	2.770	3
HD163379	8.821	0.265	0.158	0.022	0.808	0.172	2.731	2
HD163583	10.425	0.147	0.195	-0.029	0.982	0.012	2.897	3
HD163712	9.643	0.218	0.235	-0.032	0.856	0.078	2.799	3
HD163833	9.608	0.013	0.184	0.024	0.962	0.108	2.842	3
HD164231	8.609	0.117	0.234	-0.031	0.951	0.041	2.870	3
HD164258	6.378	0.098	0.189	-0.041	1.072	0.081	2.906	2
HD164485	8.292	0.333	0.218	-0.015	0.802	0.020	2.801	3
HD164827	9.301	0.178	0.140	0.063	0.944	0.040	2.867	2
HD165945	9.337	0.218	0.159	0.019	0.955	-0.001	2.891	3
HD166223	9.627	-0.012	0.174	-0.064	0.681	0.185	2.741	3
HD166469	6.476	0.003	0.141	0.064	0.860	0.058	2.811	3
HD166473	7.923	0.208	0.321	-0.118	0.514	-0.268	2.801	3
HD166808	9.244	0.093	0.205	-0.041	1.041	0.069	2.898	3
HD167024	9.177	0.097	0.212	-0.016	0.998	0.063	2.882	3
HD167288	8.572	0.065	0.147	0.034	0.500	-0.151	2.737	3
HD167700	9.515	0.234	0.175	0.011	0.981	0.035	2.887	3
HD168314	10.674	0.000	0.189	-0.064	0.895	0.046	2.847	3
HD168767	8.674	0.135	0.147	0.058	0.928	0.040	2.859	3

HD number	y	$b-y$	m_1	δm_1	c_1	δc_1	β	N
HD169380	9.852	0.014	0.256	-0.053	0.775	-0.129	2.867	3
HD169481	9.082	0.116	0.177	0.027	1.086	0.188	2.864	3
HD169852	9.462	0.102	0.185	0.015	1.006	0.076	2.880	3
HD169965	8.719	0.214	0.104	0.104	0.872	0.023	2.839	2
HD170044	10.729	0.204	0.197	-0.009	0.849	0.150	2.760	2
HD170397	6.041	-0.018	0.179	-0.058	0.897	0.084	2.831	3
HD170565	9.130	0.269	0.253	-0.047	0.628	-0.200	2.825	1
HD171279	7.367	0.070	0.169	-0.001	1.057	0.090	2.896	1
HD171771	8.471	0.245	0.144	0.054	1.025	0.093	2.881	3
HD172626	9.645	0.132	0.208	-0.006	0.988	0.076	2.871	3
HD172703	8.826	0.002	0.240	-0.037	0.845	0.059	2.803	3
HD173562	7.897	0.039	0.178	-0.008	1.105	0.140	2.895	3
HD176196	7.506	-0.035	0.165	-0.042	0.860	0.029	2.839	3
HD176519	9.673	0.000	0.249	-0.117	0.780	-0.143	2.879	3
HD177013	9.084	0.173	0.170	0.026	0.668	-0.074	2.781	4
HD177016	9.289	0.231	0.141	0.067	0.956	0.113	2.835	3
HD177268	9.034	0.059	0.210	-0.014	0.895	-0.040	2.882	3
HD177382	9.507	0.233	0.181	0.026	0.855	0.023	2.828	3
HD177765	9.152	0.248	0.261	-0.054	0.731	-0.110	2.834	3
HD178246	9.330	0.133	0.169	0.034	0.835	-0.067	2.866	3
HD180058	9.852	0.331	0.141	0.060	0.874	0.108	2.793	3
HD181810	10.502	0.058	0.204	0.002	0.932	0.060	2.851	3
HD183806	5.591	-0.024	0.173	-0.048	1.047	0.200	2.846	4
HD184120	10.220	0.051	0.229	-0.022	0.816	-0.042	2.844	3
HD184343	9.736	0.242	0.156	0.055	0.868	0.572	2.603	3
HD185204	9.534	0.178	0.266	-0.061	0.633	-0.169	2.811	3
HD185256	9.938	0.277	0.185	-0.004	0.615	-0.039	2.738	3
HD186041	9.186	0.391	0.116	0.056	0.537	0.107	2.666	2
HD186117	7.342	0.082	0.202	-0.001	1.028	0.108	2.875	4
HD186284	9.877	0.203	0.182	0.022	0.788	-0.020	2.814	2
HD187473	7.291	-0.008	0.160	-0.049	0.606	-0.005	2.768	4
HD187474	5.319	-0.063	0.220	-0.100	0.854	0.050	2.827	4
HD187761	9.617	0.161	0.218	-0.012	0.780	-0.038	2.819	3
HD188008	8.846	0.045	0.229	-0.035	0.876	-0.061	2.883	4
HD188518	9.468	0.321	0.155	0.027	0.438	0.064	2.642	2
HD188601	10.256	0.281	0.266	-0.063	0.555	-0.223	2.799	3
HD189832	6.910	0.139	0.201	0.006	0.950	0.115	2.830	4
HD189899	7.579	0.343	0.145	0.041	0.407	0.047	2.634	2
HD189963	10.005	0.237	0.203	0.002	0.864	-0.030	2.862	2
HD190290	9.912	0.289	0.293	-0.091	0.466	-0.306	2.796	4
HD190654	9.296	0.301	0.157	0.014	0.431	-0.006	2.669	2
HD191439	8.898	-0.010	0.229	-0.092	0.910	-0.063	2.899	3
HD191695	10.068	0.301	0.156	0.040	0.661	-0.081	2.781	3
HD191796	7.790	-0.025	0.202	-0.075	0.972	0.098	2.857	4
HD193644	8.642	0.236	0.160	0.014	0.591	0.033	2.708	2
HD193756	9.195	0.181	0.213	-0.008	0.760	-0.040	2.810	5
HD193941	8.943	0.295	0.153	0.018	0.421	-0.017	2.668	2
HD194623	8.724	0.255	0.181	-0.010	0.503	-0.006	2.694	2
HD194726	9.907	0.150	0.242	-0.035	0.869	0.002	2.848	2
HD194750	8.901	-0.047	0.202	-0.077	0.832	-0.006	2.842	2
HD195112	9.191	0.105	0.209	-0.007	0.681	-0.091	2.796	3
HD195961	5.336	0.254	0.273	-0.094	0.680	0.059	2.727	2
HD196470	9.721	0.211	0.263	-0.059	0.650	-0.144	2.807	4
HD197417	8.009	0.038	0.233	-0.032	0.939	0.015	2.877	4
HD200623	9.079	0.069	0.243	-0.053	0.871	-0.071	2.885	5
HD201018	8.645	0.041	0.249	-0.053	0.819	-0.116	2.882	4
HD202400	9.185	0.260	0.176	-0.006	0.437	-0.025	2.679	4
HD203006	5.081	-0.004	0.225	-0.100	0.830	-0.023	2.849	7
HD203932	8.820	0.175	0.196	0.004	0.742	-0.020	2.791	6

HD number	y	$b-y$	m_1	δm_1	c_1	δc_1	β	N
HD204018	6.419	0.212	0.264	-0.078	0.627	-0.059	2.753	1
HD204367	7.830	0.039	0.220	-0.060	0.996	0.020	2.899	2
HD207259	8.871	0.134	0.221	-0.013	0.742	-0.105	2.838	5
HD208217	7.199	0.102	0.274	-0.069	0.626	-0.186	2.816	5
HD208759	10.036	0.058	0.258	-0.062	0.877	-0.058	2.881	6
HD209364	9.976	0.207	0.238	-0.041	0.824	0.083	2.780	6
HD209605	9.576	0.174	0.243	-0.036	0.783	-0.055	2.832	6
HD212385	6.851	0.067	0.236	-0.062	0.934	-0.026	2.893	5
HD213637	9.611	0.298	0.206	-0.035	0.411	-0.031	2.670	2
HD215185	10.357	0.168	0.242	-0.054	0.732	0.032	2.760	2
HD215966	7.889	-0.036	0.178	-0.055	1.036	0.203	2.840	6
HD215983	9.664	0.076	0.232	-0.042	0.892	-0.050	2.885	6
HD217522	7.525	0.289	0.227	-0.056	0.484	-0.015	2.691	6
HD217704	10.265	0.146	0.229	-0.022	0.835	-0.031	2.848	5
HD218227	5.214	0.247	0.251	-0.071	0.660	0.027	2.731	1
HD218495	9.356	0.114	0.252	-0.049	0.812	-0.098	2.870	5
HD218994	8.565	0.154	0.196	0.008	0.826	0.032	2.807	5
HD219391	8.734	0.116	0.233	-0.027	0.873	-0.005	2.854	2
HD219831	9.988	0.109	0.235	-0.028	0.964	0.126	2.832	2
HD220003	6.029	0.259	0.267	-0.089	0.623	0.008	2.725	1
HD221127	9.099	0.307	0.184	0.002	0.323	-0.037	2.634	2
HD221531	8.342	0.285	0.173	-0.003	0.435	-0.025	2.678	5
HD221760	4.928	0.041	0.188	0.012	1.074	0.146	2.879	8
HD222638	8.666	-0.005	0.267	-0.137	0.811	-0.091	2.871	5
HD222925	9.022	0.403	0.110	0.109	0.473	0.191	2.596	5
HD223967	7.055	-0.041	0.165	-0.045	0.793	0.033	2.812	2
HD224962	10.177	0.243	0.212	-0.039	0.651	0.103	2.706	5

Table 4.3

Dereddened Strömgren photometric indices of the cool Ap stars

HD number	y	$b-y$	$[m_1]$	$[c_1]$	$[u-b]$	β
HD 2202	8.366	0.246	0.213	0.454	0.880	2.693
HD 2883	9.369	0.295	0.226	0.317	0.769	2.660
HD 2957	8.512	-0.001	0.208	0.973	1.389	2.885
HD 3980	5.719	0.068	0.299	0.743	1.342	2.876
HD 3988	8.351	0.107	0.188	0.914	1.290	2.830
HD 5823	9.846	0.190	0.245	0.623	1.113	2.767
HD 6532	8.445	0.088	0.230	0.861	1.321	2.880
HD 7676	8.402	0.113	0.314	0.607	1.236	2.832
HD 8783	7.796	0.078	0.220	1.035	1.475	2.883
HD 9050	8.965	0.147	0.244	0.793	1.282	2.808
HD 9289	9.383	0.138	0.250	0.798	1.298	2.832
HD 10081	9.615	0.004	0.182	1.028	1.392	2.877
HD 11090	10.811	0.112	0.296	0.674	1.266	2.853
HD 11346	9.922	0.156	0.233	0.911	1.377	2.854
HD 12932	10.235	0.179	0.260	0.729	1.250	2.810
HD 14944	9.732	0.114	0.197	1.121	1.514	2.846
HD 15144	5.879	0.058	0.234	0.918	1.387	2.889
HD 16002	8.962	0.080	0.230	1.020	1.481	2.857
HD 16145	7.668	0.033	0.205	1.042	1.452	2.887
HD 18610	8.162	0.124	0.370	0.549	1.290	2.828
HD 19712	7.357	-0.076	0.234	0.862	1.331	2.867
HD 19918	9.336	0.169	0.246	0.788	1.281	2.855
HD 20505	9.901	0.019	0.229	0.985	1.444	2.906
HD 20880	7.957	0.097	0.229	0.986	1.445	2.870
HD 22488	7.505	0.221	0.256	0.736	1.247	2.752
HD 23207	7.568	0.113	0.279	0.816	1.375	2.868
HD 23393	8.299	0.225	0.196	0.743	1.134	2.743
HD 23715	9.477	0.154	0.259	0.775	1.293	2.822
HD 24712	6.001	0.191	0.245	0.588	1.079	2.760
HD 24786	9.757	0.047	0.187	1.016	1.391	2.893
HD 24825	6.823	-0.046	0.179	1.052	1.410	2.831
HD 26726	9.860	0.131	0.335	0.618	1.287	2.858
HD 27211	9.468	-0.027	0.189	0.973	1.352	2.888
HD 27285	9.747	0.148	0.233	0.849	1.315	2.835
HD 27463	6.350	0.022	0.235	0.868	1.338	2.878
HD 27472	10.001	0.147	0.238	0.821	1.298	2.815
HD 28430	8.221	0.119	0.204	0.943	1.352	2.856
HD 29578	8.507	0.173	0.260	0.734	1.255	2.813
HD 30335	9.717	0.064	0.220	0.989	1.428	2.899
HD 30374	9.696	0.081	0.166	1.009	1.340	2.871
HD 30849	8.865	0.168	0.313	0.688	1.315	2.847
HD 31225	7.019	0.099	0.208	1.048	1.464	2.871
HD 31973	9.437	0.083	0.229	0.949	1.407	2.882
HD 33011	9.579	0.171	0.247	0.745	1.238	2.801
HD 33629	9.064	0.200	0.267	0.643	1.177	2.784
HD 34205	9.264	0.134	0.243	0.927	1.413	2.877
HD 34514	9.268	-0.007	0.197	1.000	1.394	2.868
HD 35361	9.959	0.154	0.188	1.031	1.407	2.828
HD 36964	9.614	0.123	0.257	0.801	1.316	2.848
HD 37308	8.728	0.128	0.256	0.871	1.383	2.829

HD number	y	$b-y$	$[m_1]$	$[c_1]$	$[u-b]$	β
HD 38719	7.510	0.017	0.210	1.024	1.444	2.892
HD 39575	7.867	-0.059	0.237	0.873	1.348	2.868
HD 40277	8.333	0.046	0.258	0.854	1.370	2.894
HD 40765	9.577	0.271	0.290	0.612	1.191	2.739
HD 40886	8.209	-0.021	0.238	0.775	1.252	2.818
HD 41385	9.434	0.154	0.309	0.650	1.268	2.840
HD 41511	4.894	0.220	0.050	1.230	1.329	2.769
HD 41613	9.689	0.202	0.195	0.893	1.283	2.845
HD 41757	8.489	-0.005	0.183	1.138	1.504	2.847
HD 42075	8.968	0.205	0.297	0.624	1.218	2.788
HD 42326	7.708	0.010	0.245	0.897	1.387	2.889
HD 42605	8.934	0.146	0.244	0.874	1.362	2.881
HD 42659	6.768	0.124	0.279	0.740	1.299	2.834
HD 42777	9.166	-0.013	0.262	0.788	1.311	2.876
HD 43226	8.961	0.102	0.266	0.792	1.324	2.876
HD 43901	8.216	0.138	0.250	0.898	1.398	2.862
HD 44226	9.492	0.161	0.288	0.739	1.315	2.842
HD 44290	8.533	-0.023	0.196	0.904	1.295	2.860
HD 44550	9.626	0.269	0.209	0.628	1.047	2.703
HD 45698	8.161	0.072	0.261	0.808	1.330	2.883
HD 45870	9.802	-0.005	0.208	0.970	1.386	2.861
HD 45961	9.424	0.062	0.213	0.952	1.378	2.870
HD 46649	9.564	0.036	0.192	0.790	1.175	2.835
HD 46665	9.441	0.039	0.262	0.694	1.218	2.840
HD 47009	9.070	0.091	0.217	0.867	1.302	2.873
HD 49686	9.798	0.063	0.208	1.029	1.446	2.878
HD 50031	9.668	0.125	0.275	0.822	1.373	2.897
HD 50143	9.781	0.145	0.273	0.671	1.217	2.810
HD 50304	7.574	0.005	0.138	1.231	1.507	2.791
HD 50620	9.743	0.085	0.258	0.885	1.402	2.892
HD 50627	10.633	0.239	0.219	0.814	1.252	2.837
HD 50861	9.718	0.150	0.201	0.885	1.287	2.830
HD 51203	10.500	0.207	0.293	0.646	1.232	2.813
HD 51684	7.950	0.139	0.281	0.774	1.336	2.842
HD 52280	9.793	0.039	0.186	1.029	1.401	2.905
HD 52539	9.507	-0.056	0.218	0.788	1.224	2.835
HD 52599	8.506	0.130	0.218	0.939	1.376	2.843
HD 52696	8.549	0.095	0.217	1.055	1.489	2.874
HD 52847	8.157	0.101	0.352	0.613	1.317	2.843
HD 54087	9.431	0.222	0.240	0.876	1.356	2.770
HD 54399	9.803	0.163	0.193	1.017	1.404	2.860
HD 55540	9.498	0.026	0.263	0.769	1.294	2.868
HD 55719	5.293	0.003	0.222	1.029	1.472	2.886
HD 56026	9.851	0.132	0.225	0.927	1.376	2.853
HD 56350	6.705	-0.079	0.194	0.797	1.184	2.813
HD 56809	7.102	0.034	0.202	1.124	1.528	2.877
HD 56882	8.378	0.111	0.254	0.835	1.343	2.872
HD 56981	10.015	0.489	0.294	0.147	0.735	2.600
HD 57040	9.207	0.259	0.372	0.367	1.110	2.785
HD 57964	9.405	0.070	0.127	0.707	0.960	2.825
HD 58368	9.592	0.086	0.246	0.825	1.318	2.877
HD 58939	10.131	0.113	0.201	1.099	1.502	2.888
HD 59164	8.365	0.002	0.200	1.067	1.467	2.877
HD 59437	9.260	0.029	0.257	0.873	1.388	2.872
HD 59660	10.033	0.067	0.186	1.019	1.391	2.871
HD 59776	8.913	0.217	0.208	0.660	1.076	2.734
HD 60435	8.891	0.136	0.264	0.806	1.335	2.855
HD 60572	9.338	0.007	0.257	0.776	1.290	2.871
HD 61468	9.844	-0.013	0.239	0.773	1.250	2.833

HD number	y	$b-y$	$[m_1]$	$[c_1]$	$[u-b]$	β
HD 61513	10.161	-0.046	0.244	0.832	1.320	2.869
HD 61731	9.767	0.123	0.305	0.624	1.235	2.843
HD 61763	7.958	0.025	0.115	1.018	1.247	2.742
HD 62244	8.276	0.035	0.219	1.036	1.475	2.886
HD 62399	9.440	-0.033	0.248	0.924	1.420	2.897
HD 62530	8.156	-0.036	0.198	0.863	1.258	2.818
HD 62553	7.857	0.045	0.214	1.032	1.460	2.885
HD 62556	7.941	0.032	0.218	0.822	1.257	2.865
HD 62562	8.926	0.078	0.259	0.820	1.338	2.889
HD 62905	9.597	0.014	0.238	0.834	1.309	2.840
HD 62953	8.940	0.260	0.158	1.397	1.713	2.760
HD 63728	9.316	0.016	0.189	0.855	1.233	2.860
HD 63745	10.683	0.020	0.272	0.724	1.267	2.856
HD 63759	8.292	0.063	0.217	1.079	1.514	2.891
HD 64288	10.171	-0.040	0.265	0.773	1.303	2.846
HD 65142	8.522	-0.026	0.193	1.018	1.405	2.841
HD 65836	6.788	0.063	0.223	0.920	1.367	2.904
HD 65963	9.281	0.006	0.186	0.922	1.294	2.853
HD 67909	8.961	0.110	0.244	0.854	1.342	2.869
HD 68013	9.185	-0.029	0.222	0.838	1.281	2.861
HD 68419	8.186	0.018	0.226	0.980	1.433	2.908
HD 68480	8.899	0.010	0.250	0.603	1.103	2.786
HD 68807	9.159	0.037	0.253	0.782	1.287	2.864
HD 68998	8.618	0.145	0.208	0.970	1.386	2.843
HD 69013	9.456	0.296	0.383	0.341	1.107	2.772
HD 69204	9.936	0.131	0.243	0.869	1.354	2.909
HD 69638	9.437	0.088	0.251	0.911	1.413	2.885
HD 69862	10.065	0.146	0.220	0.976	1.416	2.878
HD 70702	8.572	-0.076	0.291	0.857	1.440	2.904
HD 71058	9.436	0.599	0.392	0.231	1.015	2.590
HD 72316	8.804	-0.001	0.248	0.836	1.332	2.840
HD 72611	7.014	-0.062	0.189	0.732	1.110	2.805
HD 72634	7.280	-0.019	0.198	0.991	1.386	2.869
HD 72801	9.586	0.120	0.157	0.882	1.195	2.830
HD 73101	9.367	-0.003	0.166	0.891	1.224	2.827
HD 73403	8.877	-0.038	0.219	0.904	1.342	2.872
HD 73850	9.317	0.077	0.240	0.795	1.274	2.867
HD 74067	5.199	-0.052	0.228	0.898	1.354	2.856
HD 74169	7.214	-0.041	0.207	0.839	1.252	2.851
HD 74494	8.863	-0.021	0.237	0.797	1.272	2.826
HD 74555	8.956	0.010	0.205	0.927	1.337	2.854
HD 74629	9.696	0.143	0.229	0.970	1.428	2.893
HD 74636	9.210	0.027	0.164	0.896	1.223	2.835
HD 74672	9.801	0.122	0.243	0.956	1.442	2.895
HD 75049	9.090	-0.054	0.239	0.925	1.403	2.906
HD 75425	9.585	0.112	0.268	0.782	1.318	2.864
HD 75445	7.131	0.165	0.244	0.707	1.194	2.801
HD 76276	9.725	0.223	0.228	0.811	1.268	2.839
HD 76460	9.805	0.221	0.250	0.805	1.304	2.817
HD 76759	9.141	0.068	0.200	0.856	1.257	2.848
HD 76877	9.890	0.082	0.241	0.957	1.438	2.865
HD 77438	10.131	0.122	0.272	0.882	1.426	2.851
HD 77609	8.006	0.033	0.177	0.864	1.218	2.798
HD 77809	10.293	0.107	0.275	0.834	1.384	2.884
HD 77830	9.047	0.236	0.282	0.685	1.250	2.731
HD 79539	9.226	0.077	0.242	0.993	1.476	2.885
HD 79976	8.505	0.002	0.188	1.018	1.394	2.868
HD 80249	10.424	-0.081	0.289	0.901	1.480	2.890
HD 80316	7.782	0.118	0.345	0.575	1.266	2.856

HD number	y	$b-y$	$[m_1]$	$[c_1]$	$[u-b]$	β
HD 80992	9.867	0.088	0.221	1.073	1.515	2.884
HD 81076	9.546	0.147	0.156	1.056	1.369	2.797
HD 81289	8.403	-0.008	0.233	0.642	1.107	2.787
HD 81588	8.445	0.125	0.286	0.750	1.321	2.847
HD 81877	8.873	-0.008	0.238	0.851	1.326	2.819
HD 82038	9.568	0.168	0.197	1.020	1.415	2.867
HD 82093	7.095	0.065	0.203	1.056	1.461	2.872
HD 82417	9.181	0.150	0.189	1.122	1.500	2.872
HD 82562	9.213	0.014	0.198	0.939	1.334	2.870
HD 82749	9.364	0.019	0.181	0.971	1.334	2.842
HD 82989	8.320	0.418	0.239	0.579	1.058	2.720
HD 83181	9.467	0.008	0.200	0.953	1.354	2.888
HD 83368	6.168	0.159	0.259	0.734	1.251	2.825
HD 83817	9.047	0.332	0.231	0.559	1.020	2.711
HD 84041	9.330	0.177	0.265	0.762	1.291	2.844
HD 85284	9.775	0.039	0.219	0.888	1.326	2.818
HD 85453	8.144	-0.045	0.154	0.529	0.837	2.747
HD 85564	9.563	0.167	0.259	0.779	1.297	2.830
HD 85733	10.077	0.170	0.246	0.790	1.281	2.886
HD 85766	9.978	0.171	0.235	0.756	1.225	2.807
HD 86051	9.790	-0.030	0.198	0.846	1.241	2.806
HD 86181	9.323	0.172	0.236	0.723	1.195	2.819
HD 86592	7.858	0.113	0.311	0.607	1.230	2.837
HD 86976	8.345	0.127	0.317	0.737	1.370	2.883
HD 87087	9.912	0.126	0.188	1.028	1.403	2.862
HD 87488	6.987	-0.030	0.208	0.897	1.312	2.827
HD 88042	10.062	0.097	0.119	0.765	1.004	2.750
HD 88241	7.920	0.129	0.188	0.960	1.337	2.807
HD 88385	8.020	-0.007	0.272	0.761	1.305	2.838
HD 88507	9.697	0.135	0.220	0.891	1.332	2.855
HD 88701	9.258	0.002	0.225	0.830	1.280	2.846
HD 89075	8.488	0.001	0.123	0.900	1.146	2.807
HD 89192	6.850	0.019	0.189	0.976	1.355	2.889
HD 89385	8.327	0.015	0.202	0.903	1.306	2.871
HD 89519	8.266	0.032	0.156	0.832	1.143	2.791
HD 89680	8.368	0.053	0.184	1.070	1.437	2.872
HD 89840	9.855	0.156	0.191	1.016	1.398	2.870
HD 90131	9.517	0.030	0.293	0.893	1.480	2.877
HD 91087	9.426	0.058	0.271	0.816	1.359	2.883
HD 91239	7.365	-0.065	0.202	0.861	1.266	2.851
HD 91735	9.450	0.205	0.216	0.743	1.175	2.852
HD 91982	9.431	0.085	0.256	0.999	1.512	2.879
HD 92106	7.778	0.075	0.169	0.979	1.316	2.857
HD 92218	9.194	0.128	0.320	0.729	1.369	2.880
HD 92286	9.700	0.026	0.204	1.011	1.418	2.830
HD 92499	8.890	0.179	0.333	0.579	1.246	2.812
HD 92534	9.379	0.013	0.212	0.703	1.128	2.819
HD 93500	8.731	0.038	0.178	1.004	1.360	2.863
HD 94052	9.630	0.074	0.203	1.002	1.409	2.842
HD 94111	9.640	0.062	0.255	0.878	1.388	2.880
HD 94274	9.290	0.001	0.207	0.912	1.326	2.878
HD 94455	8.019	0.116	0.209	1.057	1.475	2.872
HD 94660	6.098	-0.080	0.226	0.746	1.197	2.801
HD 95158	9.224	0.159	0.239	0.868	1.345	2.824
HD 95491	9.208	0.169	0.223	0.889	1.336	2.806
HD 95508	9.521	0.005	0.206	0.954	1.366	2.874
HD 95699	7.751	0.070	0.249	0.952	1.449	2.872
HD 95811	9.502	0.281	0.296	0.644	1.235	2.739
HD 96237	9.434	0.233	0.303	0.657	1.263	2.824

HD number	y	$b-y$	$[m_1]$	$[c_1]$	$[u-b]$	β
HD 96451	6.901	0.053	0.245	0.957	1.446	2.886
HD 96616	5.155	0.001	0.198	1.031	1.427	2.873
HD 96897	10.121	0.935	0.705	0.057	1.468	2.613
HD 97132	9.727	0.121	0.251	0.934	1.435	2.871
HD 97394	8.797	0.105	0.304	0.800	1.408	2.862
HD 97987	9.806	0.522	0.303	0.249	0.855	2.713
HD 98340	7.137	-0.031	0.163	0.791	1.118	2.822
HD100357	8.973	0.029	0.213	0.743	1.170	2.815
HD100587	7.378	-0.005	0.184	0.958	1.326	2.826
HD101065	7.994	0.431	0.465	-0.084	0.845	2.641
HD101189	5.127	-0.018	0.131	0.882	1.143	2.810
HD101410	6.646	-0.001	0.150	1.076	1.376	2.856
HD102333	9.046	0.068	0.244	0.910	1.399	2.875
HD102812	10.763	0.140	0.283	0.801	1.367	2.874
HD102983	9.553	0.045	0.203	0.889	1.295	2.872
HD103210	10.189	0.128	0.224	0.957	1.405	2.866
HD103302	8.284	0.016	0.200	0.974	1.374	2.892
HD104044	9.577	-0.007	0.210	0.973	1.393	2.822
HD104402	9.506	0.091	0.227	0.974	1.429	2.893
HD105999	8.014	0.213	0.166	0.576	0.909	2.709
HD106215	9.323	0.034	0.217	0.989	1.423	2.878
HD106322	10.187	0.126	0.249	0.890	1.387	2.879
HD106374	7.360	0.123	0.236	1.005	1.478	2.829
HD107107	8.734	0.073	0.247	0.820	1.315	2.864
HD107180	9.846	0.180	0.270	0.786	1.327	2.862
HD109300	10.250	0.131	0.082	0.684	0.847	2.744
HD109426	9.217	0.227	0.215	0.860	1.289	2.846
HD109790	10.453	0.111	0.118	1.094	1.330	2.806
HD109989	9.087	0.053	0.222	0.899	1.342	2.868
HD110072	10.104	0.227	0.322	0.442	1.085	2.759
HD110274	9.328	0.195	0.243	0.766	1.252	2.853
HD110446	9.382	0.136	0.177	1.092	1.447	2.895
HD110568	9.746	0.284	0.191	0.746	1.128	2.766
HD111675	9.756	0.142	0.244	1.002	1.489	2.875
HD112528	8.249	0.199	0.252	0.779	1.283	2.839
HD112616	9.700	0.114	0.278	0.919	1.474	2.852
HD113149	10.156	0.069	0.154	1.023	1.332	2.872
HD113588	9.618	0.154	0.096	1.022	1.214	2.777
HD114035	8.292	-0.007	0.172	0.902	1.246	2.832
HD114709	9.943	0.087	0.211	1.026	1.447	2.875
HD115226	8.510	0.177	0.231	0.850	1.311	2.863
HD115285	8.326	0.075	0.170	1.090	1.429	2.860
HD115440	8.235	0.056	0.144	0.552	0.840	2.747
HD116114	7.024	0.174	0.254	0.813	1.322	2.833
HD116423	8.472	0.100	0.200	0.750	1.150	2.793
HD116458	5.654	-0.030	0.198	0.847	1.242	2.797
HD116729	8.951	0.066	0.272	0.827	1.371	2.900
HD116763	9.101	0.025	0.168	0.952	1.287	2.845
HD117025	6.106	0.044	0.239	0.850	1.328	2.884
HD117227	9.085	0.141	0.246	0.849	1.342	2.842
HD117290	9.281	0.152	0.256	0.849	1.361	2.867
HD117453	10.380	-0.032	0.274	0.763	1.312	2.848
HD117691	9.446	0.244	0.264	0.885	1.413	2.783
HD118231	8.902	0.053	0.119	0.791	1.028	2.785
HD118470	9.979	0.093	0.224	0.958	1.406	2.880
HD118683	9.824	0.213	0.232	0.844	1.309	2.832
HD118913	7.692	0.034	0.199	0.928	1.326	2.863
HD119027	10.022	0.257	0.260	0.506	1.026	2.731
HD119158	9.778	0.135	0.232	1.047	1.512	2.883

HD number	y	b-y	$[m_1]$	$[c_1]$	$[u$-$b]$	β
HD119308	7.853	0.005	0.205	0.912	1.322	2.882
HD119794	8.993	0.089	0.241	0.900	1.382	2.875
HD120346	9.813	0.121	0.164	0.971	1.298	2.833
HD121276	9.464	0.130	0.117	0.632	0.867	2.750
HD121661	8.556	0.036	0.240	0.798	1.279	2.866
HD121675	9.676	0.150	0.227	0.923	1.377	2.841
HD121788	8.761	0.164	0.233	0.839	1.304	2.793
HD121840	9.424	0.175	0.261	0.939	1.460	2.868
HD122525	8.703	0.169	0.200	1.034	1.435	2.885
HD122569	9.008	0.003	0.223	0.950	1.395	2.885
HD122659	9.024	0.005	0.205	0.977	1.387	2.875
HD123112	6.974	0.046	0.141	1.048	1.330	2.845
HD123164	9.879	0.117	0.259	0.852	1.370	2.874
HD123627	8.139	0.140	0.211	1.041	1.463	2.887
HD124437	8.925	0.086	0.186	1.000	1.373	2.842
HD124740	7.826	0.004	0.142	0.822	1.106	2.804
HD125467	8.667	0.100	0.234	0.855	1.323	2.871
HD125555	9.400	0.218	0.216	0.927	1.360	2.826
HD125735	10.070	0.097	0.242	0.884	1.369	2.885
HD126297	9.456	0.188	0.215	0.890	1.320	2.831
HD126365	8.426	0.245	0.210	0.484	0.904	2.705
HD126515	7.078	-0.052	0.269	0.868	1.406	2.907
HD126936	9.491	0.300	0.214	0.617	1.045	2.722
HD127021	9.753	0.169	0.183	0.949	1.316	2.868
HD127154	7.281	0.001	0.121	0.961	1.203	2.794
HD127159	9.707	0.189	0.208	0.872	1.288	2.847
HD127210	10.365	0.266	0.219	0.517	0.955	2.718
HD127241	8.999	0.052	0.179	0.876	1.234	2.826
HD127608	8.546	-0.053	0.218	0.861	1.298	2.837
HD128472	9.802	0.182	0.250	0.894	1.393	2.841
HD128540	9.108	0.117	0.168	1.127	1.463	2.888
HD128649	9.478	0.001	0.233	0.806	1.272	2.869
HD128843	10.334	0.115	0.157	0.908	1.221	2.887
HD129052	10.305	0.212	0.304	0.644	1.252	2.807
HD129189	8.523	0.016	0.202	0.817	1.221	2.860
HD129994	10.066	0.125	0.159	1.032	1.349	2.858
HD130336	8.870	0.012	0.113	0.585	0.811	2.763
HD130382	10.247	0.077	0.201	0.886	1.287	2.879
HD130559	5.634	0.024	0.209	0.898	1.317	2.879
HD131141	9.426	0.178	0.293	0.747	1.333	2.845
HD131750	8.549	0.121	0.282	0.686	1.249	2.847
HD131870	9.420	0.057	0.184	0.847	1.215	2.834
HD131910	9.906	0.275	0.200	0.788	1.189	2.753
HD132205	8.715	0.226	0.311	0.590	1.211	2.818
HD132322	7.357	0.129	0.250	0.917	1.418	2.894
HD132673	8.472	0.176	0.218	0.871	1.306	2.848
HD132968	8.635	0.082	0.168	1.123	1.458	2.865
HD132981	10.503	0.227	0.221	0.884	1.325	2.834
HD133792	6.255	0.035	0.182	1.094	1.459	2.869
HD133812	9.662	0.300	0.225	0.462	0.912	2.687
HD134214	7.464	0.216	0.262	0.577	1.101	2.774
HD134465	9.962	0.072	0.218	0.977	1.413	2.876
HD134507	9.629	0.187	0.205	0.953	1.362	2.853
HD134640	9.894	0.158	0.222	0.914	1.359	2.845
HD135173	9.758	0.126	0.226	0.927	1.378	2.869
HD135297	7.944	0.001	0.180	0.920	1.280	2.847
HD135396	8.279	0.259	0.183	0.763	1.128	2.754
HD135459	10.211	0.370	0.248	0.863	1.358	2.746
HD135480	8.907	0.092	0.231	0.937	1.398	2.899

HD number	y	$b-y$	$[m_1]$	$[c_1]$	$[u-b]$	β
HD135512	9.720	0.179	0.268	0.784	1.321	2.860
HD135728	8.602	0.236	0.245	0.884	1.375	2.842
HD135815	9.313	0.133	0.198	1.046	1.442	2.863
HD136575	10.222	0.129	0.209	0.997	1.416	2.884
HD137160	8.006	0.048	0.186	0.939	1.311	2.854
HD137401	9.886	0.211	0.247	0.858	1.352	2.843
HD137509	6.859	-0.085	0.165	0.373	0.702	2.711
HD137581	9.500	0.087	0.155	1.123	1.432	2.870
HD137802	9.398	0.141	0.281	0.747	1.310	2.871
HD137848	9.377	0.081	0.214	1.069	1.496	2.904
HD137949	6.673	0.196	0.346	0.541	1.233	2.818
HD138146	10.110	0.137	0.232	0.952	1.415	2.861
HD138218	9.639	0.195	0.237	0.766	1.240	2.794
HD138426	8.554	0.084	0.199	0.973	1.371	2.898
HD138497	7.161	0.020	0.219	0.850	1.287	2.840
HD138633	8.572	0.248	0.203	0.965	1.371	2.857
HD138777	9.690	0.249	0.308	0.618	1.234	2.782
HD138927	9.279	0.197	0.233	0.841	1.308	2.811
HD139474	9.163	0.021	0.183	0.851	1.216	2.838
HD139631	8.706	0.150	0.165	0.967	1.297	2.860
HD140220	7.980	0.069	0.154	1.124	1.433	2.854
HD140393	10.621	0.089	0.272	0.782	1.326	2.866
HD140748	9.214	0.089	0.247	0.908	1.402	2.877
HD140959	9.884	0.056	0.281	0.822	1.384	2.909
HD141249	10.178	0.223	0.318	0.625	1.262	2.835
HD141317	8.900	0.048	0.188	0.947	1.323	2.848
HD141981	9.853	0.136	0.203	1.055	1.462	2.885
HD142070	7.939	0.084	0.263	0.816	1.342	2.892
HD142502	9.501	0.244	0.258	0.812	1.328	2.861
HD142544	9.707	0.113	0.240	0.868	1.349	2.864
HD142823	8.946	0.104	0.166	0.841	1.173	2.861
HD143487	9.420	0.386	0.331	0.316	0.979	2.706
HD143654	8.978	0.180	0.177	0.963	1.318	2.895
HD144413	10.141	0.197	0.192	1.070	1.455	2.902
HD144748	8.612	0.094	0.215	1.043	1.473	2.886
HD144897	8.583	0.166	0.185	0.656	1.026	2.780
HD145074	10.299	0.369	0.206	0.800	1.213	2.814
HD145393	9.763	0.300	0.206	0.828	1.240	2.802
HD146631	9.526	0.214	0.231	0.911	1.372	2.825
HD146971	8.589	0.160	0.194	1.028	1.416	2.904
HD147105	8.783	0.342	0.175	0.934	1.283	2.874
HD147863	9.721	0.144	0.188	1.074	1.450	2.879
HD148593	9.111	0.348	0.278	0.628	1.184	2.827
HD148848	7.444	0.133	0.199	0.808	1.206	2.816
HD148898	5.384	0.064	0.192	1.059	1.442	2.885
HD149046	12.164	0.428	0.171	0.529	0.871	2.690
HD149250	9.263	0.033	0.203	0.734	1.140	2.814
HD149769	9.735	0.154	0.280	0.807	1.367	2.876
HD150035	8.901	0.174	0.164	1.032	1.361	2.872
HD150562	9.816	0.301	0.266	0.599	1.131	2.783
HD150715	10.010	0.119	0.170	1.051	1.392	2.874
HD150862	9.162	0.334	0.230	0.279	0.739	2.650
HD151301	8.541	0.222	0.284	0.622	1.190	2.827
HD151560	9.737	0.270	0.270	0.777	1.316	2.775
HD151860	9.031	0.258	0.196	0.534	0.927	2.733
HD151873	9.073	0.068	0.097	1.157	1.352	2.703
HD151941	9.801	0.202	0.251	0.851	1.353	2.831
HD152137	9.635	0.039	0.224	0.857	1.305	2.877
HD152387	8.925	0.153	0.192	1.078	1.461	2.908

HD number	y	$b-y$	$[m_1]$	$[c_1]$	$[u-b]$	β
HD153149	9.405	0.209	0.240	0.806	1.285	2.894
HD153183	8.968	0.142	0.193	0.978	1.363	2.846
HD153192	10.000	0.016	0.234	0.795	1.263	2.860
HD153201	6.390	0.009	0.117	0.600	0.833	2.730
HD153742	10.095	0.317	0.197	0.805	1.199	2.824
HD153953	9.422	0.312	0.170	0.909	1.249	2.818
HD154075	10.030	0.113	0.190	0.549	0.930	2.771
HD154253	9.011	0.113	0.247	0.781	1.276	2.863
HD154308	8.761	0.103	0.207	0.913	1.326	2.885
HD154645	9.027	0.056	0.163	0.930	1.256	2.814
HD154708	8.744	0.277	0.308	0.423	1.038	2.743
HD155127	8.388	0.144	0.160	1.043	1.363	2.864
HD155171	10.209	0.267	0.275	0.734	1.284	2.792
HD155188	9.877	0.050	0.244	0.761	1.249	2.854
HD156049	8.245	0.003	0.177	0.847	1.200	2.840
HD156808	8.614	0.640	0.034	1.457	1.525	2.788
HD156869	7.926	0.046	0.181	0.954	1.316	2.854
HD157289	8.929	0.129	0.238	0.898	1.375	2.874
HD158205	8.289	0.082	0.207	1.111	1.524	2.896
HD158293	8.936	0.098	0.230	0.985	1.445	2.880
HD158450	8.514	0.212	0.223	0.838	1.284	2.892
HD158979	10.258	0.124	0.179	0.940	1.299	2.855
HD159930	9.977	0.192	0.143	1.118	1.403	2.870
HD159992	9.394	-0.051	0.251	0.845	1.347	2.879
HD160127	8.089	0.134	0.204	1.043	1.451	2.876
HD160468	7.306	0.262	0.222	0.528	0.972	2.691
HD160544	9.152	0.226	0.230	0.816	1.275	2.855
HD161349	8.470	0.294	0.217	0.416	0.850	2.678
HD161380	9.653	0.436	0.239	0.324	0.803	2.625
HD161423	9.328	0.175	0.316	0.564	1.195	2.820
HD161459	10.326	0.245	0.290	0.630	1.210	2.820
HD161596	9.669	0.062	0.184	1.004	1.372	2.842
HD161704	8.368	0.298	0.225	0.370	0.820	2.666
HD161755	9.635	0.297	0.205	0.858	1.269	2.854
HD161998	9.847	0.209	0.265	0.846	1.375	2.798
HD162265	10.062	0.394	0.229	0.778	1.236	2.800
HD162316	9.338	0.262	0.321	0.524	1.166	2.809
HD162373	9.017	0.079	0.225	0.866	1.317	2.886
HD162639	9.897	0.270	0.226	0.796	1.247	2.778
HD163256	9.884	0.210	0.216	0.774	1.206	2.770
HD163379	8.821	0.265	0.206	0.755	1.166	2.732
HD163583	10.425	0.147	0.221	0.953	1.396	2.897
HD163712	9.643	0.218	0.274	0.812	1.361	2.799
HD163833	9.608	0.013	0.186	0.959	1.332	2.842
HD164231	8.609	0.117	0.255	0.928	1.438	2.870
HD164258	6.378	0.098	0.207	1.052	1.466	2.906
HD164485	8.292	0.333	0.278	0.735	1.291	2.801
HD164827	9.301	0.178	0.172	0.908	1.252	2.867
HD165945	9.337	0.218	0.198	0.911	1.308	2.891
HD166223	9.627	-0.012	0.172	0.683	1.027	2.741
HD166469	6.476	0.003	0.142	0.859	1.142	2.811
HD166473	7.923	0.208	0.358	0.472	1.189	2.801
HD166808	9.244	0.093	0.222	1.022	1.466	2.898
HD167024	9.177	0.097	0.229	0.979	1.438	2.882
HD167288	8.572	0.065	0.159	0.487	0.804	2.737
HD167700	9.515	0.234	0.217	0.934	1.368	2.887
HD168314	10.674	0.000	0.189	0.895	1.273	2.847
HD168767	8.674	0.135	0.171	0.901	1.244	2.859

HD number	y	$b-y$	$[m_1]$	$[c_1]$	$[u-b]$	β
HD169380	9.852	0.014	0.259	0.772	1.289	2.867
HD169481	9.082	0.116	0.198	1.063	1.459	2.864
HD169852	9.462	0.102	0.203	0.986	1.392	2.880
HD169965	8.719	0.214	0.143	0.829	1.114	2.839
HD170044	10.729	0.204	0.234	0.809	1.277	2.760
HD170397	6.041	-0.018	0.176	0.901	1.252	2.831
HD170565	9.130	0.269	0.301	0.574	1.177	2.825
HD171279	7.367	0.070	0.182	1.043	1.406	2.896
HD171771	8.471	0.245	0.188	0.976	1.352	2.881
HD172626	9.645	0.132	0.232	0.962	1.425	2.871
HD172703	8.826	0.002	0.240	0.845	1.325	2.803
HD173562	7.897	0.039	0.185	1.097	1.467	2.895
HD176196	7.506	-0.035	0.159	0.867	1.184	2.839
HD176519	9.673	0.000	0.249	0.780	1.278	2.879
HD177013	9.083	0.173	0.201	0.633	1.036	2.781
HD177016	9.289	0.231	0.183	0.910	1.275	2.835
HD177268	9.034	0.059	0.221	0.883	1.324	2.882
HD177382	9.507	0.233	0.223	0.808	1.254	2.828
HD177765	9.152	0.248	0.306	0.681	1.293	2.834
HD178246	9.330	0.133	0.193	0.808	1.194	2.866
HD180058	9.852	0.331	0.201	0.808	1.209	2.793
HD181810	10.502	0.058	0.214	0.920	1.349	2.851
HD183806	5.590	-0.025	0.168	1.052	1.389	2.846
HD184120	10.220	0.051	0.238	0.806	1.282	2.844
HD184343	9.736	0.242	0.200	0.820	1.219	2.603
HD185204	9.534	0.178	0.298	0.597	1.193	2.811
HD185256	9.938	0.277	0.235	0.560	1.029	2.738
HD186041	9.186	0.391	0.186	0.459	0.832	2.666
HD186117	7.342	0.082	0.217	1.012	1.445	2.875
HD186284	9.878	0.203	0.220	0.747	1.186	2.814
HD187473	7.291	-0.007	0.159	0.607	0.925	2.768
HD187474	5.319	-0.063	0.209	0.867	1.284	2.827
HD187761	9.617	0.161	0.247	0.748	1.242	2.819
HD188008	8.846	0.045	0.237	0.867	1.341	2.883
HD188518	9.468	0.321	0.213	0.374	0.799	2.642
HD188601	10.256	0.281	0.317	0.499	1.132	2.799
HD189832	6.910	0.139	0.226	0.922	1.374	2.830
HD189899	7.579	0.343	0.207	0.338	0.752	2.635
HD189963	10.005	0.237	0.246	0.817	1.308	2.862
HD190290	9.912	0.289	0.345	0.408	1.098	2.796
HD190654	9.296	0.301	0.211	0.371	0.793	2.669
HD191439	8.898	-0.010	0.227	0.912	1.366	2.899
HD191695	10.068	0.301	0.210	0.601	1.021	2.781
HD191796	7.790	-0.025	0.198	0.976	1.371	2.858
HD193644	8.642	0.236	0.202	0.543	0.948	2.709
HD193756	9.195	0.181	0.246	0.724	1.215	2.810
HD193941	8.944	0.295	0.206	0.362	0.774	2.669
HD194623	8.724	0.256	0.227	0.452	0.906	2.694
HD194726	9.907	0.149	0.269	0.838	1.376	2.848
HD194750	8.901	-0.047	0.193	0.841	1.226	2.842
HD195112	9.191	0.105	0.228	0.660	1.116	2.796
HD195961	5.336	0.254	0.319	0.629	1.267	2.727
HD196470	9.721	0.211	0.301	0.608	1.210	2.807
HD197417	8.009	0.038	0.240	0.931	1.411	2.877
HD200623	9.079	0.069	0.255	0.857	1.368	2.885
HD201018	8.645	0.041	0.256	0.811	1.324	2.882
HD202400	9.185	0.259	0.223	0.385	0.830	2.679
HD203006	5.081	-0.004	0.224	0.831	1.279	2.849
HD203932	8.820	0.175	0.227	0.707	1.162	2.791

HD number	y	$b-y$	$[m_1]$	$[c_1]$	$[u-b]$	β
HD204018	6.419	0.212	0.302	0.585	1.189	2.753
HD204367	7.831	0.039	0.227	0.989	1.443	2.900
HD207259	8.871	0.134	0.245	0.715	1.205	2.838
HD208217	7.199	0.102	0.292	0.606	1.190	2.816
HD208759	10.036	0.058	0.268	0.865	1.402	2.882
HD209364	9.976	0.207	0.274	0.782	1.330	2.780
HD209605	9.576	0.174	0.274	0.748	1.297	2.832
HD212385	6.851	0.067	0.248	0.921	1.417	2.893
HD213637	9.611	0.298	0.260	0.352	0.872	2.671
HD215185	10.357	0.168	0.272	0.698	1.243	2.760
HD215966	7.889	-0.036	0.172	1.043	1.386	2.840
HD215983	9.664	0.076	0.246	0.877	1.368	2.885
HD217522	7.525	0.289	0.279	0.426	0.984	2.691
HD217704	10.265	0.146	0.255	0.806	1.316	2.848
HD218227	5.214	0.247	0.295	0.611	1.202	2.731
HD218495	9.356	0.114	0.273	0.789	1.334	2.870
HD218994	8.565	0.154	0.224	0.795	1.243	2.807
HD219391	8.734	0.116	0.254	0.850	1.358	2.854
HD219831	9.989	0.109	0.255	0.942	1.451	2.832
HD220003	6.029	0.259	0.314	0.571	1.198	2.725
HD221127	9.099	0.308	0.239	0.261	0.740	2.635
HD221531	8.342	0.285	0.224	0.378	0.827	2.678
HD221760	4.928	0.041	0.195	1.066	1.457	2.879
HD222638	8.666	-0.005	0.266	0.812	1.344	2.871
HD222925	9.022	0.403	0.183	0.392	0.757	2.596
HD223967	7.055	-0.041	0.158	0.802	1.117	2.812
HD224962	10.177	0.243	0.256	0.602	1.114	2.706

Chapter 5

High-speed photometry of the roAp stars

5.1 Introduction

This chapter has two functions. The first is to present the new roAp stars discovered in the Cape Survey. At least one light curve and one amplitude spectrum is shown for each of the new roAp stars. This has considerable entertainment value for no two roAp star oscillation spectra are exactly alike. The light curves have, with very few exceptions, been obtained in Johnson *B* light. The second function of this chapter is to provide an observational history of the new roAp stars and to illustrate just how hard it can be to prove that these stars pulsate, or otherwise.

The oscillations in the roAp stars have been studied almost exclusively using the technique of high-speed photometry. The extremely low oscillation amplitudes, < 1 mmag in many cases, demand high photometric precision. That such precision can be routinely attained is shown by the fact that 22 of the known 25 roAp stars have been discovered at the South African Astronomical Observatory (SAAO). We find that when we participate in multisite collaborative projects, the quality of photometry from the other sites is rarely as good as the SAAO data. Why is this? In the 1983 edition of *Hvar Observatory Bulletin* **7**, p. 271, Waelkens commented in the discussion after Weiss's paper that La Silla "... is really excellent for photometry; but it is still rare to get the same impressive accuracy that Kurtz obtained at Sutherland." Breger commented that the success of the photometric observations at Sutherland could "be due to the excellent equipment and the experienced people using the site." It is true that one of our main advantages is that we are attuned to the normal behaviour of our photometers and consequently we identify malfunctions quickly.

In the first half of this chapter I will describe how we acquire our high-speed photometric observations, what the sources of error are and what manipulations we subject the data to. Common pitfalls are also discussed at some length. Although I will discuss our experiences in observing the roAp stars, much of this chapter discusses the technique of high-speed photometry rather than observations of the roAp stars, *per se*. In a sense, this chapter could be sub-titled "common pitfalls in high-speed photometry." Readers interested in a detailed exposition of high-speed photometry are referred to the monograph on this subject by Brian Warner (1988). The second half of the chapter

contains the discovery light curves for the new roAp stars. The chapter ends with an atlas of null results from the Cape Survey.

The high-speed photometry reported in this chapter was acquired by me over 28 weeks spanning 2.5 years. During this time, D.W. Kurtz also used much of his telescope time in support of the Cape Survey. He contributed about another twelve weeks' worth of high-speed photometric observations which are also presented here. UCT students R. Ashley, A Jonson, G. Kauffmann and H. Winkler also contributed small amounts of data. Most of the results presented in this chapter have already been published and, where possible, I indicate the involvement of other people by referring to the original discovery publications.

5.2 Selection of the candidate roAp stars

To enhance our chance of discovering new roAp stars we searched for oscillations mainly in the subset of stars with Strömgren photometric indices similar to those of the 14 roAp stars known prior to the start of our survey (Figs 4.6 & 4.7):

$$0.08 \leq b\text{-}y \leq 0.29;$$

$$0.20 \leq m_1 \leq 0.32$$

$$\delta m_1 \geq 0.01$$

$$0.49 \leq c_1 \leq 0.85$$

$$\delta c_1 \leq 0.04$$

$$2.70 \leq \beta \leq 2.83$$

Indices in these ranges are not an unambiguous indicator of roAp pulsation. Nonetheless, we have found this technique to be highly successful. In the three years since its inception, the Cape Survey has produced 10 confirmed new roAp stars compared to only one discovery during that time by parallel searches in both hemispheres.

The reader may object to our procedure by claiming that it is possible that the above ranges of photometric indices are a selection effect rather than astrophysically real limits of the roAp phenomenon. To test this we searched for rapid oscillations in a large number of stars which fell outside the ranges above; all these stars yielded null results. We also observed a small number of stars 'blind', that is, without any knowledge of their colours. One new roAp star discovered in this way turned out to have photometric indices in the ranges given above. All the null results of the Cape Survey are presented in section 5.9.

5.3 The instrumentation used for the high-speed photometry

The observations are acquired using the University of Cape Town Photometer (Nather and Warner 1971), St Andrews Photometer (Spencer Jones, 1983) and the Radcliffe Peoples Photometer attached to either the 0.75-m or 1.0-m telescope at the Sutherland site of the SAAO. A small number of high-speed observations were acquired using the SAAO 0.5-m telescope with the Modular Photometer, which was described earlier in section 4.3. These observations were usually acquired when conditions were deemed not good enough for all-sky photometry but usable for high-speed photometry. This is not to say that we observed in non-photometric conditions; oscillations in HD 84041 discovered on the 1.0-m telescope were subsequently confirmed with a very good light curve obtained on the 0.5-m telescope. As a rule, though, we avoided doing high-speed photometry with the 0.5-m telescope even for bright stars because the scintillation noise level for the 0.5-m telescope is about 0.6 mmag on a good night, about twice as much as that of the 1.0-m telescope. (By the term 'scintillation noise level', I mean the level of the highest scintillation noise peaks in the amplitude spectrum of the observations.) Thus the larger 0.75-m and 1.0-m telescopes were used to collect more photons and, more importantly for these relatively bright stars, to reduce the scintillation noise.

The high-speed photometric observations in the Cape Survey are usually acquired as continuous 10-s integrations through a Johnson *B* filter. To minimize the effects of seeing fluctuations and tracking errors we use apertures of 30 arcsec or larger. The use of such large apertures is not problematic for the roAp stars which are all so bright that the dominant source of noise is scintillation and *not* photon statistics and/or sky background. For some of the roAp stars which are as bright as $V = 3$, some attenuation of the light at the telescope is necessary to reduce the photometer's count rates. For this purpose the instruments are equipped with neutral density filters which allow attenuation by either 2.5 mag or 5 mag. In some cases, we reduced the count rate by observing the star in the Johnson *U* band or in Strömgren *v* rather than inserting a neutral density filter in the light path. Observing the brighter roAp stars through a narrower pass-band filter such as a Strömgren filter is desirable since it reduces the phase smearing which arises because of the well established colour dependance of the phase of the oscillations (Weiss & Schneider 1984, Kreidl & Kurtz 1986 & Kurtz 1990).

The field acquisition eyepieces on the University of Cape Town, St Andrews and Radcliffe People's photometers are mounted on X-Y slides. This allows the eyepiece to be manually moved to a

nearby guide star and locked on to it so that program star observations do not have to be interrupted for guiding purposes. The SAAO 1.0-m telescope has an autoguider which can be used in conjunction with the St Andrews and Radcliffe Peoples photometers. For the University of Cape Town Photometer, a small commercially available CCD camera is available for autoguiding purposes, but we elected not to use it as the setup time was unacceptably long (10-15 min) for the short ($\approx$ 1 - 2 hr) monitoring runs used in the Cape Survey. Moreover, the CCD camera head must be mounted in place of the acquisition eyepiece so that visual inspection of the field is no longer possible. As of this writing, no satisfactory alternative to this undesirable mode of use has been devised. Experiments with the use of an autoguider show that it can lead to an appreciable reduction in noise by reducing image motion caused by telescope tracking errors. This in turn permits the use of a smaller aperture thus improving the signal-to-noise by lowering the sky background contribution. In our experience, the quality of the photometry acquired using an autoguider is higher at the cost of a longer setup time on a star.

The observations are interrupted at irregular intervals for measurements of the sky background, the frequency of which depend on the position and phase of the moon. On a good moonless night, it is sufficient to measure the sky background every 30 - 45 min. Because we are searching for oscillations with periods ~ 10 min and we want as high a duty cycle as possible, no standard stars are observed. The data are then binned to 40-s integrations to lower the point-to-point scatter and to lower the time required to compute the Fourier transforms. We have found that this binning gives a good visual display of the light curve in the time domain. There are sufficient points per cycle to see the shape of the light curve while the high frequency noise is reasonably suppressed.

The observations are all acquired in single-channel mode. We forgo the use of simultaneous comparison star observations because the roAp stars are usually the brightest stars in their fields and it is difficult to find a comparison star of similar brightness in the limited field of the second channel. Normalization to a fainter comparison star would only degrade the quality of the program star observations. Indeed, on good photometric nights, many observers who do use two channels simply discard their comparison channel observations. We measure the noise in our time series by quoting the standard deviation σ of one observation with respect to the mean for the night; σ includes all sources of noise as well as the actual variations in the star itself. On most good photometric nights at SAAO $\sigma \leq 5.0$ mmag; this includes *all* sky transparency variations and sensitivity drifts for the whole night as well as the oscillations in the program star itself. The reduction process normally lowers σ to

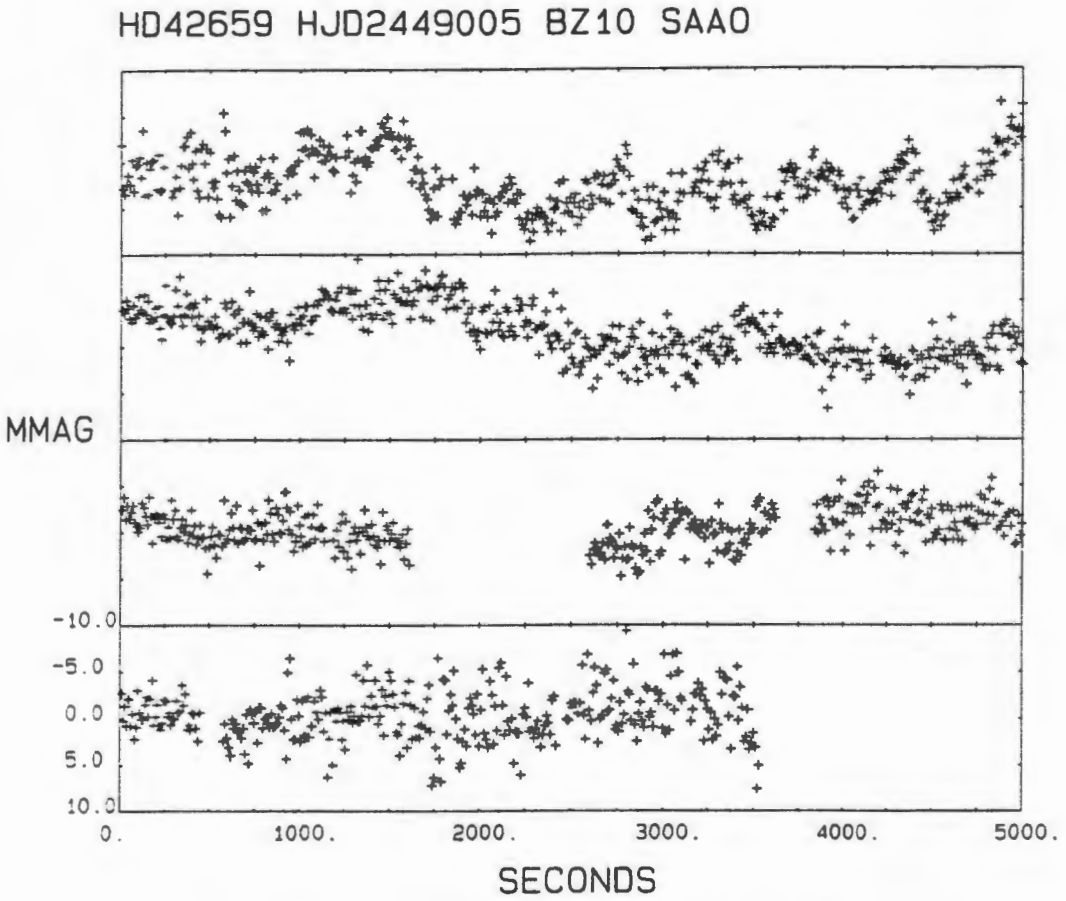

Figure 5.1 The 5-hr *B* light curve of HD 42659 obtained using the SAAO 1.0-m telescope on night JD 2449005. This light curve is continuous and is read left to right and top to bottom. The gap in the third panel is where about 1 ks of poor data was removed from the light curve.

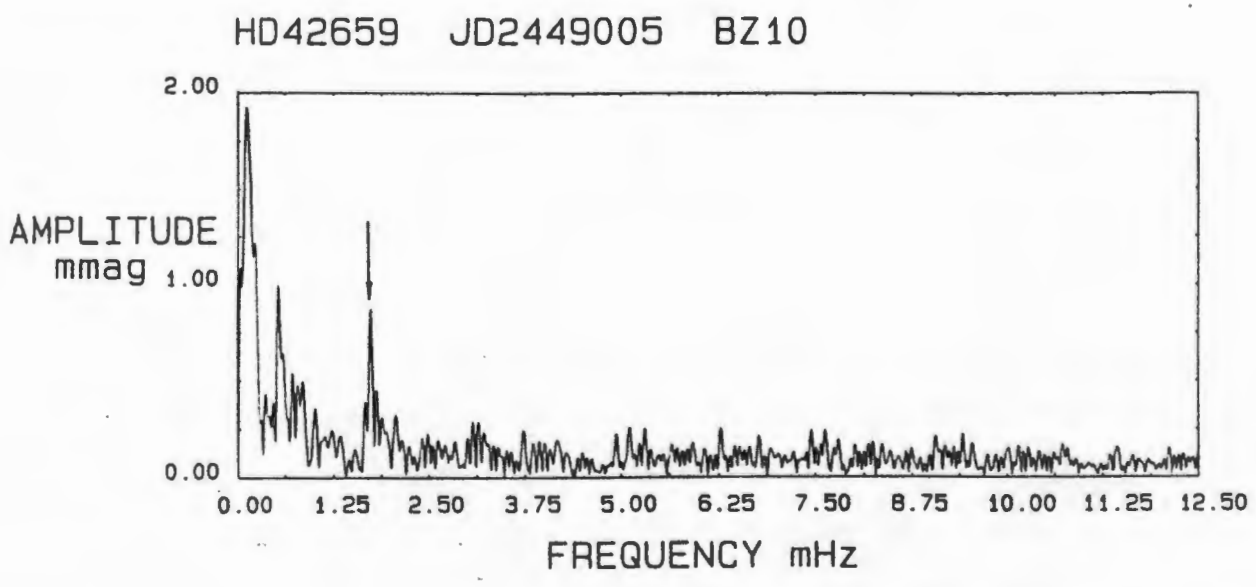

Figure 5.2 The discrete Fourier transform of the data in Fig. 5.1. Note that the ordinates are scaled in *amplitude*, not power. The arrowed peak is the oscillation eigenfrequency of the star. The peaks at low frequencies are caused by gradual sky transparency variations which are visible in Fig. 5.1.

around 2.5 mmag. Figure 5.1 is an example of a 5-hr light curve of the roAp star HD 42659 obtained on a (really) typical good night at SAAO. In Fig. 5.2 we show the Discrete Fourier Transform (DFT) (Deeming 1975, Kurtz 1985) of that light curve. This, and all other DFT's shown in this thesis have ordinates scaled in *amplitude*, not power. We use the term amplitude to mean one half of the peak-to-peak variation (*i.e.* the amplitude A in a signal varying as $\Delta m = A \cos(\omega t + \phi)$); some variable star photometrists would refer to this as the semi-amplitude. The arrowed peak in Fig. 5.2 is at the pulsation frequency of this star, ν = 1.72 mHz. The tall peaks at low frequency are caused by sky transparency variations during the observations. We will say more about these variations later.

The instrument is controlled by the acquisition program MILLY running on an IBM 80286 microcomputer (Balona 1988b). At the start of the high-speed observations, the observer specifies the run number, the filter (usually Johnson B) and the integration time. At the end of each integration the integrated raw photon count (*i.e.* not corrected for anything) is displayed both numerically and graphically. We find these real-time data displays to be indispensable aids in identifying and rectifying problems as they occur at the telescope.

5.4 Common Pitfalls

Because of the extremely low amplitudes of the roAp stars it is imperative that roAp star photometrists be aware of, and overcome, some common pitfalls such as:

(a) The use of small apertures which causes light losses from tracking errors and seeing fluctuations.

(b) Careless manual guiding which causes spurious dips in the light curve which have to be excised. Such gaps reduce the duty cycle and introduce unwanted sidelobes in the Fourier spectrum of the time series.

(c) In some telescopes, moonlight reflects off internal parts of the telescope causing problems, especially when the moon is close to the program star. This often causes step discontinuities in the light curve when the dome is rotated.

(d) Bad monitoring of sky background causes the sky subtraction process to introduce spurious trends which manifest themselves as low frequency noise. This is especially true for observations acquired near astronomical twilight or at moon rise/set.

(e) Sensitivity variations across the aperture cause guiding corrections to introduce discontinuities in the light curve. It is easy enough to test the flatness of the aperture

by positioning the star in the four quadrants of a large aperture and noting the count rates at each position. Such variations also exacerbate the deleterious effects of the periodic drive error of the telescope (see (m) below).

(f) Damp photomultiplier tube bases are often caused by power failures unnoticed by the observer during the day. Often power is restored with a minimal delay, but if the power is down for long enough, the cold-boxes start to warm up and moisture condenses on the photomultiplier tube base thus providing an electrical conduction path for inter-electrode leakage. This causes greatly increased scatter in the count rates, higher dark counts and introduces erratic excursions in the light curve. The only solution here is to bake out the moisture from the PMT. The presence of dirt or grease on the base of the PMT can lead to similar problems. Another consequence of daytime power cuts is that the PMT sensitivity may not stabilize by nightfall.

(g) Moisture can also condense on the Fabry lens or glass window of the photocathode thus fogging these surfaces. To prevent this, the Fabry lens is often heated slightly.

(h) Dirt on filter surfaces exacerbates problems with the drive error of the telescope at best and produces useless data at worst. Another good reason for checking the filters at the start of an observing run is that often the filters in the instrument are not the ones the observer thinks! The author has heard at least one credible story of an observer who spent a week observing through masking tape. Alternatively, the filters might be scratched or otherwise damaged or have deteriorated.

(i) Dirt often accumulates on the glass window of photocathode. Many observers keep their filter sets scrupulously clean only to place them in a photometer whose photocathode is dirty. In the University of Cape Town photometer, the aluminium dark slide, abraded from years of use, deposited a fine swarf on the surface of the glass envelope of the PMT. When I started observing on that occasion, a 2-minute telescope oscillation was immediately apparent in the real time display of the data. The severity of the problem had a strong hour angle effect which was probably caused by the swarf rolling around on the surface of the glass envelope. Interestingly, the previous observers had not noted any faults.

(j) Vignetting can be a frustrating source of error to find. Several years ago it was discovered that the baffle on the secondary mirror of one of the SAAO telescopes was vignetting the beam. The problem was so subtle that it took two years to find its cause.

(k) Misalignments in the photometer.

(l) The long time series acquired in high-speed photometry often reveal flexure problems in photometers. I have often noted flexure problems in runs lasting several hours. At the start of the run the program star and guide star were both well centered. Hours later the guide star was centered, but the program star had moved way off centre. The solution here is to interrupt the observations every 1.5-2 hr or so (depending on the declination) to check the centering of the program star in the aperture.

(m) Spurious periodicities are often introduced into the data by telescope drive oscillations. The most common telescope tracking errors are those with periods of 2 or 4 sidereal minutes (8.356 or 4.178 μHz, respectively) or multiples of these. In the case of HD 60435, a 4 mHz oscillation was 'studied' for several years before it was realized that this was an oscillation in the telescope and not in the star! A manifestation of the 2-minute (8.3 mHz) drive error on the SAAO 0.75-m telescope is shown in the panel for HD 31973 in Fig. 5.32. This was caused by the presence of dirt on the glass envelope of the photomultiplier tube (see (i) above). The drive error is strictly periodic, but frequent guiding corrections introduce irregular phase glitches which produce a broad Lorentzian hump of power centered on the drive frequency rather than a single spike. It should also be remembered that the apparent amplitude of the drive error goes as cos δ where δ is the declination.

(n) A telescope that is too finely balanced and 'floats' on a worn drive gear produces erratic excursions of the star in the aperture. This problem can be cured with the simple expedient of putting a small extra weight on the telescope so that it is no longer so finely balanced.

(o) Electronic malfunctions such as drifting or fluctuating HT supply introduce spurious trends in the data. The very large variation in gain produced by a small variation in voltage makes it essential to use a very well regulated voltage supply.

(p) Inadequately shielded photomultiplier tubes are affected by variations in the local magnetic field as when, for example, an iron observing ladder is moved close to the instrument.

(q) It is not uncommon to have electrical switching noise caused by coldbox coolers, lights, dome rotation motors, wind-blind motors, printers and radios causing spikes in the data stream.

(r) Poor thermal regulation in cold boxes can lead to high dark current as the PMT warms up. This often appears as a periodic oscillation in the count rates as the cooler unit switches on and off with some characteristic period. One should also remember that temperature variations cause changes in the spectral characteristics of the photocathode with a general increase in red sensitivity with increasing temperature. For *U*-band photometry this means that the red leak will increase as the PMT temperature increases.

(s) Inaccurate time is also an insidious source of error. It is vital that the observer should have reliable means of checking the time accurate to ≤ 0.1 sec independent of the data acquisition system. Most acquisition computers supply a date and time which get written to the header of the data file. Often, these dates and times are wrong by anything ranging from a fraction of a second to a day (often *exactly* 1 day), or more. In some acquisition systems, the observer enters the date, time and the RA and Dec of the star at the start of a run and *no other record is kept of the observations*. The data are logged as Heliocentric Julian Dates and counts. This is a disaster waiting to happen. In the event of a mistake being made in the entry of any of these 4 quantities, it is impossible to recover the actual times. Heliocentric corrections are also often incorrectly calculated. Computing the correct Heliocentric times is vital to producing useful roAp photometry, especially when subtle period changes or frequency shifts are being sought.

The above sources of error arise in the instrumentation and can all be eliminated or minimized by careful maintenance. We end this section by reiterating our earlier remark that an on-line data display is absolutely essential to detecting many of these problems at the telescope in time for remedial action to be taken.

5.5 Sources of noise

In addition to the sources of error that can be removed or minimized by the observer there are sources of noise which are less easy to overcome. There are two main sources of atmospheric noise that the roAp star observer has to contend with. First there are sky transparency variations that occur on a time-scale of 20 min or longer. For single-channel observations, the effect of these variations is to introduce peaks at low frequencies $\nu \leq 1.0$ mHz in the Fourier transform of the data (see Fig. 5.2). On good nights, these sky transparency peaks are well resolved from the frequencies of interest ($\nu \geq 1.0$ mHz) and the roAp oscillations can be detected without difficulty. On marginal nights, the sky transparency noise can extend above 2.0 mHz making the detection of the roAp oscillations impossible. The severity of these sky transparency oscillations depends on the quality of the night and the observer can do nothing about them. They are influenced by dust, fires, volcanic ash and temperature and humidity fluctuations during the passage of frontal weather systems.

The noise at higher frequencies is dominated by *scintillation* (Warner 1988) which is caused by rapid atmospheric density fluctuations at heights up to the tropopause. For the relatively bright roAp stars it is the level of the scintillation noise, not photon statistics, that sets the lower limit of detectability of oscillation amplitudes. The level at which the sky transparency noise reaches the scintillation noise sets the lower frequency limit at which oscillations can be detected and studied. Fortunately, the observer can reduce the scintillation noise by using a larger telescope. Young (1967) showed that the scintillation noise goes down as the -2/3 power of the telescope aperture and rises as the 3/2 power of the airmass. Kurtz (1984c) obtained observations of the roAp star HD 101065 using a 0.5-m and 1.9-m telescope which demonstrate that the larger telescope produced data with scintillation noise lower by roughly a factor 2.5.

Fossat (1984) has investigated the broad-band photometric noise at a number of good mid-latitude sites around the world (La Silla, Mauna Kea, The Canary Islands, Granada & Sutherland) and concludes that there is remarkably little variation among these sites. In Figure 5.3 I show a schematic amplitude spectrum of atmospheric noise attainable with 5 hr of observations on a good night at Sutherland with the SAAO 1.0-m telescope. The Figure shows that on good nights the level of the sky transparency noise drops down to the level of the scintillation noise somewhere between 1 - 2 mHz.

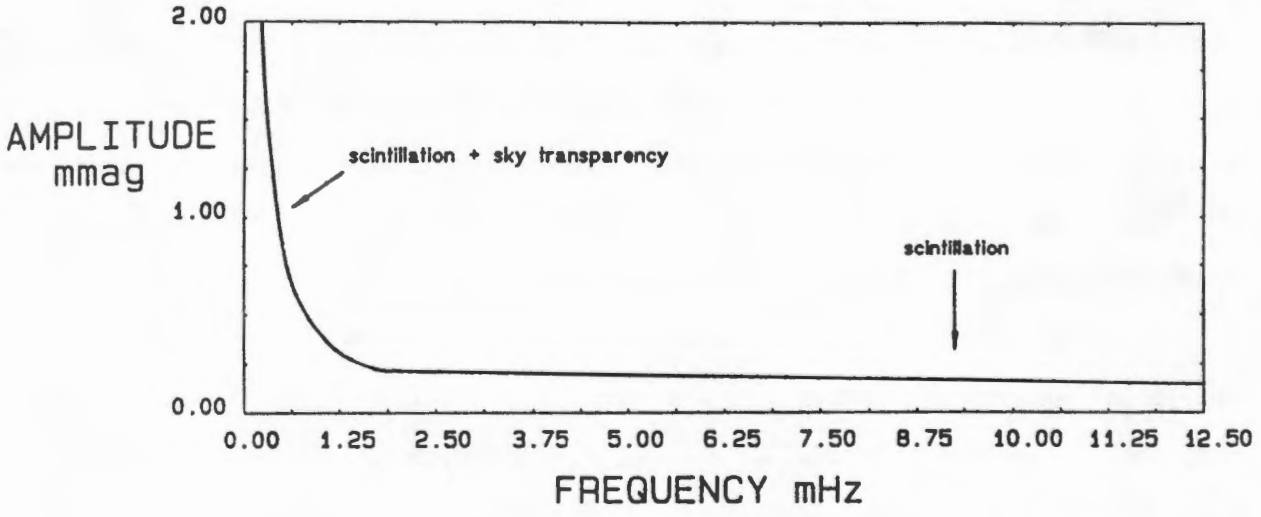

Figure 5.3 A schematic amplitude spectrum showing the typical atmospheric noise distribution obtainable with 5 hr of *B* observations on the SAAO 1.0-m telescope on a good night.

5.6 Aliasing

The daily gap in observations from a single site introduces strong 1 day^{-1} (11.57 μHz) aliases in the amplitude spectrum of data combined from several nights. Moreover, it is a perversity of nature that the eigenfrequencies in the roAp stars are often separated from each other by nearly an integral multiple of 1 day^{-1} thus making it impossible to study such frequencies from a single site. To reduce these problems, multisite observations are often acquired from sites well separated in longitude. This has the effect of increasing the duty cycle and lowering the amplitude of the daily aliases to eliminate confusion. However, even multisite observations are often gapped and one must be wary of aliases which are several sub-multiples of 1 day^{-1}.

5.7 The Reductions

The first step in the reduction process is visual inspection of the light curves to identify and remove all the obviously bad bits of data. It is not sufficient to flag only sky points at the telescope and reduce data without ever seeing the light curve. There are many ways in which spurious points get introduced into the light curve. We have already mentioned electrical switching noise above. Other sources of spurious data are cosmic rays, moonlit cirrus, contrails, lightning, aircraft lights, satellites and meteors passing through the field of the aperture. Schaefer (1985) has discussed the nature and incidence of spurious flashes in astronomical observations. After the removal of obvious bad points from the data stream, the data are corrected for coincidence counting losses, sky background and extinction in that order. The times of the midpoints of observations are converted into Heliocentric Julian Dates with an accuracy of 10^{-5} day (~1s). Since no standard stars are observed, no transformation of the resulting instrumental magnitudes to the standard system is done.

Data reduced in this way still contain noise at low frequencies $\nu \leq 1.0$ mHz caused by gradual sky transparency variations. These sky transparency variations manifest themselves in the Fourier transform as a number of high amplitude peaks at low frequencies. It is important to remove these peaks because they have relatively low amplitude sidelobes which cause perturbations to the frequencies of interest in the program star. The sky transparency variations are removed in the time domain by subtracting, or *prewhitening*, a series of low frequency sinusoids corresponding the low frequency sky transparency peaks. It is somewhat surprising that the sky transparency variations for a whole night can be modelled with remarkably few terms. On a good night, the subtraction of half a dozen peaks is sufficient to bring the low frequency noise down to the level of the scintillation noise.

The noise parameter σ is usually lowered to around 2.5 mmag by the prewhitening process on most good nights. Figure 5.4 shows the reduced and prewhitened light curve for the same data as depicted in Fig. 5.1. Figure 5.5 is the Fourier transform of these prewhitened data showing that most of the low frequency noise has been removed. These data are ready to be combined with data from other nights and Fourier analysed to reveal all the component frequencies of the oscillations.

Before going on to present the new roAp stars we will spend a few paragraphs discussing the limits of detection for oscillations in our data. We have already mentioned (Sec. 3.15) that for any given light curve the detection limits are governed by a combination of factors: the star's brightness, the duration of the run, the size of the telescope and the quality of the night. Here I will discuss these limits more quantitatively.

The first issue we will consider is the determination of the highest frequency that can be detected in the data, the so-called *Nyquist frequency*. For data sampled continuously with integration time τ this frequency is determined by the sampling frequency $1/\tau$. The periodogram of data sampled at rate $1/\tau$ contains aliases which arise because of beating between the sampling frequency and *any* frequency ν in the data. Thus the periodogram of data varying with frequency ν and sampled at frequency $1/\tau$ has peaks at ν, $1/\tau \pm \nu$, $2/\tau \pm \nu$,... (Kurtz (1983) illustrates this point graphically). The highest meaningful frequency ν that one can search up to is where ν and the first alias $1/\tau - \nu$ overlap, that is, where $\nu = 1/\tau - \nu$. This yields the Nyquist frequency $\nu_N = 1/2\tau$. Generally, one selects a sampling rate such that the frequencies of interest will fall within the first Nyquist interval. For our 10-s integrations binned to 40-s integrations, the Nyquist frequency is 12.5 mHz. This Nyquist interval is wide enough to include several harmonics of the principal frequency in roAp stars with non-sinusoidal light curves (*e.g.* Fig 2.3).

The lowest frequency at which we can search for a signal is not so well defined because the level of the sky transparency noise rises towards lower frequencies. To reduce the variance of the data and to remove the high frequency sidelobes of the sky transparency peaks from the frequency domain of interest, we prewhiten our data up to ~0.8 mHz on most nights. Thus we are insensitive to low-amplitude oscillations below ~0.8 mHz. In practice, we do not believe peaks with frequencies below 1.0 mHz; such oscillations are best studied using conventional differential photometry.

The amplitude limit for detection of oscillations on a good night for frequencies > 1.0 mHz is governed by the scintillation noise. The scintillation noise goes down as the -2/3 power of the telescope aperture (Young 1967). On a really good night one can attain a scintillation noise level of

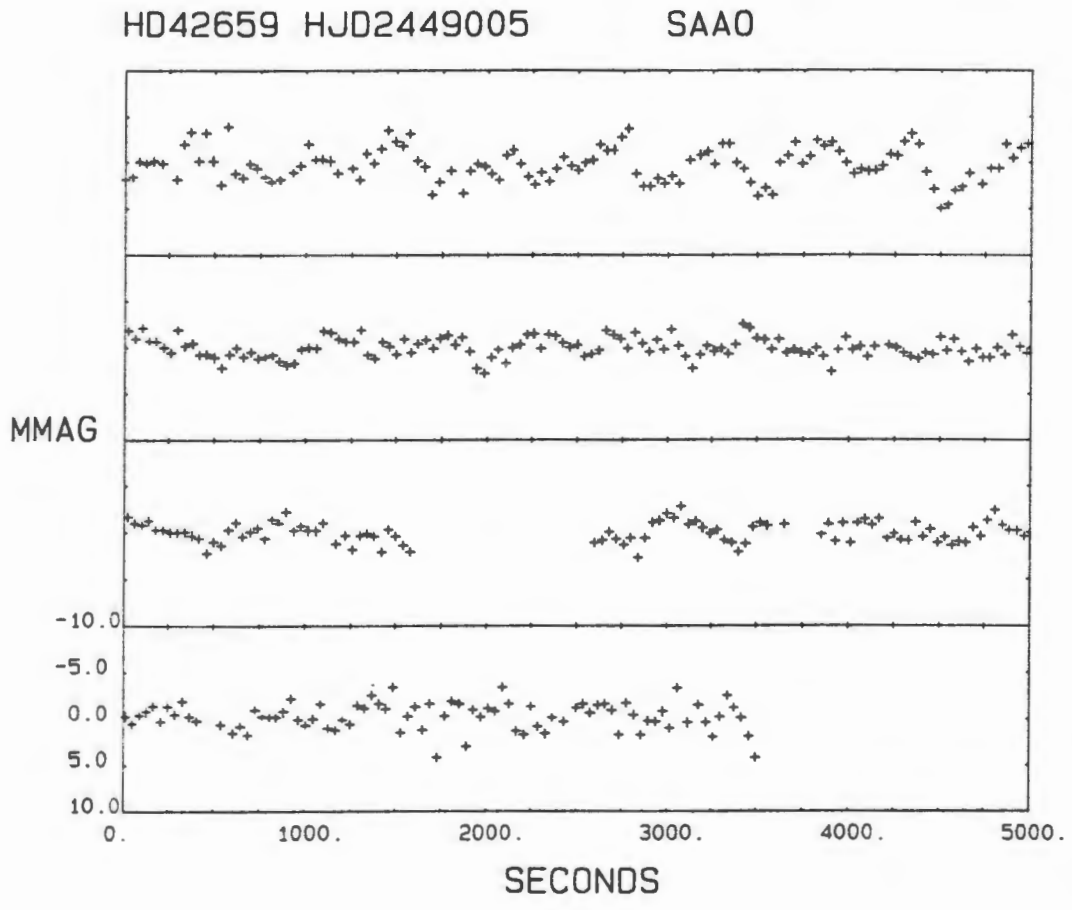

Figure 5.4 The light curve of the same data as in Figure 5.1 after the sky transparency variations have been prewhitened and the data binned to 40-s integrations.

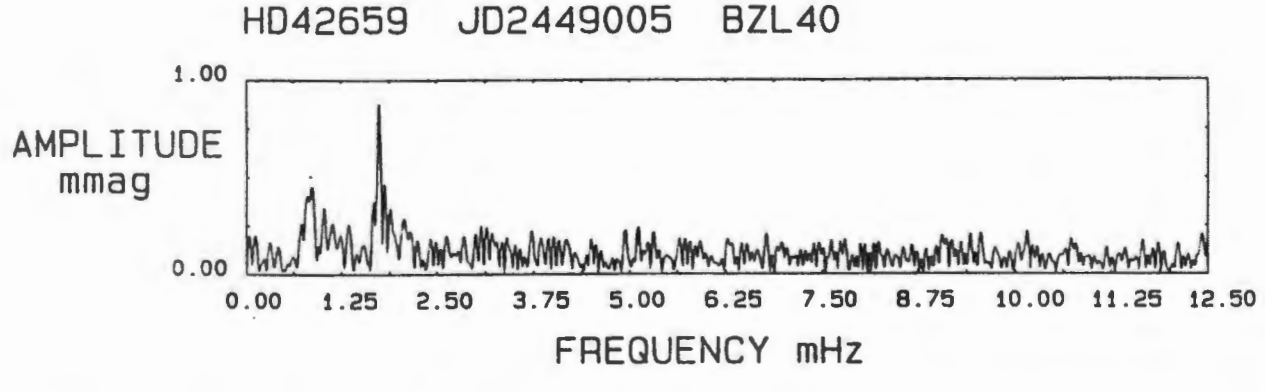

Figure 5.5 The amplitude spectrum of the light curve in Figure 5.4.

~0.2 mmag on the SAAO 1.0-m telescope. For the 0.5-m telescope the corresponding figure is about 0.4 - 0.5 mmag. The observed amplitude is also reduced because the observations are time averages, and not instantaneous measurements. It is readily shown that the amplitude reduction factor for a real frequency ν due to an integration time τ is sinc $(\nu\tau)$.

With this preamble, we now present the 10 new roAp stars to be discovered in the Cape Survey. The stars are presented in order of their HD catalogue numbers.

5.8 The new roAp stars

5.8a HD 19918

The southern (δ=-82°) Ap SrEuCr (Houk & Cowley 1975) star HD 19918 was monitored photometrically for 2.2 hr on the night of 6/7 October 1990 (JD2448171) (Martinez & Kurtz 1991a). The photometry was obtained using the University of Cape Town (UCT) photometer attached to the 0.75-m telescope of the SAAO. Figure 5.6(a) shows the discrete Fourier transform (DFT) of these observations out to the Nyquist frequency of 12.5 mHz. This amplitude spectrum was computed using Deeming's (1975) DFT algorithm as modified by Kurtz (1985) for faster execution. Normally we would remove the low frequency sky transparency peaks, but we deliberately show them in Fig. 5.6 so that the reader may judge the data. The peak marked ν_1 suggests the presence of rapid oscillations at 1.5 mHz with an amplitude of 0.9 mmag. We observed this star again on the nights JD2448172 and JD2448217 to confirm the presence of rapid oscillations at ν_1=1.5 mHz. The JD2448172 data were too noisy to confirm or refute our detection of oscillations at 1.5 mHz but on night JD 2448217 the 1.50-mHz peak appeared with a very good signal-to-noise ratio (Fig 5.6(b)). Note the difference in the amplitude of ν_1 in the two panels of Fig. 5.6. Such amplitude modulation is commonly observed in the roAp stars. It arises in the following ways: (1) through the beating of two, or more, unresolved oscillation frequencies, (2) though the oscillations being observed with changing aspect as the star rotates or (3) through intrinsic non-periodic variations in the amplitude of the oscillation frequency. Only a detailed study of the oscillations will reveal relative importance of these factors in HD 19918.

In Fig. 5.7 we present a light curve of the observations acquired on night JD2448217. To reduce the point-to-point scatter we have binned the data to 40-s integrations by taking non-overlapping 4-point averages of the data. We have also removed some low frequency sky transparency variations to

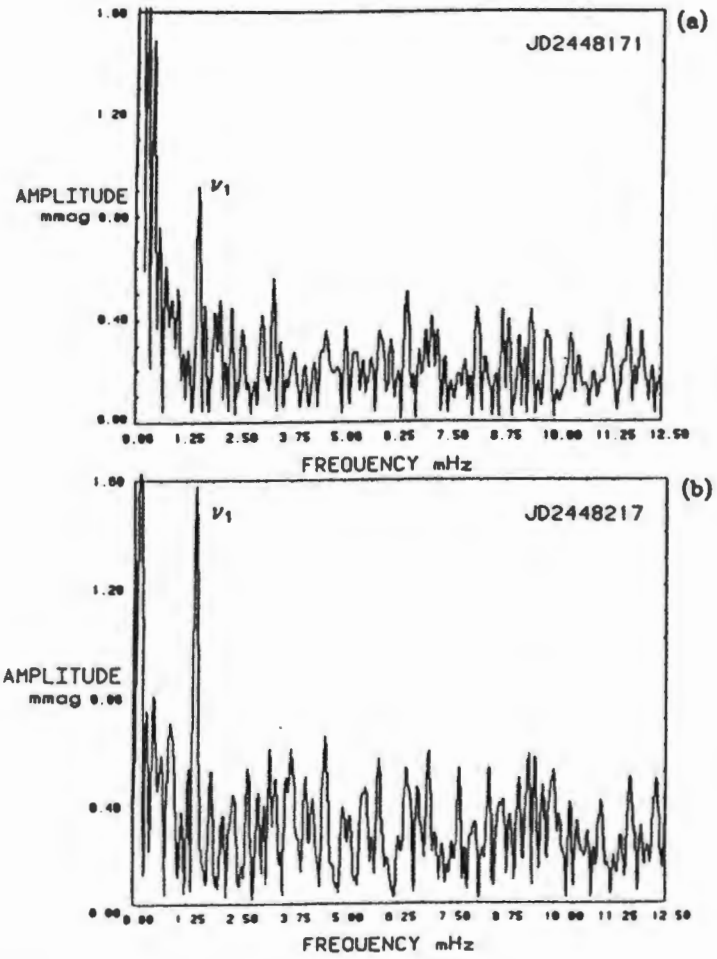

Figure 5.6 The discrete Fourier transform of the *B* light variations of HD 19918 on night JD 2448171 (a) and JD 2448217 (b). The sampling interval for both runs was 10 s binned to 40 s. This yields a Nyquist frequency of 12.5 mHz. The duration of run (a) was 2.2 hr and the duration of run (b) was 2.4 hr. The peak labeled ν_1 at 1.50 mHz marks the frequency of the rapid oscillations in HD 19918.

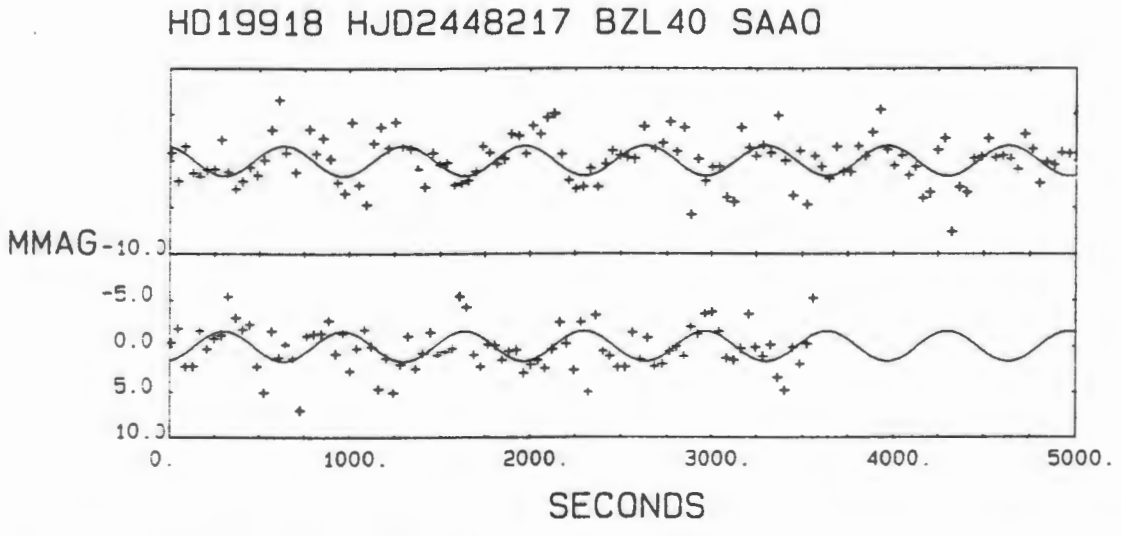

Figure 5.7 The record of the *B* light variations of HD 19918 on night JD 2448217. The sampling interval was 10 s binned to 40 s and the duration of the observations was 2.4 hr. The solid line is a least-squares fit to the observations of a sinusoid of frequency ν_1 = 1.50 mHz. This light curve is continuous from the upper left; the right edge of the top panel coincides with the left edge of the lower panel.

facilitate the reader's perception of the oscillations. The solid line is a least squares fit to the data of a sinusoid with frequency $\nu_1 = 1.50$ mHz and an amplitude of 1.61 mmag.

Table 5.1

Journal of observations of HD 19918

HJD start	T hr	N_{40}	σ mmag
8171.47550	2.20	196	1.611
8217.36385	2.39	214	2.462
8221.36284	1.84	165	3.160
8223.36059	4.28	375	2.560
8224.30791	3.97	350	3.104
8226.28137	2.76	239	3.441
8227.28528	4.35	382	2.125
8228.34903	1.65	145	2.352
8237.35652	2.11	189	3.650
8239.28299	2.39	210	3.099
8240.28448	2.04	128	2.573
8241.29512	0.83	74	2.749
8243.33618	1.39	116	3.388

We observed HD 19918 again on 11 nights from JD 2448221 to JD 2448243. On six of those nights we were able to confirm the existence of rapid oscillations at 1.5 mHz. The data for the other 5 nights were too noisy to permit a convincing detection of the oscillations. Visual inspection of the nightly amplitude spectra indicated that the oscillation amplitude is modulated on a night-to-night basis. To find the cause of this modulation and to refine our determination of ν_1 we analysed the data in groups of closely spaced nights and as a whole. All the data sets analysed suffer from severe aliasing ambiguities, so the determination of the principal frequency suffers from a 1 cycle per day alias ambiguity. With this caveat the principal frequency is $\nu_1 = 1.5102$ mHz. In keeping with the stated purpose of this chapter, namely, to present the new roAp stars and to convince the reader of the reality of the oscillations, we will not present those inconclusive frequency analyses here. The main reason why these analyses are inconclusive is that the runs are short and the noise levels in the data are fairly high. Workers planning future campaigns on HD 19918 should bear in mind that nights of excellent photometric quality are needed to study the rapid oscillations; the lowest airmass attained by this $\delta = -82^{\circ}$ star at Sutherland is 1.54.

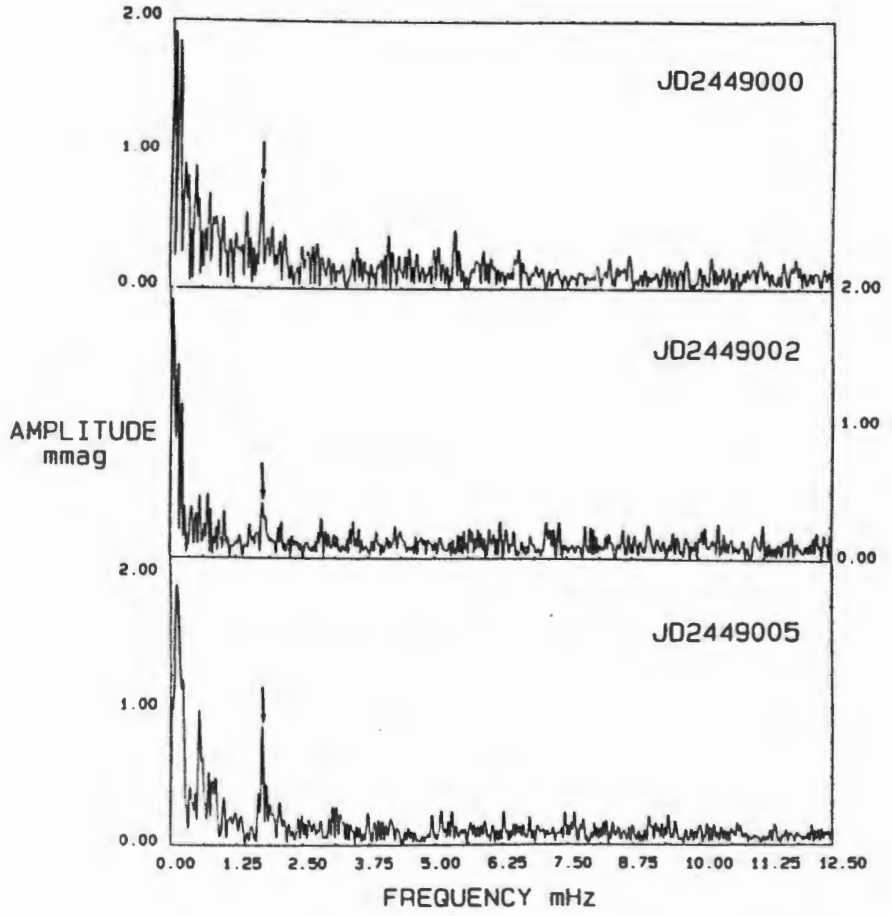

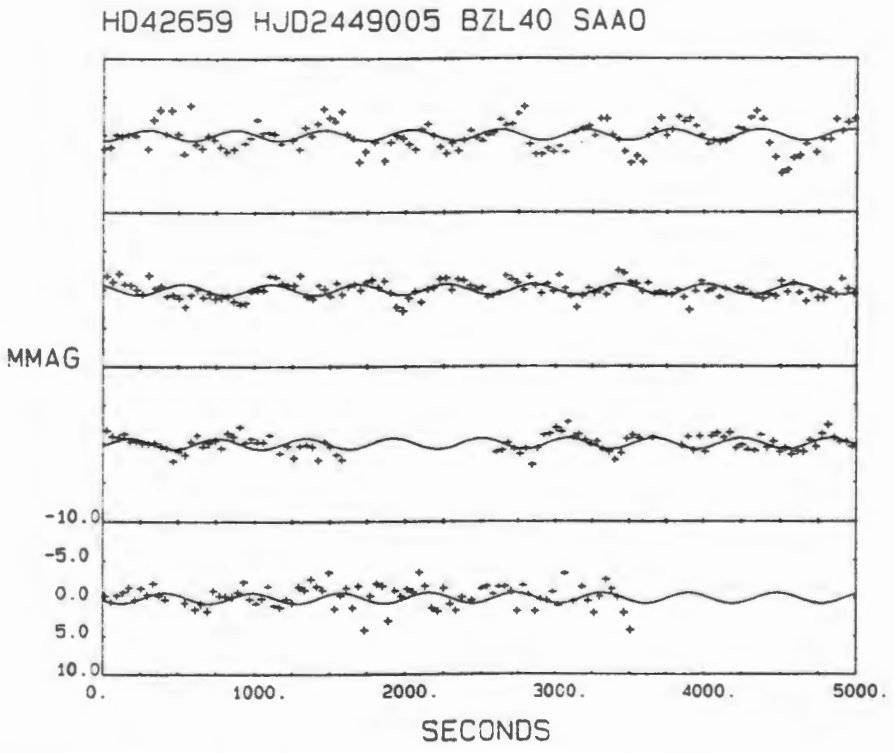

Figure 5.8 Amplitude spectra of the *B* light curves of HD 42659 acquired on nights JD 2449000, 9002 and 9005. The peaks at low frequency are caused by transparency variations in the atmosphere. The arrowed peak is the pulsation frequency ν = 1.72 mHz. Notice that in the lower two panels the level of the noise in the vicinity of ν_1 is ≈ 0.25 mmag. Below these amplitude spectra, we show the light curve for night JD 2449005. The solid line is a least-squares fit to the data of a sinusoid of frequency ν_1 = 1.72 mHz.

5.8b HD 42659

The cool Ap SrCrEu (Houk & Smith-Moore 1988) star HD 42659 was monitored photometrically for 1.59 hr on the night 22/23 November 1992 (JD 2448949) (Martinez, Kurtz & Ashley 1993). The data were acquired using the UCT photometer attached to the 0.75-m telescope of the SAAO at Sutherland. Inspection of the real-time data display at the telescope indicated the presence of rapid oscillations with a 10-minute period and a Johnson B amplitude of 0.5 mmag. A Fourier transform of the light curve showed a peak at ν = 1.7 mHz corresponding to the signal tentatively identified at the telescope.

HD 42659 has V = 6.768 so the dominant source of noise in these observations is scintillation rather than photon statistics. Because of the extremely low amplitude of these oscillations, we elected to confirm their reality on the larger SAAO 1.0-m telescope. This is an example of a case where a larger telescope was used not to increase the number of photons counted, but instead to *decrease* the scintillation noise. HD 42659 was observed again on nights JD2448965, 8966, 8967, 8968 and 8969. The 10-min oscillation was evident in the Fourier transform only on the first two nights. On nights 8967 - 8969 there were indications of the 10-min oscillations in the less noisy portions of the light curves, but there were no unambiguous peaks at ν = 1.7 mHz in the Fourier transforms of these light curves.

Further confirming observations were acquired on nights JD2449000-9002, 9004 and 9005 using the St Andrews Photometer, which has an autoguider, on the SAAO 1.0-m telescope. The continuous pointing corrections performed by the autoguider minimized the effect of light variations caused by tracking errors in the telescope. This allowed us to use smaller apertures, when conditions permitted, and produced more precise photometry than manual guiding. The 1.7 mHz signal appeared on all these nights. Table 5.2 is a journal of our high-speed photometric observations of HD 42659.

In Figure 5.8 we show the amplitude spectra acquired on three good nights without the low frequency peaks removed. The peak of interest here is the arrowed peak at ν = 1.72 mHz. Fig 5.8 shows that we have a convincing detection of the oscillations in HD 42659 even in the presence of sky transparency variations. There is evidence for amplitude modulation of the oscillations since on some nights no signal is seen. However, because the oscillations are at the limit of detectability of the equipment, this star will be very difficult to work on.

Table 5.2

Journal of observations of HD 42659

HJD start	T hr	N_{40}	σ mmag
8949.53464	1.59	142	0.987
8965.38322	3.05	271	0.951
8966.37207	3.57	314	1.102
8967.35932	3.64	326	1.608
8968.35596	2.29	201	1.095
8969.35974	5.55	492	1.101
8971.39536	1.92	282	1.982
9000.36052	4.25	341	1.273
9002.29334	5.68	476	1.289
8969.35974	5.55	492	1.101
9000.36052	4.25	341	1.273
9001.35243	4.33	366	1.212
9002.29334	5.68	476	1.289
9004.41331	2.47	213	1.291
9005.29105	5.14	420	1.418

5.8c HD 84041

The southern star HD 84041, classified as Ap SrEuCr by Houk (1982) and Ap SrEu(F) by Bidelman & MacConnell (1973), was identified as a roAp star candidate on the basis of its Cape Survey Strömgren photometric indices, b-y = 0.177, m_1 = 0.233, c_1 = 0.797, β = 2.844, which are typical of the cool Ap stars. Application of Crawford's (1979) calibration for normal A stars yields δm_1 = -0.026 and δc_1 = -0.061, both of which are indicative of heavy metal line blanketing. Recall from section 4.6 that the negative δc_1 index does not indicate a sub-dwarf luminosity for this star. It is a result of the extreme spectral abnormalities depressing the continuum redward of the Balmer jump thus affecting the c_1 index which measures the Balmer jump.

On the night JD 2448335 we acquired 1.02 hr of high-speed photometry of HD 84041 which suggested the presence of rapid oscillations with a period of 14.6 min (Martinez 1991). To confirm our detection of rapid oscillations we observed this star again on the nights JD 2448354, 8355, 8358, 8359, 8362 and 8377 using various SAAO 0.5-m, 0.75-m and 1.0-m telescope/photometer combinations. A journal of all these observations is given in Table 5.3.

From the outset, the amplitude of the oscillations in HD 84041 appeared to be strongly modulated. On some nights the amplitude was > 3 mmag and on other nights no coherent oscillations were detectable. There was also a suggestion of amplitude modulation on a time-scale of several

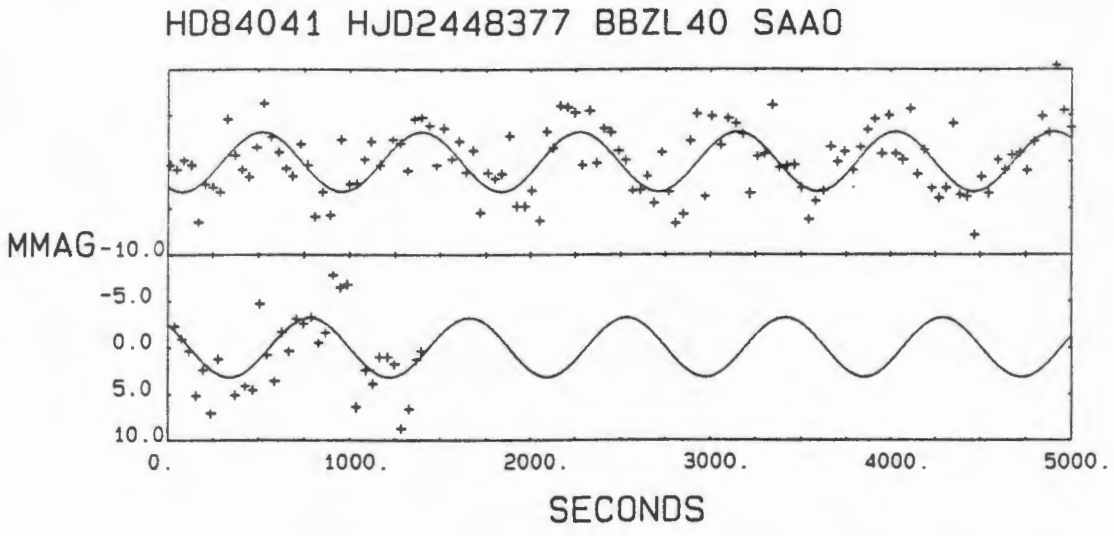

Figure 5.9 The second Johnson *B* light curve of HD 84041 acquired on night JD 2448377. The observations shown here have been binned to 40 s integrations and the sky transparency variations have been removed. The duration of the observations is 4.77 hr. The light curve shows variations with a 14.6-min period. To guide the reader's eye, we have fitted a sinusoid with a period 14.6 min to the data.

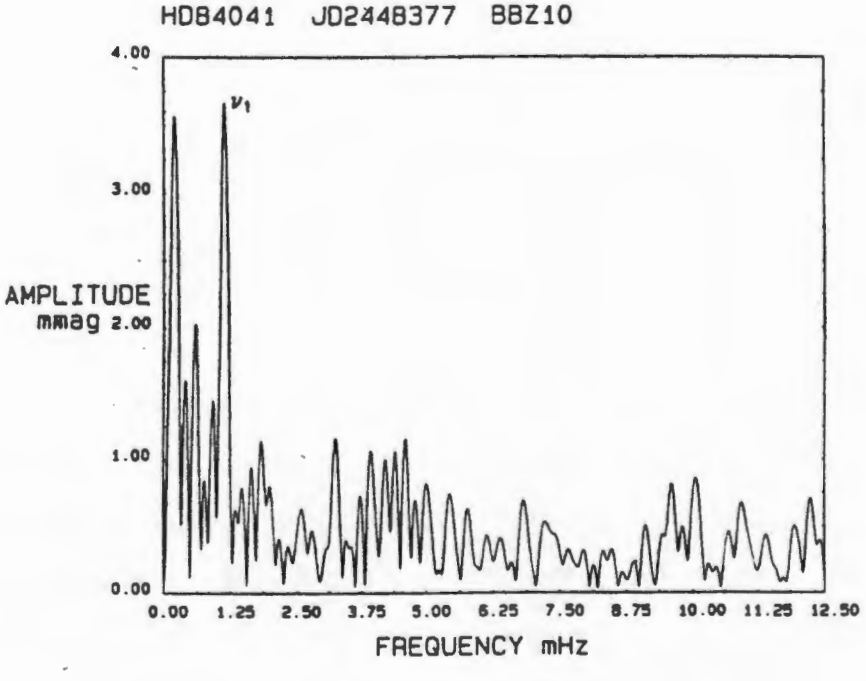

Figure 5.10 The Fourier transform of the data shown in Fig. 5.9. Here we have included the sky transparency variations so that the reader may see that we have a convincing detection of oscillations in the presence of the sky transparency variations.

hours. If a night's data were split into two halves, one half might show semi-amplitudes of 3 mmag in the amplitude spectrum while the other half might show the same oscillations at greatly reduced amplitude, or no oscillations at all!

Table 5.3

Journal of observations of HD 84041

HJD start	T hr	N_{40}	σ mmag
8335.36573	1.02	92	1.540
8354.28869	2.09	188	1.038
8355.34813	3.29	284	1.258
8358.26744	2.74	211	2.401
8359.31449	1.18	99	2.219
8362.23899	1.93	171	1.539
8377.33799	1.77	156	3.603
8377.21299	4.77	335	4.746

In Fig. 5.9 we present the light curve acquired on night JD 2448377. The amplitude spectrum of this light curve is shown in Fig. 5.10. in which the peak of interest is the one labeled ν_1 at 1.14 mHz. The solid line in Fig. 5.9 is a fit of a sinusoid of frequency ν_1 = 1.14 mHz to the data. The peaks to the left of ν_1 in Fig. 5.10 are caused by sky transparency variations which have been removed in Fig. 5.9. The noise at frequencies $\nu \geq 0.8$ mHz, the scintillation noise, is quite high in Fig. 5.9 because these observations were acquired using an 0.5-m telescope. Interestingly, these are some of the best signal-to-noise data we have on this star! As Fig. 5.10 shows, at ν_1 = 1.1 mHz, the oscillations are not clearly in the frequency regime dominated by scintillation noise and this complicates the study of the rapid oscillations in this star. The intriguing behaviour of HD 84041 during the 1991 discovery observations motivated us to organize a collaborative multi-site campaign on this star for the 1992 season. This campaign is reported in detail in chapter 6.

5.8d HD 119027

HD 119027 is classified by Houk (1982) as Ap SrEu(Cr). Its Strömgren and Hβ photometric indices have been determined as part of the Cape survey: V = 10.022, b-y = 0.257, m_1 = 0.214, c_1 = 0.557 and β = 2.731. For this β index, Crawford's (1979) A star calibration yields δm_1 = -0.034 and δc_1 = -

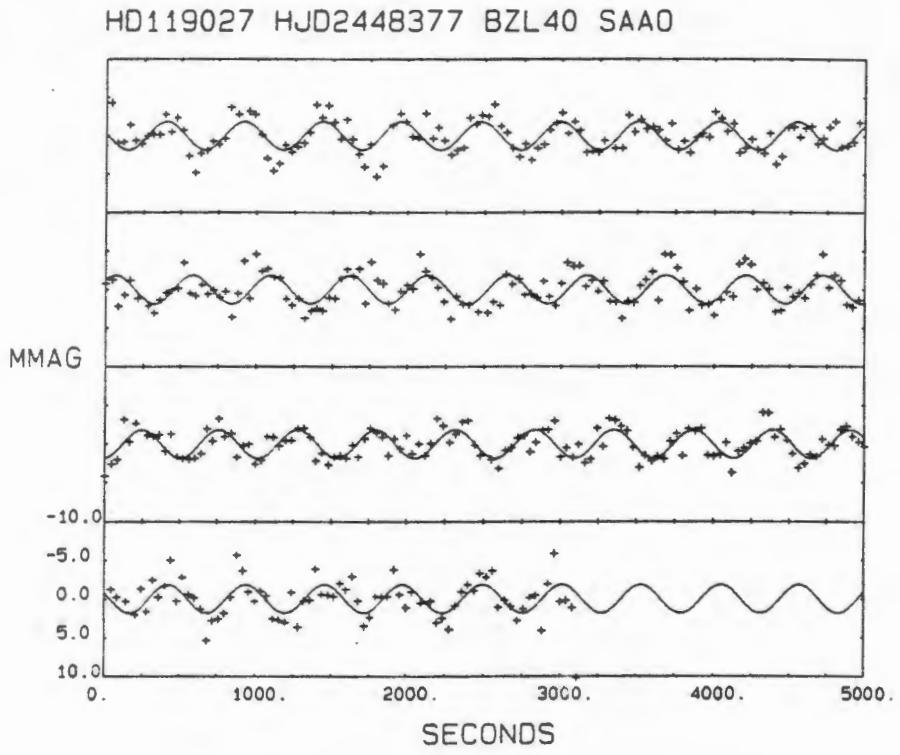

Figure 5.11 The light curve of HD 119027 in Johnson *B* light spanning 5.03 hr on night JD 2448377. The light curve is continuous from the upper left. Each point is the mean of 4 10-s integrations. The solid line is a best-fit sinusoid with a period of 8.63 min and an amplitude of 1.8 mmag.

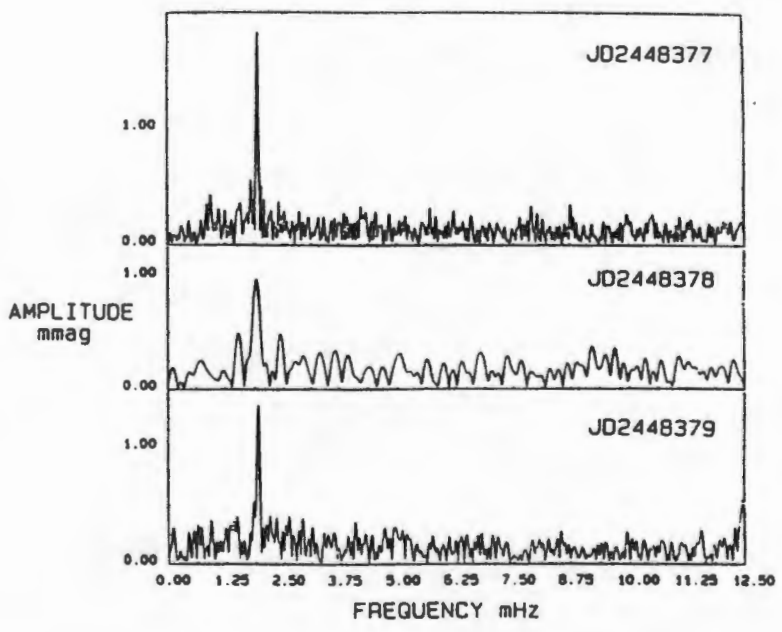

Figure 5.12 The amplitude spectra of the observations of HD 119027 acquired on the nights JD 2448377, 8378 and 8379. Notice that the amplitude of the oscillations varies from night to night by more than the level of the noise. This indicates a real amplitude modulation in the oscillations.

0.076. On the basis of these indices, we searched for rapid oscillations in this star for 5.0 hr on the night JD 2448377 (Martinez & Kurtz 1991b). Inspection of the real-time data display at the telescope revealed the presence of rapid oscillations with a period P = 8.63 min and an amplitude A = 1.8 mmag (Fig. 5.11). The observations were acquired with the UCT photometer attached to the SAAO 1.0-m telescope.

The amplitude spectrum of the data acquired on night JD2448377 is presented in the upper panel of Fig. 5.12. The prominent peak is at ν_1=1.93 mHz. We observed this star again on the following two nights, JD2448378 and 8379. These observations are all journaled in Table 5.4. The amplitude spectra of nights JD2448378 and 8379 are shown in Fig. 5.12 in the middle and lower panel, respectively. We also Fourier analyzed the three nights together to refine our determination of ν_1 to ν_1 = 1.9302 mHz. Note that the height of the peak ν_1 differs among the panels by somewhat more than the level of the noise. This suggests that the oscillations in HD 119027 are amplitude modulated on a time-scale of $\approx$ 1 day. Unfortunately the discovery observations did not have a high enough duty cycle to permit us to investigate the nature of this modulation. Because of this we obtained further observations of this star on 22 nights during a campaign in 1991 May - June. A detailed frequency analysis of those data is presented in chapter 7.

Table 5.4

Journal of observations of HD 119027

HJD start	T hr	N_{40}	σ mmag
8377.33875	5.03	445	2.097
8378.38943	1.81	161	1.358
8379.37450	4.36	378	1.946

5.8e HD 150562

The cool A/F (p Eu) (Houk 1978) star HD 150562 was monitored photometrically for 4.67 hr on the night JD 2448411 (Martinez & Kurtz 1992). Inspection of the real-time data display at the telescope indicated the presence of rapid oscillations with a period P = 10.75 min and amplitude A = 0.75 mmag (Fig. 5.13). The observations were acquired using the St Andrews Photometer attached to the SAAO 1.0-m telescope.

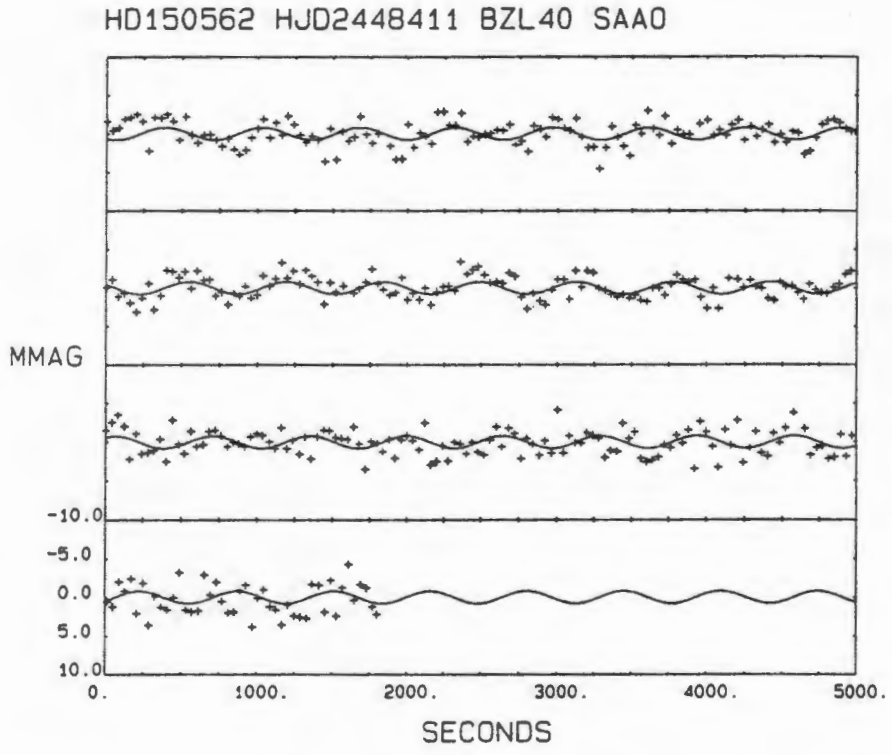

Figure 5.13 The Johnson *B* light curve of HD 150562 for 4.67 hr on night JD 2448411. The sky transparency variations have been removed from this light curve and the data have been binned to 40-s integrations.

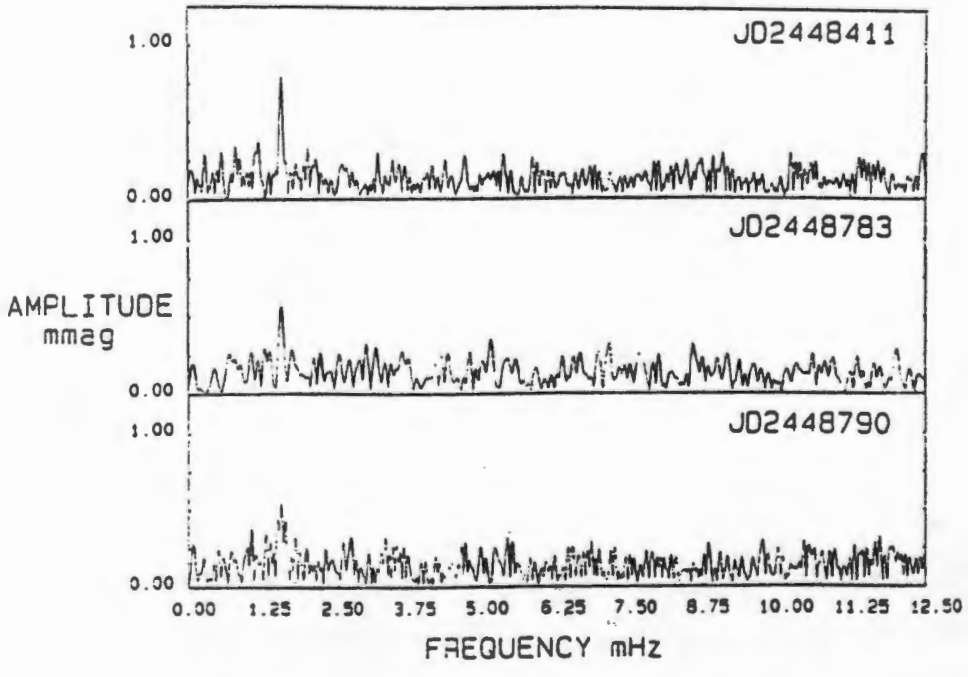

Figure 5.14 Amplitude spectra for the observations of HD 150562 acquired on one night in 1991 and two nights in 1992. The sky transparency variations have been removed from these data. Notice that the highest noise peaks in this Figure are at around 0.25 mmag.

To confirm the presence of rapid oscillations, we observed this star again on nights JD2448427, 8462, 8465, 8723, 8783, 8786, 8790 and 8792. Table 5.5 is a journal of all these high-speed photometric observations. In Figure 5.14 we show the amplitude spectra acquired on three good nights. The prominent peak is at ν_1 = 1.55 mHz. The solid line in Fig. 5.13 is a sinusoid of frequency ν_1 = 1.55 mHz, with least-squares-fitted amplitude and phase.

Inspection of all available amplitude spectra suggests that the oscillations in HD 150562 are amplitude modulated. To refine our determination of ν_1 and to search for additional frequencies, we Fourier analyzed the last four nights together. This produced an amplitude spectrum with severe aliasing ambiguities. The value of ν_1 is ambiguous by 1 cycle day^{-1} in these data; we cannot distinguish between ν_1 = 1.5585 mHz and ν_1 = 1.5470 mHz. Further observations of the rapid oscillations in HD 150562 are required in order to refine the determination of ν_1 and to check for the conjectured amplitude modulation.

Table 5.5

Journal of observations of HD 150562

HJD start	T hr	N_{40}	σ mmag
8411.47169	4.67	416	1.583
8427.44208	3.77	303	1.871
8462.32836	2.05	184	1.415
8465.22933	1.62	146	1.308
8723.41122	2.02	173	3.305
8783.37563	3.41	302	1.399
8786.32017	4.45	321	1.807
8790.33042	5.08	392	1.616
8792.41326	2.62	227	1.485

5.8f HD 161459

When the Ap EuSrCr (Houk 1978) star HD 161459 was first observed on the night of 16/17 July 1990 (JD2448089), it became evident within half an hour that the star was oscillating with a period around 12 min (Martinez & Kauffmann 1990). The discovery of rapid oscillations in this star occurred in the ideal way in that we caught it on a good night when the amplitude up above 0.8 mmag and we were able to follow it for 7.67 hr. The amplitude spectrum of these data out to the Nyquist frequency of

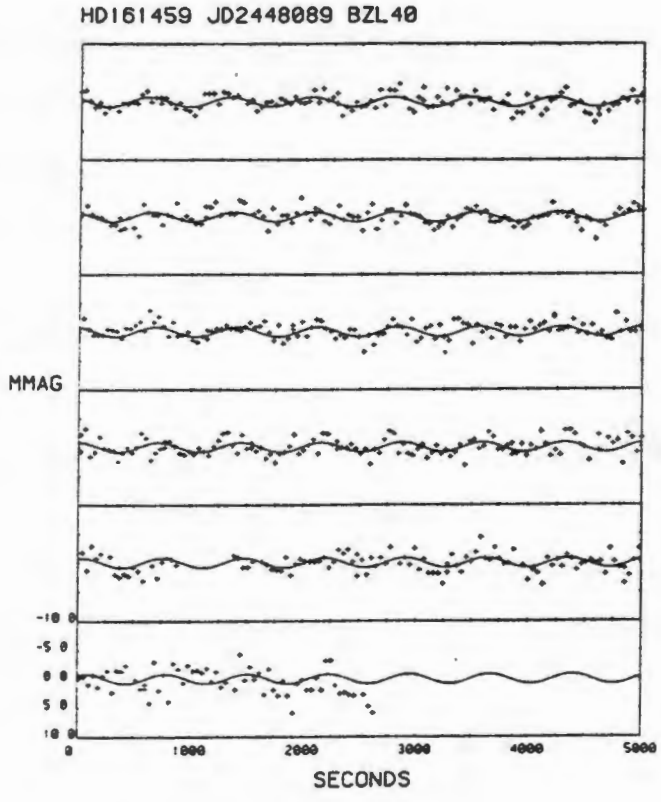

Figure 5.15 The Johnson *B* brightness record of HD 161459 on night 16/17 July 1990 (JD 2448089) when the rapid oscillations in this star were discovered. This 7.67-hr long light curve was acquired using the University of Cape Town photometer attached to the SAAO 1.0-m telescope. The observations had to be terminated when the hour angle got very close to 6 hr west. Notice that even with the telescope that far over, the quality of the photometry was still good. The sky transparency variations have been removed from this light curve and a sinusoid of period 12.0 min has been fitted to facilitate the reader's perception of the oscillations.

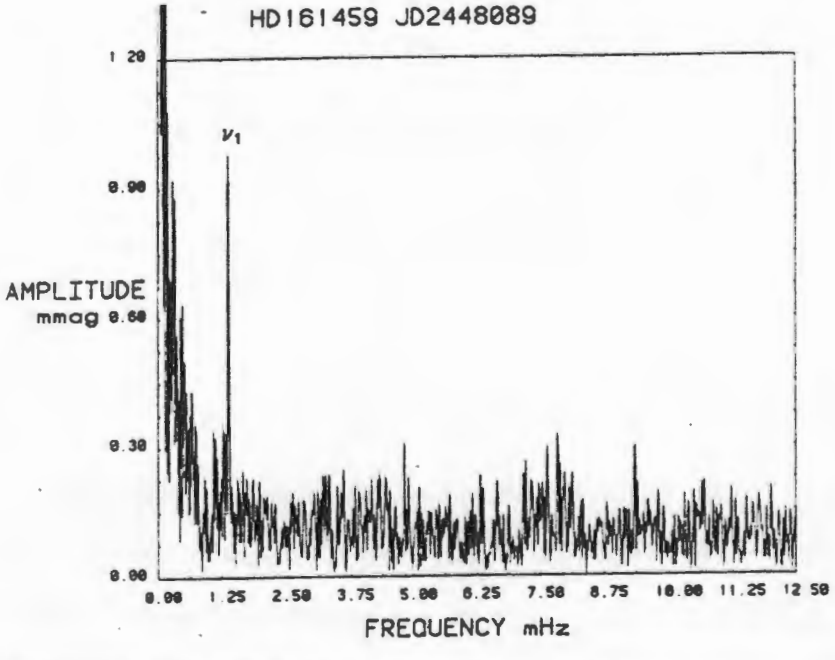

Figure 5.16 The Fourier transform of the *B* light curve of HD 161459 acquired on night JD 2448089. Even in the presence of the sky transparency variations, the oscillations in HD 161459 stand out at very good signal-to-noise.

12.5 mHz for 40-s integrations is presented in Fig. 5.15. The prominent peak is at ν_1 = 1.39 mHz (P = 12.0 min) with an amplitude of 0.84 millimagnitudes (mmag). The solid line in Figure 5.16 is a sinusoid of frequency ν_1 = 1.39 mHz which has been fitted to the data by least squares in order to optimize its amplitude and phase. Further observations of this star were acquired on 6 nights spanning JD2448104-8110 (Table 5.6).

The data were analyzed on a night-by-night basis, in groups of closely spaced nights and as a whole. In what follows, we will present a summary of these analyses. We began by inspecting the nightly amplitude spectra for obvious indications of other oscillation frequencies. In the JD2448104 data (Fig. 5.17) we discovered evidence for a harmonic of the oscillation frequency ν_1. The second-tallest peak in the amplitude spectrum of these data lies at ν = 2.78 mHz, exactly where one expects to find the first harmonic of ν_1. The same peak does not appear in the other nights' data (e.g. see Fig. 5.15), but this is not surprising given that the amplitude signal-to-noise of ν_1 was the highest of all our data on that night. On night JD2448110, the oscillations attained a similar amplitude, but the scintillation noise was more than a factor of 2 higher, so we could not confirm the presence of the conjectured harmonic. We thus regard this as a tentative identification of the first harmonic in this star requiring confirmation. In Fig. 5.18 we present the light curve acquired on night JD2448104. The solid line is a least squares fit of ν_1 and the conjectured harmonic $2\nu_1$ to the data.

The nightly amplitude spectra presented above suggest that the amplitude of the principal pulsation frequency, ν_1 = 1.39 mHz, is modulated on a night-to-night basis. In order to test for this we fitted ν_1 = 1.39 mHz to each of the nightly data sets by least squares. Depending on which nights one compares, there are amplitude differences ranging from 2σ to 5σ. To test for amplitude modulation on shorter time-scales we performed similar least squares fits to half-hour segments of the data but found no statistically significant trends in either amplitude or phase behaviour within the nightly data sets.

To search for frequencies causing amplitude modulation we Fourier analyzed the JD2448106-8109 data set out to the Nyquist frequency (Fig. 5.19). Other than ν_1 and a vague indication of the harmonic $2\nu_1$, the spectrum is flat out to the Nyquist frequency. We thus concentrated on the amplitude spectrum in the region of ν_1 (Fig. 5.20 (top)). The tallest peak lies at ν = 1.3909 mHz, but the aliasing is so severe that we are unable to refine our frequency determination of ν_1 to higher precision than 1.39 mHz with confidence. The lower part of Fig. 5.20 shows the spectral window and emphasizes the severe aliasing problem in this data set. This means that we are unable to identify

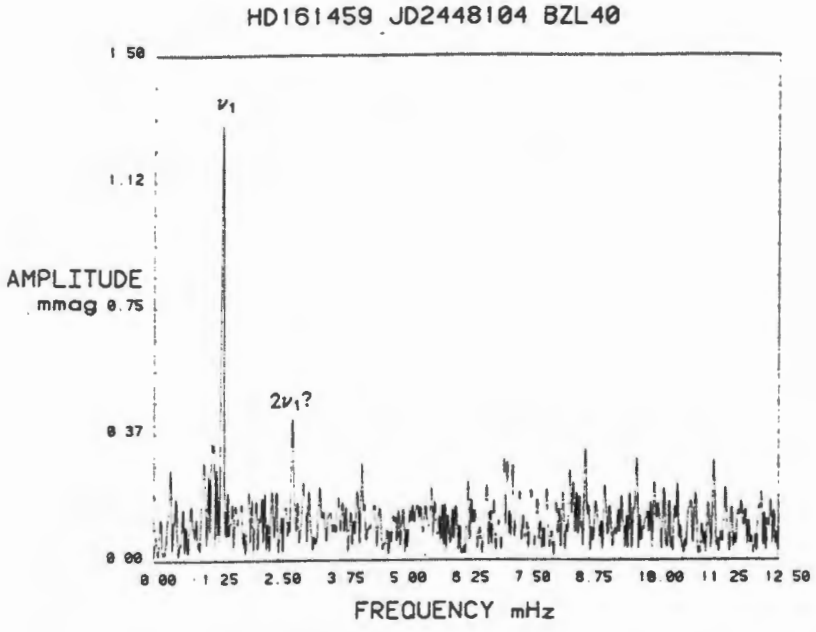

Figure 5.17 The amplitude spectrum of the *B* observations of HD 161459 acquired on night JD 2448104. The peak labeled $2\nu_1$ lies where we would expect to find the first harmonic of ν_1. The reader should not conclude from this Figure that we claim a secure detection of the first harmonic in HD 161459.

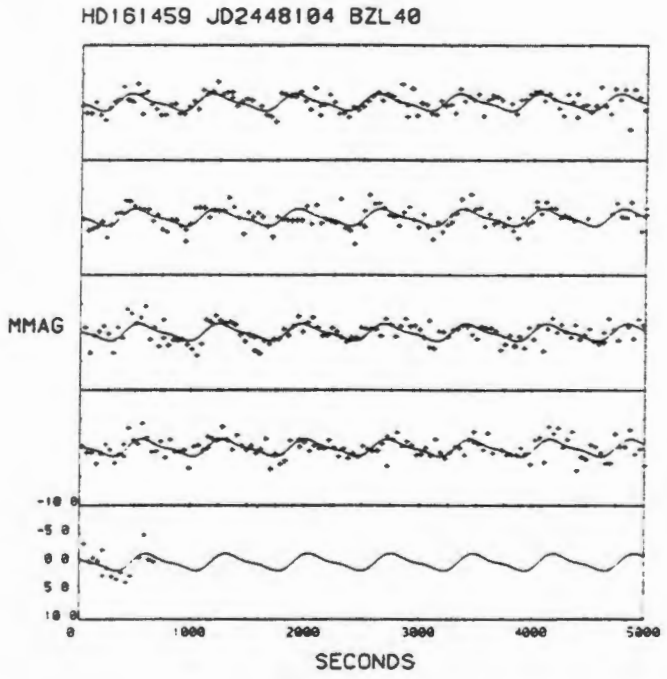

Figure 5.18 The Johnson *B* light curve of HD 161459 on night JD 2448104. The solid curve is a fit of a sinusoid of frequency ν_1 = 1.39 mHz and its first harmonic, $2\nu_1$, to the data.

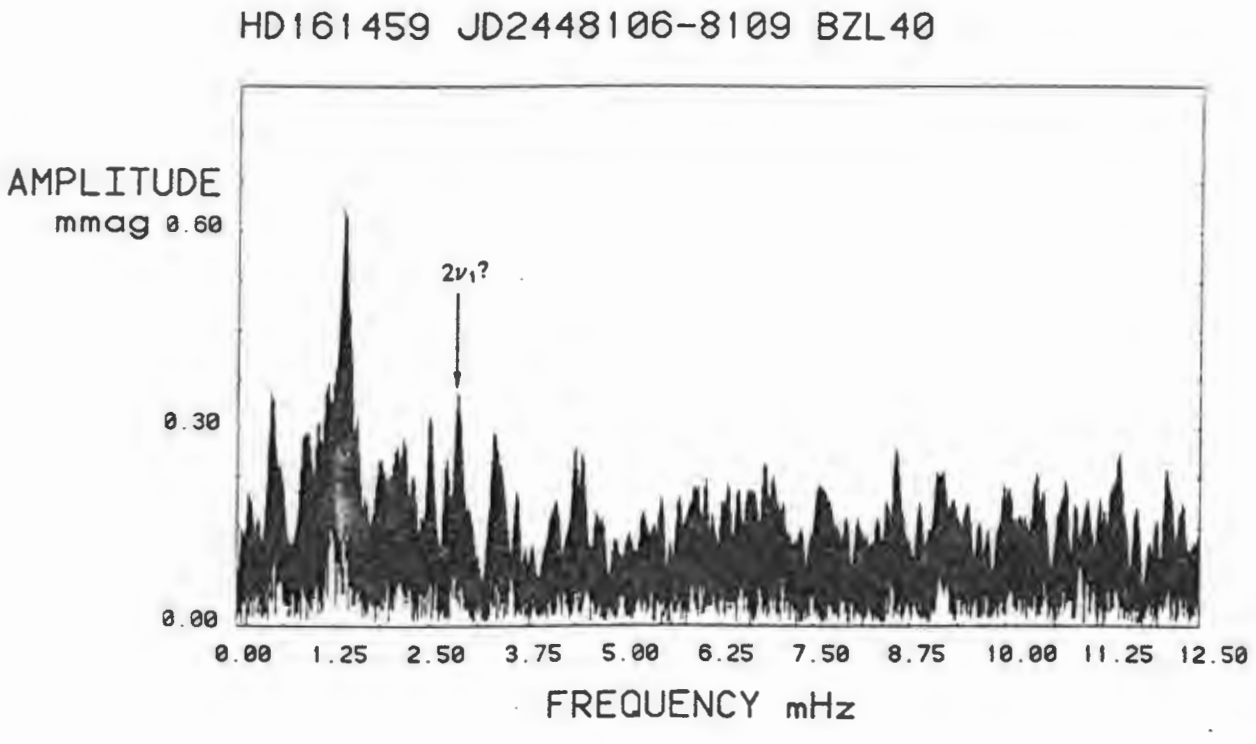

Figure 5.19 The amplitude spectrum of the combined data of HD 161459 for nights JD 2448106-8109. Note the increased amplitude at frequencies close to the expected position of the first harmonic of ν_1. The reality of the conjectured harmonic can only be tested by acquiring further observations.

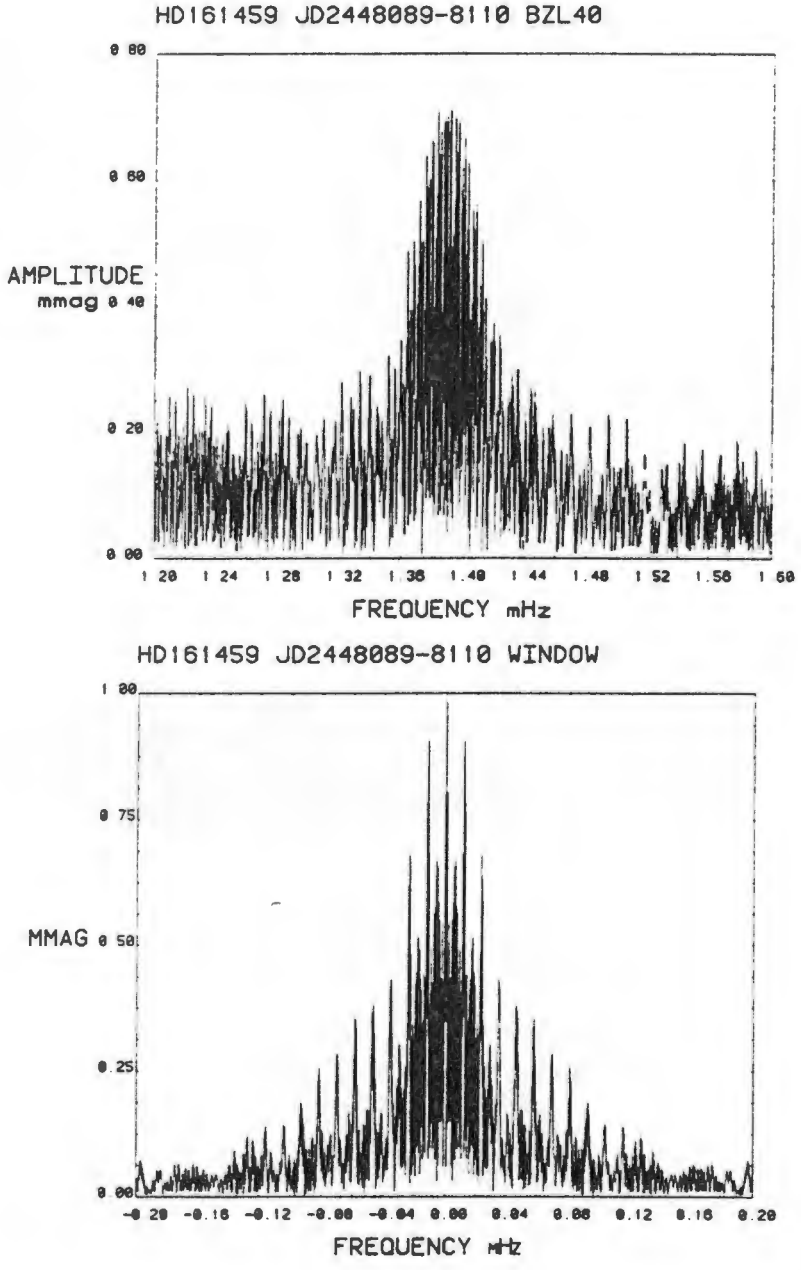

Figure 5.20 The amplitude spectrum of the entire HD 161459 data set (top) in the region of ν_1 and the spectral window (bottom) of these observations. The aliasing in the top panel is so severe that we are unable to refine our frequency determinations more precisely than 1.39 mHz.

unambiguously the other frequencies which give rise to the amplitude modulation of ν_1. The analysis of other subsets of the data proved to be similarly fruitless. Clearly, it is not possible to describe the oscillations in this star in terms of only a single, stable oscillation frequency at $\nu_1 = 1.39$ mHz. Further extensive observations will be required to characterize this star's complex oscillation behaviour more accurately.

Table 5.6

Journal of observations of HD 161459

HJD start	T hr	N_{40}	σ mmag
8089.29723	7.67	663	1.49
8104.23448	5.73	503	1.72
8106.22279	3.05	269	1.49
8107.22007	1.64	125	2.09
8108.21955	1.99	176	1.45
8109.21810	2.00	176	1.38
8110.21954	1.56	134	2.75

5.8g HD 190290 - Asteroseismology in one night

The southern ($\delta = -79^{o}$) 10th mag star HD 190290 classified as Ap EuSr by Houk & Cowley (1975) was observed on the night of 4/5 August 1990 (JD2448108) (Martinez & Kurtz 1990). Shortly after setting on this star it became evident that HD 190290 was oscillating with a 7-min period with a suggestion of beating, so we decided to continue acquiring data for as long as possible - nearly nine hours on that night. We were fortunate indeed to search for rapid oscillations in this star on an excellent photometric night; the lowest airmass attained by this circumpolar star at the SAAO is 1.4. In Figure 5.21(a) we present the amplitude spectrum of these observations out to the Nyquist frequency of 12.5 mHz for 40-s integrations. Again, we include the sky transparency variations in Fig. 5.21 so that the reader may judge the data.

The prominent peak in Fig. 5.21(a) is at $\nu_1 = 2.27$ mHz with an amplitude of 1.13 mmag. To test for further frequencies in the data we subtracted a sinusoid of frequency $\nu_1 = 2.27$ mHz from the data. The resulting amplitude spectrum in Fig. 5.21(b) clearly indicates the presence of another frequency at $\nu_2 = 2.23$ mHz with an amplitude of 0.55 mmag. In Figures 5.21(b) and 5.21(c) we have

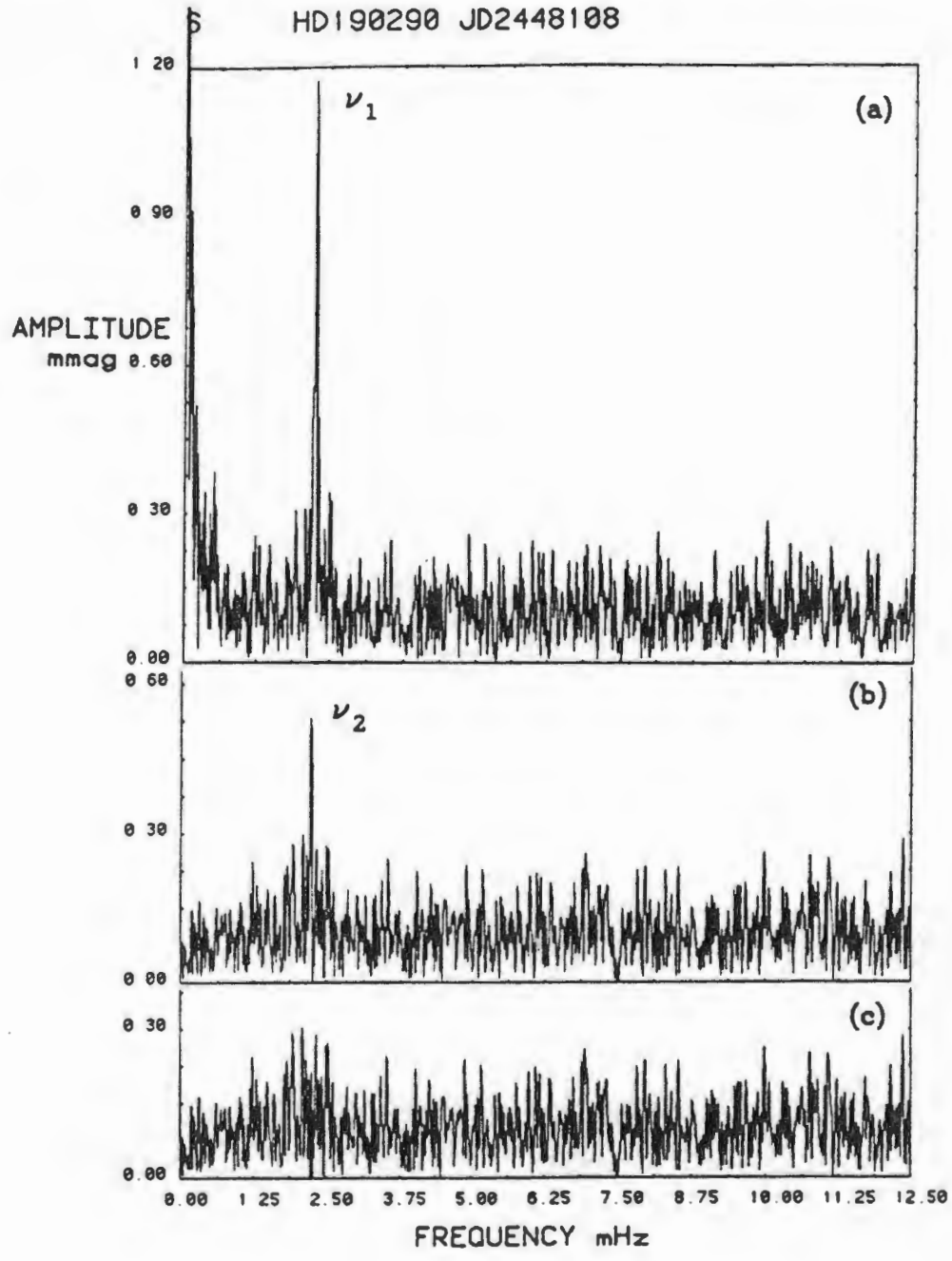

Figure 5.21 The amplitude spectrum of the *B* observations of HD 190290 acquired on night JD 2448108. Panel (a) shows the principal oscillation frequency ν_1 = 2.27 mHz in the presence of the sky transparency variations. When ν_1 and these sky transparency variations are removed from the data, we are left with the amplitude spectrum shown in panel (b) which reveals the presence of another oscillation frequency at ν_1 = 2.23 mHz. Upon removing ν_2 from the data we are left with the amplitude spectrum shown in panel (c) which suggests the possible presence of further oscillation frequencies.

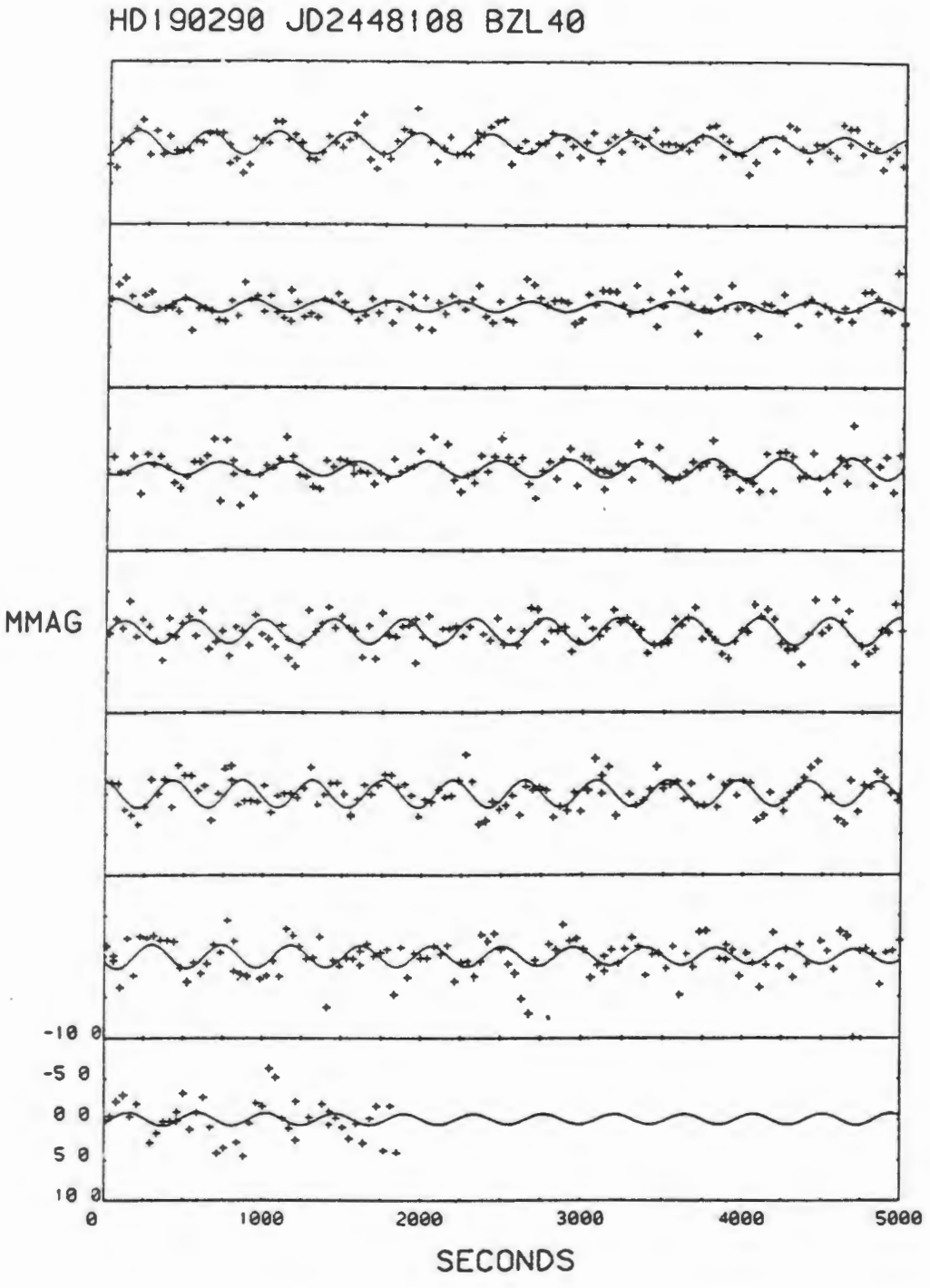

Figure 5.22 The *B* light curve of HD 190290 acquired on night JD 2448108. The solid curve is a least-squares fit of ν_1 = 2.27 mHz and ν_2 = 2.23 mHz to the observations.

removed the low-frequency sky transparency variations also. On prewhitening both ν_1 and ν_2 from the data, we are left with the spectrum shown in Fig. 5.21(c) which suggests the presence of further frequencies, but we cannot meaningfully pursue the identification of further frequencies with these data.

Table 5.7

Journal of observations of HD 190290

HJD start	T hr	N_{40}	σ mmag
8108.30738	8.85	780	1.88

The frequency separation between ν_1 and ν_2 is 40 μHz. This cannot be a rotation frequency because it would correspond to a rotation period of 6.9 hr, improbably short for an A star. We thus conclude that ν_2 is another excited p-mode. Tassoul (1980, 1990) has shown that in the asymptotic theory of stellar oscillations, high-order p-modes should have, to first order, an equal separation $\Delta\nu$ given by eq. (2.4). The spacing of 40 μHz between ν_1 and ν_2 is in good agreement with the computed values of $\Delta\nu$ for a variety of A star models. Applying the models of Shibahashi & Saio (1985), Gabriel *et al.* (1985) and Heller & Kawaler (1988) we find that $\Delta\nu$ = 40 μHz is consistent with an A star slightly evolved off the ZAMS. We do not wish to dwell on the interpretation of this 40 μHz spacing here, but merely to note that it is a crude measurement of the asymptotic p-mode spacing in HD 190290 consistent with values observed in other roAp stars. Of course, a thorough frequency analysis is required in order to refine our frequency determinations and to find possible other frequencies in this star suggested in Fig. 5.21(c). In Fig. 5.22 we present the light curve of these observations to which ν_1 and ν_2 have been fitted.

5.8h HD 193756

This star was first observed on the night JD2448072 for 48 min before the unwelcome arrival of ridge cloud brought the run to a premature end. Even in this brief run, there was a vague indication that the light curve was *not* flat and the highest peak in the amplitude spectrum of these data happened to lie in the region of 1.3 mHz, exactly the region of interest. With so few data we could not exclude sky

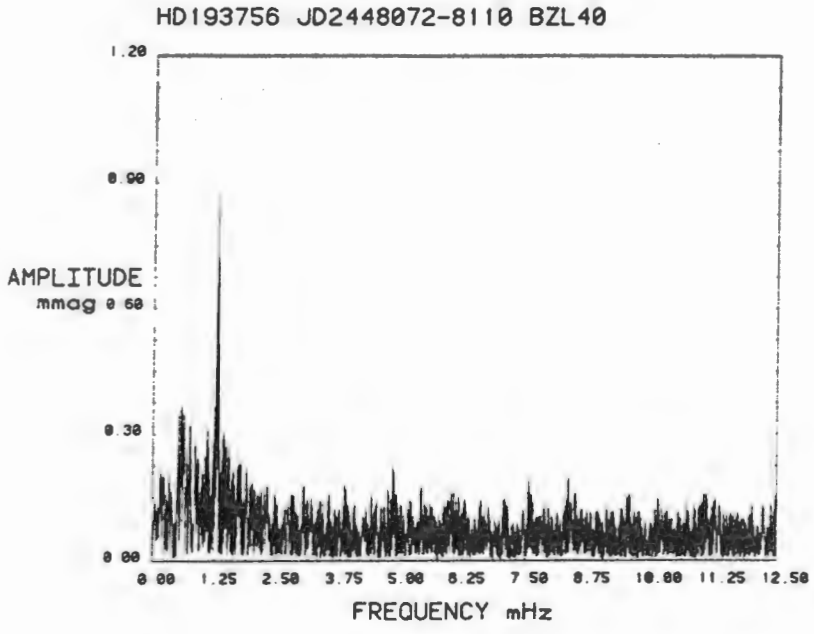

Figure 5.23 The amplitude spectrum for the entire JD 2448072 - 8110 data set for HD 193756. This spectrum shows that the oscillation frequencies in this star all lie in the region of ν_1 = 1.3 mHz.

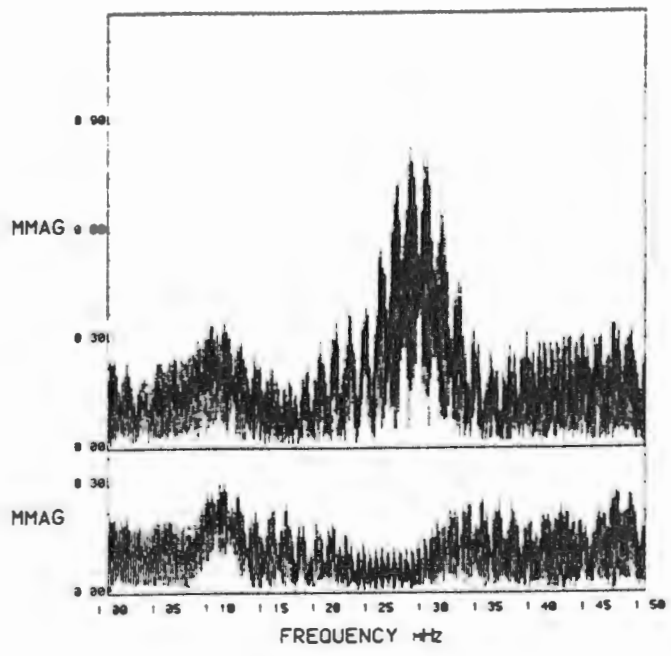

Figure 5.24 The top panel shows the amplitude spectrum of the JD 2448072 - 8110 observations of HD 193756 in the region of ν_1 = 1.284 mHz. If we remove ν_1 from these data, we are left with the amplitude spectrum shown in the lower panel which reveals that no further oscillation frequencies were excited to observable amplitudes during our observations of this star.

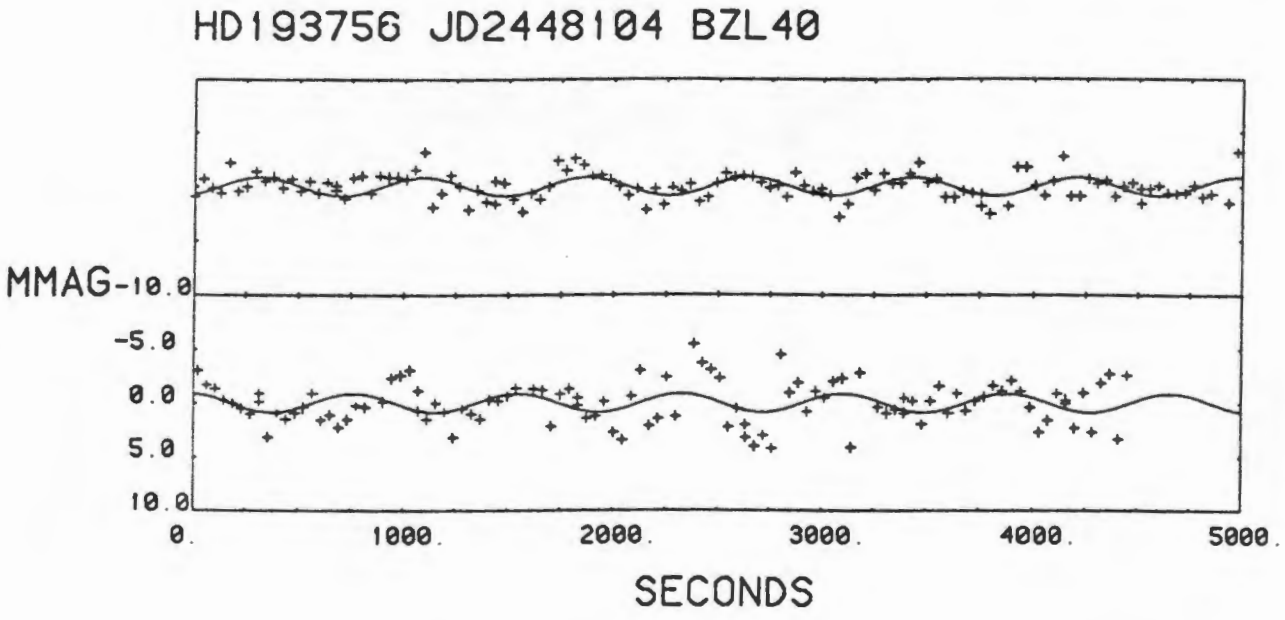

Figure 5.25 The Johnson *B* light variations of HD 193756 on night JD 2448104. This light curve is continuous from the upper left. Each point is the mean of 4 10-s integrations. The solid line is a fit of a sinusoid of frequency ν_1 = 1.284 mHz to the data.

transparency changes as the probable cause for slight excursions in brightness about the mean value so we observed this star again two nights later (JD2448074) for 1 hr. This time an even noisier amplitude spectrum was obtained, but again a 'noise' peak appeared at 1.3 mHz. Intrigued by this, we observed HD 193756 again on the nights JD2448104, 8105 and 8110 and confirmed the presence of rapid oscillations in this star (Martinez & Kurtz 1990b). The observations are journaled in Table 5.8.

The data were analysed in individual nights, in two groups of closely spaced nights and as a whole and we found convincing evidence for only one frequency at $\nu_1 = 1.284$ mHz. In Fig. 5.23 we present the amplitude spectrum for all 5 nights analysed together. Figure 5.24 shows the amplitude spectrum in the region of $\nu_1 = 1.284$ mHz. If we subtract a sinusoid of this frequency from the data we are left with the amplitude spectrum shown in the lower panel of Fig. 5.24 which indicates that there were no other oscillation frequencies in this star at the time of our observations. For completeness, we include a light curve (Fig. 5.25) of the observations on JD2448104 to which a sinusoid of frequency $\nu_1 = 1.284$ mHz has been fitted.

Table 5.8

Journal of observations of HD 193756

HJD start	T hr	N_{40}	σ mmag
8072.47030	0.79	72	1.30
8074.50368	0.99	86	0.93
8104.47918	2.62	230	1.56
8105.30462	2.06	161	2.03
8110.29281	5.99	530	1.67

5.8i HD 196470 - An equatorial roAp star

We first observed this 10th magnitude Ap SrEu(Cr) (Houk & Smith-Moore, 1989) equatorial (δ = -18°) star for 2.09 hr on the night 30 June/1 July 1990 (JD2448073) (Martinez *et al.* 1990). A visual inspection of the real-time display at the telescope suggested the presence of oscillations with a period of 10.8 min, but, since it was not an excellent night, we could not exclude the possibility that we were seeing sky transparency variations. Fig. 5.26 is an amplitude spectrum of these data in which the conjectured oscillation frequency $\nu_1 = 1.54$ mHz is indicated. In the presence of the sky transparency

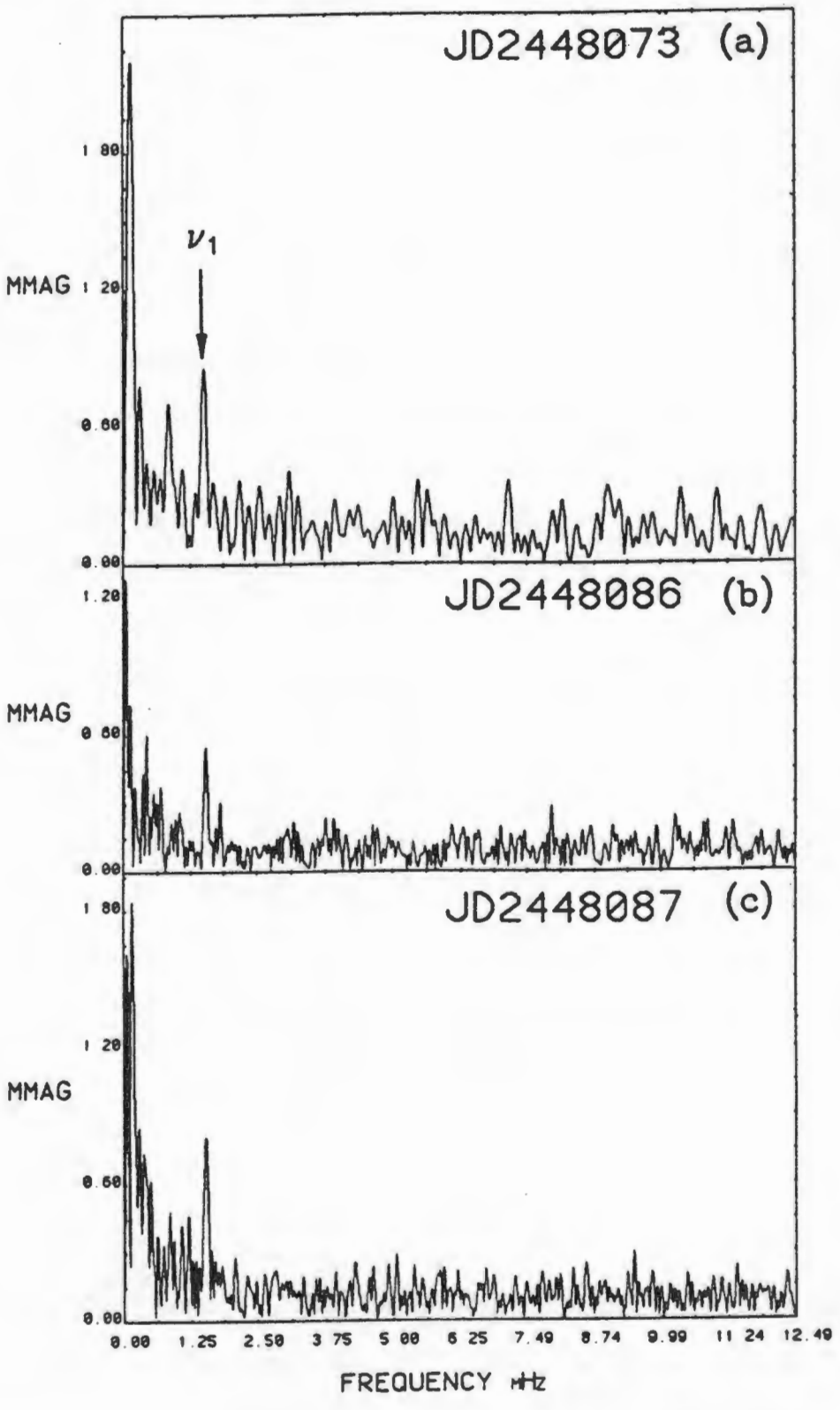

Figure 5.26 Amplitude spectra of the Johnson *B* observations of HD 196470 on the nights JD 2448073, 8086 and 8087. These amplitude spectra include the sky transparency variations to show that we have a convincing detection of the rapid oscillations in this star. The peak labeled ν_1 at 1.544 mHz is the oscillation frequency.

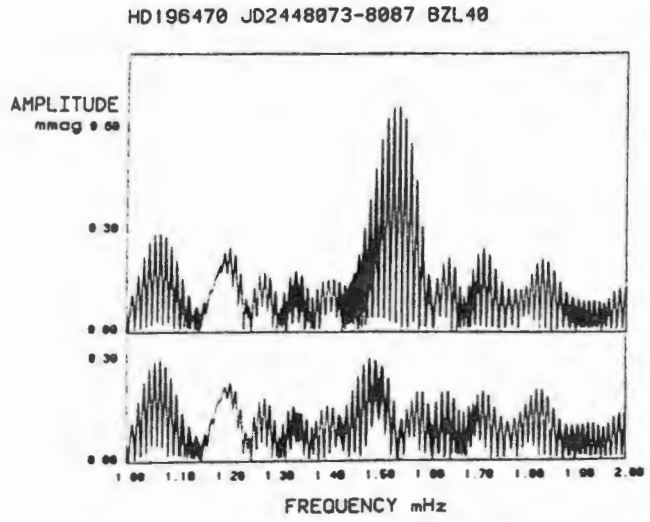

Figure 5.27 The amplitude spectrum of the JD 2448073 - 8087 observations of HD 196470 in the region of ν_1 = 1.544 mHz (upper panel). The lower panel shows the flat spectrum that results if this frequency is removed from the data.

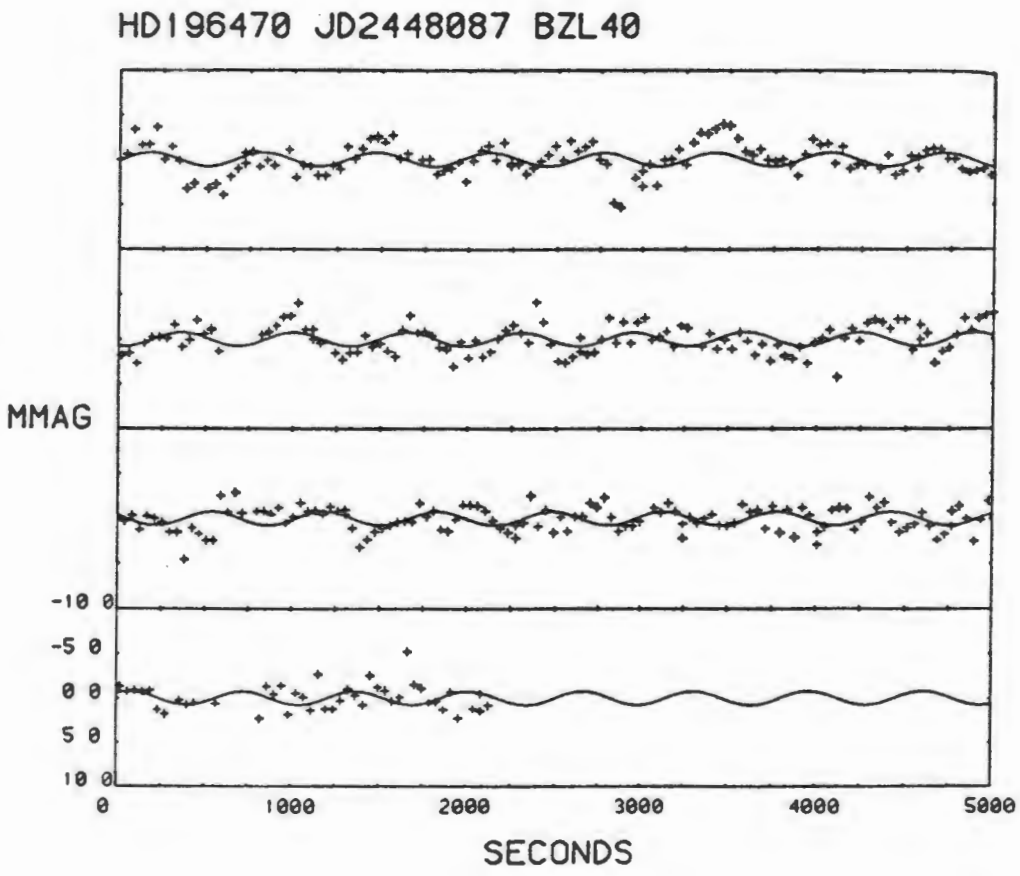

Figure 5.28 A continuous 4.8-hr record of the Johnson *B* light variations in HD 196470 on night JD 2448087. The solid curve is a fit of a sinusoid of frequency ν_1 = 1.544 mHz to the data.

variations on that night, this frequency identification is hardly convincing, so we elected to observe this star again on the nights 13/14 and 14/15 July 1990 (JD2448086-8087). Table 5.9 is a journal of these observations. The amplitude spectra for these two nights are presented in Fig. 5.26(b) and 5.26(c), respectively. There can be no doubt that the frequency $\nu_1 = 1.54$ mHz is a real oscillation frequency in the star.

There is an indication in Fig. 5.26 of amplitude modulation of ν_1. However, caution is called for as the difference in amplitude among the 3 panels is comparable to the level of the noise. If the amplitude modulation is real, it could arise from changing aspect as the star rotates, from beating with unresolved modes or from real variations in the amplitude of the mode associated with ν_1 or, indeed, through all of these effects operating together. To test for amplitude modulation, we Fourier analysed all 3 nights together (Fig. 5.27) but found no convincing evidence for further frequencies upon removing ν_1 from the data. However the higher resolution of this analysis did allow us to refine our identification of the oscillation frequency to $\nu_1 = 1.544$ mHz. In Figure 5.28 we present a light curve for the night JD2448087 to which a sinusoid of frequency $\nu_1 = 1.544$ mHz has been fitted. Further monitoring of this star is merited, because if turns out to be a multimode pulsator, it is particularly well situated to be a target object for a contemporaneous multi-site observing campaign.

Table 5.9

Journal of observations of HD 196470

HJD start	T hr	N_{40}	σ mmag
8073.51860	2.09	188	1.30
8086.43226	4.64	404	1.25
8087.46308	4.80	404	1.55

5.8j HD 218495

One of the aims of our survey is to determine the hot border of the roAp phenomenon. Prior to the discovery of roAp variability in HD 218495, HD 6532 was the only known roAp star with $\beta \approx 2.88$. We decided to search for rapid oscillations in HD 218495 because it has a similarly hot β index of 2.87 (Table 2.2). This star was observed for a total of 7.39 hr on the nights JD2448104, 8107 and 8110

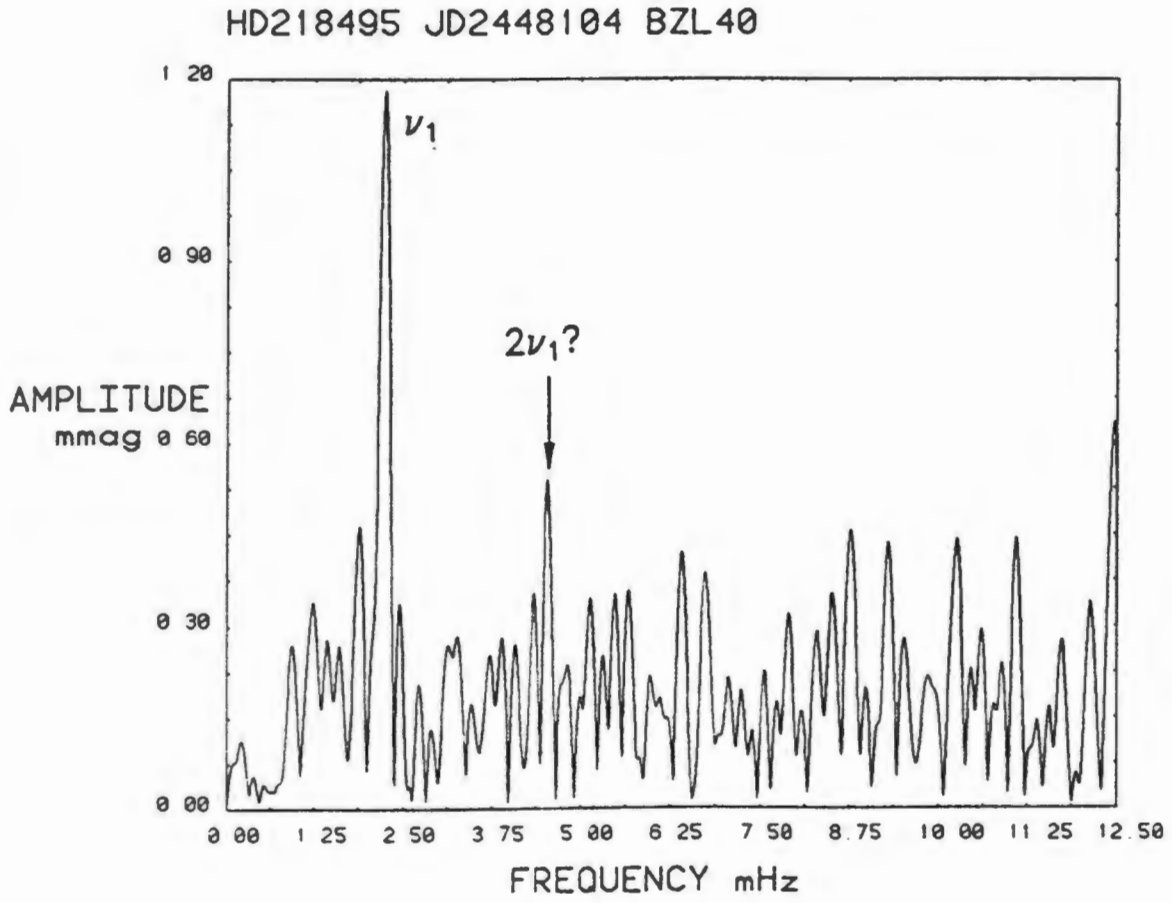

Figure 5.29 The amplitude spectrum of the JD 2448104 high-speed *B* observations of HD 218495. The presence of a possible first harmonic of ν_1 is indicated by the arrow labeled '$2\nu_1$?'

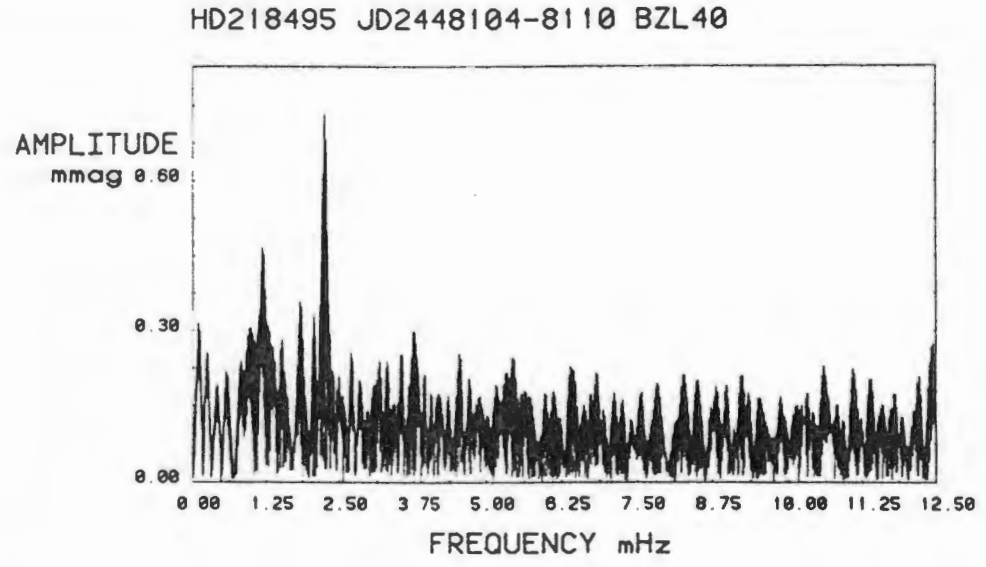

Figure 5.30 The amplitude spectrum of the JD 2448104 - 8110 high-speed *B* observations of HD 218495.

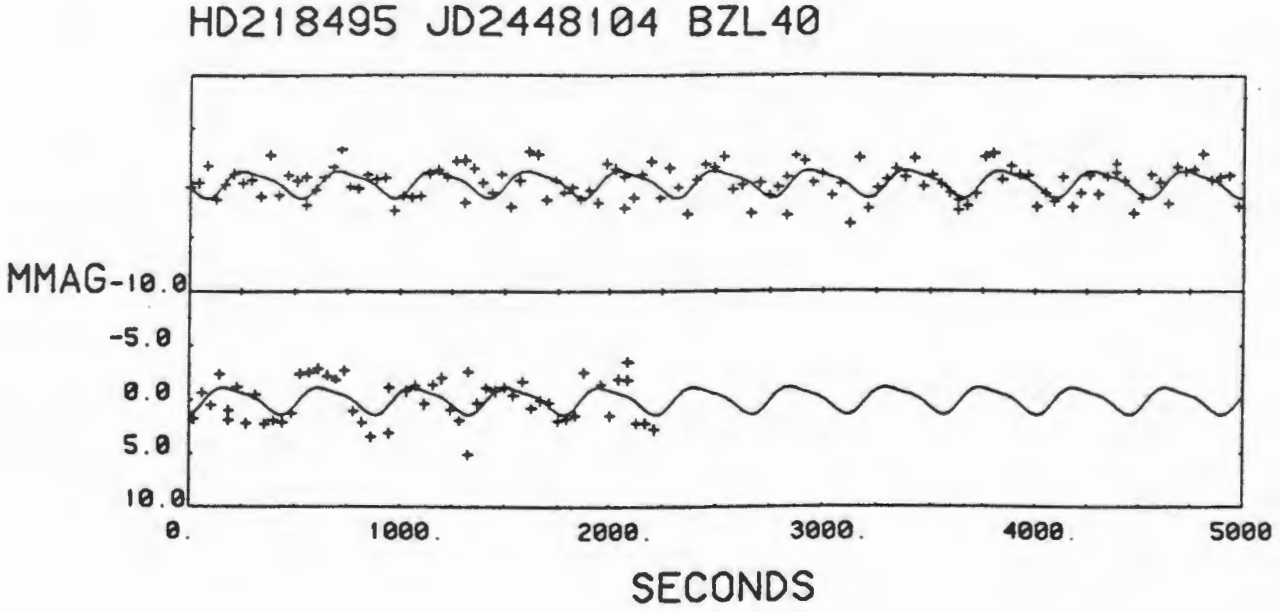

Figure 5.31 The light curve showing the discovery of rapid oscillations in HD 218459 on night JD 2448104. The sky transparency variations have been removed from these data and each point is an average of 4 10-s integrations. The solid line is a fit of ν_1 and its conjectured harmonic $2\nu_1$ to the data. The fit is reasonably good.

(Martinez & Kurtz 1990b). In Figure 5.29 we present an amplitude spectrum of the JD2448104 data which reveals the presence of oscillations at ν_1=2.24 mHz. It also suggests the presence of the first harmonic of ν_1 at $2\nu_1$=4.48 mHz; such harmonics are observed in 5 other roAp stars (Kurtz 1990). A peak appears at the *same* frequency on the other two nights but at such reduced amplitude that it does not draw attention to itself. This is not surprising given the lower amplitude of ν_1 on those nights and the lower signal-to-noise ratio which obtains in this higher frequency regime. A Fourier analysis of all three nights together (Fig. 5.30) does not show a convincing peak at $2\nu_1$. Thus, the reality of the conjectured harmonic must be verified with further observations. Figure 5.31 is the JD2448104 light curve to which both ν_1 and the conjectured harmonic $2\nu_1$ have been fitted. The discovery of rapid oscillations in this star confirms that the roAp phenomenon occurs at least as early as spectral type A3 according to Crawford's (1979) A star calibration.

Table 5.10

Journal of observations of HD 218495

HJD start	T hr	N_{40}	σ mmag
8104.59286	2.00	179	1.66
8107.58107	2.37	205	1.48
8110.54589	3.02	269	1.77

5.9 The null results

Although this chapter has focussed on the positive results of our searches for rapid oscillation in Ap stars. the null results are also of interest. For this reason, we end this chapter with a presentation of the null results from the Cape Survey. This presentation is both tabular and graphic. Lest readers be dissuaded from observing these stars we caution that the appearance of a star in our list of null results does *not* exclude it from being a roAp star. All we are entitled to conclude is that the star was constant for the duration of these particular observations. Many of the null results do not have the precision required to reveal the presence of oscillations for some of the lower amplitude roAp stars. Several of our null results have amplitude spectra with features suggestive of rapid oscillations: these stars should be investigated further. Several roAp stars may lie undiscovered in these null results

because we happened to observe them near quadrature (amplitude minimum) or during a time when several oscillation frequencies in the star interfered destructively. With these caveats we now present the null results.

Figure 5.32 is an atlas of amplitude spectra of the null result stars. There are 138 stars in this atlas of which 46% have observations on more than one night. Each panel in the atlas covers the frequency range 0 - 10 mHz and is 4 mmag high. The HD number of the star is listed above the panel and the Julian date, the duration of the observations (in hr) and the number of 10-s integrations are listed in the upper right-hand corner of the panel. If the observations are through a filter other than Johnson *B*, the filter is indicated next to the Julian date. (The letters A, B or C appearing in this position are an exception to this rule - they indicate the first, second, third, *etc* light curves of the star acquired on a given night.) Further details of any of these runs are available from the author on request. There are a few stars in the atlas which do not have Cape Survey high-speed photometry but for which older photometry exists in our archives. These stars are distinguished by the Julian dates of their observations all being earlier than JD 2448000. These previously unpublished observations were all acquired by D.W. Kurtz in his earlier searches for roAp stars.

For the reader's convenience, the null results have all been gathered together in a one-page table. Table 5.11 lists the HD numbers of the null result stars and the number of nights each star was observed. Stars which have been observed in one or more of the surveys described in chapter 3 are marked accordingly (*cf*. Table 3.2).

Table 5.11

Null results of searches for rapid oscillations in the Cape Survey

HD	N	HD	N	HD	N	HD	N
2883		59164		119308	5	164827	
2957		61731	3	119794		167024	
3980		62556		121661		170565	5
3988		65836		123164	3	172703	
5823 +	2	67909	2	125735	7	176196	
7676	3	68419	2	130336	2	177268	6
8783	2	68480		131141		177765	2
9050 +	3	69013 +		131750	3	183806	
11090		73850		132322		184120	2
18610	2	74494 +	3	132981		185204	2
19712		74555		135728		187473	
19817	2	75425		137160		187474	
22488		77809	4	137509		188008	
23207		81289		137802		188601 +	
23715		81588	6	138777		191439	4
26726	4	86592 +	3	141249		191796	
27211		86976	2	142070		194623	
27463	2	91239	3	142502		195112	
29578	6	92218	2	143487	2	197417	2
30849	2	92499	3	144748		201018	4
31973		94660	4	145393		203006	
33011 +	4	96897		148593		207259	2
33629	5	97394	2	149769		208217	8
34060	2	97987		151301	6	208759	
36964		100357		151860	2	209605	
39575	2	102333 +		154253	2	212385	3
40886	3	103302		154708	3	215983	
41385 +	3	107107		155188		217704	3
42075		107180 +		155366		218994	2
42326 +	2	110072		158450		221531 +	2
44226		110274	3	161423		222638	4
50143		112528 +	2	162316		222925	
52539 +		115440		162373	3	223967	5
52847	2	116114 +	2	162639			
57040	2	116729	2	164258			

Notes:

1. For stars observed more than once, the column marked 'N' indicates the number of times the star was observed.
2. The stars marked with a '+' also appear in the null results of other surveys listed in Table 3.2.

Figure 5.32 An atlas of amplitude spectra of 138 apparently constant Ap stars observed in the Cape Survey. Each panel covers the frequency range 0 - 10 mHz and is 4 mmag high. The annotations on the lower left panel of the page apply to all the other panels. Consult the text in section 5.9 for a description of the annotations that appear in each panel. Details on any of these observations are available from the author on request.

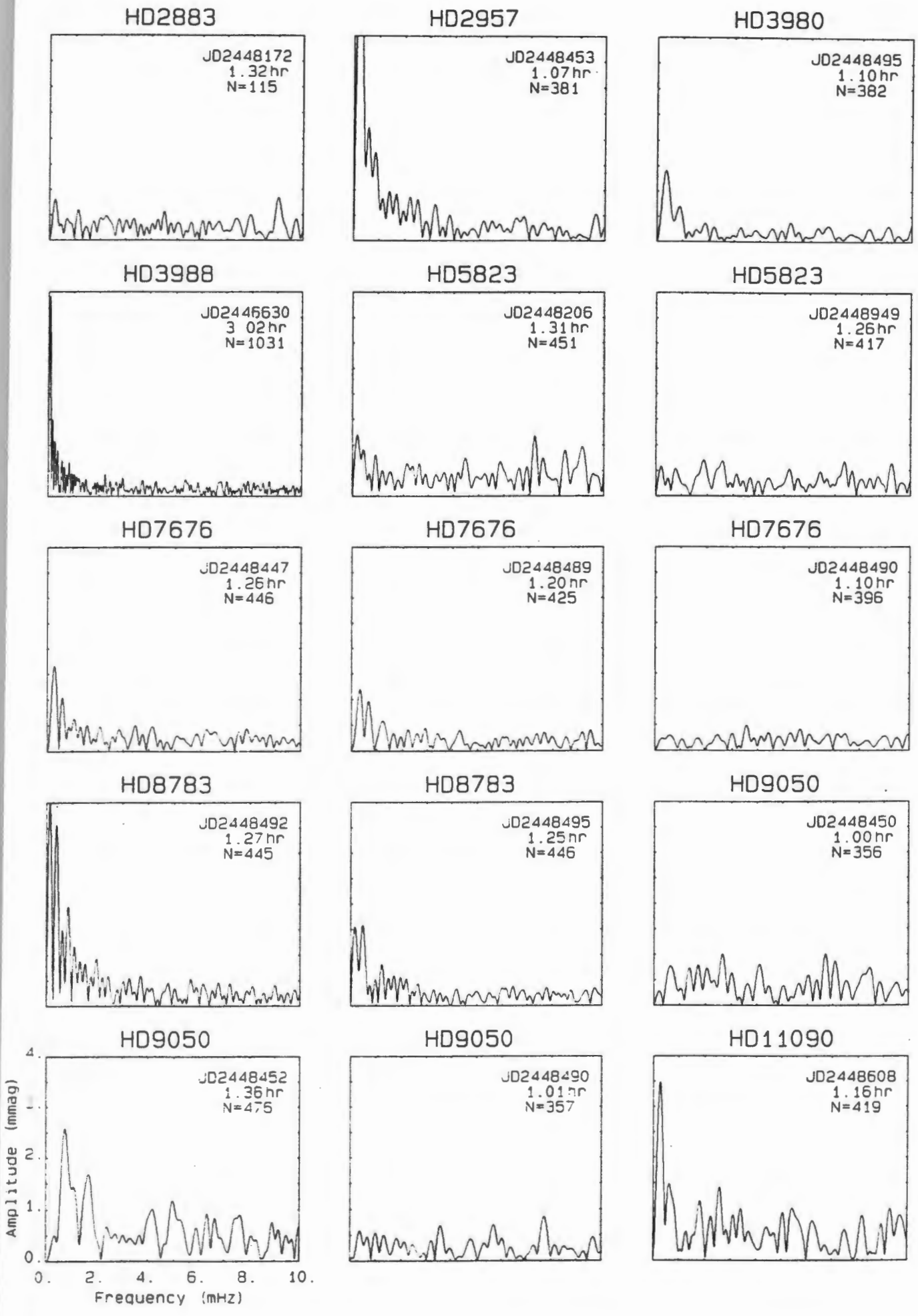
HD2883
JD2448172
1.32hr
N=115
HD2957
JD2448453
1.07hr
N=381
HD3980
JD2448495
1.10hr
N=382
HD3988
JD2446630
3.02hr
N=1031
HD5823
JD2448206
1.31hr
N=451
HD5823
JD2448949
1.26hr
N=417
HD7676
JD2448447
1.26hr
N=446
HD7676
JD2448489
1.20hr
N=425
HD7676
JD2448490
1.10hr
N=396
HD8783
JD2448492
1.27hr
N=445
HD8783
JD2448495
1.25hr
N=446
HD9050
JD2448450
1.00hr
N=356
HD9050
JD2448452
1.36hr
N=475
HD9050
JD2448490
1.01hr
N=357
HD11090
JD2448608
1.16hr
N=419
Amplitude (mmag)
4.
3.
2.
1.
0.
0.
2.
4.
6.
8.
10.
Frequency (mHz)

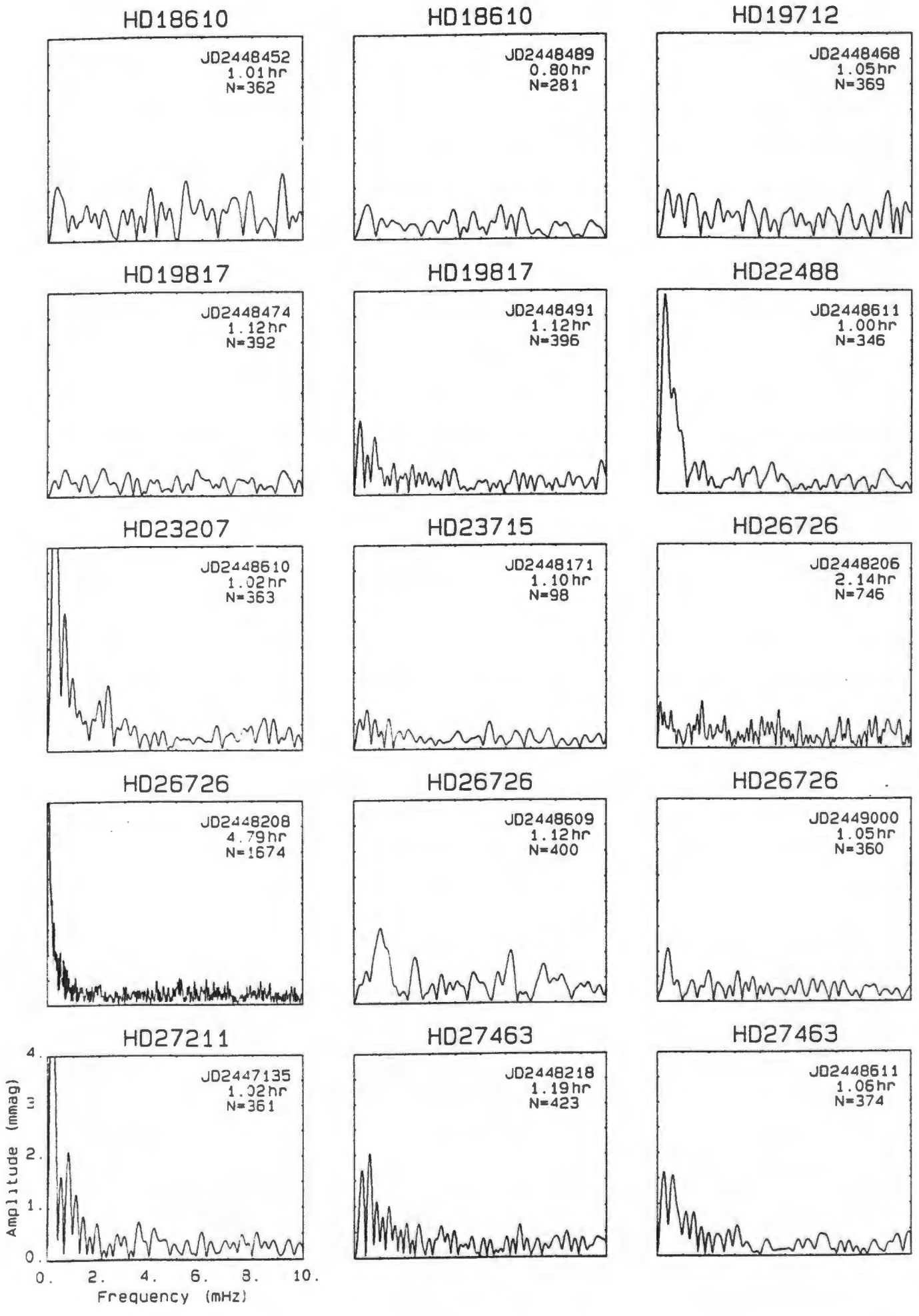
HD18610
JD2448452
1.01hr
N=362
HD18610
JD2448489
0.80hr
N=281
HD19712
JD2448468
1.05hr
N=369
HD19817
JD2448474
1.12hr
N=392
HD19817
JD2448491
1.12hr
N=396
HD22488
JD2448611
1.00hr
N=346
HD23207
JD2448610
1.02hr
N=363
HD23715
JD2448171
1.10hr
N=98
HD26726
JD2448206
2.14hr
N=746
HD26726
JD2448208
4.79hr
N=1674
HD26726
JD2448609
1.12hr
N=400
HD26726
JD2449000
1.05hr
N=360
HD27211
JD2447135
1.02hr
N=361
HD27463
JD2448218
1.19hr
N=423
HD27463
JD2448611
1.06hr
N=374
Amplitude (mmag)
4.
3.
2.
1.
0.
0.
2.
4.
6.
8.
10.
Frequency (mHz)

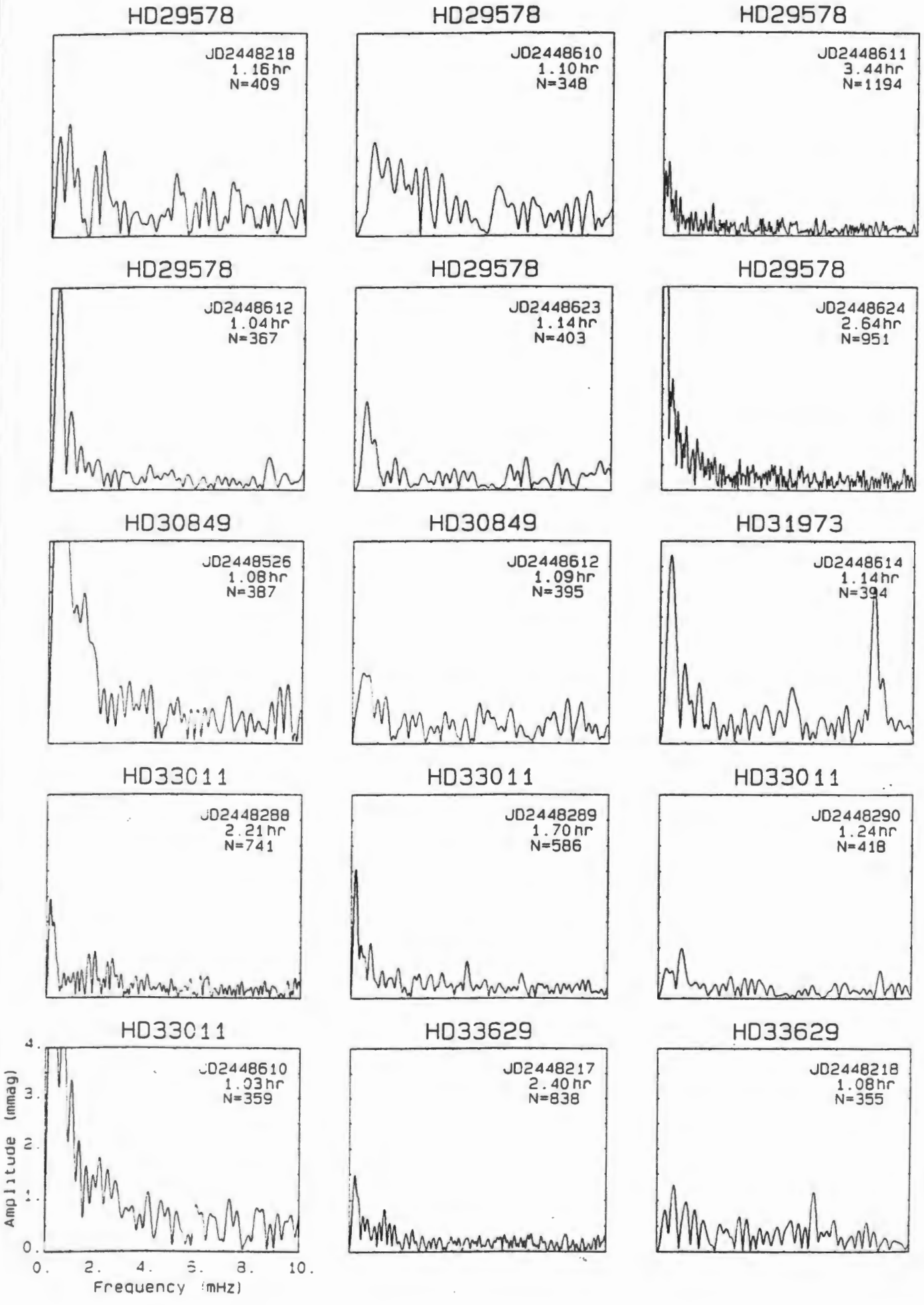
HD29578
JD2448218
1.16hr
N=409
HD29578
JD2448610
1.10hr
N=348
HD29578
JD2448611
3.44hr
N=1194
HD29578
JD2448612
1.04hr
N=367
HD29578
JD2448623
1.14hr
N=403
HD29578
JD2448624
2.64hr
N=951
HD30849
JD2448526
1.08hr
N=387
HD30849
JD2448612
1.09hr
N=395
HD31973
JD2448614
1.14hr
N=394
HD33011
JD2448288
2.21hr
N=741
HD33011
JD2448289
1.70hr
N=586
HD33011
JD2448290
1.24hr
N=418
HD33011
JD2448610
1.03hr
N=359
HD33629
JD2448217
2.40hr
N=838
HD33629
JD2448218
1.08hr
N=355
Amplitude (mmag)
0.
2.
4.
6.
8.
10.
Frequency (mHz)

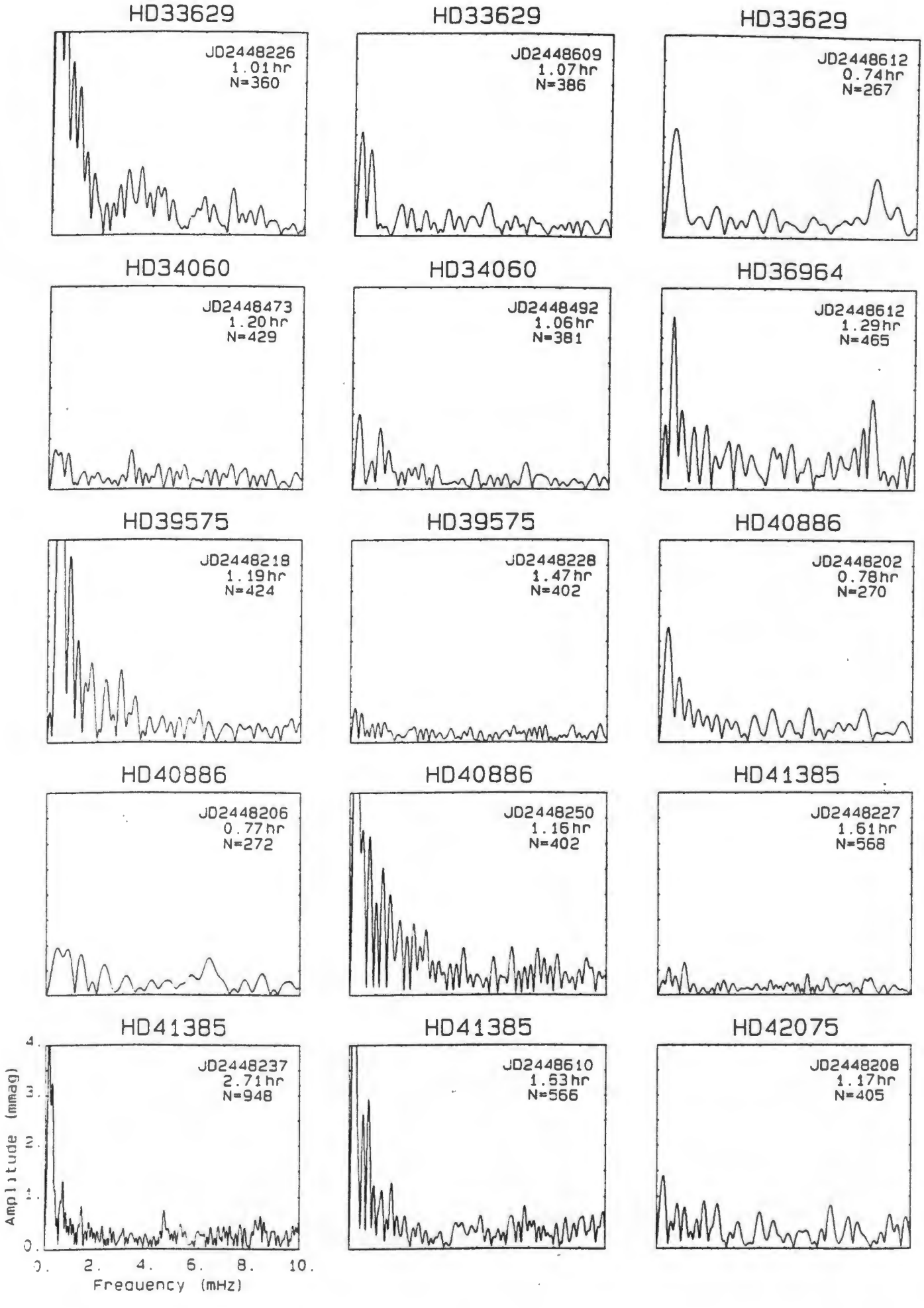
HD33629
JD2448226
1.01hr
N=360
HD33629
JD2448609
1.07hr
N=386
HD33629
JD2448612
0.74hr
N=267
HD34060
JD2448473
1.20hr
N=429
HD34060
JD2448492
1.06hr
N=381
HD36964
JD2448612
1.29hr
N=465
HD39575
JD2448218
1.19hr
N=424
HD39575
JD2448228
1.47hr
N=402
HD40886
JD2448202
0.78hr
N=270
HD40886
JD2448206
0.77hr
N=272
HD40886
JD2448250
1.16hr
N=402
HD41385
JD2448227
1.61hr
N=568
HD41385
JD2448237
2.71hr
N=948
HD41385
JD2448610
1.63hr
N=566
HD42075
JD2448208
1.17hr
N=405
Amplitude (mmag)
0.
2.
4.
6.
8.
10.
Frequency (mHz)

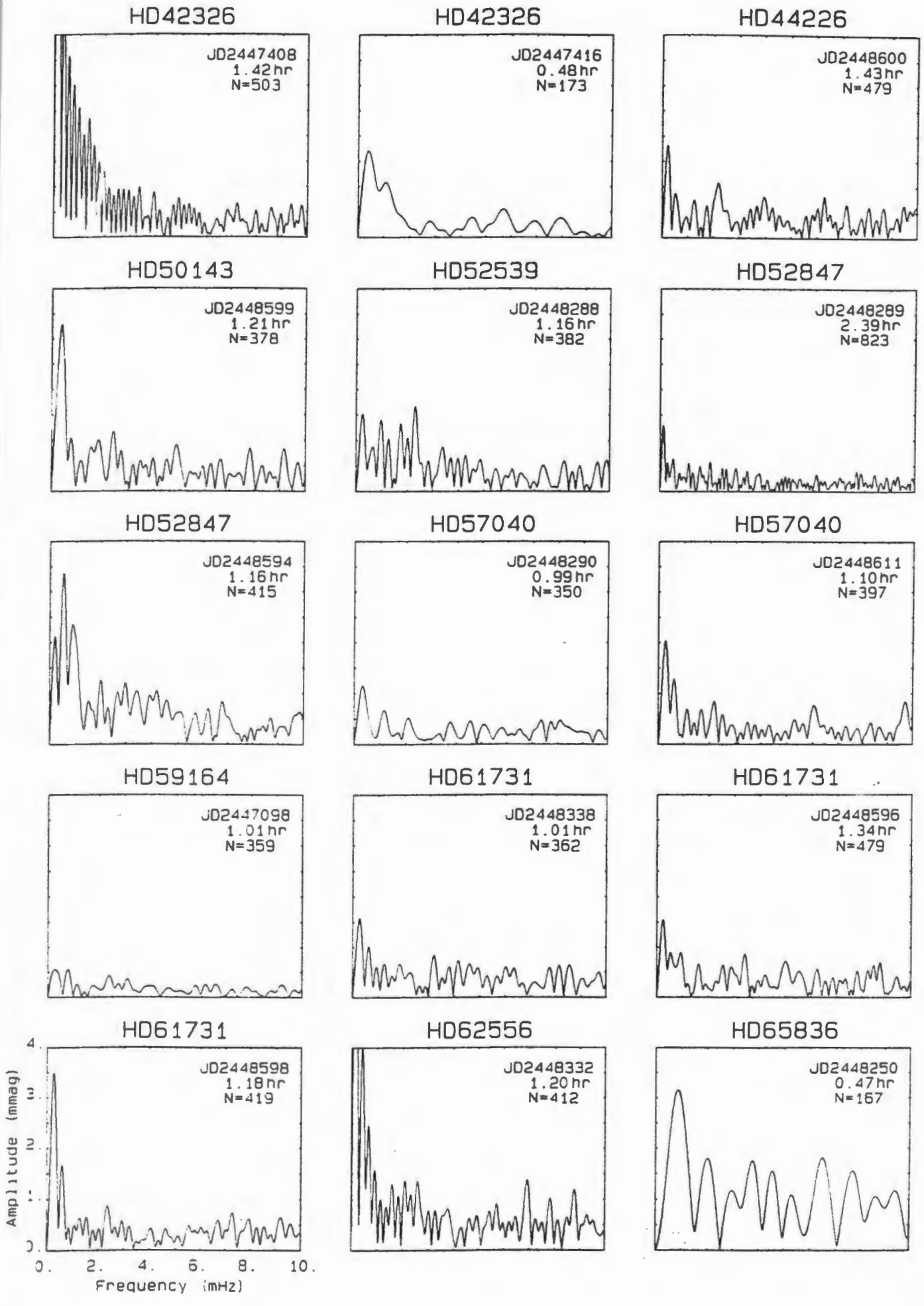
HD42326
JD2447408
1.42hr
N=503
HD42326
JD2447416
0.48hr
N=173
HD44226
JD2448600
1.43hr
N=479
HD50143
JD2448599
1.21hr
N=378
HD52539
JD2448288
1.16hr
N=382
HD52847
JD2448289
2.39hr
N=823
HD52847
JD2448594
1.16hr
N=415
HD57040
JD2448290
0.99hr
N=350
HD57040
JD2448611
1.10hr
N=397
HD59164
JD2447098
1.01hr
N=359
HD61731
JD2448338
1.01hr
N=362
HD61731
JD2448596
1.34hr
N=479
HD61731
JD2448598
1.18hr
N=419
HD62556
JD2448332
1.20hr
N=412
HD65836
JD2448250
0.47hr
N=167
Amplitude (mmag)
0.
2.
4.
6.
8.
10.
Frequency (mHz)

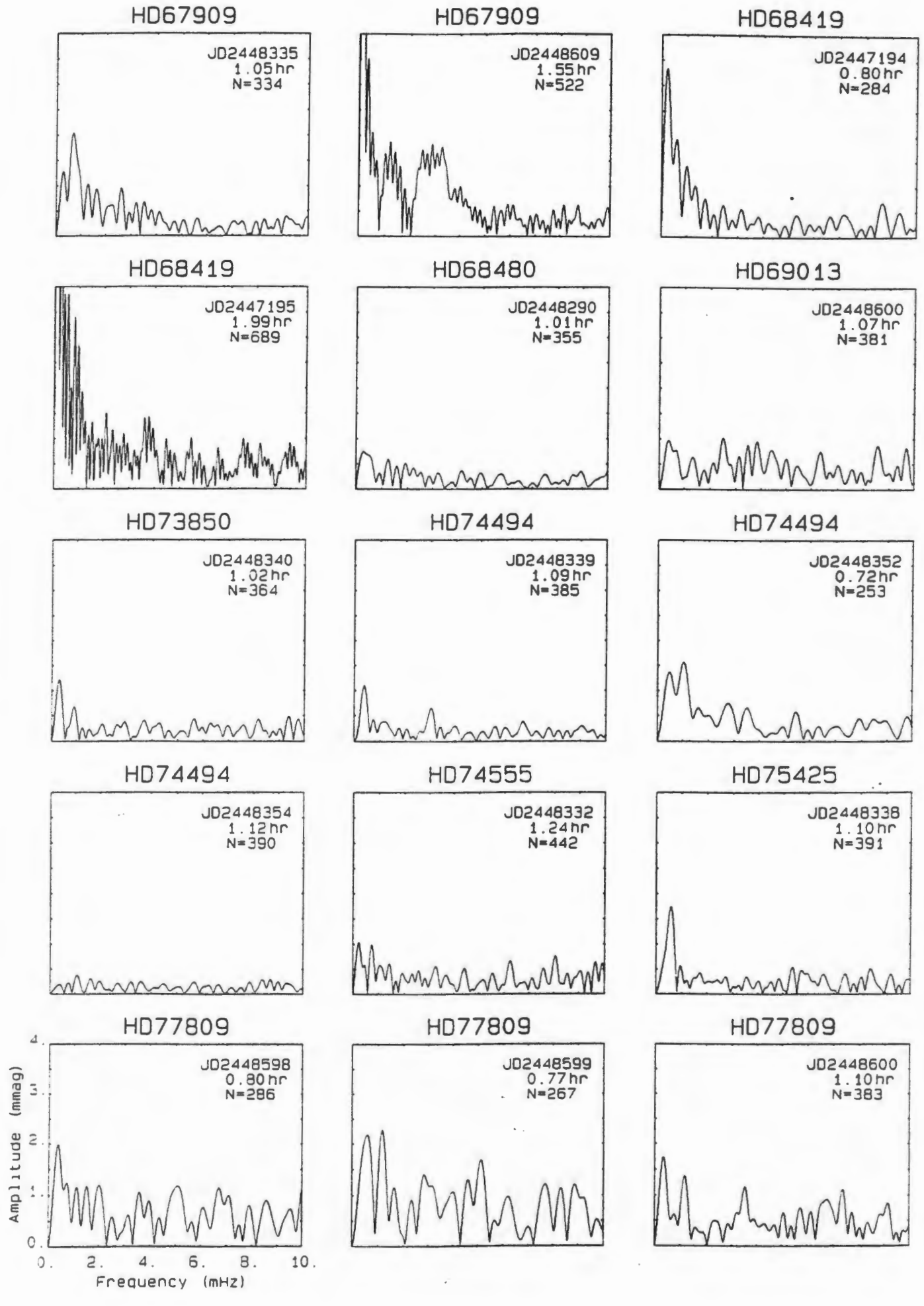
HD67909
JD2448335
1.05hr
N=334
HD67909
JD2448609
1.55hr
N=522
HD68419
JD2447194
0.80hr
N=284
HD68419
JD2447195
1.99hr
N=689
HD68480
JD2448290
1.01hr
N=355
HD69013
JD2448600
1.07hr
N=381
HD73850
JD2448340
1.02hr
N=364
HD74494
JD2448339
1.09hr
N=385
HD74494
JD2448352
0.72hr
N=253
HD74494
JD2448354
1.12hr
N=390
HD74555
JD2448332
1.24hr
N=442
HD75425
JD2448338
1.10hr
N=391
HD77809
JD2448598
0.80hr
N=286
HD77809
JD2448599
0.77hr
N=267
HD77809
JD2448600
1.10hr
N=383
Amplitude (mmag)
0.
2.
4.
6.
8.
10.
Frequency (mHz)

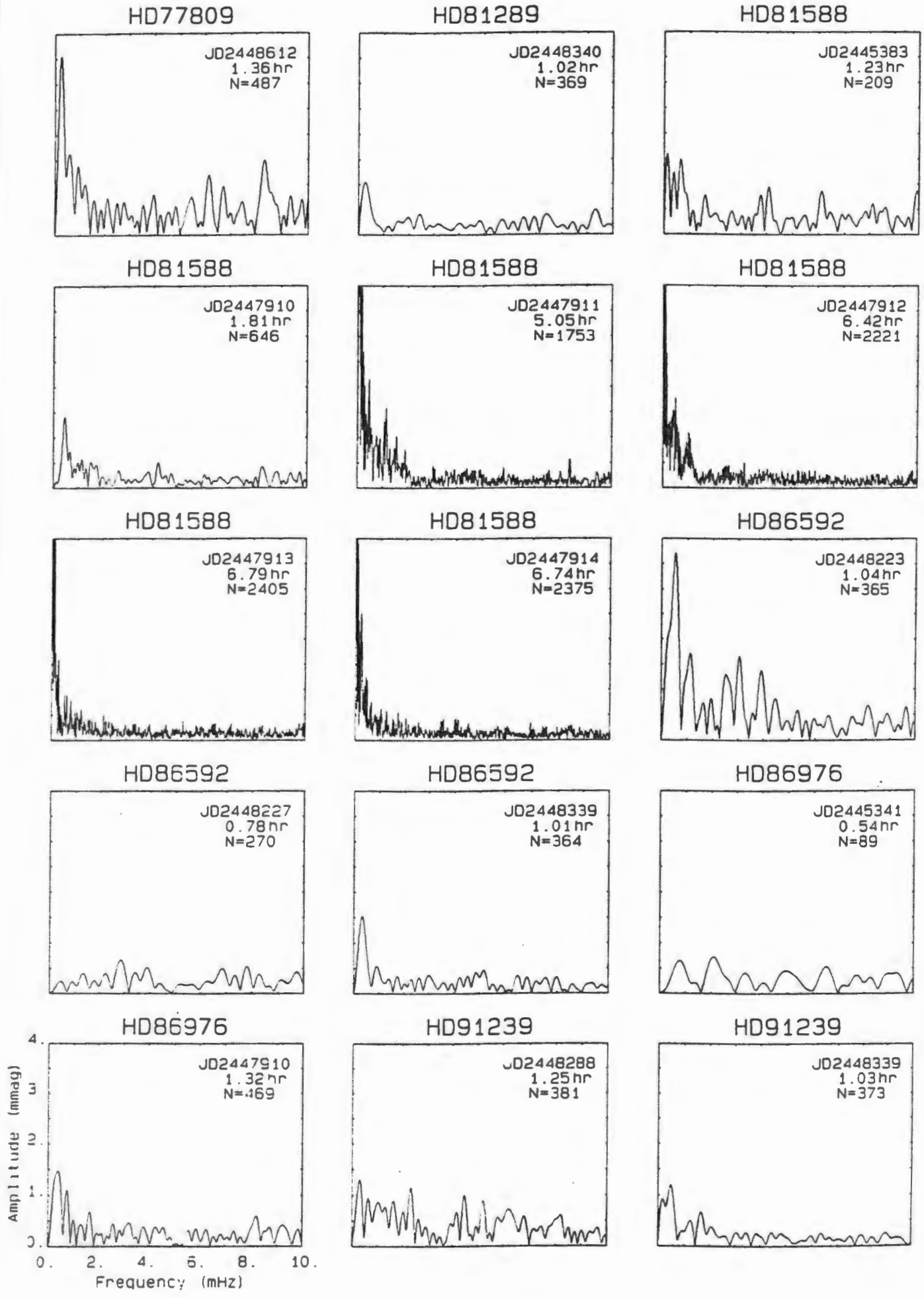
HD77809
JD2448612
1.36hr
N=487
HD81289
JD2448340
1.02hr
N=369
HD81588
JD2445383
1.23hr
N=209
HD81588
JD2447910
1.81hr
N=646
HD81588
JD2447911
5.05hr
N=1753
HD81588
JD2447912
6.42hr
N=2221
HD81588
JD2447913
6.79hr
N=2405
HD81588
JD2447914
6.74hr
N=2375
HD86592
JD2448223
1.04hr
N=365
HD86592
JD2448227
0.78hr
N=270
HD86592
JD2448339
1.01hr
N=364
HD86976
JD2445341
0.54hr
N=89
HD86976
JD2447910
1.32hr
N=469
HD91239
JD2448288
1.25hr
N=381
HD91239
JD2448339
1.03hr
N=373
Amplitude (mmag)
0.
1.
2.
3.
4.
0.
2.
4.
6.
8.
10.
Frequency (mHz)

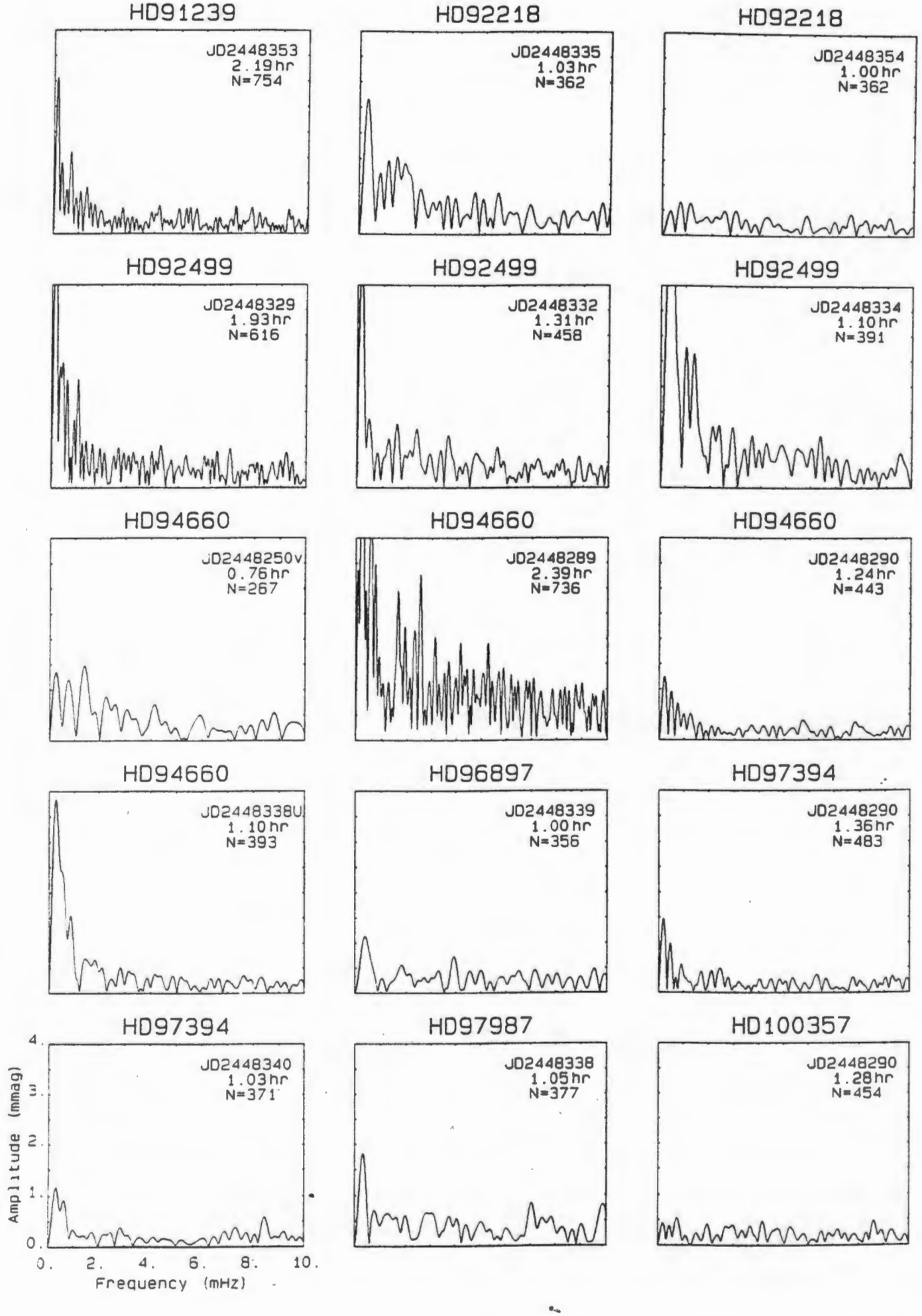
HD91239
JD2448353
2.19hr
N=754
HD92218
JD2448335
1.03hr
N=362
HD92218
JD2448354
1.00hr
N=362
HD92499
JD2448329
1.93hr
N=616
HD92499
JD2448332
1.31hr
N=458
HD92499
JD2448334
1.10hr
N=391
HD94660
JD2448250v
0.76hr
N=267
HD94660
JD2448289
2.39hr
N=736
HD94660
JD2448290
1.24hr
N=443
HD94660
JD2448338U
1.10hr
N=393
HD96897
JD2448339
1.00hr
N=356
HD97394
JD2448290
1.36hr
N=483
HD97394
JD2448340
1.03hr
N=371
HD97987
JD2448338
1.05hr
N=377
HD100357
JD2448290
1.28hr
N=454
Amplitude (mmag)
0.
1.
2.
3.
4.
0.
2.
4.
6.
8.
10.
Frequency (mHz)

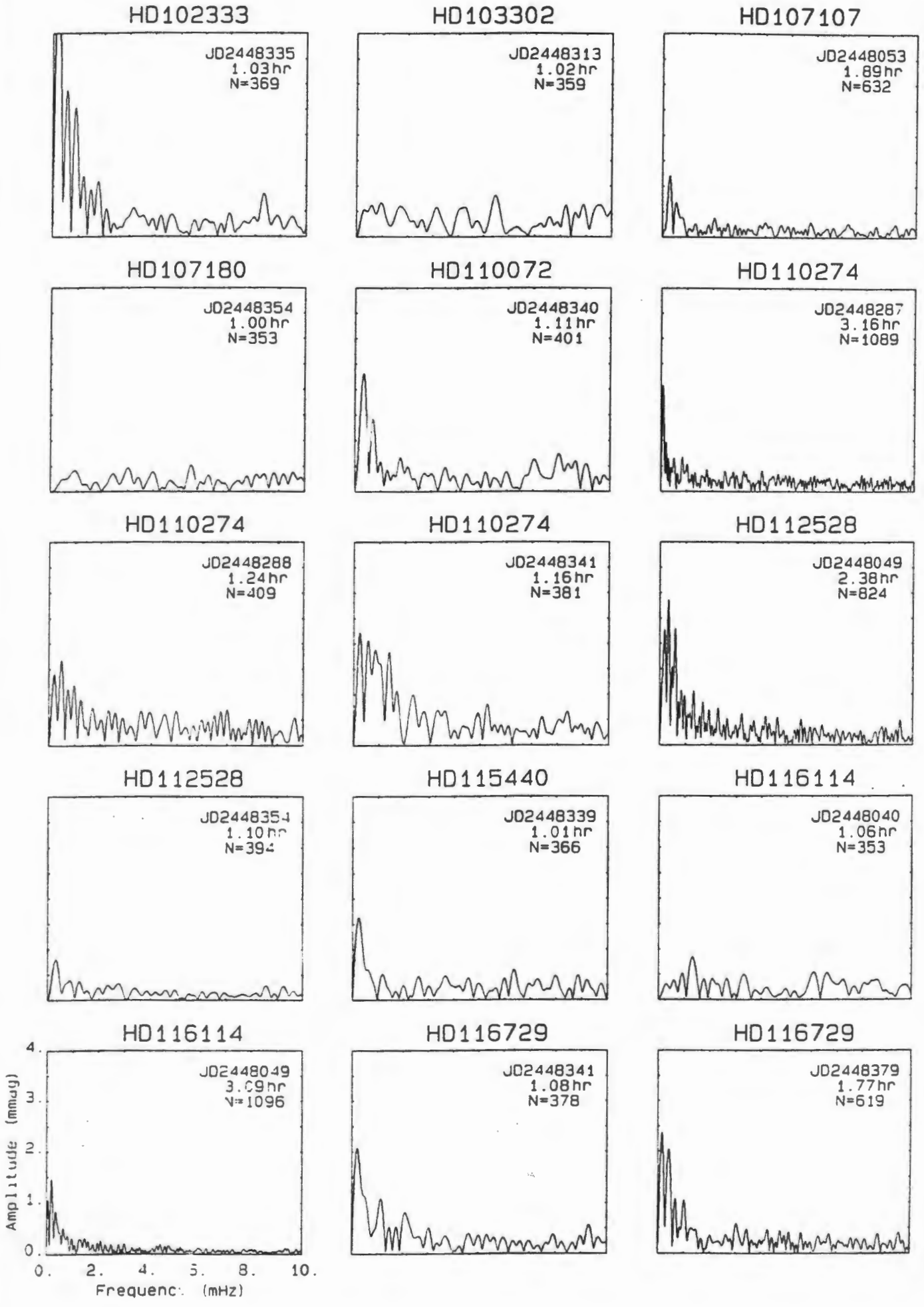
HD102333
JD2448335
1.03hr
N=369
HD103302
JD2448313
1.02hr
N=359
HD107107
JD2448053
1.89hr
N=632
HD107180
JD2448354
1.00hr
N=353
HD110072
JD2448340
1.11hr
N=401
HD110274
JD2448287
3.16hr
N=1089
HD110274
JD2448288
1.24hr
N=409
HD110274
JD2448341
1.16hr
N=381
HD112528
JD2448049
2.38hr
N=824
HD112528
JD2448354
1.10hr
N=394
HD115440
JD2448339
1.01hr
N=366
HD116114
JD2448040
1.06hr
N=353
HD116114
JD2448049
3.09hr
N=1096
HD116729
JD2448341
1.08hr
N=378
HD116729
JD2448379
1.77hr
N=619
Amplitude (mmag)
4.
3.
2.
1.
0.
0.
2.
4.
5.
8.
10.
Frequenc (mHz)

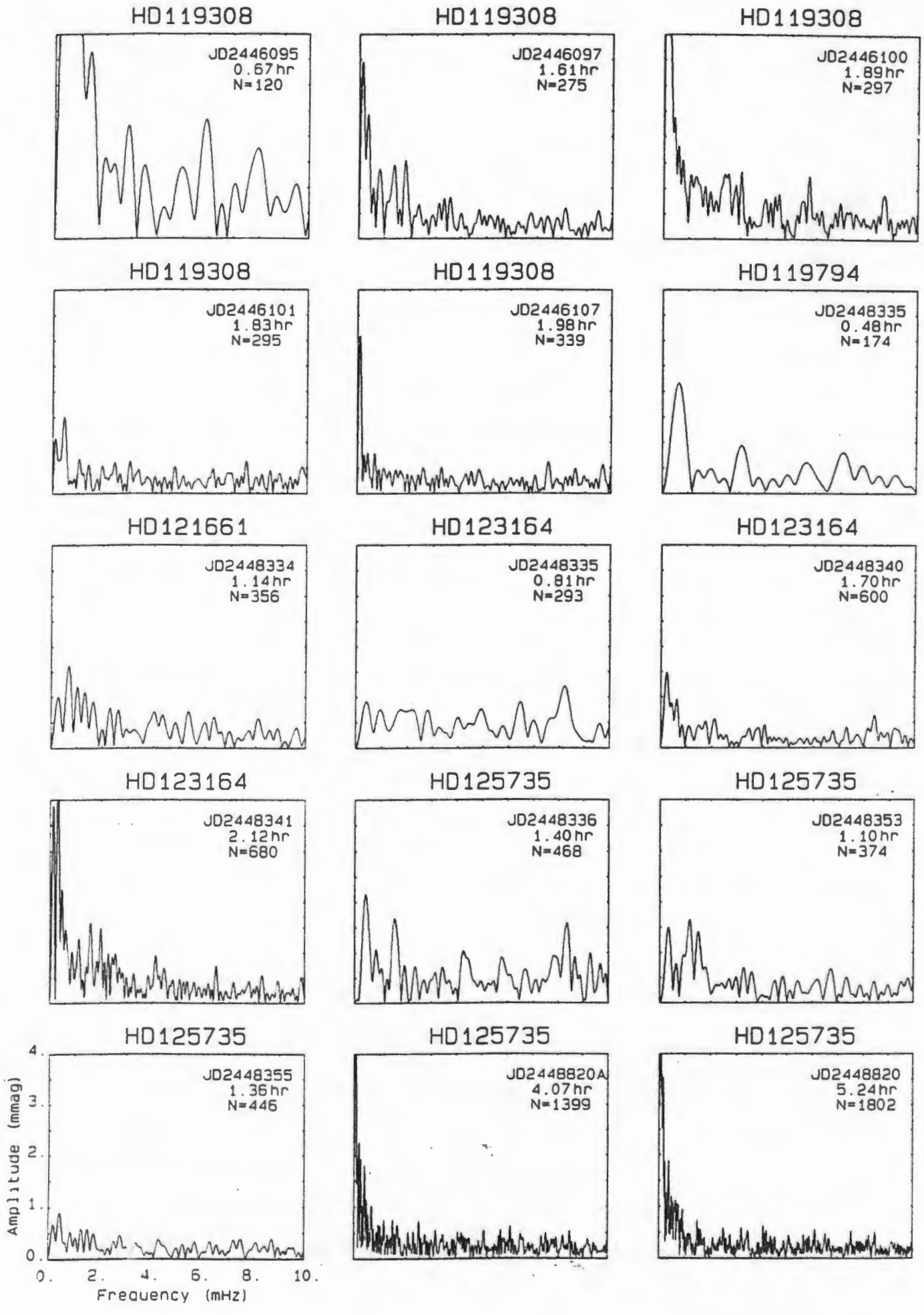
HD119308
JD2446095
0.67hr
N=120
HD119308
JD2446097
1.61hr
N=275
HD119308
JD2446100
1.89hr
N=297
HD119308
JD2446101
1.83hr
N=295
HD119308
JD2446107
1.98hr
N=339
HD119794
JD2448335
0.48hr
N=174
HD121661
JD2448334
1.14hr
N=356
HD123164
JD2448335
0.81hr
N=293
HD123164
JD2448340
1.70hr
N=600
HD123164
JD2448341
2.12hr
N=680
HD125735
JD2448336
1.40hr
N=468
HD125735
JD2448353
1.10hr
N=374
HD125735
JD2448355
1.36hr
N=446
HD125735
JD2448820A
4.07hr
N=1399
HD125735
JD2448820
5.24hr
N=1802
Amplitude (mmag)
0.
1.
2.
3.
4.
0.
2.
4.
6.
8.
10.
Frequency (mHz)

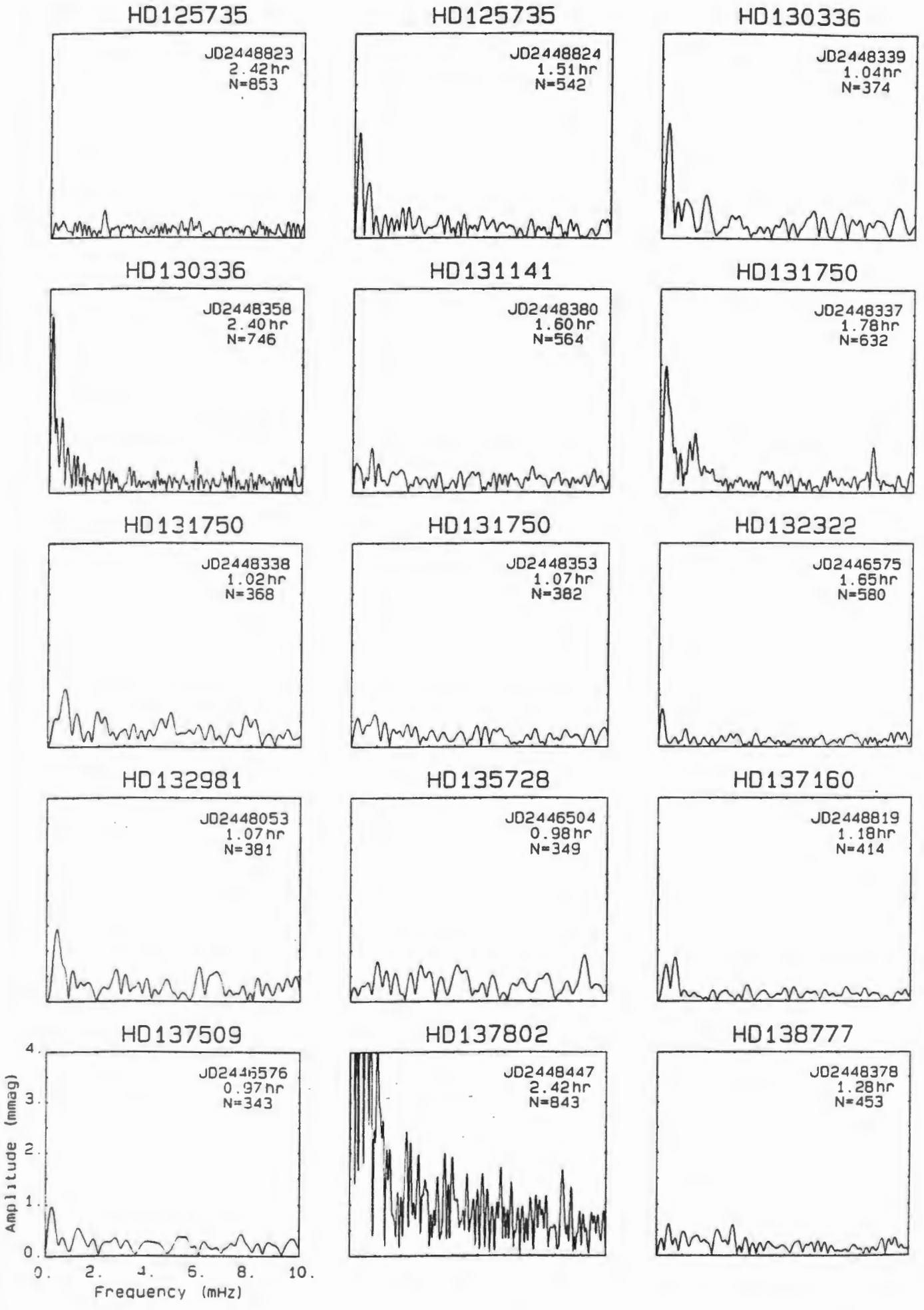
HD125735
JD2448823
2.42hr
N=853
HD125735
JD2448824
1.51hr
N=542
HD130336
JD2448339
1.04hr
N=374
HD130336
JD2448358
2.40hr
N=746
HD131141
JD2448380
1.60hr
N=564
HD131750
JD2448337
1.78hr
N=632
HD131750
JD2448338
1.02hr
N=368
HD131750
JD2448353
1.07hr
N=382
HD132322
JD2446575
1.65hr
N=580
HD132981
JD2448053
1.07hr
N=381
HD135728
JD2446504
0.98hr
N=349
HD137160
JD2448819
1.18hr
N=414
HD137509
JD2446576
0.97hr
N=343
HD137802
JD2448447
2.42hr
N=843
HD138777
JD2448378
1.28hr
N=453
Amplitude (mmag)
0.
1.
2.
3.
4.
0.
2.
4.
6.
8.
10.
Frequency (mHz)

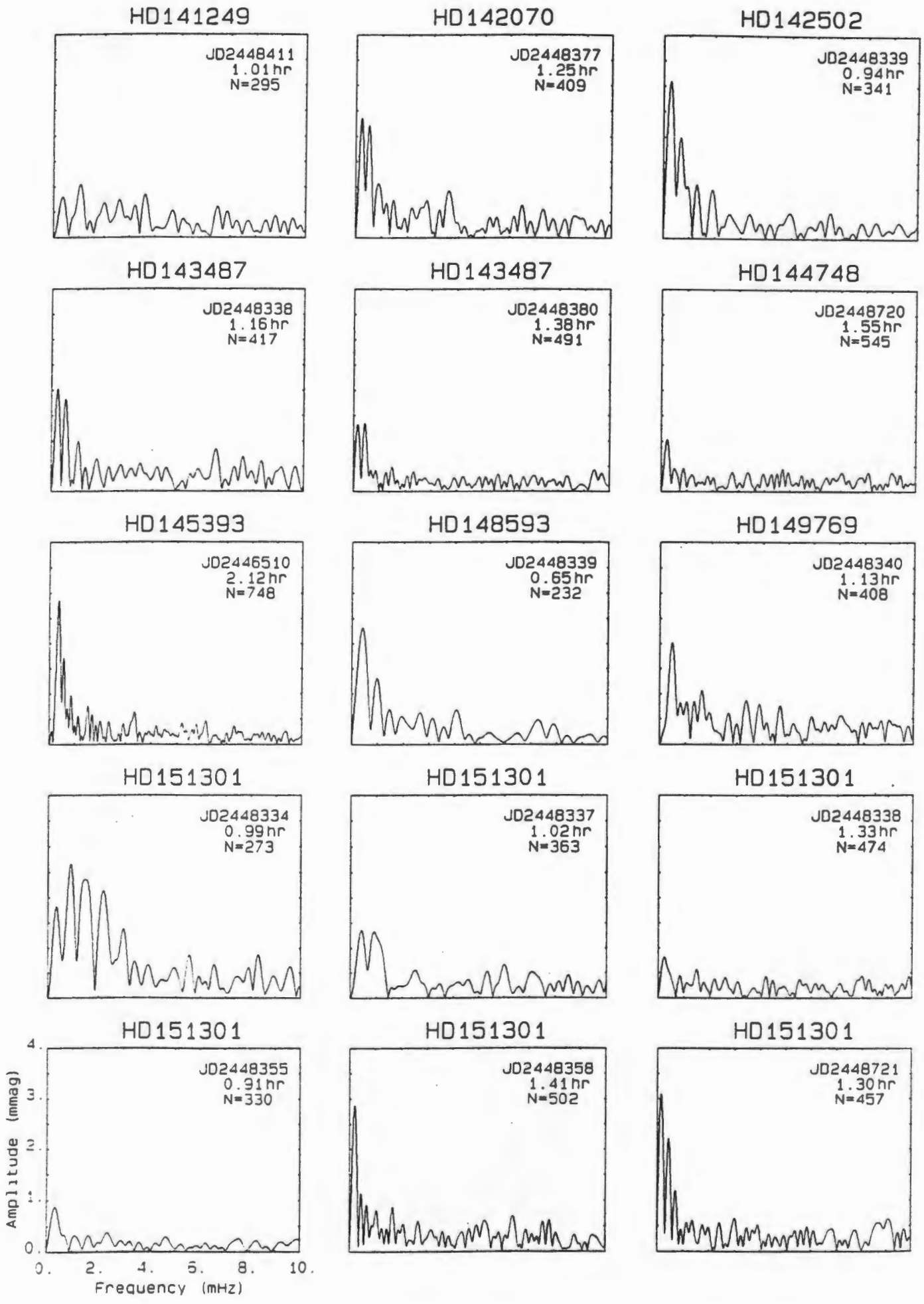
HD141249
JD2448411
1.01hr
N=295
HD142070
JD2448377
1.25hr
N=409
HD142502
JD2448339
0.94hr
N=341
HD143487
JD2448338
1.16hr
N=417
HD143487
JD2448380
1.38hr
N=491
HD144748
JD2448720
1.55hr
N=545
HD145393
JD2446510
2.12hr
N=748
HD148593
JD2448339
0.65hr
N=232
HD149769
JD2448340
1.13hr
N=408
HD151301
JD2448334
0.99hr
N=273
HD151301
JD2448337
1.02hr
N=363
HD151301
JD2448338
1.33hr
N=474
HD151301
JD2448355
0.91hr
N=330
HD151301
JD2448358
1.41hr
N=502
HD151301
JD2448721
1.30hr
N=457
Amplitude (mmag)
0.
2.
4.
5.
8.
10.
Frequency (mHz)

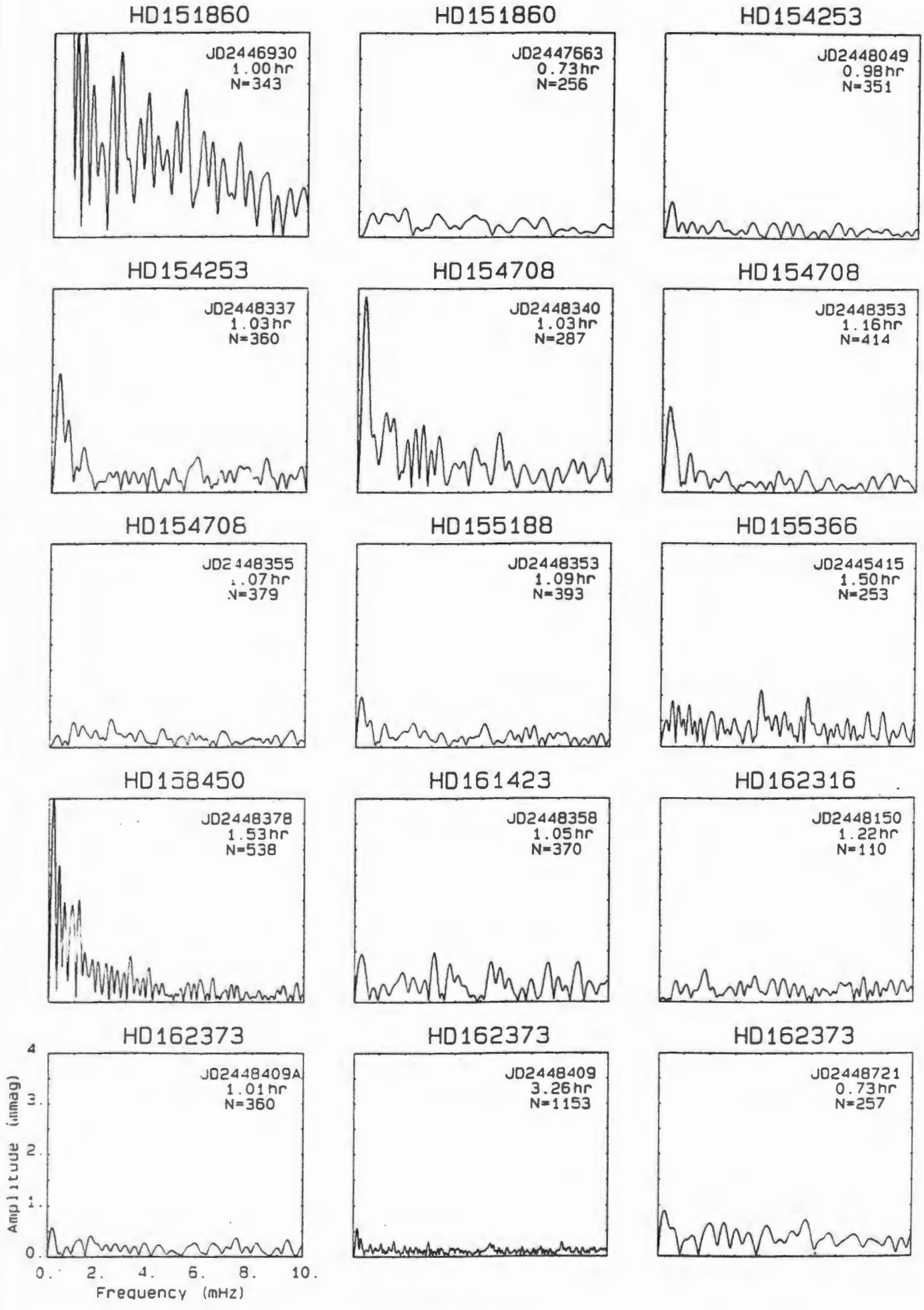
HD151860
JD2446930
1.00hr
N=343
HD151860
JD2447663
0.73hr
N=256
HD154253
JD2448049
0.98hr
N=351
HD154253
JD2448337
1.03hr
N=360
HD154708
JD2448340
1.03hr
N=287
HD154708
JD2448353
1.16hr
N=414
HD154708
JD2448355
1.07hr
N=379
HD155188
JD2448353
1.09hr
N=393
HD155366
JD2445415
1.50hr
N=253
HD158450
JD2448378
1.53hr
N=538
HD161423
JD2448358
1.05hr
N=370
HD162316
JD2448150
1.22hr
N=110
HD162373
JD2448409A
1.01hr
N=360
HD162373
JD2448409
3.26hr
N=1153
HD162373
JD2448721
0.73hr
N=257
Amplitude (mmag)
0.
1.
2.
3.
4
0.
2.
4.
6.
8.
10.
Frequency (mHz)

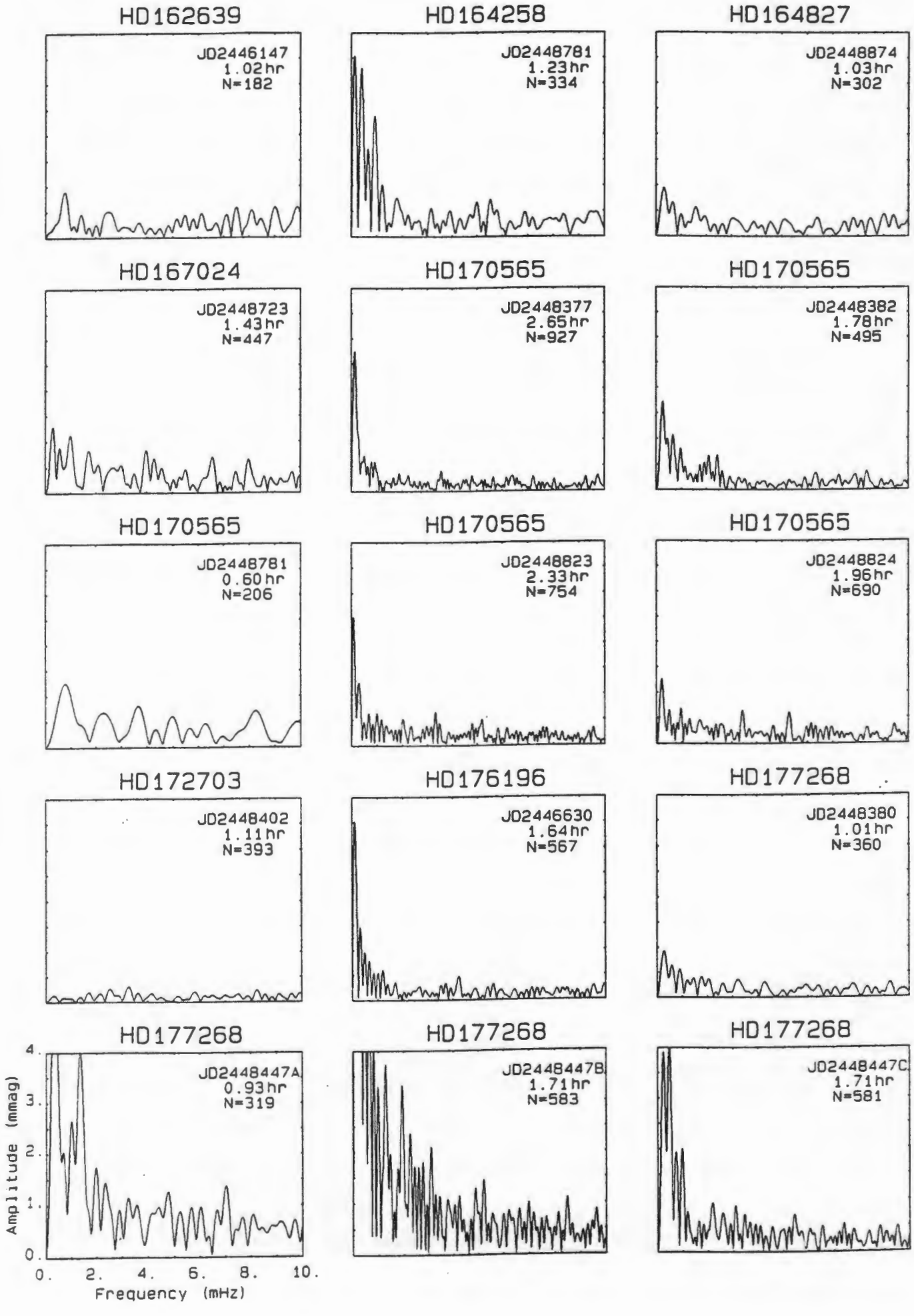
HD162639
JD2446147
1.02hr
N=182
HD164258
JD2448781
1.23hr
N=334
HD164827
JD2448874
1.03hr
N=302
HD167024
JD2448723
1.43hr
N=447
HD170565
JD2448377
2.65hr
N=927
HD170565
JD2448382
1.78hr
N=495
HD170565
JD2448781
0.60hr
N=206
HD170565
JD2448823
2.33hr
N=754
HD170565
JD2448824
1.96hr
N=690
HD172703
JD2448402
1.11hr
N=393
HD176196
JD2446630
1.64hr
N=567
HD177268
JD2448380
1.01hr
N=360
HD177268
JD2448447A
0.93hr
N=319
HD177268
JD2448447B
1.71hr
N=583
HD177268
JD2448447C
1.71hr
N=581
Amplitude (mmag)
0.
1.
2.
3.
4.
0.
2.
4.
6.
8.
10.
Frequency (mHz)

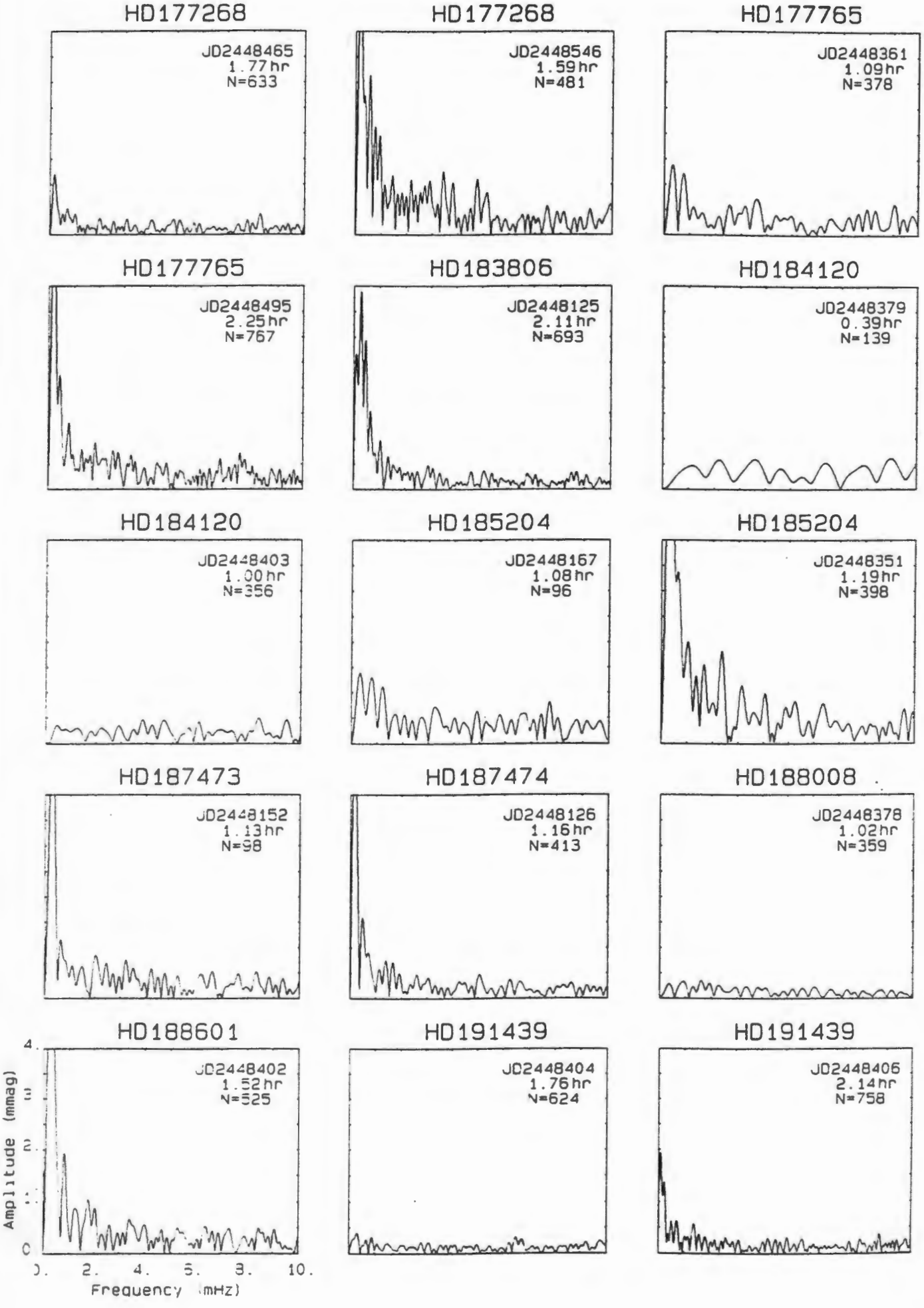
HD177268
JD2448465
1.77hr
N=633
HD177268
JD2448546
1.59hr
N=481
HD177765
JD2448361
1.09hr
N=378
HD177765
JD2448495
2.25hr
N=767
HD183806
JD2448125
2.11hr
N=693
HD184120
JD2448379
0.39hr
N=139
HD184120
JD2448403
1.00hr
N=356
HD185204
JD2448167
1.08hr
N=96
HD185204
JD2448351
1.19hr
N=398
HD187473
JD2448152
1.13hr
N=98
HD187474
JD2448126
1.16hr
N=413
HD188008
JD2448378
1.02hr
N=359
HD188601
JD2448402
1.52hr
N=525
HD191439
JD2448404
1.76hr
N=624
HD191439
JD2448406
2.14hr
N=758
Amplitude (mmag)
Frequency (mHz)

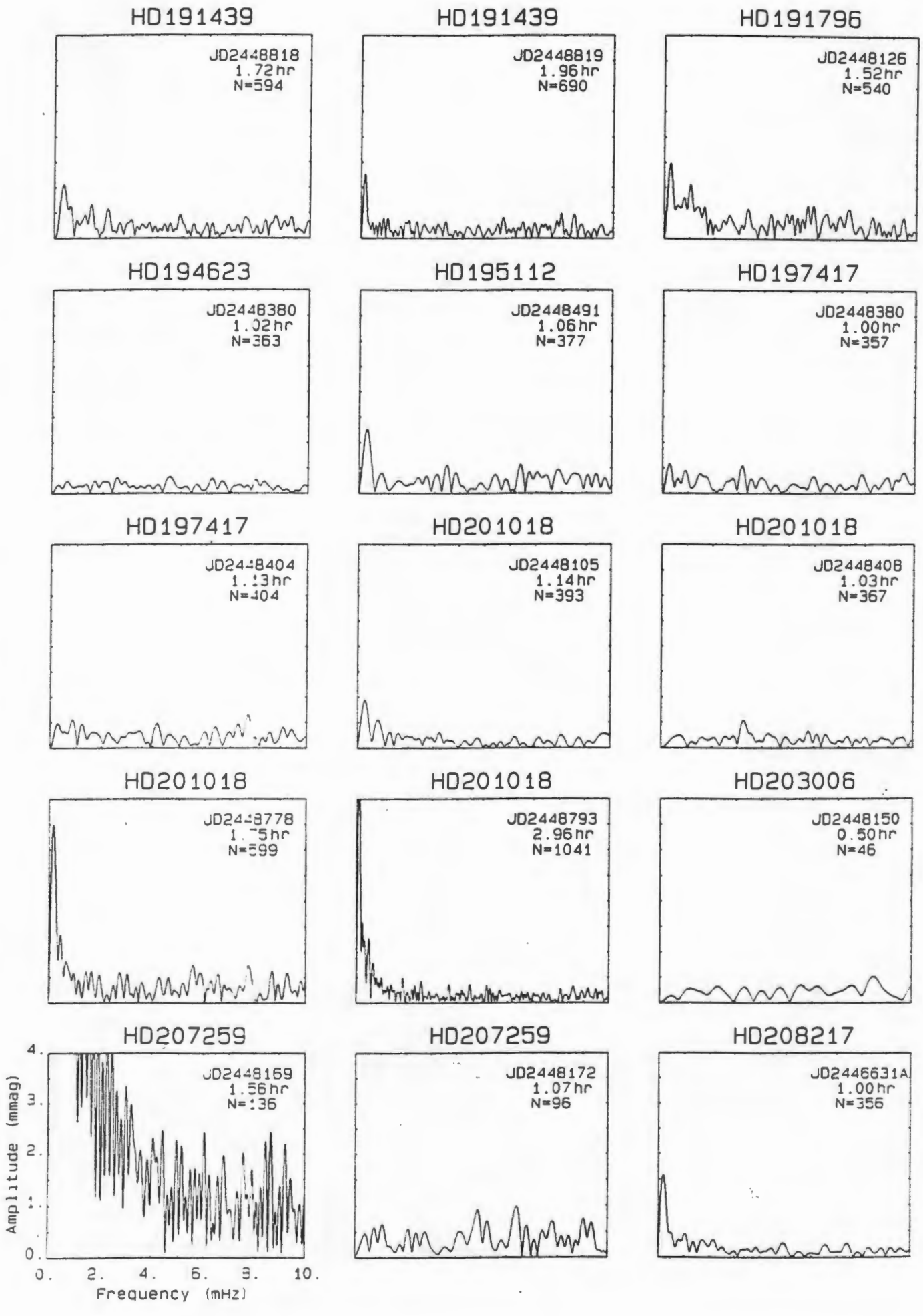
HD191439
JD2448818
1.72hr
N=594
HD191439
JD2448819
1.96hr
N=690
HD191796
JD2448126
1.52hr
N=540
HD194623
JD2448380
1.02hr
N=363
HD195112
JD2448491
1.06hr
N=377
HD197417
JD2448380
1.00hr
N=357
HD197417
JD2448404
1.13hr
N=404
HD201018
JD2448105
1.14hr
N=393
HD201018
JD2448408
1.03hr
N=367
HD201018
JD2448778
1.75hr
N=399
HD201018
JD2448793
2.96hr
N=1041
HD203006
JD2448150
0.50hr
N=46
HD207259
JD2448169
1.56hr
N=136
HD207259
JD2448172
1.07hr
N=96
HD208217
JD2446631A
1.00hr
N=356
Amplitude (mmag)
0.
1.
2.
3.
4.
0.
2.
4.
6.
8.
10.
Frequency (mHz)

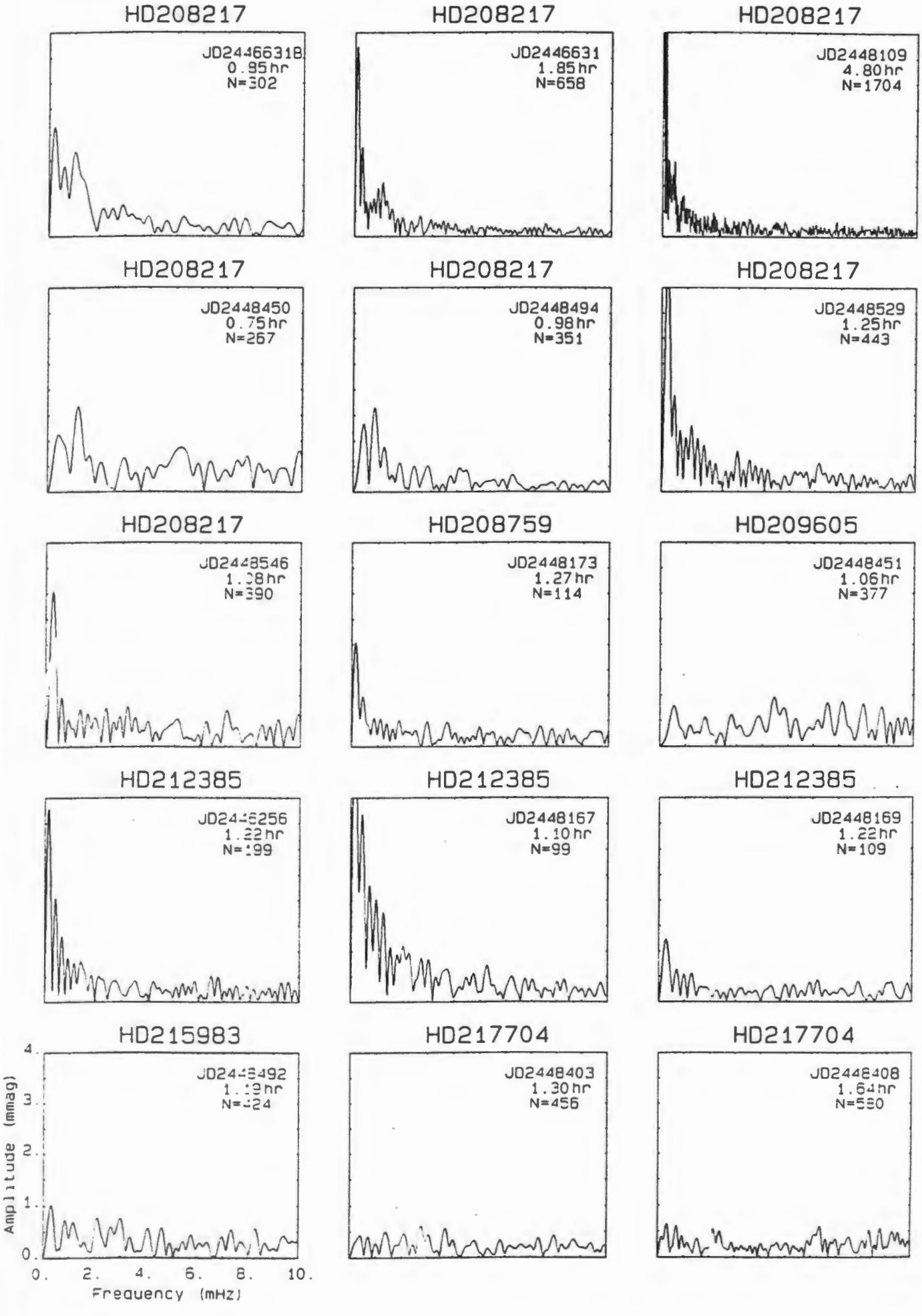
HD208217
JD2446631B
0.95hr
N=302
HD208217
JD2446631
1.85hr
N=658
HD208217
JD2448109
4.80hr
N=1704
HD208217
JD2448450
0.75hr
N=267
HD208217
JD2448494
0.98hr
N=351
HD208217
JD2448529
1.25hr
N=443
HD208217
JD2448546
1.08hr
N=390
HD208759
JD2448173
1.27hr
N=114
HD209605
JD2448451
1.06hr
N=377
HD212385
JD2448256
1.22hr
N=199
HD212385
JD2448167
1.10hr
N=99
HD212385
JD2448169
1.22hr
N=109
HD215983
JD2448492
1.19hr
N=424
HD217704
JD2448403
1.30hr
N=456
HD217704
JD2448408
1.64hr
N=580
Amplitude (mmag)
0.
1.
2.
3.
4.
0.
2.
4.
6.
8.
10.
Frequency (mHz)

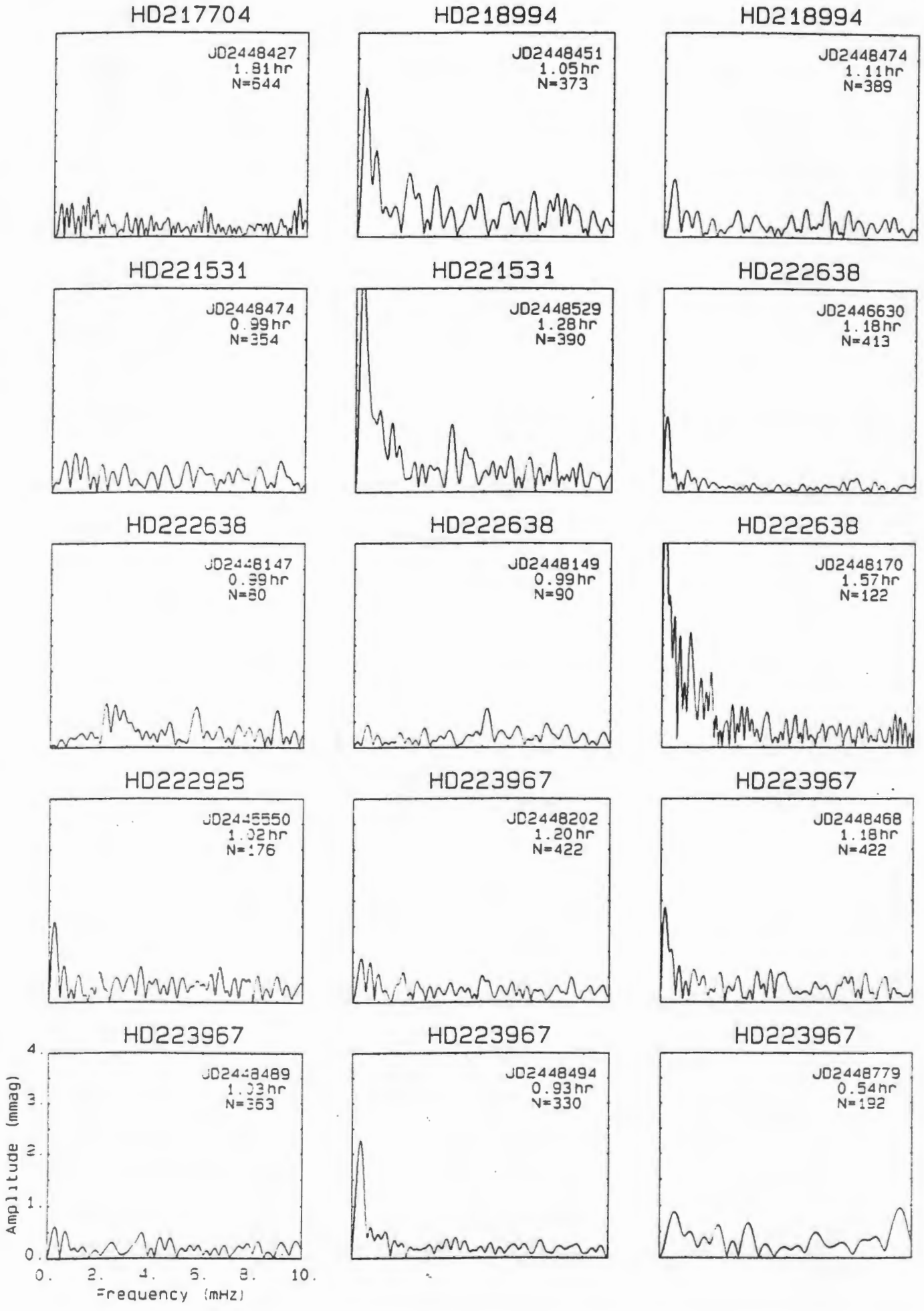
HD217704
JD2448427
1.81hr
N=544
HD218994
JD2448451
1.05hr
N=373
HD218994
JD2448474
1.11hr
N=389
HD221531
JD2448474
0.99hr
N=354
HD221531
JD2448529
1.28hr
N=390
HD222638
JD2446630
1.18hr
N=413
HD222638
JD2448147
0.99hr
N=80
HD222638
JD2448149
0.99hr
N=90
HD222638
JD2448170
1.57hr
N=122
HD222925
JD2445550
1.02hr
N=176
HD223967
JD2448202
1.20hr
N=422
HD223967
JD2448468
1.18hr
N=422
HD223967
JD2448489
1.03hr
N=363
HD223967
JD2448494
0.93hr
N=330
HD223967
JD2448779
0.54hr
N=192
Amplitude (mmag)
0.
1.
2.
3.
4.
0.
2.
4.
6.
8.
10.
Frequency (mHz)

Chapter 6

A frequency analysis of the rapidly oscillating Ap star HD 84041 and a determination of its rotation period.

6.1 Introduction

In chapter 5 we described the discovery of rapid oscillations with a period of 14.6 min in HD 84041. This star is classified as Ap SrEuCr by Houk (1982) and Ap SrEu(F) by Bidelman & MacConnell (1973). It has Strömgren photometric indices typical of the cool Ap stars: b-y = 0.177, m_1 = 0.233, c_1 = 0.797, β = 2.844. Application of Crawford's (1979) calibration for normal A stars yields δm_1 = -0.026 and δc_1 = -0.061, both of which are indicative of the heavy metal line blanketing in the Ap stars.

The amplitude of the oscillations in the discovery observations appeared to be strongly modulated on a night-to-night basis as well as on a time-scale of hours. Amplitude modulation on a time-scale of days in a roAp star is usually indicative of rotation. As the star rotates, the oscillations are seen from varying aspect. This manifests itself in the frequency spectrum as a $(2\ell + 1)$ frequency multiplet, as predicted by the oblique pulsator model (section 2.7). Amplitude modulation in roAp stars on time-scales of hours is usually indicative of the beating of two or more independent pulsation modes. Given a long enough time-base, such secondary frequencies can always be identified, at least to the level of having to discriminate among their daily aliases. If the spacing between two frequencies, ν_1 and ν_2, is close to an integral multiple of 1 day^{-1}, then one of the aliases of ν_1 sits on top of ν_2 and the only way to identify ν_2 correctly is to acquire contemporaneous multi-site observations. Moreover, the complexity of the amplitude spectrum in a star with a rich p-mode spectrum is also greatly reduced in multi-site data. An example of this is the rich p-mode star HD 60435, which has been the subject of two multi-site campaigns by Matthews *et al.* (1986, 1987).

Analyses of the sparse 1991 data on HD 84041 indicated that this star exhibits the effects of oblique rotation and the beating of several independent pulsation modes. The conjectured multi-frequency nature of HD 84041 elicits interest because of inferences of the rotational inclination and magnetic geometry that can be made using the oblique pulsator model and inferences of the luminosity and evolutionary status of this star using the techniques of asteroseismology. Clearly, further observations of HD 84041 were highly desirable. The highly complex nature of the oscillations

in this star suggested to us that a single-site campaign would prove inconclusive. Thus a multi-site campaign on HD 84041 was scheduled during January - February 1992. The campaign focussed on the rapid oscillations and also searched for more gradual mean light variations which arise with rotation.

In this chapter we present 117 hours of high-speed Johnson *B* observations of HD 84041 obtained during 1992 at the SAAO and the Cerro Tololo Inter-American Observatory (CTIO). These observations show that HD 84041 pulsates in several *p*-modes with periods near 15 min. The amplitude of the oscillations is modulated in such a complex way that the modulating frequencies cannot be identified with certainty, even with this large data set. We present 26 nights of differential *UBVRI* photometry acquired at the SAAO which we use to determine the rotation period of HD 84041, P_{rot} = 3.69±0.01 day. The mean light variations have a double-wave nature which indicates that both magnetic (pulsation) poles are seen, but from different aspect.

Many of the observations presented in this chapter were acquired by my collaborators. Tobias J. Kreidl of Lowell Observatory obtained observations at CTIO contemporaneously with observations at SAAO by Chris Koen. Unfortunately, the CTIO observations were mostly too noisy to be of much use. Don Kurtz provided SAAO observations of HD 84041 on 9 nights. SAAO astronomers Francois van Wyk, Fred Marang and Greg Roberts provided differential photometry of HD 84041 on 26 nights which was used to determine the rotation period of this star. The material presented in this chapter has been published in *Monthly Notices of the Royal Astronomical Society* (Martinez *et al.* 1993).

6.2 The high-speed photometric observations

High-speed Johnson *B* observations were acquired on 22 nights during 1992 January and February. We used the University of Cape Town photometer attached to the SAAO 0.75-m or 1.0-m telescope and the People's photometer attached to the Lowell 0.61-m telescope at CTIO. The same observing procedure was used by all observers and the data were all reduced and analyzed by the author. The observing procedures and basic reductions have already been described in sections 5.3 and 5.7, respectively.

Table 6.1 is a Journal of the observations listing the civil date, the Heliocentric Julian Date of the first and last observation, the duration of the observations in hours, the number of 40-s integrations, the standard deviation, σ, of one observation with respect to the mean for the night and

Table 6.1

A Journal of the 1991 and 1992 high-speed *B* observations of HD 84041.

	HJD start 2440000+	HJD end 2440000+	T hr	N_{40}	σ mmag	Telescope & Observer
1991						
Mar 19/20	8335.36573	8335.40826	1.02	92	1.540	SAAO 0.75-m PM
Apr 7/ 8	8354.28869	8354.37560	2.09	188	1.038	SAAO 1.00-m PM
Apr 8/ 9	8355.34813	8355.48533	3.29	284	1.258	SAAO 1.00-m PM
Apr 11/12	8358.26744	8358.38167	2.74	211	2.401	SAAO 0.50-m PM
Apr 12/13	8359.31449	8359.36385	1.18	99	2.219	SAAO 0.50-m PM
Apr 15/16	8362.23899	8362.31960	1.93	171	1.539	SAAO 0.50-m PM
Apr 30/ 1	8377.33799	8377.41194	1.77	156	3.603	SAAO 0.50-m PM
Σ			14.02	1201		
1992						
Jan 24/25	8646.56924	8646.86129	7.01	489	4.218	CTIO 0.61-m TJK
Jan 25/26	8647.57441	8647.86116	6.88	493	5.048	CTIO 0.61-m TJK
Jan 26/27	8648.56720	8648.85755	6.97	527	4.892	CTIO 0.61-m TJK
Jan 27/28	8649.69445	8649.86300	4.05	193	6.232	CTIO 0.61-m TJK
Jan 29/30	8651.36253	8651.59194	5.51	446	2.986	SAAO 0.75-m CK
Jan 29/30	8651.57406	8651.61951	1.09	81	5.688	CTIO 0.61-m TJK
Jan 29/30	8651.67601	8651.72551	1.19	96	3.358	CTIO 0.61-m TJK
Jan 30/31	8652.43263	8652.61883	4.47	361	2.902	SAAO 0.75-m CK
Jan 30/31	8652.55777	8652.78067	5.35	420	5.987	CTIO 0.61-m TJK
Jan 31/ 1	8653.32002	8653.56771	5.94	511	2.336	SAAO 0.75-m CK
Jan 31/ 1	8653.56280	8653.86392	7.23	562	4.493	CTIO 0.61-m TJK
Feb 1/ 2	8654.41929	8654.54841	3.10	272	2.687	SAAO 0.75-m CK
Feb 2/ 3	8655.42346	8655.57028	3.52	309	2.141	SAAO 0.75-m CK
Feb 3/ 4	8656.42540	8656.53043	2.52	222	2.510	SAAO 0.75-m CK
Feb 12/13	8665.28773	8665.58791	7.20	600	2.893	SAAO 1.00-m DWK
Feb 13/14	8666.29007	8666.62422	8.02	683	1.911	SAAO 1.00-m DWK
Feb 14/15	8667.28951	8667.53118	5.80	506	1.694	SAAO 1.00-m DWK
Feb 15/16	8668.30585	8668.55857	6.07	499	2.460	SAAO 1.00-m DWK
Feb 16/17	8669.28619	8669.43718	3.62	312	1.806	SAAO 1.00-m DWK
Feb 17/18	8670.27799	8670.50681	5.49	468	1.874	SAAO 1.00-m DWK
Feb 18/19	8671.42569	8671.60544	4.31	370	1.683	SAAO 1.00-m DWK
Feb 19/20	8672.28034	8672.32391	1.05	88	1.968	SAAO 1.00-m DWK
Feb 19/20	8672.34087	8672.48896	3.55	223	1.670	SAAO 1.00-m DWK
Feb 21/22	8674.47539	8674.62631	3.62	303	1.909	SAAO 1.00-m PM
Feb 22/23	8675.52273	8675.63028	2.58	215	3.271	SAAO 1.00-m PM
Feb 23/24	8676.41279	8676.44502	0.77	69	1.684	SAAO 1.00-m PM
Σ			116.91	9318		

the telescope/observer combination. For convenience, Table 6.1 also lists the 1991 discovery observations journaled in Table 5.3.

6.3 The differential photometric observations

Mean light observations of HD 84041 were obtained on 26 nights from 4/5 February to 6/7 April 1992 using the Modular Photometer (Sec. 4.3) attached to the SAAO 0.5-m telescope at Sutherland. HD 84041 and two comparison stars, $C1$ = HD 83994 (F3/5V, m_{pg} = 8.2 (Houk 1982)) and $C2$ = HD 83547 (A0V, m_{pg} = 8.5 (Houk 1982)) were observed in the Johnson $UBVRI$ system.

The observing sequence used was $C1,C2,V,V,C2,C1$ where V denotes HD 84041. For the comparison stars, we used 40-s integrations for each of the $UBVRI$ filters followed by a sequence of 10-s integrations on the sky through the same filters. For the fainter HD 84041, we used 60-s integrations per filter for star and 10-s integrations per filter for sky. As each $UBVRI$ filter sequence of HD 84041 took just under 6 min, two consecutive observations of HD 84041 were made in an attempt to average out the 15-min oscillations which can have a peak-to-peak B amplitude as much as 6 mmag at times. While this procedure did not entirely remove the effect of the rapid oscillations, it did reduce that effect.

Apertures of 30 arcsec or larger were used to avoid light losses due to telescope tracking errors and seeing fluctuations. The observations were placed on the standard system using E-region standards and were corrected for coincidence counting losses, sky background and extinction.

The comparison star observations were first checked for variability by plotting the differential $UBVRI$ magnitudes $C1$-$C2$. This also allowed us to identify any isolated bad points in either of the comparison star data before they were used to compute differential magnitudes of HD 84041. Our observational errors determined from the differential magnitudes of the two comparison stars, $C1$-$C2$, are: σ_U = 0.003, σ_B = 0.003, σ_V = 0.003, σ_R = 0.003, σ_I = 0.004.

Table 6.2 gives the differential $UBVRI$ magnitudes calculated by averaging the two HD 84041 observations and subtracting the time-interpolated average of comparison star $C2$. We chose to work with the differential magnitudes HD 84041 - $C2$ because they gave the best signal-to-noise. We also formed differential magnitudes HD 84041 - $C1$ and HD 84041 - $[(C1 + C2)/2]$ and we found that these differential magnitudes gave amplitude spectra with higher noise levels.

Table 6.2

Differential mean *UBVRI* observations of HD 84041.

HJD	ΔU	ΔB	ΔV	ΔR	ΔI
2448657.52409	1.108	1.005	0.756	0.633	0.522
2448659.48083	1.109	1.017	0.753	0.629	0.522
2448660.53703	1.125	1.022	0.755	0.636	0.525
2448662.51547	1.132	1.020	0.747	0.619	0.507
2448663.46895	1.107	1.013	0.760	0.637	0.529
2448665.52291	1.128	1.024	0.758	0.624	0.512
2448666.54799	1.120	1.019	0.747	0.620	0.514
2448667.52895	1.117	1.017	0.763	0.641	0.532
2448668.48041	1.109	1.010	0.757	0.632	0.527
2448670.48910	1.108	1.013	0.746	0.624	0.512
2448674.52395	1.112	1.013	0.757	0.635	0.520
2448681.39587	1.120	1.013	0.750	0.625	0.511
2448682.44096	1.122	1.022	0.763	0.640	0.531
2448684.45010	1.142	1.030	0.749	0.617	0.508
2448701.43558	1.119	1.014	0.754	0.630	0.515
2448702.41093	1.122	1.018	0.754	0.630	0.521
2448703.46550	1.127	1.016	0.747	0.617	0.506
2448704.39835	1.109	1.017	0.762	0.640	0.528
2448705.34392	1.109	1.008	0.755	0.631	0.524
2448706.39462	1.137	1.031	0.756	0.625	0.520
2448709.40048	1.114	1.011	0.754	0.635	0.525
2448714.44207	1.131	1.018	0.749	0.619	0.511
2448715.41802	1.110	1.017	0.763	0.641	0.530
2448716.43572	1.119	1.007	0.756	0.633	0.525
2448717.41948	1.135	1.022	0.761	0.633	0.524
2448719.43727	1.131	1.019	0.765	0.642	0.536

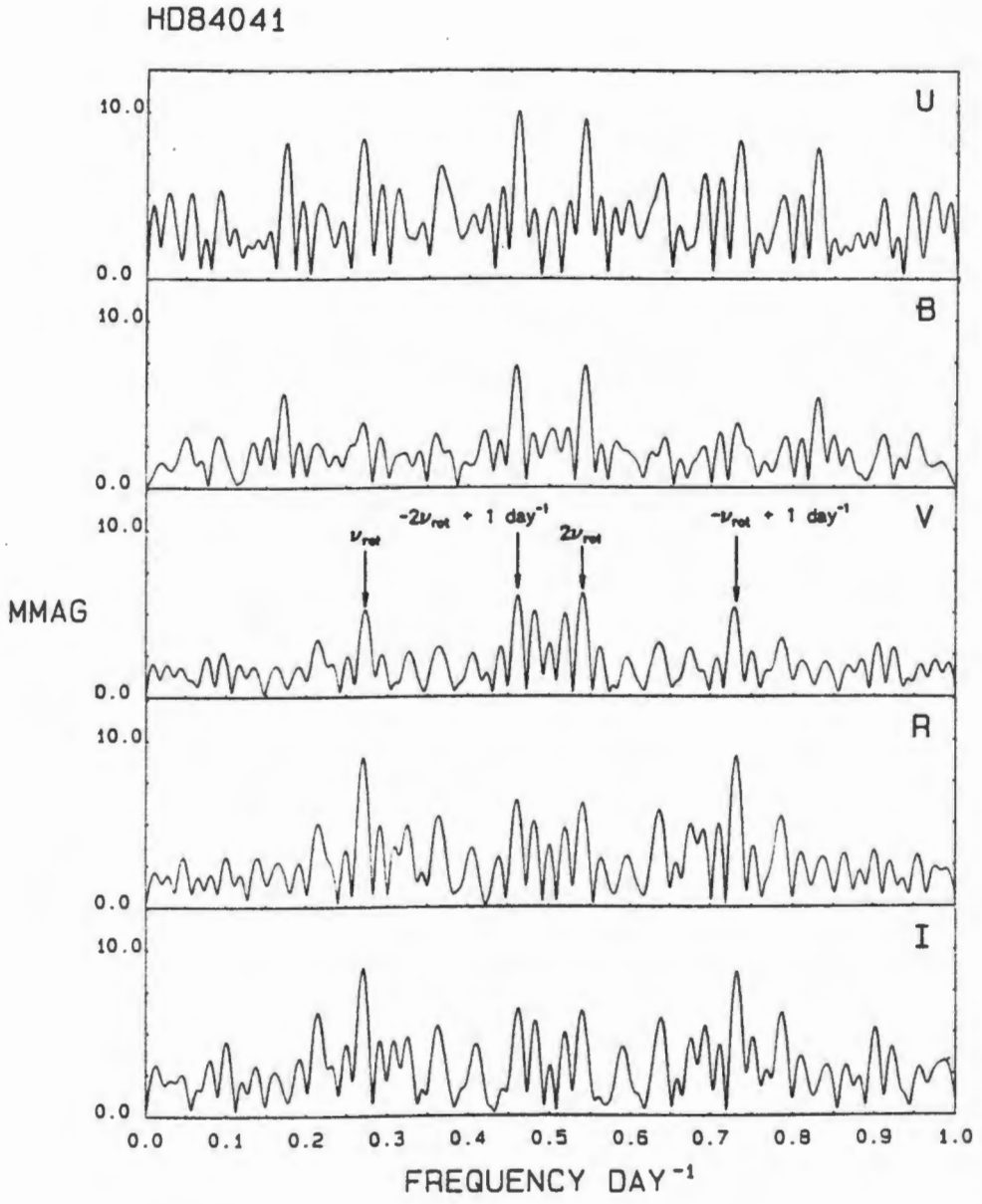

Figure 6.1 Amplitude spectra of the *UBVRI* differential photometry listed in Table 6.2. This Figure illustrates how the problem of aliases is exacerbated at frequencies close to zero where positive aliases of the negative frequencies spill over into the positive frequency domain to produce higher apparent noise levels; the real noise levels in this Figure can be gauged from Fig. 6.2. The peaks of interest are the rotation frequency, ν_{rot}, and its harmonic, $2\nu_{rot}$. Also labeled are the $+1\ day^{-1}$ aliases of the negative counterparts of these peaks.

6.4 The rotation period of HD 84041

The first step in our analysis was to determine the rotation period of HD 84041. Knowing the rotation period simplifies the analysis of the high-speed data because we can search for and identify rotation sidelobes in the amplitude spectrum of the oscillations. A frequency analysis of all available mean light observations was performed using a fast Discrete Fourier Transform algorithm (Kurtz 1985). Fig 6.1 shows the amplitude spectrum for each of the *UBVRI* pass-bands in the frequency range 0 to 1 day^{-1} for the SAAO data.

The Nyquist frequency for data consisting of one observation per night is 0.5 day^{-1}, so the reader may object to the display of frequency spectra up to 1 day^{-1}. We do this to illustrate our arguments below where we will demonstrate that the mean light oscillations at a frequency, ν_{rot}, below the Nyquist frequency produce amplitude at a frequency $2\nu_{rot}$ above the Nyquist frequency. This is because of the non-sinusoidal nature of the mean light variations which will become evident shortly. Consider the frequency range 0 - 0.5 day^{-1} in Fig. 6.1. In the *U*, *V*, *R* and *I* panels, the peak labeled ν_{rot} is at 0.270 day^{-1}. The *B* panel also has a peak at 0.270 day^{-1} although it is not as convincing as in the other panels. We note also the peak labeled $2\nu_{rot}$, at 0.540 day^{-1} = 2 × 0.270 day^{-1}, just above the Nyquist frequency. We will discuss the significance of this 1:2 ratio in the frequencies below.

To a reader unaccustomed to interpreting amplitude spectra at such low frequencies, Fig 6.1 might seem to be only an amplitude spectrum of noise: there might seem to be no compelling reason to select ν_{rot}, or any other frequency, as a possible real oscillation frequency. The key to the correct interpretation of Fig. 6.1 is to realize that amplitude spectra at frequencies close to zero are complicated by positive aliases of the negative counterpart of the spectrum spilling over into the frequency range of interest. This spill-over from negative frequencies results in asymmetrical window patterns and a great confusion of aliases in the amplitude spectrum. To demonstrate that the complexity of these amplitude spectra is produced by just the two frequencies, ν_{rot} and $2\nu_{rot}$, we optimized the amplitudes and phases of ν_{rot} and $2\nu_{rot}$ by using a linear least squares algorithm to fit a function of the form

$$\Delta F = A_0 + A_1 \cos(2\pi\nu_{rot}(t-t_0) + \phi_1) + A_2 \cos(4\pi\nu_{rot}(t-t_0) + \phi_2) \qquad (6.1)$$

to the data in Table 6.2 for each filter *F*. The amplitudes and phases thus determined were used as initial estimates for a non-linear least squares fit (in which the frequencies are also treated as variable) to the same function which yielded refined values of and uncertainties for ν_{rot} and $2\nu_{rot}$ as shown in Table 6.3. We then prewhitened sinusoids with the appropriate amplitudes and phases from

Table 6.3

A least-squares fit of ν_{rot} and $2\nu_{rot}$ to the mean light observations for each filter. The function fitted is $\Delta F = A_0 + A_1\cos(2\pi\nu_{rot}(t-t_0)+\phi_1) + A_2\cos(4\pi\nu_{rot}(t-t_0)+\phi_2)$ for each filter F and the phases are given relative to t_0 = HJD 2448662.16500. The column labeled σ gives the standard deviation per observation of the residuals on removing ν_{rot} and its harmonic from the data.

	ν day^{-1} (±0.001)	A_0 mag	A_1, A_2 mmag	ϕ radian	σ mmag
U	0.271	1.1207	8.4±1.1	-0.12±0.12	3.72
	0.542		11.8±1.1	-0.65±0.10	
B	0.271	1.0170	4.3±0.7	-0.58±0.16	2.47
	0.542		6.8±0.7	-0.19±0.12	
V	0.271	0.7554	4.7±0.7	2.58±0.14	2.33
	0.542		4.5±0.7	0.88±0.15	
R	0.271	0.6303	8.7±0.7	2.75±0.08	2.50
	0.542		5.0±0.8	1.25±0.14	
I	0.271	0.5207	8.5±1.2	2.66±0.14	4.15
	0.542		4.7±1.3	1.17±0.24	

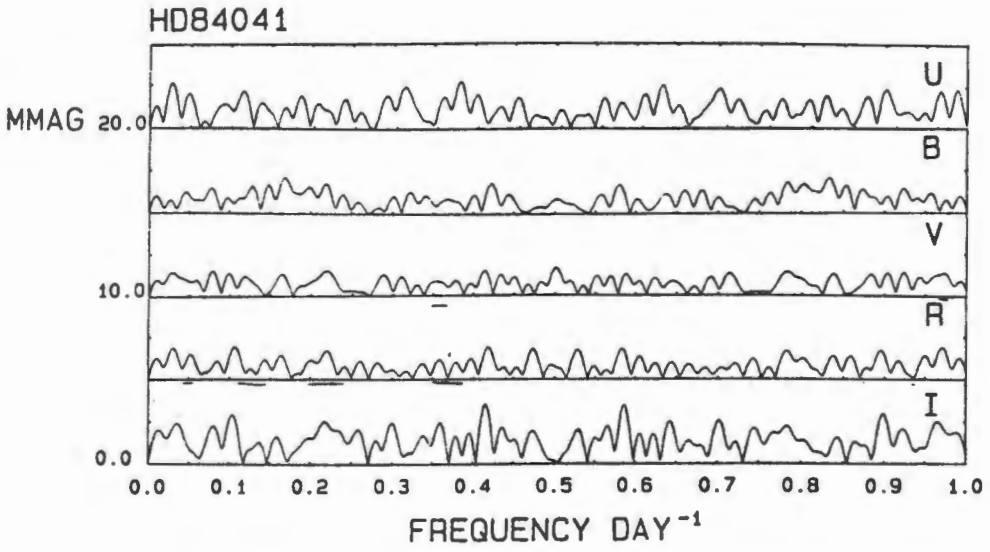

Figure 6.2 Amplitude spectra of the residuals on prewhitening ν_{rot} and $2\nu_{rot}$ from the data showing that the complexity in Fig. 6.1 was generated by just these two window patterns. The scale of the ordinates is the same for all five panels; each panel is 5 mmag high.

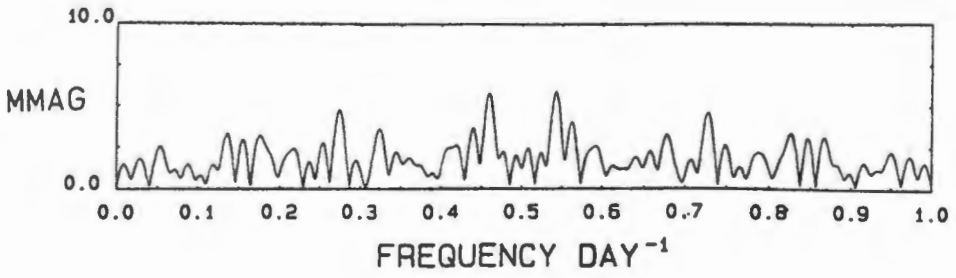

Figure 6.3 The amplitude spectrum of an artificial noise-free signal which is the sum of two pure sinusoids at frequencies ν_{rot} and $2\nu_{rot}$ sampled at the same times as the *B* mean light data in Table 6.2 and with *B* amplitudes as listed in Table 6.3. Note the striking resemblance of this amplitude spectrum to that shown in Fig. 6.1 for real data. This shows that the complexity of the amplitude spectra in Fig. 6.1 is governed by the superposition of the window patterns of ν_{rot} and its harmonic and is *not* noise.

each panel in Fig. 6.1 to produce the residuals shown in Fig. 6.2. These amplitude spectra are flat, indicating that ν_{rot} and $2\nu_{rot}$ are the only coherent oscillation frequencies in the data. Notice also that the standard deviations, σ, of the residuals (Table 6.3) are comparable to the errors found in the comparison star differential photometry (section 6.3), indicating that the two consecutive observations of HD 84041 averaged out the rapid oscillations and that there are no additional variations in these mean light observations.

For completeness, we demonstrate that the complexity of the amplitude spectra in Fig. 6.1 is indeed caused by the window patterns of the rotation frequency and its harmonic. Fig. 6.3 is the amplitude spectrum of the sum of two noise free sinusoids, ν_{rot} and $2\nu_{rot}$, sampled at the same times as the B data in Table 6.2, with amplitudes and phases as given in Table 6.3. The resemblance of Fig. 6.3 to Fig. 6.1 is excellent.

The other prominent peaks at 0.730 day^{-1} and 0.460 day^{-1} in Fig. 6.1 may be identified as +1 day^{-1} aliases of the negative counterparts of ν_{rot} and $2\nu_{rot}$, respectively. The peak at 0.171 day^{-1} in the U and B panels in Fig. 6.1 disappears when these panels are prewhitened by ν_{rot} and $2\nu_{rot}$. Examination of Fig. 6.3 shows that a peak also exists at 0.17 day^{-1} for the noise-free test signal. We thus dismiss the 0.17 day^{-1} peak as spurious; it is a feature in the spectral window of these data which has been enhanced by noise.

The presence of two peaks of unequal height in a 1:2 frequency ratio in the amplitude spectra is caused by a double-wave light curve with dips of unequal depth. Assuming a centered dipole magnetic geometry, such a light curve arises if we see both magnetic poles, but one at more favourable aspect than the other. We then expect to see amplitude at $2\nu_{rot}$ as well as ν_{rot} in the amplitude spectra as is the case in Fig. 6.1. We can show that HD 84041 has a double-wave light curve by plotting all the $UBVRI$ observations on a phase diagram. Fig. 6.4 is such a phase diagram showing the excellent fit of the frequencies ν_{rot} and $2\nu_{rot}$ to the data. Assuming that HD 84041 has a centered dipole magnetic field and that the abundance distribution is symmetrical about the magnetic poles, this light curve implies that neither the rotational inclination i, nor the magnetic obliquity β are near 90°. Fig. 6.4 also shows that there is a phase shift with filter but no π-radian phase reversal from U to I as is seen in many other Ap stars (Molnar 1973).

The ephemeris for the mean B light variations is

$$HJD(\text{mean } B \text{ minimum}) = \begin{matrix} 2448662.17 & + 3.69\,E \\ \pm 0.09 & \pm 0.01 \end{matrix} \qquad (6.2)$$

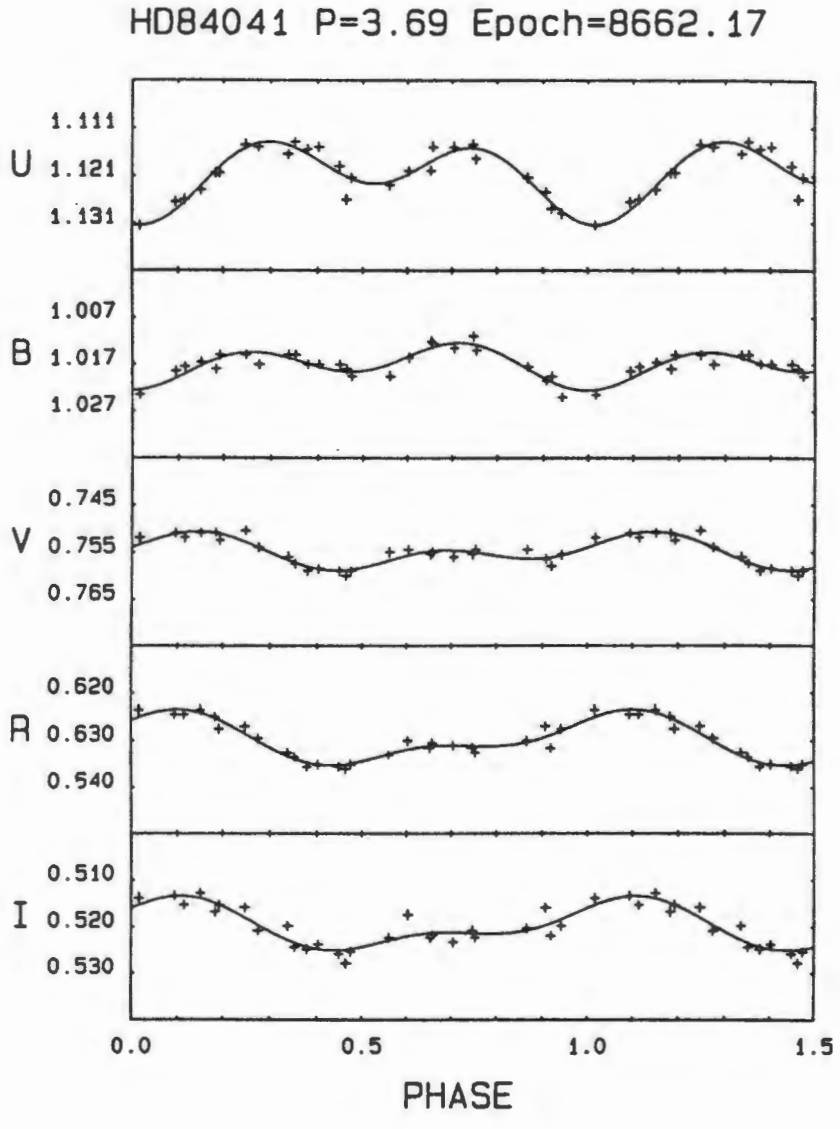

Figure 6.4 A phase diagram of the *UBVRI* data presented in Table 6.2 showing a double wave and the excellent fit of the 3.69-day rotation period to the data. Notice the phase shift with filter from *U* to *I*.

The 3.69-day rotation period of HD 84041 should give rise to $2\ell+1$ frequencies separated by 3.137 μHz in the amplitude spectrum of the high-speed photometry for each pulsation mode of spherical degree ℓ. We will discuss searches for these rotational sidelobes in section 6.5.

6.5 Frequency analysis of the high-speed photometry

The data were analyzed in individual nights, in groups of closely spaced nights, and as a whole. In what follows, we will discuss only the subset of analyses that contributed most to our understanding of the oscillations in HD 84041.

The first step in our frequency analysis was to compute the amplitude spectrum for each night of data. Fig. 6.5 shows the light curve obtained at the SAAO on night HJD 2448653, a good, but not outstanding, night at Sutherland. This Figure demonstrates that HD 84041 is a rapidly oscillating Ap star with an oscillation period near 15 min and an oscillation amplitude that is modulated over a time-scale of a few hours. Fig. 6.6 shows the amplitude spectrum of this light curve out to the Nyquist frequency. Note that but for the enhanced amplitude in the vicinity of ν_1 = 1.12 mHz, the amplitude spectrum is flat. As this is also the case in all the other nightly amplitude spectra, further analyses concentrated on the frequencies in the vicinity of ν_1. If we remove ν_1 from the data, we are left with the lower panel in Fig. 6.6 which shows residual amplitude at ν_2 = 1.08 mHz. These two frequencies were least-squares-fitted to the data to produce the solid line in Fig. 6.5.

The next step in the frequency analysis was to analyze the 1992 data as a whole to refine the value of ν_1 and to identify the frequencies causing the observed amplitude modulation. Fig. 6.7 shows the amplitude spectrum for the HJD 2448651-8676 SAAO data from 0.9 mHz to 1.3 mHz. The broad mound of amplitude in Fig. 6.7 implies that neither of these objectives can be achieved so straightforwardly. The much sparser 1991 data have a similar amplitude spectrum when analyzed as a whole. Indeed, that amplitude spectrum was one of the principal motivations for the 1992 campaign.

We then analyzed short sections of the data with high duty cycle. The multi-site HJD 2448652-8653 data span 34.35 hr and have a 60 % duty cycle. Fig. 6.8 is the amplitude spectrum of these data for the frequency range 0.9-1.3 mHz where the choice of ν_1 = 1.113 mHz is unambiguous. On prewhitening* ν_1 from these data, we are left with the amplitude spectrum of the residuals shown in Fig. 6.9 where there is a clear indication of further frequencies but the complexity of the spectrum

---

* In this chapter we use the term prewhitening to mean that each time we remove a frequency, we optimize its amplitude and phase using linear least squares, subtract from the data a cosinusoid with the appropriate frequency, amplitude and phase and then recompute the amplitude spectrum of the residuals, which is searched for further peaks.

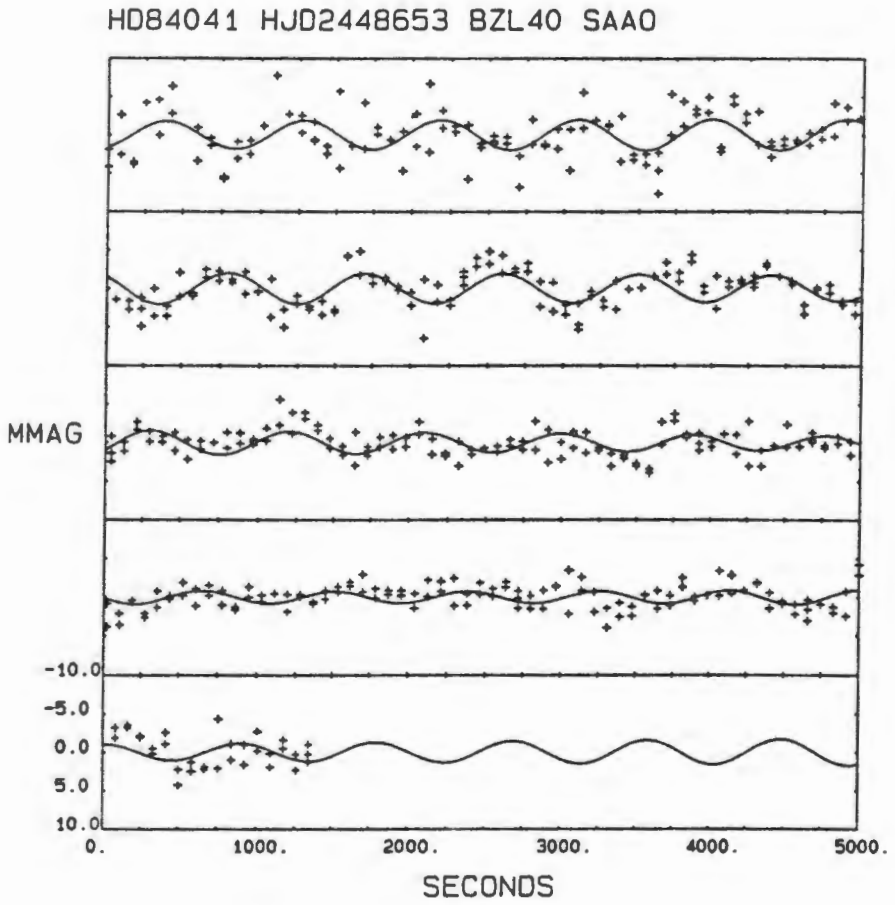

Figure 6.5 The light curve of the Johnson *B* high-speed observations acquired over 6 hr on night HJD 2448653 at the SAAO. Notice the modulation of the pulsation amplitude during the course of the run. The solid line is a least squares fit of the two frequencies beating to produce this modulation. Consult Fig. 6.6 for more details.

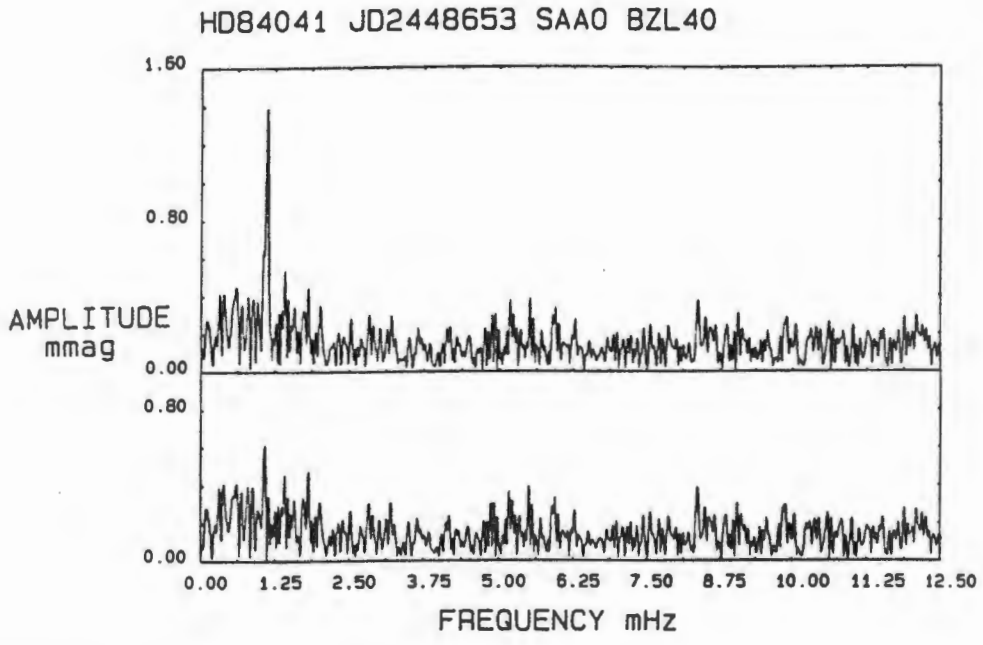

Figure 6.6 The amplitude spectrum of the light curve in Fig. 6.5. The prominent peak in the top panel lies at ν_1 = 1.12 mHz. If we remove a sinusoid of frequency ν_1, we are left with the amplitude spectrum shown in the lower panel which indicates a second frequency at ν_2 = 1.08 mHz. These two frequencies were fitted by least squares to the data to produce the solid line in Fig. 6.5.

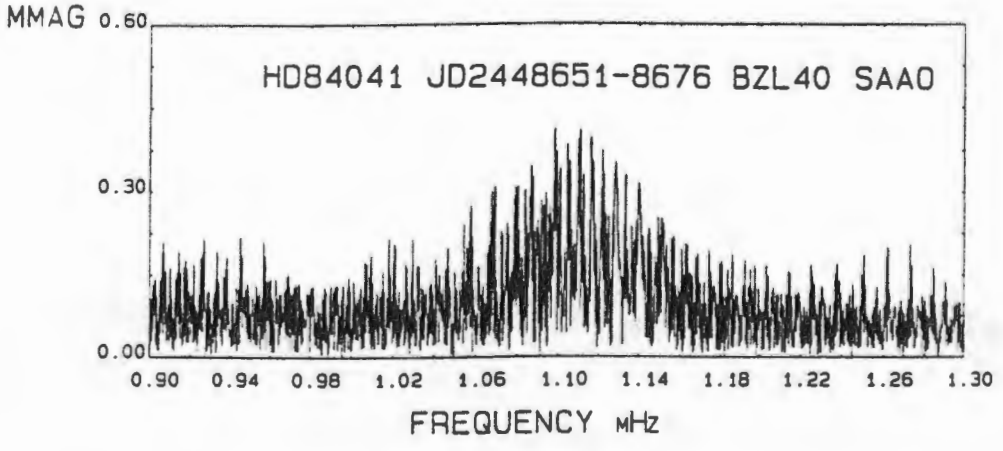

Figure 6.7 The amplitude spectrum of the HJD 2448651-8676 SAAO observations. The broad mound of amplitude suggests that the oscillations shown in Fig. 6.6 do not maintain phase coherence on time-scales comparable to the length of this data set.

does not yield unambiguous choices for those frequencies. We emphasize that the tallest peak in Fig. 6.9 is not necessarily the correct choice for the next frequency since the differences in amplitude among the peaks are smaller than the noise level in this Figure. To discriminate among the possible choices, we must examine stretches of multi-site data which are relatively free of daily alias ambiguities.

On night HJD 2448653, the SAAO and the CTIO observations overlapped to form a continuous 13-hr record of the *B* brightness variations in HD 84041 with no aliasing problems; the principal sidelobes of the sinc function for these data are only 20 per cent of the height of the central peak in the spectral window. To reduce the alias ambiguities in Fig. 6.9, we analyzed just the HJD 2448653 multi-site data alone. In Fig 6.10 we show the amplitude spectrum of the HJD 2448653 SAAO + CTIO data in the same frequency range as in Fig. 6.9. The feature of interest is the triplet of peaks at 1.085 mHz, 1.112 mHz and 1.141 mHz. The peak at ν = 1.112 mHz in Fig. 6.10 corresponds to ν_1 in Fig. 6.8. The peaks at ν_2 = 1.085 mHz and ν_3 = 1.141 mHz are separated from ν_1 and ν_2 by 27 μHz and 29 μHz, respectively. These separations are an order of magnitude more than the expected 3.137-μHz rotational sidelobes of ν_1 (which are not resolved in this data set), but they are consistent with the expected asymptotic *p*-mode spacing of alternating even and odd ℓ modes.

We then used these tentative identifications of ν_2 and ν_3 to resume our analysis of the HJD 2448652-8653 data. Panels (a) and (b) in Fig. 6.11 show the amplitude spectra of the residuals on prewhitening the amplitude spectrum in Fig. 6.9 by ν_2 = 1.085 mHz and ν_3 = 1.145 mHz, respectively. The tallest peak in panel (b) lies at ν_4 = 1.119 mHz, very close to ν_1 = 1.113 mHz. Panel (c), which results when the data are prewhitened by the tentative ν_4, shows no further amplitude. The optimized amplitudes and phases of ν_1, ν_2, ν_3 and ν_4 are shown in Table 6.4. We caution that these frequencies form a credible frequency solution *for this data set*, but they are not a unique general solution. Most other subsets of our data have such complex amplitude spectra that it is not possible to perform convincing frequency analyses. The results of those analyses depend on the frequencies selected and are hence uncertain.

The rotation period of HD 84041 has been determined to be P_{rot} = 3.69±0.01 day. If part of the amplitude modulation of ν_1 is the rotational amplitude modulation of an oblique pulsator, we expect to see the $2\ell+1$ frequency multiplets with spacing ν_{rot} as predicted by the oblique pulsator model. For a dipole mode, we would expect rotation side-lobes separated by 3.137 μHz on either side of ν_1, which we do not see in our results. However, this expectation is based on the assumption that ν_1

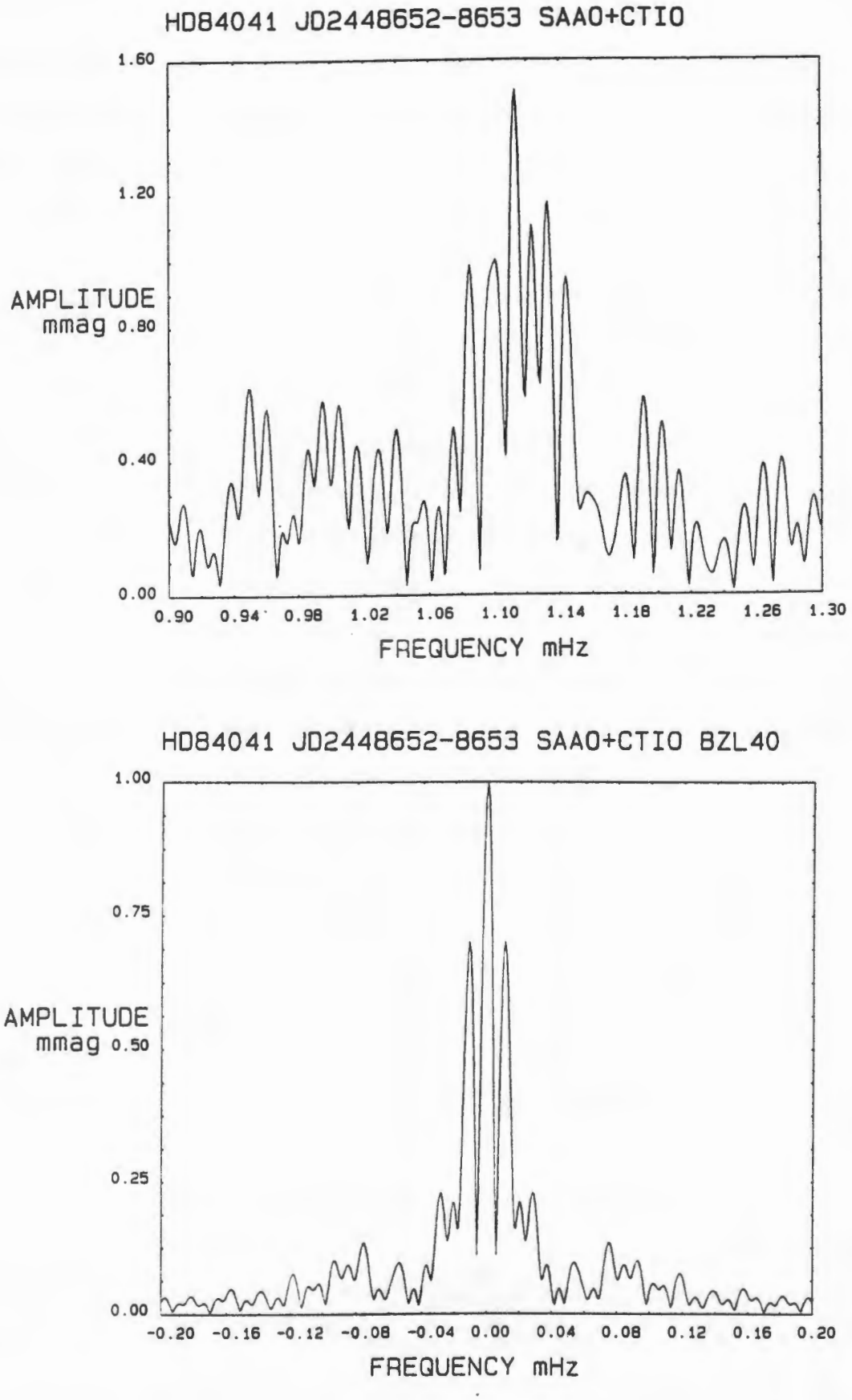

Figure 6.8 (top). The amplitude spectrum of the HJD 2448652-8653 contemporaneous SAAO and CTIO data. The prominent peak is at ν_1 = 1.113 mHz. **(bottom)** The spectral window of these data.

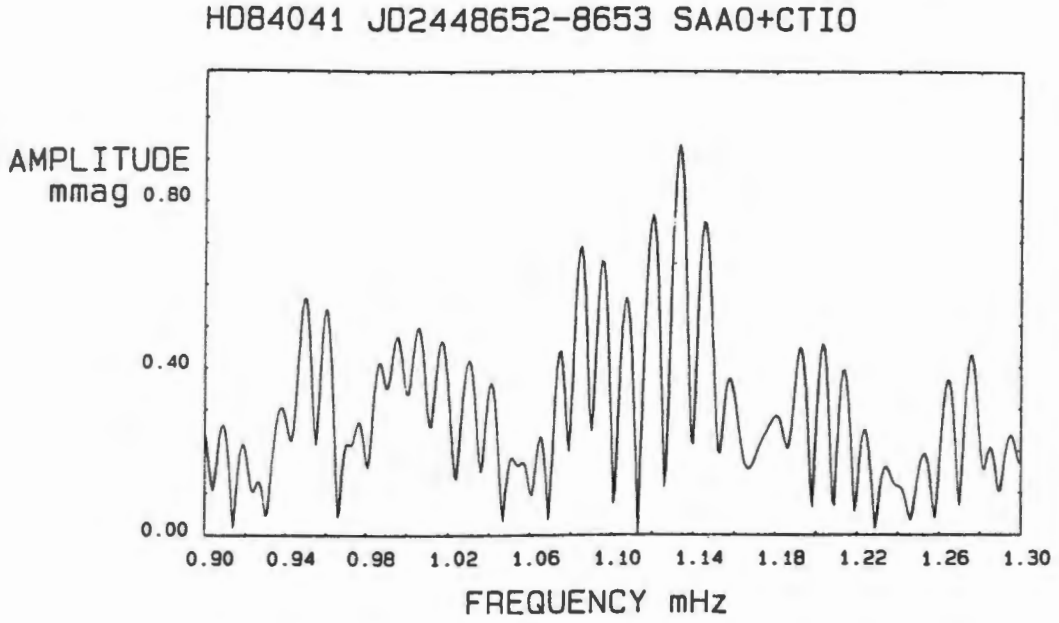

Figure 6.9 The amplitude spectrum of the residuals on prewhitening ν_1 from the HJD 2448652-8653 data. There is an indication of further frequencies here, but the correct choice of peak is not clear because the differences in height among the peaks are all less than the level of the noise.

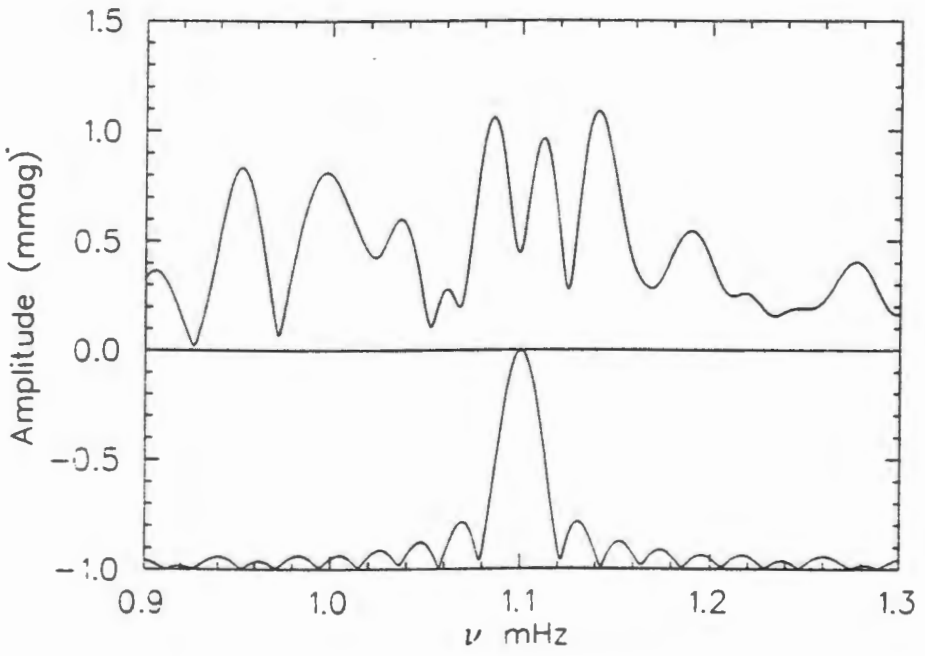

Figure 6.10 The amplitude of the continuous 13-hr *B* light curve acquired from SAAO and CTIO on night HJD 2448653. The SAAO portion of this light curve is shown in Fig. 6.5 and its amplitude spectrum is shown in Fig. 6.6. The feature of interest here is the triplet of peaks centered on 1.1 mHz. The spectral window of these data is plotted below the frequency axis for comparison and shows that the left and right peaks of the triplet are not principal sidelobes of the sinc function of ν_1.

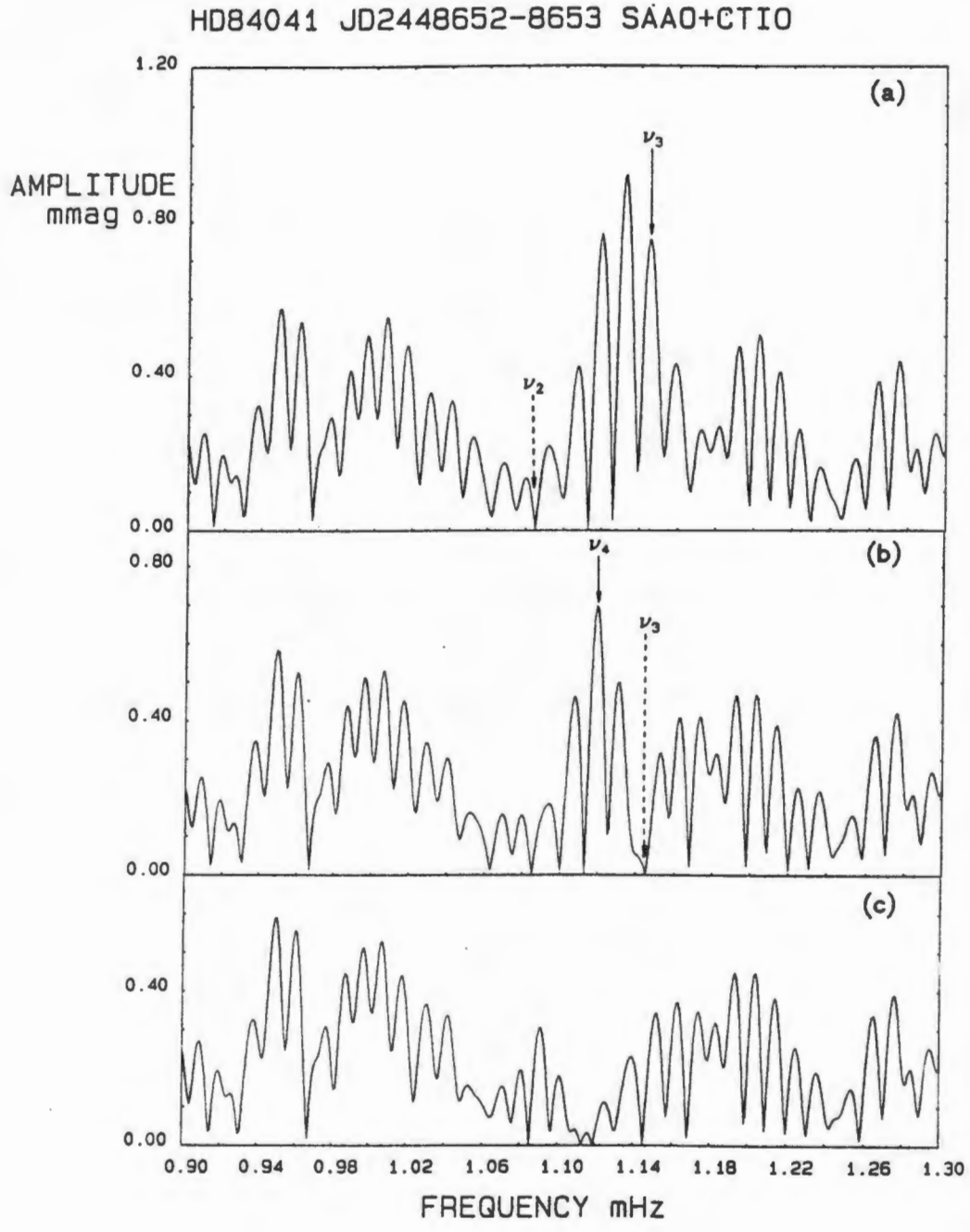

Figure 6.11 The amplitude spectra of the HJD 2448652-8653 SAAO + CTIO data for the residuals at successive stages of prewhitening following on from Fig. 6.9. Our selection of prewhitening frequencies is motivated by the alias-free HJD 2448653 SAAO + CTIO data (consult Fig. 6.10 and the text). In panel (a) we have prewhitened by ν_2 = 1.085 mHz (stippled arrow) and ν_3 = 1.145 mHz is indicated by the solid arrow. In panel (b) we have prewhitened by ν_3 = 1.145 mHz (stippled arrow) and the tallest peak remaining is at ν_4 = 1.119 mHz (solid arrow). Panel (c) shows the residuals on prewhitening by ν_4.

Table 6.4

A linear least squares fit (top) of the form $\Delta B = \Sigma A_i \cos(2\pi\nu_i(t-t_0)+\phi_i)$ to the HJD 2448652-8653 data with $t_0 = HJD\ 2448662.16500$. This fit assumes that the frequencies are perfectly determined and varies the amplitudes and phases to minimize the residuals. The results of this fit were used as the initial values for a non-linear least squares fit (bottom) of the same form. The non-linear fit varies the frequency, amplitude and phase to minimize the residuals and yields an uncertainty for the frequency. Notice how the uncertainties of the phases in the non-linear fit are large indicating either poor phase coherence or unresolved nearby frequencies. These frequencies are *not* a definitive frequency solution for the oscillations in HD 84041 and should not be used without reference to the text.

	ν mHz	A mmag	ϕ radian
ν_1	1.113	1.37±0.13	-3.11±0.10
ν_2	1.085	0.74±0.13	2.79±0.18
ν_3	1.145	0.74±0.13	-1.12±0.18
ν_4	1.119	0.74±0.13	3.11±0.18

	ν mHz	A mmag	ϕ radian
ν_1	1.1137±0.0009	1.37±0.18	0.20±4.35
ν_2	1.0842±0.0006	0.80±0.14	-1.14±3.12
ν_3	1.1468±0.0007	0.78±0.15	1.28±3.20
ν_4	1.1199±0.0015	0.95±0.18	1.35±7.01

is the principal oscillation frequency, and not one of its rotational sidelobes. Note from Table 6.4 that $\nu_4 - \nu_1 = 2\nu_{rot} = 2\times3.1\ \mu$Hz. A possible interpretation of this is that ν_1 is not the principal oscillation frequency, but rather $\nu' = (\nu_1+\nu_4)/2 = 1.1168$ mHz. The amplitude of ν' must then be so low that it is not detectable in these data. Such asymmetric frequency multiplets arise naturally in oblique pulsator models that incorporate the effects of Coriolis and Lorentz forces on the oscillations. An example of a roAp star with a depressed central frequency component is HR 3831. The reader will find it instructive to examine the schematic amplitude spectrum of that star in our atlas of roAp star oscillation spectra (Fig. 9.1). Clearly, further observations are required to test the hypothesis that ν' is the principal oscillation frequency in HD 84041.

6.6 Discussion of the results of the frequency analysis

The frequency analysis of the 1992 multi-site data produces a hump of amplitude as shown in Fig. 6.7; this is an unexpected result. There are several possible causes for this hump. One possibility is that there is a clock error in the data which destroys the phase coherence of the signal. However, we can exclude this possibility as great care was taken by the observers to ensure the correctness of the recorded times. Most weekly, or longer, subsets of the data suffer from the same problem, regardless of whether they are drawn from either the CTIO data alone, or the SAAO data alone, or both data sets combined. The hump of amplitude suggests that the oscillations do not maintain phase coherence on the time-scale of the entire data set. If so, the width of the hump is a measure of the coherence time-scale. However, the hump may also result from the sparse sampling of low signal-to-noise data. Further long, uninterrupted observations of good signal-to-noise from at least two sites are required to distinguish between these two possibilities. That the amplitude of the light variations is modulated is certain. However, the frequencies causing this modulation are not certain. We stress that the identifications of ν_1, ν_2 and ν_3 are *not* secure and require confirmation. One other possibility is that the modulation is an intrinsic modulation of the pulsation modes themselves. An observational test of this will be difficult, requiring very high duty-cycle observations for extended periods.

The oscillatory behaviour seen in HD 84041 is reminiscent of HD 60435, which has the richest p-mode spectrum of all the roAp stars. The rapid variability of that star suffers apparently stochastic amplitude and/or phase modulation on time-scales of a few days; this behaviour is well documented as a result of two multi-site campaigns (Matthews *et al.* 1986, 1987). HD 60435 oscillates with possibly up to 30 frequencies which lie in a pattern of roughly equal spacing of 26 μHz. These

frequencies are interpreted as a series of p-modes of alternating even and odd degree (ℓ = 1 and 2) with high radial overtones ($13 \leq \nu \leq 28$). Since the spacing of consecutive overtones is twice the spacing of alternating even and odd ℓ modes, the asymptotic p-mode spacing in HD 60435 is $\Delta\nu = 2 \times 26\,\mu$Hz, a spacing consistent with theoretical expectations for a slightly evolved A star (Gabriel *et al.* 1985, Shibahashi & Saio 1985). In HD 84041, the frequencies ν_1, ν_2 and ν_3 are separated equally by roughly 31 μHz (Table 6.4, bottom). If we take this as a measurement of the asymptotic p-mode spacing of alternating even and odd ℓ modes, then $\Delta\nu \approx 2 \times 31\,\mu\text{Hz} = 62\,\mu$Hz for HD 84041. This again is consistent with theoretical expectations for a slightly evolved A star. We stress that these frequency identifications are tentative and require confirmation.

In the oblique pulsator model, the pulsation axis coincides with the magnetic axis, which is inclined to the rotation axis. At, or near, the magnetic poles, there are spots or rings of enhanced rare earth abundance which give rise to mean brightness variations as the star rotates. Thus, times of quadrature (magnetic cross-over) should correspond to times of pulsation amplitude minima. Assuming dark photospheric patches are associated with the magnetic poles, as in most Ap stars (Matthews 1987), times of minimum brightness are times of magnetic extrema. Since HD 84041 has a double-wave light curve, the secondary brightness minimum should coincide with the secondary magnetic extremum and hence also secondary oscillation amplitude maximum. The real picture is probably not so simple, however. For HR 3831 Kurtz *et al.* (1992) have shown that while the times of magnetic and pulsation extrema coincide, there is a 25-s lag in the time of mean-light extremum. This argues that HR 3831 is an oblique pulsator with the pulsation and magnetic axes coincident and indicates a deviation from cylindrical symmetry which complicates the interpretation of pulsation amplitude modulation in terms of the oblique pulsator model.

Fig. 6.12 is a plot of the oscillation amplitude of HD 84041 as a function of rotation phase to permit a direct comparison of the phase difference between the mean B light curve and the B amplitude behaviour of the rapid oscillations. The scatter in Fig. 6.12 is too high to draw any conclusions regarding the relative phasing between the mean light curve and the amplitude modulation curve. According to the oblique pulsator model, for simple dipole modes, the pulsation amplitude goes to zero at quadrature. In Fig. 6.12, phases such as 0.25 and 0.75 have low oscillation amplitudes which are in some cases consistent with zero amplitude within the errors. The apparent complexity of the amplitude behaviour may be caused by the beating of several oscillations (not all pure dipole modes) which masks the systematic oscillation amplitude trends predicted for a simple

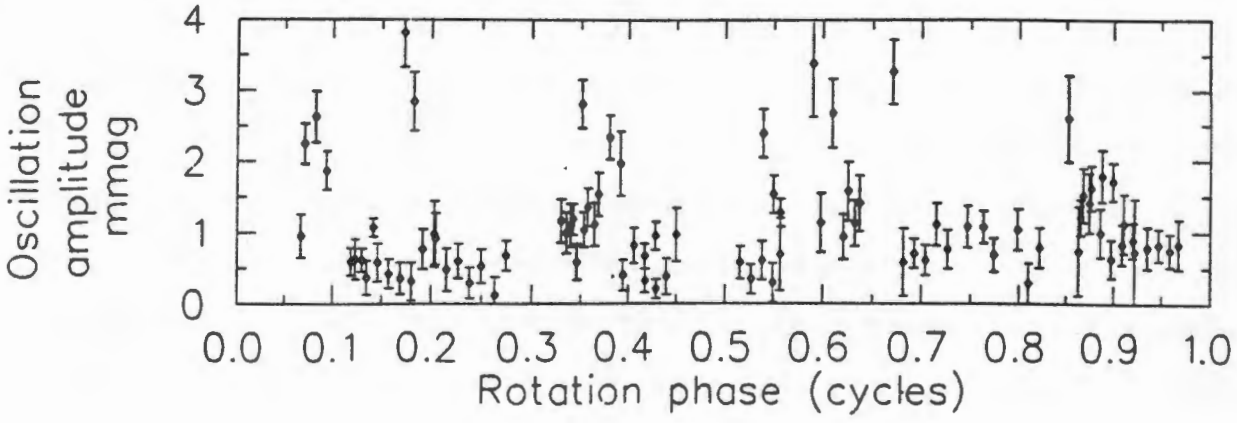

Figure 6.12 A plot of the oscillation amplitude of ν_1 as a function of rotation phase computed for 1-hr segments of data. Note that the amplitude is down at two phases, here 0.25 and 0.75, in accordance with expectations from the oblique pulsator model. The high scatter is caused by the beating of many modes masking the underlying oblique pulsator effect.

dipole. The oblique pulsator model also predicts that the oscillation phase will undergo π-radian phase reversals at quadrature. A plot of oscillation phase as a function of rotation phase (not shown) does not show these phase reversals; of present, they are masked by the beating of several frequencies.

We end this discussion with a cautionary note. The study of chaos in physical systems is topical at present and, not surprisingly, since many variable stars exhibit irregular variability, attempts at applying chaos theory to variable star data have been made (e.g. see Auvergne & Baglin (1986) and references therein). For many roAp stars, a complete description of the oscillations does not seem to be possible. Frequency solutions obtained for well-sampled data sets have little or no predictive power - sometimes even from night to night. Examples of such stars are HD 60435 (Matthews *et al.* 1987), HD 119027 (Ch. 7, this thesis), HD 134214 (Kurtz *et al.* 1991), HD 203932 (Martinez *et al.* 1990), HD 217522 (Kreidl *et al.* 1991) and HD 84041. While it may be tempting to invoke chaos to "explain" the highly complex character of pulsations in these roAp stars, it should be remembered that at the signal-to-noise levels obtaining in the roAp stars it is not possible to separate chaotic effects from noise or other forms of non-periodic variations (Auvergne & Baglin 1986). Kreidl (1992) has searched for evidence of chaos in roAp star photometry, but his results are inconclusive, largely because of the very low amplitudes of roAp pulsations. Recent work by Kurtz (in preparation) suggests that invocations of chaos to explain the non-stationary behaviour of roAp oscillations are at present premature. Kurtz has followed the non-stationary phase behaviour of HR 3831 on as many nights as possible for the past two observing seasons and he finds evidence for a periodic phase variation in the oscillations. This finding is discussed in more detail in section 9.5.

6.7 Conclusion

We have presented high-speed Johnson *B* photometric observations and mean light *UBVRI* observations of the Cape Survey Ap star HD 84041 which allow us to conclude the following:

1) HD 84041 is a rapidly oscillating Ap star oscillating with probably at least three *p*-modes in the vicinity of 1.1 mHz
2) HD 84041 exhibits mean light variations of a double-wave nature indicating that both magnetic poles are being seen and that neither the rotational inclination i, nor the magnetic obliquity β are near 90°.

3) The rotation period of HD 84041 as determined from its mean light variations is P_{rot} = 3.69±0.01 day.

4) The amplitude of the rapid oscillations is modulated in a complex way, often on a time-scale shorter than can be accounted for by rotational amplitude modulation. Certainly, part of the modulation can be accounted for by beating of multiple frequencies. There is evidence for at least two other frequencies in the region of ν_1 but we cannot identify these frequencies with confidence.

5) Although the rotation period of HD 84041 has been established in this work, the rotational frequency splitting expected in the amplitude spectrum of the rapid oscillations has not been found. We note, however, that ν_1 and ν_4 are separated by twice the rotation frequency. This leads us to speculate the perhaps the principal oscillation frequency is not ν_1, but rather $(\nu_1+\nu_4)/2$ = 1.1168 mHz. A knowledge of all the components of the rotationally split multiplet would allow an application of the oblique pulsator model. We do not engage in a speculative application of the model here, but instead point to the need for further observations to test this hypothesis.

6) In several roAp stars the harmonics of the principal oscillation frequencies are seen. In HR 3831 (Kurtz *et al.* 1992b), for example, the first, second and (probably) third harmonics are seen. A search for the first harmonic in HD 84041 yields a null result. (By way of clarification, in this thesis we use the term *harmonic*, to mean an integer multiple of the fundamental oscillation frequency, that is, simply a description of the non-sinusoidal pulse shape of the oscillations. This is not to be confused with different modes of pulsation of the stellar atmosphere which we refer to as *overtones*.)

The chief difficulty in observing *p*-modes in stars other than the Sun is their very small amplitude. Although tantalizing, the results presented here fall short of what is needed for a detailed understanding of the *p*-mode oscillations in HD 84041 and for the determination of the parameters of asteroseismological interest. Moreover, our observations suggest that the lifetimes of *p*-modes on HD 84041 may be shorter than the rotation time-scale; this has to be investigated.

A thorough multi-site study will be required to decipher the *p*-mode spectrum of this star. Multi-site observations are needed to reduce the confusing influence of the daily aliases and spurious

peaks produced by modes with short lifetimes. However, any future study will have to achieve a signal-to-noise at least as good as the best observations presented in this chapter. The CTIO data are a factor of 2 noisier than the SAAO data, partly because they were acquired on the smallest telescope used for the high-speed observations in the 1992 campaign. The scintillation noise can be reduced by using telescopes in the 1.0-m class, or larger. At 1.1 mHz, on a mediocre or poor night, the oscillations in this star are not in the frequency regime where the noise is dominated by scintillation; there is an appreciable sky transparency contribution to the noise. Future studies of this star will benefit by using two-channel observations to reduce the sky transparency component of the noise.

Chapter 7

The discovery and analysis of a rich *p*-mode oscillation spectrum in the Ap star HD 119027.

7.1 Introduction

In chapter 5 we described the discovery of rapid oscillations with a 9-min period in the southern Ap SrEu(Cr) star HD 119027. We also showed evidence for the modulation of the oscillation amplitude which indicates the presence of further frequencies. To search for and study these conjectured frequencies we monitored this star for a total of 106 hr on 22 nights during April - June 1991. The analysis of these observations forms the subject of the present chapter. Most of the observations presented in this chapter were acquired by my collaborators, Don Kurtz (University of Cape Town) and Pieter Meintjes (Potchefstroom University). As campaign coordinator, I reduced and analyzed all the observations. The material presented in this chapter has been published in the *Monthly Notices of the Royal Astronomical Society* (Martinez *et al.* 1993).

Before embarking on a full discussion of the frequency analysis, I will present an overview of the salient results of the campaign. To begin with, casual inspection of the amplitude spectra for individual nights indicates that HD 119027 shows unmistakable evidence of multiperiodicity. On some nights, as many as 4 oscillation modes were excited to observable amplitudes. Detailed frequency analyses reveal the presence of at least 5 oscillation frequencies in the region of 1.9 mHz with a roughly equal spacing of 26 μHz. However, the data cannot be adequately described with only these five frequencies. Further frequency components are required and those frequencies depend on the particular subset of data being analyzed. This indicates that some non-periodic amplitude or phase modulation of the basic pattern of 5 frequencies must be taking place. High-resolution determinations of the values of the 5 principal frequencies reveal that their spacings differ by formally significant amounts from the nominal 26 μHz spacing. Attempts to determine the rotation period of HD 119027 by searching for rotational amplitude modulation of the oscillations and mean light variations both yield null results. We also show that there is no evidence of the harmonics of the 9-min oscillations, thus indicating a sinusoidal pulse shape. We interpret the 5 equally spaced

frequencies as non-radial p-modes of high overtone ($n \approx 35$). We argue that the 26-μHz spacing indicates the presence of even and odd ℓ modes, but we are unable to obtain secure mode identifications with the data at hand.

7.2 High-speed photometric observations of HD 119027

High-speed photometric observations of HD 119027 were obtained on 22 nights in 1991 April-June using either the University of Cape Town Photometer or the St Andrews Photometer attached to the SAAO 0.75-m or 1.0-m telescope. The observing and reduction procedures employed for these observations have already been described in sections 5.3 and 5.7, respectively, so we will not describe them here. A journal of the observations is given in Table 7.1 which lists the Julian Date at the start and end of the observations, the duration of the observations in hours, the number of 40-s integrations, the standard deviation, σ, of one observation with respect to the mean for the night, the duty cycle, or 'filling factor', of the string of data and the observer/telescope/photometer combination. The quantity σ includes noise arising from scintillation, sky transparency variations, photon statistics and, of course, the actual oscillations in HD 119027 itself. A typical light curve is shown in Fig 7.1 where we draw attention to the amplitude modulation visible on a time-scale of hours. This amplitude modulation is produced by the beating of at least three frequencies, as we will show in section 7.4.

7.3 Frequency Analysis

The data were analyzed in individual nights, in groups of closely spaced nights, and as a whole. Amplitude spectra were computed using Deeming's (1975) Discrete Fourier Transform (DFT) algorithm with the modification suggested by Kurtz (1985). The subtraction of frequencies was performed in Fourier space using the technique of Gray & Desikachary (1973). This technique requires the computation of the DFT and the spectral window only once. To subtract a frequency from the data, we optimise that frequency's amplitude and phase by fitting it to the data by linear least squares. The spectral window is then scaled to this optimized amplitude and subtracted from the amplitude spectrum in Fourier space. The residuals are then examined and any further frequencies identified are subtracted in the same manner, one at a time. This results in a substantial saving in computing time because we do not have to recompute the Fourier transform of the data every time we

Table 7.1

Journal of 1991 observations of HD 119027.

Date 1991	JD start 2440000+	JD end 2440000+	t (hr)	N_{40}	σ (mmag)	duty cycle	Obs/Tel/Phot
Apr 30/ 1	8377.33875	8377.54847	5.03	445	2.10	0.98	DWK/1.0-m/UCTP
May 1/ 2	8378.38943	8378.46496	1.81	161	1.36	0.99	"
May 2/ 3	8379.37450	8379.55621	4.36	378	1.95	0.96	"
May 3/ 4	8380.40677	8380.45724	1.21	108	1.12	0.99	"
May 25/26	8402.31931	8402.53283	5.12	443	2.44	0.96	DWK/1.0-m/StAP
May 26/27	8403.21163	8403.55119	8.15	710	1.83	0.97	"
May 27/28	8404.20301	8404.52788	7.80	663	1.96	0.94	"
May 28/29	8405.21025	8405.54849	8.12	715	1.73	0.98	"
May 29/30	8406.20326	8406.53883	8.05	705	2.01	0.97	"
May 31/ 1	8408.20373	8408.53300	7.90	687	1.81	0.97	"
Jun 1/ 2	8409.20345	8409.53595	7.98	699	1.71	0.97	"
Jun 2/ 3	8410.20513	8410.51472	7.43	630	1.79	0.94	"
Jun 3/ 4	8411.20924	8411.24095	0.76	67	1.68	0.98	"
Jun 4/ 5	8412.22515	8412.38376	3.81	330	1.85	0.96	PJM/0.75-m/UCTP
Jun 5/ 6	8413.22397	8413.38657	3.90	341	3.04	0.97	"
Jun 10/11	8418.21749	8418.38560	4.03	334	1.88	0.92	"
Jun 11/12	8419.22395	8419.37765	3.69	325	2.32	0.98	"
Jun 12/13	8420.21736	8420.38558	4.04	337	1.95	0.93	"
Jun 14/15	8422.20745	8422.37497	4.02	346	2.39	0.96	"
Jun 19/20	8427.21546	8427.42950	5.14	426	1.85	0.92	PM/1.0-m/StAP
Jun 20/21	8428.22533	8428.28413	1.41	126	1.41	0.99	"
Jun 21/22	8429.19366	8429.28445	2.18	172	2.62	0.88	"
Σ			105.95	9148			

Notes:
DWK = Don Kurtz, PJM = Pieter Meintjes, PM = Peter Martinez
UCTP = University of Cape Town Photometer
StAP = St. Andrews Photometer

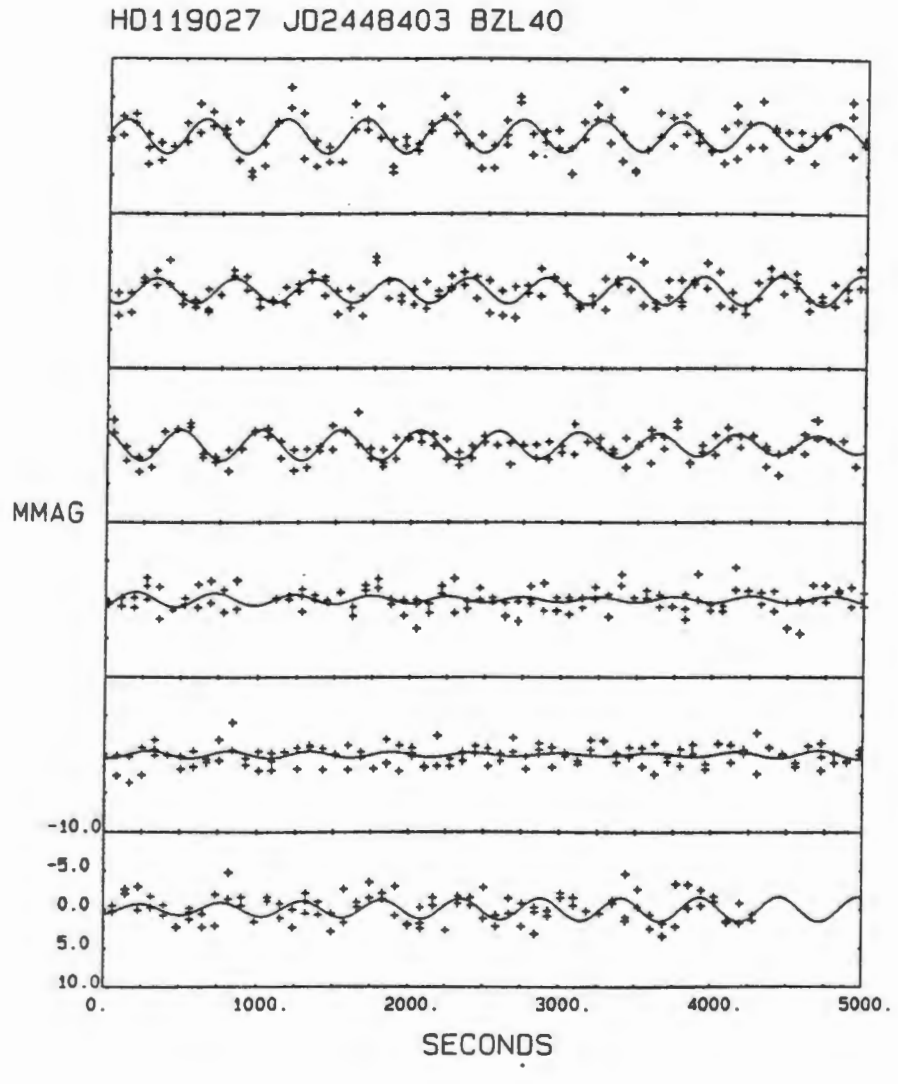

Figure 7.1 The light curve of HD 119027 obtained on JD2448403. Note how the amplitude of the oscillations is modulated on a time-scale of a few hours. This modulation is produced by the beating of at least three frequencies which we identified by prewhitening (see section 7.4). The solid line is a least squares fit of the frequencies 1.912 mHz, 1.941 mHz and 1.836 mHz to the data. At amplitude maximum, the oscillation amplitude is 2 mmag peak to peak.

subtract a frequency from the data. We term this process *dewindowing*; it is equivalent to prewhitening in the time domain.

In what follows, we will discuss the frequency analyses which contributed most to our current understanding of the oscillation spectrum of this star.

7.4 The nightly amplitude spectra

We began our frequency analysis by computing the amplitude spectra of the individual nightly data sets out to the Nyquist frequency of 12.5 mHz for 40-s integrations. Although the frequency resolution of these analyses is low, they have the advantage of being immune to the aliasing ambiguities that arise when data from several nights are analyzed together. Another advantage is that, for multi-mode pulsators, intrinsic variations in the mode amplitudes can be seen on a night-to-night basis, provided the frequency spacing is large enough that the frequencies are resolved in a single night of observations.

The nightly amplitude spectra reveal the presence of oscillations only in the region of 1.9 mHz. On most nights the peak at 1.9 mHz was broader than the central peak in the window pattern of the observations and it was also asymmetric. This broadness and asymmetry suggests the presence of further frequencies which were not resolved in those light curves. In the discussion that follows we concentrate on runs of sufficient length to resolve these other frequencies. A representative sample of such runs from night JD2448403 to night JD2448410 is shown in Fig. 7.2. For reasons of scale, we show only the frequency range 0 to 5 mHz; the amplitude spectra are all flat from 5 mHz to the Nyquist frequency of 12.5 mHz. These were all 7 to 8-hr runs of virtually 100% duty cycle (Table 7.1). What we wish to emphasize in Fig. 7.2 is that there is complex of *resolved* prominent peaks at 1.9 mHz and the dominant peak is different on different nights. The presence of multiple oscillations is most evident on night JD2448408 where 4 modes are clearly discernible. The spacing between the peaks is ≈ 50 μHz. Witness the difference in the amplitude spectra between nights JD2448404 and 8408.

As an example, we discuss the analysis of the JD2448403 data in detail. Fig. 7.1 shows how the amplitude of the variations in HD 119027 was modulated on that night suggesting the presence of at least two pulsation frequencies. A careful inspection of the amplitude spectrum of these data (Fig. 7.2) suggests the presence of at least three frequencies the values of which were determined, by

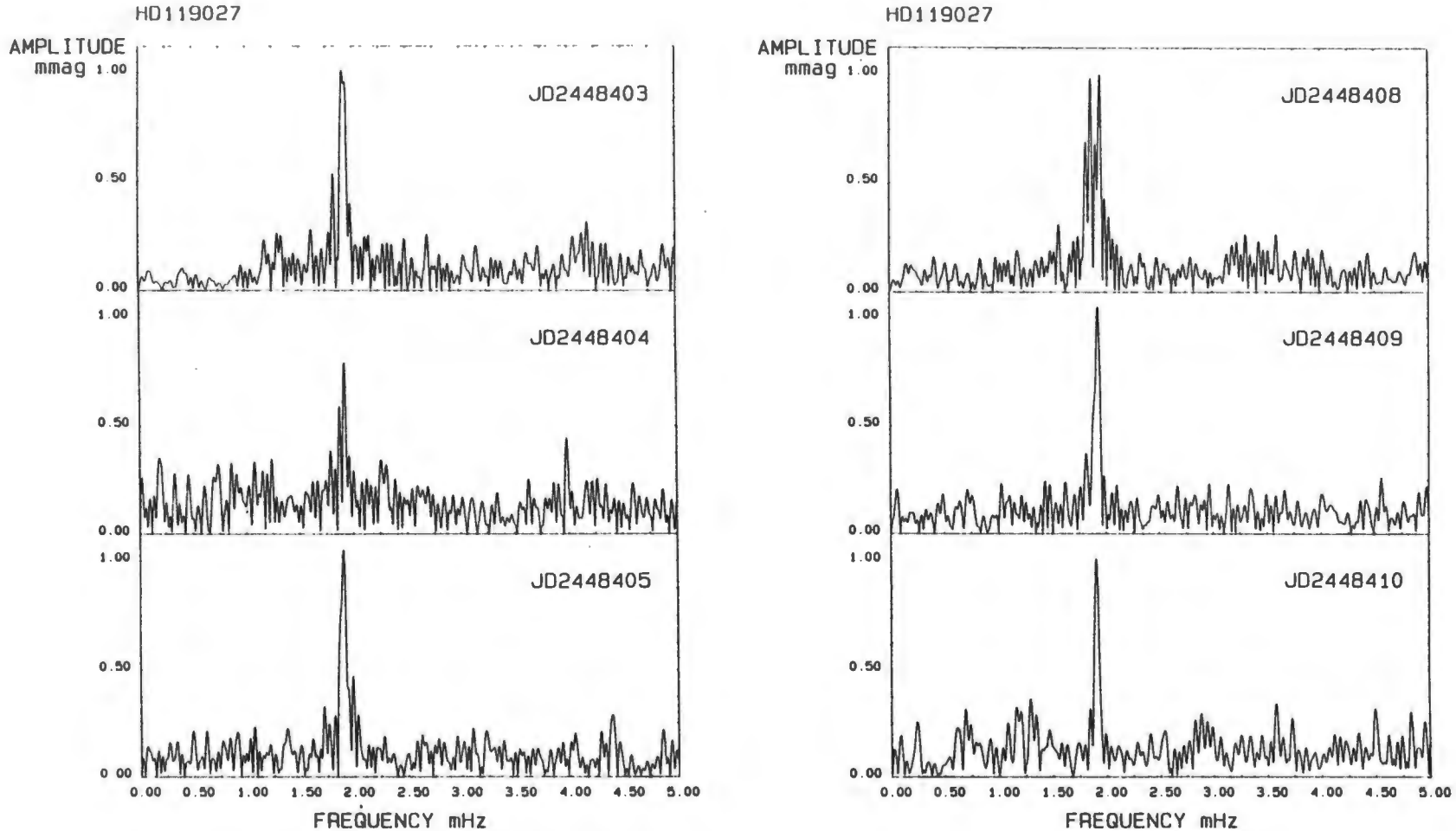

Figure 7.2 A selection of amplitude spectra of the oscillations of HD 119027 acquired on nights JD2448403-8410. Only frequencies in the range 0-5 mHz are shown because beyond 5 mHz the spectra are flat out to the Nyquist frequency of 12.5 mHz. The first panel, JD2448403, is the amplitude spectrum of the light curve presented in Fig. 7.1 which is clearly modulated in amplitude, a consequence of beating of several modes. The multi-mode character of the oscillations is especially evident in night JD2448408. Unfortunately the frequency resolution in these plots is not high enough for us to study the amplitude behaviour of the various modes. Note that there is no amplitude in the region of the harmonic 2ν. The peak at around 4 mHz in night JD2448404 does not appear in any of the other amplitude spectra and we consider it to be an abnormally high noise peak on that night.

prewhitening, to be 1.912 mHz, 1.941 mHz and 1.836 mHz. The solid line in Fig. 7.1 is a least squares fit of these three frequencies to the data.

We also note in passing that there are no prominent peaks in the vicinity of $2\nu_1$ = 3.8 mHz in Fig. 7.2. This is where the first harmonic of ν_1 would be if it were present, a point we will return to in section 7.8.

7.5 The JD2448402-8410 data

This data set combines the advantage of the fairly good resolution of an 8.2-day span of data with a good duty cycle (31%). Since there is evidence for oscillations only in the region of 1.9 mHz, we confine our attention to the frequency range 1.70 to 2.20 mHz. The amplitude spectrum for this frequency range is presented in Fig. 7.3 where we identify the principal oscillation frequency as 1.91370 mHz.

Figure 7.3 also indicates the presence of at least one additional frequency. To identify the additional frequency components we dewindowed ν_1 as described in section 7.3. This resulted in the amplitude spectrum shown in Fig. 7.4 which reveals two more frequencies at ν_2 = 1.94022 mHz and ν_3 = 1.88762 mHz, respectively. Note that the frequencies ν_1, ν_2 and ν_3 are separated by approximately 26 μHz; $\nu_2 - \nu_1$ = 26.52 μHz and $\nu_1 - \nu_3$ = 26.08 μHz.

On dewindowing ν_2 and ν_3 we are left with the residuals shown in the top panel of Fig. 7.5. The tallest peak in Fig. 7.5(a) is at ν_{2p} = 1.94217 mHz. We have chosen the notation 'ν_{2p}' to reflect the fact that this frequency lies very close to ν_2 on its positive side. In another analysis to be discussed later, we will find such frequencies close to ν_3 on its positive and negative sides which we shall denote ν_{3p} and ν_{3m}, respectively. We will discuss these ν_p and ν_m frequencies later. After dewindowing ν_{2p}, we are left with the amplitude spectrum shown in Fig. 7.5(b) in which the selection of the next frequency is confused by an alias ambiguity. In frequency analyses (not presented in this chapter) for other subsets of data, this particular alias ambiguity does not arise. We are guided by those analyses in our choice of ν_4 = 1.83522 mHz in Fig. 7.5(b).

Upon dewindowing ν_4, we are left with the amplitude spectrum shown in Fig. 7.5(c) in which the next frequency is difficult to choose. Again, we rely on the results of several other frequency analyses to select ν_5 = 1.86100 mHz; in the JD2448408-8413 data this frequency is unambiguously selectable. Admittedly, we have not selected the tallest peak in the amplitude spectrum in Fig. 7.5(c), but the difference in amplitude between the peak we have selected and the tallest peak is significantly

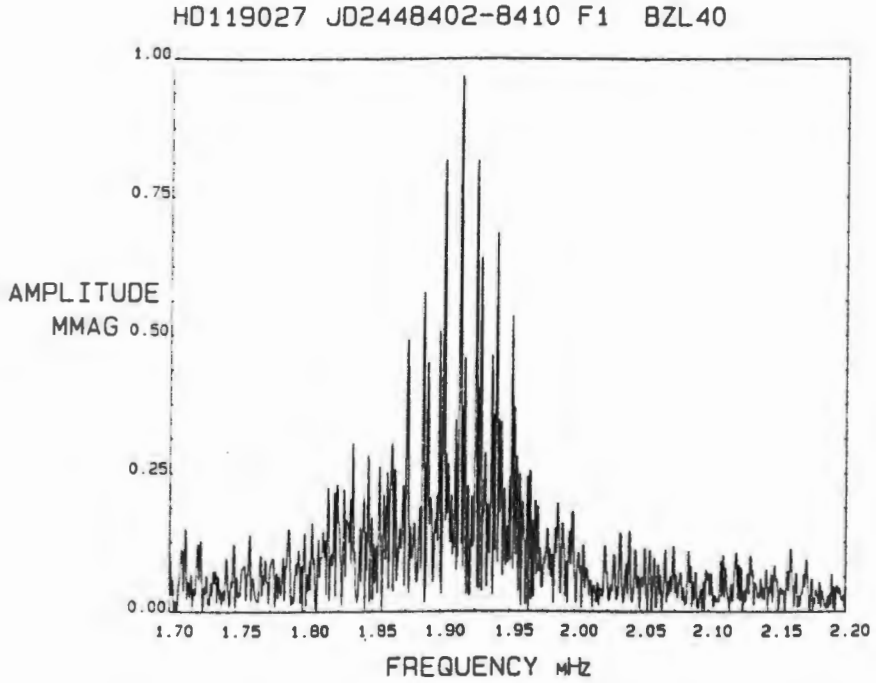

Figure 7.3 The amplitude spectrum of the JD2448402-8410 data. Since the oscillations are confined to the region of $\nu \approx 1.9$ mHz, we restricted our attention to the frequency range 1.7 - 2.2 mHz, enough to show all of the oscillations and a stretch of noise on either side. The dominant alias pattern is centered at $\nu_1 = 1.91370$ mHz.

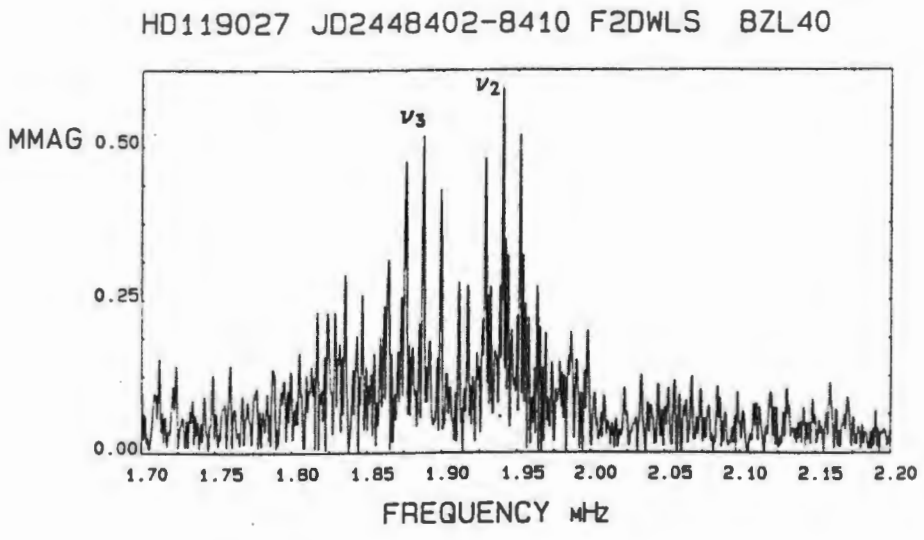

Figure 7.4 The amplitude spectrum of the JD 2448402-8410 data after dewindowing $\nu_1 = 1.91370$ mHz. The two well resolved alias patterns are at $\nu_2 = 1.94022$ mHz and $\nu_3 = 1.88762$ mHz. Note the low noise level in this plot; the tallest noise peaks are around 0.12 mmag.

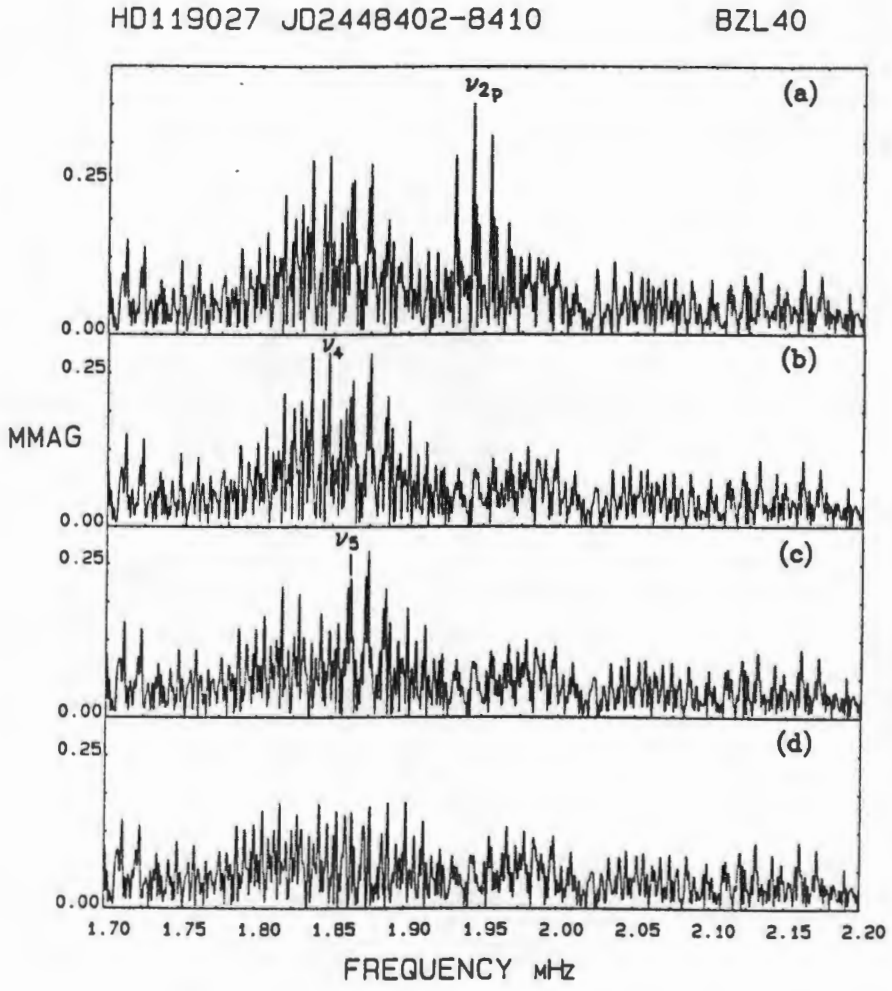

Figure 7.5 The top panel shows the residuals in the amplitude spectrum of the JD2448402-8410 data after dewindowing ν_{123}. The tallest peak in Fig. 7.5(a) at 1.94217 mHz is designated 'ν_{2p}' because it is too close to ν_2 ($+2\,\mu$Hz) to fit into the 26-μHz pattern. Consult the text for further details. The four other panels of this figure show the residuals during several successive stages of dewindowing: (b) $\nu_4 = 1.83522$ mHz, (c) $\nu_5 = 1.86100$ mHz and (d) the residuals on dewindowing ν_5. Again, note the enhanced amplitude in the bottom panel although no further peaks may be selected with confidence. As an exercise, the reader may try to identify other peaks that might coincide with the 26-μHz spacing noted in the text.

less than the level of the noise. On dewindowing ν_5 we are left with enhanced amplitudes in the region of ν_1-ν_5 as shown in Fig 7.5(d) but we are unable to select further frequencies with confidence. Table 7.2 gives linear and non-linear least squares fits of the frequencies ν_1 to ν_5. Notice how the spacings ν_2-ν_1 and ν_1-ν_3 differ by formally significant amounts. We will discuss these differences in section 7.10.

The frequencies ν_4 and ν_5 fit into the pattern of frequencies spaced by 26 μHz defined by ν_1, ν_2 and ν_3. We stress that we did not choose ν_4 and ν_5 solely because they fit into this 26 μHz spacing; these frequencies are unambiguously selectable in other data sets. Nevertheless, the reader may wonder about the statistical significance of the frequencies ν_4 and ν_5. The False Alarm probability (Scargle 1982), F, of finding a peak with power signal-to-noise z among N independent Fourier frequencies is $F = 1 - (1-e^{-z})^N$. If one naively applies this criterion to ν_4 using $z = (A/\sigma)^2 \approx (0.28/0.125)^2 \approx 5.02$ from Fig. 7.5(b) and $N = 730$ frequencies for this data set and the frequency range shown in Fig. 7.5, the calculation of $F = 0.992$ suggests that finding a peak such as ν_4 purely by chance should not surprise us.

However, ν_4 does not just lie anywhere in Fig. 7.5(b) - it is very close to an integral multiple of the 26 μHz spacing noted above. For these data, the Gaussian half-width of the central peak in the spectral window is $\sigma_\nu = 0.70$ μHz. If we ask what is the probability of there being a prominent peak within a stretch of spectrum $\pm 3\sigma_\nu$ from $\nu = \nu_1 - 3\times 26$ μHz, then $N = 6$ and $F = 3.9$ per cent, indicating that ν_4 is probably real. Similar arguments can be applied to ν_5, but we emphasize that it is our ability to recognize these same window patterns standing out above the noise continuum in different data sets that really lends credence to the identification of an oscillation peak at these low signal-to-noise levels.

7.6 The JD2448402-8429 data

In order to refine our frequency determinations we performed a high-resolution frequency analysis of our data using the long temporal baseline of the entire data set. This data set comprises 8056 40-s integrations spanning 27 days to yield a duty cycle of 14%. Because of its low duty cycle, this data set is beset by aliasing ambiguities which give rise to a complicated fine structure in the frequency spectrum. This means that we can only really use this data set to refine the values of the frequencies determined from the smaller data sets discussed earlier, rather than to search for further frequencies with confidence.

Table 7.2

Linear (top) and non-linear (bottom) least squares fits of the frequencies ν_1 to ν_5 to the JD2448402-8410 data. The functional form is $A_i\cos(2\pi\nu_i(t-t_o)+\phi_i)$ and the phases are given relative to t_o=JD2448406.42000, the centroid of the data.

	ν (mHz)	A (mmag)	ϕ (rad)
ν_1	1.91370	0.87±0.03	-1.30±0.04
ν_2	1.94022	0.69±0.03	-0.77±0.05
ν_3	1.88762	0.54±0.03	-1.97±0.06
ν_{2p}	1.94217	0.40±0.03	-2.07±0.08
ν_4	1.83522	0.29±0.03	0.64±0.11
ν_5	1.86100	0.21±0.03	1.25±0.15

$\nu_2-\nu_1$ = 26.52 μHz
$\nu_1-\nu_3$ = 26.08 μHz
$\nu_3-\nu_5$ = 26.62 μHz
$\nu_5-\nu_4$ = 25.78 μHz

$\nu_1-\nu_5$ = 52.70 μHz = 2×26.35 μHz
$\nu_1-\nu_4$ = 78.48 μHz = 3×26.16 μHz

	ν (mHz)	A (mmag)	ϕ (rad)
ν_1	1.91365±0.00003	0.87±0.03	-1.30±0.04
ν_2	1.94022±0.00003	0.69±0.03	-0.77±0.05
ν_3	1.88757±0.00004	0.56±0.03	-1.97±0.06
ν_{2p}	1.94219±0.00006	0.40±0.03	-2.08±0.09
ν_4	1.83534±0.00008	0.30±0.03	0.64±0.11
ν_5	1.86098±0.00010	0.23±0.03	1.25±0.14

$\nu_2-\nu_1$ = 26.57±0.04 μHz
$\nu_1-\nu_3$ = 25.08±0.05 μHz
$\nu_3-\nu_5$ = 26.59±0.11 μHz
$\nu_5-\nu_4$ = 25.64±0.13 μHz

$\nu_1-\nu_5$ = 52.67±0.10 = 2×26.34±0.05 μHz
$\nu_1-\nu_4$ = 78.31±0.08 = 3×26.10±0.03 μHz

$\nu_2-\nu_{2p}$ = 1.97±0.07 μHz

The 27-day timespan of these data allows us to compute high-resolution amplitude spectra with a 10 nHz step size. We thus searched 5×10^4 frequencies in the range 1.70 to 2.20 mHz (Fig. 7.6) and selected those peaks in the amplitude spectrum which conform to the 26-μHz spacing and that were closest to the ones determined in the earlier analyses. In some cases, the 1 day^{-1} aliases of these peaks had marginally bigger amplitudes, but the amplitude differences were smaller than the level of the noise outside the frequencies of interest. We summarize the results of this analysis in Table 7.3. Again, we note that the spacings of adjacent ν_i differ by formally significant amounts. The frequencies ν_{2p}, ν_{3p} and ν_{3m} are frequencies very close to ν_2 and ν_3, respectively, which do not fit into the 26-μHz spacing. Note also in Table 7.3 that the frequencies ν_{3p} and ν_{3m} are not equally spaced about $\nu_3 = 1.88780$ mHz.

The reader may argue that our frequency analysis is somewhat contrived in that we have used the conjectured 26 μHz spacing to find frequencies which fit into this spacing. We permitted ourselves to use the 26 μHz spacing only to select a frequency that was confused with its 1 day^{-1} aliases. Indeed, as Table 7.3 shows, we also selected frequencies that do not fit into the pattern when there was no compelling reason to do otherwise.

The frequencies listed in Table 7.3 are by no means a complete model of the light curve. To illustrate this, we show in Fig. 7.6 the Fourier transform of the data and beneath it the amplitude spectrum of the residuals on dewindowing all the frequencies listed in Table 7.3. This residual mound of amplitude is reminiscent of that seen in HD 101065 (Martinez & Kurtz 1990c), HD 217522 (Kreidl *et al.* 1991) and HR 1217 (Kurtz *et al.* 1989) and probably indicates changes in the pulsation amplitudes and/or phases.

7.7 The implications of residual amplitude to the least squares fits.

The linear least squares fitting procedure we employed assumes that the frequencies are precisely known and adjusts the amplitudes and phases of the frequency components to minimize the sum of the squares of the residuals. The noise is assumed to be white noise, a condition which is not met in our data. The lower panel in Fig. 7.6 shows that the local noise at ν_1 is two to three times higher than that at 2.20 mHz. Since the value of σ is computed for the entire range of the frequency spectrum, the calculated uncertainties for a given frequency can be too large or too small. As an exercise, we used the results of our linear least squares fits as the input values to a non-linear least squares fitting procedure. This procedure adjusts the frequencies, amplitudes and phases of all frequency

Table 7.3

Linear (top) and non-linear (bottom) least squares fits of the frequencies ν_1 to ν_5 to the JD2448402-8429 data. The functional form is the same as in Table 7.2 and the phases are relative to t_o=*JD*2448407.27000

	ν (mHz)	*A* (mmag)	ϕ (rad)
ν_1	1.91357	0.90±0.03	2.00±0.04
ν_2	1.94028	0.70±0.03	2.34±0.05
ν_3	1.88780	0.45±0.04	2.02±0.09
ν_{3m}	1.88661	0.32±0.04	1.80±0.11
ν_4	1.83546	0.29±0.03	-0.63±0.11
ν_{2p}	1.94216	0.42±0.03	1.86±0.08
ν_{3m}	1.88845	0.15±0.05	2.00±0.31
ν_5	1.86064	0.19±0.03	-1.10±0.17

ν_2-ν_1 = 26.71 μHz
ν_1-ν_3 = 25.77 μHz
ν_3-ν_5 = 27.16 μHz
ν_5-ν_4 = 25.18 μHz

ν_1-ν_5 = 52.93 μHz = 2×26.46 μHz
ν_1-ν_4 = 78.11 μHz = 3×26.04 μHz

	ν (mHz)	*A* (mmag)	ϕ (rad)
ν_1	1.913542±0.000010	0.80±0.03	1.94±0.04
ν_2	1.940280±0.000013	0.56±0.03	2.36±0.06
ν_3	1.887878±0.000017	0.43±0.03	2.15±0.07
ν_{3m}	1.886614±0.000021	0.43±0.03	1.61±0.08
ν_4	1.835443±0.000024	0.29±0.03	-0.66±0.10
ν_{2p}	1.942157±0.000021	0.33±0.03	1.78±0.10
ν_{3p}	1.888011±0.000102	0.19±0.03	1.50±0.47
ν_5	1.860462±0.000058	0.12±0.03	-1.47±0.24

ν_2-ν_1 = 26.738±0.016 μHz
ν_1-ν_3 = 25.664±0.020 μHz
ν_3-ν_5 = 27.416±0.060 μHz
ν_5-ν_4 = 25.019±0.063 μHz

ν_1-ν_5 = 53.080±0.059 = 2×26.540±0.029 μHz
ν_1-ν_4 = 78.099±0.026 = 3×26.033±0.013 μHz

ν_{2p}-ν_2 = 1.877±0.025 μHz
ν_{3p}-ν_3 = 0.133±0.103 μHz
ν_3-ν_{3m} = 1.264±0.027 μHz

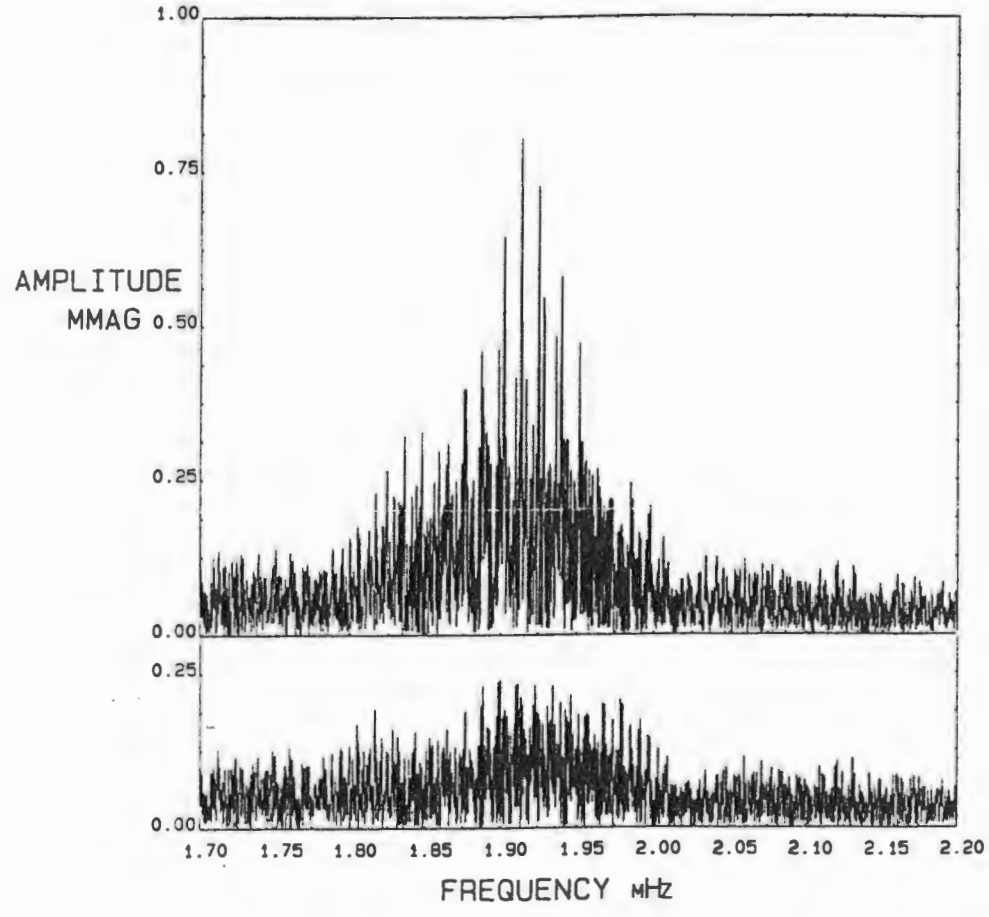

Figure 7.6 The amplitude spectrum of the entire 1991 data set. The lower panel shows the residuals on dewindowing all the frequencies listed in Table 7.3. Note the residual mound of amplitude which we interpret as evidence of non-periodic modulation of the oscillation amplitude and/or phase.

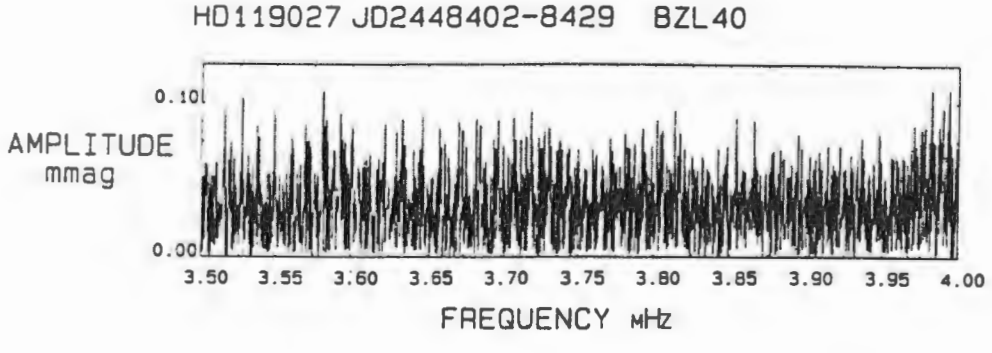

Figure 7.7 The amplitude spectrum of the JD 2448402-8429 data in the region of $2\nu_1$. There is no evidence of the first harmonic of ν_1 in this Figure.

components simultaneously in order to minimize the sum of the squares of the residuals and produces error estimates for the frequencies also. In the absence of complications such as unresolved frequencies, the non-linear least squares approach can provide frequency determinations to higher accuracy than the half-width of the peaks in the Fourier spectrum; ultimately, the accuracy depends on the signal-to-noise ratio. The problem with our data is that the noise spectrum is not flat; witness the mound in the residuals in Fig. 7.6 suggesting some form of non-periodic behaviour.

7.8 A search for the harmonic

Because several roAp stars exhibit the first harmonic of the principal oscillation frequency, we searched for evidence of the first harmonic in HD 119027. We found no indications of the harmonic in any of the nightly amplitude spectra. A high-resolution amplitude spectrum in the vicinity of $2\nu_1$ for the JD 2448402-8429 data set spanning 27 days also did not reveal any indications of the harmonic (Fig. 7.7).

7.9 The rotation period of HD 119027.

7.9a Rotational modulation of the amplitude of the rapid oscillations

The $(2\ell+1)$-fold rotational splitting predicted by the basic oblique pulsator model complicates the appearance of the amplitude spectrum and thus a knowledge of the rotation period can facilitate the frequency analysis. In attempting to identify possible rotational sidelobes in HD 119027, we considered the equally spaced frequency quintuplet as a rotationally split $\ell=2$ mode. However, the 26-μHz spacing is unlikely to be caused by rotational frequency splitting because that would imply a 10.6-hr rotation period for HD 119027, an improbably short rotation period for an Ap star.

Other candidates for the rotational sidelobes are the frequencies ν_{2p}, ν_{3p} and ν_{3m} we found in the JD2448402-8429 data. Consider first the spacing between ν_3 and ν_{3p} and ν_{3m}. The problem with ν_{3p} and ν_{3m} as rotational sidelobes is that they are not equally spaced about ν_3. From the non-linear least squares fits in Table 7.3, $\nu_3-\nu_{3m}=1.264\pm0.027$ μHz and $\nu_{3p}-\nu_3=0.133\pm0.103$ μHz. Notice the large error on ν_{3p} in Table 7.3. This frequency is almost certainly an artefact of the analysis caused by variations in the amplitude or phase of ν_3. If we consider ν_{2p} as a possible rotation sidelobe, the spacing $\nu_{2p}-\nu_2=1.877\pm0.025$ μHz differs from the $\nu_3-\nu_{3m}$ spacing by 0.613 ± 0.037 μHz, a 16σ result. This argues against ν_{2p} and ν_{3m} both being rotation sidelobes of ν_2 and ν_3 respectively, but does not

exclude either one in particular. There is no corresponding ν_{2m} sidelobe either, a result confirmed by force-fitting $\nu_{2m} = \nu_2 - 1.877$ mHz to the data by linear least squares.

We conclude that rotational sidelobes cannot be identified in our pulsation data thus implying that either the star is seen nearly (rotation) pole-on, or the magnetic obliquity, β, is small or that HD 119027 has a rotation period much longer than the time-scale of the observations. We can use the oblique pulsator model to constrain ι and β further if we use the amplitude of the highest noise peaks in Fig. 7.6 as an upper limit on the amplitude of the conjectured rotation side-lobes, A_{rot} = 0.20 mmag. From eq. (2.17), we have $(A_{+1} + A_{-1})/A_0 = 0.4/0.9 = 0.44 = \tan \iota \tan \beta$. Thus, ι and β can each be at most 34°.

7.9b A study of the mean light variations

Because the Ap stars are spotted rigid rotators, differential photometry of their mean light variations can be used to determine their rotation periods for stars with favourable inclination. We obtained differential *UBVRI* photometry of HD 119027 and two local comparison stars, HD 118646 (F3V) and HD 118394 (F5V) on 19 nights from May to October 1991 using the 0.5-m telescope of the SAAO at Sutherland. These observations are being prepared for publication, but a preliminary analysis indicates a null result for rotation in all colours. This is consistent with the absence of rotational sidelobes in the amplitude spectra and suggests that either HD 119027 is not strongly spotted or the rotation axis is viewed pole-on or $\beta \approx 0°$ or this star has a rotation period much longer than the time-scale of the observations.

7.10 The *p*-mode spectrum of HD 119027

In section 2.6 we described how the asymptotic theory of low-degree, high overtone ($n >> \ell$) *p*-mode pulsation predicts a spectrum of equally spaced frequencies with a characteristic separation, $\Delta\nu$, as given in eq. (2.3). Physically, $\Delta\nu$ is the reciprocal of the time for sound to cross the star. To first order, eq (2.3) says that modes with the same value of $(n + \ell/2)$ will be nearly degenerate since $\nu_{n\ell} \approx \nu_{n-1,\ell+2}$ and $\nu_{n\ell} \approx \nu_{n+1,\ell-2}$. Thus, consecutive overtones $(n, n+1)$ of modes of exclusively even or odd ℓ will be spaced by $\Delta\nu$, whereas alternating even and odd ℓ modes will be spaced by $\Delta\nu/2$. The problem is to decide whether the observed spacing corresponds to $\Delta\nu$ or $\Delta\nu/2$. The A star models of Shibahashi & Saio (1985), Gabriel *et al.* (1985) and Heller & Kawaler (1988) predict values of $\Delta\nu \approx$ 50 - 80 μHz for a slightly evolved $2M_\odot$ star. Their results indicate that the observed frequency spacing

of 26 μHz in HD 119027 corresponds to the spacing between alternating even and odd ℓ modes, $\Delta\nu/2$. Thus in HD 119027, we are probably seeing both even and odd ℓ modes with a spacing of $\Delta\nu = 52$ μHz. This is comparable to the asymptotic p-mode spacings seen in several other roAp stars: 52 μHz in HD 60435, 34 μHz or 68 μHz in HR 1217, 58 μHz in HD 101065, 68 μHz in HD 166473, 51 mHz in HD 176232, 58 μHz in HD 201601 (Kurtz 1990), and 66 μHz in HD 203932 (Martinez, Kurtz & Heller 1990)*.

We cannot exclude the possibility that $\Delta\nu = 26$ μHz until an independent luminosity estimate for this star becomes available. There is weak corroboration for our choice of $\Delta\nu = 52$ μHz in the finding by Matthews (1989, 1991) that the ratios $\Delta\nu/\langle\nu\rangle$ for the known roAp stars cluster about the values 0.025 and 0.04. For $\Delta\nu = 52$ μHz, $\Delta\nu/\langle\nu\rangle \approx 0.027$, whereas for $\Delta\nu = 26$ μHz, $\Delta\nu/\langle\nu\rangle \approx 0.014$.

Having decided that the spectrum has alternating even and odd ℓ modes allows us to estimate the overtones n of the frequencies ν_1 to ν_5. Using eq. (2.3) and the values in Table 7.3 we find $n \approx 35$. For comparison, in HD 60435 Matthews *et al.* (1987) found that $n \approx$ 26 to 28 for the highest frequencies and $n \approx$ 13 to 15 for the lowest. In HD 101065, Martinez & Kurtz (1990c) found that $n \approx$ 20 - 25. In HR 1217, Kurtz *et al.* (1989) found $n \approx$ 80 if consecutive overtones of $\ell = 1$ are excited, and $n \approx 40$ if alternating even and odd ℓ-modes are excited.

The 26 μHz spacing and the character of the oscillations in HD 119027 is reminiscent of HD 60435 which has a rich p-mode spectrum (Matthews *et al.* 1987) with a 26.3 μHz spacing. This star, too, changes the structure of its amplitude spectrum from night to night. Examples of the oscillations seen in HD 60435 on 8 nights are shown in Fig. 2.6. It is instructive to compare Fig. 2.6 to Fig. 7.2.

A star that has been observed to mode-switch is HD 217522 (Kreidl *et al.* 1990). From 1982 to 1989, the principal oscillation frequency in this star shifted from $\nu(1982) = 1.21529 \pm 0.00004$ mHz to $\nu(1989) = 1.1999 \pm 0.0001$ mHz, a difference of 15.4 ± 0.1 μHz. Moreover, there is a another frequency in the 1989 data at $\nu = 2.0174 \pm 0.0001$ mHz which was not seen in the 1982 data. At its 1989 signal-to-noise, there is no chance that this frequency could have been missed in the 1982 data had it been present then.

Libbrecht (1988) has noted similar behaviour in γ Equ. In his 1987 radial velocity observations of that star, Libbrecht found two frequencies, 1.366 and 1.427 mHz, but could not confirm Kurtz's 1983 detection of a single oscillation frequency at 1.339 mHz. Unpublished high-

* The observed $\Delta\nu/2 \approx 33$ *m*Hz spacing in HD 203932 is a tentative result requiring confirmation.

speed photometry of γ Equ obtained on Mauna Kea in August 1988 with a narrow band filter at λ4120 (FWHM 30Å) (Matthews, private communication) confirms the presence of the 1.366-mHz oscillation reported by Libbrecht. There is no evidence in these data for the 1.339-mHz oscillation, but it is worth noting that 1.366 mHz - 2 day^{-1} = 1.343 mHz.

In the star HD 203932, Martinez *et al.* (1990) have identified 4 frequencies with roughly equal spacing $\Delta\nu/2$ = 33 μHz and they have presented evidence for transient oscillatory behaviour here as well.

In contrast to the apparent transience of modes in multi-mode pulsators, the singly periodic roAp stars have remarkably stable amplitude spectra, a characteristic which makes them excellent candidates to search for evolutionary frequency changes. The best-studied roAp star, HR 3831, is singly periodic with harmonics. The basic structure of HR 3831's frequency spectrum, a rotationally split ℓ = 1 mode, is stable in amplitude, but not in phase (Kurtz *et al.* 1993). The phase instabilities, which appear to be periodic, are discussed more fully in section 9.5. In the ostensibly singly periodic roAp star HD 134214, Kurtz *et al.* (1990) cannot phase together 1985 and 1990 data with a single frequency. However, the difference between the best-fit frequencies for the two data sets is $\approx$0.1 μHz, too small to be a mode-switch to a neighbouring overtone. Further observations are required to investigate the stability of the amplitude spectrum in that star.

The pattern that is emerging is that the roAp stars which have only one pulsation mode are stable in amplitude, but not necessarily phase, for years whereas the multi-mode pulsators can switch modes with growth/decay time-scales of days. It is important to characterize the growth and decay patterns of these transient oscillation modes because this knowledge is of relevance to an understanding of the mode selection and excitation mechanisms operating in the roAp stars.

The frequency ν_{2p} appears with a good signal-to-noise in the JD 2448402-8413 data. This frequency is of considerable interest if it can be shown to be a real oscillation frequency in the star rather than just the Fourier transform's way of modelling some non-periodic modulation of ν_2 in our data. If ν_{2p} is a real frequency in the star, the spacing ν_{2p}-ν_2 = 1.89 μHz is a measure of the second-order term $\delta\nu$ in the Tassoul relation (eqn. 2.3) and has considerable diagnostic potential.

Christensen-Dalsgaard (1988) and Ulrich (1986) have used the parameters $\Delta\nu$ and $\delta\nu$ to construct an oscillation H-R diagram which at present is calibrated only by the Sun. The 1.89 μHz separation between ν_{2p} and ν_2 is lower than Christensen-Dalsgaard's (1987) predictions for the Solar

case, but may agree with theoretical expectations scaled to the mass and radius of Ap stars as discussed in section 9.8. Further observations to test the reality of ν_{2p} are thus highly desirable.

We note in Table 7.3 that the separations of the principal frequencies ν_1 to ν_5 are not exactly equal. If we assume an alternating even and odd ℓ-mode interpretation of the principal frequencies then we expect inequalities in the frequency spacings,

$$(\nu_{n,1} - \nu_{n,0}) < (\nu_{n+1,0} - \nu_{n,1}) \tag{7.1}$$

$$(\nu_{n,1} - \nu_{n-1,2}) > (\nu_{n,2} - \nu_{n,1}) \tag{7.2}$$

as pointed out by Shibahashi & Saio (1985). We can test these inequalities with our frequencies derived for HD 119027 in Table 7.3 by adopting self-consistent n and ℓ values and substituting them where appropriate. Such an exercise shows that inequality (4) cannot be satisfied for such n,ℓ values and that inequality (3) is satisfied if ν_1 is identified with an $\ell = 1$ mode and ν_2 is identified with an $\ell = 0$ mode, and so on. Although these results are consistent with alternating $\ell = 0$ and $\ell = 1$ modes, we emphasize that this exercise does not constitute a secure mode identification of the frequencies observed in HD 119027*.

7.11 Conclusion

We have presented observations of the new rapidly oscillating Ap star HD 119027 which show that:

1) HD 119027 pulsates with at least five nearly equally spaced frequencies in the vicinity of 1.9 mHz. The spacing between these frequencies is 26 μHz.
2) The data cannot be completely described by these five frequencies. There is a residual mound of amplitude in the vicinity of 1.9 mHz no matter which subset of the data is analyzed. This suggests that there must be some amplitude or phase modulation of these 5 frequency components.
3) Attempts to determine the rotation period of this star have yielded null results. Analyses of the rapid oscillations constrain ι and β to be $\leq 34^{\circ}$. The lack of mean light variations indicates that HD 119027 is either viewed (rotation) pole-on or the magnetic obliquity $\beta \approx 0^{\circ}$ or it has a rotation period much longer than the time spanned by the data, or it has an unusually homogeneous surface for an Ap star.

---

* In Table 7.3, ν_{3m} has the same amplitude as ν_3, so either peak could be selected as a mode frequency for the star. A quick test of (ℓ,n) combinations will show that our discussion is sensitive to the choice of ν_3 or ν_{3m}, and that it is no longer possible to discriminate between $\ell = 0$, $\ell = 1$ and $\ell = 1$, $\ell = 2$ modes. However, the frequency ν_{3m} does not arise in other data sets and its reality as a stable oscillation frequency rather than as a modulation artefact has yet to be established.

4) There is no indication of the first or higher harmonics of the frequencies at 1.9 mHz.

5) The spacings of the principal frequencies ν_1 to ν_5 are not exactly equal and satisfy the inequalities $(\nu_1-\nu_3) < (\nu_2-\nu_1)$ and $(\nu_5-\nu_4) < (\nu_3-\nu_5)$ in agreement with the inequality expected in the spacing of alternating $\ell=0$ and $\ell=1$ modes. The basic 26-μHz frequency spacing is also consistent with theoretical expectations for the spacing of alternating even and odd ℓ modes. The spacing of consecutive overtones in HD 119027 is thus $\Delta\nu$ = 52 μHz.

HD 119027 joins a growing number of roAp stars with non-stationary amplitude spectra. The non-stationary behaviour of the oscillations in HD 119027 needs to be further investigated and the reality of ν_{2p}, ν_{3m} and ν_{3p} needs to be tested. To resolve the 26-μHz spacing requires over ten hours of continuous monitoring of HD 119027. To test the reality of ν_{2p}, the time-span of the observations should be at least 7 days. Multi-site observations will permit the data to be analyzed in frames thus allowing the variations in amplitude and phase to be followed. Ultimately, it is the lifetimes of the transient modes rather than the time-span of the observations which will dictate the frequency resolution attainable. For short-lived modes, the width of the peak will provide a measure of the mode life-time.

On good nights the dominant source of noise at 1.9 mHz for a star as bright as HD 119027 is scintillation. Since scintillation noise scales as the -2/3 power of the aperture of the telescope, future studies should use apertures as large as possible. Given the above requirements of frequency resolution and amplitude signal-to-noise ratio, a multi-site campaign of some two weeks' duration using $\geq$ 1.0-m class telescopes offers the best hope of improving our knowledge of the oscillation spectrum of this intriguing star.

Chapter 8

The photometric limits of the roAp phenomenon

8.1 Introduction

In chapter 1 we described how the discovery of rapid oscillations in HD 101065 prompted Kurtz to search for similar oscillations in other Ap stars. With the discovery of the first half-dozen roAp stars it became apparent that the roAp phenomenon is confined to the Ap SrCrEu stars, the coolest of the Ap stars. To maximize the probability of finding new roAp stars subsequent searches concentrated on the SrCrEu stars. These searches revealed that the spectroscopic designation Ap SrCrEu is a necessary but not sufficient indicator of the roAp phenomenon in any given A star. Because in general roAp stars have much lower δc_1 indices than constant luminosity Ap SrCrEu stars, the δc_1 index has often been used to select roAp star candidates. This selection procedure introduces a bias against the more luminous roAp stars because such stars have δc_1 indices which are too low for their luminosities but typical of the less luminous Ap stars. In the absence of other luminosity indicators, such stars will be overlooked in the selection of roAp star candidates.

It was Matthews (1990) who first sought to define the photometric limits of the roAp phenomenon by investigating the positions of the roAp stars in various Strömgren photometric diagrams. His sample consisted of the 14 roAp stars then known, 51 SrCrEu stars extracted from the photometric catalogue of Vogt & Faundez (1979) and 75 δ Scuti stars extracted from Breger's (1979) review article. Matthews' diagrams show that the $[c_1]$ - $[u\text{-}b]$ and $[c_1]$ - $(b\text{-}y)$ planes provide a better indicator of the roAp phenomenon than does the δc_1 index alone.

Nelson & Kreidl (1993) used the results of the Lowell - Wisconsin Survey (described in chapter 3) to investigate the positions of the roAp stars in the Johnson, Strömgren and Geneva photometric systems. Their sample comprised 120 mostly peculiar B8 - F4 stars and the 24 roAp stars known by late 1992. Nelson and Kreidl conclude from their diagrams that there are no obvious means of using colour indices to differentiate roAp stars from non-pulsating Ap stars. The Cape Survey, as we have seen, indicates that this is not really so; colour indices within a certain range can be used as a probabilistic indicator of the roAp phenomenon.

From the outset, the Cape Survey attempted to delineate the extent of the roAp phenomenon. To this end we studied a broad, homogeneous sample of SrCrEu stars. We obtained $uvby\beta$ photometry for 549 Ap SrCrEu stars selected from Tables 3.3 and 3.5 and high-speed photometry for 148 stars. Of the stars monitored for oscillations, 10 proved to be new roAp stars. Of the remaining 138 apparently constant stars, 136 stars have $uvby\beta$ photometry listed in Table 4.2. The difference of 2 stars arises because, to avoid selection effects, we searched for rapid oscillations in many stars without prior knowledge of their Strömgren colours. As of this writing, these 2 stars have not yet been observed in the $uvby\beta$ system as part of the Cape Survey.

Before presenting the photometric diagrams that form the main body of this chapter, we remind the reader of a caveat discussed in chapter 4. One must remember when looking at the diagrams below that the scatter is increased by the intrinsic variations in chemical peculiarity from star to star as well as colour variations caused by oblique rotation. These diagrams also illustrate a strange perversity of nature which often confounds the definition of new astrophysical phenomena. This is the uncanny ability of astronomers to discover a prototypical object which later turns out to be atypical of the phenomenon it originally defined. In good astronomical tradition, the roAp stars are no exception to this. In the photometric diagrams to be shown in this chapter there is one roAp star that is always an outlier. This star is Przybylski's star, HD 101065, the prototype of the class!

8.2 The $(b-y)$ - $[c_1]$ diagram and β - c_1 diagram

In the chemically normal A- to F- type stars the index $[c_1]$ is a luminosity indicator and the index $(b-y)$ is a temperature indicator affected by reddening. Thus for normal stars a $[c_1]$ vs $(b-y)$ diagram is essentially a temperature - luminosity diagram. In chapter 4 we saw how the c_1 index in an Ap star is lower than in a chemically normal A star of the same luminosity. Briefly, the reason for this is that the continuum on the redward side of the Balmer jump is depressed by the severe blanketing and the star appears to have a smaller Balmer jump, and hence a higher surface gravity, than is really the case. For this reason, the c_1 index is not a reliable luminosity indicator for the Ap stars.

Figure 8.1 shows $(b-y)$ - $[c_1]$ diagram for all the Cape Survey stars. The axes have been chosen to portray the data in the customary fashion for HR diagrams. Temperature increases to the left and luminosity increases upwards. The filled circles represent the roAp stars, the open circles are the 136 stars (with $uvby\beta$ photometry) for which we obtained null results during searches for rapid oscillations and the dots represent the stars for which only $uvby\beta$ photometry exists. These three

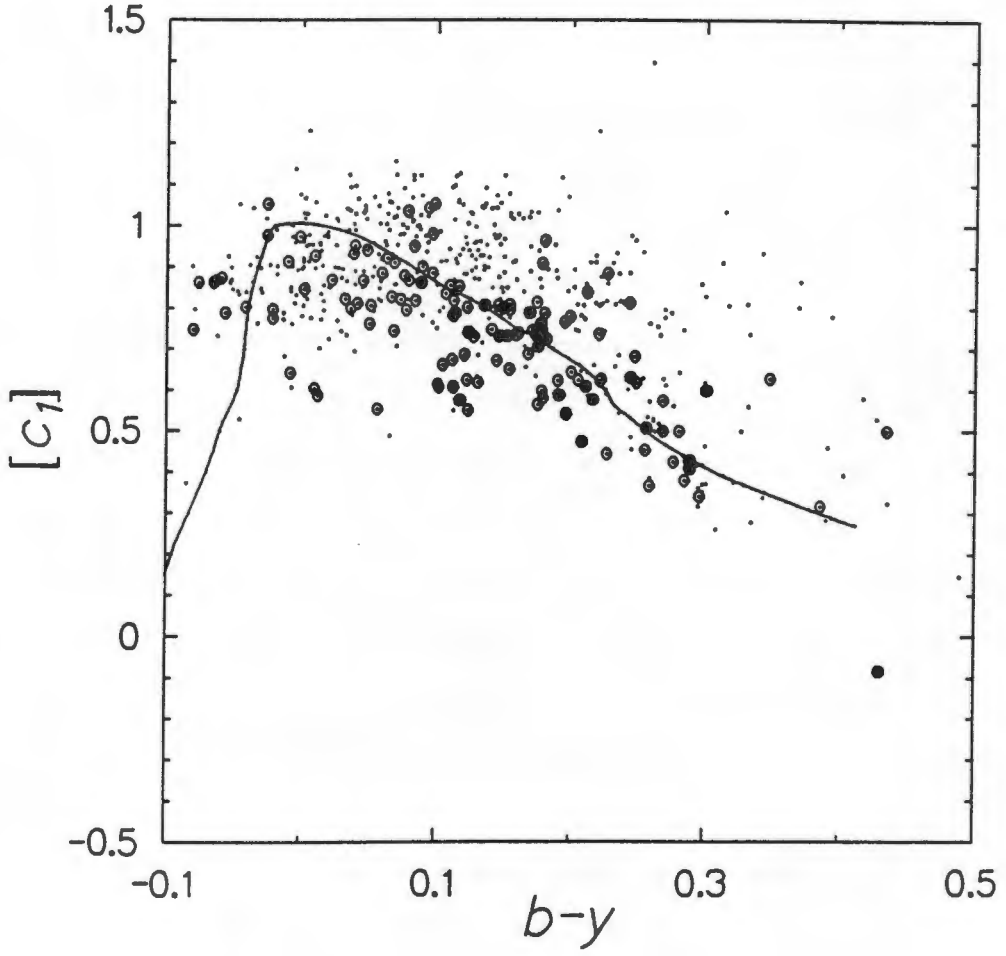

Figure 8.1 The $[c_1]$ versus $(b\text{-}y)$ diagram for the Cape Survey Ap SrCrEu stars. The dots represent all the stars for which only $uvby\beta$ photometry exists at present. The open circles represent those stars in which we searched for rapid oscillations. The filled circles represent the roAp stars. The solid line is the main sequence calibration line from Crawford's (1975, 1978, 1979) calibration of the B-, A- and F-type stars. This plot shows that the abundance variations from star to star are not so severe that they obliterate the underlying main sequence trend.

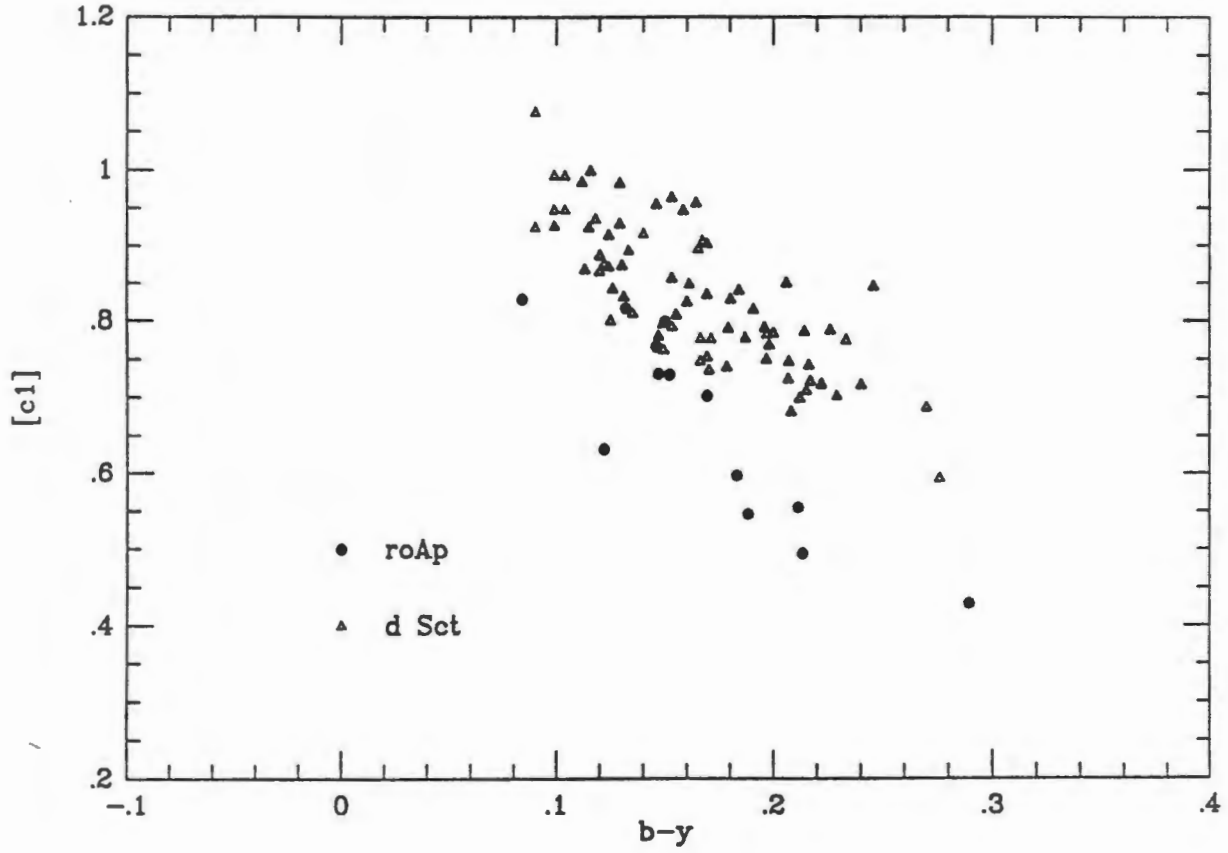

Figure 8.2 The relative positions of the chemically peculiar roAp stars and the chemically normal δ Scuti stars in the $[c_1]$ - $(b\text{-}y)$ plane. Notice that the two types of star fall on parallel sequences and that the δ Scuti stars have a tighter distribution than the roAp stars. The downward shift of the roAp stars relative to the δ Scuti stars is due to severe blanketing which depresses the c_1 index. Consult the text for more details. (Taken from Matthews 1990.)

symbols are used throughout the rest of this chapter in the same context. The solid line in Fig. 8.1 is Crawford's (1975, 1978, 1979) empirical standard main sequence relation for the chemically normal B-, A- and F-type stars. Because of metallicity effects on $[c_1]$ and reddening effects on $(b\text{-}y)$, the reader should not pay too much attention to the positions of stars relative to the main sequence relation. What *is* significant, however, is that the distribution of stars follows the same slope as the standard relation. Evidently the metallicity differences among the Ap stars are not so great as to obscure the underlying main sequence trend. The effect of the abundance anomalies is to shift the stars to higher values of $[c_1]$ than they would have had were they chemically normal. Matthews (1990) has illustrated this point graphically in a $[c_1]$ vs $(b\text{-}y)$ plot (Fig 8.2) of the roAp stars and the chemically normal δ Scuti stars. The two groups of stars lie on parallel sequences with the roAp stars on the lower sequence.

The distribution of open circles in Figure 8.1 shows that the Cape Survey has accomplished its objective of searching for rapid oscillations in the Ap SrCrEu stars over a wide range of temperature and luminosity. From the Figure we can see that $(b\text{-}y)$ for the roAp stars ranges from 0.08 to 0.31. The roAp stars are confined to the coolest Ap SrCrEu stars and, for a given $(b\text{-}y)$, they are confined to the smaller values of $[c_1]$. This result is confirmed for the northern Ap stars observed by Nelson & Kreidl (1993) in the Lowell - Wisconsin Survey (see their Fig. 3).

We have already noted that the metallicity differences in the Ap stars are not so large that they totally obscure the main sequence trend in the data. On closer inspection one finds that the roAp stars form a narrower band than the general distribution of SrCrEu stars. If we interpret this to mean that abundance differences are not large among the roAp stars, then relative differences in c_1 could be used as an indicator of relative luminosity differences among roAp stars of similar β. It should be possible to test this conjecture using independent luminosity estimates derived from studies of the rapid oscillations. As an exercise, one can select roAp stars of similar β for which the asymptotic p-mode spacing $\Delta\nu$ has been measured. The stars with higher $\Delta\nu$ are less luminous (see Fig. 2.10) so they should have a lower $[c_1]$ index. Table 8.1 contains a number of roAp stars suitable for such a comparison. We did not include in this Table stars for which the measured p-mode spacing is < 50 μHz. The reason for this is the factor-of-two ambiguity in determining $\Delta\nu$; in stars where alternating even and odd ℓ modes are excited, the measured spacing is $\Delta\nu/2$ (see section 2.6). The A star models of Gabriel *et al.* (1985), Shibahashi & Saio (1985) and Heller & Kawaler (1988) show that

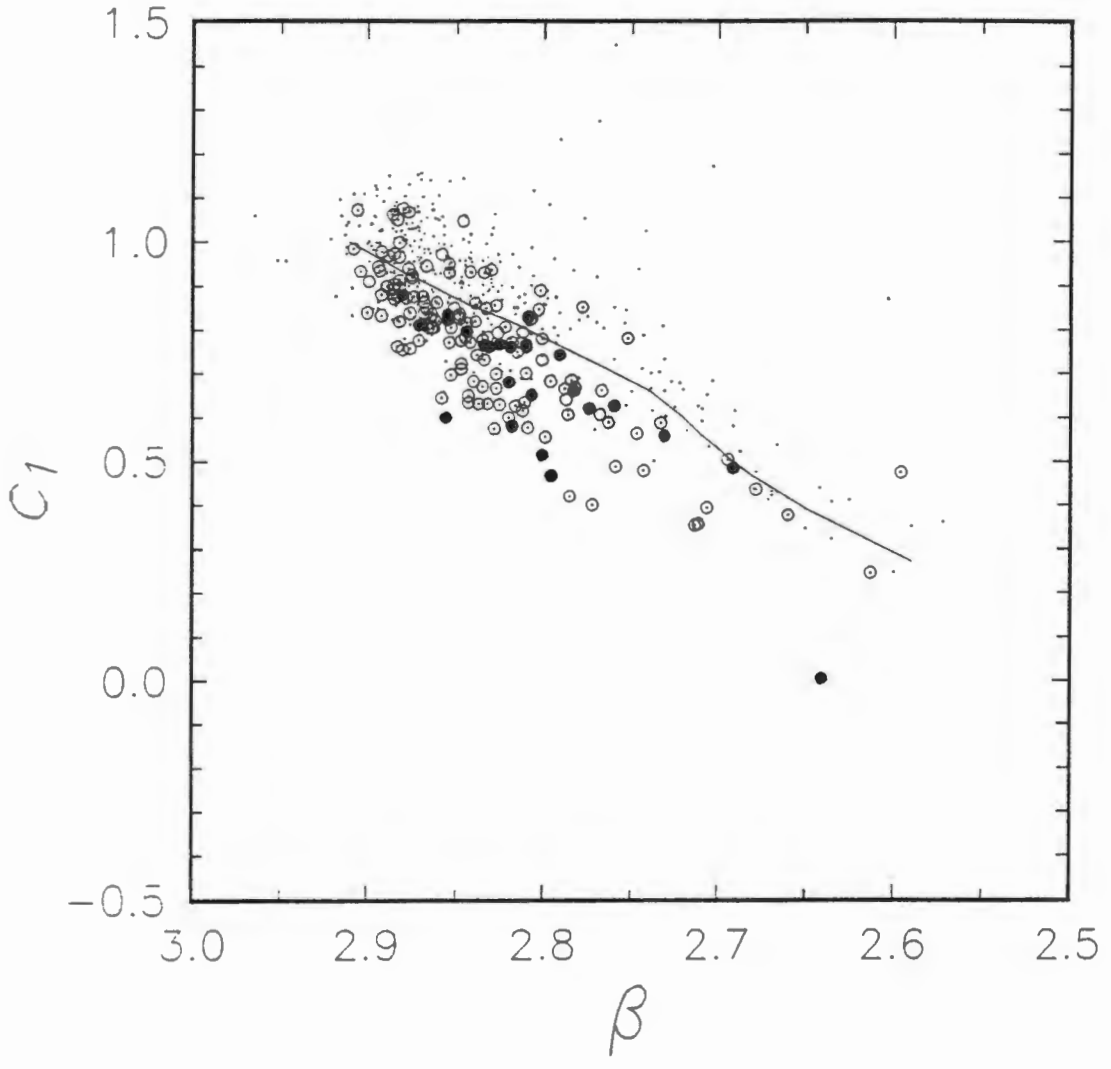

Figure 8.3 The c_1 - β diagram for the Cape Survey stars. The meaning of the symbols is explained in the caption of Fig. 8.1

$\Delta\nu \approx 100$ μHz on the ZAMS. Thus by taking only stars with measured p-mode spacings > 50 μHz we could be sure that our $\Delta\nu$ values are not wrong by a factor of two.

Table 8.1

Star	β	$[c_1]$	$\Delta\nu$ (mHz)
HD 176232	2.809	0.799	50.6
HD 201601	2.819	0.731	58
HD 203932	2.791	0.707	66
HD 166473	2.801	0.472	68

Table 8.1 shows that the stars with higher asteroseismological luminosities (lower $\Delta\nu$) have higher values of $[c_1]$. We note that this comparison serves only as evidence in favour of our conjecture, and not proof of it. In time, the p-mode spacings of more roAp stars will be determined and it will be possible to perform more comparisons of this nature.

Since β is also a temperature indicator, a plot of $[c_1]$ vs β is also a temperature - luminosity diagram. For completeness, we show in Fig. 8.3 the $[c_1]$ - β diagram of the Cape Survey stars. The symbols in this plot have the same meaning as in Fig. 8.1. Because β is free of reddening effects, the distribution of stars is tighter than in the $[c_1]$ - $(b\text{-}y)$ diagram. The Figure also shows that although most roAp stars lie below the standard main sequence relation because of metallicity effects (chapter 4), some more luminous roAp stars lie above it. Since several previous searches for roAp stars have concentrated on SrCrEu stars with apparent subdwarf c_1 indices (*i.e.* $\delta c_1 < 0$), the Cape Survey sampled a large number of stars lying above the standard relation. No rapid oscillators were found in this search; the single roAp star lying above the standard line in Fig. 8.3 is HD 176232 which has $\delta c_1 = +0.031$.

8.3 The $[m_1]$ - $[c_1]$ diagram

The $[m_1]$ - $[c_1]$ diagram for the Cape Survey stars is shown in Fig 8.4. The open circles in this diagram show that the general distribution of $([m_1],[c_1])$ values has been well sampled in the search for new rapid oscillators. One of the earliest systematic investigations of the distribution of different types of chemically peculiar stars in the m_1 - c_1 diagram was conducted by Cameron (1967). Using Cameron's data, Golay (1974) prepared a schematic m_1 - c_1 diagram showing the positions of the different

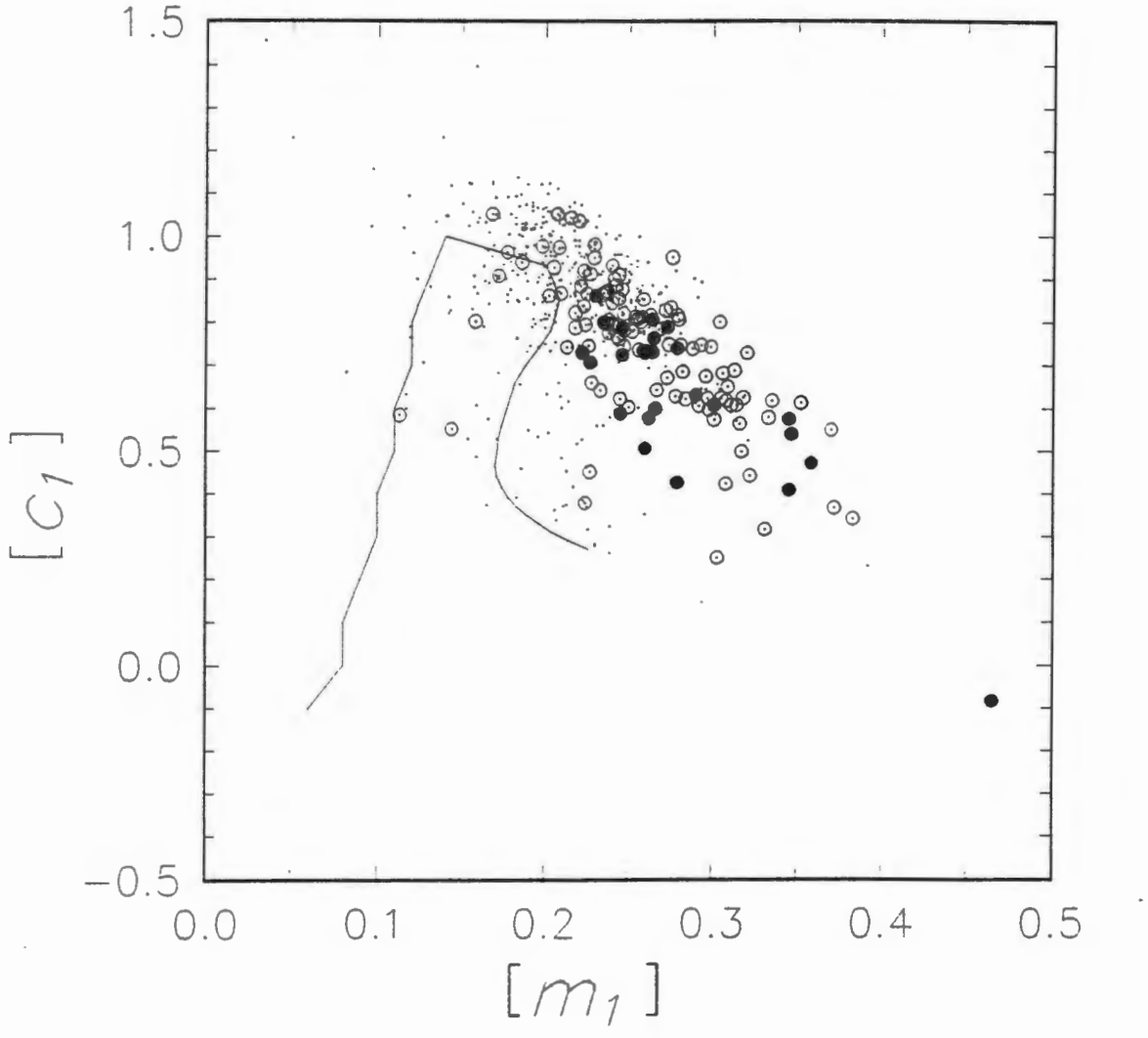

Figure 8.4 The $[c_1]$ - $[m_1]$ diagram for the Cape Survey stars. The symbols in this plot have the same meaning as in Figure 8.1. This diagram should be compared with Figure 8.5, a schematic m_1 - c_1 diagram of the position of the Ap SrCrEu stars.

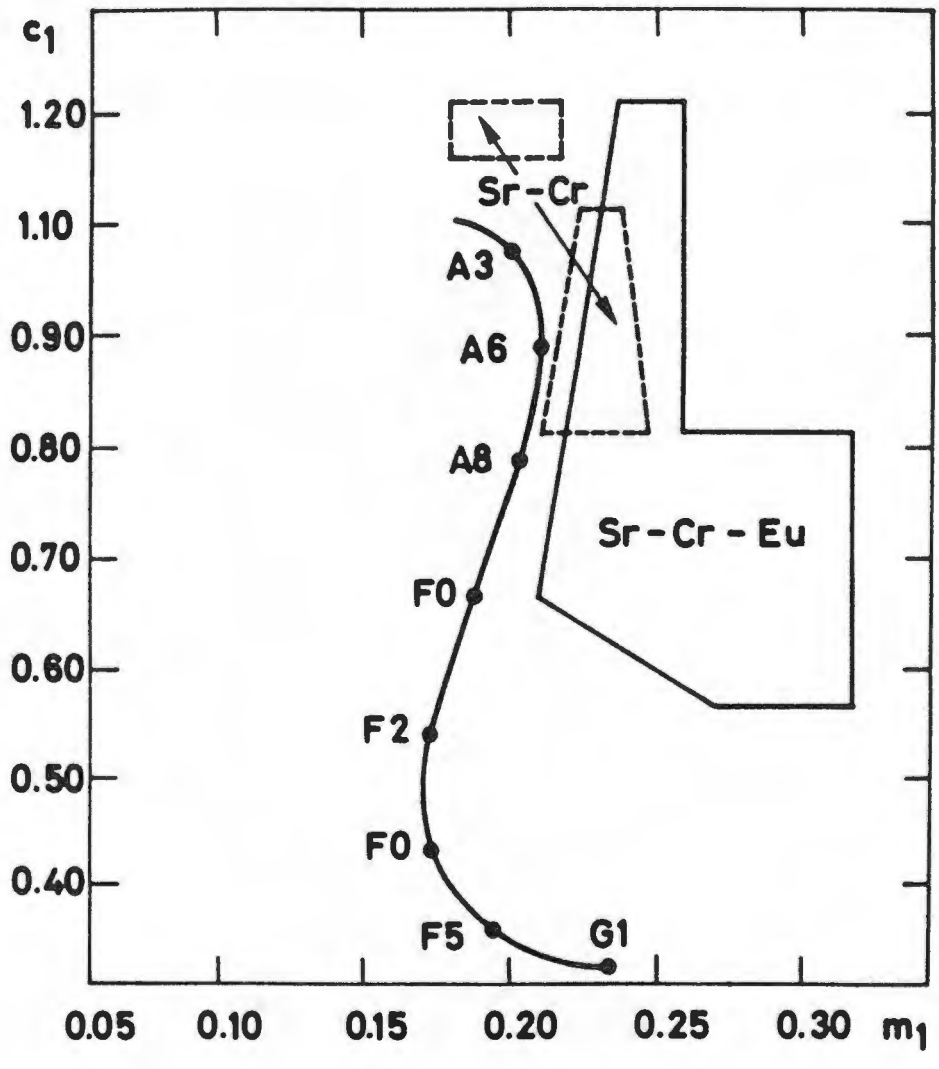

Figure 8.5 A schematic m_1 - c_1 diagram showing the region occupied by the Ap SrCrEu and SrCr stars. (Taken from Golay 1974.)

classes of Ap stars. Golay's diagram is reproduced here as Figure 8.5. The distribution of Ap SrCrEu stars in my $[m_1]$ - $[c_1]$ diagram is essentially in agreement with Golay's although it does extend closer to the bend in the ZAMS at around F0 - F5 than indicated in his schematic m_1 - c_1 diagram.

The known roAp stars are confined mostly to the lower right of the general distribution of stars. In a similar diagram presented by Matthews (1990) there was a dearth of SrCrEu stars to the left of the roAp stars (see his Fig. 4). Fig. 8.4 shows that the distribution of SrCrEu stars extends well to the left of the roAp stars. A curiosity about the positions of the roAp stars in Fig. 8.4 is that there seems to be a gap in $[c_1]$ values of the roAp stars for $0.6 < [c_1] < 0.7$. I could find no systematic differences in any observed photometric or asteroseismological quantity among roAp stars on either side of the gap. A search for rapid oscillations in 10 stars lying inside this "$[c_1]$ gap" yielded null results. Further work is required to establish whether this gap is a sampling artefact or whether it is astrophysically significant.

8.4 The δm_1 - δc_1 plane

An inspection of the δm_1 and δc_1 trends (Fig. 8.6) indicates that a correlation exists between these two indices in the sense that stars with higher δm_1 tend on average to have higher δc_1. Figure 8.6 also reiterates the fact that the roAp stars have negative δm_1 and δc_1 indices relative to Crawford's (1975, 1978, 1979) calibration. The distribution of roAp stars is fairly tight compared to the general distribution of SrCrEu stars. The observer searching for roAp stars may be tempted to restrict the search to stars with $\delta c_1 < 0.0$, but this would introduce a strong selection effect because the more luminous stars can have δc_1 indices that are positive in spite of the fact that they are depressed by line blanketing. One such star is HD 176232, which has $\delta c_1 = +0.031$; this is the one star lying above the standard main sequence relation in Fig 8.3

8.5 The $[c_1]$ - $[u-b]$ diagram

In the temperature range of the roAp stars the index $[u-b]$ is a luminosity indicator related to $[c_1]$ by the relation $[u-b] = [c_1] + 2[m_1]$. In the absence of blanketing, the $[c_1]$ and $[u-b]$ indices are about equally sensitive to the Balmer jump. To appreciate this intuitively, the reader may wish to consult Fig. 4.2, which is a schematic representation of the effects of line blanketing and the Balmer discontinuity on the intensity. Thus, to some extent, the $[c_1]$ - $[u-b]$ diagram indicates line blanketing differences independent of luminosity differences.

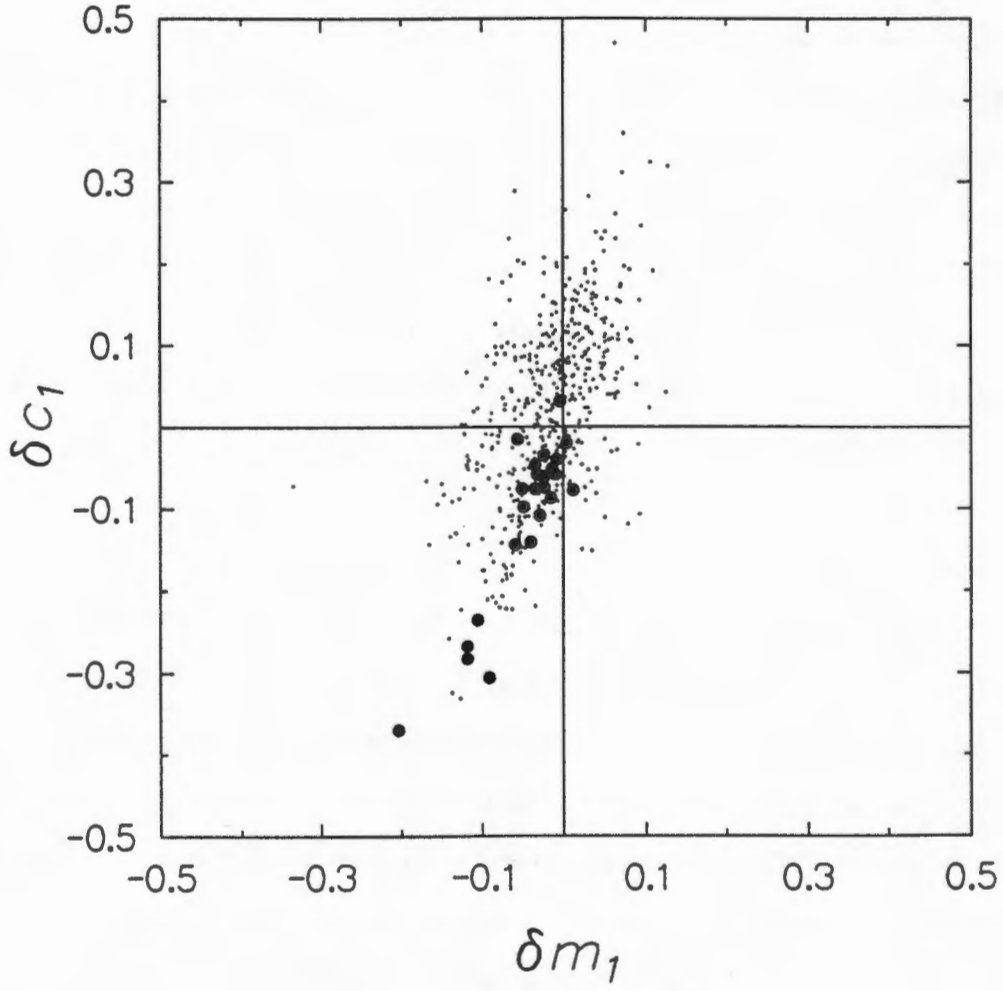

Figure 8.6 The relation between δc_1 and δm_1 for the Cape Survey stars. The filled circles represent the 25 known roAp stars

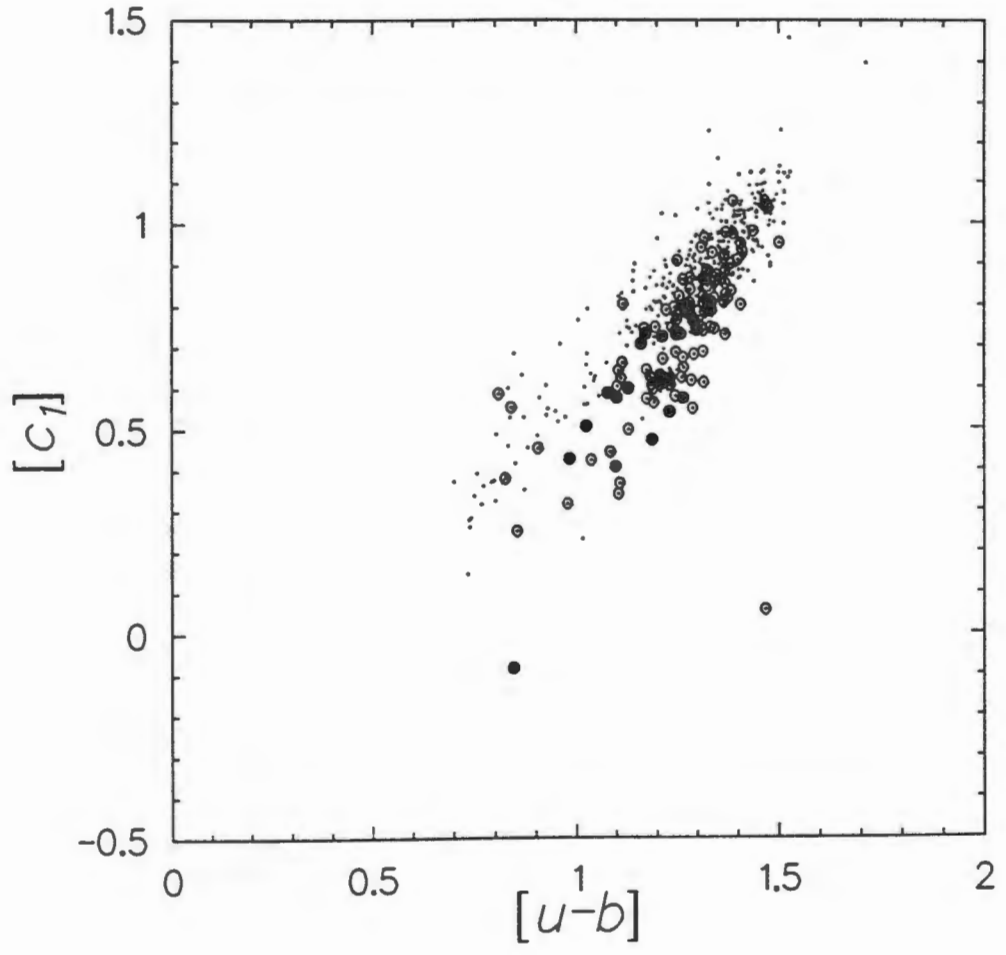

Figure 8.7 The relationship between $[c_1]$ and the luminosity parameter $[u\text{-}b]$ for the Cape Survey stars. The different symbols are explained in Fig. 8.1.

Matthews (1990) was the first to examine the positions of the roAp stars in the $[c_1]$ - $[u\text{-}b]$ diagram. His finding that the roAp stars seemed to be well separated from the general distribution of Ap SrCrEu stars prompted us to examine our stars in this diagram also. Figure 8.7 shows the $[c_1]$ - $[u\text{-}b]$ diagram for the Cape Survey stars. As expected, $[c_1]$ and $[u\text{-}b]$ are strongly correlated but the roAp stars form a tighter band than the general distribution of SrCrEu stars. This roAp band is confined to the lower half of the general distribution of SrCrEu stars. While most SrCrEu stars are concentrated towards the higher values of $[c_1]$ and $[u\text{-}b]$, the roAp stars tend towards the opposite end of the distribution. Evidently the roAp stars are among the more extremely peculiar SrCrEu stars so that the $[c_1]$ and $[u\text{-}b]$ indices are strongly depressed. What is clear from Fig. 8.7 is that the roAp stars are not as well separated from the general distribution of SrCrEu stars as appears to be the case in Fig. 1 of Matthews' paper. In his $[c_1]$ - $[u\text{-}b]$ diagram there are no SrCrEu stars below $[u\text{-}b] = 1.2$ whereas in Fig. 8.7 the SrCrEu stars extend down to $[u\text{-}b] = 0.7$. I conclude that the separation noticed by Matthews is an artefact of the small sample of SrCrEu stars he used.

In sections 8.2 & 8.4 we have shown the danger of using a negative δc_1 index as the sole criterion when selecting roAp star candidates. This is because this criterion introduces a selection effect against high-luminosity stars which have positive δc_1 indices. In the $[c_1]$ - $[u\text{-}b]$ plane such a bias does not arise. An example of a star which would be excluded by this bias is HD 176232, which has $\delta c_1 = +0.031$ and thus lies above the standard relation in the δc_1 - δm_1 and c_1 - β planes. Notice, though, that this star is not really well separated from the main band of roAp stars; if the standard relation were not drawn in Fig. 8.3, HD 176232 would not seem to be well separated from the rest of the roAp stars. In the $[c_1]$ - $[u\text{-}b]$ plane this star lies within the band defined by the other roAp stars.

8.6 The m_1 - β and $[m_1]$ - $[u\text{-}b]$ diagrams

For completeness, and for its entertainment value, we examine the metallicity index m_1 against the temperature indicator β and the luminosity indicator $[u\text{-}b]$. Figure 8.8 shows the m_1 - β diagram for the Cape Survey stars. This Figure should be contrasted with Fig. 4.7, which is a similar diagram showing the roAp stars known prior to the Cape Survey. The open circles show that the β - m_1 plane was well sampled in the search for new oscillators. The $[m_1]$ - $[u\text{-}b]$ diagram (Fig. 8.9) shows that the roAp stars (excluding HD 101065) are confined to $0.98 \leq [u\text{-}b] \leq 1.34$ and $0.22 \leq [m_1] \leq 0.36$.

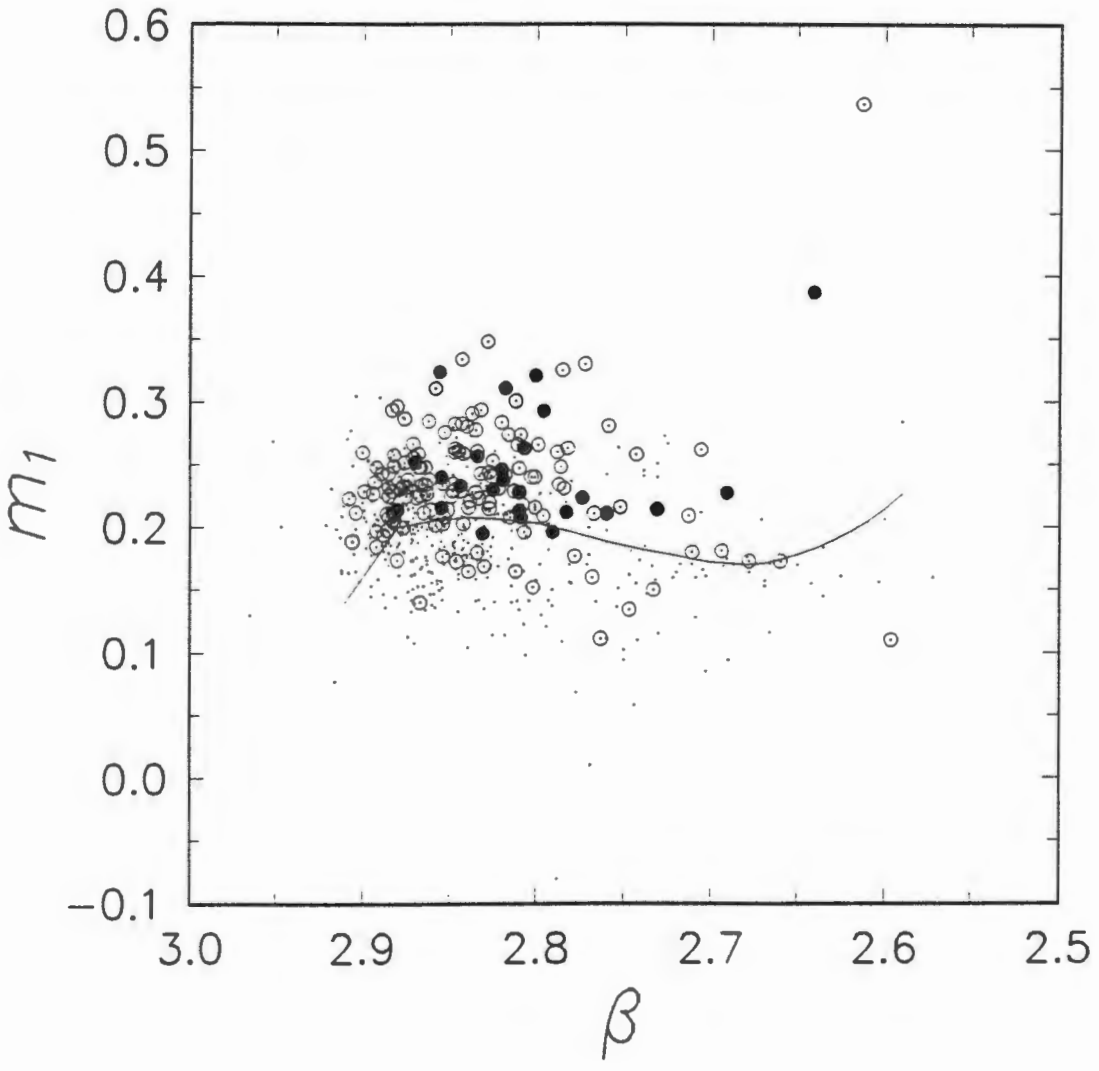

Figure 8.8 The relationship between the metallicity index m_1 and the effective temperature indicator β for the Cape Survey stars. The plot symbols are explained in Fig. 8.1. The line drawn is Crawford's standard main sequence relation for the A- and F- type stars.

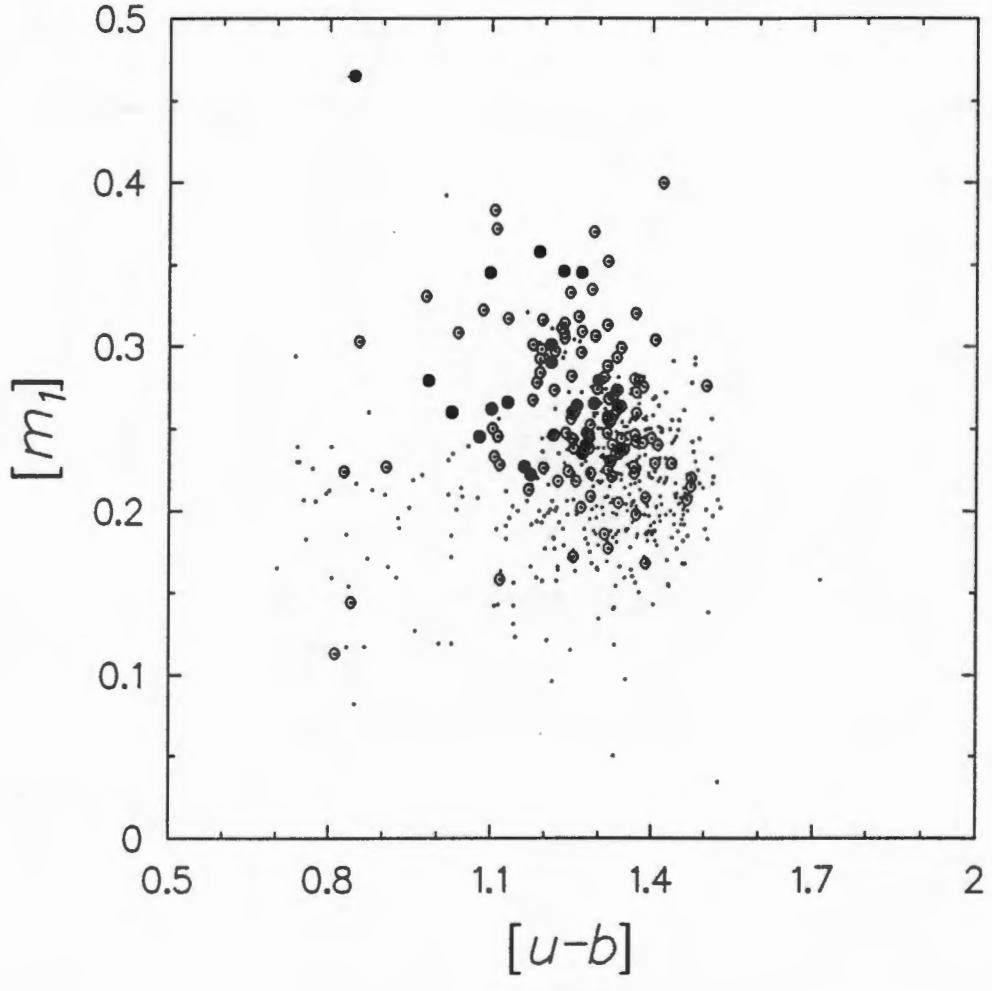

Figure 8.9 The relationship between the dereddened metallicity index $[m_1]$ and the luminosity index $[u-b]$ for the Cape Survey stars. Consult Fig. 8.1 for an explanation of the plot symbols.

8.7 The photometric limits of the roAp phenomenon

Having presented and discussed these diagrams, we are now in a position to list the photometric limits of the roAp phenomenon:

$$2.69 \leq \beta \leq 2.88$$

$$0.08 \leq b\text{-}y \leq 0.31$$

$$0.19 \leq m_1 \leq 0.33$$

$$-0.12 \leq \delta m_1 \leq 0.02$$

$$0.46 \leq c_1 \leq 0.88$$

$$-0.31 \leq \delta c_1 \leq 0.04$$

In terms of the dereddened parameters, the limits are:

$$0.22 \leq [m_1] \leq 0.36$$

$$0.40 \leq [c_1] \leq 0.87$$

$$0.98 \leq [u\text{-}b] \leq 1.34$$

These limits do not include Przybylski's star because it is an extreme outlier in most cases.

Chapter 9

The asteroseismology of the roAp stars

9.1 Introduction

We begin this chapter by presenting an atlas of amplitude spectra of the roAp stars. The atlas will serve as the basic reference for the rest of this chapter which discusses the results that have been obtained from the asteroseismology of the roAp stars. The first such result (section 9.3) is the determination of the asteroseismological luminosities of the roAp stars. The results of this luminosity determination lead to a discussion in section 9.4 of possible driving mechanisms for the roAp stars. In section 9.5 we discuss frequency changes due to evolution, binary motion, or other causes, and section 9.6 deals with pulsation mode changes and mode lifetimes. In section 9.7 we discuss the possibility of using the oscillations to probe the atmospheric structure of the roAp stars. The chapter ends with a discussion in section 9.8 on the estimation of the main sequence ages of the roAp stars and a comparison of data from our atlas with a theoretical oscillation HR diagram for the roAp stars.

9.2 An atlas of roAp star oscillation spectra

In this section we present an atlas of the oscillation spectra of the roAp stars. Fig. 9.1 is a series of schematic amplitude spectra for the roAp stars listed in order of HD number. The ordinate is scaled in units of mmag and the abscissa is scaled in units of mHz. Each pulsation frequency is represented by a vertical line. The point where the line crosses the frequency axis is the frequency of that mode and the length of the line is the amplitude of that mode. We will refer to these schematic lines as *peaks* for the purposes of this discussion; the origin of the term is clear and its use here creates no confusion. Some peaks are annotated with one of two symbols, an arrow or a question mark. An arrow pointing to a peak indicates that that peak has a harmonic at twice its frequency. A stippled arrow indicates that the presence of the harmonic requires confirmation. A question mark above a peak indicates that the identification of that frequency is insecure. In several stars the $(2\ell + 1)$ frequency splitting caused by oblique rotation is seen. This rotational splitting is denoted by the Ω symbol and the rotation frequency is usually listed alongside it in units of μHz. Other frequency spacings of interest are also indicated in the atlas. In all cases frequency spacings are given in units of

μHz. The frequencies depicted in each panel of Fig. 9.1 are tabulated below the panel with a reference to the most recent frequency analysis available for that star. Frequencies in parentheses are insecure and require confirmation. For cross-referencing purposes, the schematic amplitude spectra are all collectively referred to as Fig. 9.1 and the frequencies tabulated under these amplitude spectra are all collectively referred to as Table 9.1.

9.3 Asteroseismological luminosities of the roAp stars

The luminosities of the roAp stars are not well known because the normal photometric calibrations of temperature and luminosity are not valid for the heavily blanketed flux distributions in the cool Ap stars. The deviation from the standard relation for normal stars is most pronounced in stars with extreme abundance anomalies and in the cooler Ap stars. We saw in chapter 4 how a naive application of the δc_1 index implies that the roAp stars are well below the ZAMS (*e.g.* see Fig. 8.3), a result not confirmed for two roAp stars with parallax luminosities (α Cir = HD 128898 and γ Equ = HD 201601).

Fortunately, asteroseismology permits determinations of the luminosities of those roAp stars in which several modes are observed. Recall from chapter 2 that the asymptotic frequency spacing for a star undergoing high-overtone p-mode pulsation is given by the Tassoul (1990) relation

$$\nu_{n\ell} = \Delta\nu(n + \ell/2 + \epsilon) + \delta\nu$$

where ϵ is a constant dependant on the surface layers of the star and $\delta\nu$ is a second-order term $<<$ $\Delta\nu$. To first order, the Tassoul relation is degenerate for modes (n,ℓ) and $(n+1,\ell\text{-}2)$ in the sense that a mode (n,ℓ) has the same frequency as a mode $(n+1,\ell\text{-}2)$. The second-order term, $\delta\nu$, lifts this degeneracy as described in chapter 2 and is a measure of the sound speed gradient inside the core, essentially an age indicator. The first-order frequency spacing $\Delta\nu$ is the frequency spacing of consecutive overtones for the p-modes. This corresponds to the reciprocal of the sound crossing time of the star. Given a long enough time span of observations, both these frequency spacings can be observed.

Heller and Kawaler (1988), Shibahashi & Saio (1985) and Gabriel *et al.* (1985) have computed series of A star models which show how $\Delta\nu$ varies with age. Given a knowledge of T_{eff}, one should be able to derive asteroseismological luminosities for the roAp stars using these models. As an exercise, I used the observed frequency spacings and T_{eff} estimated from the photometry to derive tentative luminosities for the roAp stars (Table 9.2). The Hβ index was used to estimate T_{eff} using

Table 9.1 and Figure 9.1

An atlas of roAp star oscillation spectra

Table 9.1

Oscillation frequencies and amplitudes of HD 6532

(Kurtz and Cropper MNRAS 228, 125, 1987)

ν (mHz)	A (mmag)
(2.378678)	(0.18)
2.396215	0.98
2.402165	0.73
2.408120	0.59
(2.425649)	(0.14)
2.804299	0.11

Notes: Further studies of the distorted dipole of this star are highly desirable. The rotation period is close to 2 days, so a multi-site study is required.

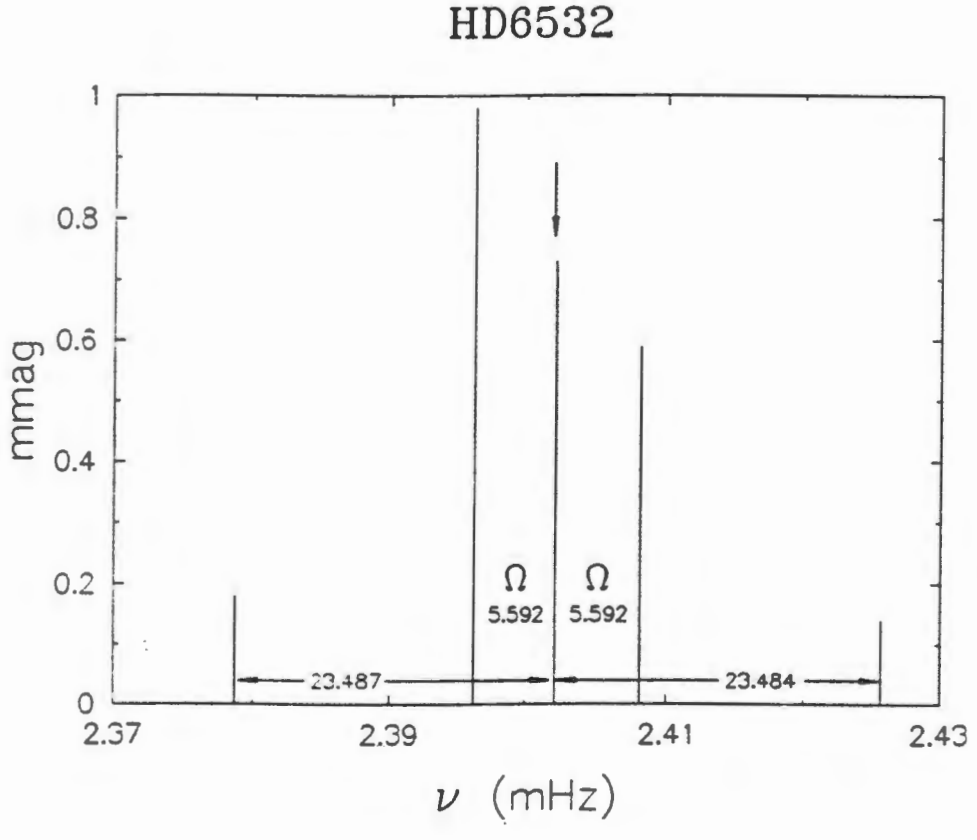

Table 9.1 (cont'd)

Oscillation frequencies and amplitudes of HD 12932

(Martinez and Kurtz - unpublished)

ν (mHz)	A (mmag)
1.43630	2.282

Notes: At V = 10.2 this star could benefit from studies with telescope of aperture ≥ 1.5 m to improve photon statistics.

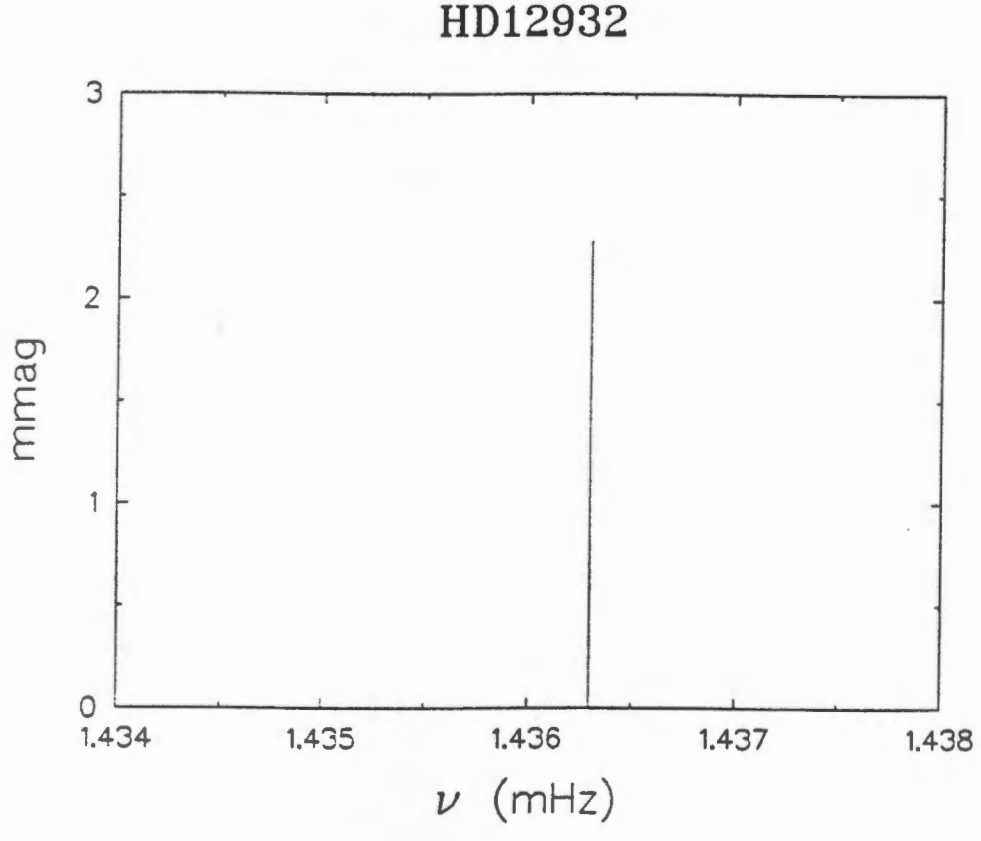

Table 9.1 (cont'd)

Oscillation frequencies and amplitudes of HD 19918

(Martinez and Kurtz - in preparation)

ν (mHz)	A (mmag)
1.5101	1.275
3.0200	0.305

Notes: New Cape Survey roAp star. An intensive exploratory study from a single site is required.

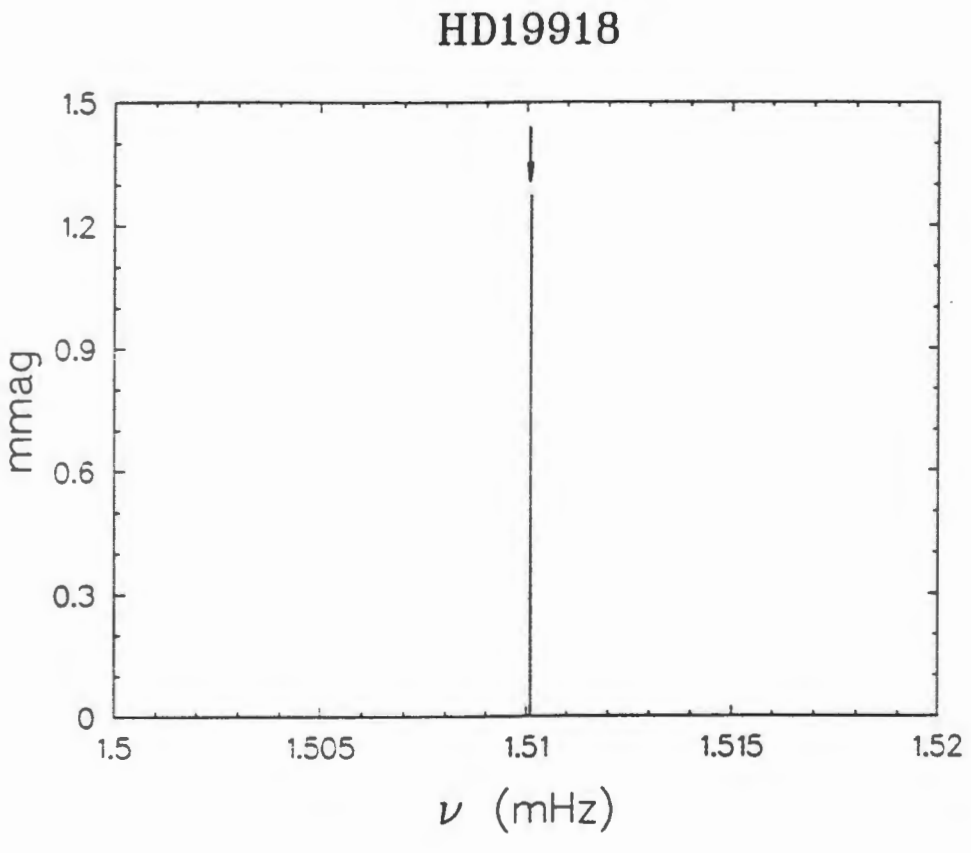

Table 9.1 (cont'd)

Oscillation frequencies and amplitudes of HD 24712

(Kurtz *et al.* - MNRAS, 240, 881, 1989)

ν (mHz)	A (mmag)
2.61965	0.193
2.65201	0.343
2.65294	0.770
2.65387	0.183
2.68667	0.442
2.68760	1.046
2.68853	0.418
2.71992	0.156
2.72085	0.818
2.72178	0.266
2.75476	0.170
2.75569	0.288
2.75662	0.176
2.80568	0.160
2.80661	0.148

Notes: Further progress in our understanding of this star will require an intensive 3-week multi-site campaign.

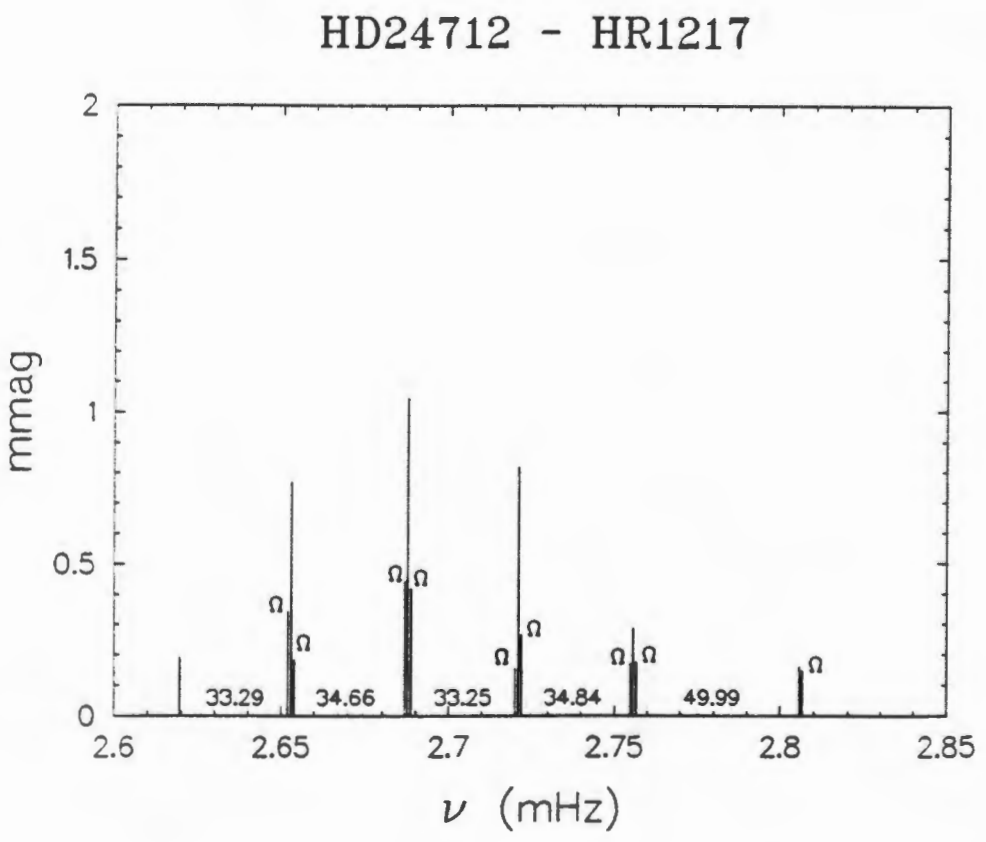

Table 9.1 (cont'd)

Oscillation frequencies and amplitudes of HD 42659

(Martinez, Kurtz & Ashley 1993, IBVS #3844)

ν (mHz)	A (mmag)
1.72	0.75

Notes: New Cape Survey roAp star. An intensive exploratory study from a single site is required. Telescopes of aperture ≥ 1.0 m should be used.

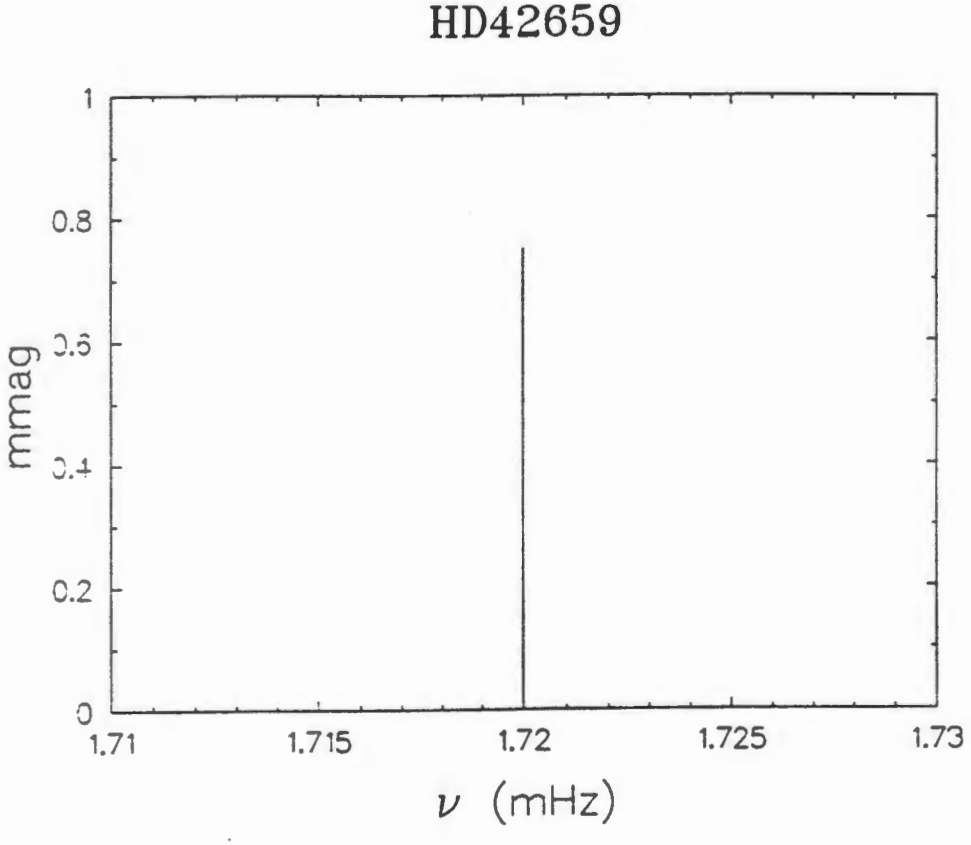

Table 9.1 (cont'd)

Oscillation frequencies and amplitudes of HD 60435

(Matthews *et al.* 1987, ApJ 313, 782)

ν (mHz)	A (mmag)
0.7090	
0.7614	
0.8428	
0.9397	
0.9906	
1.0433	
1.0990	
1.1482	
1.1734	
1.2250	
1.2848	
1.3281	
1.3525	
1.3810	
1.4073	
1.4334	
1.4572	

Notes: No amplitudes are listed because the amplitudes are strongly modulated from night to night. The 4 mHz oscillations studied by Matthews *et al.* are a telescope artefact and are not listed here.

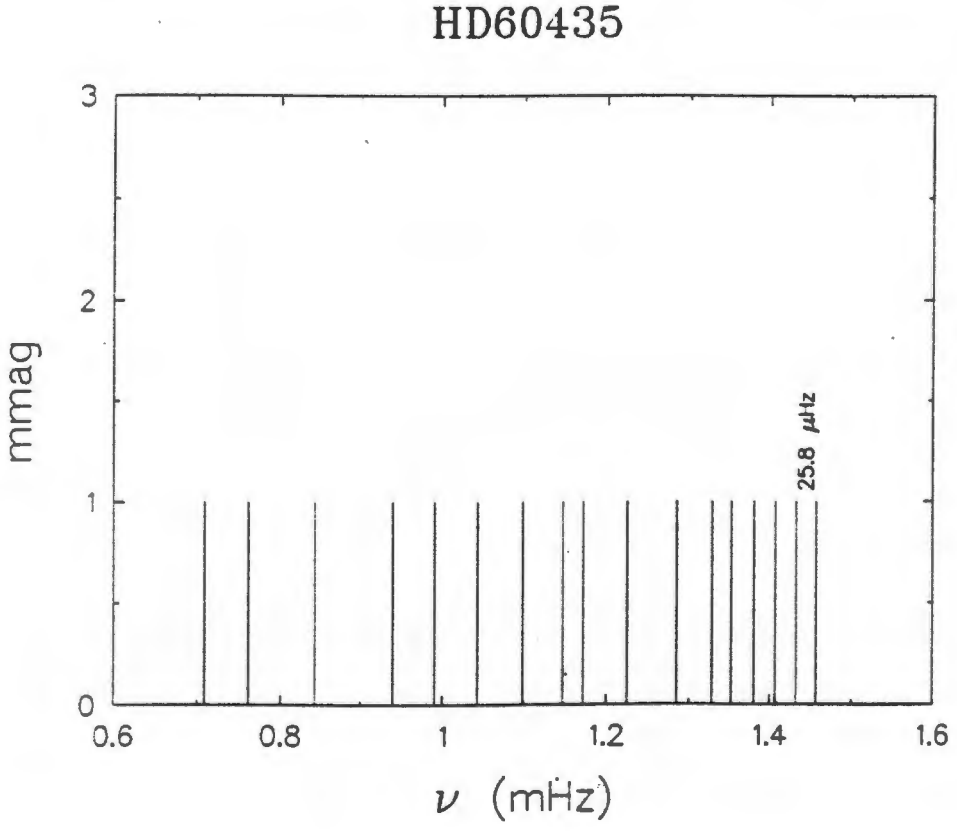

Table 9.1 (cont'd)

Oscillation frequencies and amplitudes of HD 80316

(Kurtz 1990, MNRAS, 242, 489)

ν (mHz)	A (mmag)
(2.2460)	(0.40)
2.2516	0.44
(2.2572)	(0.21)

Notes: This star appears to be a dipole pulsator. It is of interest to determine whether it has a distorted dipole mode like HD 83368 and HD 6532. The rotation period is near 2 days, so a multi-site study

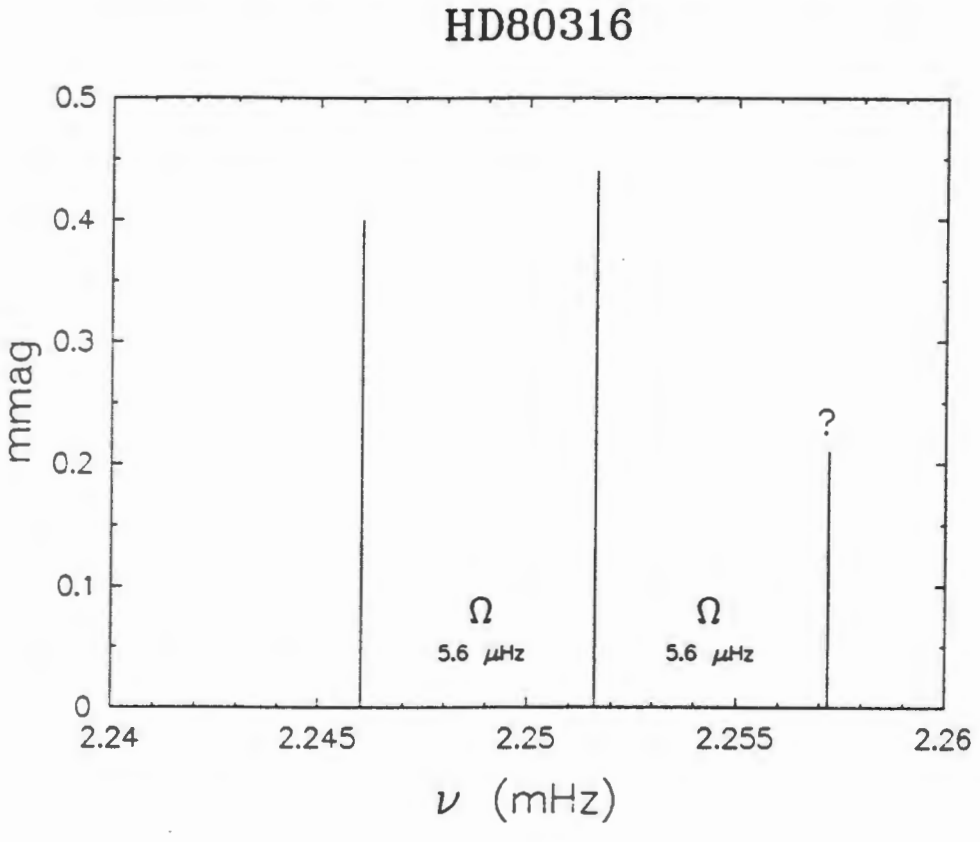

Table 9.1 (cont'd)

Oscillation frequencies and amplitudes of HD 83368

(Kurtz, Shibahashi & Goode, 1990 MNRAS 247, 558)
(Kurtz, Kanaan & Martinez, 1993 MNRAS 260, 343)

ν (mHz)	A (mmag)
1.42395445	2.09
1.42801257	0.40
1.43207097	1.71
2.84790845	0.19
2.85602534	0.42
2.86414166	0.19
4.28809652	0.10

Notes: This star is already the subject of intensive ongoing scrutiny to study its distorted dipole pulsation. Any additional high quality observations are useful.

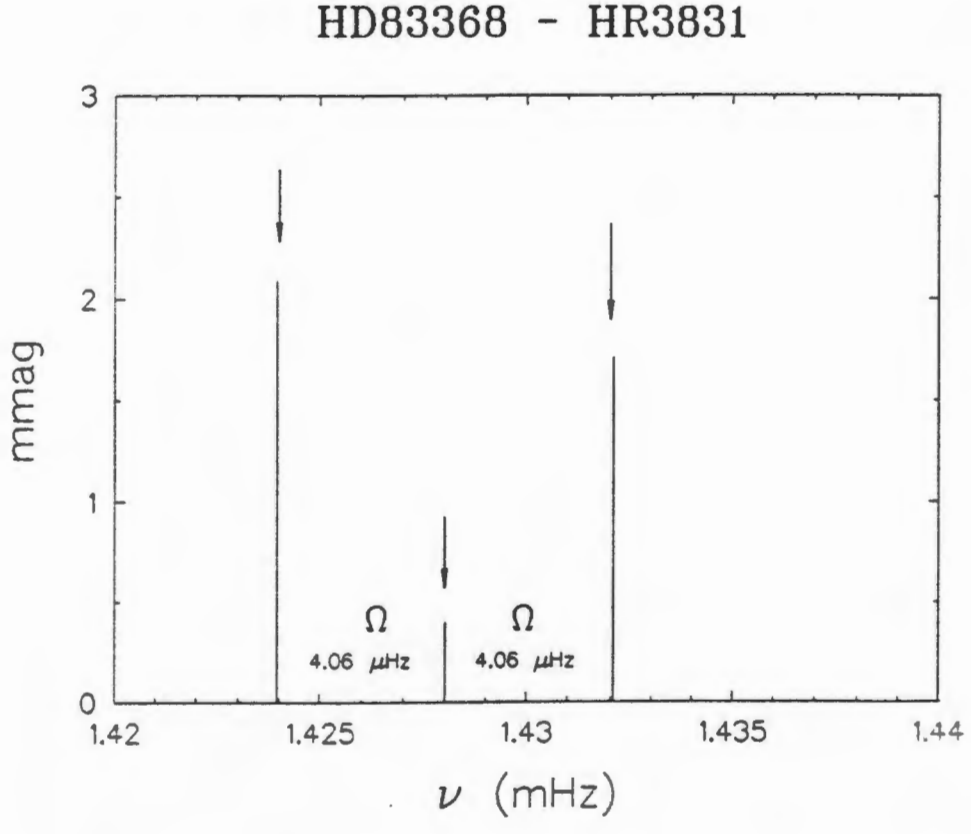

Table 9.1 (cont'd)

Oscillation frequencies and amplitudes of HD 84041

(Martinez *et al.* 1993, MNRAS, in press)

ν (mHz)	A (mmag)
1.0842	0.80
1.1137	1.37
1.1199	0.95
1.1468	0.78

Notes: The structure of this star's amplitude spectrum changes on a time-scale of days. A multi-site study using telescopes of aperture ≥ 1 m is required.

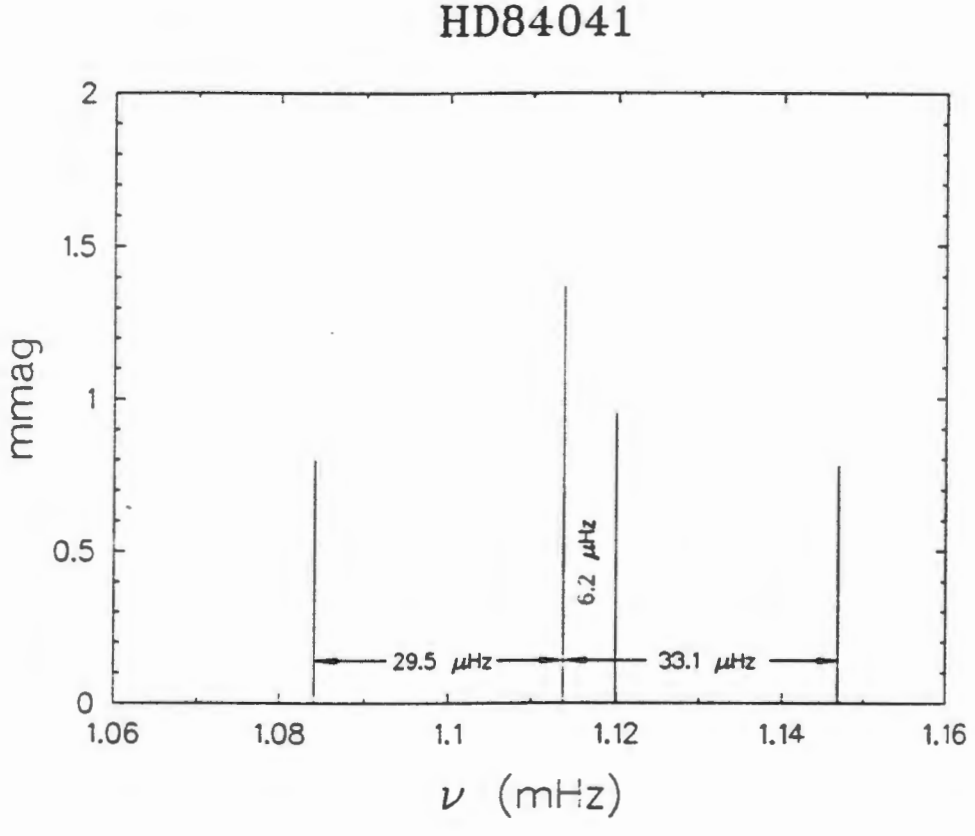

Table 9.1 (cont'd)

Oscillation frequencies and amplitudes of HD 101065

(Martinez and Kurtz 1990, MNRAS 242, 636)

ν (mHz)	A (mmag)
1.3150340	0.62
1.3699260	0.90
1.3728660	4.50
2.7457355	0.18

Notes: A campaign to monitor the phase of the principal frequency is desirable. To split the two pulsation modes separated by 58 μHz requires a full night of observations. Observations one full night per week over a season would suffice.

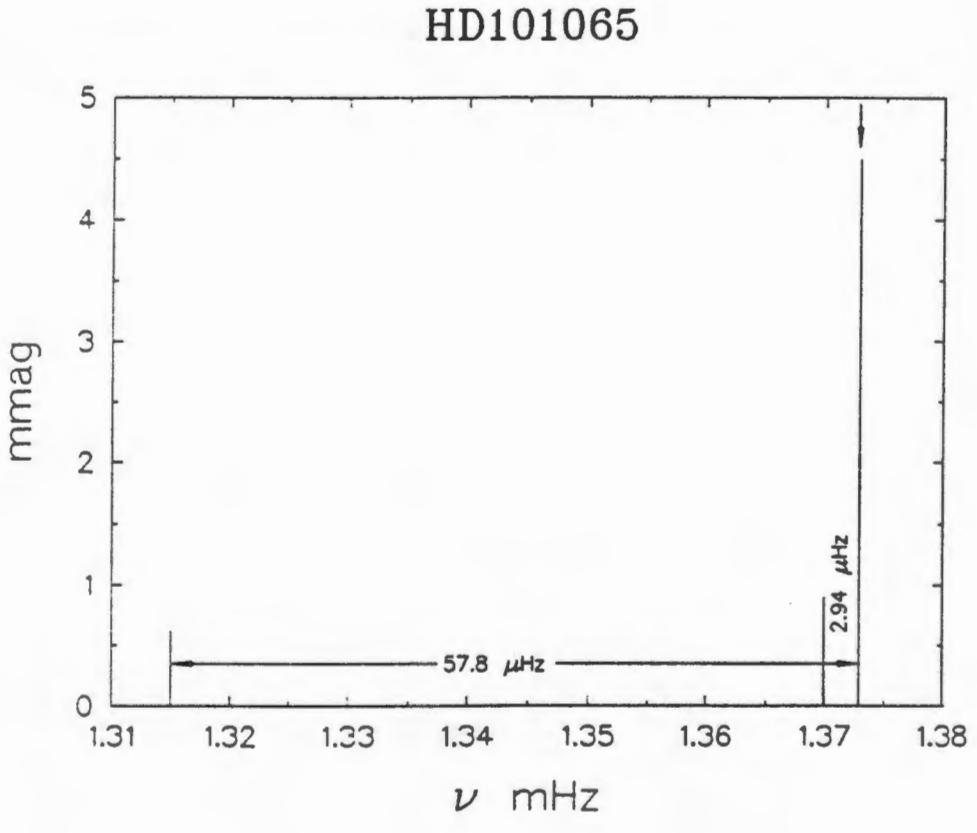

Table 9.1 (cont'd)

Oscillation frequencies and amplitudes of HD 119027

(Martinez *et al.* 1993, MNRAS, 260, 9)

ν (mHz)	A (mmag)
1.83534	0.30
1.86098	0.23
1.88757	0.56
1.91365	0.87
1.94022	0.69
1.94219	0.40

Notes: This star is obviously of asteroseismological interest. A multi-site study is highly desirable.

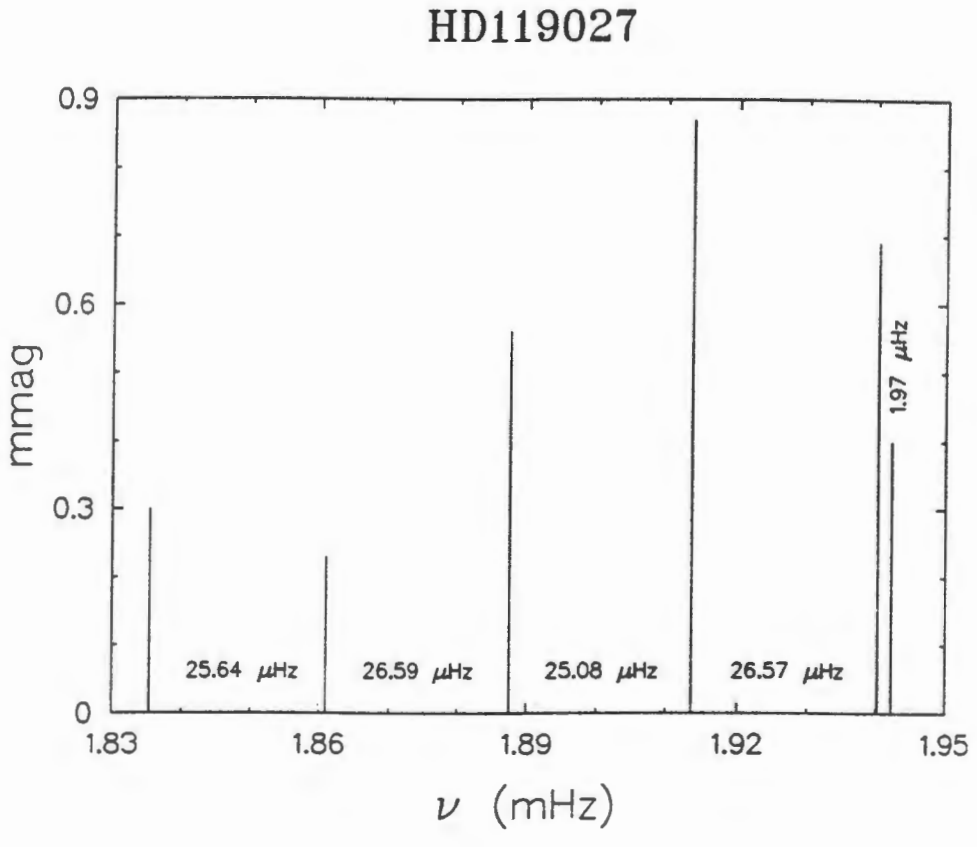

Table 9.1 (cont'd)

Oscillation frequencies and amplitudes of HD 128898

(Kurtz *et al.* in preparation)

ν (mHz)	A (mmag)
2.2654283	0.14
2.3417913	0.16
2.3669447	0.14
2.4394034	0.24
2.4419999	2.55
2.4445900	0.29
2.5664893	0.12
4.8840105	0.19

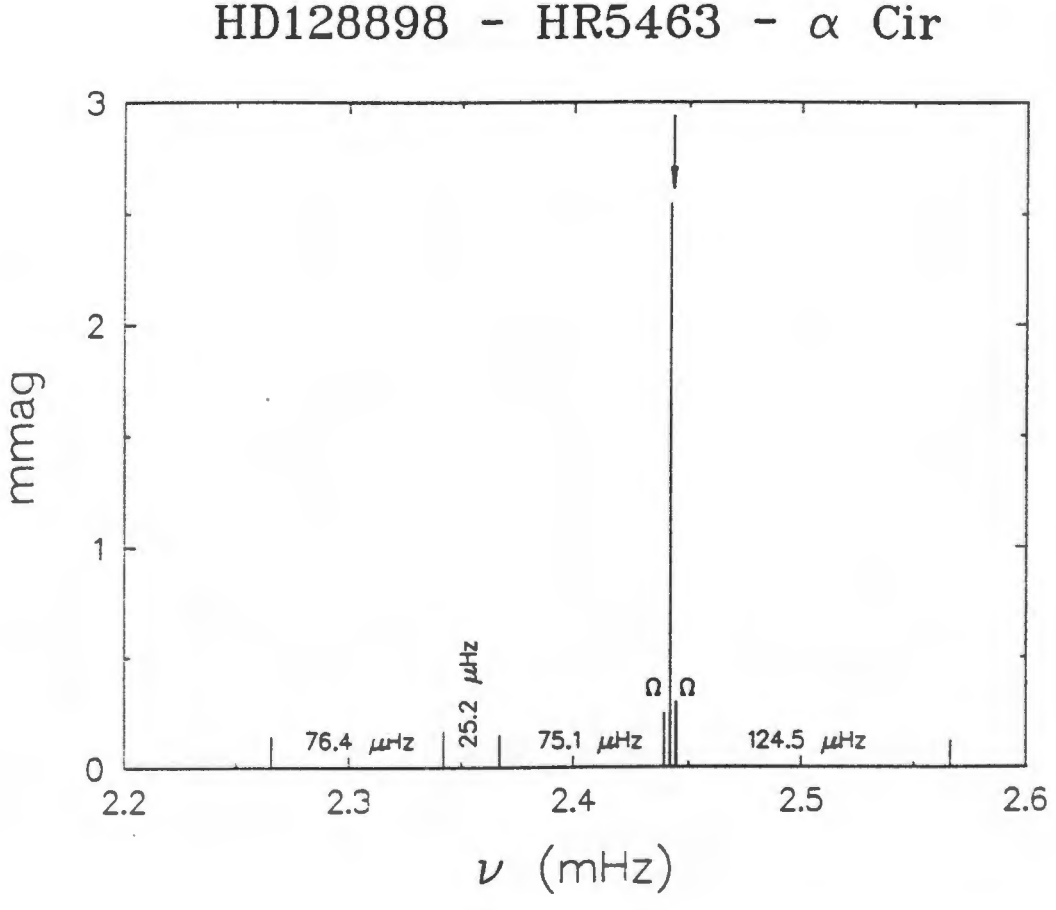

Table 9.1 (cont'd)

Oscillation frequencies and amplitudes of HD 134214

(Kurtz *et al.* 1991 MN 251, 152)

ν (mHz)	A (mmag)
2.949574	3.37

Notes: The single frequency in this star can be used to monitor the phase behaviour and the rate of frequency change. A one-hour light curve once per week during a season would suffice to monitor the phase stability.

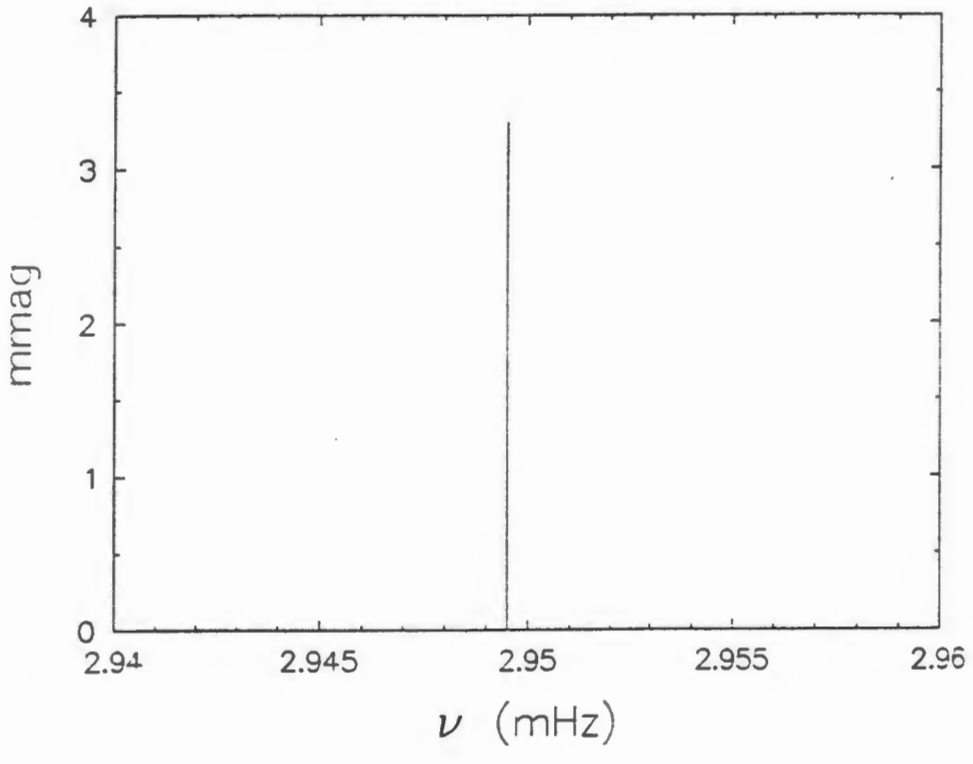

Table 9.1 (cont'd)

Oscillation frequencies and amplitudes of HD 137949

(Kurtz *et al.* 1991 MN 249, 468)

ν (mHz)	A (mmag)
(1.97521)	(0.15)
2.014781	1.50
4.029559	0.18

Notes: Large change of frequency from 1981 to 1987. $\nu(1987) - \nu(1981) = -.04$ nHz gives d(lnP)/dt two orders of magnitude larger than expected from evolutionary models.

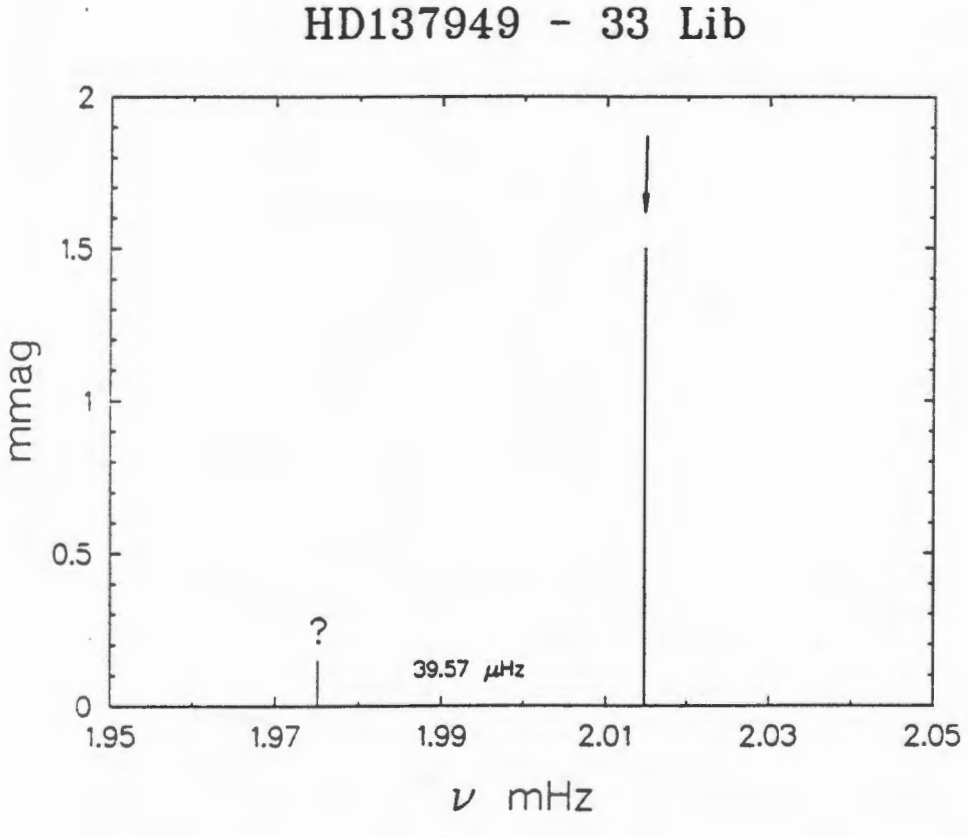

Table 9.1 (cont'd)

Oscillation frequencies and amplitudes of HD 150562

(Martinez 1992, IBVS #3750)

ν (mHz)	A (mmag)
1.55	~0.75

Notes: New Cape Survey roAp star. An intensive exploratory study from a single site is required.

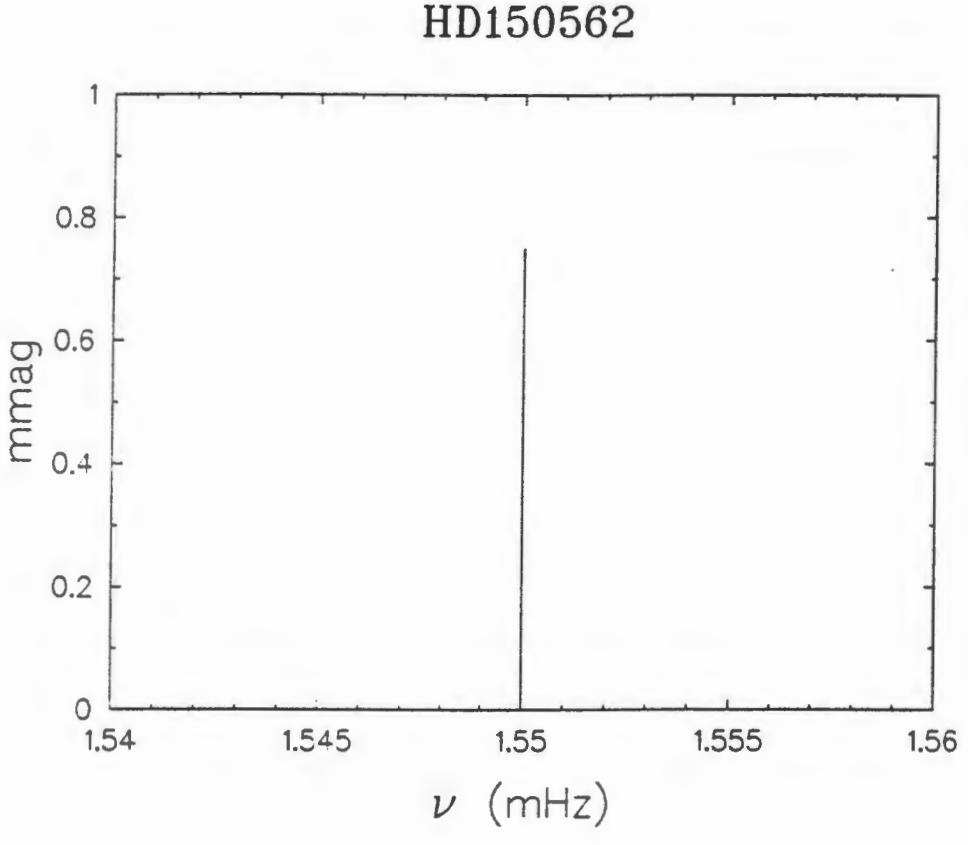

Table 9.1 (cont'd)

Oscillation frequencies and amplitudes of HD 161459

(Martinez *et al.* 1991, MNRAS, 250, 666)

ν (mHz)	A (mmag)
1.39	~1.0

Notes: New Cape Survey roAp star. An intensive exploratory study from a single site is required.

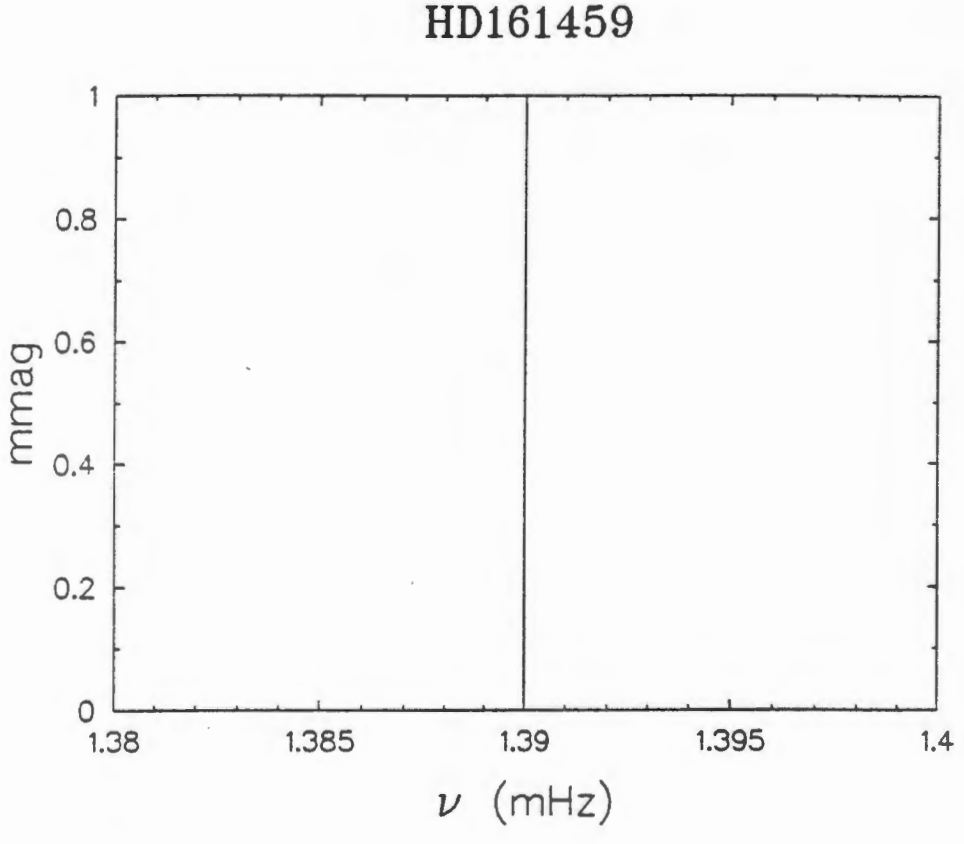

Table 9.1 (cont'd)

Oscillation frequencies and amplitudes of HD 166473

(Kurtz & Martinez 1987 MN 226 187)

ν (mHz)	A (mmag)
1.823890	0.27
1.891944	0.49
1.928169	0.25

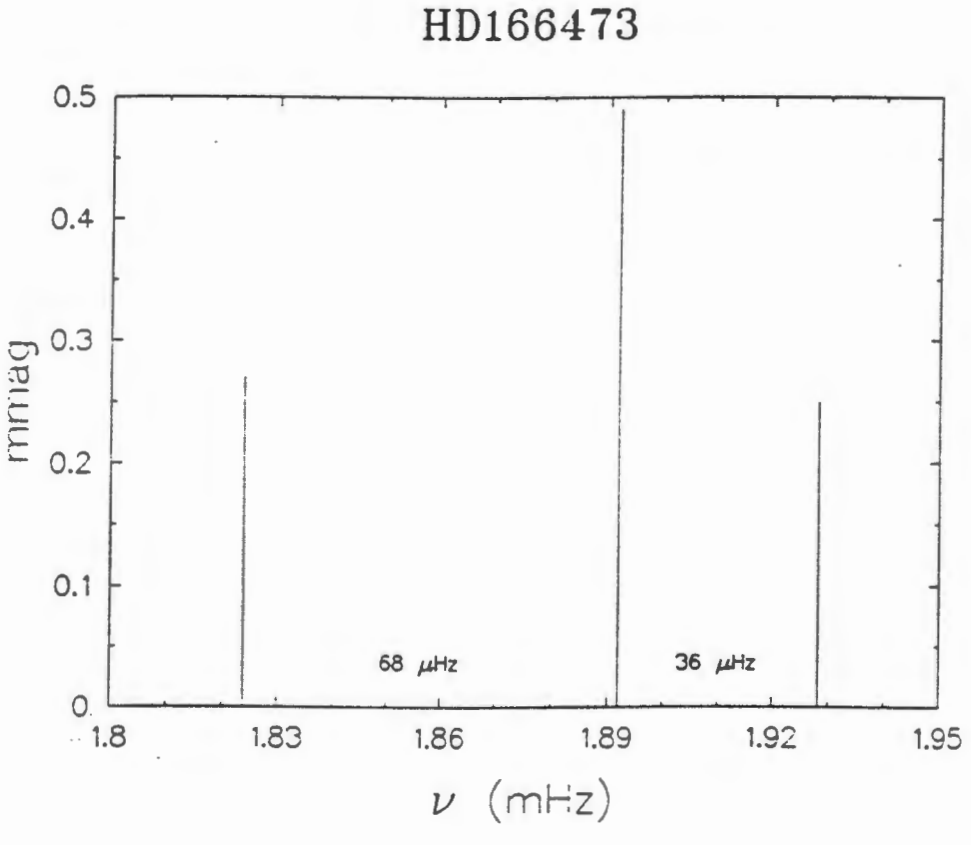

Table 9.1 (cont'd)

Oscillation frequencies and amplitudes of HD 176232

(Heller & Kramer 1990, MNRAS, 244, 372)

ν (mHz)	A (mmag)
1.239261	0.28
1.385373	0.33
1.435996	0.44

Notes: The relatively long periods and low amplitudes make this a difficult star to work on. Confirmation of the frequency spacings is desirable.

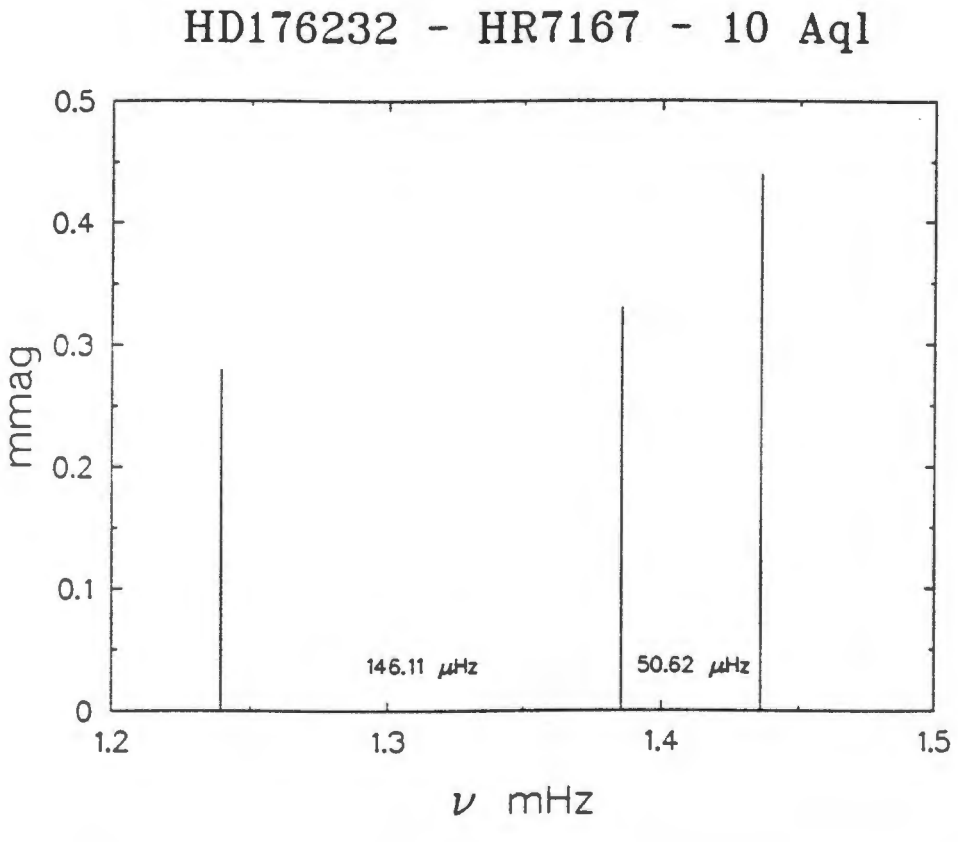

Table 9.1 (cont'd)

Oscillation frequencies and amplitudes of
HD 190290

(Martinez and Kurtz - unpublished)

ν (mHz)	A (mmag)
2.246	0.46
2.275	1.24

Notes: This star is obviously of asteroseismological interest. At δ = -79°, this austral winter season object can be observed for very long times. The extreme southern declination means that this star is a high-airmass object, however, and difficult to work on.

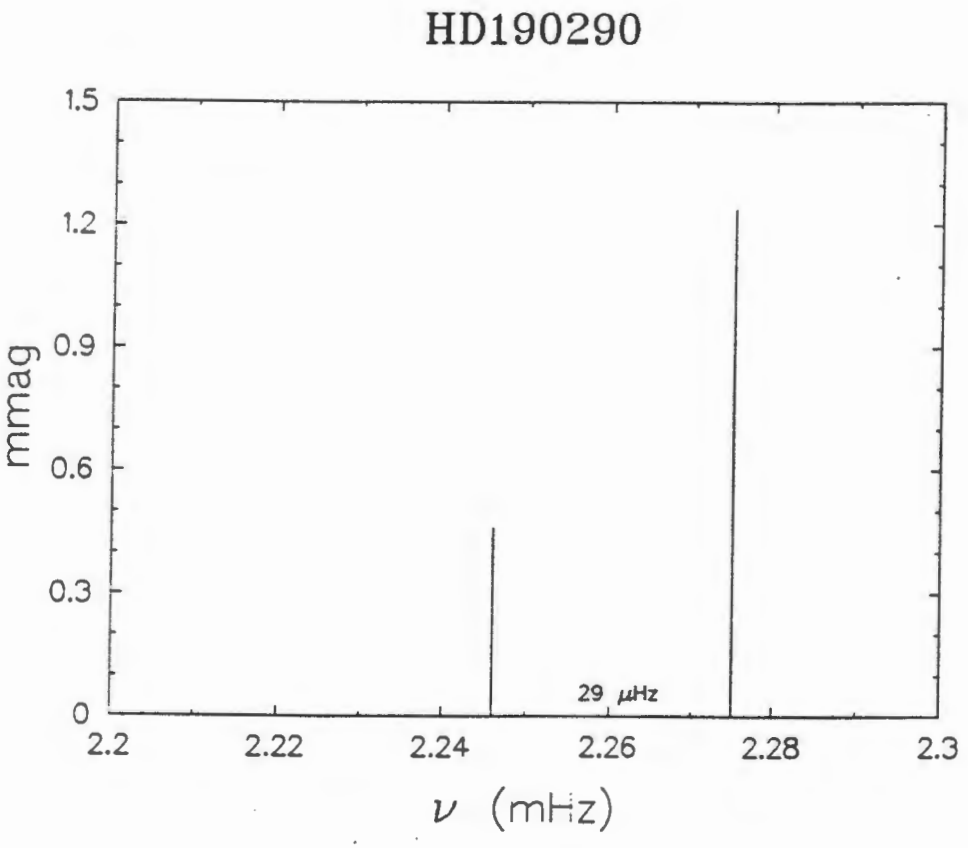

Table 9.1 (cont'd)

Oscillation frequencies and amplitudes of HD 193756

(Martinez *et al.* 1991, MNRAS, 250, 666)

ν (mHz)	A (mmag)
1.284	0.9

Notes: New Cape Survey roAp star. An intensive exploratory study from a single site is required.

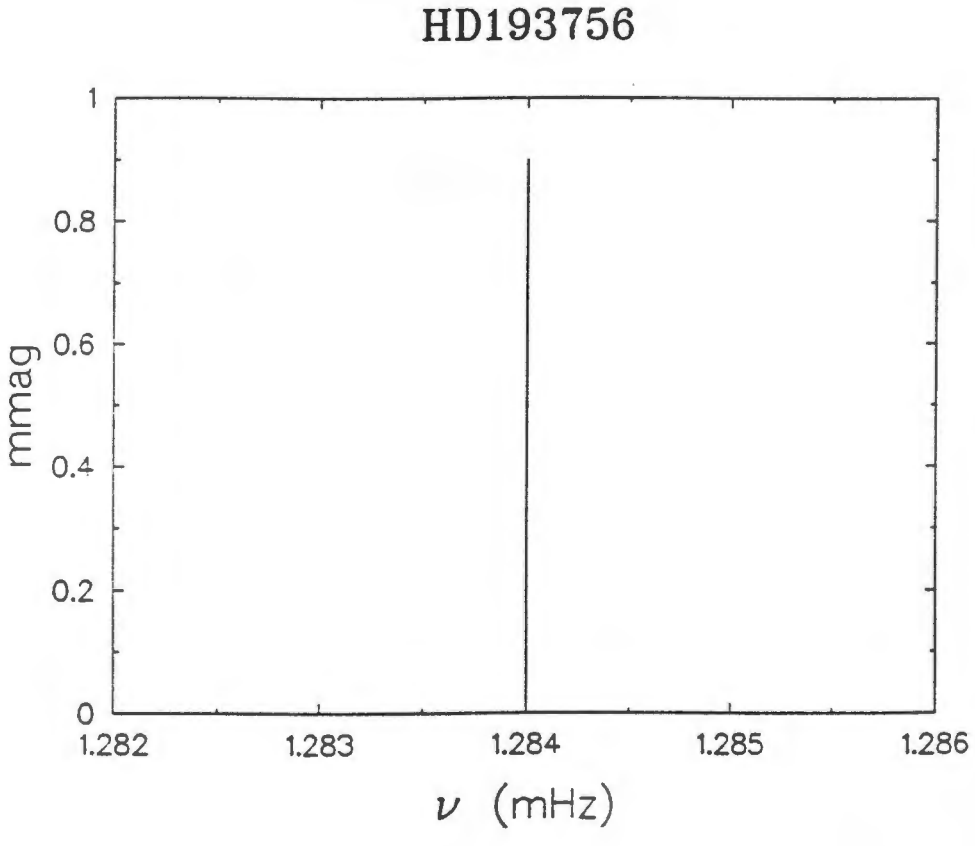

Table 9.1 (cont'd)

Oscillation frequencies and amplitudes of HD 196470

(Martinez *et al.*, 1991, MNRAS, 250, 666)

ν (mHz)	A (mmag)
1.544	≈0.7

Notes: New Cape Survey roAp star. An intensive exploratory study from a single site is required. At δ = -18°, this star is also accessible to northern observers.

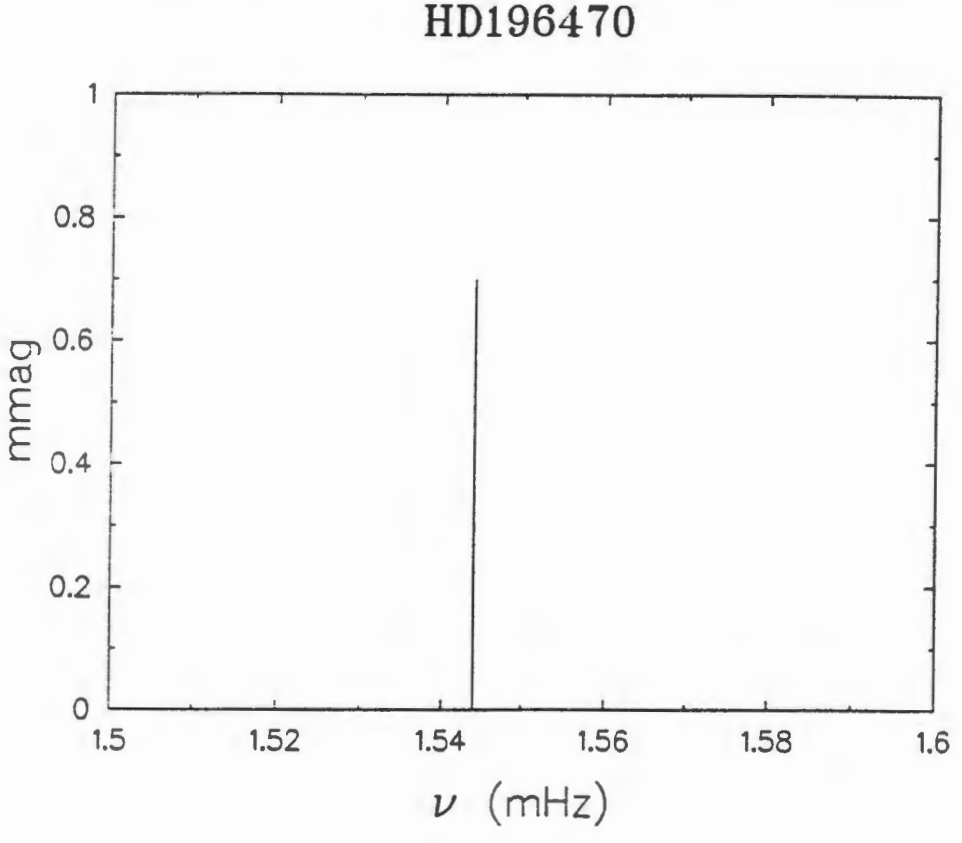

Table 9.1 (cont'd)

Oscillation frequencies and amplitudes of HD 201601

(Kurtz, 1983, MNRAS, 202, 1)
(Libbrecht, 1988, ApJ, 330, L51)

ν (mHz)	A (mmag)
1.339	0.88
1.366	0.25
1.427	0.25

Notes: A thorough study is required. At δ = +10°, this star can be observed from both hemispheres.

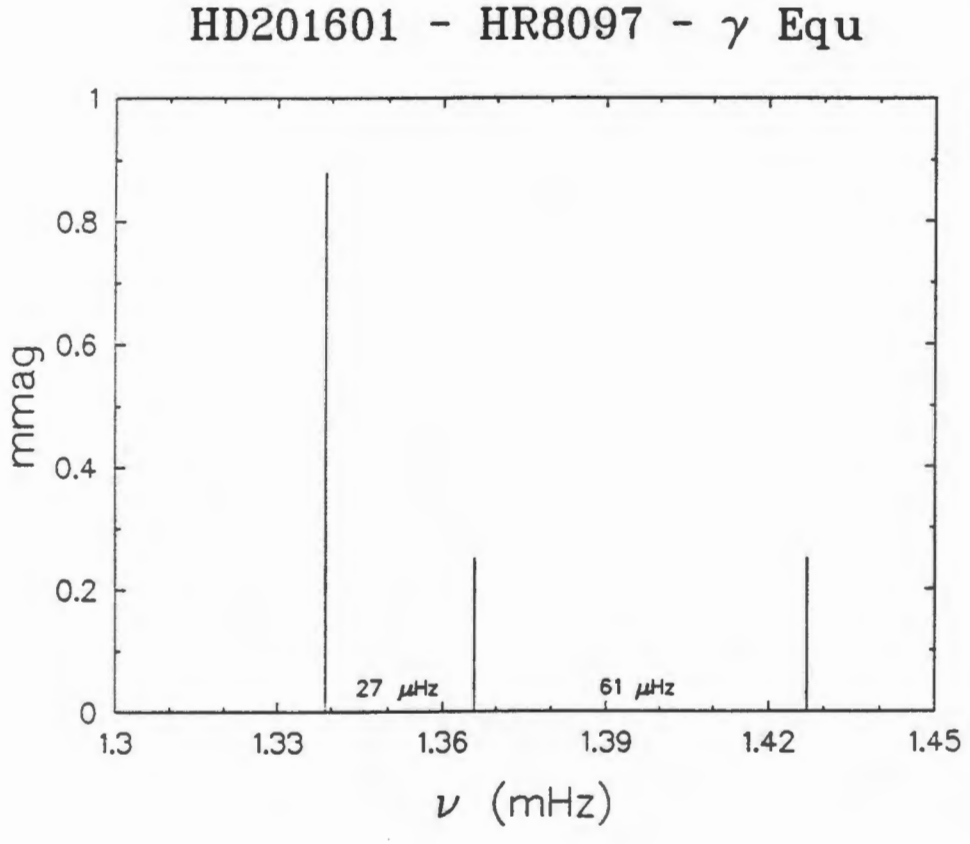

Table 9.1 (cont'd)

Oscillation frequencies and amplitudes of HD 203932

(Martinez *et al.* 1990, MNRAS, 246, 699)

ν (mHz)	A (mmag)
2.7373	0.15
2.7723	0.17
2.804774	0.64
2.8380	0.17

Notes: The amplitude spectrum of this star is non-stationary on a time-scale of days. A further multi-site study is desirable.

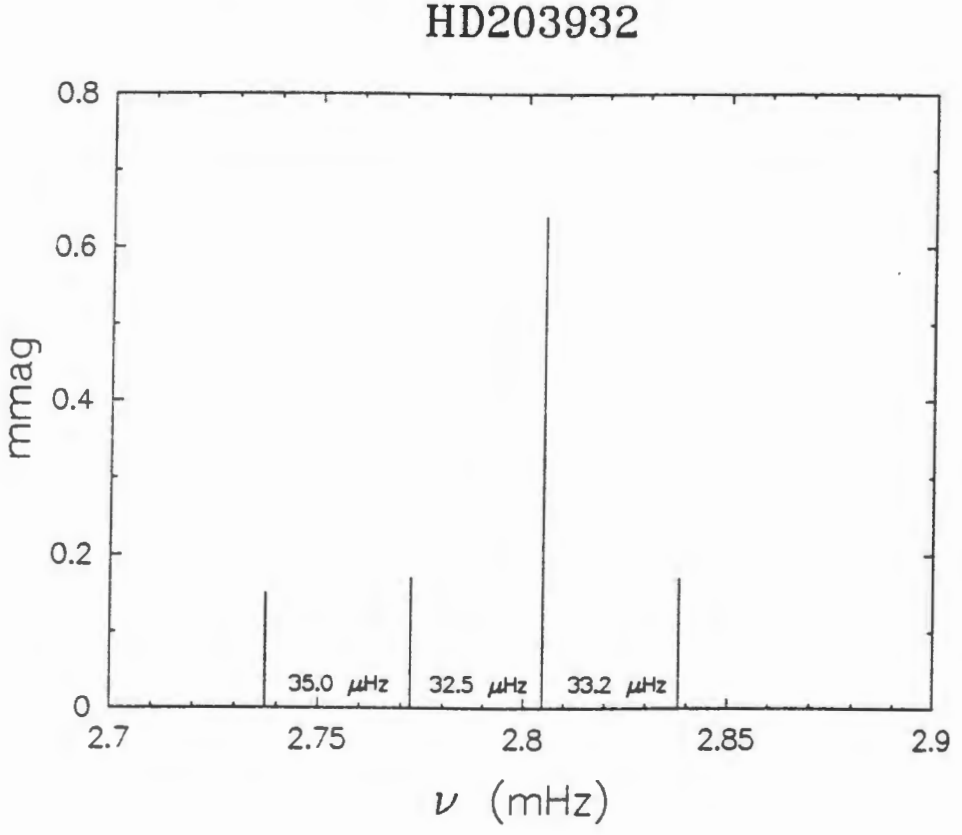

Table 9.1 (cont'd)

Oscillation frequencies and amplitudes of HD 217522

(Kreidl *et al.* 1991, MNRAS, 250, 477)

ν (mHz)	A (mmag)
1.1999	2.26
1.21529	2.14
2.0174	1.02

Notes: Evidence for mode switching. $\nu(1982) - \nu(1989) = 15.4 \pm 0.1$ μHz

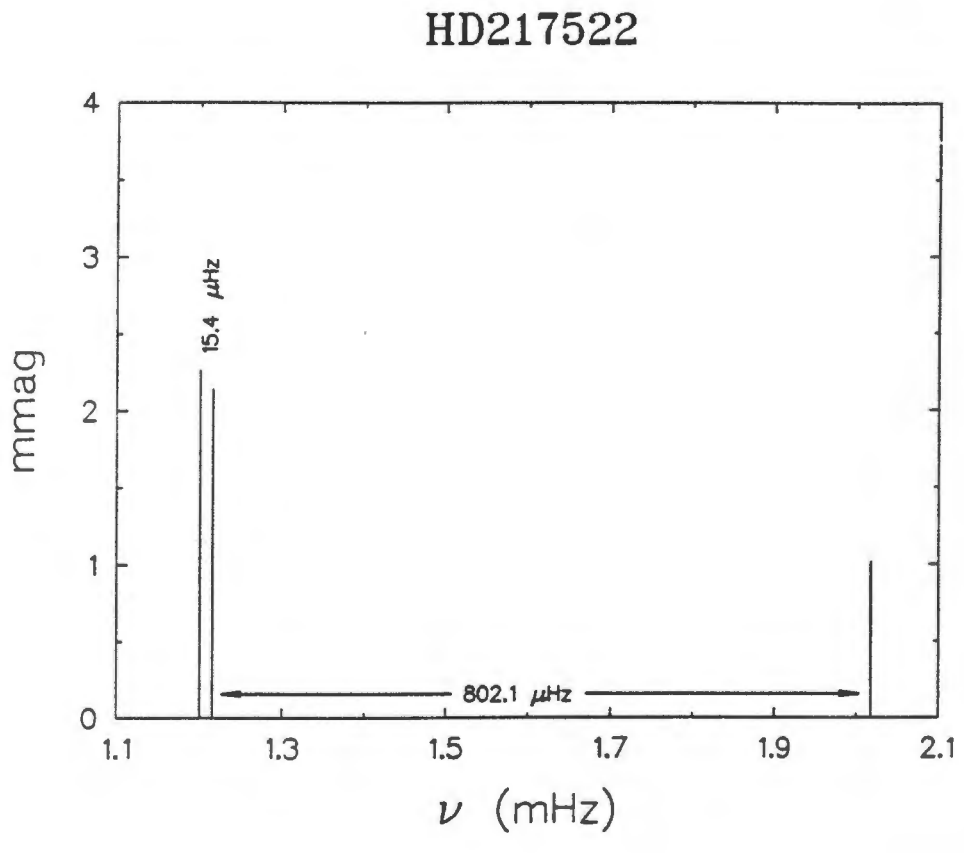

Table 9.1 (cont'd)

Oscillation frequencies and amplitudes of HD 218495

(Martinez *et al.* 1991, MNRAS, 250, 666)

ν (mHz)	A (mmag)
2.24	1.1
(4.48)	(0.5)

Notes: New Cape Survey roAp star. An intensive exploratory study from a single site is required.

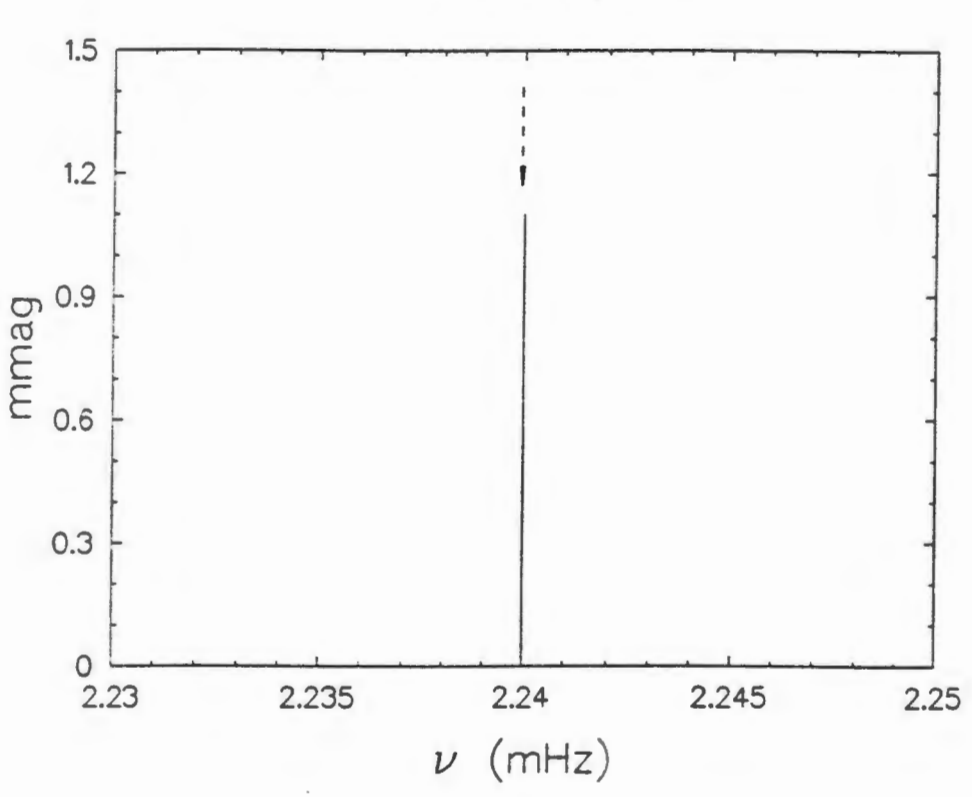

the T_{eff} - $log\ g$ grids of Moon & Dworetsky (1985). The effective temperatures thus determined for the roAp stars range from 6800 K to 8400 K. These temperatures are less well determined than for normal stars because in the Ap stars the continuum flux distributions differ substantially from those of the normal stars. An extreme example of this is Przybylski's star, HD 101065, where the line blanketing is so severe that the continuum is not seen in the visible part of the spectrum. For HD 101065, we have adopted T_{eff} = 7400 K based on the arguments presented by Martinez & Kurtz (1990c).

Fig 9.2 shows an HR diagram with the evolutionary tracks of the normal A star models of Heller & Kawaler (1988). On this diagram I have plotted the roAp stars for which we have $\Delta\nu$ values, no matter how tentative. The observed borders of the lower instability strip (Breger 1979) are also indicated. The results of this exercise are interesting. Figure 9.2 indicates that the roAp stars all lie within the instability strip and are all *above* the ZAMS. The presence of the roAp stars within the instability strip implicates the κ mechanism operating on He II in the He II ionization zone as a probable driving mechanism. It is highly unlikely that the roAp stars all lie in the instability strip because of a selection effect. From the outset, we have searched for oscillations in stars spanning a wide range of temperature and luminosity, as shown in the Figures in chapter 8.

How do these asteroseismological luminosities fare when compared with independent luminosity estimates? At present, we can check our asteroseismological luminosity for only one roAp star, γ Equ (HD 201601), which has a parallax luminosity $M_V(\pi) = 1.9$ that agrees with its asteroseismological luminosity of $M_V(\Delta\nu) = 1.8$. However, we must mention the caveat that our value of $\Delta\nu = 58\ \mu$Hz for this star is not secure and needs to be confirmed. For the roAp star HD 128898 (α Cir), we do not have an asteroseismological luminosity, but the available parallax luminosity $M_V(\pi) = 1.9$ and $T_{eff} = 8000$ K place it inside the instability strip. Some readers may argue that the roAp stars all lie within the instability strip because of a fortuitous choice of $\Delta\nu$ values. For HD 217522, a choice of $\Delta\nu$ = 62 μHz instead of $\Delta\nu$ = 31 μHz, would place this star outside the red border of the instability strip. When the HIPPARCOS parallaxes for the roAp stars become available, we will be able to confirm or refute more of these asteroseismological luminosities.

We end this section by pointing out another way in which the study of roAp star oscillations can shed light on the physics of the Ap phenomenon. We have often alluded to the difficulty of obtaining reliable effective temperature estimates for the Ap stars. The oscillations in the roAp stars may offer a way to estimate T_{eff} to high accuracy given good luminosity estimates. When accurate

Table 9.2

Effective temperatures and asteroseismological luminosities for the rapidly oscillating Ap stars.

HD	y	$b-y$	m_1	δm_1	c_1	δc_1	β	T_{eff} K	$\Delta\nu$ μHz	ΔM_V	M_V
6532	8.445	0.088	0.214	-0.014	0.879	-0.051	2.880	8400			
12932	10.235	0.179	0.228	-0.024	0.765	-0.035	2.810	7800			
19918	9.336	0.169	0.216	-0.010	0.822	-0.058	2.855	8200			
24712	6.001	0.191	0.211	-0.023	0.626	-0.074	2.760	7400	68	0.7	2.4
42659	6.768	0.124	0.257	-0.050	0.765	-0.076	2.834	8100			
60435	8.891	0.136	0.240	-0.034	0.833	-0.047	2.855	8200	52	1.1	1.4
80316	7.782	0.118	0.324	-0.118	0.599	-0.283	2.856	8300			
83368	6.168	0.159	0.230	-0.024	0.766	-0.062	2.825	7950			
84041	9.330	0.177	0.233	-0.026	0.797	-0.061	2.844	8100			
101065	7.994	0.431	0.387	-0.204	0.002	-0.370	2.641	7400	58	1.0	2.1
119027	10.022	0.257	0.214	-0.034	0.557	-0.076	2.731	7150	52	1.2	2.1
128898	3.198	0.152	0.195	0.012	0.760	-0.077	2.831	8000			
134214	7.464	0.216	0.223	-0.029	0.620	-0.108	2.774	7550			
137949	6.573	0.196	0.311	-0.105	0.580	-0.236	2.818	8000	40	1.4	1.2
150562	9.816	0.301	0.212	-0.015	0.659	-0.087	2.783	7600			
161459	10.326	0.245	0.246	-0.040	0.679	-0.141	2.820	7950			
166473	7.923	0.208	0.321	-0.118	0.514	-0.268	2.801	7850	68	0.6	2.1
176232	5.89	0.150	0.208	-0.004	0.829	0.031	2.809	7800	51	1.1	1.7
190290	9.312	0.289	0.293	-0.091	0.466	-0.306	2.796	7900	40	1.4	1.2
193756	9.195	0.181	0.213	-0.008	0.760	-0.040	2.810	7800			
196470	9.721	0.211	0.263	-0.059	0.650	-0.144	2.807	7850			
201601	4.68	0.147	0.238	-0.032	0.760	-0.058	2.819	7900	58	0.8	1.8
203932	8.820	0.175	0.196	0.004	0.742	-0.020	2.791	7650	66	0.6	2.2
217522	7.525	0.289	0.227	-0.056	0.484	-0.015	2.691	6800	31	2.3	1.4
218495	9.356	0.114	0.252	-0.049	0.812	-0.098	2.870	8350			

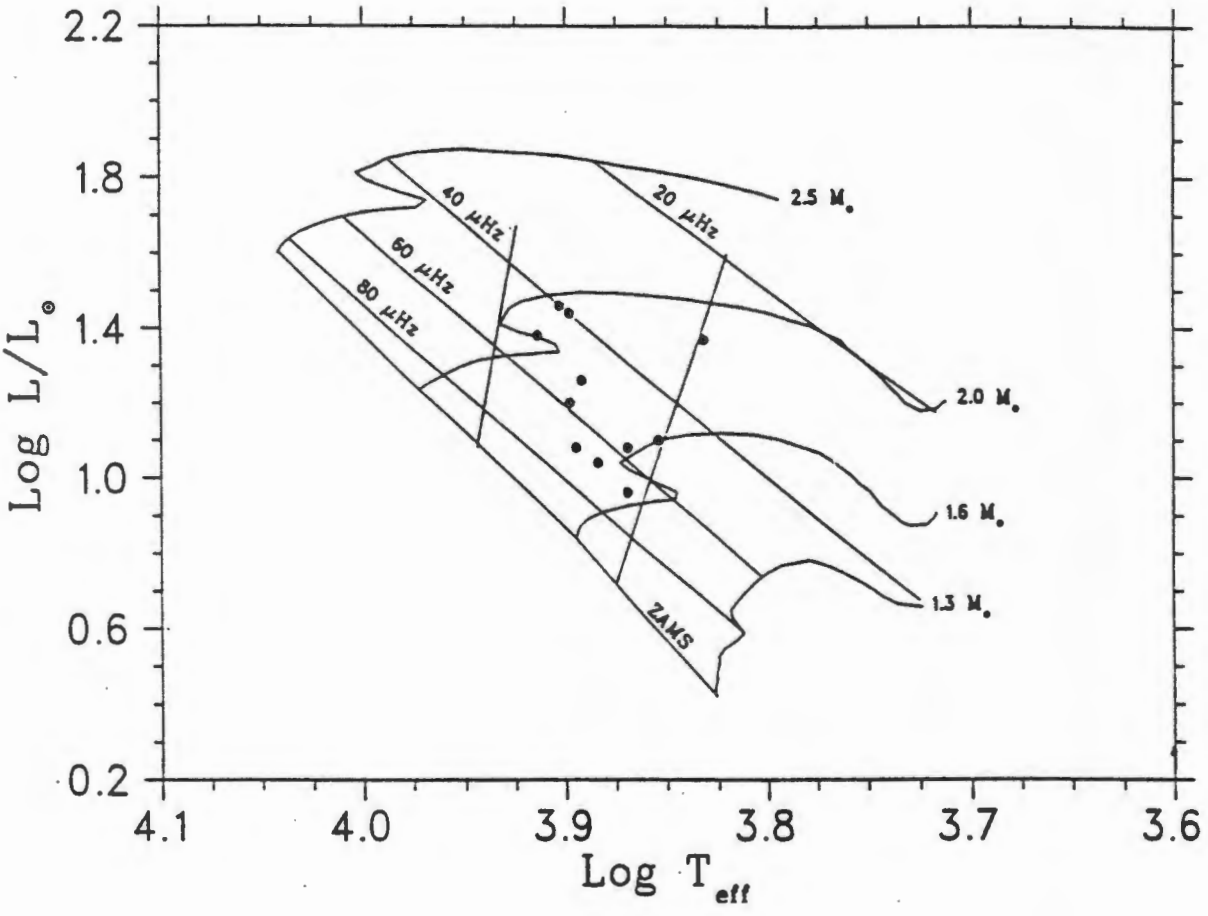

Figure 9.2 A theoretical HR diagram showing the roAp stars for which $\Delta\nu$ is known. The evolutionary tracks of Heller & Kawaler (1988) are shown for a range of masses appropriate to the roAp stars. Also shown are the observed borders of the instability strip.

HIPPARCOS parallaxes become available, it should be possible to use the parallax luminosity and $\Delta\nu$ to determine T_{eff}. This would in turn permit one to check the validity of the Hβ calibration for the Ap stars.

9.4 Driving Mechanisms

Much has been written about the possible pulsation driving mechanisms in the roAp stars. It is not the function of this section to review all of these models in detail, but merely to present and discuss some of the alternatives. The apparent confinement of the roAp stars to the instability strip indicates that the κ mechanism is a possible driving mechanism. Invoking the κ mechanism has substantial implications for the diffusion theory but is not necessarily inconsistent with it. As noted in chapter 1, "classical" diffusion theory predicts that helium will have settled out of the He II ionization zone which drives the pulsations in the δ Scuti stars. Vauclair *et al.* (1991) have developed a series of models of diffusion in magnetic stars with stellar winds in which they vary the mass loss rate as a free parameter. These models indicate that He is depleted at the magnetic equator while it accumulates at the magnetic poles in the He I ionization zone (Fig 9.3). The depletion of He at the equator is by a factor of ~3 for cool ($\leq 10^5$ K) Ap stars. For hotter stars, Vauclair *et al.* find that the He abundance should be normal to slightly under-abundant at the magnetic equator, depending on the strength of the magnetic field. The accumulation of He at the magnetic poles occurs at small mass loss rates comparable to those in the solar wind ($\sim 10^{-13} M_\odot\,\mathrm{yr}^{-1}$). If the mass loss rate at the magnetic poles is significantly greater, He may accumulate in a ring at some intermediate magnetic latitude.

In the cool Ap stars, the He accumulation is not visible as it lies below the photosphere. It becomes visible in the hotter stars at the same temperature as the Bp "He rich" stars are observed. In the cool stars, the He II ionization zone contains the tail of the He enhancement profile which peaks in the He I ionization zone. This "tail-end" enhancement may provide sufficient He in the He II ionization zone to drive the pulsations in the roAp stars. Further work is required to show whether there is sufficient He enhancement to drive the oscillations. Perhaps the most significant result of Vauclair *et al.*'s paper is that they point out that the roAp stars are not chemically spherically symmetric because of He abundance and molecular weight gradients. Thus the acoustic cavity within which the oscillations resonate is not spherically symmetric either and this must be taken into account when making detailed comparisons of theory to the observations.

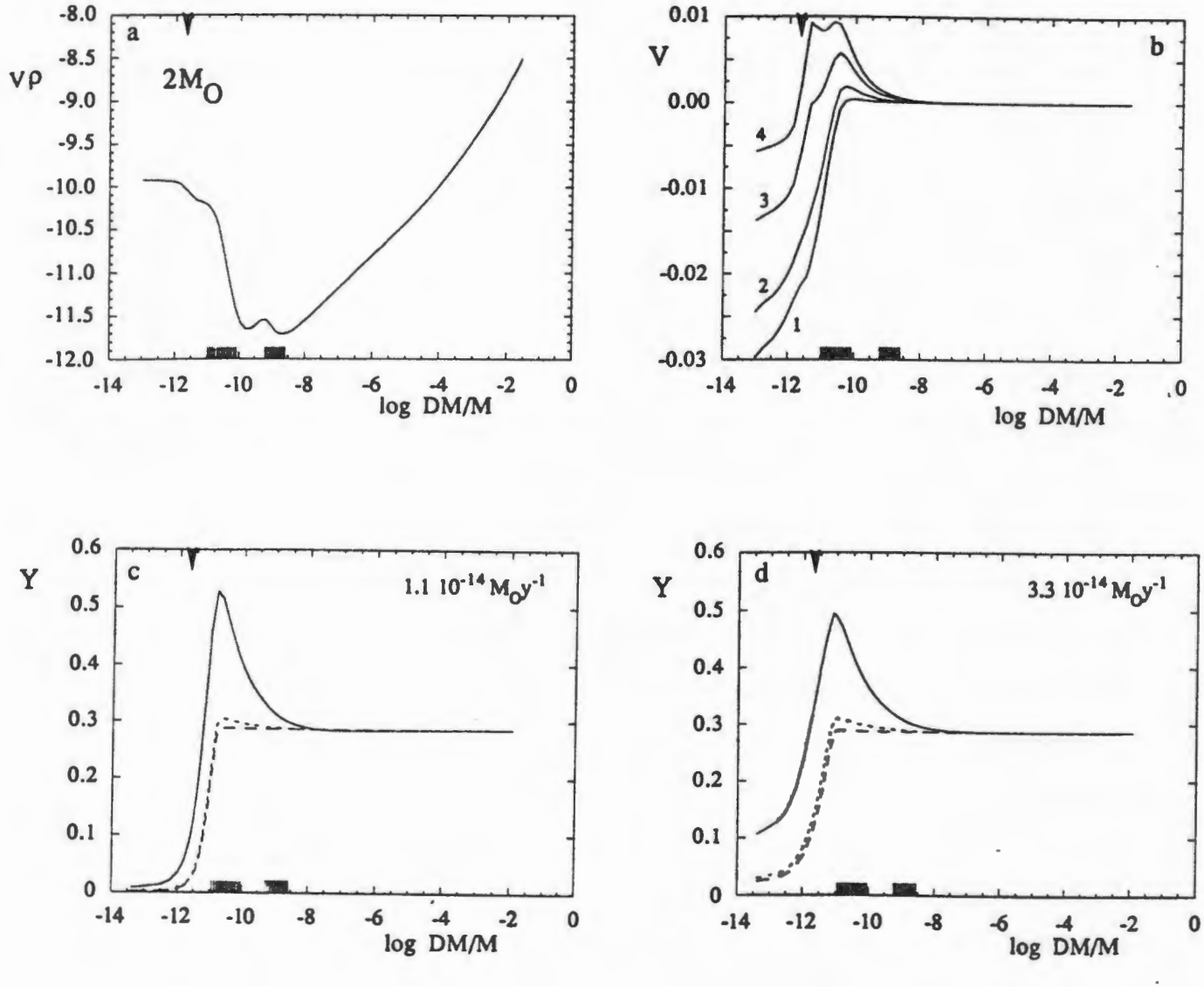

Figure 9.3 Results of He diffusion calculations by Vauclair *et al.* (1991) for a $2.0M_{\odot}$ star with T_{eff} = 9660 K. The abscissa is the outer mass fraction of the star. The arrowhead at the top of each panel indicates where the Rosseland optical depth = 1 and the two shaded zones at the bottom are the two He ionization zones.

Panel (a) shows the He diffusion flux. The flux drops when He becomes singly ionized, increases a bit like $T^{3/2}$, then falls at the second ionization and finally increases monotonically like $T^{3/2}$.

Panel (b) shows the net He velocity, which is the sum of the diffusion velocity and the wind velocity. The four curves are for four different values of outward flux corresponding to mass loss rates of 1.1×10^{-14}, 3.3×10^{-14}, 7.7×10^{-14}, 1.1×10^{-13} $M_{\odot}$/yr, from 1 - 4, respectively. The wind velocity goes as ρ^{-1}, so deep in the star the velocity is small. As one rises up through the atmosphere, the wind velocity begins to dominate and the total velocity is positive, meaning the He moves upwards. Even higher, the He becomes neutral and the diffusion velocity becomes larger than the wind velocity and the total velocity becomes negative, meaning the He moves down.

Panel (c) is the He abundance profile for a mass loss rate of 1.1×10^{-13} $M_{\odot}$/yr for a series of macroscopic diffusion coefficients of 2×10^{5} (solid line), 2×10^{6} (short dashes) and 2×10^{7} (long dashes) cm^2s^{-1}.

Panel (d) is the He abundance profile for a mass loss rate of 3.3×10^{-14} $M_{\odot}$/yr for a series of macroscopic diffusion coefficients of 10^{6} (solid line), 7×10^{6} (short dashes) and 7×10^{7} (long dashes) cm^2s^{-1}.

Another potential difficulty for the diffusion hypothesis in pulsating stars is the surface pulsation velocity. Fortunately, observations show that the pulsation velocities in the roAp stars are not big enough to be a problem for the diffusion hypothesis. The surface pulsation velocities are 20 - 200 m/s for HR 1217 (Matthews *et al.* 1988) and γ Equ (Libbrecht 1988). Since velocity amplitude falls off rapidly with depth in the atmosphere there is no turbulent mixing of the surface layers with lower layers.

The discovery of rapid oscillations in a star well outside the instability strip would present a problem for the hypothesis that driving is via the κ mechanism operating in the He II ionization zone. We have searched for rapid oscillations in many such stars and have only null results. The detection of non-pulsating Ap stars inside the roAp instability strip is also problematic, although the same problem arises for the δ Scuti stars.

Of course, the κ mechanism is not restricted to He and will operate on any element with a sharp opacity drop from one stage of ionization to the next. The ionization region of such an element must also coincide with the transition region between the quasi adiabatic interior layers and the non-adiabatic outer layers. Matthews (1988) has proposed a κ mechanism based in the Si IV ionization zone which operates even if He is depleted from the surface layers. Matthews argues that Si enhancement is greater at the magnetic poles than at the magnetic equator so that the dominant source of driving is at the poles. In this way the magnetic and pulsation axes coincide to modulate the pulsation amplitude in phase with the magnetic curve, as observed. It remains to be shown that sufficient Si can be concentrated in the Si IV ionization zone to drive the pulsations. One way to test Matthews' hypothesis observationally is to conduct a spectroscopic survey to see whether there is significant Si enhancement in the roAp stars versus well-established constant luminosity Ap stars.

Shibahashi (1983) has avoided the problem of He depletion in the He II ionization zone by proposing an alternative to these opacity-drop driving mechanisms, *magnetic overstable convection*. Because this is a somewhat esoteric mechanism, Cox (1984) has presented a more physically intuitive exposition of the theory. The discussion presented here follows Cox's treatment. The crux of this driving mechanism is the interaction of the magnetic field with convective motions in the superadiabatic region of the envelope. It is well known that magnetic field lines embedded in a plasma exert a tension along their length which constrains motions of that plasma. The motions of particular interest here are the convective motions in the superadiabatic region. Suppose that a parcel of gas in this region is given an upward displacement. This parcel is hotter and less dense than its

surroundings and it experiences an upwards buoyant force. That is, the buoyant force is in the same direction as the original displacement. Thus in the absence of a magnetic field or a chemical gradient this region is convectively unstable. In the presence of a magnetic field the tension of the field lines will provide a restoring force that resists the convective motions. The result of this is that what would be a monotonic motion in the absence of a magnetic field becomes an oscillatory motion in the presence of a magnetic field.

Because of gradual heat losses by the parcel to its surroundings, the upward buoyant force slowly decreases so that the net downward (magnetic) restoring force increases. This means that the amplitude of the oscillations gradually increases; that is, they are *overstable*. In describing this, Cox uses the apt analogy of a simple harmonic oscillator whose spring constant gradually increases. For a dipole magnetic geometry, convection is unstable at the magnetic equator and overstable at the magnetic poles. The magnetic restoring force causes the convective motions to become oscillatory and the few modes observed are the resonances of the global eigenmodes and the overstable convective oscillations. The oscillation periods are set by the convective timescale. The coincidence of the magnetic and pulsation axes is readily explained in this model since the driving takes place at the poles.

If overstable magnetic convection is the driving mechanism in the roAp stars then one would expect that they should not be confined to the δ Scuti instability strip. Yet nature may have conspired to keep them there, as pointed by Kurtz (1990). The cool border of the δ Scuti instability strip more or less coincides with the cool end of the Ap phenomenon. In the early F stars the κ-mechanism cuts off because the He II ionization zone is too deep to drive pulsation; the magnetic Ap phenomenon (and thus, magnetic overstable convection also) cuts off because of the onset of large convective envelopes. For the hotter Ap stars, the degree of superadiabicity at the poles is lower, so presumably the blue border is set by an observational cutoff where the pulsation amplitude drops below observational limits. Perhaps this observational cutoff more or less coincides with the observed blue border of the instability strip. Figure 9.1 indicates that none of the roAp stars is hotter than the observed blue border of the instability strip. We note, however, that this blue border is not well determined.

9.5 Frequency changes

From an asteroseismological standpoint, the richer the oscillation spectrum of the star, the more information we can extract from it. However, there is one very important parameter which is best studied in singly periodic stars - it is the rate of frequency change. The way in which a frequency changes is an important clue to the cause of the change. A frequency change can be gradual or abrupt; it can be secular or periodic. Two of the most probable causes of gradual frequency change in a pulsating star are evolution and orbital motion. Evolution affects a star's pulsation frequencies because as the star evolves, its radius and mean density change, so its resonant frequencies change. Orbital motion causes the observed pulsation frequency to change because of the Doppler effect. For stars with well determined pulsation frequencies this is an accurate way to measure binary orbits. By observing for long enough, it is always possible to discriminate between orbital and evolutionary frequency change. Evolutionary frequency changes are secular and quadratic whereas orbital Doppler shifts are periodic and sinusoidal (for circular orbits).

The roAp stars exhibit a bewildering variety of frequency changes ranging from abrupt changes on a timescale of days to gradual secular changes on a timescale of a year and probably even periodic or quasi-periodic frequency changes on a timescale of a decade. An abrupt frequency change by an integral multiple of the p-mode spacing $\Delta\nu$ or $\Delta\nu/2$ is interpreted as a pulsation mode change. Such frequency changes form the subject of section 9.6. In this section we will discuss changes of frequency which are not attributable to pulsation mode changes.

Heller & Kawaler (1988) have investigated evolutionary period changes theoretically for a series of A star models which they allowed to evolve off the main sequence. The evolutionary tracks of their models are portrayed in Fig. 9.2. The models yield values of $|\,dP/dt\,| \sim 10^{-12} - 10^{-13}$ and thus dP/dt should be detectable in roAp stars with about 6 yr of observations. For a given T_{eff}, models with a smaller p-mode spacing, $\Delta\nu$, have a higher luminosity and a higher $|\,dP/dt\,|$. By using the measured values of dP/dt it should be possible to resolve ambiguities in the determination of $\Delta\nu$. In HR 1217, for example, there are two possible values of $\Delta\nu$, 34 μHz and 68 μHz (Kurtz *et al.* 1989). According to Heller & Kawaler's models, dP/dt should be detectable with the 6 yr of observations available if $\Delta\nu$ = 34 μHz whereas it should not be detectable if $\Delta\nu$ = 68 μHz. Unfortunately, Kurtz *et al.* (1989) find that alias ambiguities and the interaction of the many frequencies in HR 1217 preclude this. This illustrates the importance of the remark made in the opening paragraph of this section that dP/dt is more readily determined in singly periodic stars.

Several other roAp stars with less complicated oscillation spectra than HR 1217 have data sets long enough to permit a determination of dP/dt. In HD 101065, which oscillates with three frequencies, Martinez & Kurtz (1990c) find a rate of frequency change 10 - 100 times higher and of the opposite sign than expected for a hydrogen-core-burning A star. Either HD 101065 is a unique highly evolved object (as suggested by Przybylski), and not an Ap star, or the measured frequency change is caused by binary motion. If so, the companion has a mass < 0.1 $M_{\odot}$ unless the orbit is within 2° of pole-on. However, I hasten to add that one cannot exclude a series of abrupt frequency changes with the data at hand. Further concerted monitoring of this star is warranted. Observations over several years spanning at least one week per season (in order to resolve the three frequencies) should allow us to follow the frequency changes more carefully.

HD 137949 is another star that shows a period change ($dP/dt = (4.9\pm0.3)\times10^{-11}$) orders of magnitude larger than theoretical expectations for evolutionary effects (Kurtz, 1991). Interestingly, some δ Scuti stars also show period changes much larger than expected from evolutionary effects. For example, Breger (1990) has measured $dP_1/dt = -3.4\times10^{-10}$ and $dP_2/dt = -1.4\times10^{-9}$ for the two principal periods in 4 CVn. It is therefore not clear whether all these reported frequency changes, if real, are evolutionary.

The resolution of this problem may be in sight, for the roAp stars, at least. Kurtz *et al.* (in preparation) have made a careful study of 12 yr of data on the oblique pulsator HR 3831 which shows that the frequency of the principal pulsation mode varies by about 0.1 μHz on a time-scale of two years. This again is orders of magnitude higher than expected from evolutionary effects. Figure 9.4 is a series of (O-C) diagrams showing how the principal frequency of HR 3831 varied during six observing seasons. Through careful analysis, Kurtz *et al.* were able to exclude abrupt phase changes, a drift of the pulsation pole with respect to the magnetic pole and orbital motion as the cause of the frequency variations. They can exclude evolutionary changes because $|dP/dt|$ is too high and its sign changes from season to season contrary to all expectations of the way an evolutionary frequency change should behave. Interestingly, the magnitude of these frequency variations is of the same order as the magnetically induced changes in the frequencies of solar 5-min oscillations. This motivated Kurtz *et al.* to suggest that the frequency variations in HR 3831 may be caused by variations in the stellar magnetic field, possibly in a stellar magnetic cycle. Inference from the Sun suggests that the magnetic variations in HR 3831 are orders of magnitude lower than can be detected in conventional

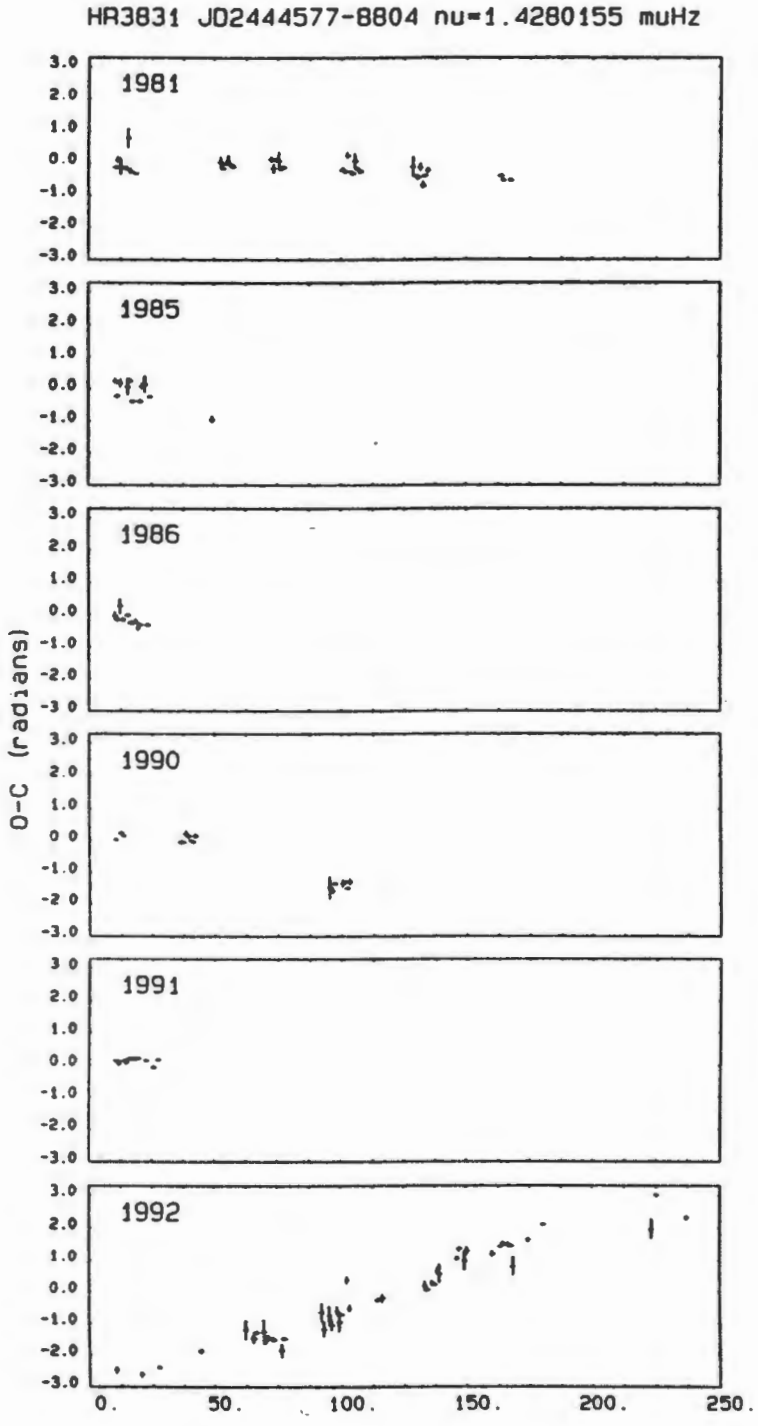

Figure 9.4 Plots of (O-C) for the principal oscillation mode in the roAp star HR 3831. In this diagram, a sloping line indicates a changing frequency. Abrupt vertical jumps indicate abrupt changes of phase. The frequency fitted in all the panels was the frequency obtained from the 1991 data; hence the 1991 data lie on a horizontal line, by definition. By changing the fitted frequency it is possible to make the data in any given panel lie on a horizontal line, but then the slopes in the other panels all change. It is not possible to find a single frequency that fits the data in all years and makes them all lie on horizontal lines. Kurtz *et al.* (in preparation) exclude evolution and orbital motion as causes of the frequency variations and argue that they constitute evidence for a stellar magnetic cycle in HR 3831. (Figure courtesy of D.W. Kurtz.)

magnetic measurements. If these frequency variations are really magnetically induced, then a study of them may offer the only way to investigate magnetic variations in these stars.

For many of the roAp stars the analysis of large data sets always culminates in a residual mound of amplitude after all the principal frequencies have been extracted. Examples of stars where this is the case are HD 101065 (Martinez & Kurtz 1990c) and HR 3831. Significantly, the analysis just described for HR 3831 succeeded in 'cleaning up' the amplitude spectrum of the residuals to the point where there are no indications of further frequencies. Perhaps a magnetic cycle, or some other common mechanism, is causing the long-term mode instabilities observed in the well-studied roAp stars. A program to monitor several previously well studied roAp stars like HD 101065 has commenced and monitoring of HR 3831 is continuing. The important point here is that Kurtz *et al.*'s elegant frequency analysis of HR 3831 should serve as a reminder that attempts to invoke chaos to explain non-stationary phenomena in roAp star oscillation spectra (*e.g.* Kreidl 1992) are at present premature.

9.6 Mode changes and mode lifetimes

Several roAp stars are observed to switch their principal pulsation frequency abruptly. Such frequency shifts are usually commensurate with some integer multiple of the p-mode spacing $\Delta\nu$ and they are interpreted as shifts to a nearby overtone. An example of a star where abrupt frequency shifts have been noted is HD 217522 (Kreidl *et al.* 1991). Observations in 1982 showed pulsation with a frequency ν_1 = 1.21529 mHz whereas observations in 1989 showed that the principal pulsation frequency had shifted to ν_1 = 1.1999 mHz, a shift of 15.4±0.1 μHz. Moreover, the 1989 data showed a new frequency at ν_2 = 2.0174 mHz at such a significance level that there was no chance it could have been missed in the 1982 observations. Such a frequency shift is orders of magnitude too high to arise from evolutionary changes in HD 217522. Kreidl *et al.* have interpreted the frequency shift as a mode change and have used the size of the shift to estimate the luminosity of HD 217522 as we did in section 9.3.

In HD 217522, the mode change has not actually been observed, but for the roAp star HD 60435 a transition from one pulsation mode to another was well observed (*e.g.* Figure 2.6). HD 60435 has the richest p-mode spectrum of the roAp stars. It pulsates with many frequencies having a basic spacing of 25.8 μHz. This spacing is interpreted as $\Delta\nu/2$, the spacing of alternating even and odd ℓ modes. During a multi-site observing campaign from Chile and South Africa in 1985

(Matthews *et al.* 1987) this star was observed to undergo a transition from one mode to another. Since then, many mode changes in this star have occurred. In fact, there are so many mode changes that one cannot meaningfully talk about a principal oscillation frequency for HD 60435. The lifetimes of some of the modes seem to be as short as a few days. A rotation period of 7.6793±0.0006 days has been determined for HD 60435 by Kurtz *et al.* (1990) from a study of its mean light variations. In many cases the modes have lifetimes shorter than one rotation cycle. These conclusions are secure. They were obtained from over 400 hr of contemporaneous multi-site data and there is no chance that they are artefacts produced by aliasing and frequency resolution problems.

There are other roAp stars with mode instabilities on time-scales on days. Examples of such stars are HD 203932 (Martinez *et al.* 1990), HD 84041 (chapter 6) and HD 119027 (chapter 7). These stars are not as well studied as HD 60435, but there is strong evidence that they pulsate in several modes and perhaps their behaviour is qualitatively similar to that of HD 60435.

Kurtz (1990) has pointed out that the pulsation mode lifetimes appear to be longer in those stars which pulsate in few modes and shorter in the rich *p*-mode stars. An example of a mode-stable star is HR 3831 which is singly periodic with harmonics. The principal dipole oscillation is amplitude-stable over more than 10-yr. There are slight changes in phase from one season to the next which are discussed in section 9.5. Another example of a well studied mode-stable star is HD 101065 which pulsates with one large amplitude mode and at least one other much smaller amplitude mode (Martinez & Kurtz 1990c). The large-amplitude mode seems to suffer some amplitude or phase instability on time-scales of 10 yr but is stable on shorter time-scales. HR 1217 pulsates with 6 modes (Kurtz *et al.* 1989) that are stable over one rotation cycle, but variable on a time-scale of 4 rotation cycles.

9.7 Atmospheric structure

Asteroseismology promises to yield accurate knowledge not only about stellar interiors, but also stellar atmospheres. For the roAp stars, the possibility that we can learn something about the atmospheric structure by studying the oscillations is particularly exciting in view of the difficulties in determining even basic parameters like the effective temperature and surface gravity. This diagnostic possibility is a consequence of the requirements for maintaining standing waves in the stellar acoustic cavity. For a standing wave to be reflected at the surface, the temperature gradient must be steep enough that the sound speed gradient changes significantly over a radial distance short compared to

the wavelength of the mode. This is just a statement of the requirement of a sharp boundary to maintain reflective phase coherence in a standing wave. The shortest wavelength (equivalently, highest overtone n) that can be maintained is the one where the wavelength becomes comparable to the height of the reflecting layer. The frequency of this mode is called the critical frequency ν_{crit}.

Shibahashi & Saio (1985) were the first to point out that many roAp stars pulsate with frequencies above the critical frequency for the relevant standard A star model atmospheres. Since these pulsation frequencies are long lived, they cannot be evanescent modes. From this they inferred that in these Ap stars the temperature gradient is markedly steeper than in the standard models thus resulting in a sharper reflection boundary, and hence a higher critical frequency. The idea that the $T(\tau)$ relation might be steeper in Ap stars than in chemically normal A-type stars is not new. In the late 1970's, Muthsam (1979a, b), who was modelling Ap star atmospheres, found that his models produced $T(\tau)$ relations significantly steeper than those of normal A stars. If one does not accept the notion of a steeper $T(\tau)$ relation in Ap stars, then one has to believe that the modes with $\nu > \nu_{crit}$ are being driven extremely hard. In the case of hard driving, one might expect to see the harmonics of frequencies with $\nu > \nu_{crit}$, but this is not always the case.

It has been known from the earliest work on roAp stars (Kurtz 1982, Schneider & Weiss 1989) that the pulsation amplitude drops rapidly towards the red. To investigate this trend in the infrared Matthews *et al.* (1990) observed the roAp star HR 3831 in the K-band at the time of B-band pulsation amplitude maximum. They obtained an upper limit for the K-band pulsation amplitude significantly lower than one would expect for a star pulsating like a blackbody. Matthews *et al.* then studied the effect of differential limb darkening in the visible and infrared on the integrated amplitude of the $\ell = 1$, $m = 0$ mode in HR 3831. They found that limb darkening enhances the observed amplitude of such a mode by under-weighting the low-amplitude and/or antiphase sectors on the disk for all orientations except equator-on where the net amplitude is zero. Moreover, limb darkening is stronger at shorter wavelengths thus leading lead to higher observed amplitudes at those wavelengths. By measuring the amplitude at a range of wavelengths from the ultraviolet to the infrared, one should be able to infer the limb darkening coefficients and produce an empirical T - τ relation for an Ap star atmosphere. Matthews *et al.* (1992) have applied this approach to HR 3831 and they find that this star must have a steeper temperature gradient in agreement with the prediction of Shibahashi & Saio (1985) and the model atmosphere calculations of Muthsam (1979a, b).

Several observers besides Matthews *et al.* have attempted to detect rapid oscillations in roAp stars in the infrared (e.g. α Cir (Weiss *et al.* 1991), HD 134214 (Belmonte *et al.* 1992a), 10 Aql (Belmonte *et al.* 1992b)). What struck me about these infrared observations is that they were essentially all null results, placing only an upper limit on the possible pulsation amplitude. I decided that if we were going to attempt similar observations at Sutherland to determine $T(\tau)$ for roAp stars, I should at least demonstrate that *some* signal is detectable in the infrared. On the night 17/18 August 1992 (JD 2448852), the SAAO 1.9-m Radcliffe telescope and Mk III InSb photometer were made available to me for 3 hr to search for rapid oscillations in any suitably placed roAp stars. At my request, Dr Kazuhiro Sekiguchi of the SAAO obtained 2.4 hr of high-speed K-band observations of the roAp star HR 1217. The $f/50$ secondary mirror on that telescope chops between two apertures to measure the quantities $(star+sky1)-sky2$ and $sky1-(star+sky2)$. Subtraction of these quantities yields twice the stellar signal minus the sky background contribution. Since we were searching for rapid oscillations with periods around 6 min., no standard stars were observed and we did not attempt to put the observations on the standard system. The resulting instrumental magnitudes were corrected for mean extinction.

Figure 9.5 is the light curve of these data which shows that there was a gradual improvement in sky transparency during this run. Fig. 9.6 shows the Fourier transform of those data up to the Nyquist frequency of 6.0 mHz. The peaks at low frequency are caused by sky transparency variations. The peak labeled 'ν_1' lies at 2.73 mHz, exactly the frequency of the well-studied B-band oscillations (Kurtz *et al.* 1989). Removing the low-frequency noise lowers the general level of the peaks but does not otherwise change the appearance of the spectrum much in the vicinity of ν_1. When the 4 highest peaks in the frequency range 0 - 0.92 mHz are removed, the highest peak remaining is at 2.72 mHz. A least squares fit of ν_1 = 2.72 mHz to the prewhitened data yields an amplitude of 1.3±0.4 mmag for ν_1.

Without prior knowledge of the optical oscillations at 2.72 mHz, this peak would be statistically insignificant. However, the chance of finding a peak of z signal/noise in power at exactly the right frequency is $\sim e^{-z}$ (Scargle 1982). Taking A_1 = 1.3±0.4 mmag and the level of the noise in the amplitude spectrum of the prewhitened data to be a conservative 0.8 mmag, $z = (1.3/0.8)^2$ which yields a False Alarm probability of 7% for this peak, *i.e.*, the peak ν_1 is significant at the 93% level.

Unfortunately, the beating of the principal oscillation modes in HR 1217 does not allow us to predict the instantaneous B amplitudes on any given night. Thus we cannot compare our tentative

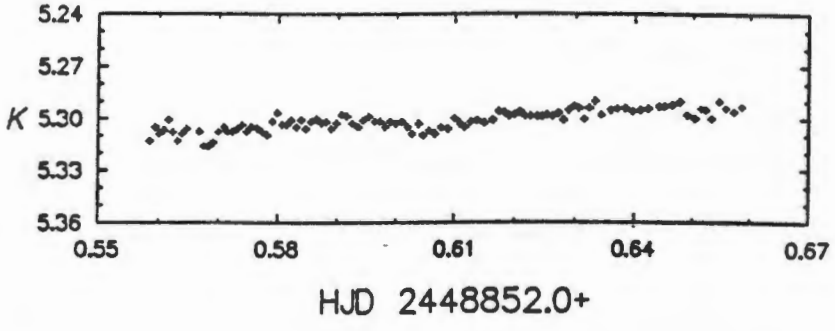

Figure 9.5 The *K*-band light curve of HR 1217 obtained over 2.4 hr on JD2448852.

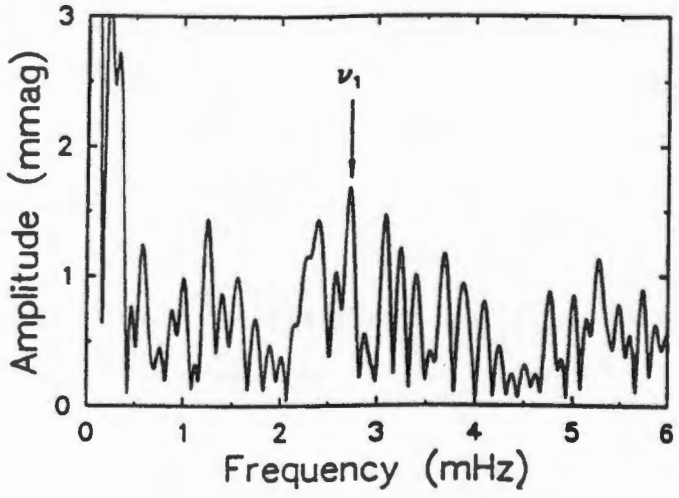

Figure 9.6 The amplitude spectrum of the data shown in Fig. 9.5. The peak labeled 'ν_1' is at the optical oscillation frequency of 2.72 mHz.

measurement of A_K to any expectations of the K amplitude. For this, simultaneous multicolour photometry will be necessary. These observations were done as an experiment to determine the feasibility of studying roAp star oscillations in the infrared with the existing facilities at SAAO. They are the first high-speed observations done on the SAAO 1.9-m telescope using instrumentation and software really designed for all-sky observations. With some work it should be possible to improve our signal-to-noise ratio so that the study of rapid oscillations in the infrared becomes a real prospect at SAAO.

9.8 Estimation of main sequence ages

As a pulsating star evolves the sound speed in the core changes gradually in response to the change in core composition during core H-burning. In chapter 2 we described how the asymptotic p-mode spacing $\Delta\nu$ is a mean density indicator and the second order term $\delta\nu$ is a main sequence age indicator. Christensen-Dalsgaard (1984) and Ulrich (1986) have used these two parameters to create a sort of asteroseismological mass - age diagram as shown in Fig. 2.11 for solar-type stars. There are very few roAp stars for which we have both $\Delta\nu$ and $\delta\nu$ estimates, and for those stars the observed $\delta\nu$ is a factor of 10 smaller than theoretical expectations for the solar-type stars. It is only very recently that models in the roAp star mass range have been computed. In private communication Matthews has informed me that "Audard & Provost have generated eigenfrequency spectra for 2.0 $M_\odot$ models which yield $\delta\nu \sim 3\ \mu$Hz, in much better agreement with observed values than the solar models of Christensen-Dalsgaard. Dziembowski has also noted that the magnetic field seems to introduce perturbations of order 1 - 2 μHz to this parameter."

Figure 9.7 shows the first crude asteroseismological HR diagram for stars in the roAp mass range. The solid lines are evolutionary tracks for 1.0, 1.5 and 2.0$M_\odot$ models calculated by Audard & Provost (Matthews, private communication). In this diagram, the models evolve from the ZAMS at the top to near the end of the main sequence stage at the bottom. The position of the Sun is indicated and it is interesting to note that the Sun does not lie on the locus of points defined by the 1.0 $M_\odot$ model; clearly these models need further refinement. The filled circles indicate *tentative* ($\Delta\nu$,$\delta\nu$) values for 4 roAp stars obtained from Table 9.1: HD 60435, HD 24712, HD 101065 & HD 119027. In the case of HD 101065 and HD 119027, the rotation periods are not known. We have attempted without success to find rotation periods for both stars by studying the amplitude modulation of the pulsations and by studying the mean light variations. It is nonetheless conceivable that these fine

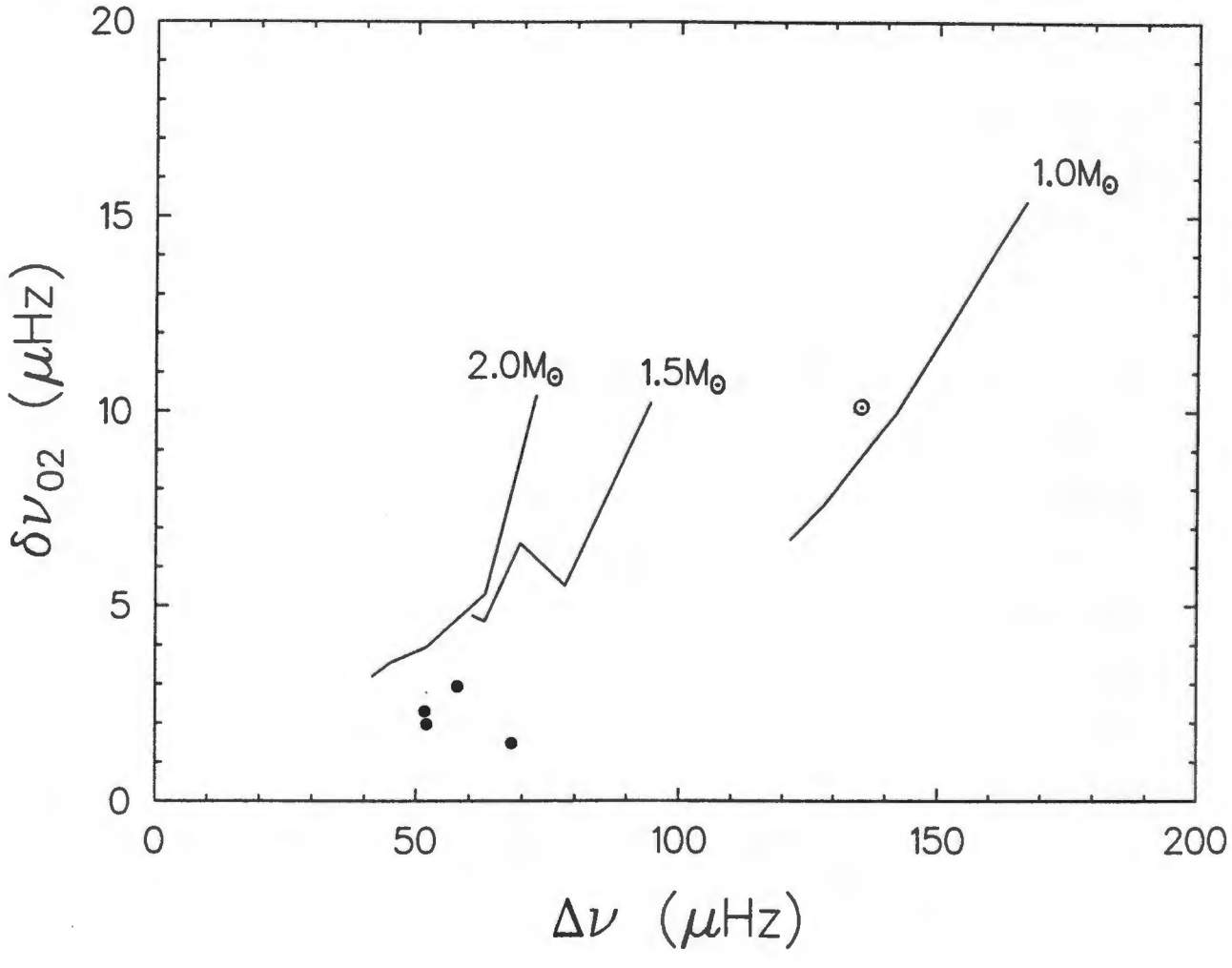

Figure 9.7 An asteroseismological HR diagram for the roAp stars. The solid lines are the models of Audard & Provost (Matthews, private communication) for 1.0, 1.5 and 2.0 $M_\odot$ stars. In this diagram the ZAMS runs along the tops of the model trajectories. The filled circles indicate the observed positions of the roAp stars. These positions are tentative; consult the text for further details. The observed position of the Sun is also indicated. Notice that this does not fall on the theoretical $1.0M_\odot$ track.

frequency splittings may turn out to be a measure of the rotation period rather than a measure of the parameter $\delta\nu$. This confusion occurred in the case of the roAp star α Cir (HD 128898) whose amplitude spectrum revealed two closely spaced frequencies separated by 2.6 μHz in an early study by Kurtz & Balona (1984). If this were a rotationally split frequency, one would expect to see at least one other frequency forming a triplet. Since they could find no evidence of another rotation sidelobe frequency, Kurtz & Balona concluded that they had observed two independent pulsation modes. Kurtz (1988) later proposed that this was a measurement of $\delta\nu$ = 2.6 μHz in α Cir. In contrast to this, the latest unpublished observations (May 1993) reveal a pure dipole oscillation which manifests itself as a rotationally split frequency triplet with a spacing of 2.6 μHz.

With the above caveats in mind, we now consider Fig. 9.7. The roAp stars seem to lie about 2 - 3 μHz below the end points of the 1.5 $M_\odot$ and 2.0 $M_\odot$ models. This implies that these particular roAp stars are highly evolved objects, something which is testable by determining the rate of frequency change in these stars. However, in light of the comment by Dziembowski above that magnetically induced perturbations of 1 - 2 μHz in $\delta\nu$ are possible, we see again that more detailed model calculations are required. The 10 new roAp stars should yield a few more points for this diagram once their oscillation spectra have been studied in detail.

Chapter 10

Conclusion

10.1 An overview

We have come to the end of our discussion of the Cape Survey and an overview is in order. The roAp stars pulsate in low order ($\ell \leq 3$), high-overtone ($n \approx 10 - 80$) nonradial p-modes with periods in the range 6 - 15 minutes and amplitudes $\leq$ 16 mmag peak-to-peak in Johnson B. They are oblique pulsators whose magnetic and pulsation axes are co-aligned. The best examples of oblique pulsators are HR 3831 and HD 6532, which show the clear signature of distorted oblique dipole pulsation. Application of the oblique pulsator model constrains the rotational inclination i, the magnetic obliquity β and the internal magnetic field strength.

The Cape Survey has produced a catalogue of Strömgren $uvby\beta$ photometry of all the southern Ap SrCrEu stars with declinations $\delta \leq -12^{\circ}$ in the Michigan Spectral Catalogue. Our catalogue also includes 71 SrCrEu stars in the equatorial strip from $\delta = -12^{\circ}$ to the equator. The Cape Survey is an ongoing project and as more volumes of the Michigan Spectral Catalogue become available, the survey will proceed northwards to cover the equatorial strip above the equator. The photometric catalogues produced in the Cape Survey will be especially useful to observers searching for new roAp stars.

We have searched for high-overtone pulsations in 148 SrCrEu stars and discovered 10 new roAp stars. Several of the new roAp stars are multimode pulsators with amplitude spectra suitable for asteroseismological studies. Asteroseismology can potentially allow the determination of mass, luminosity and age of the roAp stars from analyses of their frequency spectra. Exploratory frequency analyses of the new roAp stars HD 84041 and HD 119027 reveal the existence of rich oscillation spectra with evidence of non-stationary behaviour. These stars should be the subject of a multisite campaign of about two weeks' duration with preferably at least three sites well spaced in longitude. Telescopes $\geq$ 1 m should be used. The null results of our survey and similar earlier surveys are presented in this thesis. The intention of this systematic compilation of null results is to record which

stars have been observed and, in most cases, to draw attention to how little they have been observed. Observers should *not* be dissuaded from searching for rapid oscillations in most of these stars.

Plots of the positions of the roAp stars and the apparently constant Ap stars in various Strömgren photometric diagrams show that the parameter space has been well explored in an attempt to determine the photometric limits of the roAp phenomenon. Virtually all the roAp stars fall below the main sequence in a photometric temperature - luminosity plot. The apparent subdwarf luminosities of the roAp stars are caused by the severe abundance anomalies which depress the photometric luminosity indicator c_1. Estimates of the luminosity derived from asteroseismology (see below) indicate that the roAp stars are slightly evolved main sequence objects. In the case of α Cir, the available parallax luminosity indicates that this star is slightly *above* the main sequence in agreement with the luminosity estimates for other Ap stars (chapter 1).

The Cape Survey Hβ photometry was used to estimate the effective temperatures of the roAp stars. These estimates of T_{eff} were then used in conjunction with the observed values of $\Delta\nu$, the frequency spacing of consecutive overtones, to infer the luminosities of several roAp stars. At present it is possible to check our asteroseismological luminosities for only one star, γ Equ (HD 201601). For this star, the parallax and asteroseismological luminosities are in good agreement. When the HIPPARCOS results are published, it should be possible to verify more of the asteroseismological luminosities. When these effective temperature and luminosity estimates are used to plot the roAp stars on an HR diagram, they all lie within the classical instability strip. This implicates the κ-mechanism in the He II ionization zone, but does not exclude magnetic overstable convection. This uncertainty arises because magnetic overstable convection may be confined to operate within limits similar to those of the instability strip.

The pulsations in the roAp stars can also be used to probe their outer layers and thereby shed light on the Ap phenomenon. Studies of the pulsation amplitude of HR 3831 from the ultraviolet to the infrared have allowed tentative inferences of the $T(\tau)$ relation for this star. This relation appears to be steeper in HR 3831 than in normal A stars in support of the results of model atmosphere calculations done in the late 1970's. This means that the surface temperatures of Ap stars may be much lower than implied by their effective temperatures. Work of this nature requires an excellent photometric site, especially for the infrared high-speed photometry. In this thesis I have explored the possibility of doing such work at Sutherland and the results were encouraging.

10.2 The future

As is often the case in research, the Cape Survey has not answered all the questions that were posed at its inception. The excitation mechanism is not known with certainty. The fact that the roAp stars are confined to the instability strip strongly suggests that the κ-mechanism operating in the He II ionization zone is the driving mechanism. However, magnetic overstable convection is also a contending mechanism, especially if it operates within a region that coincides with the instability strip. Further observational work is required to sharpen the observed borders, especially the blue border, of the instability strip. Theoretical work is required to explore the question of whether magnetic overstable convection is confined to a similar temperature range as the instability strip.

We still do not know what distinguishes the apparently constant Ap stars from the roAp stars. We have unsuccessfully searched for oscillations in a number of Ap stars which are the photometric twins of known roAp stars. Because of the low amplitudes and long rotation periods in some stars, many of the null results are really inconclusive rather than negative. In this regard, it is important to establish a number of definitely constant Ap stars with known magnetic/rotation periods. Such a star is β CrB, which shows no evidence of rapid oscillations at magnetic maximum. Perhaps spectroscopic observations will reveal systematic differences between the pulsating and constant Ap stars. A medium- to high-resolution spectroscopic survey of roAp stars and well established, secure constant luminosity stars should be conducted as the next logical step. Such a survey might also constrain the choice of pulsation driving mechanisms.

Campaigns such as those described in chapters 6 and 7 indicate that multisite observations are critical to the future success of the asteroseismology of roAp stars. Astronomers studying δ Scuti stars have reached similar conclusions and perhaps a union of the networks of roAp star observers and δ Scuti star observers could better serve the interests of both communities. The Global Network of Automatic Telescopes proposed by David Crawford of Kitt Peak National Observatory is also an exciting potential source of multisite data. What we have learned from participating in multisite campaigns is that it is no good to have a roAp star as a secondary target in a campaign. In our experience, secondary target data have proved to be inadequate when it comes to unravelling the oscillation spectra of stars that clearly require high duty-cycle multisite observations.

Studying the rapid oscillations of Ap stars from space is an exciting prospect, but as none of the proposed missions dedicated to asteroseismology have received approval yet, ground-based

techniques will continue to be important in the 1990's. Another idea that could be explored is the possibility of observing roAp stars in the infrared from the Kuiper Airborne Observatory.

It is a curious fact that since the 1980's theoretical $\delta\nu$ - $\Delta\nu$ diagrams have been produced for solar-type models, for which only one observational point exists (*i.e.* the Sun), while similar diagrams have only just started coming out for the roAp stars, for which there are more observational points. The observers should concentrate on producing more secure determinations of $\delta\nu$ to provide data for such diagrams.

More and more roAp stars are beginning to display nonstationary behaviour on timescales ranging from days to years. Much observational work is needed to study the mode lifetimes and growth/decay timescales in the multimode stars. Such questions are coupled to the question of the excitation mechanism.

For the singly periodic stars, measurement of dP/dt values can potentially be used to determine the evolutionary timescale and to remove ambiguities in the measurement of $\Delta\nu$. In some roAp stars the frequencies are very accurately known. Doppler shifts in these frequencies can reveal the presence of low-mass companions. The careful frequency analysis done for HR 3831 by Kurtz (chapter 9) suggests that the principal frequency in that star may vary periodically on a two-year timescale. The origin of these variations is unclear since Kurtz is able to exclude evolution and an orbital companion. If, as Kurtz speculates, they reflect intrinsic magnetic variations in the star, then the oscillations offer us yet another glimpse of otherwise unobservable physics. Whatever the origin of the variations, similar effects should be sought in other stars. Such a program requires a less intensive, but longer effort, say, a few hours one night every week for several seasons. Such a project is already under way at Sutherland.

The mode selection mechanism is unknown. It is a reasonable assumption that the magnetic field selects modes of low degree, but no convincing explanations have been advanced for the particular choice of frequencies excited in a given star. Some roAp stars seem to pulsate only in exclusively even or odd ℓ modes, whereas others pulsate in alternating even and odd ℓ modes simultaneously. Mode identifications have thus far been made only from analyses of the frequency spectra. Studies of line profiles are an additional source of mode identifications.

The Cape Survey is an ongoing project. The immediate priorities of the Survey are to do exploratory frequency analyses of more of the new roAp stars and to keep searching for new roAp stars. As more volumes of the Michigan Catalogue are published, the Survey will push northward to

cover the declination band just north of the equator. This should reduce the imbalance which exists at present in which most roAp stars are in the southern hemisphere and most roAp star observers are in the northern hemisphere. Such equatorial stars would also be excellent candidates for multisite collaborations. We have no doubt that the Cape Survey will continue yielding interesting roAp stars and that as the sample size of the roAp class grows, so will our understanding of the roAp phenomenon.

References

Abt, H.A., 1961. *Astrophys. J. Suppl.*, **6,** 37.

Abt, H.A., 1965. *Astrophys. J. Suppl.*, **11,** 429.

Abt, H.A., 1975. *Astrophys. J.*, **195,** 405.

Abt, H.A., 1979. *Astrophys. J.*, **230,** 485.

Abt, H.A. & Bidelman, W.P., 1969. *Astrophys. J.*, **158,** 1091.

Abt, H.A. & Cardona, O., 1983. *Astrophys. J.*, **272,** 182.

Abt, H.A. & Moyd, K.I., 1973. *Astrophys. J.*, **182,** 809.

Abt, H.A. & Snowden, M.S., 1973. *Astrophys. J. Suppl.*, **25,** 137.

Adelman, S.J., 1985. *Pubs. Astr. Soc. Pacific*, **97,** 970.

Alecian, G., 1986. In: *Upper Main Sequence Stars with Anomalous Abundances,* IAU Colloq. No. 90, p. 381, eds. Cowley, C.R., Dworetsky, M.M. & Megessier, C., Reidel, Dordrecht.

Alecian, G. & Artru, M.-C., 1987. *Astron. Astrophys.*, **186,** 223.

Alecian, G. & Michaud, G., 1981, *Astrophys. J.*, **245,** 226.

Aller, L.H., 1963. In: *Astrophysics: The atmospheres of the sun and stars,* 2nd Edition, The Ronald Press Co., New York, p. 62.

Ando, H., Watanabe, E., Yutani, M., Shimizu, Y. & Nishimura, S., 1988. *Pubs. Astr. Soc. Japan,* **40,** 249.

Angel, J.R.P. & Landstreet, J.D., 1970. *Astrophys. J. Letters,* **160,** L147.

Auvergne, M. & Baglin, A., 1986. *Astron. Astrophys.*, **168,** 118.

Babcock, H.W., 1947. *Astrophys. J.*, **105,** 105.

Babcock, H.W., 1947b. *Pubs. Astr. Soc. Pacific*, **59,** 260.

Babcock, H.W., 1947c. *Pubs. Astr. Soc. Pacific*, **59,** 112.

Babcock, H.W., 1949. *Observatory*, **69,** 191.

Babcock, H.W., 1951. *Astrophys. J.*, **114,** 1.

Babcock, H.W., 1956. *Astrophys. J.*, **124,** 489.

Babcock, H.W., 1962. In: *Astronomical techniques,* ed. W.A. Hiltner, University of Chicago Press. p. 107.

Babel, J. & Michaud, G., 1991. *Astron. Astrophys.*, **241,** 493.

Babel, J. & Michaud, G., 1991b. *Astron. Astrophys.*, **248,** 155.

Babel, J. & Michaud, G., 1991c. *Astrophys. J.*, **366,** 560.

Babel, J., 1992. *Astron. Astrophys.*, **258,** 449.

Balona, L.A., 1988a. LUCY user's manual, South African Astron. Obs.

Balona, L.A., 1988b. MILLY user's manual, South African Astron. Obs.

Baxandall, F.E., 1913. *Observatory,* **36,** 440.

Belmonte, J.A., 1989. PhD thesis, Universidad de La Laguna, Tenerife.

Belmonte, J.A. *et al.*, 1991. *Astron. Astrophys.*, **246,** 71.

Belmonte, J.A., Jones, A.R., Pallé, P.L. & Roca Cortés, T., 1990. *Astrophys. J.*, **358,** 595.

Belmonte, J.A., Pérez, F. & Roca, T. 1991. *Investigacion y ciencia,* 178, 76.

Belmonte, J.A., Martinez Roger, C. & Vidal, I., 1992a. *Inf. Bull. Var. Stars,* 3751.

Belmonte, J.A., Kreidl, T.J. & Martinez Roger, C., 1992b. *Inf. Bull. Var. Stars,* 3752.

Belopolsky, A., 1913. *Astron Nachr.*, **196,** 1.

Bidelman, W.P. & MacConnell, D.J., 1973. *Astron. J.*, **78,** 687.

Bohlender, D.A., Brown, D.N., Landstreet, J.D. & Thompson, I.B., 1987. *Astrophys. J.*, **323,** 325.

Bohlender, D.A. & Landstreet, J.D., 1990. *Astrophys. J.*, **358,** 274.

Bohlender, D.A. & Landstreet, J.D., 1990b. *Astrophys. J.*, **358,** L25.

Bonsack, W.K. & Wolff, S.C. 1980. *Astron. J.*, **85,** 599.

Borra, E.F. & Landstreet, J.D., 1980. *Astrophys. J.Suppl.*, **42,** 421.

Borra, E.F., Landstreet, J.D. & Thompson, I., 1983. *Astrophys. J. Suppl.*, **53,** 151.

Borra, E.F. & Vaughan, A.H., 1977. *Astrophys. J.*, **220,** 924.

Borsenberger, J., Michaud, G. & Praderie, F., 1979. *Astron. Astrophys.*, **76,** 287.

Borsenberger, J., Michaud, G. & Praderie, F., 1981. *Astrophys. J.*, **243,** 533.

Borsenberger, J., Michaud, G. & Praderie, F., 1984. *Astron. Astrophys.*, **139,** 147.

Boyarchuk, A.A. & Savanov, I.S., 1986. In: *Upper Main Sequence Stars with Anomalous Abundances,* IAU Colloq. No. 90, p. 433, eds. Cowley, C.R., Dworetsky, M.M. & Megessier, C., Reidel, Dordrecht.

Brancazio, P.J. & Cameron, A.G.W., 1967. *Canadian J. Physics,* **45,** 3297.

Breger, M., 1970. *Astrophys. J.*, **162,** 597.

Breger, M., 1979. *Pubs. Astr. Soc. Pacific,* **91,** 5.

Breger, M., 1990. In: *Communications in asteroseismology,* No. 12, Computing centre of the Austrian academy of sciences, Vienna.

Breger, M., 1991. *Astron. Astrophys.*, **250,** 107.

Breger, M. *et al.*, 1989. *Astron. Astrophys.*, **214,** 209.

Breger, M. *et al.*, 1990. *Astron. Astrophys.*, **231,** 56.

Brown, S.F., Donati, J.-F., Rees, D.E. & Semel, M., 1991. *Astron. Astrophys.*, **250,** 463.

Brown, T.M., Gilliland, R.L., Noyes, R.W. & Ramsey, L.W., 1991. *Astrophys. J.*, **368,** 599.

Cameron, R.C., 1967. In: *The magnetic and related stars,* ed. R.C. Cameron, Mono Book Corp., Baltimore, p. 471.

Catalano, F.A., Renson, P. & Leone, F., 1993. *Astron. Astrophys. Suppl.* **98,** 269.

Christensen-Dalsgaard, J., 1984. In: *Space Research Prospects in Stellar Activity and Variability,* p. 11. eds Mangeney, A. & Praderie, F., Publ. Observatoire de Paris.

Christensen-Dalsgaard, J., 1987., In: *Advances in Helio- and Asteroseismology,* Proc. IAU Symp. No. 123, p. 295, ed. Christensen-Dalsgaard, J. & Frandsen, S., Reidel, Dordrecht, Holland.

Christensen-Dalsgaard, J., 1989. *Lecture notes on stellar oscillations,* Aarhus University.

Christensen-Dalsgaard, J., Gough, D. & Toomre, J., 1985. *Science,* **229,** 4717.

Conti, P.S. & Barker, P.K., 1973., *Astrophys. J.*, **186,** 185.

Cousens, A. 1983. *Mon. Not. R. astr. Soc.*, **203,** 1171.

Cousins, A.W.J., 1987. *South African Astron. Obs. Circulars,* **11,** 93.

Cousins, A.W.J., 1989. *South African Astron. Obs. Circulars,* **13,** 15.

Cousins, A.W.J., 1990. *South African Astron. Obs. Circulars,* preprint.

Cowley, C.R., 1977. *Astrophys. Space Sci.*, **51,** 349.

Cowley, C.R., 1991. In: *Evolution of stars: The photospheric abundance connection,* eds. G. Michaud & A. Tutukov, Kluwer Academic Publishers, Dordrecht, Netherlands. p. 183-193.

Cox, A.N., 1955. *Astrophys. J.*, **121,** 628.

Cox, A.N., King, D.S. & Hodson, S.W., 1979. *Astrophys. J.*, **231,** 798.

Cox, J.P., 1980. *Theory of stellar pulsation,* Princeton University Press.

Crawford, D.L., 1966. In: *Spectral classification and multicolour photometry,* Eds: K. Lodén, L.O. Lodén & U Sinnerstad, IAU Symposium 24, p. 170.

Cox, J.P., 1984. *Astrophys. J.*, **280,** 220.

Crawford, D.L., 1975. *Astron. J.*, **80,** 955.

Crawford, D.L., 1978. *Astron. J.*, **83,** 48.

Crawford, D.L., 1979. *Astron. J.*, **84,** 1858.

Crawford, D.L. & Barnes, J.V., 1969. *Astron. J.*, **74,** 818.

Crawford, D.L. & Barnes, J.V., 1970. *Astron. J.*, **75,** 946.

Crawford, D.L. & Barnes, J.V., 1974. *Astron. J.*, **79,** 687.

Crawford, D.L. & Mander, J., 1966. *Astron. J.*, **71,** 114.

Deeming, T.J., 1975. *Astrophys. Space Sci.*, **36,** 137.

Deutsch, A.J., 1947. *Astrophys. J.*, **105,** 283.

Deutsch, A.J., 1952. *Transactions of the IAU*, **8,** 801.

Deutsch, A.J., 1958. In: *Electromagnetic phenomena in cosmical physics,* IAU Symp. No. 6, ed. B. Lehnert, Cambridge, p. 209.

Dolez, N. & Gough, D.O., 1982. In: *Pulsations in classical and cataclysmic variables*, eds. J.P. Cox & C.J. Hansen, JILA, Boulder, Colorado, p. 248.

Donati, J.-F., Semel, M. & del Toro Iniesta, J.-C., 1990. *Astron. Astrophys.*, **233,** L17.

Drake, S.A. *et al.* 1987. *Astrophys. J.*, **322,** 902.

Dziembowski, W. & Goode, P.R., 1985. *Astrophys J.*, **296,** L27.

Dziembowski, W. & Goode, P.R., 1986. In: *Seismology of the Sun and Distant Stars,* p. 441, ed. Gough, D.O., Reidel, Dordrecht, Holland.

Eddignton, A.S., 1926. *The internal constitution of the stars,* Cambridge University Press, Cambridge.

Faraggiana, R., 1987. *Astrophys. Space Sci.*, **134,** 381.

Floquet, M., 1983. In: *Les journées de Strasbourg,* Vème Réunion, ed. Observatoire de Strasbourg, p. 83.

Fossat, E., 1984. In: *Proceedings of the workshop on improvements to photometry,* eds W.J. Borucki & A.T. Young, NASA Conference Publication 2350, p. 56.

Fowler, W.A., Burbidge, E.M., Burbidge, G.R., & Hoyle, F., 1965. *Astrophys. J.*, **142,** 423.

Gabriel, M., Noels, A., Scuflaire, R. & Mathys, G., 1985. *Astron. Astrophys.*, **143,** 206.

García, J.R. *et al.*, 1993. *Delta Scuti Star Newsletter,* No 6, p. 14. Ed. M. Breger, Türkenschanzstr. 17, A-1180, Wien, Austria.

Gerbaldi, M., Floquet, M., Hauck, B., 1985. *Astron. Astrophys.*, **146,** 341.

Golay, M., 1974. *Introduction to astronomical photometry,* Reidel Publishing Co., Dordrecht, Holland.

Gough, D. & Toomre, J., 1991. *Annual Reviews of Astron. Astrophysics.*, **29,** 627

Gray, D.F. & Desikachary, K., 1973. *Astrophys. J.*, **181,** 523.

Gray, R.O. & Garrison, R.F., 1989. *Astrophys. J. Suppl.*, **69,** 301.

Grønbech, B. & Olsen, E.H., 1976. *Astron. Astrophys. Suppl.*, **25,** 213.

Grønbech, B. & Olsen, E.H., 1977. *Astron. Astrophys. Suppl.*, **27,** 443.

Guthnick, P. & Prager, R., 1914. *Veroff. K. Sternw. Berlin Babelsberg,* **1,** 1.

Guthrie, B.N.G., 1971, *Astrophys. Space Sci.*, **13,** 168.

Hale, G.E., 1908. *Astrophys. J.*, **28,** 315.

Hartoog, M.R., 1976. *Astrophys. J.*, **205,** 807.

Hartoog, M.R., Cowley, C.R., & Cowley, A.P., 1973. *Astrophys. J.*, **182,** 847.

Hatzes, A.P., Penrod, G.D. & Vogt, S.S., 1989. *Astrophys. J.*, **341,** 456.

Hauck, B. & Slettebak, A. 1983. *Astron. Astrophys.*, **127,** 231.

Havnes, O. & Conti, P.S., 1971. *Astron. Astrophys.*, **14,** 1.

Heller, C.H. & Kawaler, S.D., 1988. *Astrophys. J.*, **329**, L43.

Heller, C.H. & Kramer, K.S., 1988. *Pubs. Astr. Soc. Pacific*, **100**, 583.

Hensberge, H., Van Rensbergen, W. & Blomme, R., 1991. *Astron. Astrophys.*, **249**, 401.

Hensler, G., 1979. *Astron. Astrophys.*, **74**, 284.

Hildebrandt, G., 1992. *Astron. Nachr.* **313**, 233.

Houk, N & Cowley, A.P., 1975. Michigan Spectral Catalogue of Two-Dimensional Spectral Types for the HD Stars Volume 1, Dept of Astronomy, University of Michigan.

Houk, N., 1978. Michigan Spectral Catalogue of Two-Dimensional Spectral Types for the HD Stars Volume 2, Dept of Astronomy, University of Michigan.

Houk, N., 1982. Michigan Spectral Catalogue of Two-Dimensional Spectral Types for the HD Stars Volume 3, Dept of Astronomy, University of Michigan.

Houk, N & Smith-Moore, M., 1988. Michigan Spectral Catalogue of Two-Dimensional Spectral Types for the HD Stars Volume 4, Dept of Astronomy, University of Michigan.

Hric, L., 1988. In: *Magnetic stars*, eds. I.M. Kopylov & Yu. V. Glagolevskij, Nauka, Leningrad, p. 111.

Jaschek, C. & Jaschek, M., 1958. *Z. Astrophys.*, **45**, 35.

Jones, T.J., Wolff, S.C., & Bonsack, W.K., 1974. *Astrophys. J.*, **190**, 579.

Joss, P.C., 1974. *Astrophys. J.*, **191**, 771.

Khokhlova, V.G., 1975. *Soviet Astron*, **19**, 576.

Kilkenny, D., Balona, L.A., Carter, D.B., Ellis, D.T. & Woodhouse, G.F.W., 1988. *Mon. Not. Astr. Soc. Southern Africa*, **47**, 69.

Kreidl, T.J., 1986. *Lecture Notes in Physics*, **274**, 134.

Kreidl, T.J., 1991. *Mon. Not. R. astr. Soc.*, **248**, 701.

Kreidl, T.J., 1992. In: Proceedings of IAU colloquium 139, Victoria, Canada., in press.

Kreidl, T.J. & Kurtz, D.W., 1986. *Mon. Not. R. astr. Soc.*, **220**, 313.

Kreidl, T.J., Kurtz, D.W., Bus, S.J., Kuschnig, R., Birch, P.B., Candy, M.P. & Weiss, W.W., 1991. *Mon. Not. R. astr. Soc.*, **250**, 477.

Krishna-Kumar, C., Davila, J.M. & Sundar Rajan, R., 1989. *Astrophys. J.*, **337**, 414.

Kroll, R., 1989. *Reviews in modern astronomy*, **2**, 194.

Kurtz, D.W., 1976. *Astrophys. J. Suppl.*, **32**, 651.

Kurtz, D.W., 1978. *Astrophys. J.*, **221**, 869.

Kurtz, D.W., 1978b. *Inf. Bull. Var. Stars*, 1436.

Kurtz, D.W., 1979. *Mon. Not. R. astr. Soc.*, **189**, 1.

Kurtz, D.W., 1980b. *Mon. Not. R. astr. Soc.*, **193**, 29.

Kurtz, D.W., 1982. *Mon. Not. R. astr. Soc.*, **200**, 807.

Kurtz, D.W., 1983. *Inf. Bull. Var. Stars*, 2285.

Kurtz, D.W., 1984. *Mon. Not. R. astr. Soc.*, **206,** 247.

Kurtz, D.W., 1984b. *Mon. Not. R. astr. Soc.*, **206,** 253.

Kurtz, D.W., 1984c. In: *Proceedings of the Workshop on Improvements to Photometry,* p. 56, ed. Borucki, W.J. & Young, A., NASA Conference Publication 2350.

Kurtz, D.W., 1985. *Mon. Not. R. astr. Soc.*, **213,** 773.

Kurtz, D.W., 1986. *Astrophys. Space Sci.*, **125,** 311.

Kurtz, D.W., 1988. *Mon. Not. R. astr. Soc.*, **233,** 565.

Kurtz, D.W., 1988b. In:*Procs. Symposium on Multimode Stellar Pulsations*, p. 107, Editors: Kovács, G., Szabados, L. & Szeidl, B., Konkoly Observatory, Kultura, Budapest, 1988.

Kurtz, D.W., 1988c. In:*Procs. Symposium on Multimode Stellar Pulsations*, p. 95, Editors: Kovács, G., Szabados, L. & Szeidl, B., Konkoly Observatory, Kultura, Budapest, 1988.

Kurtz, D.W., 1989. *Mon. Not. R. astr. Soc.*, **238,** 261.

Kurtz, D.W., 1989b. *Mon. Not. R. astr. Soc.*, **238,** 1077.

Kurtz, D.W., 1990. *Annual Reviews of Astronomy & Astrophysics,* **28,** 607.

Kurtz, D.W., 1991. *Mon. Not. R. astr. Soc.*, **249,** 468.

Kurtz, D.W., 1992. *Mon. Not. R. astr. Soc.*, **259,** 700.

Kurtz, D.W. & Balona, L.A., 1984. *Mon. Not. R. astr. Soc.*, **210,** 779.

Kurtz, D.W., Kanaan, A. & Martinez, P., 1993. *Mon. Not. R. astr. Soc.*, **260,** 343.

Kurtz, D.W., Kanaan, A., Martinez, P. & Tripe, P., 1992. *Mon. Not. R. astr. Soc.*, **255,** 289.

Kurtz, D.W., Kreidl, T.J., O'Donoghue, D.O., Osip, D.J. & Tripe, P., 1991. *Mon. Not. R. astr. Soc.*, **251,** 152.

Kurtz, D.W., Matthews, J.M., Martinez, P., Seemann, J., Cropper, M., Clemens, J.C., Kreidl, T.J., Sterken, C., Schneider, H., Weiss, W.W., Kawaler, S.D., Kepler, S.O., van der Peet, A., Sullivan, D.J. & Wood, H.J., 1989. *Mon. Not. R. astr. Soc.*, **240,** 881.

Kurtz, D.W. & Shibahashi, H., 1986. *Mon. Not. R. astr. Soc.*, **223,** 557.

Kurtz, D.W., van Wyk, F. & Marang, F., 1990. *Mon. Not. R. astr. Soc.*, **243,** 289.

Kurtz, D.W. & Wegner, G., 1979. *Astrophys. J.*, **232,** 510.

Landstreet, J.D., 1980. *Astron. J.*, **85,** 611.

Landstreet, J.D., 1982. *Astrophys. J.*, **258,** 639.

Landstreet, J.D., 1988. *Astrophys. J.*, **326,** 967.

Landstreet, J.D., Barker, P.K., Bohlender, D.A. & Jewison, M.S., 1989. *Astrophys. J.*, **344,** 876.

Lanz, T., 1985. *Astron. Astrophys.*, **144,** 191.

Lebedev, V.S., 1989. Astrophys. Issledov., Izvestia SAO **27,** 54.

Ledoux, P., 1951. *Astrophys. J.*, **114,** 373.

Ledoux, P. & Renson, P. 1966. *Annual reviews in astronomy and astrophysics,* **4,** 293.

Leone, F., 1991. *Astron. Astrophys.*, **252,** 198.

Leroy, J.-L., Landi Degl'Innocenti, E. & Landolfi, M., 1992. In: *Proceedings of Paris Workshop on Determination of Stellar and Solar Magnetic Fields*, eds N Mein, H Frisch & M. Faurobert-Scholl.

Libbrecht, K.G., 1988. *Astrophys. J.*, **330,** L51.

Ludendorff, H., 1906. *Astron. Nachr.*, **173,** 1.

Maitzen, H.M., 1981. In: *Les Étoiles de composition chimique anormal du debut de la séquence principale*, Université de Liège, Liège, p. 51.

Maitzen, H.M., 1984. *Astron. Astrophys.*, **138,** 493.

Maitzen, H.M., 1989. *Reviews in Modern Astronomy*, **2,** 205.

Manfroid, J. & Sterken, C., 1987. *Astron. Astrophys. Suppl.*, **71,** 539.

Manfroid *et al.*, 1991. *Astron. Astrophys. Suppl.*, **87,** 481.

Martinez, P., 1989. *Mon. Not. R. astr. Soc.*, **238,** 439.

Martinez, P., 1991. *Inf. Bull. Var. Stars*, 3621.

Martinez, P. & Kauffmann G., 1990. *Inf. Bull. Var. Stars*, 3507.

Martinez, P. & Kurtz, D.W., 1990. *Inf. Bull. Var. Stars*, 3510.

Martinez, P. & Kurtz, D.W., 1990b. *Inf. Bull. Var. Stars*, 3509.

Martinez, P. & Kurtz, D.W., 1990c. *Mon. Not. R. astr. Soc.*, **242,** 636.

Martinez, P., Kurtz, D.W. & Heller, C.H., 1990. *Mon. Not. R. astr. Soc.*, **246,** 699.

Martinez, P., Kurtz, D.W., Kauffmann, G. & Jonson, A.C., 1990. *Inf. Bull. Var. Stars*, 3506.

Martinez, P. & Kurtz, D.W., 1991a. *Inf. Bull. Var. Stars*, 3553.

Martinez, P. & Kurtz, D.W., 1991b. *Inf. Bull. Var. Stars*, 3611.

Martinez, P. & Kurtz, D.W., 1992. *Inf. Bull. Var. Stars*, 3750.

Martinez, P., Kurtz, D.W. & Kauffmann, G., 1991. *Mon. Not. R. astr. Soc.*, **250,** 666.

Martinez, P., Kurtz, D.W. & Meintjes, P., 1993. *Mon. Not. R. astr. Soc.*, in press.

Martinez, P. & Ashley, R.A., 1993. *Inf. Bull. Var. Stars*, 3844.

Martinez, P., Kurtz, D.W., Ashley, R.A., 1993. *Inf. Bull. Var. Stars*, 3844.

Martinez, P., Kurtz, D.W. & Meintjes, P.J., 1993. *Mon. Not. R. astr. Soc.*, **260,** 9.

Martinez, P., Kurtz, D.W., Kreidl, T.J., Koen, C., van Wyk, F., Marang, F. & Roberts, G., 1993. *Mon. Not. R. astr. Soc.*, **263,** 273.

Mathys, G., 1985. *Astron. Astrophys.*, **151,** 315.

Mathys, G., 1989. *Fundamentals of Cosmic Physics*, **13,** 143.

Mathys, G., 1990. *Astron. Astrophys.*, **232,** 151.

Mathys, G. & Lanz, T. 1990. *Astron. Astrophys.*, **230,** L21.

Mathys, G. & Lanz, T. 1992. *Astron. Astrophys.*, **256,** 169.

Matthews, J.M., 1987. In the PhD Thesis *Frequency analysis of the rapidly oscillating Ap star HD 60435.*, University of Western Ontario, London, Ontario.

Matthews, J.M., 1988. *Mon. Not. R. astr. Soc.*, **235,** 7P.

Matthews, J.M., 1989. In: *Seismology of the Sun and Sun-like stars,* ESA Special Publication 286, p. 547.

Matthews, J.M., 1990. In: *Progress of seismology of the Sun and stars,* eds. Y. Osaki & H. Shibahashi, Springer Verlag, Berlin, *Lecture Notes in Physics,* **367,** 385.

Matthews, J.M., 1991. *Pubs. Astr. Soc. Pacific,* **103,** 5.

Matthews, J.M., Kreidl, T.J. & Wehlau, W.H., 1988. *Publs. Astr. Soc. Pacific,* **100,** 255.

Matthews, J.M., Kurtz, D.W. & Wehlau, W.H., 1986. *Astrophys. J.*, **300,** 348.

Matthews, J.M., Kurtz, D.W. & Wehlau, W.H., 1987. *Astrophys. J.*, **313,** 782.

Matthews, J.M. & Wehlau, W.H. 1985. *Pubs. Astr. Soc. Pacific,* **97,** 841.

Matthews, J.M., Wehlau, W.H., Walker, G.A.H.& Yang, S., 1988. *Astrophys. J.*, **324,** 1099.

Matthews, J.M., Wehlau, W.H. & Walker, G.A.H. 1990. *Astrophys. J.*, **365,** L81.

Matthews, J.M., Wehlau, W.H., Rice, J. & Walker, G.A.H. 1992. preprint.

Maury, A.C., 1897. *Harvard Annals,* **28,** 96.

Mégessier, C., 1984. *Astron. Astrophys.*, **138,** 267.

Mégessier, C., 1988. *Astron. Astrophys. Suppl.*, **72,** 551.

Mégessier, C., Khokhlova, V.L. & Ryabchikova, T.A., 1979. *Astron. Astrophys.*, **71,** 295.

Michaud, G., 1970. *Astrophys. J.*, **160,** 641.

Michaud, G., 1980. *Astron. J.*, **85,** 589.

Michaud, G., 1986. In: *Upper Main Sequence Stars with Anomalous Abundances,* IAU Colloq. No. 90, eds. Cowley, C.R., Dworetsky, M.M. & Megessier, C., Reidel, Dordrecht, p. 459.

Michaud, G., Mégessier, C. & Charland, Y., 1981. *Astron. Astrophys.*, **103,** 244.

Michel, E. *et al.*, 1992. *Astron. Astrophys.*, **255,** 139.

Molnar, M.R., 1973. *Astrophys. J.*, **179,** 527.

Molnar, M.R. & Wu, C.-C., 1978. *Astron. Astrophys.*, **63,** 335.

Moon, T.T. and Dworetsky, M.M., 1985. *Mon. Not. R. astr. Soc.*, **217,** 305.

Morgan, W.W., 1933. *Astrophys. J.*, **77,** 330.

Moskalik, P., 1986. *Acta Astron* **36,** 333.

Moss, D., 1986. *Physics Reports,* **140,** 1.

Moss, D., 1989. *Mon. Not. R. astr. Soc.*, **236,** 629.

Muthsam, H., 1979a. *Astron. Astrophys. Suppl.*, **35,** 107.

Muthsam, H., 1979b. *Astron. Astrophys.*, **73,** 159.

Muthsam, H. & Stepien, K., 1980. *Astron. Astrophys.*, **86,** 240.

Nather, R.E. & Warner, B., 1971. *Mon. Not. R. astr. Soc.*, **152,** 209.

Nelson, M.J. & Kreidl, T.J., 1993. *Astron. J.*, **105,** 1903.

North, P. 1984. *Astron. Astrophys.*, **141,** 328.

North, P. & Cramer N., 1981. In: *Les Étoiles de composition chimique anormal du debut de la séquence principale*, Université de Liège, Liège, p. 55.

North, P. & Kroll, R., 1989, *Astron. Astrophys. Suppl.*, **78,** 325.

Noyes, R.W., Baliunas, S.L., Belserene, E., Duncan, D.K., Horne, J. & Widrow, L., 1984. *Astrophys. J. Letters,* **285,** L23.

Percy, J.R., 1975. *Astron. J.*, **80,** 698.

Perry, C.L., Olsen, E.H. & Crawford, D.L., 1987. *Pubs. Astr. Soc. Pacific,* **99,** 1184.

Preston, G.W., 1967. *Astrophys. J.*, **150,** 547.

Preston, G.W., 1974. *Annual Reviews Astron. Astrophys.*, **12,** 257.

Renson, P., 1989. *Inf. Bull. Var. Stars,* 3452.

Rice, J.B., 1988. *Astron. Astrophys.*, **199,** 299.

Rice, J.B. & Wehlau, W.H., 1990. *Astron. Astrophys.*, **233,** 503.

Rice, J.B. & Wehlau, W.H., 1991. *Astron. Astrophys.*, **246,** 195.

Rice, J.B., Wehlau, W.H. & Khokhlova, V.L., 1989. *Astron. Astrophys.*, **208,** 179.

Ryabchikova, T.A., 1991. In: *Evolution of stars: The photospheric abundance connection,* ed. G. Michaud & A. Tutukov, Kluwer Academic Publishers, Dordrecht, p. 149.

Sargent, W.L.W., 1967. In: *The magnetic and related stars.* ed. R.C. Cameron, Mono Book Corp, Baltimore, p. 329.

Scargle, J.D., 1982. *Astrophys. J.*, **263,** 835.

Schaefer, B. 1985. *Astron. J.*, **90,** 1363.

Schneider, H. & Weiss, W.W., 1989. *Astron. Astrophys.*, **210,** 147.

Schneider, H. & Weiss, W.W., 1990. *Inf. Bull. Var. Stars,* 3520.

Schutt, R.L., 1991. *Astron. J.*, **101,** 2177.

Schwarzchild, M., 1950. *Astrophys. J.*, **112,** 222.

Semel, M., 1989. *Astron. Astrophys.*, **225,** 456.

Shibahashi, H., 1983. *Astrophys. J.*, **275,** L5.

Shibahashi, H., 1991. In: *Challenges to theories of the structure of moderate-mass stars,* ed. Gough, D.O. & Toomre, J., Springer, Berlin, p. 393.

Shibahashi, H. & Saio, H., 1985. *Publs. astr. Soc. Japan,* **37,** 245.

Shibahashi, H. & Takata, M. 1993. preprint.

Spencer Jones, J., 1983. *South African Astron. Obs. Facilities Manual.*

Stepien, K., 1989. *Astron. Astrophys.*, **220,** 105.

Stepien, K. & Dominiczak, R., 1989. *Astron. Astrophys.*, **219,** 197.

Stepien, K. & Muthsam, H. 1981. *Astron. Astrophys.*, **100,** 159.

Stepien, K. & Muthsam, H. 1987. *Astron. Astrophys.*, **185,** 225.

Stibbs, D.W.N., 1950. *Mon. Not. R. astr. Soc.*, **110,** 395.

Stift, M.J., 1975. *Mon. Not. R. astr. Soc.*, **172,** 133.

Strömgren, B. 1966. *Annual Reviews Astron. Astrophys.*, **4,** 433.

Tassoul, M., 1980. *Astrophys. J. Suppl.*, **43,** 469.

Tassoul, M., 1990. *Astrophys. J.*, **358,** 313.

Ulrich, R.K., 1986. *Astrophys. J.*, **306,** L37.

Unno, W., Osaki, Y., Ando, H., Saio, H. & Shibahashi, H. 1989. *Nonradial oscillations of stars (2nd Edition)*, Univ. of Tokyo Press, Tokyo.

van den Heuvel, E.P.J., 1967, *Bull. Astron. Inst. Netherlands,* **19,** 11.

Vauclair, S., 1983. In: *Astrophysical Processes in Upper Main Sequence Stars,* Eds. Hauck, B. & Maeder, A., Geneva Observatory, p167.

Vauclair, S., Dolez, N. & Gough, D.O., 1991. *Astron. Astrophys.*, **252,** 618.

Vauclair, S. & Vauclair, G., 1982. *Annual Reviews of Astronomy & Astrophysics,* **20,** 37.

Vauclair, G., Vauclair, S. & Michaud, G., 1978. *Astrophys. J.*, **223,** 920.

Vogt, N. & Faundez, M., 1979. *Astron. Astrophys. Suppl.*, **36,** 477.

Warner, B., 1988. *High-speed astronomical photometry,* Cambridge University Press, Cambridge.

Wegner, G., 1981. *Astrophys. J.*, **247,** 969.

Wegner, G., Cummins, D.J., Byrne, P.B., & Stickland, D.J., 1983. *Astrophys. J.*, **272,** 646.

Weiss, W.W., 1978. *Astron. Astrophys. Supp,* **35,** 83.

Weiss, W.W. & Schneider, H., 1984. *Astron. Astrophys.*, **135,** 141.

Weiss, W.W., Schneider, H., Kuschnig, R. & Bouchet, P., 1991. *Astron. Astrophys.*, **245,** 145.

Wolff, S.C., 1981. *Astrophys. J.*, **244,** 221.

Wolff, S.C., 1983. *The A-Type Stars: Problems and Perspectives*, Nasa Special Publication 463.

Wolff, S.C. & Hagen, W., 1976. *Publs. astron. Soc. Pacif.*, **88,** 119.

Wolff, S.C. & Wolff, R.J., 1976. In: *The Physics of Ap stars,* ed. Weiss, W.W., Jenkner, H. & Wood, H.J., Universitatssternwarte, Wien, p.503.

Young, A.T., 1967. *Astron. J.*, **72,** 747.